ISTITUTO NAZIONALE DI FISICA NUCLEARE
Laboratori Nazionali di Frascati

FRASCATI PHYSICS SERIES

INFN Commissione Scientifica Nazionale 1 (CSN1)

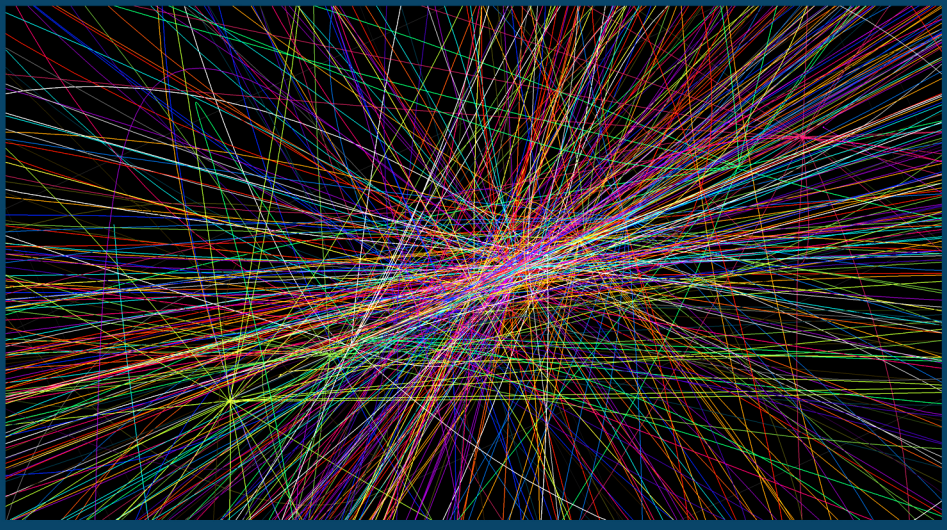

What Next: White Paper of CSN1

Proposal for a long term strategy for accelerator based experiments

Editors
F. Bedeschi, R. Tenchini, J. Walsh

INFN Commissione Scientifica Nazionale 1 (CSN1)

What Next: White Paper of CSN1

Proposal for a long term strategy for accelerator based experiments

May 29, 2015

FRASCATI PHYSICS SERIES

Series Editor: *Rossana Centioni*

Series Editor: *Debora Bifaretti*

Cover illustration: high-pileup LHC collisions. Copyright CERN, for the benefit of the CMS Collaboration.

Volume LX

Istituto Nazionale di Fisica Nucleare - Laboratori Nazionali di Frascati
SIDS - Servizio Informazione e Documentazione Scientifica
Ufficio Biblioteca e Pubblicazioni (sis.publications@lnf.infn.it)
P.O. Box 13, I-00044 Frascati Roma Italy

ISBN 978-88-864-0999-5

Commissione Scientifica Nazionale 1

F. Bedeschi, A. Andreazza, W. Baldini, C. Biino, P. Camarri, G. Carlino, A. Colaleo, M. Grassi, A. Lai, S. Malvezzi, S. Passaggio, A. Passeri, M. Pepe, G. Polesello, M. Rescigno, G. Sguazzoni, F. Simonetto, T. Spadaro, S. Spagnolo, A. Tricomi, V. Vagnoni, A.M. Zanetti.

Conveners Working Group Standard Model

S. Forte, A. Nisati, G. Passarino, R. Tenchini.

Conveners Working Group Beyond Standard Model

G. Polesello, S. Rahatlou, A. Romanino, A. Wulzer.

Conveners Working Group Flavour Physics

C. Bozzi, G. De Nardo, L. Silvestrini, C. Tarantino.

Conveners Working Group Non Perturbative QCD

M. Anselmino, M. Ruspa, L. Trentadue.

Conveners Task force on new technologies

M. Ferrario, F. Forti, D. Lucchesi, G. Punzi.

Editors

F. Bedeschi, R. Tenchini, J. Walsh.

List of Authors

A. Andreazza[10a,b], M. Anselmino[20a,b], P. Azzi[13b], W. Baldini[5], R. Barbieri[37,16b], F. Bedeschi[16b], E. Bertuzzo[38], C. Biino[20b], M. Bochicchio[17b], W. Bonivento[3], C. Bozzi[5], F. Bradamante[21a,b], D. Buttazzo[26], S. Camarda[35], P. Camarri[18], L. Cappiello[12a,b], G. Carlino[12b], C.M. Carloni Calame[14a], N. Cartiglia[20b], A. Castro[2a,b], F. Ceccopieri[36], P. Checchia[13b], M. Chiesa[14b], M. Cobal[22a,b], A. Colaleo[1], P. Colangelo[1], F. Cossutti[21b], G. Corcella[8], G.M. Dallavalle[2b], G. D'Ambrosio[12,23], S. De Curtis[6b,a], M. D'Elia[16a,b], F. De Fazio[1], G. De Nardo[12a,b], G. Degrassi[19a,b], F. Dettori[23], B. Di Micco[19a,b], F. Donato[20a,b], L. Fanò[15a,b], P. Ferrarese[27], M. Ferrario[8], G. Ferrera[10a,b], F. Ferro[7], S. Forte[10a,b], F. Forti[16a,b], R. Franceschini[23], A. Gennaro[21a,22b], P. Giacomelli[2b], M. Grassi[16b], E. Graverini[28], D. Greynat[12a,b], G. Isidori[8], A. Lai[3], G. Lanfranchi[8], I. Lax[2b], P. Lenisa[5a,b], P. Lipari[17b], D. Lucchesi[13a,b], S. Malvezzi[11b], U. Marconi[2b], G. Maron[24], A. Martin[21a,b], B. Mele[17b], S. Miscetti[8], G. Montagna[14a,b], M. Moulson[8,23], R. Mussa[20b], P. Nason[11b], N. Neri[10b], O. Nicrosini[14b], A. Nisati[17b], C. Oleari[11a,b], F. Palla[16b], G. Panico[25], G. Panizzo[21a,22b], S. Passaggio[7], G. Passarino[20a,b], A. Passeri[19b], D. Pedrini[11b], M. Pepe[15b], F. Piccinini[14b], M. Pinamonti[29,22b], G. Polesello[14b], G. Punzi[16a,b], M. Radici[14b], M. Raggi[8], S. Rahatlou[17a,b], M. Rescigno[17b], A. Romanino[29,21b], M. Ruspa[20b,33], L. Rossi[23], F. Sala[30], E. Santopinto[7], N. Serra[28], G. Sguazzoni[6b], G. Signorelli[16b], L. Silvestrini[17b], F. Simonetto[13a,b], M. Sozzi[16a,b], T. Spadaro[8], S. Spagnolo[9], N. Tantalo[18], C. Tarantino[19a,b], R. Tenchini[16b], A. Tesi[31], A. Thamm[32], R. Torre[13a,b], D. Treleani[21a,b], L. Trentadue[11b,34], A. Tricomi[4], A. Urbano[29], V. Vagnoni[2b], P. Valente[17b], A. Vicini[10a,b], J. Walsh[16b], A. Wulzer[13a,b], A.M. Zanetti[21b].

[1] INFN, Sezione di Bari,
Via Orabona 4, I-70125 Bari, Italy

[2] Dipartimento di Fisica e Astronomia, Università degli Studi Di Bologna (a) and
INFN, Sezione di Bologna (b),
Via Irnerio 46, I-40126 Bologna, Italy

[3] INFN, Sezione di Cagliari,
Complesso Univ. di Monserrato, S.P. per Sestu Km 0.7, I-09042 Monserrato, Cagliari, Italy

[4] Dipartimento di Fisica e Astronomia, Università di Catania and INFN, Sezione di Catania,
Via Santa Sofia 64, I-95123 Catania, Italy

[5] INFN, Sezione di Ferrara,
Polo Scientifico e Tecnologico ed. C - Via Saragat 1, I-44122 Ferrara, Italy

[6] Dipartimento di Fisica e Astronomia, Università degli Studi di Firenze (a) and
INFN, Sezione di Firenze (b),
Via G. Sansone 1, I-50019 Sesto Fiorentino, Firenze, Italy

[7] INFN, Sezione di Genova,
Via Dodecaneso 33, I-16146 Genova, Italy

[8] INFN, Laboratori Nazionali di Frascati,
Via E. Fermi 40, I-00044 Frascati, Roma, Italy

[9] Dipartimento di Matematica e Fisica, Università del Salento and INFN, Sezione di Lecce,
Via Arnesano, I-73100 Lecce, Italy

[10] Dipartimento di Fisica, Università di Milano (a) and INFN, Sezione di Milano (b),
Via Celoria 16, I-20133 Milano, Italy

[11] Dipartimento di Fisica, Università di Milano-Bicocca (a) and INFN, Sezione di Milano-Bicocca (b),
Piazza della Scienza 3, I-20126 Milano, Italy

[12] Dipartimento di Fisica, Università di Napoli (a) and INFN, Sezione di Napoli (b),
Complesso Univ. di Monte S. Angelo ed. C, Via Cintia, I-80126 Napoli, Italy

[13] Dipartimento di Fisica, Università di Padova (a) and INFN, Sezione di Padova (b),
Via Marzolo 8, I-35131 Padova, Italy

[14] Dipartimento di Fisica, Università di Pavia (a) and INFN, Sezione di Pavia (b),
Via A. Bassi 6, I-27100 Pavia, Italy

[15] Dipartimento di Fisica e Geologia, Università degli studi di Perugia (a) and
INFN, Sezione di Perugia (b),
Via A. Pascoli, I-06123 Perugia, Italy

[16] Dipartimento di Fisica, Università di Pisa (a) and INFN, Sezione di Pisa (b),
Polo Fibonacci ed. C, Largo B. Pontecorvo 3, I-56127 Pisa, Italy

[17] Dipartimento di Fisica, Università di Roma (a) and INFN, Sezione di Roma (b),
P.le Aldo Moro 2, I-00185 Roma, Italy

[18] Dipartimento di Fisica, Università di Roma Tor Vergata and INFN, Sezione di Roma Tor Vergata,
Via della Ricerca Scientifica 1, I-00133 Roma, Italy

[19] Dipartimento di Matematica e Fisica, Università Roma Tre (a) and INFN, Sezione di Roma Tre (b),
Via della Vasca Navale 84, I-00146 Roma, Italy

[20] Dipartimento di Fisica, Università di Torino (a) and INFN, Sezione di Torino (b),
Via P. Giuria 1, I-10125 Torino, Italy

[21] Dipartimento di Fisica, Università degli Studi di Trieste (a) and INFN, Sezione di Trieste (b),
Via Valerio 2, I-34127 Trieste, Italy

[22] Dipartimento di Chimica, Fisica e Ambiente, Università di Udine (a) and
INFN, Gruppo Collegato di Udine (b),
Via delle Scienze, 206 - I-33100 Udine, Italy

[23] CERN,
1121 Genève 23, Switzerland

[24] INFN-CNAF,
Viale Berti Pichat 6/2, 40127 Bologna, Italy

[25] Universitat Autonoma de Barcelona
Institut de Fisica d'Altes Energies (IFAE)
Campus UAB, Edifici Cn E-08193 Bellaterra, Barcelona, Spain

[26] Technische Universität München (TUM)
Institute for Advanced Study (IAS)
Lichtenbergstrasse 2a, 85748 Garching Germany

[27] Georg-August-Universität Göttingen
II. Physikalisches Institut
Friedrich-Hund-Platz 1, 37077 Göttingen Germany

[28] Universität Zürich, Physik Institut
Winterthurerstrasse 190 CH-8057 Zürich Switzerland

[29] Scuola Internazionale Superiore di Studi Avanzati (SISSA)
via Bonomea, 265 I-34136 Trieste Italy

[30] Institut de Physique Théorique
Orme des Merisiers batiment 774 Point courrier 136
CEA/DSM/IPhT, CEA/Saclay F-91191 Gif-sur-Yvette Cedex France

[31] University of Chicago
Department of Physics 5720 So. Ellis Ave., KPTC 201 Chicago, IL 60637-1434 USA

[32] Johannes Gutenberg-Universität Mainz (JGU)
Saarstr. 21, 55122 Mainz Germany

[33] Universitá del Piemonte Orientale

via Solaroli 17, I-28100 Novara, Italy

[34] Universitá di Parma
Viale G. P. Usberti 7/A, I-43124 Parma, Italy

[35] Deutsches Elektronen-Synchrotron (DESY)
Notkestrasse 85, 22607 Hamburg, Germany

[36] IFPA (Interactions Fondamentales en Physique et en Astrophysique), Universitè de Liège,
19A Allèe du 6 Août, 4000Liège, Belgium

[37] Scuola Normale Superiore (SNS)
Piazza dei Cavalieri 7, I-56126 Pisa, Italy

[38] Instituto de Fisica, Universidade de Sao Paulo,
Sao Paulo, Brazil

Foreword

The CSN1 (Commissione Scientifica Nazionale 1) is the INFN committee which manages experiments at high energy particle accelerators. This document describes our understanding of the current scientific scenarios and proposes a strategy for the next 10 years in the context of a 20-year global vision for this field of research.

The idea for this document was born during 2013. Many excellent experimental results had been obtained, including the newly discovered low mass Higgs boson, but there was still no hint of new physics both in direct and indirect searches. The future was full of proposals for new experiments and research infrastructures, and major upgrades of the existing ones, but all motivations had to be evaluated in a global context. In general there was a clear need to re-analyze in depth our science drivers and then find a consensus within our community about the strategy for the future. This need was reinforced by the perception that funding in our field was becoming more difficult. Since potential new programs are expensive, choices were going to be needed and priorities would need to be set.

During the November 2013 meeting of CSN1 there was a discussion on how to deal with this situation. In the end we decided to start a process leading to the proposal of a long term strategy to be published in a "White Paper" on the time scale of approximately a year. We decided that the whole community should be involved with the help of many well known theorists [1]. This required some organization, so we formed four working groups covering the following scientific topics: "Direct searches of new physics", "Precise Standard Model measurements", "Flavour physics" and "Non-perturbative QCD". These topics cover completely all scientific activities present in CSN1. Each working group is coordinated by four conveners: two theorists and two experimental physicists.

A similar process involving all INFN activities was started one month later by the INFN top management under the name of "What Next" and the CSN1 working groups morphed quite naturally into this extended organization, while retaining also their original scope. In addition to its use for CSN1, this document represents our main contribution to the more global "What Next" process.

Two widely attended workshops have been organized to discuss the activities ongoing within the working groups. First a kick off meeting of the whole "What Next" in Rome on April 7-8, 2014; then a dedicated CSN1 workshop in Elba on May 22-24, 2014.

Thereafter an editorial committee was setup to coordinate the writing of the document and a preliminary draft was discussed during the December 2014 meeting of CSN1. An updated version was released shortly afterwards for comments from the members of CSN1, the conveners and participants of the working groups. After inclusion of the suggestions received, an open meeting was held on January 15^{th} to discuss the document and in particular its conclusions. The conclusions were approved during the CSN1 meeting of January 19-20, 2015 and the full document has been released for public distribution in May 2015.

President of CSN1,
Dr. Franco Bedeschi

[1] We thank CSN4, the INFN committee handling theoretical physics, for its strong support and active collaboration.

Contents

1 Introduction

Particle physics at accelerators has entered a new historical phase with the discovery of what seems to be, to all effects, the first fundamental scalar field. This phase encompasses three aspects already present in fundamental science in the past two hundred years. The *discovery of the Higgs boson* recalls the excitement of the discovery of the positron in the thirties, which proved that the anti-electron of Dirac's equation was not just a mere mathematical artifact. The *triumph of the Standard Model* recalls the success of classical electrodynamics at the end of the XIX century, which made scientists believe that a model, which could potentially explain all phenomena in a laboratory, was at hand. The evidence of phenomena, which cannot be explained by the Standard Model, recalls the experimental evidence of radioactivity, *new physics* at the time, in Curie's laboratory at the dawn of the XX century.

There is no doubt that *new physics* exists, beyond the Standard Model, as indicated by the inconsistency with a few experimental observations:

- Standard Model fermions constitute only about one sixth of the total matter in galaxies, according to astrophysical observations;
- neutrinos oscillate and therefore have a mass, while within the Standard Model they are predicted to be strictly massless.

This evidence for new physics is further reinforced by the lack of *natural explanations* for some observed phenomena:

- baryons in our known universe are not matched by an equal amount of anti-baryons, this asymmetry cannot be dynamically explained within the Standard Model (it must be postulated as a peculiar asymmetric initial condition);
- the hierarchical pattern of quark and lepton masses, and the approximate symmetries exhibited by their mixing matrices, are completely unexplained (they are mere free parameters of the model);
- the lightness of the Higgs boson mass compared to the Planck scale (the fundamental mass scale associated to gravitational interactions) requires an unnatural fine-tuning of the mass term in the Higgs potential.

The three aspects mentioned above, *i) important discovery, ii) precise verification of a model, iii) unexplained phenomena* co-exists at the present time, making this period a special one. There is a fourth aspect that, again, is not new to fundamental physics. Having found experimental evidence of all the building blocks of the Standard Model, we have somewhat lost guidance in the search for new fundamental constituents, and we must rely, rather than on model-dependent prejudices, on the traditional way of discovering new physics by exploring new frontiers; *i.e.,* making new experimental measurements or improving the precision of existing measurements.

From the above considerations, two main drivers for particle physics at accelerators can be identified, on a time scale relevant for this report. The first one is, rather obviously, to understand the role of the new discovered scalar in electroweak symmetry breaking. The properties of the Higgs boson must be studied with high precision, similarly to what has been done, in the past, for vector bosons. It is of paramount importance to understand if the newly discovered scalar particle is indeed the Higgs boson responsible for the Brout-Engler-Higgs mechanism in the Standard Model or if it is something else, *e.g.,* composite or part of a doublet. Furthermore, the role of the scalar in its interactions with other particles should be clarified. Is the coupling of the scalar boson to fermions, in particular to the most massive fermion, the top quark, as predicted by the Standard Model? Is the unitarity of WW scattering really preserved as foreseen if the new boson is the Standard Model Higgs boson? These questions, together with other related ones, must be answered.

The second major physics driver is evident, too, and it is related to the need to clarify the experimental observations and the theoretical arguments, which are pointing to the existence of physics

beyond the Standard Model. As an example, experiments at accelerators have a considerable potential to reveal the nature of dark matter (DM) by producing it in high energy interactions. Indeed, the search for DM at accelerators is complementary to direct and indirect detection of cosmic DM. Another example is the search for supersymmetric top partners (stop) or other new particles that could shed light on the stabilization mechanism of the Higgs mass parameter. In this perspective, the search for third generation partners has gained considerable momentum and is expected to be a very active field of research in the coming years. Last but not least, the search for deviations from the Standard Model predictions in flavour-changing transitions of quarks or leptons could reveal new dynamics responsible for the approximate flavour symmetries observed in nature. More generally, precise studies of flavour-changing transitions provides an effective tool for indirect searches of new particles, even at mass scales well above those directly accessible at the LHC.

While the two main physics drivers can be easily defined, the identification of relevant subjects is more complex. To this end four dedicated working groups have been formed and their conclusions are reported in this document. The status of Standard Model physics and the main expected developments are described in Chapter 4. Obviously, a large fraction of this chapter is dedicated to the prospect for measurements of Higgs boson properties, including precision measurements of couplings and searches for rare Higgs boson decays. Improved measurements of the W boson and top quark masses are discussed next, together with other key electroweak parameters and the strong coupling constant. Electroweak fits have historically anticipated the top and Higgs boson mass values, they are now a powerful test of consistency of the Standard Model and, with increasing precision, they could give important indications for new physics. Di-boson physics is another important subject, giving insight to new phenomena at energy scales much higher than the accelerator centre-of-mass. The study of top quark properties is promising for detecting new physics, because of the large top-Higgs Yukawa coupling and because top is the only quark that decays before hadronisation takes place, allowing unique measurements to be made. Monte Carlo simulations have progressed enormously in recent years, and they represent an essential tool for precision measurements and searches; perspectives for further progress are discussed. Chapter 5 is dedicated to physics beyond the Standard Model. The driving principle of naturalness is reviewed and emphasis is given to scenarios taking into account the most recent experimental results. Supersymmetry is examined taking as examples the minimal and next-to-minimal models; composite-Higgs models are also examined. The previously-mentioned interplay between accelerator and non-accelerator-based searches for dark matter is explored. Naturalness-independent searches, e.g. experimental signatures of a "dark sector", are also presented. Chapter 6 is dedicated to the discussion of flavour physics. The experimental program for beauty, charm and tau physics in the next ten years is reviewed, with emphasis on the sensitivity to new physics and complementarity with direct searches. Prospects for lepton flavour violation experiments are presented. Dedicated experiments in the kaon sector are also considered. The possibility of a very-high statistics flavour experiment at LHC (*extreme flavour*) is also described in some detail. Chapter 7 is dedicated to experimental measurements and theoretical studies related to non-perturbative QCD. Prospects for improved measurements of the nucleon structure function are given here, including studies of the 3-D structure function of the proton. Diffractive physics is reviewed. The interplay between cosmic ray measurement and related measurements at accelerators is discussed in this chapter.

Before discussing physics prospects, the scenario for present and future accelerators must be established. The relevant accelerator parameters expected for LHC upgrades and for possible future colliders, in particular ILC and FCC, are given in Chapter 2. This chapter establishes a common ground for the discussions in the working group chapters, where technical limitations of future accelerators must be taken into account. Perspectives for developments in the computing, detector and data acquisition areas are presented in Chapter 3, where potential bottlenecks are highlighted.

Conclusions and recommendations are presented in the last chapter. Material comprising in-depth analysis and additional contributions can be found in Appendices A and B.

Executive reading

This document includes a considerable amount of information, in particular in Chapters 4, 5, 6 and 7: a *Summary and Outlook* section is provided at the end of each of these chapters. We suggest to readers who wish to have a broad and general view of the subjects to read these summaries and the final recommendations in Chapter 8.

2 Present and Future Accelerators

Advancement in particle physics has always been linked with the availability of particle beams of ever increasing energy or intensity. Given the scope of this report, which is to propose a strategy for particle physics experiments at accelerators for the next 10 years in the context of a much longer global vision (20 years or more), a concise description of current facilities, future projects and potential developments in the field of particle accelerator is required. First the present and near-future landscape of accelerators dedicated to fundamental science will be briefly reviewed. Subsequently the current plans for future facilities world-wide will be discussed and the key performance of the future machines as presently foreseen will be given. New ideas and concepts that may bring more powerful machines for particle physics in the more distant future will be reviewed in the last paragraph.

2.1 Current facilities and planned evolution

2.1.1 LHC and its future

The Large Hadron Collider at CERN, the most powerful and complex accelerator ever built, is currently our only tool for the exploration of the energy frontier, and offers the means to explore the forefront of Standard Model physics and beyond, as discussed in this report. The LHC started initial commissioning with beam at the end of 2009 and has established excellent operational performance, reaching in 2012 a bunch spacing of 50 ns and a β^* of 0.6 m and $\sqrt{s} = 8$ TeV. The integrated luminosity collected by the two general purpose experiments at LHC was around $6\,\text{fb}^{-1}$ in 2011 and around $25\,\text{fb}^{-1}$ in 2012, more than enough to enable ATLAS and CMS to announce the discovery of a Higgs boson. The LHC also enabled LHCb to collect 1.2 and 2.2 fb^{-1} in 2011 and 2012 respectively, with luminosity limited at around $4 \times 10^{32}\,\text{cm}^{-2}\text{s}^{-1}$ via transverse separation. The versatility of the machine is proved also from the successful lead-lead and proton-lead runs in 2011 and early 2013, as well as several high β^* runs culminating in the operation at 1 Km β^* run for the TOTEM and ALFA experiments. The main machine parameters for LHC are displayed in Table 1, together with their foreseen evolution for the next decade towards the High-Luminosity LHC.

Table 1: LHC operation parameters in 2012 run and foreseen evolution towards the HL-LHC. $^{(1)}$ Leveled.

Parameter	LHC 2012	LHC post LS1	LHC design	HL-LHC
Beam Energy [TeV]	4	6.5	7	7
β^* [m]	0.6	<0.5	0.55	0.15
Bunch spacing [ns]	50	25	25	25
Number of bunches	1380	2590	2808	2736
Max proton/bunch [$\times 10^{11}$]	1.7	1.15	1.15	2.2
Crossing angle [μm]	-	300	285	590
Normalized emittance	1.8(?)	1.8	3.75	2.5
Peak luminosity [$10^{34}\,\text{cm}^{-2}\text{s}^{-1}$]	0.77	1.7	1	$5^{(1)}$
Pileup	37	49	27	$138^{(1)}$

After a long shutdown (LS1) and extensive consolidation work on the dipole splices, the LHC is expected to start a new run in 2015 reaching 13 TeV centre-of-mass energy. The integrated luminosity goal for proton-proton collisions is 10 fb^{-1} in the first year dedicated to establishing operation at 25 ns bunch spacing. In the following two years a luminosity goal of 100-120 fb^{-1} has been indicated. The planned LS2 (see Fig.1) involves several upgrades to the detectors and to the injector complex, which will enable an increase in beam current and to reach a total of 300 fb^{-1} of proton-proton collisions by 2022. At that point the LHC machine as well as the ATLAS and CMS detectors are expected to undergo an extensive upgrade phase in order to cope with an integrated luminosity 10 times higher than design

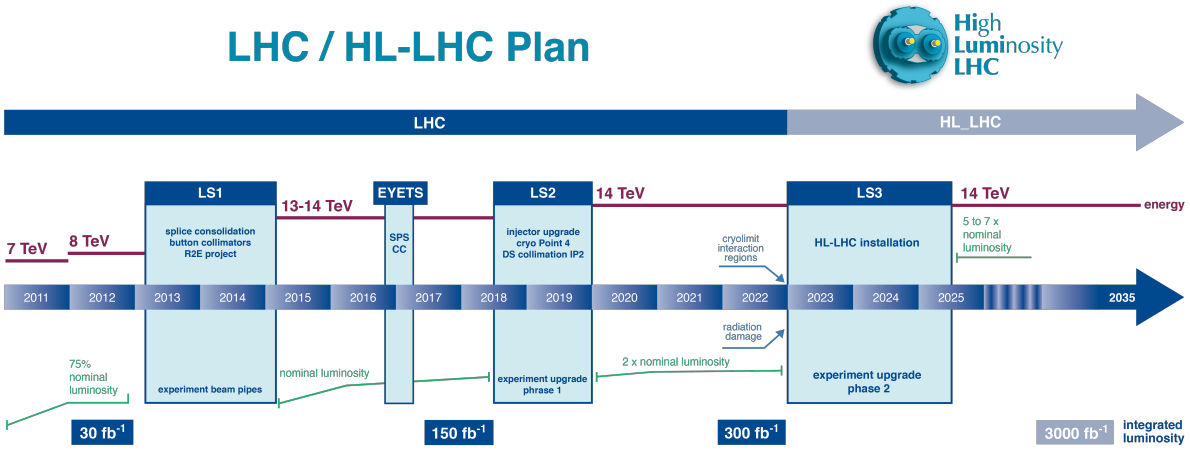

Fig. 1: LHC evolution plan.

and bring the total integrated luminosity to 3000 fb^{-1} by the mid 2030's (HL-LHC).

At HL-LHC the maximum instantaneous luminosity is kept below $5 \times 10^{34}\,\text{cm}^{-2}\text{s}^{-1}$ in order to increase beam lifetime and integrated luminosity (*luminosity leveling* [1]), corresponding to around 140 pileup events per bunch crossing. Options employing 50 ns bunch spacing are still discussed in case of difficulties in establishing operations at 25 ns in 2015 because of electron cloud build-up or other factors, at the price of allowing much higher event pile up ($\sim$ 250). Other beam structures are under investigations, for example a scheme based on 25 ns spacing with 8 bunches and 4 empty bunches can alleviate the e-cloud problem while keeping the pile up at 140, at a price of relatively small loss of luminosity. The main features of the upgrade are listed below:

- Wide aperture niobium-tin (Nb_3Sn) quadrupoles will be used to replace the present inner triplet quadrupole magnets. Given the aperture (150 mm) and the peak field (> 12 T) these quadrupole have a stored energy per unit length twice as larger as the one of the LHC dipoles.
- Wider aperture and revision of the insertion optics and layout will allow a squeeze to β^* of 15 cm. In order to reach such a low β^* value, a new optics scheme called ATS (Achromatics Telescopic Scheme) will be employed to overcome the limitation of the matching section and of the sextupole correction circuits.
- 11 T Nb_3Sn dipoles will be used to make room for collimators in the cold dispersion suppressors.
- Enhanced collimators will be installed for the 500 MJ beams.
- Wide aperture niobium-titanium (NbTi) separator magnets (the first twin aperture magnets moving away from the interaction point) will be employed.
- Crab cavities, which are high-frequency RF transverse deflectors providing quasi head-on-collisions at the interaction point, will be used to compensate the luminosity reduction factor caused by the large crossing angle.

A novel scheme, named *crab-kissing* [2] is also under investigation to alleviate the pile up density issue. By turning the bunches also in the perpendicular plane (beside rotating them in the crossing plane to reduce the angle), the longitudinal pile up density can be reduced by a factor 2. This enhanced set of parameters may enable to run with a leveled instantaneous luminosity of $7.5 \times 10^{34}\,\text{cm}^{-2}\text{s}^{-1}$ and a total pile up of 200. In such a case an integrated luminosity in excess of 4000 fb^{-1} could be reached over the ten years of HL-LHC operations.

2.1.2 Muon and kaon beams for rare processes

Facilities providing intense muon or kaon beams currently exist or are being upgraded at Fermilab, CERN, PSI and J-PARC laboratories.

At Fermilab the 40 year old accelerator complex underwent a first upgrade phase, the Proton Improvement Plan, which allowed the doubling of the Booster repetition rate and addressed various reliability concerns. Muon beams for the g-2 and, later on, for the Mu2e experiments will be available, starting in 2016. Protons from the Booster with 8 GeV kinetic energy will be extracted to produce secondary muon beams for the g-2 and Mu2e experiments through new dedicated beam lines. The upgrade path for the Mu2e experiment is centred on the Proton Improvement Plan-II (PIP-II) [3] project. The main goal is to deliver 1.2 MW of proton beam power from the Main Injector at 120 GeV, for the start of the foreseen long baseline neutrino experiments (LBNF), but also to enable an order of magnitude increase in beam power on the Mu2e target. The upgrade can potentially provide intense kaon beams. The heart of PIP-II is an 800-MeV superconducting linear accelerator, which capitalises on the lab's expertise in superconducting radio-frequency technologies. Along with modest improvements to Fermilab's existing Main Injector and Recycler accelerators, the superconducting linac, called SCL, will provide the megawatt proton beam that is needed for the Long-Baseline Neutrino Facility. PIP-II is planned to deliver beam in the early part of the next decade.

Kaon beams at CERN are provided by the SPS, which can deliver 400 GeV protons at a 30% duty cycle. About 3×10^{12} protons per 16.8 second spill are impinging on the North Area targets, yielding a high intensity hadron beam. As an example, a fixed momentum (75 GeV/c) beam is delivered to the NA62 experiment at 750 MHZ with an average kaon content of 6%. The SPS fixed-targed running depends on the LHC schedule and corresponding upgrades, as the SPS fills the LHC with protons. The current run is expected to end in 2018, two additional runs are expected for the periods 2020-2023 and 2025-2028.

The Swiss Muon Source at the Paul Scherrer Institute (PSI) is currently the world's most intense continuous beam muon source. It is powered by the PSI 590 MeV cyclotron with a proton current of 2200 mA. The proton beam hits two graphite targets, followed by seven beamlines for muon (or pion) extraction, with available muon energies ranging from 0.5 keV to 120 MeV. For LFV current or proposed experiments, such as MEG, MEG-II and Mu3e, muons from pions decaying at the surface of the pion production target are collected (*surface muons*) and delivered to the detectors with beam transport systems including superconducting solenoids. The beam line currently available for particle physics (πE5) provides muons at 1.6×10^8 Hz; an upgraded beam line with a rate of 4×10^{10} Hz (HiMB) is under study.

The J-PARC accelerator complex at Ibaraki comprises three proton accelerators; the 50 GeV high-intensity main ring (MR) is used for particle physics applications. The MR feeds two extraction ports. The slow extraction (SX) port directs the high-energy protons to the Hadron Experimental Facility where experiments are carried out with kaon beams. Protons from the fast extraction (FX) port are guided by a superconducting magnetic array towards the pion production target. Neutrinos generated in pion decay processes are sent as part of the T2K experiment to the Super-Kamiokande facility. High-intensity muon beams generated in the same process can be used for LFV experiments, muons rates in excess of 10^{11} Hz are foreseen for the years 2019/2020.

2.1.3 Electron-positron colliders

Current facilities taking the role of ϕ, charm/tau and b factory are, respectively, DAFNE, BEPC-II and SuperKEKB.

The ϕ-factory DAFNE is located in Frascati; it provides colliding beams of 510 MeV, with up to 120 bunches per beam and a maximum stored current per ring of 5.2 A. Each Main Ring of the DAFNE collider consists of two 180 degrees bends of different length, the "short arc" and the "long

arc", reaching a maximum diameter of 32.5 m. The maximum achieved luminosity by DAFNE (2009) is 4.36 $\times 10^{32}\,\mathrm{cm}^{-2}\mathrm{s}^{-1}$, with electron and positron beam currents of 1.47 and 1.00 A, respectively.

The BEPC-II accelerator in Beijing consists of a 202 m long electron-positron linac injector, a storage ring with circumference of 240.4 m, and in connection with each other, 210 m transport lines. It has a design luminosity of $1 \times 10^{33}\,\mathrm{cm}^{-2}\mathrm{s}^{-1}$ at the beam energy of 1.89 GeV, with 93 bunches and a beam current of 1.1 A. Its installation was completed in the summer of 2005 and it has reached most of the design specifications. First beams were provided in 2009 to the BES-III experiment and about 8 fb^{-1} have been collected to date at various centre-of-mass energies, from the J/ψ resonance to the Λ_c production threshold.

SuperKEKB is a very high-luminosity asymmetric b-factory located at the KEK site in Japan. It consists of a low energy ring (LER) hosting a beam of 4 GeV and a high energy ring (HER) where the beam energy is 7 GeV. It's a multi-bunch machine with 2500 bunches with bunch currents of 1.44 mA (1.04 mA) for the LER (HER), respectively. The design luminosity is $8 \times 10^{35}\,\mathrm{cm}^{-2}\mathrm{s}^{-1}$. In order to achieve such a very high luminosity crab cavities are employed, together with strong focusing and large crossing angle at the interaction point (nano-beam scheme). The SuperKEKB project was approved in 2010 and the collider is under commissioning at the moment of writing this report.

2.2 Future projects for the energy and intensity frontier

2.2.1 The International Linear Collider

The idea of a high-energy linear collider based on superconducting RF cavities dates back to the pioneering work done by the TESLA collaboration in the nineties. The current project, the International Linear Collider (ILC) [4–6], foresees a high-luminosity linear electron-positron collider based on 1.3 GHz superconducting radio-frequency (SCRF) accelerating technology. The possibility of obtaining high-gradient with SCRF has been demonstrated at the TESLA test facility at DESY where 35 MV/m have been reached. The same technology foreseen for the ILC is being employed at the European X-ray free-electron laser (XFEL), a 17.5 GeV linear accelerator currently under construction, and whose commissioning is expected in 2016.

The centre-of-mass-energy range foreseen for the ILC is from 200 to 500 GeV, extendable to 1 TeV. At the ILC beams are produced by a polarised electron source based on a photocathode DC gun and a polarised positron source in which positrons are obtained from electron-positron pairs by converting high-energy photons. These photons are produced by passing the high-energy main electron beam through an undulator. Electron and positron damping rings (DR) with a circumference of 3.2 km are housed in a common tunnel and host beams of 5 GeV. Beams are transported from the damping rings to the main linacs, where are injected after bunch-compression. The two main linacs utilise the already mentioned 1.3 GHz SCRF cavities operating at an average gradient of 31.5 MV/m, with a pulse length of 1.6 ms. Two beam-delivery systems, each 2.2 km long, bring the beams into collision with a 14 mrad crossing angle, at a single interaction point which can be occupied by two detectors in a so-called push-pull configuration.

The total length of the ILC complex, expected to be hosted in Japan, is 31 km. The electron source, positron source and the electron and positron damping rings are expected to be centrally located around the interaction region. The damping-ring complex is displaced laterally to avoid interference with the detector hall. The electron and positron sources themselves are housed in the same (main accelerator) tunnels as the beam-delivery systems, in order to reduce the overall cost and size of the central-region underground construction.

Table 2: Summary table of the 250 - 500 GeV baseline and luminosity and energy upgrade parameters. Also included is a possible 1st stage 250 GeV parameter set (half the original main linac length)

			Baseline 500 GeV Machine			1st Stage	L Upgrade	E_{CM} Upgrade	
								A	B
Centre-of-mass energy	E_{CM}	GeV	250	350	500	250	500	1000	1000
Collision rate	f_{rep}	Hz	5	5	5	5	5	4	4
Electron linac rate	f_{linac}	Hz	10	5	5	10	5	4	4
Number of bunches	n_b		1312	1312	1312	1312	2625	2450	2450
Bunch population	N	$\times 10^{10}$	2.0	2.0	2.0	2.0	2.0	1.74	1.74
Bunch separation	Δt_b	ns	552	553	554	554	366	366	366
Pulse current	I_{beam}	mA	5.80	5.79	5.79	5.8	8.75	7.6	7.6
Main linac average gradient	G_a	MV/m	14.7	21.4	31.5	31.5	31.5	38.2	39.2
Average total beam power	P_{beam}	MW	5.2	7.3	10.5	5.2	21.0	27.2	27.2
Estimated AC power	P_{AC}	MW	122	121	163	129	204	300	300
RMS bunch length	σ_z	mm	0.3	0.3	0.3	0.3	0.3	0.250	0.225
Electron RMS energy spread	$\Delta p/p$	%	0.190	0.158	0.124	0.190	0.124	0.083	0.085
Positron RMS energy spread	$\Delta p/p$	%	0.152	0.100	0.070	0.152	0.070	0.043	0.047
Electron polarisation	P_-	%	80	80	80	80	80	80	80
Positron polarisation	P_+	%	30	30	30	30	30	20	20
Horizontal emittance	$\gamma\epsilon_x$	μm	10	10	10	10	10	10	10
Vertical emittance	$\gamma\epsilon_y$	nm	35	35	35	35	35	30	30
IP horizontal beta function	β_x^*	mm	13.0	16.0	11.0	13.0	11.0	22.6	11.0
IP vertical beta function (no TF)	β_y^*	mm	0.41	0.34	0.48	0.41	0.48	0.25	0.23
IP RMS horizontal beam size	σ_x^*	nm	729.0	683.5	474	729	474	481	335
IP RMS veritcal beam size (no TF)	σ_y^*	nm	7.7	5.9	5.9	7.7	5.9	2.8	2.7
Luminosity (inc. waist shift)	L	$\times 10^{34}\ cm^{-2}s^{-1}$	0.75	1.0	1.8	0.75	3.6	3.6	4.9
Fraction of luminosity in top 1%	$L_{0.01}/L$		87.1%	77.4%	58.3%	87.1%	58.3%	59.2%	44.5%
Average energy loss	δ_{BS}		0.97%	1.9%	4.5%	0.97%	4.5%	5.6%	10.5%
Number of pairs per bunch crossing	N_{pairs}	$\times 10^3$	62.4	93.6	139.0	62.4	139.0	200.5	382.6
Total pair energy per bunch crossing	E_{pairs}	TeV	46.5	115.0	344.1	46.5	344.1	1338.0	3441.0

Table 2 shows the ILC parameters for several centre-of-mass energies, including possible upgrades and staging. These parameters have been optimised taking into account the constraints imposed by the various accelerator sub-systems. For example, the bunch charge, bunch spacing and the total number of bunches in the damping rings are limited by various instability thresholds (most notably the electron cloud in the positron ring), realistic rise-times for the injection and extraction kickers, and the desire to minimise the circumference of the rings. The beam current is further constrained by the need to minimise the number of klystrons (peak power) and higher-order modes (cryogenic load and beam dynamics). Dynamic cryogenic load (refrigeration) is also a cost driver, which limits the repetition rate of the machine. Both the electron and positron sources constrain the achievable beam current and total charge: for the laser-driven photocathode polarised electron source, the limits are set by the laser; for the undulator-based positron source, the limits are set by the power deposition in the photon target. Finally, at the interaction point, single-bunch parameters are limited by the strong beam-beam effects and requirements on both the beam-beam backgrounds and beam stability.

2.2.2 CLIC

The CLIC scheme [7] represents to date the only available technology to build an electron-positron collider in the multi-TeV energy range keeping reasonable accelerator length, cost and power consumption. In this scheme the required RF power is provided by a low-energy high-intensity drive beam, which is decelerated in dedicated *power-extraction and transfer structures* (PETS) feeding accelerating structures for the main high-energy beam.

In the current design [8] the two main accelerators of CLIC accelerate electrons and positrons from 9 GeV to 1.5 TeV in one pass, reaching a centre-of-mass energy of 3 TeV. An accelerating gradient of 100 MV/m is foreseen to limit the length of the machine to less than 50 km. The kinetic energy of a 2.4 GeV drive beam of 100 A intensity is used to generate an RF power of about 270 MW by means of low-impedance PETS, which decelerate the drive beam and high-impedance accelerating structures. The two beam lines run parallel at a distance of 60 cm. The main beam is pre-accelerated to 9 GeV in an injection linac and enters damping rings for emittance reduction before entering the high-energy accelerating structure. In order to avoid breakdown at such an high gradient the beam pulse has to be limited to 150 ns, about 300 high-charge bunches (3.7×10^9 $\mathrm{e}^{\pm}$) spaced by only 0.5 ns have to be accelerated to yield a peak luminosity of 5.9×10^{34} $\mathrm{cm}^{-2}\mathrm{s}^{-1}$. Such a short bunch interval makes the detector design particularly challenging. The vertical (horizontal) beam size at the interaction point is 1 (40) nm. An initial phase at a centre-of-mass energy of 500 GeV and lower luminosity is foreseen, which corresponds to a 13 km long machine.

A dedicated CLIC test facility at CERN (CTF3) is devoted to prototyping and technological studies. At CTF3 a high-current drive beam generates the 12 GHz RF power for accelerating structures, with a drive beam of 4 A and up to 120 MeV. An accelerating gradient of 145 MeV/m has been achieved, demonstrating the CLIC concept.

2.2.3 Future Circular Colliders

In February 2014 an initiative for a Future Circular Collider has been launched in Geneva in order to perform preparatory studies and an initial design for a very large circular machine, tentatively to be located in the Geneva area, located in an underground tunnel of up to 100 km circumference running below the lake and the Saleve mountain range [9]. The aim is to bring together the HEP and accelerator physics community to define a Conceptual Design Report (CDR) and a cost review for the next European Strategy Update in 2018. The project comprises a proton-proton collider (FCC-hh) defining infrastructure requirements, an e^+e^- collider (FCC-ee) as potential intermediate step and also a proton-electron collider (FCC-he) option.

In order to explore the several tens of TeV energy scale with a proton-proton collider a goal of

100 TeV collision energy in the centre-of-mass has been set. One of the main technological challenges is the development of the capability to construct the large number of magnets required. A dipole field of 16 T, which is envisaged as the ultimate goal for low temperature superconducting alloys, will require a machine with a circumference as large as 100 km. A shorter machine (80 km) would be possible if high temperature superconducting (HTS) magnets become available. A selection of machine parameters as defined in [10] is shown in Table 3, compared to the HL-LHC. In the same table a high energy upgrade for the LHC machine is displayed (HE-LHC). This option has been discussed in the past, but is currently not not anymore the CERN baseline. Nevertheless is always kept as a possible alternative, would physics requirements endorse a 33 TeV centre-of-mass collider. The technology development for HE-LHC is the same as FCC-hh, the infrastructure is largely there, so a decision in favour of HE-LHC can be postponed to the next decade.

Table 3: FCC-hh current design parameters from [10] compared to HL-LHC and HE-LHC design. $^{(1)}$ Leveled.

Parameter	HL-LHC	HE-LHC	FCC-hh (25 ns)	FCC-hh (5ns)
Beam Energy [TeV]	7	16,5	50	50
Dipole field [T]	8.33	20	16 (20)	16 (20)
Circumference [Km]]	26.7	26.7	100 (83)	100 (83)
Peak luminosity [$10^{34}\,\mathrm{cm}^{-2}\mathrm{s}^{-1}$]	$5.0^{(1)}$	5.0	5.0	5.0
Pileup	$135^{(1)}$	147	171	34
β^* [m]	0.15	0.35	1.1	1.1
Number of bunches	2736	2736	10600 (8900)	53000 (44500)
Max proton/bunch [$\times 10^{11}$]	2.2	1.0	1.0	0.2
Normalized emittance	2.5	1.38	2.2	0.44
Crossing angle [μm]	590	185	7.4	–
RMS IP spot size [μm]	7.1	5.2	6.8	3
RMS bunch length [cm]]	7.55	7.55	7.55(8)	7.55(8)
Stored energy per beam [GJ]	0.7	0.7	8.4 (7.0)	2.4 (7.0)
SR power per ring [MW]	0.33	4.35	28.4 (44.3)	28.4 (44.3)

Table 4: Parameter for the FCC-ee project [11].

Parameter	Lep 2	FCC-ee Z	FCC-ee W	FCC-ee H	FCC-ee $t\bar{t}$
Bending radius	3.1	11	11	11	11
Beam Energy [GeV]	104	45.5	80	120	175
Current [mA]	3.0	1450	152	30	6.6
Total Sincroton Radiation [MW]	22	100	100	100	100
n. bunches	4	16700	4490	1360	98
particle per bunch [10^{11}]	4.2	1.8	0.7	0.46	1.4
Transverse emittance H [nm]	22	29	3.3	0.94	2.0
Transverse emittance V [pm]	250	60	1	2	2
Betatron function at IP H [m]	1.2	0.5	0.5	0.5	1.0
Betatron function at IP V [μ m]	50	1	1	1	1
σ_x^* [μm]	182	121	41	22	45
σ_y^* [nm]	3200	250	84	44	45
$\sigma_{z,tot}$ [mm]	11.5	2.56	1.49	1.17	1.49
Hourglass factor	1	0.64	0.77	0.83	0.78
Luminosity/IP [$10^{34}\,\mathrm{cm}^{-2}\mathrm{s}^{-1}$]	0.012	28.0	12.0	6.0	1.8
Luminosity lifetime [min]	434	298	73	29	21

As already mentioned, in a first phase the FCC tunnel could host an $\mathrm{e}^+\mathrm{e}^-$ collider (FCC-ee). The potential of a very large $\mathrm{e}^+\mathrm{e}^-$ circular collider has drawn considerable attention following the Higgs boson discovery. Synchrotron energy loss per turn goes as E^4/r, where E is the beam energy and r the

Table 5: Parameter for the CEPC machine [12] and FCC-ee project [11].

Parameter	CEPC	FCC-ee H
Bending radius	6.1	11
Beam Energy [GeV]	120	120
Current [mA]	16.6	39
Total Sincroton Radiation [MW]	103	100
n. bunches	50	1360
particle per bunch [10^{11}]	3.8	0.46
Transverse emittance H [nm]	6.12	0.94
Transverse emittance V [pm]	18	2
Betatron function at IP H [m]	0.8	0.5
Betatron function at IP V [μ m]	1200	1
σ_x^* [μm]	70	22
σ_y^* [nm]	150	44
$\sigma_{z,tot}$ [mm]	2.14	1.17
Hourglass factor	0.64	0.83
n. Interaction Points	2	4
Luminosity/IP [$10^{34}\,\mathrm{cm}^{-2}\mathrm{s}^{-1}$]	2.0	6.0
Luminosity lifetime [min]	47+51	29

radius of the ring. An increase of the radius by a factor three, which is roughly the ratio between the proposed FCC and the LEP radii, would be sufficient to produce the 125 GeV Higgs boson with about one half of the RF power utilised at LEP. The present conceptual design of the machine foresees a power consumption a factor of five higher than LEP, still manageable, with a multi-bunch scheme. A collider with such a large ring would also give the opportunity to perform precision measurements at the Z pole, at the WW production threshold and at the $t\bar{t}$ production threshold.

The FCC-ee design is based on an accelerator ring with a storage ring delivering continuous top-up injection. The storage ring compensates for the small beam lifetime caused by Bhabha scattering and loss of particles in collisions, providing a constant level of luminosity [13]. The multi bunch operation foresees more than 16000 bunches with beams of 45.6 GeV (Z Pole) and about 100 bunches with beams of 175 GeV ($t\bar{t}$ production threshold). Figure 2 shows the FCC-ee expected instantaneous luminosity as a function of the centre-of-mass energy, if the luminosity is delivered at four interaction points. The highest luminosity is reached at the Z pole, as expected from the previous considerations. The behaviour is clearly complementary to linear colliders: much higher luminosity can be reached at a centre-of-mass energy up to $t\bar{t}$ threshold, while linear colliders can potentially reach a much higher centre-of-mass energy.

At the same time a similar project is under development in China. The CEPC-SppC study group aims at developing a Circular Electron-Positron Collider for Precision Higgs physics and, later, a proton-proton collider in the same 50-70 Km circumference tunnel. The envisaged time-line is rather aggressive, with an R&D phase and engineering design to be completed in 2020, construction of the tunnel and e^+e^- collider in 2021-2027 and data taking at the end of the decade to be concluded in 2035 for the construction of the pp collider. Parameters for the CEPC machine are shown in Table 5, together with those at the same energy for the FCC project. The proton-proton collider is less studied so far, but several options exist depending on the availability of high field dipoles and the tunnel length. Centre-of-mass energy of 50 to 90 TeV is envisaged with a luminosity for each of the two interaction regions of order 2 to 3 $\times 10^{35}\,\mathrm{cm}^{-2}\mathrm{s}^{-1}$ [14].

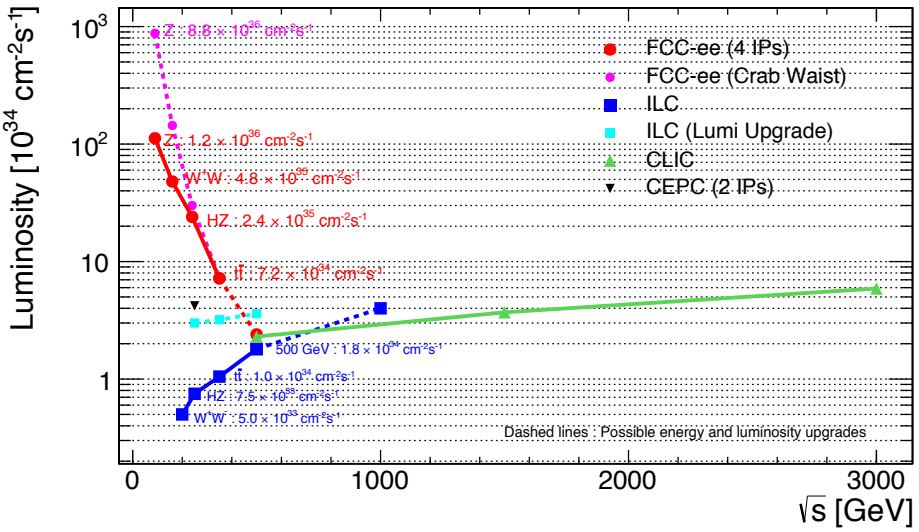

Fig. 2: Instantaneous luminosity, in units of $10^{34}\mathrm{cm}^{-2}\mathrm{s}^{-1}$, expected at FCC-ee (full red line), in a configuration with four interaction points operating simultaneously, as a function of the centre-of-mass energy. For illustration, the luminosities expected at linear colliders, ILC (blue line) and CLIC (green line), are indicated in the same graph. The plot includes further luminosity and energy upgrades for ILC and FCC-ee (dashed lines), under discussion at the time of writing.

2.3 Novel techniques for particle acceleration

Because of electrical breakdown of metals in the presence of high electric fields, conventional particle accelerators, which consist of metal cavities driven by high-power microwaves, typically operate with accelerating fields up to $\sim$ 100 MV/m at 12 GHz. To overcome this limitation a tremendous effort is ongoing towards the development of novel high gradient acceleration techniques based on laser or particles beam driven accelerating structures, operating in vacuum structures [15] or in plasma wakes produced in gas filled capillaries [16]. Since Plasma-based concepts presently offer the highest gradient acceleration compared to other novel acceleration techniques (high frequency metallic structures, dielectric wake field structures) they will be discussed in detail in the following.

Plasma based accelerators replace the metallic walls of conventional RF structures with a plasma. The damage problems faced in high-gradient metallic structures are therefore not an issue. Laser beams (laser wakefield accelerator LWFA) or charged particle beams (particle wakefield accelerator PWFA) are used to excite space-charge oscillations in the plasma. The resulting longitudinal fields can be used for particle acceleration. Plasma structures have been built from the mm to the meter scale. Accelerating gradients up to 160 GV/m have been demonstrated in experiments [17] with increasing accelerated beam quality as the one required to drive advanced light sources (FEL, Compton, etc.) in the next decade [18].

For any variant of wake field accelerator to be practical as a linear collider (LC), several feasibility and practicality issues must be resolved in the context of an integrated system test. Most importantly, wake field accelerators, like standard accelerator modules, must be capable of being staged in a series of phase-locked segments. Both PWFA and LWFA approaches must demonstrate simultaneous electron and positron acceleration and focusing in plasma densities consistent with preserving electron and positron beam quality. Both must demonstrate timing, pointing, and focusing control consistent with the high luminosities required in a lepton collider. Finally, both must demonstrate that multi-bunch plasma instabilities (such as convective hose instability) can be overcome with operation at the tens of kHz repetition rate required for high luminosity. Beyond the feasibility issues are questions of practicality related

to overall cost, efficiency, and reliability.

A number of small scale facilities are in operation or under construction in Europe (France, Italy, Germany) and two large R&D facilities are spearheading this research in the U.S., FACET at SLAC and BELLA at LBNL, with the goal to achieve high quality beams, stability, efficiency and staging. During the last year (2014) two important milestones have been achieved:

- At BELLA (LWFA) multi-GeV electron beams with energy up to 4.2 GeV, 6% rms energy spread, 6 pC charge, and 0.3 mrad rms divergence have been produced from a 9-cm long capillary discharge waveguide with a plasma density of about 10^{17} cm^{-3}, powered by laser pulses with peak power up to 300 TW. Preformed plasma waveguides allow in this case the use of lower laser power compared to unguided plasma structures to achieve the same electron beam energy [19].
- At FACET (PWFA) acceleration of about 74 pC of charge contained in the core of the trailing bunch in an accelerating gradient of about 4.4 GV/m has been demonstrated. The core particles gain about 1.6 GeV of energy per particle, with a final energy spread as low as 0.7%, and an energy transfer efficiency from the wake to the bunch that can exceed 30%. The acceleration of a distinct bunch of electrons containing a substantial charge and having a small energy spread with both a high accelerating gradient and a high energy-transfer efficiency represents a milestone in the development of plasma wakefield acceleration into a compact and affordable accelerator technology [20].

These results make plasma wake field accelerators promising candidates for HEP applications also. Parameters covering a wide range of colliding beam energies from 250 GeV (Higgs Physics) up to 10 TeV have been elaborated for both LWFA and PWFA concepts resulting in the required luminosity $\sim 10^{34}$ cm^{-2}s^{-1} and efficiency as high as 30% as summarized hereafter.

A 2-TeV electron-positron collider based on LWFA might be less than 1 km long [21]. Its electron arm could be a string of 100 acceleration modules, each with its own laser. A 30-J laser pulse drives in each module a plasma wave in a 1 meter-long capillary channel of preformed plasma. Bunched electrons or positrons from the previous module gain 10 GeV by riding the wave through the channel. To achieve the desired collider luminosity, a laser-plasma collider would need a repetition rate of about 13 kHz. That means an average laser power of half a megawatt per module, which is still far beyond the performance of lasers available today. Current high-peak-power lasers can operate with an average power of 100 W at most, with a wall-plug efficiency of about 0.1%. Reaching the high average-power levels required for particle-physics colliders is a daunting but not insurmountable task that requires a revolution in laser technology. Excellent candidates to this end are diode-pumped fiber amplifiers, where the active medium is confined within the core of an optical fiber and pumped using semiconductor laser diodes. In the past 10 years diode-pumped fiber amplifiers have attained unprecedented increase in both average power and efficiency. For instance, continuous-wave fiber lasers with average powers in the kW regime were first demonstrated in 2004 and are now commonplace. Their efficiency can reach $50-60\%$. A laser composed of a large number of fibers across the beam, which can be individually addressed, pumped and phased with extreme precision, i.e. 1% in amplitude and in phase at a kHz bandwidth is now under development [22]. Laser pulse energies of 32 J at 13 kHz corresponding to 400 kW average power with 240 TW peak power were identified as being reasonable target values. Ideally the laser wall plug efficiency would be 50%, giving an overall efficiency from laser to beam of 20%. For a 1 TeV collider, 100 of these stages would be necessary. To produce a single stage using this technique requires the addition of pulses from around 10 000 fiber lasers. The key questions are (a) could so many fibers be phased? (b) can such a system be produced for a reasonable cost? The next decade will hopefully bring us a positive answer.

For HEP applications a promising medium term solution is based on the beam driven (PWFA) linear collider scheme where the laser power source is replaced by a conventional RF linac producing

a high charge driving beam. This linear collider solution is certainly less compact than a LWFA based scheme but has some important advantages:

- timing and synchronization are rather simpler issues compared to LWFA schemes since both drive and witness bunches are generated by the same source (the RF linac),
- existing RF electron linacs can achieve repetition rates as high as GHz in pulsed mode in normal conducting structures or MHz in continuous wave operation in superconducting structures,
- two limiting factors for energy gain and efficiency in LWFA schemes such as laser diffraction and electron beam-plasma wave dephasing are absent in PWFA schemes. With state of the art drive bunch emittance and energy, the only common unavoidable limitation is the driver pulse energy depletion.

Two alternative concepts have been elaborated for PWFA linear collider schemes with different time scales and maximum energies:

- A PWFA-LC design uses a conventional 25 GeV electron drive beam accelerator to produce trains of drive bunches distributed to 20 PWFA cells for both the electron and the positron arms of the collider to reach an energy of 500 GeV for each beam [23]. Each cell provides 25 GeV of energy to the main beam in about a meter of plasma. This drive beam system is very similar to the CLIC drive beam concept (two beam accelerator concept). Once the possibility to generate high quality electron and positron beams is demonstrated, an upgraded version of the existing SLAC linac could be conveniently used.
- Another concept, on a longer time scale, foresees beam acceleration up to an initial energy with ILC SC technology [24]. The beam could be further accelerated with PWFA modules at low cost and high efficiency. Alternatively and as first step of the ILC energy upgrade, the PWFA technology could be used as an ILC after-burner: each ILC bunch would be split in two, one with 2/3 of the charge used as drive bunch and a second with 1/3 of the charge used as main bunch. The ILC beam energy could then be doubled without any drive beam injector complex and without substantial additional power. Replacing the last 250 meters of ILC structures by PWFA allows TeV beam collisions without extension of the ILC tunnel. The ILC energy upgrade could then be pursued by adding a drive beam injector and progressive replacement of ILC structures by PWFA. The above concept assumes similar behavior of the electron and positron beams, which remains to be demonstrated.

Despite the fast progress, new acceleration techniques, such as those based on dielectric or plasma wake fields are unlikely to become capable of producing the high luminosity electron/positron beams needed for HEP on the time scale of the next twenty years. A feasibility experimental study of a HEP collider based on advanced acceleration techniques is expected to be completed only within the next 15 years. Nevertheless the history of accelerator science is full of unexpected bright ideas that allowed tremendous and fast progresses in science. Starting with the present solid backgrounds a strong effort in the field of novel accelerator research will certainly provide the HEP community of the desired tools.

2.4 High Field Magnets for post-LHC hadron colliders

The progress in magnet performance over the years from the resistive magnet era through the jump in performance required by High Luminosity LHC and the development towards a higher energy machine, is summarised in Fig. 3 [25].

The first key factor for sustaining the increase in magnetic field is superconductor performance. As clearly shown in Fig. 3, LHC dipole are near the limit of possibility for Nb-Ti technology. The HL-LHC project explores the use of Nb3Sn, which is much more complex and difficult superconductor.

However, it enables reaching 12 Tesla and beyond, up to 15-16 Tesla. To go toward higher fields, HTS (High Temperature Superconductors) based technology is needed. Nb3Sn has been developed in these last 10 years for HL-LHC, which provides also an ideal demonstrator on a reasonable scale of such technology, so far never used in accelerators. However, to push the Nb3Sn technology toward its limit of 15-16 T, a further important step in Nb3Sn performance is needed, improving its critical current by 50%. Obtaining this performance step is among the main objectives of the FCC-hh design and R&D phase, to be concluded around 2020 with a 16 T dipole magnet demonstrator.

The second key factor for reaching very high field, in the 15-16 T regime and beyond, is the stress and energy management. Electromechanical forces and stored energy increases with the square of the field: a 16 T dipole will need a mechanical structure able to withstand four times the forces of the LHC dipoles, and twice the ones of the HL-LHC magnets. No wonder that a phase of exploration of innovative mechanical lay-outs and structure concepts, as well of new protection systems, is needed and it will take not less than 5 years or more. This exploration of new structure and the advanced Nb3Sn wire development are the primary goals of the magnet R&D for FCC-hh for the next future.

In parallel, thanks to an European program partly funded by EC-FP7-Eucard2, a basic activity of development of HTS for accelerator magnet is going on [26]. The Eucard2 program aims at establishing the viability of HTS for collider magnets, and should reach the goal of producing and validating a HTS cable, suitable for collider magnet quality, by 2017. It will take a further 2-3 years period, before a real full size magnet prototype for FCC-hh could be ready and validated. Then the collaboration will concentrate on cost reduction: the HTS materials are five time more expensive than Nb3Sn, which in turn is ten times more expensive than LHC Nb-Ti, making the cost of a ring based on hybrid Nb3Sn/HTS technology too expensive. However, would this effort be successful, this would seriously open the way toward the 20-25 T regions, making attractive also an accelerator like HE-LHC, which can count on an existing well-tested infrastructure. By 2020-2022 all these questions can be addressed and, given the fact that LHC will have probably exhausted the first part of his life, before being re-birth as HL-LHC, that seems a good time for making the choice about a future hh collider technology.

2.5 Muon Colliders and Muon Cooling

Muon beams represent an attractive choice for high energy lepton colliders because of the negligible level of synchrotron radiation, compared to electron beams. The physics potential of muon colliders is well known since a long time [27, 28]; muon colliders have recently received renewed attention [29–31] with the discovery of the Higgs boson thanks to their possible role as a Higgs factory of relatively small size. For muons the Higgs Yukawa coupling is 4.3×10^4 larger than for electrons, opening the possibility to produce Higgs bosons by muon annihilation in the s-channel and potentially measure the Higgs boson natural width with a line shape scan.

The use of muon beams in a collider is challenging for several reasons, not the least of which is that muons are unstable particles. Muons should be produced in sufficient amount by the decay of pions produced via fixed-target collisions of an intense proton beam (in the one-to-several MW range). A liquid-metal target seems preferred for such high intensities, and the MERIT experiment at CERN [32] has demonstrated the feasibility of a 4 MW mercury-jet proton target for pion production. Pions must then be captured by superconducting solenoids in a drift region for their subsequent decay to muons. The resulting muon beam has a very large spread in energy, which has to be reduced by phase-rotation techniques [33], which trade energy spread by spread in time, in order to obtain a muon beam of typical momentum of 200 MeV/c and energy spread of 10%, preparing the beam for muon cooling.

Muon cooling is a crucial component of muon colliders. In particular, collider operation as an s-channel Higgs factory requires a relative energy spread as low as 3×10^{-5}, because the Higgs width is expected to be about 4 MeV in the Standard Model. Traditional beam-cooling methods (electron, stochastic, laser) are not viable on the microsecond timescale of the muon lifetime. A promising technique is based on ionisation cooling [34], which builds on the penetrating character of the muon and

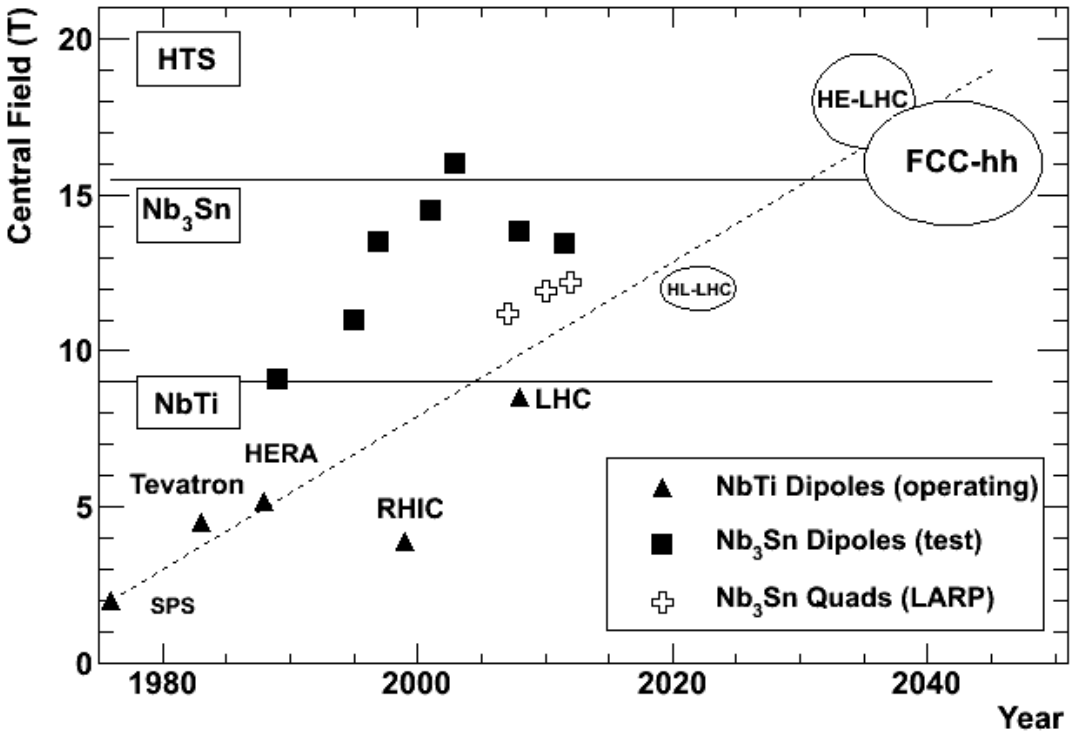

Fig. 3: Evolution of the maximum dipole field for large hadron colliders.

cooling by means of ionisation loss. In ionisation cooling, particles pass through a material medium and lose energy through ionisation interactions, followed by beam re-acceleration in RF cavities. The losses are parallel to the particle motion, and therefore include transverse and longitudinal momentum losses; the re-acceleration restores only longitudinal momentum. The loss of transverse momentum reduces particle emittances, therefore cooling the beam. In a dedicated storage ring both transverse and longitudinal muon emittances are progressively reduced, until an equilibrium condition is reached where dE/dx losses are balanced by multiple scattering. For the dE/dx loss low Z absorbers can be exploited (e.g. liquid hydrogen or LiH) in a wedged-shape geometry for emittance exchange (i.e. higher momentum muons cross more absorbing material). Dedicated experiments to develop muon ionisation cooling are underway [35] and a full-scale demonstrator has been proposed [29].

After muon cooling, in order to achieve sufficient muon survival, acceleration must occur at high average gradient. As muons are exiting the cooling step at low energy (100 MeV kinetic energy) a linac must be used to achieve sufficient time dilatation, followed by rapid-cycling recirculating accelerators (e.g. RLAs). When the muon beam has reached the nominal energy (62.5 GeV for the Higgs factory) it is transported to a storage ring, which should have minimal straight sections in order to increase the number of turns (and collisions) before the muons decay. The typical radius of such a storage ring could be about 50 m. While the physics backgrounds of a muon Higgs factory are expected to be low, particular care should be taken for beam-related backgrounds in the interaction region and in the storage ring itself: a bunch of 6×10^{12} muons at 62.5 GeV in a 50 m ring yields 5×10^{11} electrons/s/m in a narrow cone. The goal would be to achieve a luminosity of $\sim 10^{32}$ $\mathrm{cm}^{-2}\mathrm{s}^{-1}$ with several tens of thousands of Higgs bosons produced over one year of collider operation.

3 Technological aspects

Detector and computing technologies play an essential role in determining what can be measured at future accelerators. This chapter discusses the most relevant aspects of detector technology, trigger and data acquisition, and computing.

3.1 Detector technology

In this section we try to summarize the most relevant directions for development of detector technology to enable the physics programs at future accelerators [36].

In most cases the basic sensor technology is available and understood, although significant R&D and engineering is still required to make the detectors sufficiently robust, reliable, and affordable for application in real experiments. For HL-LHC, the emphasis is mostly on high rate/high occupancy capability, readout speed, and radiation hardness. For ILC, and other electron machines, the emphasis is instead on the material budget and extreme granularity. In both cases, cost and ease of fabrication are essential elements in the detector engineering.

The possible development of detectors with local reconstruction capability, extreme radiation hardness, and/or ps-level time resolution may open up new experimental horizons especially in dedicated flavour physics experiments.

Tracking and Vertexing

Solid state (silicon) detectors provide the most precise tracking device a modern experiment can use. Today's silicon trackers provide excellent performance, but many developments are in progress or planned to cope with future accelerator requirements:

- Pixels: small radius, O(1 m^2)
  - $< 50\,\mu\mathrm{m}$ pitch and $< 0.2\% X_0$ per detection layer
  - Potential for new sensor technologies
  - Hybrid pixels (more radiation hard, $10 \div 200 \cdot 10^{14}\ \mathrm{n_{eq}\ cm^{-2}}$): n-in-p silicon, diamond, 3D silicon sensors
  - Monolithic pixels (thinner and with smaller pitch): CMOS MAPS, HV-CMOS MAPS, DEPFET, CCD
  - Multi-tiered structures: high density interconnects for added functionality
  - Picosecond time resolution detectors: high rate applications
- Silicon Strips: large radius, O(10–100 m^2)
  - $> 50\,\mu\mathrm{m}$ pitch and $0.2 - 0.3\% X_0$ per detection layer
  - Established and reliable technology ($1 \div 10 \cdot 10^{14}\ \mathrm{n_{eq}\ cm^{-2}}$)
  - Smart detector structures for local p_T reconstruction and triggering; reduction of ambiguities in high occupancy environments
  - System engineering to reduce cost and production time
- Electronics, interconnections, services
  - CMOS 65 nm electronics: essential for all chip development
  - Advanced interconnection technologies such as vertical integration, through-silicon-vias, micro bump-bonding: needed to increase density and local functionality
  - Local intelligence to sparsify, build clusters, track stubs, trigger primitives: needed to cope with high occupancy/high rate and to limit bandwidth and computing requirements
  - Module design, power distribution, and cooling require careful engineering

- Equipment protection measures require a more systematic and integrated approach.

Gas Detectors

Gaseous detectors have been the workhorse of tracking systems: being low mass and relatively inexpensive, they can be used to cover large volumes, although with smaller rate capability than solid state detectors. The possibility of large internal charge amplification using elevated electric fields is a key advantage of gaseous detectors.

- Small chambers. Micro Pattern Gas Detectors can provide high resolution charged particle or photon detection. Based on fine pitch lithography
  - Many kinds in constant evolution: Micro Strip Gas Chambers, Micro Megas, Gas Electron Multipliers
  - Very powerful as tracking devices for moderate rate environments
  - Readout element of TPCs or PID devices
  - Readout element of fine grained sampling calorimeters
  - Ion backflow control essential for high rate operations
- Large chambers
  - Wired-based drift chambers still essential for moderate rate
  - Time Projection Chamber for ultra low-mass tracking at low rate.

Particle Identification

Particle identification plays an essential role in detector design and can provide an invaluable background rejection tool for many physics analyses.

- π/μ separation: relies on penetration depth measurement. Basic technology established
  - Developments of large area, high speed, cost-effective detector systems. Essential also for trigger
  - Resistive Plate Chambers (gas); scintillator/WLS fibers (solid)
  - Engineering to improve performance/cost, triggering capabilities
- e/π, π/K, and K/p identification: relies on a velocity measurement based on three technologies with different ranges of momentum sensitivity. These technologies are often combined in the same experimental apparatus
  - dE/dx: traditionally in gas detectors, but extending to solid state sensor with good energy resolution
  - Time-of-flight: depends critically on the maximum obtainable time resolution
  - Cherenkov and transition detectors: essential in the high momentum region. Many extremely clever developments with different radiator types (gas, aerogel, quartz) and light transport and detection arrangements.

Photon Detection

Photon detectors are essential components in many particle identification and calorimetry systems. The most relevant performance requirements are: high gain in magnetic field ($> 5 \cdot 10^5$); good time resolution ($\ll 100\,\mathrm{ps}$); fine granularity, long lifetime; very high detection efficiency (often down to single photon); high rate capability (several MHz/cm^2). Many developments exist that can significantly improve the overall detector performance:

- PhotoMultiplier Tube (PMT) technology evolution, such as the Multi-Anode PMT (MaPMT) and the Multi-Channel-Plate PMT (MCP-PMT): expensive and typically limited to small areas
- Gas based detectors such as MPGDs, possibly combined with large area MCP foils can provide picosecond-level time resolution on large areas
- Solid state detectors are a cost effective alternative to PMTs: photodiodes with no internal amplification; linear avalanche photodiodes (APD); silicon photomultipliers (SiPM), formed by a large array of very small avalanche photodiodes operated in Geiger mode and reaching a gain of 10^5.

Calorimetry

Energy measurement is a central element in modern detector design, providing essential physics tools such as photon and π^0 reconstruction, electron identification, jet and energy flow measurements. Although the basic technologies are established, developments are necessary to cope with high rate and high pileup environments retaining the energy resolution.

- Homogeneous crystals: NaI, CsI, PWO, LYSO, etc.
  - offer the best possible energy resolution for electromagnetic showers at lower energy
  - small decay time is an essential element to fight pileup
  - expensive: difficult balance between cost and performance; studies to find cheaper production strategies
  - critically depending on photon detector: extensive studies to optimize the overall system performance
  - calibration and radiation damage tracking can be critical
- Sampling calorimeters: absorber (W, Fe, Pb) interleaved with active layers (scintillator, liquid, gas or solid state detectors)
  - only practical solution for higher energy ranges and for hadronic calorimetry
  - established technology and long-standing experience in the community
  - not ideal performance in linearity and e/h
  - imaging calorimeters employ high granularity readout and particle flow algorithms to improve the energy resolution and correct for non-linearities
  - great efforts to engineer and industrialize the global system to reduce cost ($10^7 \div 10^8$ readout channels)
- Other approaches: various techniques are being tried to improve the performance of calorimeters
  - independent measurement of scintillation and Cherenkov light in showers to apply an event-by-event e/h correction, applicable to both sampling and homogeneous calorimeters
  - a combination of crystals and absorbers organized in shashlik geometry, with wavelength shifting fibers traversing the crystal tiles through holes along the depth of the calorimeter, providing a better resolution than scintillator readout
  - high resolution timing for both homogeneous and sampling calorimeters is also being explored to improve the pile-up rejection capabilities in high rate environment.

Electronics

Without electronics detectors are deaf, dumb and blind (trigger and DAQ are discussed in the next section). An integrated approach to electronics design will be required for the future detectors:

- Need for integrated design tools from ASIC to system integration, for example by extensive use of hardware description languages
- CMOS 65 nm electronics: essential for all chip development, sharing of knowledge and tools distribution is essential
- Distributed processing and local intelligence (for example using FPGAs) can radically change the overall system performance
- many directions are being explored: local hit clustering for strip and pixel detectors, local energy summing for calorimeters, local track segment finding, track triggers, etc.

Summary and outlook

The basic technology for the next generation detectors (HL-LHC, ILC) is mostly available, but significant focused R&D and engineering studies must be performed to optimize cost and performance of the detectors.

New systems combining advanced detectors, extreme resolution, local intelligence, and direct reconstruction of physics quantities have the potential to open new experimental horizons and should be pursued on a longer time scale.

3.2 Trigger and Data Acquisition

Trigger and Data Acquisition (TDAQ) are important elements of the technology required by the experimental study of particle physics. Most experiments make use of detectors producing a large flow of data, sustained for periods from months to years, generally exceeding the capabilities of any practical permanent storage system. The word "Trigger" is used in a wide sense to indicate any methodology for regulating and reducing this flow of data to a manageable level, by deciding which parts of the detector information should be acquired and at what time. This function most often requires performing substantial computations at high speed, in order to choose the information to retain in the way that is most advantageous for the physics. The word "DAQ" is generally used to indicate the whole process of carrying the data from the detector, up to the final destination of a permanent storage system, often also including the flow to and from the trigger system. The issues regarding the permanent storage and any further data treatment after the final selection of information are discussed separately in Section 3.3.

Trigger and DAQ systems of some kind have been part of particle physics experiments throughout the history of the field. While electronic technology has undergone huge advancements over the years, becoming cheaper and more powerful by large factors, the data handling demands in HEP have been growing at an even faster rate. As a consequence, the TDAQ system still represents today a major cost item in modern experiments, and in the most data-hungry experiments (hadronic collisions at high luminosity), it may amount to a major technical limitation to the experiment performance.

Most modern TDAQ systems are event-oriented and have a multi-layered structure. This means that the decision to permanently record a particular collision event is taken in a sequence of stages, with progressively decreasing data flow, and increasing computational cost per event. The lowest-level trigger decision is usually based on a low-complexity processing of a limited amount of event data, within low latencies, while the last level before permanent storage is now universally performed by commodity CPU systems running code written in high-level programming languages. Performance and complexity of these selection algorithms are generally only a small factor below the computations performed offline for the final analysis of the data.

All these features were already present in the pre-LHC generation of experiments (Tevatron, PEP, KEKB), but in moving to the LHC, the overall DAQ bandwidth has been increased, taking advantage of the fast internet growth that pushed telecommunication technology quickly forward, allowing large data handling systems to be built at reasonable prices, based on commercial technologies. In this process, much of the functionality of the intermediate levels of the trigger has been absorbed in the High Level Trigger implemented on commercial CPUs , and custom-developed electronics does not find much use anymore beyond the first trigger level. Most of the resources in the intermediate level are now devoted to event-building functions to prepare for high-level trigger (HLT) processing, rather than selection of events. The architecture of the first level of the trigger has not evolved as strongly as the higher levels. The technological evolution is mainly just an the update of the basic electronic components available on the market. Figure 4 shows a comparison of data rates and event sizes of a number of past and present experiments, after the first trigger level.

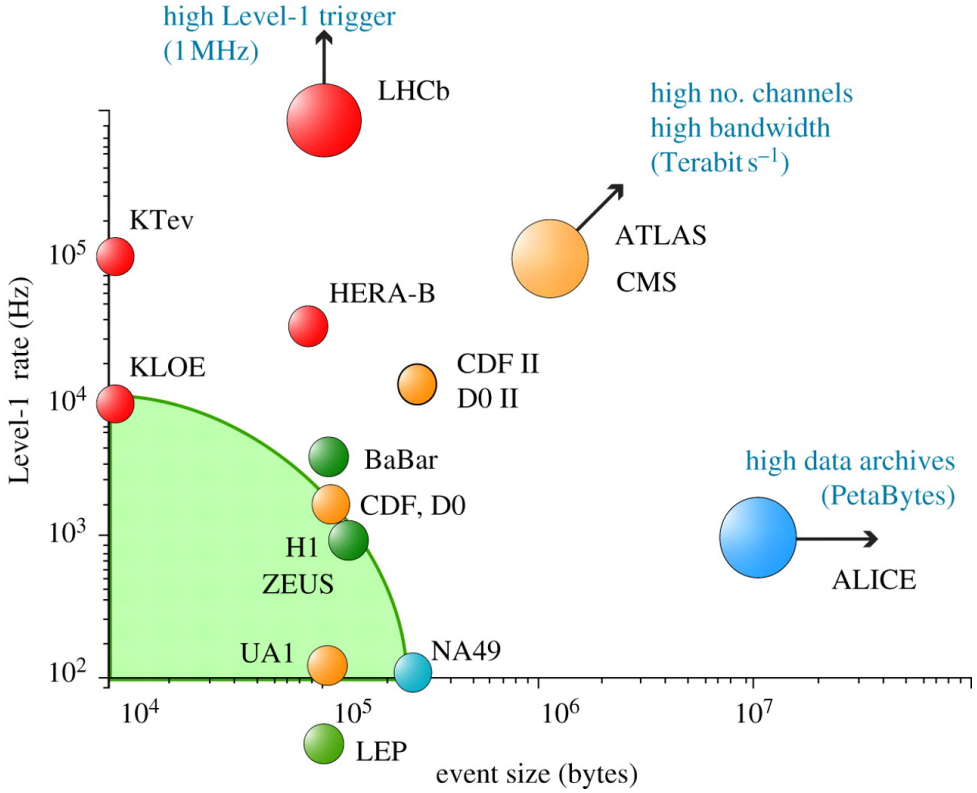

Fig. 4: Event size and data rate of major HEP experiments. (Reproduced with permission from Ref. [37].)

From the point of view of the event-selection functionality, the triggers of the LHC experiments have not evolved much from the previous generation. Event selection in ATLAS, CMS and LHCb experiments is mainly based on traditional muon and calorimetric requirements at level-1, followed by a nearly offline-like reconstruction in the HLT. In fact, some functionalities that have characterized the previous generation of experiments, like track-based triggering, or even zero-suppression in the front-end (LHCb), have been traded off in exchange for simplicity and larger system size at reasonable cost.

The demands of flavour physics require a more complete analysis of events before a trigger decision is made. Thus, LHCb has a trigger with a much higher L1 accept rate and an oversized HLT farm with respect to ATLAS and CMS. The greater demands are partly compensated by a smaller event size (see Fig 4).

In moving towards the High-Luminosity phase (Phase 2) , the ATLAS and CMS experiments are

now looking at ways to improve their L1 selection, which is expected to become their largest roadblock in the future. No obvious upgrade path from commercial products is easily visible there. CMS and ATLAS are looking at reintroducing tracking triggers, which characterized the Tevatron experiments of the previous generation — but this time under much more severe constraints in size/complexity and latency requirements, which will be at the level of a few μs.

ATLAS is introducing a track trigger in the second trigger level already in the upcoming run 2 (FTK). For phase 2, both ATLAS and CMS are considering a track trigger in the first trigger level. R&D efforts in this direction are already well represented inside CSN1 with a specific project, and are mostly relying in exploiting the Associative Memory methodology originally developed for CDF, but re-implemented with the latest gate technology (this requires custom ASICs development). Amongst the challenges in this process, are the need for a large number of cells ($> 10^8$), and the need to reduce the latency of the AM architecture in order to fit with buffering time in the front end. An R&D activity in CSN5 is also ongoing to study the feasibility of a L1 tracking trigger at 40 MHz for low-p_T physics, i.e. capable of reconstructing most of the tracks, also at low-p_T, and recognize secondary vertexes from weakly-decaying particles. There is however, no demonstrated solution yet for tracking at L1 at the time of this writing.

The upgrade of the LHCb experiment is planned for an earlier timescale (run 3, 2018+, rather than run 4) than ATLAS and CMS. This is motivated by the need to move beyond the current TDAQ system, that has already reached plateau performance. LHCb is not pursuing an improved L1 for this short-term upgrade. The experiment already works at the highest L1 accept rate amongst all LHC experiments, as the rate reduction factor from the crossing frequency is only 1:10. The LHCb chosen approach has been to limit its operating luminosity to $1 - 2 \times 10^{33}$ so that the data flow can be handled by the HLT with no help from L1, which will be eliminated. The upgraded HLT will use a much bigger processor farm, leveraging on Moore's law to year 2018 for increased computing power. The implication for the DAQ system is that it must be able to move the entire data flow of 4 TB/s from the front-end to the farm with no reduction. This is handled by connecting the fiber optic readout on the FE directly to a system of 500 PC nodes, each of them equipped with a FPGA card for data formatting, communicating with the PC with a 100Gb/s connection (16-lane PCIe Gen3). These PCs perform the event building by exchanging data amongst themselves, and then transfer the assembled events to the farm, each of them at a 80kHz event rate.

Belle II is innovating by preparing a significantly more complex trigger than has been usual in past e^+e^- experiments. The new Belle trigger includes calorimetry, muon, and track triggers right from the first trigger level, which however with its 200 ns bunch spacing is much less demanding than the LHC at high-lum.

The TDAQ path towards a future, larger circular collider (FCC) is not yet clear. The multiplicities expected at FCC-hh are not too much larger than at the HL-LHC, and given the time scale involved, one might assume that if something is possible at HL-LHC, it will also be possible at FCC. Physics rates, however, and high pileup, will make it a challenge to trigger on anything else than the highest energy events. As an example, top production occurs at 3kHz at the FCC, putting the top in the "low-p_T physics" category. It is possible that this kind of physics will not be doable at FCC, unless a dedicated "high-intensity" experiment is devised. There is a school of thought that in year 2035 and beyond, the TDAQ problems will become trivial at FCC—but it is far from obvious that Moore's law will continue to run as fast as it does today, so the need for R&D in this area is unlikely to go away, particularly for low-p_T, high-intensity physics.

3.3 Computing

3.3.1 LHC Distributed Computing

The Worldwide LHC Computing Grid (WLCG) is an HTC (High Throughput Computing) distributed system of resources based on the Grid paradigm that has been serving the LHC experiments very well. It is organized in a tiered hierarchy of sites, and those belonging to each tier level have different computational duties and service levels.

The Tier-0 centre at CERN is the central hub of the system, providing about 20% of the total WLCG computing and disk storage capacity, and 30% of the tape storage capacity. It is mainly responsible for first-pass reconstruction and for the safe keeping of the raw data. The Tier-0 distributes the raw data and the reconstructed output to the Tier-1s. There are 13 Tier-1 sites around the world, responsible for storing a proportional share of raw and reconstructed data as a second custodial copy. They also perform large-scale reprocessing, store the corresponding output, and provide archival capability of simulated datasets. The aggregated resources of all Tier-1 centres are roughly double in size those of the Tier-0 centre. Both Tier-0 and Tier-1 centres operate robotic tape libraries and must provide 24/7 operation support. A dedicated network of 10 Gbps optical-fibre links connects the Tier-0 to each of the 13 Tier-1 centres. The Tier-1 centres distribute the data to a third level: the Tier-2 centres. Tier-2s are typically smaller sites that can store sufficient data and provide adequate computing power for specific analysis tasks, handling a proportional share of the production and reconstruction of simulated events. The total amount of Tier-2 resources is roughly equal to that of Tier-1 resources, but distributed amongst more than 150 sites around the world. Tier-2 centres must provide business-hour operation support within their time zone. Finally, individual scientists can access the Grid through local computing resources, which can consist of local clusters in a university department (also known as Tier-3s) or even of an individual workstation. However, there is no formal engagement between WLCG and this fourth level of resources.

The glue between the sites is the Grid infrastructure with its CPU and data management services. Users submit computing jobs to the Grid using dedicated tools which form the middleware developed and maintained by Grid operators. Data storage and management are much more challenging than job submission, due to the very large scale of LHC datasets. Furthermore, it is anticipated that there will be a scaling problem as the LHC datasets continue to grow, and this is an issue that has to be solved mainly by the experiments themselves. The tiered structure of LHC computing was designed to be as efficient as possible with data movements. The speed and reliability of wide-area network interconnections has been constantly improving, allowing for increasingly fast file transfers, also opening the possibility of direct remote access to the data. As a consequence, nowadays jobs do not have to run necessarily on CPU resources close to the data. This implies that the original tiered hierarchy of the sites is gradually being smoothed out, as almost all of the activities can be done at every tier, with the notable exception of permanent data archiving, which still requires robotic tape libraries at the Tier-0 or Tier-1s.

It must be emphasized that all of the LHC experiments have managed to build higher levels of home-grown middleware tools on top of those originally provided by the Grid, in order to improve flexibility and stability of the overall computing infrastructure. Without this specialized work, the success of LHC computing would have been much less striking, as the reliability of the plain Grid infrastructure has proven to be too low to fulfill the requirements of the LHC experiments.

3.3.2 Current INFN infrastructure

The present INFN WLCG infrastructure comprises one Tier-1 centre, hosted at CNAF in Bologna, and 11 Tier-2 centres located at Bari (ALICE, CMS), Catania (ALICE), CNAF (LHCb), LNF (ATLAS), LNL/Padua (ALICE, CMS), Milan (ATLAS), Naples (ATLAS), Pisa (CMS), Rome (ATLAS), Rome (CMS), and Turin (ALICE). A summary of the pledged INFN resources, available for each of the four experiments at the Tier-1 and Tier-2 centres, is reported in Table 6. For completeness, the resources of

the Tier-0 centre are also shown. As of 2014, unitary costs for purchasing in Italy each sub-component

Table 6: Aggregated INFN resources available at the Italian Tier-1 and Tier-2 centres for each of the four experiments in 2015 and the overall value for WLCG. For completeness, the Tier-0 at CERN with the total WLCG resources are also reported.

Tier-1							
Resource	ALICE	ATLAS	CMS	LHCb	INFN	WLCG	INFN/WLCG
CPU [HS06]	22800	40500	39000	23600	125900	1051710	12.0%
Disk [TB]	3382	3500	3380	2720	12982	94850	13.7%
Tape [TB]	4182	5850	9620	6870	26522	179192	14.8%
Tier-2							
Resource	ALICE	ATLAS	CMS	LHCb	INFN	WLCG	INFN/WLCG
CPU [HS06]	38600	46800	65000	7875	158275	1332889	11.9%
Disk [TB]	4381	3710	3770	0	11861	105347	11.3%
Tier-0							
Resource	ALICE	ATLAS	CMS	LHCb	CERN	WLCG	CERN/WLCG
CPU [HS06]	175000	205000	271000	36000	687000	3071599	22.4%
Disk [TB]	14500	14000	15000	5500	49000	249197	19.7%
Tape [TB]	16200	33000	35000	11200	95400	274952	34.7%

(excluding infrastructural, operational and personnel costs) are about 10 Euro/HS06 (CPU), 200 Euro/TB (disk) and 30 Euro/TB (tape). This leads to a total integrated value of running resources in Italy of about 8.5 MEuro.

3.3.3 Needs for HL-LHC

The scale of computing resources needed by the LHC experiments in the HL-LHC era is expected to grow significantly, although a detailed estimate is very difficult as the future computing models are not yet designed, only seminal ideas on how to evolve them are being put forward by the experiments. A rough estimate can be obtained by extrapolating the current usage. Relevant parameters to be taken into account are the trigger rates and the complexity of HL-LHC events. The trigger rates are assumed to lie in the ranges 5-10 kHz for ATLAS and CMS, 100 kHz for LHCb and 50 kHz with Pb-Pb collisions for ALICE (200 kHz for p-Pb collisions). Accounting for the increase in event complexity is much more difficult, because even if the expected number of multiple interactions is known, strategy and code used to reconstruct the events are improving very quickly. In the latest years the reconstruction time has been reduced by a factor three or four, and new reconstruction strategies are constantly being proposed. Figures 5 and 6 show the extrapolated CPU and disk needs considering only the increased trigger rate: in

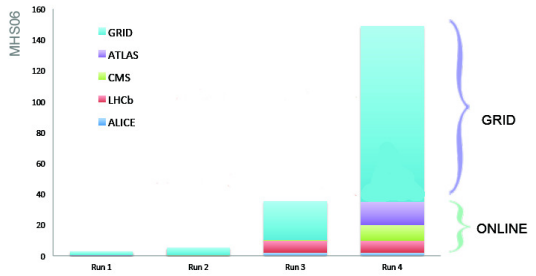

Fig. 5: Estimate of the CPU power needed by the LHC experiments.

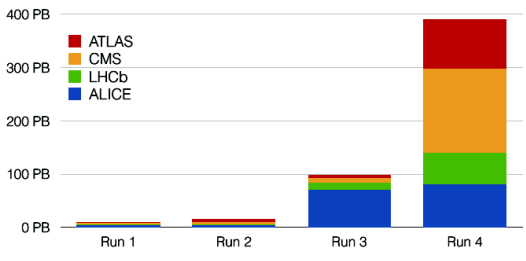

Fig. 6: Estimate of the disk space needed by the LHC experiments.

Run 4 roughly a factor of sixty increase of CPU power and a factor of 40 more disk space are necessary

with respect to Run 1. For the estimation of the disk needs, note that only RAW data are considered, *i.e.,* excluding any derived data. The technological evolution by 2020 is expected to give an increase of about a factor four for CPU power and disk space, assuming a constant monetary budget. This is about 2-3 times lower than the requirement. The situation is even worse when projecting to 2025, where a shortfall of a factor 5 is expected. On the other hand, the growth of the network capability has been increasing by an order of magnitude every four years, and it is expected to keep the same pace in the next 10 years too. The expected growth in CPU, disk and network resources are the key elements on which the strategy for the future has to be built.

3.3.4 Evolution of the distributed computing model

At present, the major funding agencies state that funds to procure computing resources will not increase in the next years, and that the optimistic scenario foresees a flat budget. This poses the problem of how to guarantee not only detector upgrades and data taking for the LHC experiments, but also data processing and analysis. Right now there is not a clear way to solve this problem, in contrast to the preparation and startup of the LHC when the development of the Grid and the ongoing technological evolution provided enough resources to process data almost in real time and produce all simulated data that were needed.

Seminal ideas on how to evolve the computing models are being put forward by the experiments. As already pointed out, the network speed increase allows data movements to happen more quickly allowing direct data access also via wide area network routes. This is changing the way data are organized on disk following the logic of removing what is seldom accessed. For this purpose, the necessary tools to monitor disk usage are being developed and tuned by the experiments.

The need for robotic libraries for tape archives is a debated question, although no alternative solutions are easily available at the moment. It is evident that at the time of Run 4 it will no longer be possible to reprocess the full sets of RAW data acquired by the detectors. For this reason, reconstruction and archival processes have to be carefully designed.

3.3.4.1 Technology Evolution

The technology is evolving, but in a different way with respect to the past. The evolution of processors is following three main avenues:

- New architectures based on accelerators; there are boards based on slightly modified graphics cards (e.g. Nvidia, AMD) or the new x86 based Xeon Phi (Intel).
- System-on-a-Chip (SoC) designs used mainly for low cost processors (e.g. smartphones, tablets). The tight coupling of the CPU with the graphics unit including direct memory sharing allows for better energy saving measures and higher performance.
- New server category based on lower-end processor designs (e.g. ARM, Atom) which couple large enough performance with a much better performance/watt ratio.

All of these developments in server architectures could be potentially relevant to the HEP use of commodity architectures. Most likely in ten years there will be only one kind of product with many cores, high performance and low energy consumption. For this reason the HEP community should invest some effort in understanding how best to make use of them.

The major disk storage technological improvement is expected to come with Heat Assisted Magnetic Recording (HAMR), a magnetic storage technology that will increase the amount of data that can be held on a standard disk platter by a factor between one and two orders of magnitude. The market for solid-state disks shows large growth rates, but the volume of units shipped is still about one order of magnitude lower than that of hard disks and the prices per unit storage are a factor 5-10 higher. In addition it must be noted that, while the capacity of hard disks has been continuously increasing, the sequential and random I/O performance has improved only very little.

3.3.4.2 Grid, cloud and HPC centers

The WLCG infrastructure will remain the main computational resource for LHC experiments. Meanwhile, computing architectures are changing, and the experiment software must evolve to keep up with them. Adapting the software to take advantage of new processor architectures is therefore a crucial aspect. The collaborations have already taken several actions with this respect. They have modified the infrastructural software framework in order to be able to submit to almost any architecture. The WLCG e-infrastructure is starting now to move toward an almost native cloud computing, and when the process is over it will be easier to access dedicated resources and opportunistic ones at the same time. Moreover there will be more efficient tools to access commercial clouds such as Amazon or Google if that will turn out to be economically advantageous, at least in certain cases.

Another important player is represented by the High Performance Computing (HPC) centers, both public and private. In the next years they are expected to continue their roles supporting the communities currently using these facilities, but as supercomputers usually have periods of low load, part of their CPU share can be opportunistically reused by the HEP world. Their use by the LHC experiments is difficult for activities that involve data movement, but it can be beneficial for simulation, where a limited amount data I/O of is involved. LHC experiments are actively porting elements of their software stacks, like Monte Carlo generators, to run on HPC resources. The benefits lie in the availability of increased amounts of simulated data, thus freeing up WLCG resources that can be used for data driven activities, and the possibility to speed up the software development taking advantage of new computational architectures.

3.3.4.3 New Strategies

Cloud computing facilitates the access to opportunistic resources, including HPC centers and this can mitigate the procurement of dedicated CPU power. However the amount of such resources at a given moment is not easily predictable, therefore they should be considered only for low priority activities.

As already pointed out the experiments are starting to evaluate new models for data storage and distribution, exploiting the increased network speed. This will reduce the data to be kept on disk, thus leading to a reduction of disk storage needs. As already said, the employment of tape devices for long term storage is being discussed. Already in Run 2, the amount of raw data collected every year will require at least two months to be reprocessed. Extrapolating to Run 4 data sizes even considering possible improvements, it will be impossible to reprocess full data sets, even not taking into account any derived or simulated data. This poses the question of permanently storing reconstructed data alone, and discard raw data. One possible strategy is to combine trigger DAQ and data processing in order to have already production level datasets after the data acquisition. Such a new model has to be studied in detail and will require a new approach to data selection and management processes.

The evolution in CPU, network and data access is modifying the old tiered structure of the WLCG infrastructure. The differences between Tier-1 and Tier-2 are already quite minimal and in the future will vanish if tape archiving is used only as backup system. The geographical distribution of computing centers will also be conditioned also by the running costs, among which electrical power and manpower are the dominant ones. A possible way to reduce such costs would be to group the computing resources in fewer bigger centers, and take advantage of the economy of scale. This strategy is being pursued by private companies like e.g. Google, that has only twelve data centers (at least in the official list) to serve the entire world. The internals of the data centers are not publicly available, but it is known that they are based on a modular approach, where each module is engineered with all components. Modular data centers are a form of emerging infrastructure allowing for substantial economies of scale.

LHC, and in particular INFN, are going to elaborate a similar strategy taking into account the peculiarity of being part of a scientific infrastructure and the important synergies with the Universities. Such a strategy implies that the number of computing centers has to be reduced and federated with common choices for infrastructure and equipment, paying particular attention to energetic efficiency

issues in order to minimize electrical power costs. However, it is worth mentioning that this approach poses non-trivial problems in reusing existing manpower distributed throughout several departments. As such, it would require a high level of remote management of resources and distributed organization of personnel and associated duties, well beyond what is customary today. The process of building up a unique e-infrastructure is under discussion in Italy and it is in progress in Europe among the major WLCG centers.

4 Standard Model Physics

In the past twenty years we have witnessed two important successes of the Standard Model: the matching between the predicted top mass and its actual value measured at the Tevatron [38–40] (Fig. 7) and the indication of a light Higgs in the mass region where it has been observed at LHC [41–43] (Fig. 8). With the Higgs discovery electroweak precision measurements are becoming a crucial test of our "standard model" and have the potential of developing into important tools for indirect information on new physics. Another success is the amazing capability of describing, often within small uncertainties, the wealth of collider data.

In the present chapter we regard at Standard Model physics as a major tool for discovering new physics. The chapter starts with a discussion on Higgs physics, which is central for the experimental programme at high energy accelerators in the next decades. Then a brief report on the status and prospects of vector bosons physics follows, including a description of key points related to our understanding of strong interactions. Furthermore, because of their relevance for the present discussion, top-quark physics prospects are presented. Perspectives in the field of theoretical calculations and Monte Carlo generators, which are essential to analyse the data and interpret the measurements, conclude the chapter.

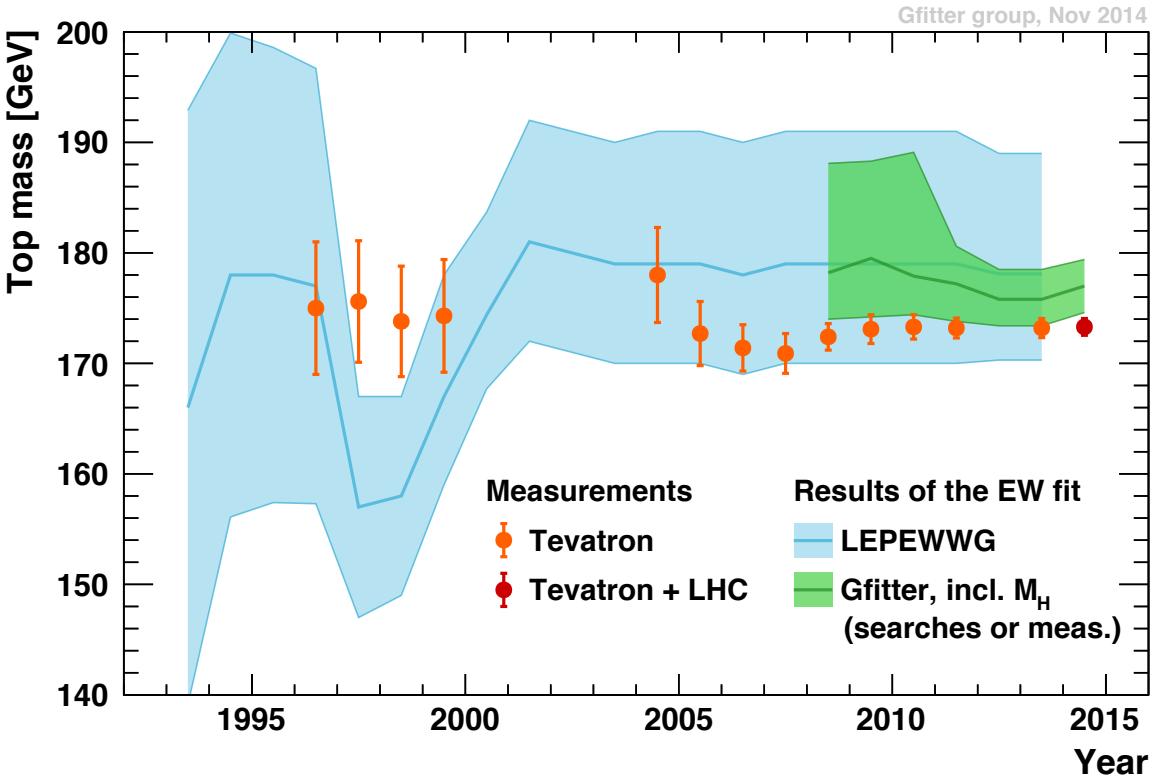

Fig. 7: The bands show the indirect determination of the top mass from electroweak fits as a function of time. The light blue band and green band are without and with the information coming from the Higgs boson mass, respectively. The points represents the combinations of direct measurements of the top mass in various years. Courtesy of Roman Kogler.

4.1 Higgs Properties and Couplings

The discovery of a scalar boson at the LHC [42, 43] has started up a new phase in the experimental exploration of the electroweak symmetry-breaking (EWSB) mechanism of the Standard Model (SM).

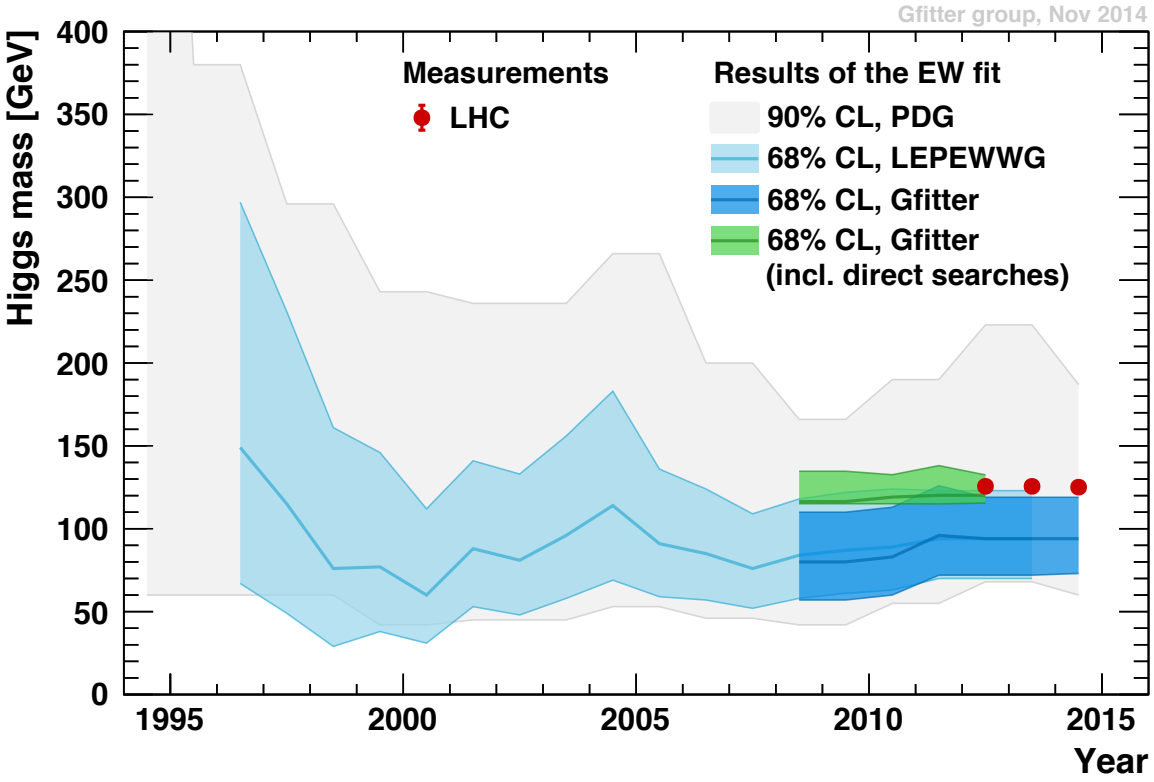

Fig. 8: The bands show the indirect determination of the Higgs boson mass from electroweak fits as a function of time. The light blue bands and green band are without and with the information coming from direct Higgs searches, respectively. The grey band shows the 90% CL interval (without direct searches). The points with error bars represents the combinations of direct measurements of the Higgs boson mass in various years. Courtesy of Roman Kogler.

The observed resonance is, within present experimental errors, well compatible with a minimal structure of the Higgs sector. Nevertheless, the determination of the different properties of the new particle with increasing precision is expected to be a powerful tool to explore what could be beyond the SM description of fundamental interactions. In particular, on the one hand, deviations in the scalar boson couplings to the electroweak vector bosons $V = W, Z$ would require further degrees of freedom to keep the VV scattering unitary. On the other hand, anomalies in the Yukawa couplings to matter fields could possibly point to a non-standard mechanism for the generation of quark and charged-lepton masses.

The key role of the Higgs sector in elementary particle physics makes it an important goal to understand the properties of the LHC resonance as accurately as possible [44, 45] and to clarify the real nature of the newly discovered Higgs-boson particle, in particular relevant questions are

- is the new boson really the SM Higgs boson?
- is it an elementary or a composite particle?
- is it the only one, or are there other Higgs fields?
- is it natural?
- is it really responsible for the masses of all elementary particles?
- is it at the origin of the matter-antimatter asymmetry?
- is it responsible for the inflationary expansion of the Universe?

The size of the deviation in the Higgs couplings to SM particles depends in general on the energy scale where the New Physics becomes relevant. For instance, in the MSSM (with $\tan\beta = 5$), one expects a deviation in the Yukawa couplings of the heaviest down-type fermions of the order $g_{hbb}/g_{hbb}^{SM} = g_{h\tau\tau}/g_{h\tau\tau}^{SM} \simeq 1 + 1.7\,\% \ (1\ \mathrm{TeV}/m_A)^2$ (where m_A is a heavy pseudoscalar mass), while, in minimal composite Higgs models, the Higgs coupling to vector bosons is affected according to $g_{hVV}/g_{hVV}^{SM} \simeq 1 - 3\,\% \ (1\ \mathrm{TeV}/f)^2$, (where f is the composite scale) [46]. The solution of the SM hierarchy problem, which in general implies the NP scale to be of the order of 1 TeV, entails then coupling deviations of at most a few percents. Hence, a percent-level accuracy on Higgs couplings is needed in order to pinpoint relevant NP effects in the Higgs precision measurements.

A list of relevant measurements discussed in this section is

- Precision in measuring couplings
- Rare and “invisible" decay modes
- Search for CP mixing in the Higgs sector
- New trends to measure natural width.

4.1.1 Precision coupling measurements

As already stated, the recently discovered “125 GeV" Higgs particle by ATLAS and CMS at LHC, is compatible within current experimental and theoretical uncertainties with the properties of the Higgs boson predicted by the Standard Model. It is of paramount importance to clarify the nature of this new object and its role in EWSB. Deviations of physics properties from those predicted in the Standard Model would unambiguously indicate new physics beyond this theory. Hence, the precise measurement of this particle's properties represent a major goal of future experiments.

The results presented here are relative to what was presented at the ECFA LC2013 Workshop (May 2013), the ECFA HL-LHC Workshops (October 2013 and October 2014) and the kick-off Workshop on FCC (February 2014).

Following the approach and benchmarks recommended in [44], measurements of couplings are currently implemented using a leading-order tree-level motivated framework. Other frameworks, based on SM Effective Field Theory (EFT), are currently in development and are discussed in [47]. The present framework is based on the assumption that the width of the Higgs boson is narrow, justifying the use of the narrow-width approximation. Hence the predicted rate for a given channel can be decomposed in the following way:

$$\sigma \cdot BR\,(i \to \mathrm{H} \to f) = \frac{\sigma_i \cdot \Gamma_f}{\Gamma_\mathrm{H}} \tag{1}$$

where σ_i is the production cross section through the initial state i, BR and Γ_f are the branching ratio and partial decay width into the final state f, respectively, and Γ_H the total width of the Higgs boson.

The coupling scale factors κ_j associated with the SM particle j are defined in such a way that the cross sections σ_j and the partial decay widths Γ_j scale with κ_j^2 compared to the SM prediction (i.e., $\kappa_i \equiv g_{hii}/g_{hii}^{(SM)}$, where g_{hii} represents the coupling). Table 7 shows the precision on Higgs boson coupling κ_i for several elementary particles that can be achieved by ATLAS and CMS independently, assuming 300 fb^{-1}of data at LHC, and 3000 fb^{-1}of data at HL-LHC. The necessary reduction of theory uncertainties which is required to have an impact of less than 10% on the total uncertainty, at LHC and HL-LHC, it is shown in Table 8. The factors λ_{ij} express the ratio of coupling scale factors, so that for example $\lambda_{\tau Z} = \kappa_\tau/\kappa_Z$; the κ_{gZ} parameter is defined as $\kappa_g \cdot \kappa_Z/\kappa_H$, where κ_H^2 is the scaling factor with respect the total Higgs boson width.

Table 7: Precision on the measurements of κ_γ, κ_W, κ_Z, κ_g, κ_b, κ_t, κ_τ, $\kappa_{Z\gamma}$, and κ_μ. These values are obtained at $\sqrt{s} = 14$ TeV using an integrated dataset of 300 fb^{-1}at LHC, and 3000 fb^{-1}at HL-LHC. Numbers in brackets are % uncertainties on the measurements estimated under [no theory uncertainty, current theory uncertainty] for ATLAS and [optimistic, pessimistic] systematic experimental and theoretical uncertainties for CMS.

L(fb^{-1})	Exp.	κ_γ	κ_W	κ_Z	κ_g	κ_b	κ_t	κ_τ	$\kappa_{Z\gamma}$	κ_μ
300	ATLAS	[9, 9]	[9, 9]	[8, 8]	[11, 14]	[22, 23]	[20, 22]	[13, 14]	[24, 24]	[21, 21]
	CMS	[5, 7]	[4, 6]	[4, 6]	[6, 8]	[10, 13]	[14, 15]	[6, 8]	[41, 41]	[23, 23]
3000	ATLAS	[4, 5]	[4, 5]	[4, 4]	[5, 9]	[10, 12]	[8, 11]	[9, 10]	[14, 14]	[7, 8]
	CMS	[2, 5]	[2, 5]	[2, 4]	[3, 5]	[4, 7]	[7, 10]	[2, 5]	[10, 12]	[8, 8]

Table 8: Estimation of the deduced size of theory uncertainties, in percent (%), for different Higgs coupling measurements, requiring that each source of theory systematic uncertainty affects the measurement by less than 30% of the total experimental uncertainty and hence increase the total uncertainty by less than 10%. A dash "-" indicates that the theory uncertainty from existing calculations [44,48,49] is already sufficiently small to fulfill the condition above for some measurements. The same applies to theory uncertainties not mentioned in the table for any measurement. The impact of the jet-bin and p_T related uncertainties in $gg \to H$ depends on analysis selections and hence no single number can be quoted. Therefore the range of uncertainty values used in the different analysis is shown. (MHOU stands for missing higher-order uncertainties. Note that these uncertainties have been recently further reduced thanks to N3LO calculations [50].)

Scenario	Status	Deduced size of uncertainty to increase total uncertainty							
	2014	by $\lesssim$10% for 300 fb^{-1}			by $\lesssim$10% for 3000 fb^{-1}				
Theory uncertainty (%)	[44, 48, 49]	κ_{gZ}	λ_{gZ}	$\lambda_{\gamma Z}$	κ_{gZ}	$\lambda_{\gamma Z}$	λ_{gZ}	$\lambda_{\tau Z}$	λ_{tg}
$gg \to H$									
PDF	8	2	-	-	1.3	-	-	-	-
incl. QCD scale (MHOU)	7	2	-	-	1.1	-	-	-	-
p_T shape and 0j $\to$ 1j mig.	10–20	-	3.5–7	-	-	1.5–3	-	-	-
1j $\to$ 2j mig.	13–28	-	-	6.5–14	-	3.3–7	-	-	-
1j $\to$ VBF 2j mig.	18–58	-	-	-	-	-	6–19	-	-
VBF 2j $\to$ VBF 3j mig.	12–38	-	-	-	-	-	-	6–19	-
VBF									
PDF	3.3	-	-	-	-	-	2.8	-	-
$t\bar{t}H$									
PDF	9	-	-	-	-	-	-	-	3
incl. QCD scale (MHOU)	8	-	-	-	-	-	-	-	2

In the fit [51, 52], it is assumed that no particles other than those in SM are contributing to NLO electroweak loops, nor decay modes contribute to the full width of this particle other than those predicted by SM. As it can be seen, depending on the type of coupling, an accuracy of a few % can be achieved for bosons, and of about 5% for fermions, by each of the two experiments. Ratio of couplings allow a test free from assumptions on the total width; the findings are reported in Fig. 9 for ATLAS [51]; similar results are expected by CMS.

The precision on couplings can considerably increase at ILC, as pictorially shown in Fig. 10. Colliders such as ILC or FCC-ee are indeed Higgs-boson factories in a very clean environment. The dominant Higgs production cross sections are shown in Fig. 11 (left plot). They correspond to the associated production $e^+e^- \to ZH$ (dominant at 250 GeV), and to the vector-boson-fusion (VBF) scattering $e^+e^- \to H\nu\nu\,, He^+e^-$ (that gets the upper hand at $\sqrt{s} > 450$ GeV). At $\sqrt{s} \simeq 250$ GeV, a statistics of 8×10^4 Higgs bosons will be collected in a first stage (3.7×10^5 after full program with 1.15 ab^{-1}). At

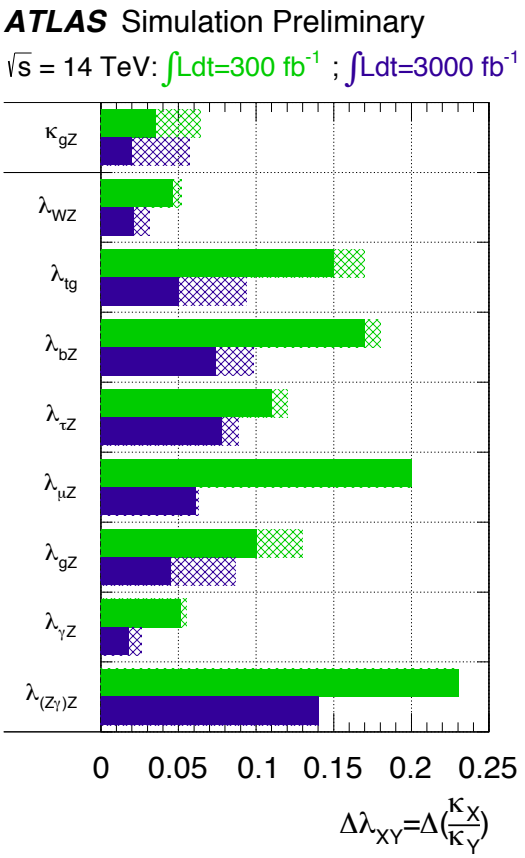

Fig. 9: Relative uncertainty on the expected precision for the determination of coupling scale factor ratios λ_{XY} in a generic fit without assumptions on the total Higgs boson width [51], assuming a SM Higgs Boson with a mass of 125 GeV and LHC at 14 TeV, 3000 fb^{-1}. The κ_{gZ} parameter represents the ratio $\frac{\kappa_g \cdot \kappa Z}{\kappa_H}$, where κ_H^2 is the scaling factor with respect the total Higgs boson width. The hashed areas indicate the increase of the estimated error due to current theory systematics uncertainties

$\sqrt{s} \simeq 500$ GeV (where the lower total cross section is more than compensated by the larger integrated luminosity), an additional statistics of 1.2×10^5 will be collected in a second stage (4×10^5 after full program with 1.6 ab^{-1}), with a dominant contribution from VBF.
The associated production $e^+e^- \to ZH$ is the key process that allows e^+e^- colliders to make a model-independent measurement of the Higgs couplings (unaffected by assumptions on the production mechanism), which is not attainable at hadron colliders. Thanks to the excellent signal-to-background (S/B) ratio, by applying the four-momentum conservation to the two-body ZH final state, one can indeed reconstruct the Higgs-system production properties just through the observation of its recoil Z system, independently from the Higgs decay mode. Notably any possible Higgs *invisible* decay would contribute to this measurement just as any *visible* Higgs decay. The outcome of these features is that one can make an absolute (that is independent from the Higgs decay BR's) determination of g_{HZZ}, the Higgs coupling to the Z. Indeed, the Higgs production cross section $\sigma(ZH) \sim g^2_{HZZ}$ can be measured in a model-independent way through the normalization of the Z recoil-mass distribution with no assumption on the Higgs interaction with other particles. In Fig. 11 (right plot), the recoil-mass distribution for the process $e^+e^- \to ZH \to \mu\mu X$ is shown as obtained by a full detector simulation [53]. A precise measurement of the Higgs mass ($\Delta m_H \lesssim 100$ MeV) can also be obtained from the shape of the distribution.

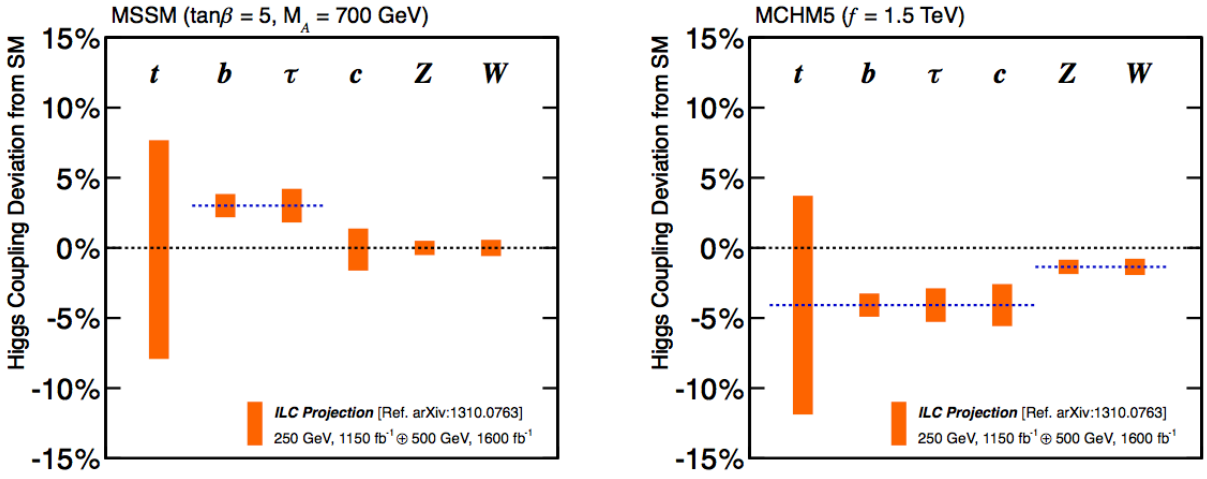

Fig. 10: Projected precision on Higgs-boson couplings, with regard to ILC capability to distinguish between different models of more complex Higgs sectors: SUSY multiple Higgs model (left) and Minimal Composite Higgs boson (right) [5].

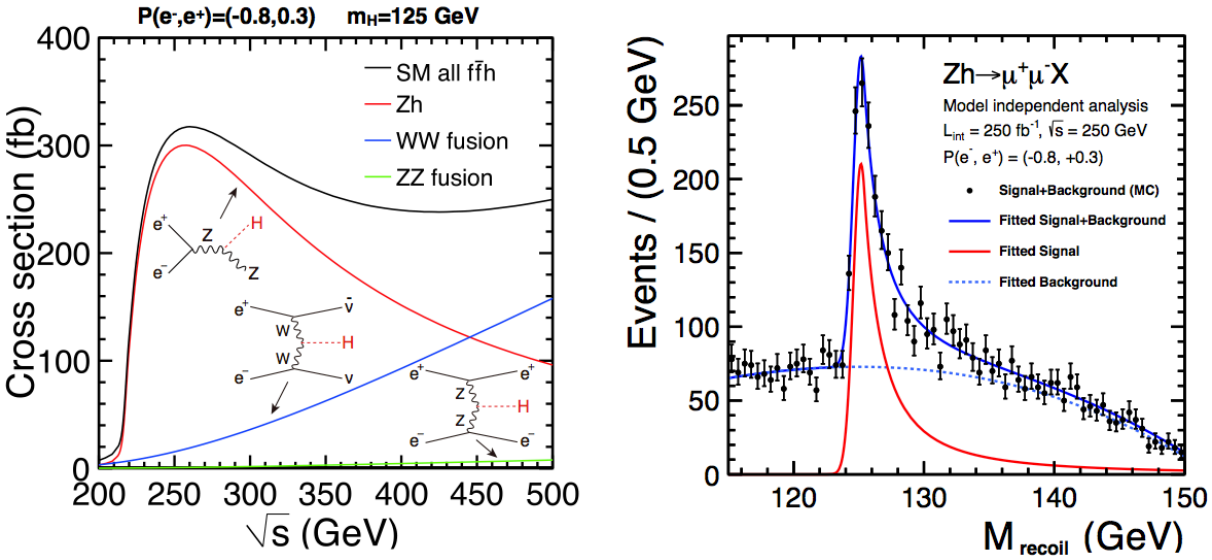

Fig. 11: Cross sections for the main Higgs production mechanisms in e^+e^- (left). Recoil-mass distribution in $e^+e^- \to Zh \to \mu\mu X$ (right) [5].

An absolute measurement of Higgs BRs for all possible decay channels (including invisible and exotic decays, as well as SM decays which are overwhelmed by background at the LHC, like $H \to jets$) can then be made by tagging different Higgs final states, thus obtaining a model-independent determination of the quantities $\sigma(ZH) \cdot \mathrm{BR}(H \to ii)$ for different Higgs decays, and hence an absolute measurements of $\mathrm{BR}(H \to ii)$ (here i stands for any boson or fermion coupled to H). The latter in turn can be combined with the direct coupling measurement from the production cross section in order to obtain a direct (model independent) determination of the Higgs total width. For instance, starting from the $H \to ZZ$ branching ratio, one has $\Gamma_H = \Gamma(H \to ZZ)/\mathrm{BR}(H \to ZZ) \propto \sigma(ZH)/\mathrm{BR}(H \to ZZ)$. Similarly, at larger collision energies, one can use the $e^+e^- \to H\nu\nu$ cross section to get a different

Table 9: Model-Independent (top) and Model-Dependent (bottom) precision on Higgs-boson couplings [5]. For the latter, the fitting technique most closely matches that used at the LHC, and no non-SM production or decay modes are assumed.

	ILC(250)	ILC(500)	ILC(1000)	ILC(LumUp)
$\sqrt{s}$ (GeV)	250	250+500	250+500+1000	250+500+1000
L (ab^{-1})	0.25	0.25+0.5	0.25+0.5+1	1.15+1.6+2.5
$\gamma\gamma$	18%	8.4%	4.0%	2.4%
gg	6.4%	2.3%	1.6%	0.9%
WW	4.8%	1.1%	1.1%	0.6%
ZZ	1.3%	1.0%	1.0%	0.5%
$t\bar{t}$	–	14%	3.1%	1.9%
$b\bar{b}$	5.3%	1.6%	1.3%	0.7%
$\tau^+\tau^-$	5.7%	2.3%	1.6%	0.9%
$c\bar{c}$	6.8%	2.8%	1.8%	1.0%
$\mu^+\mu^-$	91%	91%	16%	10%
$\Gamma_T(h)$	12%	4.9%	4.5%	2.3%
hhh	–	83%	21%	13%
BR(invis.)	$< 0.9\%$	$< 0.9\%$	$< 0.9\%$	$< 0.4\%$

	ILC(250)	ILC(500)	ILC(1000)	ILC(LumUp)
$\sqrt{s}$ (GeV)	250	250+500	250+500+1000	250+500+1000
L (ab^{-1})	0.25	0.250+0.5	0.25+0.5+1	1.15+1.6+2.5
$\gamma\gamma$	17%	8.3%	3.8%	2.3%
gg	6.1%	2.0%	1.1%	0.7%
WW	4.7%	0.4%	0.3%	0.2%
ZZ	0.7%	0.5%	0.5%	0.3%
$t\bar{t}$	6.4%	2.5%	1.3%	0.9%
$b\bar{b}$	4.7%	1.0%	0.6%	0.4%
$\tau^+\tau^-$	5.2%	1.9%	1.3%	0.7%
$c\bar{c}$	6.8%	2.8%	1.8%	1.0%
$\mu^+\mu^-$	91%	91%	16%	10%
$\Gamma_T(h)$	9.0%	1.7%	1.1%	0.8%
hhh	–	83%	21%	13%
BR(invis.)	$< 0.9\%$	$< 0.9\%$	$< 0.9\%$	$< 0.4\%$

(and more accurate) Γ_H determination via the relation $\Gamma_H = \Gamma(H \to WW)/\mathrm{BR}(H \to WW) \propto \sigma(H\nu\nu)/\mathrm{BR}(H \to WW)$. Finally, by inserting Γ_H in the measured value of $\mathrm{BR}(H \to ii) \propto g^2_{Hii}/\Gamma_H$, one can obtain an absolute measurement of the Hii coupling g_{Hii}.

The final precision presently expected for the Higgs couplings at the ILC is reported in Table 9, as summarized in [5], for the various ILC staging scenarios. These results assume (e^-, e^+) polarizations of (-0.8, 0.3) at 250 and 500 GeV, and (-0.8, 0.2) at 1 TeV, plus a 0.5% theory uncertainty. A comparison with the HL-LHC potential is presented in Fig. 12. The top part of Table 9 refers to a model-independent fit, with no assumption on or between g_{HWW} and g_{HZZ}, nor on the saturation of the total width by invisible decays. It requires the measurement of the recoil HZ process at low energies. For $\mathrm{BR}(H \to invis.)$, the numbers quoted are the 95% confidence upper limits on the branching ratio. Note that the measurement of the g_{Htt} and of the trilinear g_{HHH} coupling requires $\sqrt{s} \gtrsim 500$ GeV. The corresponding accuracies presented in Table 9 are quite preliminary, and considerable improvements are foreseen in the ongoing analyzes [54].

As already mentioned, at hadron collider some level of model-dependence is needed to determine the Higgs couplings. In order to make a fair comparison between facilities of the attainable precisions, ILC *model-dependent* fits are reported in the lower part of Table 9. In this case, the fitting technique most closely matches that used at the LHC, and no non-SM production or decay modes are assumed. In Fig. 12, the expected precisions on the κ_i scaling factors are shown, as from a constrained 7-parameter fit that assumes fermion-generation universality. The two ranges (light and dark green, respectively) shown for the HL-LHC represent the conservative and optimistic scenarios for systematic and theory uncertainties. Table 10 presents a summary including a comparison with the CLIC and the TLEP (FCC-

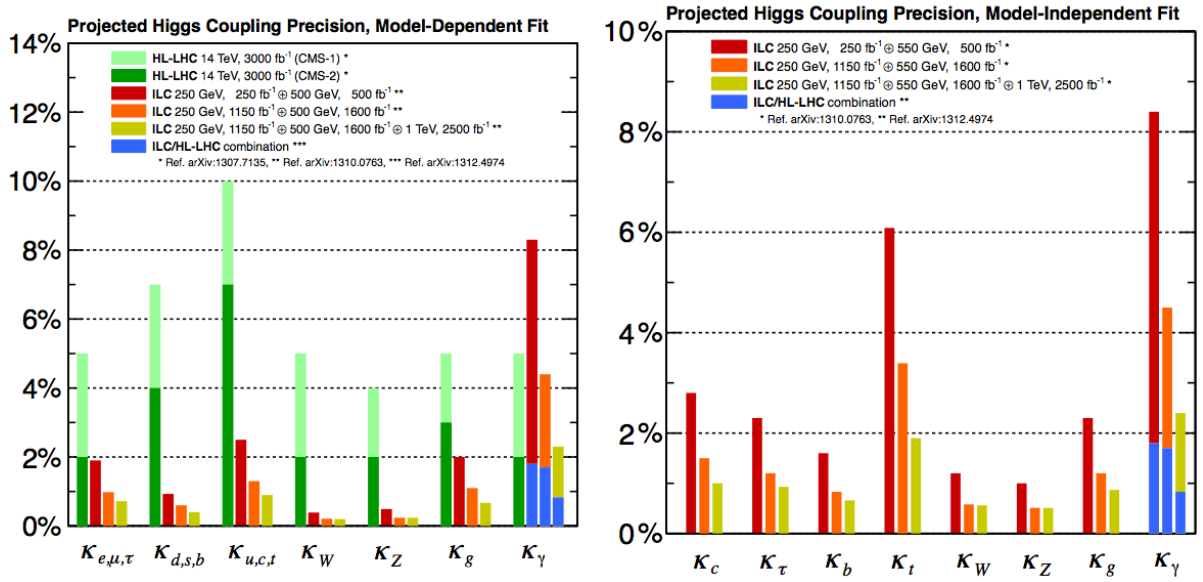

Fig. 12: Model-Dependent (left) and Model-Independent (right) projected precision on Higgs-boson coupling scaling factors. Here $\kappa_i \equiv g_{hii}/g_{hii}^{(SM)}$. Green bands refer to HL-LHC projections; blue bands refer to combinations of ILC and HL-LHC outputs.

Table 10: Expected precisions on the Higgs coupling scaling factors from a constrained 7-parameter fit assuming no non-SM production or decay modes. The fit assumes generation universality [46]. The range of values shown for LHC and HL-LHC corresponds to a conservative scenario (current theory uncertainties) and an optimistic scenario (theory uncertainties scaled by a factor 1/2).

Facility	LHC	HL-LHC	ILC500	ILC500-up	ILC1000	ILC1000-up	CLIC	TLEP (4 IPs)
$\sqrt{s}$ (GeV)	14,000	14,000	250/500	250/500	250/500/1000	250/500/1000	350/1400/3000	240/350
$\int \mathcal{L}dt$ (fb^{-1})	300/expt	3000/expt	250+500	1150+1600	250+500+1000	1150+1600+2500	500+1500+2000	10,000+2600
κ_γ	$5-7\%$	$2-5\%$	8.3%	4.4%	3.8%	2.3%	$-/5.5/<5.5\%$	1.45%
κ_g	$6-8\%$	$3-5\%$	2.0%	1.1%	1.1%	0.67%	3.6/0.79/0.56%	0.79%
κ_W	$4-6\%$	$2-5\%$	0.39%	0.21%	0.21%	0.2%	1.5/0.15/0.11%	0.10%
κ_Z	$4-6\%$	$2-4\%$	0.49%	0.24%	0.50%	0.3%	0.49/0.33/0.24%	0.05%
κ_ℓ	$6-8\%$	$2-5\%$	1.9%	0.98%	1.3%	0.72%	$3.5/1.4/<1.3\%$	0.51%
$\kappa_d = \kappa_b$	$10-13\%$	$4-7\%$	0.93%	0.60%	0.51%	0.4%	1.7/0.32/0.19%	0.39%
$\kappa_u = \kappa_t$	$14-15\%$	$7-10\%$	2.5%	1.3%	1.3%	0.9%	3.1/1.0/0.7%	0.69%

ee) prospects on Higgs-coupling accuracies [46]. CLIC numbers assume polarizations of (0.8, 0) for energies above 1 TeV. TLEP (FCC-ee) numbers assume unpolarized beams.

Additional information on the TLEP (FCC-ee) potential is given in Table 11. The prospects shown in the table assume $\sqrt{s} = 350$ GeV, four experiments and 2600 fb^{-1}of data each (plus a data sample of 10000 fb^{-1}taken at 240 GeV), and negligible theoretical uncertainties with respect the experimental ones. It is expected to measure the Higgs couplings to bosons with less than 1% uncertainty, while couplings to fermions should be measured with an uncertainty from about 0.4% ($Hb\bar{b}$) to 13% ($Ht\bar{t}$) [55].

Table 11: Relative statistical uncertainty on the Higgs boson couplings, as expected from the physics programme at $\sqrt{s} = 240$ and 350 GeV at TLEP. (The first column indicates the expected precision at TLEP when the sole 240 GeV data are considered. The substantial improvement with the inclusion of the 350 GeV data – in the second column – mostly stems from the precise total Higgs boson width measurement, which constrains all couplings simultaneously.) The numbers between brackets indicates the uncertainties expected with two detectors instead of four. For illustration, the uncertainties expected from the ILC baseline programme at 250 and 350 GeV are also given. The first three columns give the results of a truly model-independent fit, while the last two include the two assumptions made in Ref. [56] on the W/Z couplings and on the exotic decays, for completeness and easier comparison. The column labelled "TLEP-240" holds for the sole period at 240 GeV for TLEP. The last line gives the *absolute* uncertainty on the Higgs boson branching fraction to exotic particles (invisible or not).

	Model-independent fit				Constrained fit		
Coupling	TLEP-240	TLEP		ILC	TLEP		ILC
g_{HZZ}	0.16%	0.15%	(0.18%)	0.9%	0.05%	(0.06%)	0.31%
g_{HWW}	0.85%	0.19%	(0.23%)	0.5%	0.09%	(0.11%)	0.25%
$g_{\mathrm{H\bar{b}b}}$	0.88%	0.42%	(0.52%)	2.4%	0.19%	(0.23%)	0.85%
$g_{\mathrm{H\bar{c}c}}$	1.0%	0.71%	(0.87%)	3.8%	0.68%	(0.84%)	3.5%
g_{Hgg}	1.1%	0.80%	(0.98%)	4.4%	0.79%	(0.97%)	4.4%
$g_{\mathrm{H\tau\tau}}$	0.94%	0.54%	(0.66%)	2.9%	0.49%	(0.60%)	2.6%
$g_{\mathrm{H\mu\mu}}$	6.4%	6.2%	(7.6%)	45%	6.2%	(7.6%)	45%
$g_{\mathrm{H\gamma\gamma}}$	1.7%	1.5%	(1.8%)	14.5%	1.4%	(1.7%)	14.5%
$\mathrm{BR}_{\mathrm{exo}}$	0.48%	0.45%	(0.55%)	2.9%	0.16 %	(0.20%)	0.9%

4.1.2 Rare and invisible decay modes

Measurements of Higgs boson decay rates suppressed in the Standard Model give crucial information on the structure of new physics. In this respect, final states such as $H \to \mu^+\mu^-$ and $H \to Z\gamma$ are very attractive (in the SM, BR $H \to \mu^+\mu^- \sim 2.2 \times 10^{-4}$ and $H \to Z\gamma \sim 1.5 \times 10^{-3}$, respectively [57]). A high luminosity collider such as HL-LHC is the ideal machine for the production and the measurement of these final states.

The study of the $H \to \mu^+\mu^-$ decay channel is of particular importance as it allows the investigation of the Higgs boson coupling to second generation fermions, and can contribute to the final mass measurement. Several BSM models predict a Higgs boson $H \to \mu^+\mu^-$ decay rate significantly higher than in the SM case [58, 59]. In addition, at hadron colliders, the $H \to \mu^+\mu^-$ channel offers the best experimental mass resolution for fermionic final states, comparable to the one of $H \to \gamma\gamma$ and $H \to \ell^+\ell^-\ell^+\ell^-$. The production of the SM Higgs boson in the decay $H \to \mu^+\mu^-$ at HL-LHC is expected to be measured with an accuracy of about 12% with 3000 fb^{-1}, a factor three better than expected at LHC. Even with 3000 fb^{-1}, the uncertainty on the $H \to \mu^+\mu^-$ branching ratio (and other rare final states) will be limited by statistics, implying that a combination of results from ATLAS and CMS will yield even more precise measurements.

In the Standard Model the $H \to Z\gamma$ decay rate is about two third of the already observed $H \to \gamma\gamma$ process; current measurements from ATLAS and CMS are based on the one photon + two lepton final state, with a cross section limit ten times higher than the SM expectation. This final state can be either enhanced or suppressed in BSM models [60]; a precision on the $H \to Z\gamma$ rate of $20\% - 30\%$ can be obtained with 3000 fb^{-1}at LHC [52,61]. Studies made for ILC predict an accuracy for the $H \to Z\gamma$ rate larger than 30%, even in case of the highest centre-of-mass energy and integrated luminosity considered in the analyses that have been made; at FCC-ee this rate is expected to be measured with an uncertainty of about 12%.

Higgs boson decays, which are forbidden or strongly suppressed in the Standard Model, provides and unambiguous signature of physics beyond the SM. Among the first ones, lepton-flavour-violating decays [62, 63], such as $H \to \tau\mu$ [64] or $H \to \tau e$, play an important role because of the distinct experimental signature and their link to the flavour sector (Section 6.6.7). Exclusive hadronic decays, for example decays to a vector boson and a narrow resonance (e.g. $H \to Z\ J/\Psi$ or $H \to \gamma\Upsilon$) [65] have SM branching ratios in the $10^{-5} - 10^{-6}$ range and give complementary information on the couplings, providing a unique probe of the Higgs-Goldstone-vector coupling [66]. A comprehensive survey of other exotic Higgs boson decays is given in [67].

A further key study, performed by ATLAS and CMS at the HL-LHC, is the search for decays of the Higgs boson to particles that leave the experimental apparatus without being detected, e.g. to dark matter WIMPs. The process considered in the study performed is the associated ZH production, with $Z \to \ell^+\ell^-$ and the Higgs boson decaying invisibly. Limits on the "invisible final state" branching ratio of the Higgs boson at the level of $6-8\%$ can be set at the 95% confidence level; in a more conservative scenario this limit would degrade by about a factor of two. Measurements using the VBF and gluon fusion production modes can further improve the results.

The search for invisible decay modes (and other final states suppressed by Standard Model) at e^+e^- colliders can be covered by the measurement of the total width, compared with the SM prediction, whose uncertainty is predicted to be a few $\%$ (see also Section 4.1.4).

4.1.3 CP mixing studies

Studies on the measurement of properties of the Higgs boson decay vertex $H \to \ell^+\ell^-\ell^+\ell^-$ in 14 TeV proton-proton collisions have been performed [68]. Though this channel has low sensitivity to CP mixed states in the MSSM because the ZZ system has defined positive CP properties, in more general BSM models such constraint vanishes increasing the channel sensitivity. The sensitivities on the HZZ vertex tensor couplings have been determined for an integrated luminosity of 300 fb^{-1}at LHC and 3000 fb^{-1}at HL-LHC. The decay amplitude has been described following ref. [44], where the HZZ scattering amplitude has been parameterized as a function of 4 complex coupling constants: g_1, g_2, g_3 and g_4. The result of the studies are shown in Table 12, where the 95% confidence level intervals on the couplings have been reported. Such results show that a substantial improvement of our knowledge of the tensor structure of the HZZ vertex can be achieved.

Table 12: Expected values excluded at 95% C.L. for the real and imaginary part of g_4/g_1 and g_2/g_1 couplings, assuming the Standard Model. These values are obtained at $\sqrt{s} = 14$ TeV using an integrated dataset of 3000 fb^{-1}at HL-LHC.

$\mathrm{Re}(g_4)/g_1$		$\mathrm{Im}(g_4)/g_1$		$\mathrm{Re}(g_2)/g_1$		$\mathrm{Im}(g_2)/g_1$	
<-0.34	>0.26	<-0.34	>0.48	<-0.30	>0.11	<-0.71	>0.68

4.1.4 New trends in measuring the Higgs boson natural width

The natural width of the 125 GeV Higgs boson is an important physics property that could reveal new physics. In particular, decays of the Higgs boson to dark matter objects, WIMPs and other possible BSM particles would increase the natural width with respect to what predicted by SM, and indicate the production of new physics. A direct measurements of this quantity is possible only at muon colliders via line shape scan in the s-channel (Section 2.5), while at the LHC/HL-LHC and at e$^+$e$^-$ colliders the experimental mass resolution for detected Higgs candidates is significantly larger than the expected

width from Standard Model [1]. As an example, the mass resolution of the $\gamma\gamma$ system at LHC experiments is about 400 time the SM predicted natural width for $m_{\gamma\gamma} \sim 125$ GeV.

Nevertheless, an indirect determination of the Higgs boson width is possible by using the interference of the Higgs boson signal ($H \to \gamma\gamma$ or $H \to ZZ$)) with the same final state ($\gamma\gamma$ or ZZ) in the continuum [69]. In the first case the interference is studied with the on-shell peak, because the interference modifies the $H \to \gamma\gamma$ line shape, in the second case the interference happens on the off-shell side, in particular in the region where the invariant mass of the four leptons is larger than twice the Z mass. Constraints from data have been recently studied by CMS [70] and ATLAS [71] on the total width of the 125 GeV Higgs boson, using its relative on-shell and off-shell production and decay rates to a pair of Z bosons [72] [73], where one Z boson decays to an electron or muon pair, and the other to an electron, muon, or neutrino pair. This leads to an upper limit on the Higgs boson width of about 20 MeV at 95% C.L.. More studies are needed to investigate possible routes to reduce the experimental and theory uncertainties.

4.1.5 HH pair production

After the discovery of a light resonance at 125 GeV, Higgs pair production is drawing a lot of attention in the community. Indeed, among the measurements which need to be performed in future projects, the assessment of the Higgs self-coupling in processes where the Higgs boson is produced in pairs is of paramount importance. In many BSM models, double Higgs boson is significantly different from what predicted in SM. Also, Higgs boson self-coupling is strongly connected with the vacuum stability, and it has therefore important cosmological implications [47]. Early discovery of HH production in RUN-2/HL-LHC would represent another major result, hopefully followed by subsequent Higgs self-coupling measurements. The Higgs self-coupling is accessible thanks to the production diagram involving a triple Higgs vertex.

With a Higgs boson at the mass measured at LHC, examples of the most promising channels are $HH \to \bar{b}b\gamma\gamma$ and $\bar{b}b\tau^+\tau^-$. The challenging $HH \to \bar{b}bW^+W^-$ channel, initially thought to be inaccessible due to the large $\bar{t}t$ background, is now currently also been investigated. The final state with the largest branching fraction, $HH \to bbbb$, could be an interesting channel if boosted topologies (that offer better signal-to-background ratio) are considered. The channel $HH \to \bar{b}bZZ \to \bar{b}b2\ell2\nu$ could be another interesting final state to investigate, if the Z mass constraint proves sufficient to reduce the large background.

At hadron colliders, the dominant production mechanism is gluon-gluon fusion, and at the HL-LHC is estimated to have a cross-section of $34^{+37\%}_{-30\%}$ fb at NLO [74] assuming $m_{\rm H} = 125$ GeV. Due to the destructive interference of the diagrams involving di-Higgs production, this cross-section is modified to be $71(16)$ fb if the self-coupling is assumed to be zero (twice the SM prediction). Recent calculations of next-to-next-to-leading order (NNLO) QCD corrections suggests an increase of the SM cross-section by a factor $\mathcal{O}(20\%)$ [75, 76], thus enhancing its value to about 41 fb.

Preliminary studies on di-Higgs boson production in the $HH \to \bar{b}b\gamma\gamma$ decay have been recently released by ATLAS and CMS [51, 77]. A cut based analysis has been performed using Monte Carlo samples for signal and several background processes that are expected to contribute to the production of this final state. These samples have been processed through a simplified or full detector simulation. Figure 13 shows the distribution of the diphoton invariant mass, $m_{\gamma\gamma}$, after all other selection cuts are applied. A total of 8.4 events are expected with a 3000 fb^{-1} data sample, with a background contamination of 47 events, yielding a significance on HH production of $S/\sqrt{B} \simeq 1.3$. A higher significance is predicted by the analysis performed by CMS, with slightly lower background expected, that would allow a measurement of the HH yield with an accuracy of about 60 %; see Fig. 14. ATLAS and CMS are

[1] At the e^+e^- colliders, an indirect measurement is possible combining the measurements of the Higgs boson production from "Higgsstrahlung" and Vector Boson Fusion processes, as described in Section 4.1.1.

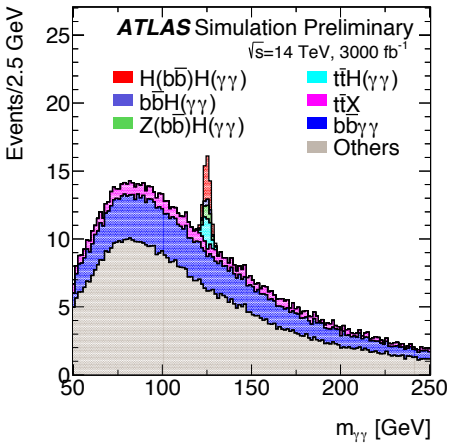

Fig. 13: The distribution of the two-photon invariant mass ($m_{\gamma\gamma}$) from the $\gamma\gamma bb$ channel after applying all selection cuts (except the one on that variable) [78].

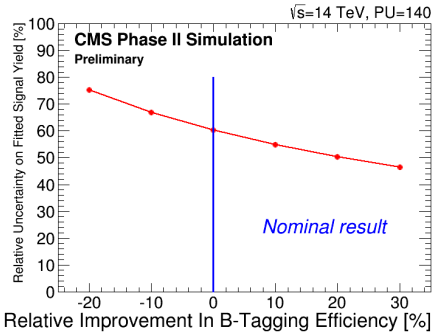

Fig. 14: The average expected relative uncertainty on the di-Higgs cross-section measurement is shown as a function of the b-tagging efficiency [77].

currently working to better understand these residual differences, and to investigate potential avenues for improving the sensitivity. Studies on $HH \to \bar{b}b\tau^+\tau^-$ final states are in progress. More detailed results from ATLAS and CMS on Higgs pair production measurement prospects at HL-LHC will be available a few months after the publication of this document.

Higgs boson pair production at e^+e^- colliders requires a centre-of-mass energy of at least the kinematic limit (~ 340 GeV). Therefore only colliders such as ILC in the version with $\sqrt{s} = 1000$ TeV and 1000 fb^{-1}can expect to measure the triple Higgs coupling with an uncertainty of about 13%.

4.2 Experimental measurements with W and Z bosons and QCD

Precision measurements in the electroweak sector of the Standard Model (SM), studying the properties of W and Z vector bosons, keep their own interest even after the discovery of the SM-like Higgs boson and in view of future experimental programs. These studies are a tool for the indirect discovery of physics beyond SM, through the search for deviations from the properties predicted by the model itself induced by quantum loop corrections. In case new physics is independently discovered, they may help in characterizing it.

There are two main classes of measurements which are interesting for the next future:

- the study of precision observables related to the vector boson properties, that enter directly as input to the electroweak global fits, together with the top quark mass $\mathrm{m_t}$ and the Higgs boson mass $\mathrm{m_H}$. Under the assumption that the new 125 GeV boson discovered at the LHC is the SM Higgs boson, all the parameters are known and this fit can now over-constrain the model for the first time [79];
- the study of the couplings in the gauge boson sector, aiming to search for anomalous contributions to the triple (TGC) and quartic (QGC) gauge boson couplings. This is a sector of measurements tightly related to the understanding of the properties of the Higgs boson, through the detailed study of the vector boson scattering (VBS), whose theoretical explanation is one of the reasons for introducing the Higgs boson itself.

As it will be noticed, besides the direct study of the vector bosons' properties and couplings, a number of additional inputs are required by the global fit. The precise knowledge of the electromagnetic and QCD coupling constants $\alpha_{\mathrm{em}}, \alpha_{\mathrm{S}}$, directly affects the fit predictions. Moreover, since hadronic colliders will keep playing a fundamental role for a while in these measurements, the improved knowledge of the initial state through a precise measurement of the proton parton distribution functions (PDFs, Section 7.3.1) is of the utmost importance.

4.2.1 Precision observables

The SM parameters mostly sensitive to the Higgs boson mass value are the W boson mass m_W, and the couplings of the Z boson described by the Weinberg angle, $\sin^2\theta_{\mathrm{W}}$ [80]. The current experiment uncertainty on $m_W = 80.385 \pm 0.015$ GeV is driven by the measurements performed at the Tevatron [81], while the uncertainty on the Weinberg effective angle is dominated by the measurements performed at LEP1/SLC $\sin^2\theta^{\mathrm{eff}}_{\mathrm{W}} = 0.23113 \pm 0.00016$ [82]. The discrepancies in the latter results obtained at the two $\mathrm{e^+e^-}$ colliders constitutes one of the most intriguing legacies of that experimental program.

The indirect determination of m_W from the global electroweak fit provides at present an uncertainty of 8 MeV [83], already smaller than the experimental precision, and that will be likely further reduced in next future through the progresses in theoretical calculations and other SM parameters knowledge [84]. This motivates the push for a reduction of the experimental uncertainty in this measurement, that can be achieved both at hadronic and leptonic colliders. The expected final precision by the analysis of the full Tevatron data sample could be of about 9 MeV, with the statistical and PDF-induced uncertainties playing a leading role. The use of data control samples to understand the detector behaviour and calibration has proved to be at the Tevatron an essential tool in reducing the other sources of systematic uncertainties, and therefore a similar result can be expected at LHC. The studies in [85] show that the m_W uncertainty coming from PDFs at LHC can be even similar to the one at Tevatron, provided the effects on the cross section normalisation are removed. Therefore an improvement of the results clearly requires a corresponding improved knowledge of the PDFs themselves. The relative importance of various PDFs depends on the observables used for the m_W extraction. Given the relevance of a precise determination of the W mass at LHC, a special section is dedicated to the subject in this report (Section A.1). Its conclusions, based on the current trend in the development of calculations and understanding of the impact of PDFs, suggest that the 10 MeV uncertainty level is reachable, at least for measurements based on the transverse mass. Extrapolations in [84] push the target for an uncertainty at LHC towards 5 MeV in the long term, exploiting for these studies the samples collected up to the HL-LHC data taking.

Better results are expected to come from the precise knowledge of the $e^+e^- \to W^+W^-$ cross section around the production threshold, which is very sensitive to m_W. This would be the main observable to study at future leptonic machines, both linear (ILC) and circular ones (ee-FCC). In both cases the dominant source of uncertainty would be the detailed knowledge of the beam energy (determining the value of $\sqrt{\mathrm{s}}$ at which the cross section is evaluated). Studies for the ILC physics case [84, 86] suggest

that a threshold scan would allow to reach an *in-situ* energy calibration sufficient to achieve a $\simeq 2.5$ MeV total uncertainty on m_W. Crucial ingredients of the measurement would be the beam energy calibration in situ with $Z\gamma$ events and the use of polarised beams to evaluate background from data. Other techniques, like the full event kinematic reconstruction à la LEP2 or the study of the hadronic mass in single W production, can complement this result but they are unlikely to provide a precision better than 3 MeV. The ultimate precision in a leptonic machine could be reached by a WW threshold scan at a circular collider: studies performed for the TLEP physics case [87] claim that the resonant depolarisation method, used at LEP1 for the precise measurement of the beam energy, could be pushed to work up to 80 GeV. This could turn into a corresponding precision on m_W of about 1 MeV.

The current theoretical precision on $\sin^2\theta^{\rm eff}_{\rm W}$ is at the level of $\simeq 7\times10^{-5}$, and it is reasonable to imagine it could be halved in next future mostly through an improved knowledge of the main input parameters. The effort of moving the experimental precision at the 10^{-5} level, and understand the current discrepancy among the values obtained by LEP1 and SLC separately is therefore important. The most precise result at an hadronic collider has been obtained by CDF [88] exploiting innovative procedures to analyze $Z\to\mu\mu$ decays, which have allowed to bring the uncertainty at the 10^{-3} level. The addition of th electron channel and of D0 similar measurement can likely bring the Tevatron combined result at the level of precision of the LEP/SLC one. Recent ATLAS results [89] show that the usage of forward electrons, in the detector acceptance $|\eta|>2.5$, can improve the precision, even with a smaller statistics compared to the central region, thanks to a smaller dilution of the information on the quark direction, confirming the smaller sensitivity to PDFs already noticed in the study [90]. All these facts suggest that LHC could achieve a comparable level of precision as LEP1/SLC as well, within the HL-LHC completion [84]. Alternative methods to explore the $Zb\bar{b}$ vertex, the basis for the LEP1 measurement of the Weinberg angle, have been suggested in [91], studying the associated production of Z and b-quark at LHC.

The ultimate precision reachable on $\sin^2\theta^{\rm eff}_{\rm W}$ is nevertheless achievable at a lepton collider, at present the only environment in which it can be expected to break the 10^{-4} precision barrier. Both for circular and linear machines, the use of longitudinally polarized beams is essential to obtain the best results. Repeating the SLC measurement of the left-right polarisation asymmetry with both beams polarised can provide a jump in precision provided all the possible polarisation combinations are used to compute it in the so called "Blondel scheme" [92]. The precision in the beam energy determination also matters, given the strong $\sqrt{\rm s}$ dependence of the γZ interference term. The projections presented in [84] shown the 10^{-5} uncertainty achievable at ILC, and even better at an ee-FCC.

A lepton collider running at the Z peak can allow to repeat the LEP1 studies of the Z line shape with possibly improved precision. It is worthwhile to notice that the Z mass determination is strongly dependent on the precise knowledge of the beam energy. The use of the resonant depolarisation technique, possible in a circular collider, might push the precision beyond the LEP1 level, as shown in the projections presented in [87].

4.2.2 Boson couplings and vector boson scattering measurements

The study of triple and quartic gauge couplings among bosons, a fundamental prediction of the SM, relies on the study of multi-boson final states at both hadron and lepton colliders. The smallness of the cross section for these processes, compared to the production of single bosons, implies the need for high integrated luminosities in order to reach a sufficient statistical precision to improve the currently available limits on anomalous contributions, that are signatures of physics beyond the SM. Among the mechanisms producing multi-boson final states, VBS plays a special role, as its unitarization is achieved by the introduction of the Higgs mechanism. A deviation from the SM predictions for these processes would be an important evidence for the need of an extension of the minimal SM. The sensitivity to non SM contribution of the observables related to VBS increases with the centre of mass energy, and this explains why hadronic machines are the main environment where this study must be performed.

Concerning charged triple gauge couplings, as shown in [93], LHC is already competitive with earlier LEP2 and Tevatron results on the parameters $\Delta\kappa$ and λ, used to describe anomalous couplings: the former is mostly sensitive to differential distributions, and the cleaner environment provided by lepton colliders can help in the precision of the determination, and ILC at 800 GeV is clearly winning over LHC, even assuming the full HL-LHC foreseen statistics (Fig. 15). On the contrary, the latter can profit from the $\sqrt{\mathrm{s}}$ dependence; furthermore, the sensitivity to it resides mostly in the high $\mathrm{p_T}$ tail of diboson system, and can benefit from large statistics. This explains why HL-LHC is expected to reach performances comparable to ILC at 800 GeV, while a h-FCC hadron collider at high energy could push further this precision.

Quartic gauge boson couplings can be extracted by the study of both di and triboson final states, like WW, WZ, ZZ and $Z\gamma\gamma$ respectively. Vector boson scattering processes contributing to these final states are characterised by emission of very forward jets, large jet-jet invariant mass, and large rapidity gaps (since they produce colourless objects in the central region). With the typical experimental selections used, the cross section for electroweak vector boson pair production is of $\mathcal{O}(10)$ fb. The study of the vector boson pair mass in the VBS processes can probe the need for physics beyond the SM Higgs mechanism at higher scale. In practice there is also the transverse polarization to take into account, and the PDFs suppress the growth, so a precise measurement of the production rate at high mass is needed. These facts combined explain why HL-LHC is needed in order to have a detailed investigation of VBS, studying in details several differential distributions sensitive to non SM contributions.

Both ATLAS [94] and CMS [95] have provided preliminary studies of sensitivity of HL-LHC to QGC, using the effective field theory approach to parameterise the possible anomalous contributions. As summarised in [84], there is a clear gain in sensitivity reach by moving from the integrated luminosity of 300 fb^{-1} expected by the end of LHC to the 3000 fb^{-1} expected at the end of the full HL-LHC program. Limits in the new physics scale are model dependent, but in general they reach or exceed the 2 TeV. In general, lepton colliders are not competitive in this sector, where hadronic machines can give better results by one or two orders of magnitude. It is worthwhile to notice that tribosons are specially sensitive to $\sqrt{\mathrm{s}}$, and could provide even better limits at energies beyond the HL-LHC ones.

In parallel to these studies, another interesting process providing access to anomalous QGC is the $\gamma\gamma \rightarrow WW$ scattering. The very weak limits on new physics established by LEP2 are already improved at LHC, and can be pushed further by order of magnitudes before any lepton collider enters into operation. The experimental technique used to study this very rare process is based on the tagging of very forward protons emerging from the scattering in the so called central exclusive production mechanism, that can be achieved with the proton spectrometers situated at about 200 m from the interaction point that both ATLAS and CMS are building at present. Results are presented in [96], showing a very interesting physics potential.

4.2.3 Parton distribution functions and the strong coupling constant

From the previous discussion it is clear that the precision in the knowledge of the proton PDFs is a limiting factor for the program of precision measurements in the electroweak sector in the next 15/20 years, when it will be dominated by LHC and HL-LHC. In particular the gluon PDF is still poorly constrained by data, while becoming of crucial importance (for instance in the description of the Higgs boson production).

LHC measurements have started to be used to complement those of HERA in constraining the proton PDFs: inclusive jet and dijet production, W charge asymmetry, $W + c$ production. But a quite larger program can be envisaged. The gluon PDF can be constrained by studying many different final states:

- isolated photons, or photon+jets, constraining medium x gluons through QCD Compton scattering;
- vector bosons + jets (high $\mathrm{p_T}$): small to medium x gluons (qg dominating at $\mathrm{p_T} > 100$ GeV);

– low mass Drell-Yan: small x gluons (if resummed calculations available; LHCb might be particularly sensitive in its acceptance);
– $\mathrm{t\bar{t}}$ production (known at NNLO): large x gluons (important for high mass BSM).

Quark PDFs understanding can benefit from measurements of the ratio of W and Z production at high $\mathrm{p_T}$, useful to study the quark-antiquark separation, or of the Drell-Yan process at high mass, sensitive to large x quark PDFs.

It is important to notice that the proposed electron-proton collider option suggested for LHC, the so called LHeC program, could be the ultimate tool to gain the deepest understanding on the PDFs, according to the projections made in the proposal [97].

Together PDFs, the precise knowledge of the strong coupling constant α_S is also essential to the precision physics program, as a basic input in the global electroweak fits. At present lattice calculations are driving the uncertainty on the average. The recent calculation of the $pp \to t\bar{t}$ cross section at NNLO opens a very interesting possibility to get an $\mathcal{O}(1)\%$ measurement at high Q^2. In future perspective, the most promising measurement can be provided by the study of $R_l = \Gamma(Z \to hadrons)/\Gamma(Z \to ll)$ at lepton colliders. ILC or ee-FCC could reach precisions of 0.0004 or 0.0001 respectively, exploiting the current precise knowledge of m_H.

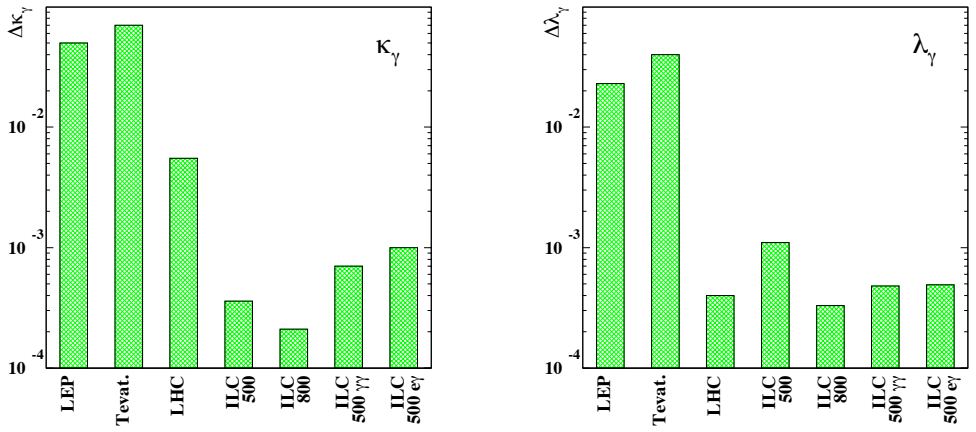

Fig. 15: Prospects for the measurements of the κ_γ and λ_γ TGC couplings at LHC and ILC, from [98].

4.3 Top quark physics

The top quark, discovered in 1995 [99, 100], is nowadays the heaviest elementary particle. It plays a crucial role in the Standard Model phenomenology and the electroweak symmetry breaking because, thanks to its large mass, it exhibits the largest Yukawa coupling with the Higgs boson. The top-quark mass m_t is a fundamental parameter of the Standard Model: even before the Higgs discovery [42, 43], it was used, together with the W mass, to constrain the Higgs mass in the global fits. With the exception of few open problems which will be discussed in the following, all measurements for both $t\bar{t}$ and single-top production are in agreement with the Standard Model expectations. Nevertheless, top quark phenomenology will remain one of the main fields of investigation in both theoretical and experimental particle physics, at any present and future facility, i.e. both lepton and hadron colliders, as well as linear and circular accelerators. Hereafter, we shall discuss the future perspectives regarding the measurement of the top-quark properties, taking particular care about its mass, couplings and final-state kinematic distributions.

4.3.1 Top quark mass

The mass of the heaviest fermion (m_t) is a physical quantity of central importance at the electroweak scale; its current world average is $m_t = 173.34 \pm 0.27$ (stat) $\pm$ 0.71 (syst) GeV [101]. The role of the top mass in precision tests has been already mentioned, besides electroweak fits the value of the top mass is used as a key input in several other important cases. As an example [102], using the current values of the measured Higgs and top masses and assuming that possible new physics interactions at the Planck scale do not affect the stability phase diagram and the electroweak vacuum lifetime, the Standard Model vacuum is found to lie on the border between stability and metastability regions ([103] discusses the robustness of the underlying hypotheses). In addition, the top mass plays a role in inflationary universe theories and in the open issue regarding whether the inflaton can be the Higgs field or not. As discussed, e.g. in [104], in inflationary theories the running of the couplings is important and, once the the Yukawa coupling is determined from the top mass, the spectral index depends on both top and Higgs masses.

A crucial assumption employed in all calculations using the top mass as an input is that the measured mass corresponds to the top-quark pole mass. However, as will be clarified later on, the connection between the top mass measured in current analyses of experimental data and the pole mass is not straightforward and, although the two values should be reasonably close, any effort to clarify the top mass interpretation is important in order to validate or modify the outcome of electroweak fits or other studies [102].

The standard methods to measure the top mass at hadron colliders, where $t\bar{t}$ pairs are produced in $q\bar{q}$ (dominant at the Tevatron) or gg (dominant at the LHC) annihilation, are based on the the investigation of the properties of the final states in top decays ($t \to bW$), which, according to W decays, are classified as double-lepton, leptons+jets or all jets. In all cases, there are two b-tagged jets, whereas the W decay products are reconstructed as isolated leptons (muons or electrons) or as jets (for $W \to q\bar{q}'$ processes). After requiring energy-momentum conservation and constraining the W mass, the final-state invariant-mass distribution exhibits a peak, which is interpreted as the production of a top quark.

The conventional techniques to reconstruct the top mass are likelihood-type such, e.g, the matrix-element and template methods. The matrix-element method compares the measured quantities with predictions obtained by convolving the LO $t\bar{t}$ cross section with the detector response. The template method is based on investigating several distributions of observables depending on m_t, under the assumption that the final state is $WbWb$ and the W mass is known; the data are then confronted with Monte Carlo templates and m_t is the value which minimizes the χ^2. Matrix-element and template methods are those used in the world average determination, based on the updated measurements from D0, CDF, ATLAS and CMS Collaborations. The projections for the LHC run at 14 TeV, i.e. a $t\bar{t}$ cross section of about 951 pb, according to the template/matrix-element methods, foresee, for a luminosity $\mathcal{L} = 100$ fb^{-1}, a systematic uncertainty of 700 MeV and a statistical error of 40 MeV. With $\mathcal{L} = 300$ fb^{-1}, the estimated systematic and statistical errors are 600 and 30 MeV, respectively [105].

Other techniques have been developed, for example the so-called endpoint [106, 107], J/ψ [108, 109] and decay-length [110] methods. These alternative techniques are presently less precise than the conventional methods, however they turn out to be very promising in view of the high statistics to be collected at LHC, because statistical uncertainties, together with several systematic uncertainties reducible with statistics, will decrease, as discussed in [107].

Generally speaking, in most analyses the experimental results are compared with simulations based on Monte Carlo generators (an exception is the endpoint method) and, strictly speaking, the reconstructed top mass cannot be precisely identified with theoretical definitions like, e.g., the pole mass.

In fact, programs like HERWIG or PYTHIA are equivalent to LO QCD calculations, with the resummation of all leading (LL) and some next-to-leading soft/collinear logarithms (NLL) [111]. In order to fix a renormalization scheme and get the pole or $\overline{\rm MS}$ mass, one would need at least a complete NLO computation, while parton showers only contain the soft/collinear part of the NLO corrections.

Furthermore, any observable yielded by such codes depends on parameters which are to be tuned to experimental data, in particular non-perturbative quantities, such as the shower cutoff or the parameters entering in the hadronization models, namely the cluster [112] (HERWIG) or string (PYTHIA) [113] models.

In the non-perturbative phase of the event simulation, the b quark in top decay hadronizes, e.g., in a meson $B^{\pm,0}$, by combining with a light (anti) quark $\bar{q}$, which may come from final- as well as initial-state radiation. Since the b quark likely radiates gluons before hadronizing, the initial colour and part of the four-momentum of the top quark may well be transferred to light-flavoured hadrons, rather than only B-hadrons. As a result, there is no unique way to assign the final-state particles to the initial (anti) top quark and this leads to another contribution to the uncertainty on the top mass, when reconstructed from the invariant mass of the top-decay products. As for colour flow and reconnection, a phenomenon already investigated at e^+e^- colliders in $e^+e^- \to W^+W^- \to 4$ jets processes, this is typically studied by varying the non-perturbative parameters of the Monte Carlo program and it leads to an uncertainty that amounts to about 300 MeV in the current top mass world average. Moreover, parton shower algorithms neglect the top width ($\Gamma_t \simeq (2.0 \pm 0.5)$ GeV [81]) and top-production and decay phases factorize: although $\Gamma_t << m_t$, for a precise mass definition with an uncertainty below 1 GeV, even width effects should be taken into account. Therefore, one often refers to the measured mass as a 'Monte Carlo mass', which must be related to a given theoretical definition. Indeed, definitions like the pole mass work well for leptons, which are colourless particles, whereas, in the case of coloured quarks, it exhibits a non-perturbative uncertainty, proportional to $\Lambda_{\rm QCD}$, due to the infrared renormalons which are contained in the higher-order corrections to the heavy-quark self energy, proportional to $\alpha_S^{n+1} n!$. Nevertheless, up to this intrinsic ambiguity, since the top mass is extracted from final-state top-decay observables, relying on the on-shell kinematics of its decay products (leptons and jets), one should reasonably expect the measured mass to be close to the pole mass. In fact, calculations based on Soft Collinear Effective Theories (SCET) [114] have proved that, assuming that the Monte Carlo mass is the SCET jet mass evaluated at a scale of the order of the shower cutoff, i.e. $Q_0 \sim \mathcal{O}$ (1 GeV), it differs from the pole mass by a small amount $\sim \mathcal{O}(\alpha_S \Gamma)$. A foreseen investigation, which may help to shed light on this issue, is based on the simulation of fictitious top-flavoured hadrons, e.g. $T^{\pm,0}$ mesons [115]. It is well known how to relate the mass of a meson to a quark mass in any renormalization scheme. Therefore, a comparison of final-state quantities with the top quark decaying before or after hadronization, and the subsequent extraction of the top mass from their Mellin moments, can be a useful benchmark to address the nature of the reconstructed m_t and the uncertainty due to non-perturbative effects, such as colour reconnection. In standard top-quark events the top quark gets its colour from an initial-state quark or gluon and, after decaying, gives it to the bottom quark; on the contrary, if it forms t-hadrons, it is forced to create a colour-singlet.

For the reasons explained above, it is of paramount importance to verify the description of key features of the experimental data by the simulation used to derive the top mass. In addition, the uncertainty related to modelling of, e.g. colour reconnection, can potentially be reduced by comparing sensitive observables in data and Monte Carlo simulation. To this end recent studies are described in [116, 117], based on the use of several distributions differential with respect to m_t. The present conclusion is that the predictions of all generators are in agreement with the data and therefore there is no bias due to the choice of the generator used to describe $t\bar{t}$ events. Differential measurements are limited by statistics, therefore these techniques will profit a lot by the foreseen increase of integrated luminosity at LHC.

In order to weaken the dependence on the shower algorithms and non-perturbative corrections, other methods have been proposed to measure the top mass at the LHC. One is based on the measurement of the total $t\bar{t}$ cross section, recently computed in the NNLO+NNLL approximation using the pole mass in [118], and extract the top mass from the comparison [119, 120]. The very fact that the mass determined from the cross section is in agreement with the value yielded by the likelihood-based standard techniques, confirms the hint that the extracted top mass should be close to the the pole mass, used in

the NNLO+NNLL calculation of [118]. Another possible strategy consists of using the $t\bar{t}$ invariant mass in events with a hard jet (j), since it is an observable more sensitive to the top mass than the inclusive cross section [121, 122]. These methods, together with the alternative and differential techniques mentioned above, will be used used to exploit the large statistics to be collected in the future LHC runs, and eventually provide a robust assessment of the uncertainty and possible biases in our determination of m_t.

Future lepton facilities will be an excellent environment to measure the top mass, because of the colourless initial state. As described in Section 2, we have several proposals for lepton colliders, mainly e^+e^- machines: the International Linear Collider (ILC), the Compact Linear Collider (CLIC) as well as circular colliders (FCC-ee, CEPC). The potential for top-quark physics at ILC and CLIC has been studied in depth, with simulations of the luminosity spectra and detector response. The key challenge at CLIC is the pile-up of the background due to $\gamma\gamma$ annihilation into hadrons, while at ILC there is no pile-up but there are more $\gamma\gamma \to \mathrm{hadrons}$ processes per bunch crossing. At a circular collider such as FCC-ee similar and even higher instantaneous luminosities can be obtained with a much lower level of beamstrahlung, a narrow beam energy spectrum having a very low tail and lower $\gamma\gamma$ backgrounds.

At e^+e^- colliders, top-pair production near threshold is an interesting process, where two main contrasting effects play a role: because of the strong interaction, the t and the $\bar{t}$ can form a Coulomb bound state, whereas the electroweak interaction smears the peak of the cross section out. The resonance cross section, computed up to NNLO accuracy [123] by using Non Relativistic QCD, is peaked at $\sqrt{s} \simeq 2m_t$ and behaves like $\sigma_{\mathrm{res}} \sim \alpha_s^3/(m_t\Gamma_t)$; the NNNLO calculation is nowadays among the main challenges in perturbative QCD. The top mass can thus be reconstructed through the so-called threshold scan. Besides pole and $\overline{\mathrm{MS}}$ masses, a particularly suitable mass definition at threshold is the 1S mass [124] m_t^{1S}, a short-distance mass defined as half the mass of a fictitious $^3S_1$ toponium ground state for stable top quarks.

In order to estimate the uncertainty on the measurement of the top mass at a lepton collider, a simulation scanning the range 346 GeV$< m_t <$ 354 GeV in steps of 1 GeV, by using the TOPPIK program [124] and assuming an integrated luminosity $\mathcal{L} = 300$ fb^{-1} was carried out in [125]. The overall uncertainty is gauged to be about 100 MeV, after summing in quadrature the errors due to statistics (30 MeV), luminosity (50 MeV), beam energy (35 MeV) and on the functional form of $f(\sqrt{s_{\mathrm{res}}}, m_t)$ (80 MeV). The luminosity spectrum of the machine affects the (statistical) uncertainty of the measurement: passing from CLIC to ILC the uncertainty on the mass should improve by 10-20%. The theoretical error, due to missing higher orders and uncertainties on the quantities entering in the calculation, such as m_t, Γ_t and α_S, is predicted to be 3% of the full error. Furthermore, a 2D template fit to the cross section can be performed as well, measuring simultaneously m_t. and α_s. Through this method, one can reach an error on the pole m_t of 60 MeV and on the 1S mass of 30 MeV.

At circular colliders such as FCC-ee the cross section just above threshold is essentially independent on the top mass, which is a useful feature for combined fits of the top mass and other parameters (e.g. the top width, α_s or the top-Higgs Yukawa coupling). This expected behaviour has been recently checked with tools developed in the context of ILC studies, where typical FCC-ee beam parameters have been included [126, 127], as shown in Fig. 16.

Above threshold, the top mass can still be determined by using final-state distributions, in the same manner as at hadron colliders: with $\sqrt{s} = 500$ GeV and $\mathcal{L} = 500$ fb^{-1}, current estimates foresee an experimental uncertainty of 100 MeV [127].

4.3.2 Top quark couplings

The determination of the coupling of top quarks to W, Z and Higgs bosons, as well as to photons and gluons, is an important challenge in top-quark phenomenology. These measurements are complementary to the Higgs coupling measurements previously described in this chapter. In particular, possible direct measurements of the Yukawa coupling will be a crucial test of the Standard Model and will help to shed

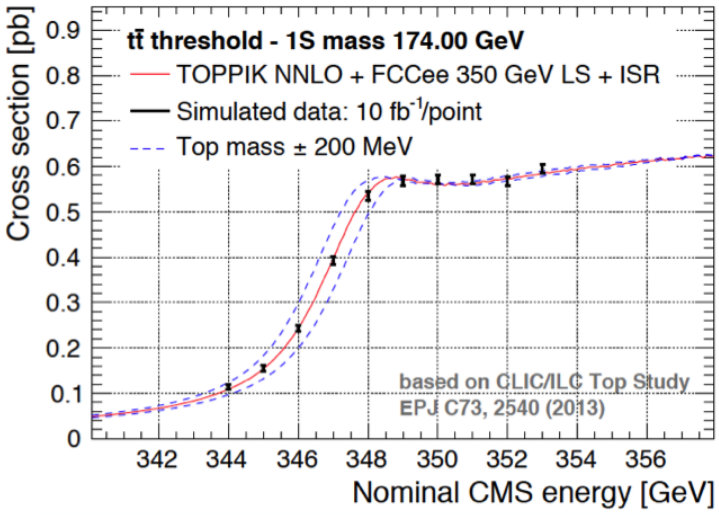

Fig. 16: Simulation of a scan around the $t\bar{t}$ threshold at FCC-ee [126, 127]. Each centre-of-mass energy point corresponds to 10 fb^{-1}, about one week of running at FCC-ee with the expected instantaneous luminosity. The solid curve is taken from a NNLO calculation [124, 128], where QED ISR and FCC-ee beam parameters have been included. It assumes a top mass of 174 GeV in the 1S mass scheme, which is shifted by 200 MeV in opposite directions in the two dashed curves.

light on some new physics models.

The strong coupling constant α_S can be extracted from the measurement of the $t\bar{t}$ and $t\bar{t}j$ cross sections. Ref. [119] compared the NNLO calculation [118] with the measured $t\bar{t}$ cross section in terms of m_t and $\alpha_S(m_Z)$. Once the top pole mass in the computation is fixed to the world average, one can extract the strong coupling constant from the comparison, obtaining the value $\alpha_S(m_Z) = 0.1151^{+0.0033}_{-0.0032}$, which is at present the first α_S determination in top-quark events and within a NNLO analysis. The experimental (about 3.5%) and theory (about 5%) errors are of similar order of magnitude and are not expected to change dramatically in the future LHC operation, namely centre-of-mass energy 13 TeV and luminosity 300 fb^{-1}. At future e^+e^- colliders, through a threshold scan of the total cross section, it will be possible to extract α_S with an uncertainty smaller than 1% and the width Γ_t with an accuracy of a few percent [125].

The coupling of the top quarks to W bosons can be measured through top decays and single-top production. The helicity fractions of W bosons in top decays have been calculated in the NNLO approximation in [129], and therefore the theory uncertainty is by far smaller than the experimental one (see the CMS and ATLAS measurements of the $t\bar{t}W$ cross section in [130, 131]). A higher level of precision of the measurement of such helicities, by exploiting the leptonic angular distributions, is thus mandatory in the next LHC operations, in order to test the Standard Model in the top-decay sector as well. As for single-top production, the LHC cross sections in the s- and t-channel, as well as in the Wt associated-production mode, are in agreement with the Standard Model expectations. In the t-channel case, for example, CMS reports a cross section measurement $\sigma_{t-\mathrm{ch}}(t) = [83.6 \pm 2.3(\mathrm{stat}) \pm 7.4(\mathrm{syst.})]$ pb [132], whereas the ATLAS result is $\sigma_{t-\mathrm{ch}}(t) = [68 \pm 8]$ pb [133]. Increasing the energy and the luminosity of the LHC will not improve too much the accuracy of this measurement, but nevertheless a precision of 5% in the determination of the single-top cross section and of 2.5% in the measurement of the CKM matrix element V_{tb} is foreseen [134].

Future e^+e^- colliders will be able to measure the tWb coupling with an accuracy about 2%, by scanning the centre-of-mass energy between m_t and $2m_t$ [135]. Furthermore, a γe collider is predicted

to have a reach for the tWb coupling between 10^{-1} and 10^{-2} [136], while an ep accelerator using the LHC facility at 1.3 TeV may aim at a sensitivity within 10^{-2} and 10^{-3} [137].

As for the top coupling to photons, although measurements of the top charge [138] and of the inclusive $t\bar{t}\gamma$ cross section [139] are available, with the results being in agreement with the Standard Model predictions, it would be desirable to determine the $t\bar{t}\gamma$ coupling with a much higher level of precision. In fact, this process suffers from large QCD backgrounds, and it is therefore necessary to set strong cuts to suppress them; the NLO calculation for $t\bar{t}\gamma$ production [140] is an important ingredient for an improved measurement at the LHC. At 14 TeV, with a luminosity of 300 fb^{-1}, the coupling to photons will be measured with a precision of 4%, whereas at 3000 fb^{-1} the expected accuracy will be about 1%.

The $t\bar{t}Z$ production cross section, sensitive to the coupling of top quarks with Z bosons, has been measured by CMS ($\sigma_{t\bar{t}Z} = [200^{+80}_{-70}(\mathrm{stat})^{+40}_{-30}(\mathrm{syst})]$ fb [130]) and ATLAS ($\sigma_{t\bar{t}Z} = [150^{+55}_{-50}(\mathrm{stat})] \pm 21(\mathrm{syst})]$ fb [131]). Improving this measurement will be important for the next LHC run; another key measurement will be the detection of single top production in association with a Z. With 300 fb^{-1} at LHC, the $t\bar{t}Z$ axial coupling can be measured with an uncertainty of about 10%, while the vector one only with an accuracy of 50%; increasing the luminosity to 3000 fb^{-1} the achievable limits will improve typically by a factor 2–3 [141].

An e^+e^- collider will be the ideal environment to test the coupling of top quarks with γ and Z bosons. As the $e^+e^- \to t\bar{t}$ process mixes photon and Z exchanges, having polarized beams, or measuring top-quark polarization in the final state, will be important to measure independently such couplings. Ref. [86] described the reach of the linear colliders ILC and CLIC, with polarizations of electrons and positrons equal to 80% and 30%, respectively, and $\sqrt{s} = 500$ GeV, finding that the expected precision is at the level of 0.1%, namely 2×10^{-3} for the coupling to photons and between 3×10^{-3} and 5×10^{-3} for $t\bar{t}Z$. FCC-ee is expected to measure the couplings with an even better sensitivity, thanks to a higher luminosity, by measuring the top polarization in the final state from angular distributions at $\sqrt{s} = 365$ GeV [142].

Top couplings are sensitive to deviations from the SM as expected in various BSM schemes like Randall-Sundrum models, Little Higgs, and composite Higgs scenarios which assume that the top carries a great deal of compositeness. These models either assume mixing between the top quark and new heavy fermions or mixing between the SM gauge bosons with new heavy vector states which couple to the top quark and can induce variations of EW couplings. In [143] a wide spectrum of predictions for deviations of the Ztt couplings in various models is considered. They are expressed as deviations in the Zt_Lt_L and Zt_Rt_R couplings since various models predict different contributions for the two top helicity components (Table 1 of [143], and references therein). These deviations, for a NP scale around 1 TeV, are pictorially drawn in Fig. 17 (left-panel), where the purple points represent different BSM models and the black ones correspond to natural choices for Composite Higgs Model parameters [144]. The possibility to distinguish the left- and right-handed couplings allows to disentangle various models. The region within the dashed red lines represents the sensitivity which can be reached by the LHC (HL-LHC) with 300 fb^{-1} (3000 fb^{-1}) [135, 145] through the Ztt cross-section, while the ILC sensitivity (detailed by dashed dark-blue lines) for $\sqrt{s}$=500 GeV with 500 fb^{-1} and polarized beams goes down to sub-percent level [146]. The sensitivity at FCC-ee for $\sqrt{s}$=365 GeV with 2.4 ab^{-1} is represented by the solid (dashed) green ellipse, obtained with the angular and energy distributions of leptons (b-quarks) in $t\bar{t}$ events [142]. At ILC and FCC-ee all top EW couplings, including Wtb, could be measured allowing full separation between axial and vector couplings, and between the Ztt and γtt couplings. These analyses are described in [142,147]; Fig. 17 (right-panel) recalls these performances in terms of the CP conserving axial and vector form factors of the Xtt vertex. The ILC expected accuracies for the t_L and t_R couplings to the Z are $\Delta(Zt_Lt_L)/Zt_Lt_L(\%) = 0.6$, $\Delta(Zt_Rt_R)/Zt_Rt_R(\%) = 1.4$.

As shown in ref. [148], the total cross-section $\sigma(e^+e^- \to t\bar{t})$, the forward-backward asymmetry A_{FB}, and the spin asymmetry $A_L = \frac{N(-,-)+N(-,+)-N(+,+)-N(+,-)}{N_{tot}}$ are powerful observables to dis-

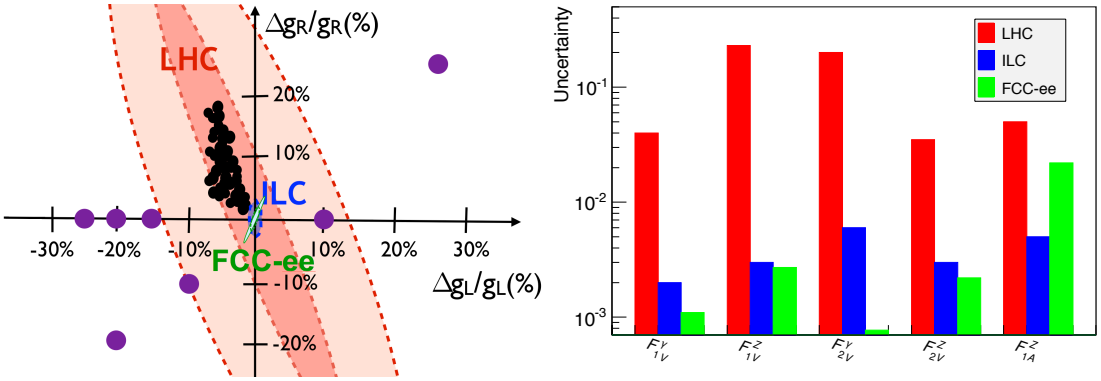

Fig. 17: *Left: Predicted deviations of Z couplings to t_L and t_R in various NP models [143, 148]. Also shown are the expected sensitivities of LHC (300 $fb^{-1}$and 3000 fb^{-1}), ILC and FCC-ee. Right: Comparison of statistical precisions on CP conserving axial and vector form factors expected at LHC with 300 fb^{-1} [145] at ILC500 with 500 fb^{-1} [147] and at FCC-ee with 2.4 ab^{-1} [142]. The FCC-ee (ILC) projections are obtained at $\sqrt{s} = 365$ GeV ($\sqrt{s} = 500$ GeV). In the case of FCC-ee lepton-angular and energy distributions are used, while ILC projections are based on the use of beam polarization.*

criminate among different scenarios. In the definition of the spin asymmetry N denotes the number of observed events and its first (second) argument corresponds to the helicity of the final state top (antitop), whereas N_{tot} is the total number of events. Figure 18 shows the deviation from the Standard Model expectation for these observables in composite Higgs models where the Higgs is a PNGB (pseudo-Nambu Goldstone boson) of $SO(5) \to SO(4)$ breaking.

The determination of the Yukawa coupling of top quarks is clearly a crucial one, since the coupling to the Higgs boson provides the highest corrections to the Higgs mass at one loop, leading to the well known naturalness problem. In order to extract the Yukawa coupling, one would need to measure the cross section of the process $pp \to t\bar{t}H$. Though only upper limits on $pp \to t\bar{t}H$ production have been determined in the first LHC run at 7 and 8 TeV, a measurement of the top-Yukawa coupling is foreseen for the forthcoming run at 13 and 14 TeV, with an expected uncertainty of about 15% at 300 fb^{-1} and then 10% at 3000 fb^{-1} [46]. Even better measurements of the Yukawa coupling are among the goals of lepton colliders: for 1000 fb^{-1} collected at ILC, the foreseen uncertainties are 10% at $\sqrt{s} = 500$ GeV and 4% at 1 TeV, respectively, under the assumption that the polarization rates are 80% for electrons and 30% for positrons. As for CLIC, the note [149] investigates the potential for a direct measurement of the top Yukawa coupling. The relative error scales like $0.53 \times \Delta\sigma/\sigma$, σ being the cross section for $t\bar{t}H$ production, so that, for e^+e^- annihilation at 1.4 TeV, a precision of 4% can be achieved without beam polarization. At FCC-ee centre-of-mass energies no direct $t\bar{t}H$ production is possible, however the Yukawa coupling can be determined by a threshold scan of the $e^+e^- \to t\bar{t}$ cross section, in order to be sensitive to Higgs exchange, besides the Z and photon contributions. The projected sensitivity is about 30%, thus below the expectations of ILC and CLIC [146]. A very precise measurement is expected at FCC-hh, thanks to a $t\bar{t}H$ production cross section 60 times higher than at LHC(14 TeV): a precision of 1% on value of the top-Higgs Yukawa couplings is achievable.

4.3.3 Measurements of other top quark properties

A complete discussion of measurements of top properties at present and future colliders is beyond the scope of this document. Here two additional relevant examples are briefly mentioned: the search for flavour changing neutral current (FCNC) top decays and the measurement of top dipole moments.

The fact that in the standard model top quarks decay essentially 100% to bW makes $t\bar{t}$ pairs an

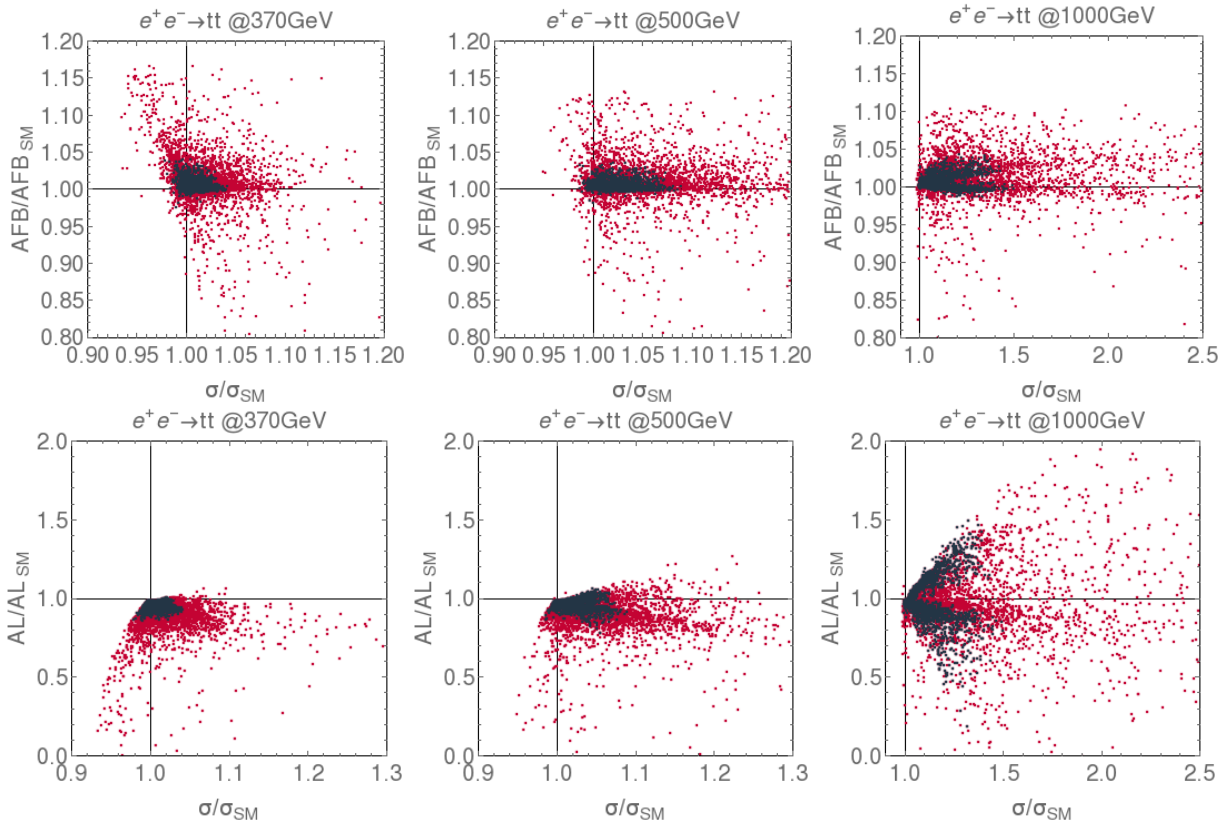

Fig. 18: *Predicted deviations [148] for the total cross-section and A_{FB}, for the process $e^+e^- \to t\bar{t}$ at 370, 500, 1000 GeV in a composite Higgs model (4DCHM) compared with the SM (top panel). In the bottom panel the total cross section is shown together with the spin asymmetry A_L. The red points correspond to a scan with $0.75 < f(\mathrm{TeV}) < 1.5$, $1.5 < g_\rho < 3$ and on the extra-fermion sector parameters as described in [144]. The black points correspond to $M_{Z'} > 2$ TeV and $M_T > 800$ GeV with T the lightest extra-fermion in the spectrum.*

ideal system to detect new physics by selecting a standard top decay and searching for a rare decay mode for the other top in the pair. Similarly, single top production occurs via electroweak interaction only through the tWb vertex, making the search for other production modes an unambiguous signature of physics beyond the standard model. The search for FCNC top interactions exploits both methods (top decay and single top production) and it is particularly relevant as FCNC are heavily suppressed in the standard model because of the unbroken QED and QCD symmetries and the GIM mechanism, while new-physics models often predict their enhancement. Signatures involving a Z boson or a photon are particularly clean and the expected sensitivity essentially scales with statistics. The reach attainable at HL-LHC for FCNC top processes is evaluated in ref. [150] and a study of the potential of FCC-ee is given in ref. [151] and summarised in Fig. 19, left panel, showing that there is considerable potential to cover unexplored territory.

In the standard model chromomagnetic (d_V) and chromoelectric (d_A) dipole moments of the top quark are expected to be small (O(10^{-3}), however their value can significant increase in extensions of the standard model [152]. Anomalous dipole moments modify observables related to $t\bar{t}$ production (e.g. spin correlations [153]) and they can be observed with enhanced sensitivity if high p_T top candidates, in the TeV range, are selected [154]. The large integrated luminosity to be collected at the LHC can be exploited, in this respect, and even higher sensitivity can be obtained at FCC-hh because one trillion $t\bar{t}$ pairs are expected for 10 ab^{-1} at a centre-of-mass energy of 100 TeV, with a large amount of pairs whose invariant mass lies in the multi-TeV range. The current bounds on the d_V and d_A values and the expected

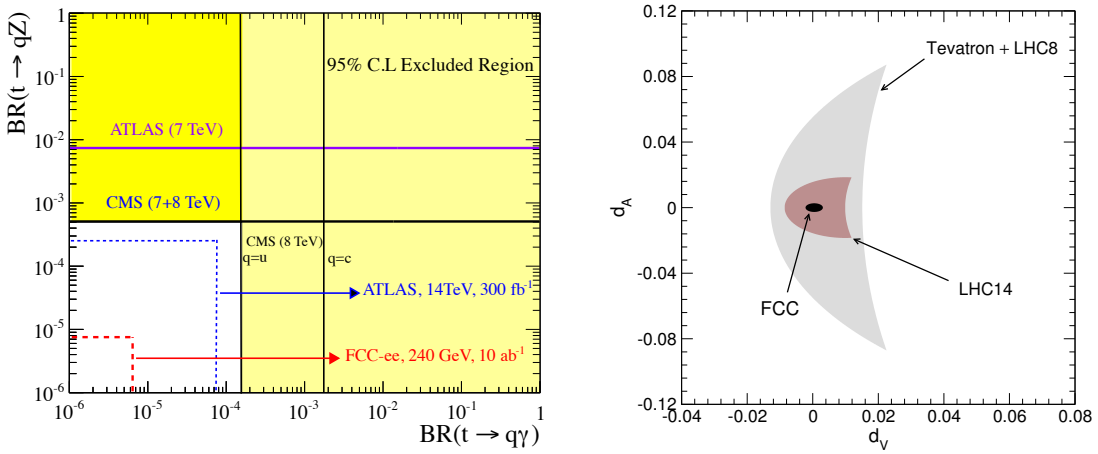

Fig. 19: *Left panel: limits on FCNC top decays into a neutral vector boson and a lighter quark. Current LHC bounds are indicated, together with the FCC-ee expectation for 10 ab^{-1} at a centre-of-mass energy of 240 GeV (from [151]). Right panel: constraints on the top dipole moments derived from measurements at the Tevatron and LHC (gray), from prediction at LHC(14 TeV) (red) and at FCC-hh (black) (from [154]).*

reach at LHC(14 TeV) and FCC-hh are shown in Fig. 19, right panel.

4.3.4 Final-state kinematics

Studying kinematic distributions relying on top production and decay does provide important tests of the Standard Model and allows one to investigate several new physics scenarios. The complete differential process $pp \to t\bar{t} \to W^+bW^-b$ has been computed in the NLO approximation, with [155, 156] and without [157] including top width effects.

Among the observables which have been investigated, the top transverse momentum spectrum has been calculated by means of resummed calculations, carried out using standard techniques [158] and in the framework of SCET [159], wherein even the $t\bar{t}$ invariant mass $m_{t\bar{t}}$ has been computed. Although such computations generally agree with the experimental data, it was found [160], by using the NLO MCFM program [161], that the uncertainty on the p_T spectrum in the boosted regime, i.e. the top decay products clustered into a single jet, is about twice larger than in the unboosted case. Such a result clearly calls for a full NNLO calculation.

An important final-state observable is the forward-backward asymmetry, which has represented for some time an open issue, since it exhibited a two-standard-deviation excess at the Tevatron [162], when compared with NLO QCD predictions. However, the recent calculation [163] of the full NNLO corrections to the asymmetry, which is also the first differential NNLO computation for $2 \to 2$ QCD processes, has shown agreement with the D0 data [164], whereas the disagreement with CDF [162] is reduced to 1.5 standard deviations.

At the LHC, such a measurement, which needs a $q\bar{q}$ initial state, is more difficult, since it is a pp collider and $t\bar{t}$ production is mostly driven by gg annihilation. In fact, ATLAS and CMS performed measurements of the asymmetry, in agreement with the Standard Model, but affected by large errors [164, 165]. Enhancing the energy to 14 TeV will increase the production of $t\bar{t}$ pairs through gg annihilation, which does not produce any forward-backward asymmetry. However, as discussed in [160], the uncertainties due to background modelling and lepton identification scale with the luminosity as $1/\sqrt{\mathcal{L}}$ and therefore, after setting appropriate cuts on the $t\bar{t}$ invariant mass and centre-of-mass rapidity, the fraction of $q\bar{q}$ annihilation will increase, thus allowing an improved measurement of the asymmetry.

Two alternatives to the standard forward-backward asymmetry have been proposed in [166] in events $t\bar{t}$+jet: they are the energy and incline asymmetries, expressed in terms of the energy difference of t and $\bar{t}$ and of the rapidity of the $t\bar{t}j$ system. After setting suitable cuts, such asymmetries should be about -12% and -4%, respectively, at the 14 TeV LHC.

At a linear collider, the main kinematic properties which are foreseen to be measured are the top production angle θ_t and the helicity angle θ_h. In this way, one will be able to determine the forward-backward asymmetry and the slope of the helicity angle λ_t with an accuracy of 2% in semileptonic events, as obtained in the simulations at $\sqrt{s} = 500$ GeV carried out in [147]. In the $t\bar{t}$ threshold regime, where a number of measurements at the linear collider are planned, at present only the total cross section has been computed at NNLO, whereas the calculation of NNLO differential distributions is highly desirable, in order to take full advantage of such a machine.

4.4 Status of Monte Carlo generators for high energy colliders

The development of high energy physics experiments carried out at colliders with increasing centre-of-mass energy, has seen a parallel development in the tools for the calculation and simulation of hard processes. In the 1980's, calculation of collider processes were typically performed at tree level, and full simulation of the events relied upon the Leading-Log (LL) shower approximation. Next-to-leading order calculations were only available for a handful of processes.

In the last few years, prompted by the perspective of the LHC runs, a remarkable progress has taken place in several areas. Fully automated techniques have been developed for the calculation of Next-to-Leading Order (NLO) cross sections, by several collaborating and competing groups. Techniques for combining fixed order calculations with parton shower generators have appeared, and have been widely applied to collider processes. Intensive work on Next-to-Next-to-Leading Order (NNLO) calculations has been carried out by several groups, with several new NNLO results having appeared since a little more than a year. Methods for interfacing NNLO calculations to shower Monte Carlo generators have also appeared for relatively simple processes.

This section summarizes what is available at present, and illustrates what can be considered to be frontier research in this field. Although it is impossible to predict what will be available ten years from now, we believe that it may be safely assumed that current frontier research will have turned into commonly used tools by that time. Additional information on perspectives for advanced QCD calculations for future colliders can be found in [47], while a thorough discussion of Monte Carlo tools for electroweak measurements is given in section A.2.

4.4.1 Presently available results

Parton Shower Monte Carlo generators (PS) fully simulate hadronic production processes by merging together a QCD component (the Shower itself) and a model for hadron formation. The QCD component is typically given in the collinear approximation. When applied to infrared finite observables, PS generators are accurate only in the collinear and soft regions, failing to predict hard, large angle emissions even at leading order. In ref. [167] a procedure was developed for matching matrix element calculations with PS generators (ME+PS), such that the production of hard, widely separated jets could be improved to LO accuracy. This prompted the application of ME+PS techniques to various ME generation tools, like, for example in `ALPGEN` with the MLM matching procedure (for a list of available ME+PS generators see [168]).

In the past 10 years, considerable effort has gone in building NLO-improved PS generators (NLO+PS). Methods like MC@NLO [169] and `POWHEG` [170, 171] allow to interface fixed order NLO calculations to parton shower generators like `PYTHIA` [172, 173] and `HERWIG` [174, 175]. In essence, for a given process, these techniques extend the precision of the generator to NLO level for inclusive processes, and to tree level for the given process in association with one jet. For example, an NLO+PS generator for Higgs

production (a process of order α_s^3 at the Born level) will yield distributions accurate up to order α_s^4. That amounts to NLO accuracy for inclusive quantities (i.e. quantities that do not depend upon the emission of associated jets, like the rapidity distribution of the Higgs, and already receive contributions at order α_S^2), and to LO accuracy for processes involving the emission of an associated jet that start at order α_S^3. These techniques have seen recently considerable progress, due to the appearance of computer frameworks that automatize some or all aspects of the calculation: the virtual contributions, the implementation of a subtraction framework for the real corrections, and the interface to a PS. In the `MadGraph5_aMC@NLO` framework [176], all aspects of an NLO calculation are automatized, starting from the generation of the LO and NLO matrix element, down to the event generation interfaced to a PS program. The `GoSam` [177], Recola [178] and Open Loops [179] frameworks deal with the automatic generation of general purpose virtual amplitudes. The Black Hat [180] generator provides virtual corrections for selected processes (vector Boson in association with jets) and is capable to deal with fairly high jet multiplicities. In fact it was recently used to compute W production with five associated jets at NLO [181]. The `Sherpa` generator [182] implements a framework for NLO calculations and for NLO+PS generation based upon a variant of the MC@NLO method. The so-called MatchBox framework [183] implements NLO+PS generators within the `Herwig++` [175] PS generator. The `POWHEG BOX` framework automatizes all aspects of the NLO calculation interfaced to a PS generator, except for the computation of the matrix elements. For these it relies upon other programs, like `MadGraph` and GOSAM.

Electroweak corrections are not presently included in publicly available automatic NLO calculators. It is however clear that the same techniques that have been applied for automated NLO QCD can be extended to the full Standard Model, as well as to any renormalizable model. Interfacing calculations including Electro-Weak corrections to Shower Monte Carlo requires the ability to handle together QED and QCD collinear showers, but it does not present new conceptual problems with respect to QCD corrections alone. In fact, in few simple cases NLO calculation matched with Shower generators have appeared in the literature [184, 185].

4.4.2 NNLO calculations

Next-to-next-to-Leading Order calculations (NNLO) for collider processes have first appeared in 1990 for the Drell-Yan process [186], followed more than ten years later by the NNLO computation of the total Higgs cross section in gluon fusion [187–189], and of the Higgs differential distributions in [190, 191]. We have witnessed since then a steady increase in the complexity of the processes for which NNLO calculations have become available: 3 jet cross sections in e^+e^- annihilation [192], WH and ZH production [193, 194], $\gamma\gamma$ production [195]. In a little more than a year from now, several new results for complex $2 \to 2$ processes have become available: Higgs production in association with a jet [196], $t\bar{t}$ production [118], a partial result on inclusive jets production [197], $Z/W + \gamma$ production [198], ZZ production [199], W^+W^- production [200] and t-channel single top production [201]. Important results have also been obtained for decay processes [202].

There are several components that make up a NNLO calculation, besides the two loop corrections. One must also supply the square of 1-loop contribution (double virtual), the virtual correction to one real emission (real-virtual) and the two-real-emission contributions. Each contribution contains soft and collinear divergences, that must cancel in the sum. This also constitutes a challenging aspect of NNLO calculations. There are several techniques currently developed for implementing these cancellations. The q_T subtraction method [191] has been used for Higgs production, Drell-Yan, $\gamma\gamma$, WH, ZH and ZZ processes. It is particularly useful for processes where the final state is a colour neutral system. The Antenna subtraction method [203] has been used for the computation of $e^+e^- \to 3\,\text{jets}$ and for dijets, and is presently also used in an effort to compute fully differential $t\bar{t}$ production at NNLO [204]. The so-called STRIPPER method (Sector Improved Phase sPaCe for real Radiation) [205, 206] has been used for $t\bar{t}$, $H + j$ and t-channel single top production. Another method being developed is described in a sequel of publications (see [207] and references therein).

The computation of the double virtual contribution is very demanding. Recent progress with integrals including massive particles [208–210] have opened the possibility of computing NNLO corrections to pairs of massive vector bosons. In general, it seems that today two loop virtual corrections to generic $2 \to 2$ processes are feasible. A recent groundbreaking technique introduced by Henn [211] is among the developments that have made this possible.

4.4.3 Current developments: NLO+PS merging and NNLO+PS generators

NLO+PS merging deals with the merging of NLO+PS generators of different associated jet multiplicity. Consider for example Higgs production in gluon fusion, a process of order α_S^2 at the Born level. Let us call `H`, `HJ` and `HJJ` the NLO+PS generators for the production of a Higgs, of the Higgs in association with a jet, and of the Higgs in association with two jets respectively. The `H` generator will yield α_S^3 accuracy; that is to say NLO accuracy for inclusive observable, like the Higgs rapidity distribution, that include terms of order α_S^2 (LO terms) plus terms of order α_S^3 (NLO terms), and LO accuracy for observables requiring an associated jet, that are given at the lowest order by terms of order α_S^3. Observable requiring more than two associated jets will be generated by the Shower Monte Carlo in the collinear approximation. The `HJ` generator is capable of yielding NLO accuracy (i.e., α_S^4 accuracy) for observables involving the Higgs plus one jet, and LO accuracy for those requiring two jets. It would be however unpredictive for fully inclusive observables. A merged `H-HJ` generator would have in addition NLO (i.e. α_S^3) accuracy for fully inclusive observables. In general one may ask to merge even more NLO+PS generators, for example `H+HJ+HJJ`, in order to have NLO accuracy (i.e. α_S^5) accuracy also for observables involving two associated jets, and thus LO accuracy for those involving three associated jets.

Notice that NLO+PS merging can be seen as an intermediate step in the construction of an NNLO+PS generators. Thus, for example, if we have an `H+HJ` merged generator, we know that it is already accurate at the α_S^4 level for all observable, except those that are totally inclusive in the emission of associated partons, where the accuracy is instead α_S^3. If we could reach α_S^4 accuracy for inclusive observables, we would have full NNLO accuracy.

Several methods have been proposed for NLO+PS merging, although the accuracy that they really meet is still a debated matter [212–217]. In particular, in refs. [212,213], carried out in the frameworks of the SHERPA and MC@NLO collaborations respectively, merging is performed using a merging scale. One clusters the event using some jet clustering procedure, characterized by a merging scale Q_0, and uses the generator with the appropriate number of jets. In [213], stability under variations of the merging scale is interpreted as an indication of accuracy. In ref. [215], NLO accuracy is adjusted by forcing the inclusive distribution to agree with the NLO one, by subtracting appropriate terms, with a procedure dubbed UNLOPS (standing for "Unitary" NLOPS). In ref. [216] (within the so-called GENEVA collaboration) the merging scale is defined in such a way that resummation can be carried out up to the NNLL level. In refs. [218] (the MiNLO method) a method was proposed to improve the accuracy of a generator in such a way that it becomes reliable also after integrating out a radiated parton. In ref. [219] it was also shown that in certain simple cases the MiNLO method applied to generators for a Boson (Higgs, Z or W) plus one jet, can be refined in such a way that it becomes NLO accurate also for inclusive quantities.

In ref. [220] a fist NNLOPS accurate generator for Higgs production in gluon fusion was presented, based upon the MiNLO procedure of ref. [219]. The same method discussed above was also applied recently to the Drell-Yan process [221]. In refs. [222, 223] NNLOPS generators were built for the Drell Yan process and for Higgs production respectively.

In ref. [224], a general strategy for NNLOPS generators based upon the GENEVA framework was outlined. No complete application of this method to physical processes has been published, although preliminary results on the Drell-Yan process have been shown to conferences [225].

4.4.4 Conclusions

In conclusion, at present generators for NLO calculations matched to shower are obtainable with a certain ease for processes with up to four particles in the final state. It is conceivable to imagine that automated generators for electroweak corrections for generic processes may become available soon. While generators for merged mutlijet samples (i.e. for processes with an arbitrary number of associated jets), with LO accuracy, have been available for quite some time, NLO accurate merged generators are now beginning to appear, and are still subject of debate. NNLO calculation for processes with up to two particles in the final state have recently appeared for a considerable number of processes, and NNLO calculation matched to shower generators have appeared only for Higgs production in gluon fusion and Drell-Yan processes. It is conceivable that within the next decade NNLO calculations matched with shower will become generally available, and that the problem of merging for NLO generators will be solved.

4.5 Standard Model Physics: Summary and Outlook

With the discovery of a scalar boson, candidates for all constituents of the Standard Model have been experimentally detected. The predictive power of the model looks impressive: no significant deviation from the model expectations has been found by experiments over the past 30 years. Nevertheless, as mentioned in the introduction of this report, there are several unexplained effects at the sub-nuclear and astrophysical level, which indicate existence of physics beyond the Standard Model. Precise measurements of standard processes have historically opened the road to the detection of new phenomena and new physical states: the guiding principle of Standard Model measurements should be their potential to add building blocks to our understanding of physics.

The Standard Model Working Group of What Next has reviewed the prospects for new measurements at existing and future colliders, with particular attention to the sensitivity for indirect detection of new physics and the potential to add important pieces to our global understanding of particle physics. The main measurements in key sectors are summarised below, keeping in mind that the working group considered both a 10-year timescale, roughly corresponding to the 300 fb^{-1} LHC phase, and a 20-year and even farther horizon, corresponding to the HL-LHC phase followed by new particle colliders.

- **Higgs boson couplings, total width.** The measurement of properties of the newly discovered scalar boson is a major subject for the next decades. A detailed investigation of the Higgs boson couplings to bosons and fermions is particularly relevant because of their sensitivity to new degrees of freedom and to non-standard mechanisms for the generation of quark and lepton masses. Precisions of the order of 10% , depending on the coupling, can be attained with the first 300 fb^{-1} at LHC; these uncertainties can be reduced to 2%–5% in the High Luminosity phase. At lepton colliders absolute measurements of the couplings are possible because the Z recoil-mass distribution in the Higgstrahlung process provides the normalization (only relative couplings are model-independent at LHC). Uncertainties at the 1% level are expected at ILC and well below 1% at FCC-ee. The natural width of the Higgs boson resonance ($\sim$ 4 MeV) is too narrow to be directly measured at LHC, however it can be inferred from the interference of a specific decay mode, e.g. ZZ, with the continuum. Prospects for interference measurements at HL-LHC look very promising in view of the current upper limit (22 MeV). At ILC/FCC-ee the Higgs width can be determined by the total HZ cross section and $\sigma \times \mathrm{BR}$ of a specific final state.
- **Higgs boson spin-parity, CP violation.** Measurements of H spin-parity and tensor structure are based on the angular analysis of decays to vector boson pairs. The presence of anomalous non-scalar components would indicate a mixed state and new physics. Very relevant measurements can be made with high statistics, as an example at HL-LHC the sensitivity for a CP-odd component in Higgs decays can be pushed below 10%.
- **Higgs boson rare production and rare decay modes.** Higgs pair production deserves special attention because of its connection with Higgs self-couplings. The search for anomalous HH production has already started, but to reach a sensitivity corresponding to the Standard Model production an integrated luminosity corresponding to the full HL-LHC phase, with the combination of several channels, is required. Several rare Higgs decay modes, such as $H \to \mu^+\mu^-$ or $H \to Z\gamma$, are sensitive to new physics. Decay modes forbidden in the Standard Model, such as $H \to \tau\mu$, can provide a clean signature of new phenomena. Again, to reach sensitivities for SM-like rates, or to probe extensively new physics models, high luminosity is required.
- **W (and Z) boson mass, electroweak couplings.** The W mass is a crucial electroweak parameter still loosely constrained by direct measurements, its uncertainty should be reduced to take full advantage of the predictive power of electroweak fits. On a 10-year time scale W mass measurements at LHC could reach an uncertainty of $\sim$ 5 MeV if a broad program of LHC measurements of observables sensitive to PDF is put in place. A further reduction of the uncertainty on the W mass can be reached at ILC and FCC-ee, with the potential to cross the 1 MeV barrier. With such

a precision improvement of the Z mass determination from a high statistics scan at the Z pole is required. A precise measurement of another crucial parameter, $\sin^2\theta_{\mathrm{W}}$, can be performed at LHC if our uncertainties on the PDF are significantly improved by means of dedicated measurements. Also in this case lepton colliders can provide a jump in precision, for both lepton and quark electroweak couplings, shedding light on the apparent discrepancy of $\mathrm{A_{LR}}$ / $\mathrm{A_{b\bar{b}}}$.

– **Triple and quartic gauge couplings, vector boson scattering.** Precision measurements of triple and quartic gauge couplings are sensitive to physics beyond the Standard Model. LHC results have already reached or surpassed the sensitivity obtained at LEP, and future data can considerably improve the present sensitivity. Possible anomalies detected with the first 300 fb^{-1} at LHC can be studied with a precision of a few percent during the High Luminosity LHC phase. Another order of magnitude in sensitivity can be gained at ILC and FCC-ee. In the QGC sector vector boson scattering is particularly relevant, because of its sensitivity to the mechanism of electroweak symmetry breaking. A precise measurement of VBS requires the integrated luminosity expected for the HL-LHC phase.

– **Top quark mass.** The top quark mass is experimentally measured at hadron colliders with a precision of $\sim 0.5\%$, however the interpretation of the measurements in terms of pole mass is subject to many discussions. Given the importance of this parameter in electroweak fits and given its connection to the stability of the electroweak vacuum, any effort to shed light on measurement interpretations and to assess in a robust way systematic uncertainties at hadron colliders is worthwhile. Efforts in this direction have already started, with new analysis techniques, which will exploit the large top quark statistics to be collected in the next years at LHC. Nevertheless it looks very difficult to cross the ~ 0.5 GeV uncertainty barrier at hadron colliders, because the coloured nature of the top quark affects any measurement aimed at reconstructing the final state. The problem can be overcome at lepton colliders, such as ILC or FCC-ee, because the top mass can be measured in a cross section scan at the $t\bar{t}$ threshold.

– **Top quark properties.** As the top quark plays a special role in the Standard Model and in many models of new physics, the potential of LHC as a top factory must be fully exploited. Differential $t\bar{t}$ and single top production cross sections should be measured with high precision in the 300 fb^{-1} phase; the study of top production should include precise measurements of polarisation, spin correlations and charge asymmetries, because of their sensitivity to new physics. The large samples of top quarks should also be used to make precise measurements of top decays, and in particular to perform precision studies of the tWb vertex. Associate production of top with other objects, such as Z or H is particularly interesting for both the single top and $t\bar{t}$ cases. Precision measurements in this sector require high integrated luminosity, as an example 3 ab^{-1} at HL-LHC are required to collect enough ttH statistics for a 10% measurement of the top-Higgs Yukawa coupling, while 1 ab^{-1} is required for a 4% measurement at a lepton collider running at a c.m. energy of 1 TeV.

5 Physics Beyond Standard Model

5.1 Introduction

The discovery of the Higgs particle and the first measurements of its properties strongly support the validity of the SM as a phenomenological description of all aspects of EW and Strong interactions including, and this is the novelty, the Higgs sector responsible for EWSB.

In spite of its phenomenological success, we do have compelling theoretical and experimental reasons to extend the SM. The SM does not account for gravity within a coherent quantum theory, it does not account for the observed amount of dark matter (DM), it does not account for the baryon asymmetry in the universe, it does not account for the homogeneity of the universe. Neutrino masses hint at the existence of new degrees of freedom, possibly related with lepton number violation, and the structure of the SM gauge quantum numbers hints at the possibility of the unification of strong and electroweak forces explaining their pattern. The SM does not provide an understanding of the distance between the Planck and electroweak scale, of the replication of families, of the peculiar pattern of masses and mixings (quarks and leptons). The presence of Landau poles represents a theoretical problem, and the dynamics of strong CP violation, of the Higgs mass, and of the cosmological constant lead to naturalness problems.

While some of the above are incontrovertible experimental facts, none of them sharply points to a specific SM extension within the reach of accelerators, nor tells us by which kind of experiments new physics will be discovered. Therefore, the current situation is rather different from that in the past decades, where a detailed path of "guided" discoveries could be identified in the exploration of particle physics at the energy frontier. Relevant examples of guided discoveries are those of the W and Z bosons, of the top quark and recently of the Higgs particle. This condition was not only fortunate, but also unusual in the long history of Fundamental Physics and science, where progress has often been unexpectedly made thanks to the mere exploitation of the capability of exploring new experimental territories. Ambitious experimental programs are more than ever essential to make progress in our understanding of Fundamental interactions.

The situation might radically change with the next LHC run, which will double the reach in energy ever achieved in accelerator experiments, thus entering previously unexplored regions of the energy frontier. This represents a tremendous opportunity for new discoveries at the forefront of particle physics. The discovery of one or more new particles would play the leading role in defining the next steps of an extensive research program at the energy frontier, to be carried out in the medium and long term by existing or new complementary experiments. In the event of no discovery we will still learn important lessons on the naturalness principle, which is and remains the key issue as extensively discussed in what follows. While hard to be ruled, its failure would question basic principles underlying our understanding of hierarchies of scales in quantum field theory, and lead us towards new paradigms, with possible far reaching consequences.

In this document, we will provide a critical assessment of the current status of selected well–motivated hypothetical extensions of the SM and of the future perspectives for their experimental study. Motivated by naturalness we will discuss Composite Higgs and Supersymmetric models. Ignoring naturalness we will consider Minimal models and Dark Sector scenarios. We will also give a brief assessment of DM searches at colliders, focusing on the complementarity with direct and indirect detection experiments. The general picture that underlies our work is described below.

5.1.1 The case for TeV scale new physics after Run 1 at LHC

The topic in BSM physics that is most directly relevant to this WG is understanding why the Higgs field condenses, why it acquires a non-vanishing value in the ground state that breaks the electroweak symmetry. This is a necessary milestone in the path towards the understanding of the constituents of matter and their laws, a key to further progress in other directions, and arguably one of the central issues in particle physics.

The SM accounts of course for such a phenomenon through the negative value of one of its parameters, the Higgs mass parameter. On the other hand, the SM does not provide an explanation for the value and the sign of that parameter. On the contrary, it prevents computing it because of the long-standing problem associated to the quadratic corrections. Any attempt at a complete understanding of EWSB in the sense above must address the latter problem.

The expectation of TeV-scale BSM Physics is mainly associated to the desire to make the electroweak scale calculable in terms of the parameters of more fundamental physics at much shorter distances. The scale at which such new physics is expected to appear is determined by the naturalness argument. In all complete UV theories where the Higgs mass is predicted and originates from new Physics at a scale $m_{\rm NP}$, in order to obtain the observed mass of $m_H = 126\,\text{GeV}$, a cancellation of order

$$\Delta \gtrsim \left(\frac{m_{\rm NP}}{450\,\text{GeV}}\right)^2 , \tag{2}$$

is required among terms which are larger than m_H^2 by a factor Δ, which is a measure of the fine-tuned cancellation required to reproduce the measured value of the Higgs mass. Since a large, and accidental, cancellation is unlikely, New Physics is expected to be present at a scale $m_{\rm NP}$ not too far from half a TeV. For example, in order to avoid a cancellation of ~ 10, $m_{\rm NP}$ should not be larger than about $1.5\,\text{TeV}$[2].

It is worth noting that:

- The above argument does not set a precise bound on $m_{\rm NP}$: while, on one hand, a smaller $m_{\rm NP}$ is better, on the other hand the largest value of $m_{\rm NP}$ that one is willing to tolerate is subjective. Even if the value of $m_{\rm NP}$ cannot be precisely predicted, the relevance of the TeV scale is clear.
- For a given amount of "acceptable" cancellation, the bound on $m_{\rm NP}$ can be stronger or weaker in specific models. For example supersymmetric models with heavy messengers lead to stronger bounds while focus point-like scenarios may lead to weaker bounds.
- The above argument rests on a number of assumptions: 1) the cancellation is accidental and not due to unknown mechanisms or environmental selection; 2) the existence of superheavy physics gives a physical meaning to the quadratic divergence of the Higgs mass.

While the lack of new physics signal so far at the LHC is disappointing, should there be no evidence of new physics at run 2 of the LHC, one could conclude that:

- Vanilla benchmark models, such as minimal supergravity, which have so far been extensively searched for in the data, are either not viable or have suffered from a significant amount of bad luck. This would reduce the interest on such models for our purposes.
- Naive expectations did not take into account several caveats to the assumptions of vanilla benchmark models. This may point to new avenues for the remainder of the LHC run at high luminosity.
- Some of the assumptions underlying the naturalness argument may be violated, and alternative motivations for new physics within the reach of the foreseeable experiments should be considered.

The above discussion can be summarized as follows:

- First, searching for "natural" new physics is and remains a priority. Even a negative result, establishing that the Higgs mass, and hence the EWSB scale, is indeed finely tuned, will have a deep impact on our understanding of Fundamental Physics.
- Second, also implicit in the first point, the naturalness argument does not provide an absolute guarantee of new physics discovery, nor provides an incontrovertible indication of the energy and the nature of the new phenomena.

[2]Note that $m_{\rm NP}$ represents the scale of the degrees of freedom making the Higgs mass "calculable", e.g. the stops in supersymmetry or the fermionic top partners in composite Higgs models. Other new physics degrees of freedom are not necessarily bound to be that light.

In conclusion, the discovery of the Higgs boson not only completed the incredibly successful story of the SM; by sanctioning the well known conceptual challenges that the SM Higgs sector brings along, it also set the foundations of the new quests to pursue. One of the purposes of the current document is to assess how and to what extent the foreseeable post-LHC experimental program can address such a challenge.

5.1.2 Physics at superheavy scales?

The lack of indirect evidence for new physics discussed above refers to new physics within the reach of realistic accelerator experiments. There actually exist two solid and precise indirect experimental hints for new physics beyond the EW scale, the unification of the SM gauge quantum numbers and neutrino masses, but they are likely to point to much higher scales. Still, the latter are relevant to our purposes because they play an indirect role in the naturalness argument (see Section 5.1.3.1) and in the theoretical investigation of the TeV scale. Let us then shortly review them.

The gauge interactions of the SM fermions are fully described by a table of 15 quantum numbers, specifying the representation of the 5 SM gauge multiplets (Q, L, u_R, d_R, e_R) under the three factors of the SM gauge group. The fact that those 15 quantum numbers, and therefore all SM fermion gauge interactions, can be exactly predicted within a Grand Unified Theory (GUT) such as SO(10) is a truly impressive success, representing one of the most compelling quantitative hints for physics beyond the EW scale.[3] Note that this powerful hint is more model-independent than the one following from the unification of the values of the three SM gauge couplings. The latter depends in fact on the unknown degrees of freedom present between the EW and the unification scale, while the former essentially only follows from group theory. Of course the successful gauge coupling unification within a specific model then adds to the evidence for GUTs (and for the specific model). If the above hints for a theory unifying the three SM interactions are correct, they imply the existence of new degrees of freedom well above the EW scale. The lower bound on the mass M_V of the new gauge bosons from the limits on proton decay is in fact $M_V \gtrsim 10^{15}\,\mathrm{GeV}$, compatible with the scale at which the gauge couplings unify in realistic models.

Another appealing indirect hint for the existence of new degrees of freedom at superheavy scales is the smallness of neutrino masses. The latter hints at new, lepton number violating degrees of freedom well above the EW scale. This is best seen within effective QFT. Under the sole hypothesis that the new degrees of freedom necessary to account for neutrino masses live at a scale Λ much larger than the EW scale, it is possible to describe their low energy effect (including neutrino masses), in terms of SM degrees of freedom and symmetries only, by adding higher dimensional operators suppressed by Λ to the SM lagrangian. It turns out that the most relevant (lowest dimensional) operator one can write does precisely that, it gives masses to the SM neutrinos and it accounts for their smallness (compared to the other SM fermion masses) in terms of the smallness of the EW scale compared to Λ. From this point of view, the see-saw mechanism is just a specific example of high scale dynamics generating that operator.[4]

The connection between the smallness of neutrino masses and their high scale origin is so simple and general that it might be considered as a hint of the existence of new degrees of freedom well above the EW scale. The exact position of that scale depends however on their couplings. If they are of the order of the SM couplings, the scale lies well above the EW scale ($\Lambda \sim 0.5 \cdot 10^{15}\,\mathrm{GeV}$ for a coupling of the size of the top Yukawa coupling). On the other hand, it is also possible that the couplings are small

[3] Note that the number of degrees of freedom involved in that prediction is limited. The viable unified gauge groups can be identified by very general requirements and the minimal choices (in each simple group series) are SU(5) and SO(10) (plus E_6 in the "exceptional" series). The prediction for the SM quantum numbers then follows, for example in the SO(10) case, from the embedding of the SM fermions in its simplest complex representation.

[4] In that context, Λ corresponds to the scale of new singlet neutrinos and the heaviness of their mass is easily associated to the fact that, unlike all SM fermions, their mass is not protected by the EW symmetry.

enough to bring Λ closer to the EW scale, with possible consequences for collider physics that will not be investigated here. In this case, the smallness of neutrino masses compared to the other SM fermions must be attributed to their smaller couplings. It is even possible that the couplings are so small that the origin of neutrino masses lies below the EW scale, as in the model discussed in Section 5.4.2 or in the case of Dirac neutrinos.

5.1.3 Theoretical benchmark models

5.1.3.1 A critical appraisal of the naturalness problem

The naturalness problem can be formulated as follows. Suppose that, motivated by one of the many issues of the SM described above, the Higgs interacts with degrees of freedom characterized by a superheavy scale M. As discussed in Section 5.1.2, this is the case for example in GUT models, where the Higgs interacts with the superheavy gauge bosons with mass $M \sim M_{\rm GUT} \sim 10^{16}\,{\rm GeV}$; or in see-saw models for neutrino masses the Higgs interacts with right-handed neutrino with mass $M \lesssim 10^{15}\,{\rm GeV}$.[5] Then it is possible to compute the physical Higgs mass in terms of the parameters of the microscopic lagrangian at the scale M. For dimensional reasons, the radiative corrections to the physical Higgs mass will involve terms proportional to the physical scale M^2, which are so large to make the Higgs mass practically not calculable.

We see that the naturalness problem arises in the assumption that the SM is the low energy remnant of a more fundamental theory characterised by a superheavy scale, and because of the desire to be able to understand the Higgs potential by being able to compute its parameters. We also see that the problem is independent of the regularisation scheme one uses to compute radiative corrections.

Let us stick to the above assumptions for the time being (as we will discuss later on, in the last decade the above assumptions have been reconsidered). All models addressing the naturalness problem along those lines introduce new physics at a scale $m_{\rm NP}$ not far from the electroweak scale, whose purpose is to keep the sensitivity of the Higgs mass to superheavy scales under control. The sensitivity to M^2 is now replaced by a sensitivity to $m_{\rm NP}^2$ (the mass of appropriate resonances in composite Higgs models or of the mass of the stops in supersymmetric models) and in order for the Higgs mass to be computable, $m_{\rm NP}$ should not be too far from the TeV scale. The dependence of the Higgs mass on the parameters at the scale $m_{\rm NP}$ and on M is model dependent, but a contribution to the Higgs mass from the radiative corrections involving the SM particles in unavoidable. Depending on the form of the latter, in particular on the dependence on the M, models addressing the naturalness problem can schematically (and qualitatively) be classified in two classes:

$$\Delta \approx \frac{\delta m_H^2}{m_H^2} \approx \left(\frac{m_{\rm NP}}{0.5\,{\rm TeV}}\right)^2 \qquad \text{supersoft theories,} \tag{3}$$

$$\Delta \approx \frac{\delta m_H^2}{m_H^2} \approx \left(\frac{m_{\rm NP}}{0.5\,{\rm TeV}}\right)^2 \log\left(\frac{M^2}{m_{\rm NP}^2}\right) \qquad \text{soft theories,} \tag{4}$$

where Δ is a measure of the fine-tuned cancellation required to reproduce the measured value of the Higgs mass. Clearly, the lack of signal at the LHC is most puzzling for soft theories with very large M, for which the radiative correction to the Higgs mass is enhanced by a large logarithm. This is the case of supersymmetric models with large messenger scale, such as supergravity, in which M is to be identified with the Planck scale ($\log(M_{\rm Pl}^2/\,{\rm TeV}^2) \sim 70$). From this point of view supersoft models and soft models with low M are preferable. Examples of the latter are supersymmetric theories with low messenger scale M. Composite Higgs models are supersoft because the Higgs potential is completely generated at the strong sector confinement scale, $m_{\rm NP}$, with no residual logarithmic sensitivity to superheavy scales. However they can also be interpreted as soft theories if $m_{\rm NP}$ is identified with the mass of the lighter resonances that cancel the quadratic top loop divergence, while M is the confinement scale, *i.e.* the

[5] Ultimately, one can expect the Higgs boson to interact with gravity at the Planck scale.

typical mass of the other bound states. In the presence of a little hierarchy among $m_{\rm NP}$ and M, which is welcome because electroweak precision tests (EWPT) generically require $M \gtrsim 2.5$ TeV and thus a considerable tuning $\Delta \sim 30$, the tuning follows Eq. (4) $\Delta \lesssim 10$ for $m_{\rm NP} \lesssim 1$ TeV (barring possible fine-tunings necessary to enforce the little hierarchy between $m_{\rm NP}$ and M).

5.1.3.2 Composite Higgs models

The idea of a Composite Higgs boson is as old as the naturalness problem, which is typical of theories with elementary scalar particles. All the scalars aside from the Higgs, which we have just discovered, have turned out to be composite particles with a compositeness scale not far from their mass and the same could be true for the Higgs. For a composite scalar, like the QCD scalar hadrons, there is no naturalness problem because their mass is generated through the mechanism of Dimensional Transmutation and thus it is insensitive to energies much above the confinement scale. As of today, we have developed a rather specific framework implementing the general idea of a Composite Higgs, based on two paradigms. The first one is that the Higgs is not a generic bound state, but a Goldstone boson associated with a spontaneous symmetry breaking taking place in a new strong sector above the electroweak scale. Alternatives might also be considered, but they typically suffer from large fine-tuning to explain why the Higgs is lighter than the other resonances. Furthermore a non-Goldstone Higgs is by now disfavoured by the LHC Higgs coupling measurements. Both these issues are addressed in the Goldstone boson case at the price of a mild tuning. The second paradigm is a specific mechanism giving mass to the fermions, which is called "Partial Compositeness". Focusing in particular on the top sector, this leads to predict the existence of fermionic coloured particles with vector-like mass, the "Top Partners" responsible for the generation of the top quark mass and of the Higgs potential.[6]

The most relevant characteristic signatures of the Composite Higgs scenario, which are common to a wide set of explicit models of this class, can be grouped in three categories.

1. **Higgs coupling modifications** with respect to the SM are absolutely unavoidable for a Composite Higgs. Furthermore the deviations can be sharply predicted up to few discrete model–dependent ambiguities. This makes them the most robust model–independent tests of Higgs Compositeness. The size of the departures from the SM is controlled by a parameter $\xi = v^2/f^2$ which measures the new physics scale f of Goldstone symmetry breaking in units of the EWSB one $v \simeq 246$ GeV. Making them small requires f large and costs fine–tuning since it is possible to show (see below) that $\Delta \gtrsim 1/\xi$. Measuring the Higgs couplings at the LHC and at future colliders is therefore an indirect but "direct" (robust) test of naturalness in this context.
2. **EW–charged spin one resonances**, with a mass $m_V = g_V f$ and coupling $g_V \in [1, 4\pi]$ are also universal predictions. Their masses and production rates depend on the new parameter g_V and not just on $\xi = v^2/f^2$, however by studying them at the LHC, at High Luminosity and at future high–energy hadronic machines we could eventually cover their parameter space fully for a given Goldstone scale f.
3. **Top Partners** come third in the list of the most robust signatures of Higgs compositeness. This is because their existence and physical properties depend on the assumption of Partial Compositeness and on some detail in its implementation. However at the current stage of our understanding Partial Compositeness seems unavoidable at least in the top sector and Top Partners are present in all known models. Furthermore the Top Partners are normally colored particles and therefore they are relatively easy to produce at hadron colliders. As mentioned above, Top Partners play a key role in the generation of the Higgs potential and thus their mass directly controls the level of tuning in the theory. Namely, the tuning scales like in Eq. (3) but with $m_{\rm NP} = m_{\rm Partner}$. Top Partners

[6] A spin–$1/2$ fermion is said to be "vector–like" if both its chirality components come in the same representation of the SM group. This allows them to have a vector–like (Dirac) mass before EWSB, differently from SM matter. Being vector–like marks an essential difference between Top Partners and fourth–family quarks and makes the Top Partners not excluded by the Higgs production rate measurement unlike the latter particles.

are thus necessarily light in a Natural Composite Higgs model, similarly to the stops in Natural SUSY and this makes them the ideal channel to test naturalness. Higgs couplings are also valid probes of naturalness because the scale f is found to be necessarily smaller than the Partners mass, $f < m_{\text{Partner}}$. Therefore an indirect limit on f sets a lower bound on m_{Partner} and thus on Δ.

Below we will describe the current and future sensitivity to the three items above by proceeding with the following logic. In Section 5.2.1 we will focus on "1)" and "2)" which provide, respectively, indirect and direct signatures of Higgs compositeness. Higgs coupling modifications are best detected by precise lepton colliders while an high–energy hadron machine would be needed for the direct resonance search. By comparing the reach in these two channels we will outline the complementarity of leptonic and hadronic experimental options for the coverage of the Composite Higgs scenario parameter space.

In Section 5.2.2 we will summarise the reach on Top Partners of current and future hadronic machines, which we can immediately interpret as the reach on the level tuning. While tentative estimates already exist, a careful assessment requires a certain amount of work because the Top Partner production mechanism which is dominant at high mass—namely, single production—has not yet been studied even at the LHC–8, and therefore we don't have robust experimental results to be extrapolated to higher energies and luminosities. A dedicated search strategy for one of the most promising channels is being developed for the purpose of the present document and is currently at a preliminary stage.

These elements will flow together to develop a picture on the current status and the future perspectives of Composite Higgs searches on the basis of our present–day theoretical understanding of this scenario. It is important to remark that this assessment might be affected by future theoretical developments. One direction which is currently under investigation is to construct non–minimal Composite Higgs models based on the "Twin Higgs" mechanism in which the Top Partners might not be colored and thus much harder to detect. While those constructions are not yet completely satisfactory and the study of their phenomenology is still at a primitive stage, theoretical progress is expected to come in the next few years. If this model–building program succeeds, the tuning reach of Top Partner searches will have to be reconsidered and radically different search strategies will have to be devised.

5.1.3.3 Supersymmetry

The appeal of supersymmetry follows not only from the (partial) solution it offers to the naturalness problem. As a weakly coupled, self-consistent theory, supersymmetry is fully calculable and can be extrapolated much above the EW scale, where the solution of some of the SM shortcomings and puzzles may lie. It is this very feature that allows us for example to follow the evolution of the SM gauge couplings and observe their precise crossing around $2 \cdot 10^{16}\,\text{GeV}$. As discussed in Section 5.1.2, such a non-trivial prediction confirms and reinforces the model-independent hint for unification contained in the structure of the SM quantum numbers. Such a double success is considered as an indication in favour of both unification and supersymmetry. Another interesting feature of supersymmetry is that it provides a dark matter candidate. More precisely, its phenomenological consistency (requiring the absence or strong suppression of baryon and lepton number violating effects) may be associated to a discrete parity, the so called "R-parity", that makes the lightest supersymmetric particle (LSP) stable. The latter, if neutral, can play the role of dark matter particle. R-parity also underlies the classic experimental signature of supersymmetry: missing energy. In any event in which susy particles are produced, the final state contains two LSP particles, which escape detection and produce an imbalance in the measured energy budget of the event.

The prototypical example of supersymmetric models is minimal supergravity (msugra), or the constrained MSSM with soft terms given at M_{Pl}. For historical and practical purposes, this has for a long time been the case most widely studied. However, as luck would have it, it happens to maximise the fine-tuning problem. The fine-tuning necessary to accommodate the measured value of the Higgs mass

is in fact in this case (from eq. (4))

$$\Delta = \left(\frac{m_{\rm NP}}{0.5\,{\rm TeV}/\sqrt{\log}} \right)^2 , \tag{5}$$

where $\log = \log(M_{\rm Pl}^2/m_{\rm NP}^2) \approx 70$ for $m_{\rm NP} = 1\,{\rm TeV}$. Natural ($\Delta \sim 1$) supergravity would therefore require new physics to live around $m_{\rm NP} \sim 0.5\,{\rm TeV}/\sqrt{70} \approx 60\,{\rm GeV}$, which underlay the confidence that supersymmetry could be found at LEP2. On top of that, the fine-tuning problem is stressed by the fact that $m_{\rm NP}$, the stop mass, is most tightly constrained in msugra (and in general in supersymmetric models with the most minimal viable field content), as the measured value of the Higgs requires (depending on the value of the A-terms) large stop-induced loop corrections. For the above reasons, supergravity has been known to be in bad shape since 1998 [226, 227]. The most recent bounds from the LHC and the measurement of a not-so-light Higgs mass have exacerbated a known problem.

On the other hand, supersymmetry is not only supergravity, on the contrary, and the assumptions exacerbating the fine-tuning problem identify at the same time the directions favoured by data in the models parameter space. Among the several possible directions, three are particularly appealing because they are simple, plausible, and effective: i) *low messenger scale*: lowering M in eq. (4) from the Planck scale [228–235] to, say, $100\,{\rm TeV}$ [236–243] or less [244,245] considerably reduces the importance of the logarithm and of the fine-tuning problem; ii) *an extra singlet*: the constraint on stop masses following from the measurement of the Higgs mass can be relaxed in the presence of an extra singlet field in the spectrum (NMSSM). This is a minimal, harmless (it does not spoil gauge coupling unification, for example), and welcome (it provides a solution to the μ-problem [246]) extension of the very minimal field content of a viable supersymmetric theory (MSSM); iii) *lighter stops*: the singlet above allows to have lighter stops, just above the present direct experimental bounds. This helps with the fine-tuning problem (remember that $m_{\rm NP}$ in eq. (4) is the stop mass) but needs to be reconciled with the stronger bounds on the first two families of squarks. The difference can be due to the sizeable negative radiative corrections to the stop mass or to a built-in hierarchy among the soft terms of different families.

We will therefore consider a model with low mass messengers, an extra singlet, and relatively light stops as our "quasi-natural" supersymmetry benchmark in Sections 5.3.2–5.3.5. Other possibilities can be considered to address the lack of supersymmetric signals at the first LHC run. They allow an additional moderate gain in fine-tuning, sometimes at the price of additional theoretical effort. We will consider them in Section 5.3.6.

5.1.3.4 Alternative BSM paradigms

The naturalness argument, whose far-reaching conceptual and practical implications will be extensively discussed, is one of the central paradigms of BSM physics. It is therefore interesting, and certainly useful in the case of experimental results disfavouring it, to consider alternatives. As mentioned in Section 5.1.1, there are at least two ways in which the naturalness argument might fail. One possibility is that the quadratic corrections to the Higgs masses are physical, because associated to physical superheavy degrees of freedom, and an accurate cancellation takes place, fine-tuning the Higgs mass to be much lighter, as we measure it. On the other hand, in the absence of physical scales associated to superheavy degrees of freedom, the radiative corrections to the Higgs mass are not huge but infinite, and their cancellation is just a mathematical problem, brilliantly solved by the renormalisation theory. A second way out of the naturalness argument therefore arises if no superheavy degrees of freedom, making the radiative corrections to the Higgs mass physical, exist. Of course, some new physics must exist in any case to address the other shortcomings of the Standard Model. In particular, it is not clear whether the existence of degrees of freedom at the Planck scale, associated to quantum gravity, could be avoided.

In the first case, the challenge is to understand the origin of the enormous cancellation underlying the determination of the Higgs mass. The possibility mostly discussed so far is to rely on an Anthropic mechanism of vacuum selection, see Section 5.3.8. One assumes the existence of a vast "landscape" of

vacua in the underlying microscopic theory, each characterised by different values of the physical constants. Depending on these values, the evolution of the Universe might be radically different, possibly preventing the formation of galaxies or other structures, eventually forbidding the creation of an environment suited for the development of intelligent life. This is essentially the only understanding available of the smallness of the cosmological constant. If a small EWSB scale, of the order of 100 GeV, is also a crucial condition for the very existence of the observer, it is not surprising that this will be the observed value no matter how unlikely it is to obtain it, by fine-tuning, in the landscape of vacua. Differently from naturalness, the Anthropic argument in itself does not give clear indications on how the SM should be extended. Its main implication is that we should not worry about fine-tuning in the Higgs mass or in other observables, provided this fine-tuning is justified by environmental selection. The concrete directions to extend the SM should be indicated, in this framework, by independent considerations. For instance, the theoretical expectations for high-energy SUSY from superstring theory, the need of DM and the quest for coupling unification can be combined in the so-called "Split-SUSY" framework [247–249], which will be discussed in Section 5.3.8.

The second case, in which no cancellation is needed in m_H, is still "under construction". While we do perfectly understand, technically, how the Higgs mass could be reduced by tuning, in a generic theory, it is hard to imagine how the high scale contribution to m_H could be avoided in a complete theory of Quantum Gravity. One proposal is that the new dynamics should be conformal, i.e. without fundamental scales to start with, while still capable to give rise dynamically to the Planck constant (to our understanding, a theoretically viable model is not available at present). Alternatively, one might claim, generically, that the UV theory contains no fundamental high mass scale or, in some sense, that it "behaves like dimensional regularisation". Interesting, speculative work has being developed in this direction. As examples of a theoretical scenario that find their collocation in this context, we will discuss models in which the naturalness problem has no relevant implications on the open problems of the SM, which are then addressed independently by physics at scales at the electroweak scale or below. In this context, the paradigm of Minimality is sometimes advocated. The idea is to identify the Minimal extensions of the SM, with a minimal number of new fields and renormalisable interactions capable to explain all the observed phenomena. On top of DM, also Baryogenesis, Inflation and neutrino masses can be addressed. In Section 5.4 we will describe models in this class and outline their possible experimental implications.

5.1.3.5 Dark Matter

The existence of a neutral DM particle with a lifetime comparable with the age of the Universe is established by cosmological and astrophysical observations, however not much is known of its properties. Several DM candidates have been proposed, with radically different masses and coupling strengths, each of which is capable of explaining the observed relic abundance by its own specific mechanism. The case of a WIMP particle with a mass in the GeV to TeV range, weak–sized coupling to SM particles and the relic generated by thermal freeze out is one of the simplest options and it can be tested at high–energy colliders, providing one of their physics objectives. For this reason it is important to compare the reach of WIMP DM collider searches with the one of existing and future dedicated observational experiments, based on either the Direct detection of DM scattering on nucleons or on the Indirect detection of its annihilation (or decay) products. This is the purpose of Section 5.5, where we will outline the complementarity of those different detection strategies.

5.2 Composite Higgs

5.2.1 Direct vs indirect searches

The goal of this section is a comparison of the prospects for direct and indirect searches at the LHC and future colliders in the context of Composite Higgs (CH) models. While the strongest indirect constraints on New Physics (NP), except for those involving the Higgs boson, come from an e^+e^- collider, LEP, the

strongest direct constraints come from hadronic colliders such as the Tevatron ($p\bar{p}$) and the LHC (pp). In fact, while hadron colliders can reach much higher energies, lepton colliders provide a much cleaner environment, suitable for precision measurements. The complementarity of direct vs indirect NP effects can therefore be translated in the complementarity of different colliders. A quantitative comparison of the physics possibilities of different machines, both in direct and indirect searches, is thus at the basis of any discussion aimed at planning the future of particle physics, at least in its collider physics incarnation.

Comparing direct vs indirect NP searches also requires a clear theoretical understanding of their model dependence/independence. Indirect searches are usually completely agnostic about the nature of NP and require only very mild assumptions on the possible underlying UV theory. On the other hand, direct searches usually require a few more assumptions on the nature and the origin of the new particles, necessary to drive their search at experiments. However, despite the larger model independence of indirect searches, their interpretation within theoretical models, which is necessary to infer their relevance (*e.g.,* to translate the bounds into the level of fine tuning of a given model), always introduces some model dependence. A clear example of this fact is given by the interpretation of indirect searches in terms of effective operators weighed by a coupling divided by a scale $g_{\rm NP}/\Lambda_{\rm NP}$: such constraints can not be interpreted as constraints on the scale of new physics, since they depend on the coupling strength $g_{\rm NP}$ of the new physics model under scrutiny. For instance, for a weakly coupled model with $g_{\rm NP} \sim 1$, an indirect bound $g_{\rm NP}/\Lambda_{\rm NP} < 1/(10\text{TeV})$ means that the scale of new physics is expected to lie above 10 TeV. The same bound, when interpreted in a strongly coupled model with $g_{\rm NP} \sim 4\pi$, instead means that the scale of new physics is expected to lie in the 100 TeV region. This illustrates very well how model dependent the interpretation of indirect constraints usually is.

Let us now specialize the discussion to CH models. Aside from being a well–motivated theoretical possibility, CH is the ideal framework for our investigation since it predicts both indirect and direct effects which could both be sizable enough to be detected. Determining which strategy could be more effective to test the CH idea is non–trivial and requires a dedicated study. Indirect effects, in the form of corrections to SM couplings or of new BSM vertices [250, 251], unavoidably emerge due to the pseudo–Nambu–Goldstone nature of the Higgs leading to deviations proportional to $\xi \equiv v^2/f^2$ where f is the Goldstone boson Higgs decay constant and v the EWSB scale. Further corrections come from the virtual exchange of new heavy resonances mixing with the SM particles at tree level, giving contributions of order $m^2_{\rm SM}/m^2_{\rm NP}$. The latter resonances can also be produced at high enough energies, giving rise to a number of possible direct signatures. The most studied and promising ones are the production of spin–one EW–charged vectors [252–256] and of the Top Partners, which will be discussed in Section 5.2.2.

The strongest indirect constraints on CH models currently come from ElectroWeak Precision Tests (EWPT), where those models could have already shown up in the form of oblique corrections or modifications of the $Zb\bar{b}$ vertex. Even restricting to custodially symmetric cosets and to fermionic operator representations which implement the so-called P_{LR} protection symmetry for $Zb\bar{b}$ [257], EWPT are still the dominant indirect constraint on the CH scenario. In spite of this, we will not take EWPT and their possible improvements at future colliders as a central pillar of our investigation. The reason is that we judge their impact too model–dependent to be quantified in a robust way.[7] Namely, as pointed out in Ref. [258], the EWPT observables are sensitive to a number of effects which can be computed only within specific and complete models and therefore they are to a large extent unpredictable at the level of generality we aim to maintain here. Instead, we decided to focus on indirect effects associated to the modifications of the Higgs boson couplings because they have the great virtue of being largely insensitive to many details of the specific model and thus predictable in a fairly model–independent way. This is particularly true for the trilinear Higgs coupling to EW gauge bosons which, at least for models based on the minimal coset $SO(5)/SO(4)$, is universally predicted to deviate from the SM expectation by a relative correction $k_V = \sqrt{1-\xi}$. We will thus take the sensitivity to k_V of future leptonic colliders as a good model–independent measure of their reach on CH models, to be compared with direct searches at

[7] This is even more true for flavour constraints, which can be stronger than EWPT, but considerably more model–dependent.

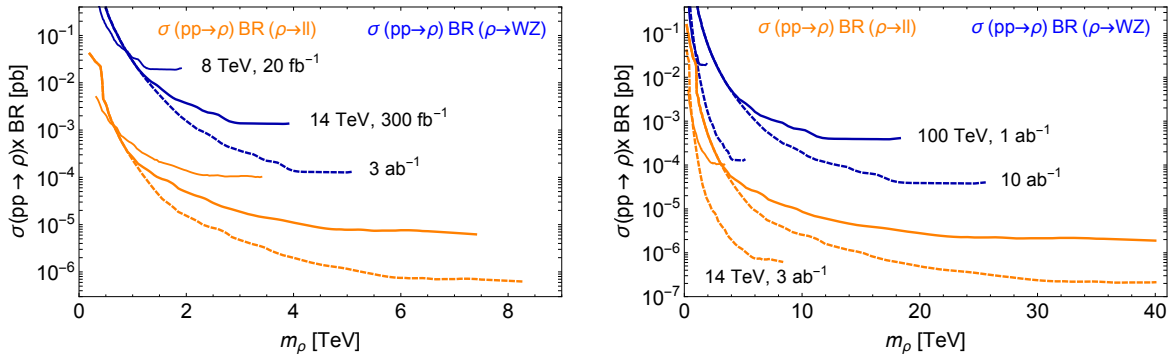

Fig. 20: Bounds on $\sigma \times$ BR from LHC at 8 TeV with 20 fb^{-1} (solid) and corresponding extrapolations to LHC at 14 TeV with 300 fb^{-1} (solid) and 3 ab^{-1} (dashed) and to FCC at 100 TeV with 1 ab^{-1} (solid) and 10 ab^{-1} (dashed). The two analyses of refs. [260] (CMS di-leptons, orange) and [261] (CMS fully leptonic di-bosons, blue) are considered.

hadron colliders.

Similar considerations underlie our choice of the representative direct signatures. Top Partners are very sensitive probes of CH models because their mass directly controls the generation of the Higgs potential and thus the level of fine–tuning required to achieve EW symmetry breaking and a light enough Higgs boson. However their properties and their very existence is, to some extent, model–dependent and therefore we did not consider Top Partner signatures but focused instead on EW vector resonances. The existence of the latter is very robust because they are associated with the current operators of the SM group, which needs to be a global symmetry of the composite sector eventually made local by the gauging of external sources. In particular, we consider the particles associated with the SM $\mathrm{SU}(2)_L$ currents, which form a $(\mathbf{3},\mathbf{1})$ triplet of the unbroken strong sector group $\mathrm{SO}(4)$. We describe this vector triplet by Model B of ref. [256], a simplified model which depends on two parameters only: the vector triplet mass m_ρ and its intrinsic coupling g_ρ controlling the interaction with the SM fermions and the EW gauge bosons. The two parameters are related to ξ by

$$\xi = \frac{g_\rho^2}{m_\rho^2} v^2 \,, \tag{6}$$

out of which the indirect reach on ξ is immediately compared with direct searches, which set limits on the (m_ρ, ξ) or (m_ρ, g_ρ) planes.

In order to perform the comparison we need an assessment of the indirect and direct search sensitivities. While a considerable literature exists on the former ones, summarized in Table 13 for various experimental setups, little is known on the latter. We will use here an estimate of direct search sensitivity based on parton luminosity re-scaling of the currently available LHC bounds to higher energies and integrated luminosities, described in Ref. [259].

5.2.1.1 Results

Figure 20 shows the comparison between the current 8 TeV LHC limits (95% CL exclusions) on $\sigma \times$ BR with 20 fb^{-1} and the corresponding bounds extrapolated to the LHC at 14 TeV with 300 fb^{-1} and 3 ab^{-1} and to the FCC at 100 TeV with 1 ab^{-1} and 10 ab^{-1} obtained by the procedure of Ref. [259]. For illustration we consider the CMS search into di-leptons of ref. [260], and the fully leptonic di-boson search of ref. [261]. The figure shows how the LHC mass reach is clearly limited by the c.o.m. energy. A luminosity upgrade by a factor of ten, from 300 fb^{-1} to 3 ab^{-1}, can merely improve the mass reach by $\sim$ 1 TeV. It does, however, increase the sensitivity on $\sigma \times$ BR by almost one order of magnitude, which translates into a two to three times more stringent bound on the new physics coupling. In fact,

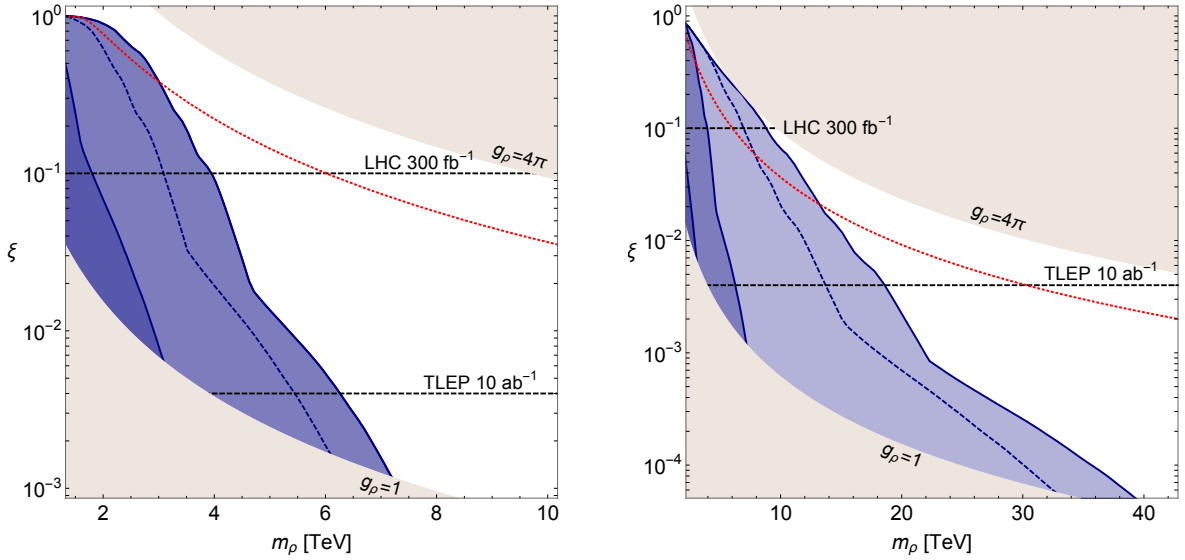

Fig. 21: Comparison of direct and indirect searches in the (m_ρ, ξ) plane. Left panel: region up to $m_\rho = 10$ TeV showing the relevance of LHC at 14 TeV with 300 fb^{-1} and 3 ab^{-1}; right plot: region up to $m_\rho = 35$ TeV showing the comparison between the LHC reach and FCC reach with 1 and 10 ab^{-1}. See Section 5.2.1.1 for additional details.

partial compositeness in CH models dictates the coupling to fermions to scale as $1/g_\rho$, while the coupling to (longitudinal) gauge bosons is proportional to g_ρ. The Drell-Yan production cross section therefore scales as $1/g_\rho^2$. Since the BR is almost constant in g_ρ in the region where the channel under consideration dominates (small values of g_ρ for di-leptons and large values of g_ρ for di-bosons), $\sigma \times$ BR scales roughly as $1/g_\rho^2$. Hence a stronger bound on $\sigma \times$ BR pushes g_ρ to larger and larger values [256]. The FCC at 100 TeV is expected to reach much higher masses, while being less sensitive to small values of $\sigma \times$ BR than the LHC in its accessible mass regime. This is due to the much larger background expected at low masses at the 100 TeV collider, which does not allow one to exclude values of $\sigma \times$ BR as small as the corresponding ones at the LHC. However, the reduced sensitivity of the FCC compared to the LHC does not affect the reach of the FCC in the relevant parameter region of composite Higgs models, as will be clear from Figs. 21 and 22.

The bounds on $\sigma \times$ BR shown in Fig. 20 can be translated into allowed and excluded regions in the parameter space of the model. As discussed in the previous section, the most illustrative two dimensional planes are (m_ρ, ξ) and (m_ρ, g_ρ), where a direct comparison between constraints from cross section limits and from Higgs coupling sensitivity at the LHC and future colliders is possible. In Figs. 21 and 22 we show the 95% CL exclusion limits in these planes. The left panels of both figures depict the region relevant for the LHC, while the right panels show the full reach of the FCC at 100 TeV. The theoretically viable region of the CH parameter space lies in between the two curves $g_\rho = 1$ and $g_\rho = 4\pi$, the upper limit $g_\rho \leq 4\pi$ is required by the internal consistency of the construction, the lower one $g_\rho \geq g_w \simeq 1$ is needed in these models to obtain the correct Weak coupling. The violet shaded regions are excluded by direct searches at different collider configurations: the shadings correspond to the LHC at 8 TeV with 20 fb^{-1} (darkest), the LHC at 14 TeV with 3 ab^{-1} (medium dark) and the FCC with 10 ab^{-1} (lightest). The violet dashed lines depict the 14 TeV LHC with 300 fb^{-1} (left plots) and the FCC with 1 ab^{-1} (right plots). The small kink in the exclusion limits present at all colliders originates from the superposition of searches in di-lepton [260] and the di-boson [261] final states at 8 TeV.[8] As discussed before, partial

[8]Note that we use the most recent CMS searches for illustration, but verified that the ATLAS searches in di-leptons [262] and dibosons [263] yield comparable results. For a complete list of relevant and most recent searches for heavy vectors see refs. [256].

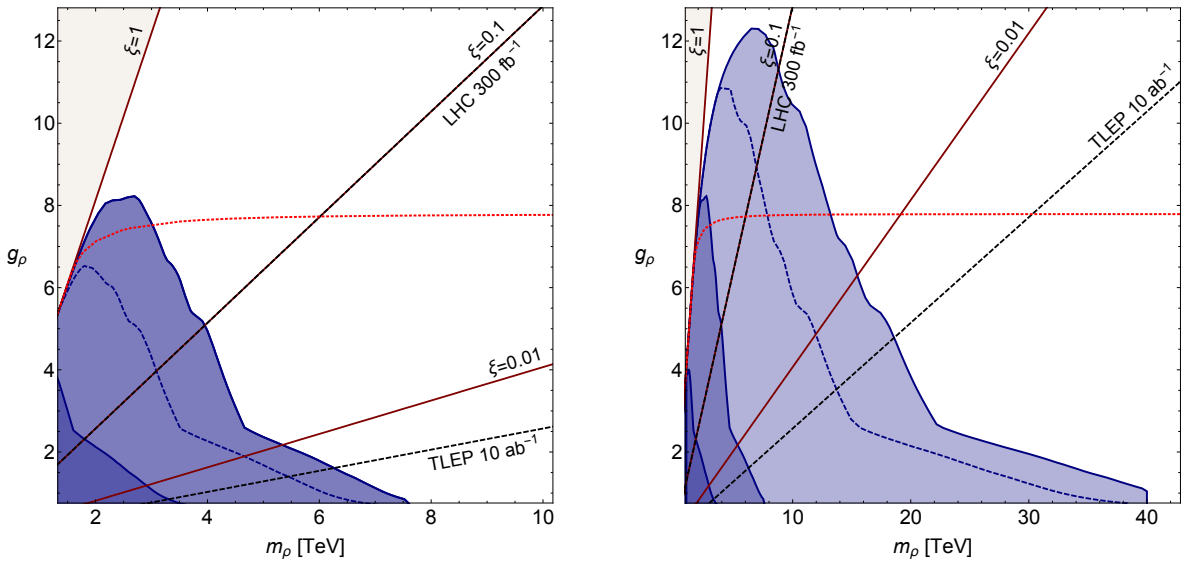

Fig. 22: Comparison of direct and indirect searches in the (m_ρ, g_ρ) plane. Left panel: region up to $m_\rho = 10$ TeV showing the relevance of LHC at 14 TeV with 300 fb^{-1} and 3 ab^{-1}; right plot: region up to $m_\rho = 35$ TeV showing the comparison between the LHC and FCC reach with 1 and 10 ab^{-1}. See Section 5.2.1.1 for additional details.

compositeness implies that the di-lepton search has a larger mass reach in the region of small g_ρ and small ξ, while the di-boson search dominates for larger couplings and values of ξ. For a clear distinction between the two regions see ref. [256]. Above the fine red dotted curve, the total width takes values larger than 20% of the mass. Since we use the narrow width approximation to compute the excluded regions from direct searches for heavy vectors (see ref. [256] for details), our bounds are not reliable beyond this limit.

The reach on ξ originating from Higgs coupling measurements are summarized in Table 13 and represented by black dashed curves in both planes (excluded region above the line). In the (m_ρ, ξ) plane,

Collider	Energy	Luminosity	ξ $[1\sigma]$	References
LHC	14 TeV	300 fb^{-1}	0.1	[264, 265]
ILC	250 GeV + 500 GeV	250 fb^{-1} 500 fb^{-1}	0.6-1.2 $\times 10^{-2}$	[56, 86, 266, 267]
CLIC	350 GeV + 1.4 TeV + 3.0 TeV	500 fb^{-1} 1.5 ab^{-1} 2 ab^{-1}	1.1-2.4 $\times 10^{-3}$	[268]
TLEP	240 GeV + 350 GeV	10 ab^{-1} 2.6 ab^{-1}	2×10^{-3}	[46]

Table 13: Summary of the precision on ξ (defined in this literature as the absolute error on the measured ξ in the SM ($\xi = 0$) hypothesis) at various experiments from the study of single and double Higgs processes.

the reach simply corresponds to horizontal lines and translates into linear curves with varying inclination in the (m_ρ, g_ρ) plane. In particular, we show the LHC reach at 300 fb^{-1}, obtained from single Higgs production, corresponding to $\xi < 0.1$, and the expected reach of TLEP at $\sqrt{s} = 350$ GeV corresponding to $\xi < 0.004$ [46]. Note that CLIC with 2 ab^{-1} is expected to have a comparable sensitivity on ξ [268].

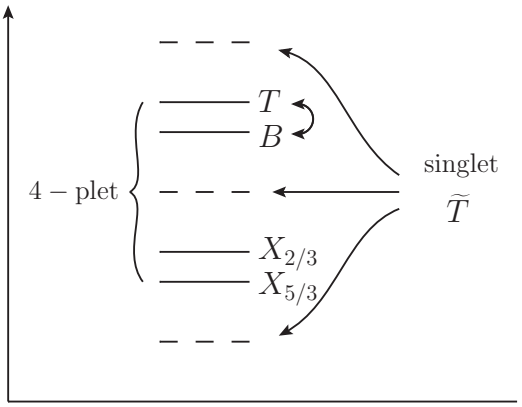

Fig. 23: Schematic structure of the spectrum of top partners in the quadruplet and singlet representations of $SO(4)$.

5.2.2 Top Partners

Light top partners are an essential ingredient of natural composite Higgs scenarios. Being charged under QCD and strongly coupled to third generation quarks they constitute a good target to probe the composite Higgs idea in collider experiments. Differently from the composite bosonic sector, whose properties are determined to large extent by the symmetry structure of the theory, the fermionic sector has considerably more freedom. The Goldstone symmetry pattern only implies that the fermionic resonances appear in multiplets of the unbroken global group. In the minimal models we are interested in this document the symmetry pattern $SO(5)/SO(4)$ implies that top partners can be classified according to their quantum numbers under the unbroken $SO(4)$ subgroup. In the most popular scenarios (motivated by the presence of accidental symmetries that protect the EW precision parameters), the top partners belong to two irreducible representations of $SO(4)$, namely the fundamental (the $\mathbf{4}$) and the trivial representation (the $\mathbf{1}$).

The spectrum of the top partners follows a simple pattern dictated by the Goldstone symmetry, depicted in Fig. 23. The one in the $\mathbf{4}$ split into two $SU(2)_L$ doublets, the (T, B) doublet with quantum numbers analogous to the (t_L, q_L) SM quark doublet, and an exotic doublet $(X_{2/3}, X_{5/3})$ with hypercharge $7/6$ and thus an exotic charged particle. Inside each doublet the mass splitting is rather small being due only to EWSB effects. The exotic doublet is always the lightest of the two and is expected to be the most interesting one for collider searches. The second state we consider, the $\widetilde{T}$ singlet, is a completely independent state, its mass is free and not connected to the 4-plet one.

Being charged under QCD, the top partners can be pair produced via QCD interactions. A remarkable aspect of this production channel is the fact that its cross section is universal, that is it depends on the mass of the resonances but not on their quantum numbers or the details of the model. In addition, the top partners can also be singly produced in association with a top or a bottom quark by the diagrams in Fig. 24. Differently from pair production, single production is not universal and its size is determined by the "flavour changing" gauge couplings that mix the top partners with the SM quarks. Single production is favoured for high resonance masses with respect to pair production because of the smaller kinematical threshold. For natural values of the production couplings single production in association with a top overcomes pair production, at the 14 TeV LHC, for $m_\psi \gtrapprox 1$ TeV. Single production in association with a bottom quark is competitive with pair production even at lower masses.

The decays of the top partners are controlled by the same couplings that determine single production and, in addition, by the interactions mediated by the physical Higgs. The branching fractions are insensitive to the overall coupling strength and are rather model–independent, determined to a large extent by the quantum numbers of the resonances. The main decay channels for the 4-plet and singlet states are listed in Table 14.

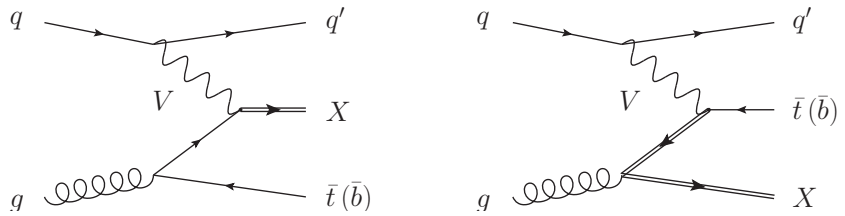

Fig. 24: Leading diagrams contributing to top partners single production.

	Wt	Zt	ht	Wb
$X_{5/3}$	100%			
$X_{2/3}$		50%	50%	
T		50%	50%	
B	100%			
$\widetilde{T}$		25%	25%	50%

Table 14: Branching ratios for the main decay channels of the top partners.

At the present and future collider experiments basically all top partners can be used as reasonable search targets. For instance at the 8 TeV LHC searches for charge $5/3$, charge $2/3$ and charge $-1/3$ states have been performed that obtained comparable bounds on the mass of the resonances. The typical structure of the spectrum, however, suggests that the most promising search channels are the ones involving the exotic $X_{5/3}$ or $X_{2/3}$ resonances, in the case of a light 4-plet, or the $\widetilde{T}$, in the case of a light singlet.

From Table 14 we can guess that the $X_{5/3}$ resonance, which decays exclusively into Wt, can lead to a more visible signature with two leptons in the final state with respect to the $X_{2/3}$, which has to pay the small leptonic BR of the Z boson plus the intrinsic 50% BR. This is confirmed by the present experimental analyses, which, focusing purely on pair production, obtain the bounds $m_{X_{5/3}} \gtrsim 800$ GeV and $m_{X_{2/3}} \gtrsim 750$ GeV [269–271]. Furthermore the $X_{5/3}$ partner leads to a clean final state with two same–sign leptons. Given that the $X_{5/3}$ is nearly degenerate with the $X_{2/3}$ we will focus on it and we will ignore $X_{2/3}$ searches in what follows. As we saw before, single production can also contribute significantly to the production cross section for the top partners. However at the moment there exist no dedicated experimental analyses for the detection of the single production signal and in order to estimate its impact on the exclusion we must rely on theory recasting or projections which we take from Ref. [272].

Let us start from the $X_{5/3}$ partner. In this case the singly produced resonances contribute to the same (same–sign dileptons) final states as the pair produced ones, and the current experimental limits can be reinterpreted by taking the additional contribution of single production into account. The result is shown in the left panel of Fig. 25, we see that the mass reach can overcome 1 TeV for relatively large but still reasonable value of the parameter c_R which controls, in the parametrization of Ref. [272], the single production coupling strength. Notice that the typical value of c_R (and of c_L introduced below) is $c_R \sim \sqrt{\xi}$, *i.e.* $c_R \sim 1/3$ for the values of ξ we are currently interested in testing. This was for the 8 TeV LHC data with 20 fb^{-1} of integrated luminosity, projections for the 13 TeV run are shown in the right panel of Fig. 25, we see that the bounds could be significantly improved and reach the 2 TeV region. As can be seen from this plot, the effect of an higher integrated luminosity for the 13 TeV LHC is not negligible. Going from 300 fb^{-1} to 3 ab^{-1} at fixed coupling there is an enhancement in the bounds of the order of 200 GeV, while moving at fixed mass the reach on the coupling improves by a factor of two. As expected on general grounds, HL–LHC has a moderate impact on the mass reach ($10 - 15\%$) and a very strong one on the coupling strength reach. Its impact is thus best visualized on a coupling–mass

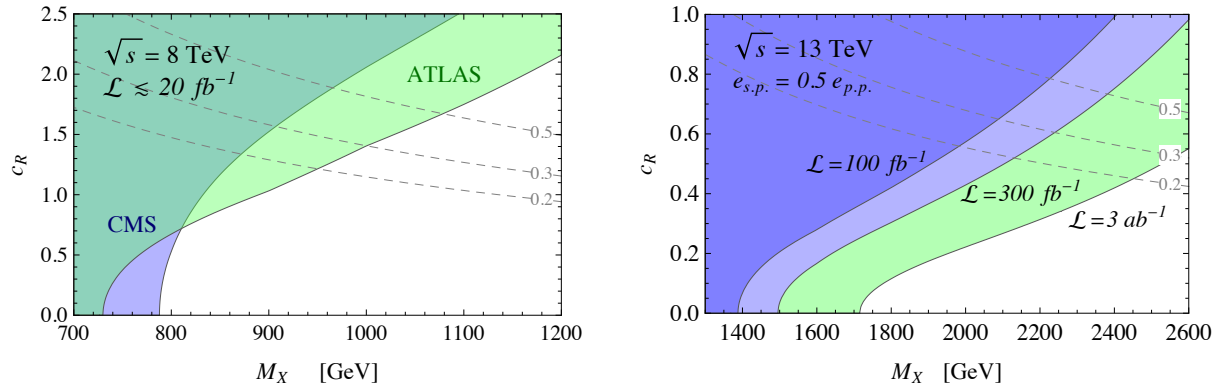

Fig. 25: Bounds on the mass of a charge-$5/3$ top partner as a function of the single production coupling c_R. Left panel: bounds derived from the 8 TeV LHC data. The green (blue) region corresponds to the ATLAS (CMS) search. Right panel: estimate of the bounds for the 13 TeV LHC for various integrated luminosities. In both plots the dashed gray lines show the contours with $\Gamma_X/M_X = 0.2, 0.3, 0.5$. The plots are taken from Ref. [272].

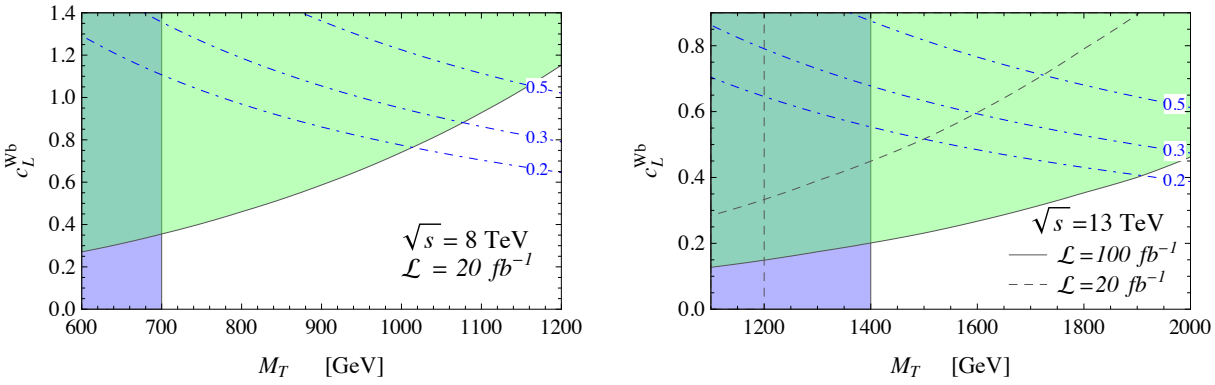

Fig. 26: Bounds on the $\widetilde{T}$ resonance for the 8 TeV LHC data (left panel) and for the 13 TeV run (right panel). The blue region denotes the exclusion from pair production only. The green region shows the estimated exclusions reach taking into account single production (the estimate is based on the analysis of Ref. [274]). The plots are taken from Ref. [272].

plane like the one we are describing here.

Searches for pair-produced singlet resonances, the $\widetilde{T}$, have also been performed at the 8 TeV LHC, leading to a bound $m_{\widetilde{T}} \gtrsim 700$ GeV. [269–271] The bound has been obtained by combining the various three main decay channels according to the $\widetilde{T}$ BR reported in table 14. Although no experimental analysis has been presented so far, it has been noticed that single production in association with a bottom quark can be used to significantly improve the bounds on the $\widetilde{T}$ [273] and an estimate of the possible reach has been presented in Ref. [274]. Based on the latter study, which however represents an expected limit and does not correspond to an actual experimental exclusion, 8 TeV limits are shown on the left panel of fig. 26 in the mass/coupling (c_L, in this case) plane. The expected reach in the next LHC run is shown in the right panel of the same figure.

We conclude by discussing the top partners reach at a hypothetical 100 TeV hadronic collider. At such a machine, the production cross sections for top partners are greatly increased and multi-TeV resonances can be easily tested. A rough estimate of the possible reach for the exotic $X_{5/3}$ and for the singlet $\widetilde{T}$ is shown in fig. 27. By relying on pair production only, one could test top partners with a mass up to order 7 TeV. If the single-production coupling is non-negligible resonances with a mass ~ 15 TeV could be probed. Notice that the huge increase in the reach also implies a much better test of Naturalness.

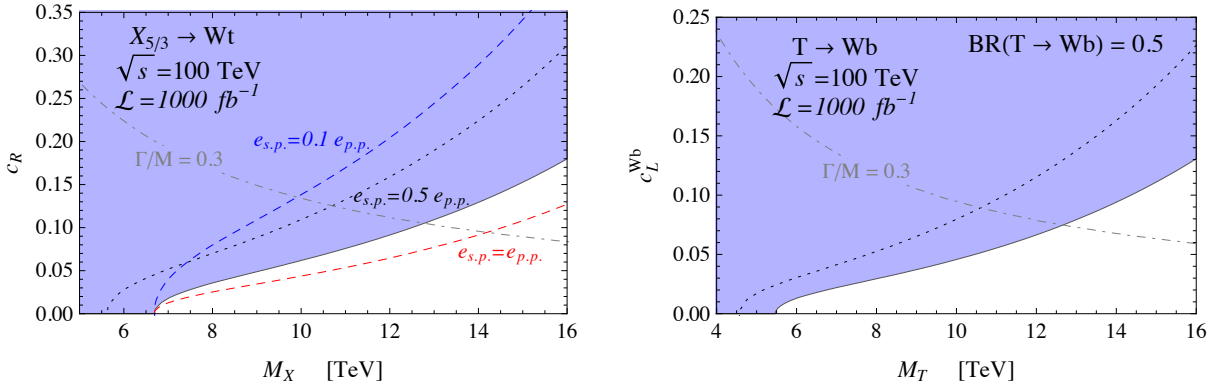

Fig. 27: Estimate of the exclusion reach for top partners at a future 100 TeV hadronic collider. The left plot corresponds to the $X_{5/3}$ resonance, while the right one to the $\widetilde{T}$. The plots are taken from Ref. [272].

Excluding top partners at a mass of order 2 TeV, as can be done at the LHC, implies a lower bound on the fine-tuning of order 5%. Extending this bound to 10 TeV, as could be done at an high-energy collider, would push the minimal amount of tuning to order 0.2%.

We stress once again that the results presented in this subsection, especially those for the 13 TeV LHC and the 100 TeV FCC, are based on rather crude estimates of the sensitivity of future experimental searches. The most problematic ones are the limits on the $\widetilde{T}$, for which a robust experimental analysis or projection is not available even for the 8 TeV LHC. Providing a careful phenomenological analysis of this particle at the 13 TeV LHC and the 100 TeV FCC, by focusing on the dominant production mode in association with a bottom quark, is the goal of the next section.

5.2.3 Single production of the Top Partner singlet at hadron colliders

Singlet top partners decay to Wb, tZ or tH in the approximate ratio 2:1:1 respectively, and the significant branching fractions to tZ and tH have attracted previous attention [273,275,276]. Here, we have chosen to focus on the most abundant expected decay: $\tilde{T} \to Wb$, with subsequent decay of the W-boson to leptons or hadrons (leptonic and hadronic channel respectively).

The enormous background which afflicts these final states can be reduced by exploiting the jet substructure to suppress top-pair production and by requiring the presence of the forward jet which characterizes the signal topology. This simple strategy has already been shown to produce a sensitive search for single top-partner production, in the context of composite Higgs models [274]. The search has competitive mass reach with respect to the existing searches for top-partner pair production at a pp collider working at 14 and 100 TeV center of mass energy. The present experimental limits are weakest for large values of the $\tilde{T} \to Wb$ branching ratio [271].

Signal and background samples

Signal events at partonic level are generated using the `MadGraph 5` [277] Monte Carlo, interfaced with `PYTHIA 6.4` [173] for the parton-shower and hadronization, and with `Delphes` [278] for the detector simulation.

Top-partner single production and decay are simulated through the processes $pp \to \tilde{T}bq$ and $\tilde{T} \to Wb$ for different mass values, ranging from 1 to10 TeV. Events are simulated at $\sqrt{s} = 14$ TeV and $\sqrt{s} = 100$ TeV. An integrated luminosity $\mathcal{L} = 3000$ fb^{-1} is assumed for both energies. For the hadronic channel the effect of 140 overlapping pile-up interactions is also included.

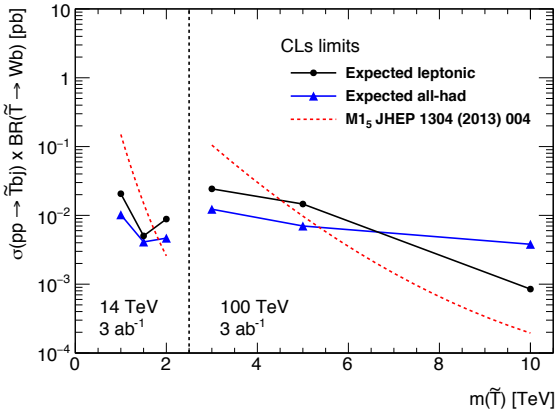

Fig. 28: Exclusion limit curves at 95%CL as a function of the $\tilde{T}$ mass for the l+jets and hadronic analysis at 14 TeV and 100 TeV for $\mathcal{L} = 3\ ab^{-1}$ of accumulated statistics.

Event selection

Background samples for W/Z+jets, $t\bar{t}$ and t+jets processes have been taken from the "Snowmass Energy Frontier studies" [279] [280] [281]. These are the dominant sources of physics background in the analysis. In the time period allowed for this specific study it has not been possible to include the background from QCD multi-jets production and the effects of fakes and instrumental backgrounds. In order to isolate the top-partner signal from the other backgrounds, partly common strategies are applied for the lepton plus jets and the hadronic case. The signal final state topology is characterized by highly energetic W-decay products (either an electron/muon or a boosted hadronic jet), b-tagged jet from the $\tilde{T}$ decay and a light forward jet. The b-quark produced in association with the $\tilde{T}$ is too soft to be seen. The lepton should be also isolated and the presence of significant missing transverse energy would account for the presence of a neutrino. In the case of the W hadronic decay, the boosted W is tagged via an algorithm which makes use of the substructure information contained in large radius jets. A boosted top-jet tagging veto is applied in the hadronic channel in order to reduce the $\mathrm{t\bar{t}}$ background which is orders of magnitude larger than the signal. However, it is important to note that the W and top tagging algorithms currently available are not optimized for highly energetic jets of several TeV, both for the case of a 100 TeV machine or very large masses of the $\tilde{T}$. Alternative solutions based on simpler jet characteristics have been devised for the 100 TeV case. More details are available in [282].

Results

The final limits are extracted in both cases from the distribution of the reconstructed mass of the $\tilde{T}$ comparing the signal and the sum of the backgrounds. In the lepton plus jets case the mass of the candidate particle $\tilde{T}$ is computed from the four-momenta of the sum of the isolated lepton, the neutrino and the b-tagged jet. The longitudinal component of the neutrino is obtained by imposing the W-boson mass constraint on the lepton plus the missing transverse energy system [274][9].

In the case of the all hadronic final state the mass of the $\tilde{T}$ is reconstructed using the invariant mass of the leading W-tag jet and the b-jet system: $m(\widetilde{T}) = m(W_{tag}, b_{tag})$. The limits are obtained using the RooStats (for the leptonic channel) or Theta (for the hadronic) framework using statistical uncertainties only. The analyses presented here are able to exclude (individually) masses of the $\tilde{T}$ up to 1.7 TeV at 14 TeV with 3 ab^{-1}, and up to 5 TeV at 100 TeV with 3 ab^{-1}, see Fig. 28. No combination has been performed at this point. The leptonic analysis limit for 10 TeV mass at 100 TeV is reported for

[9] Whenever two real solutions are found, the one with lower absolute value is chosen. If there is only one real solution, it is used. If no real solution is found, the event is rejected.

completeness in the figure, however it is not reliable because the background samples at our disposal are too poor in the hard kinematical region for a reliable estimate of the reach. For this reason this point has been excluded by the summary plot of the exclusion limits in the coupling-mass plane shown in Fig. 29. Of course, these analyses could be made more accurate. In particular the effect of pile-up in the leptonic analysis and the multi–jet QCD background in the hadronic one should be estimated. Furthermore they should be revised once new optimized algorithms become available for the different kinematical regime of a 100 TeV machine. The experience of attempting a realistic analysis for these conditions has shown the limits of the current reconstruction algorithms and the need for a significant development work to fully recover, and possibly increase, the efficiency of the analyses at an 8 TeV collider. In the meantime, this is compensated by considering statistical uncertainties only for the limit extraction.

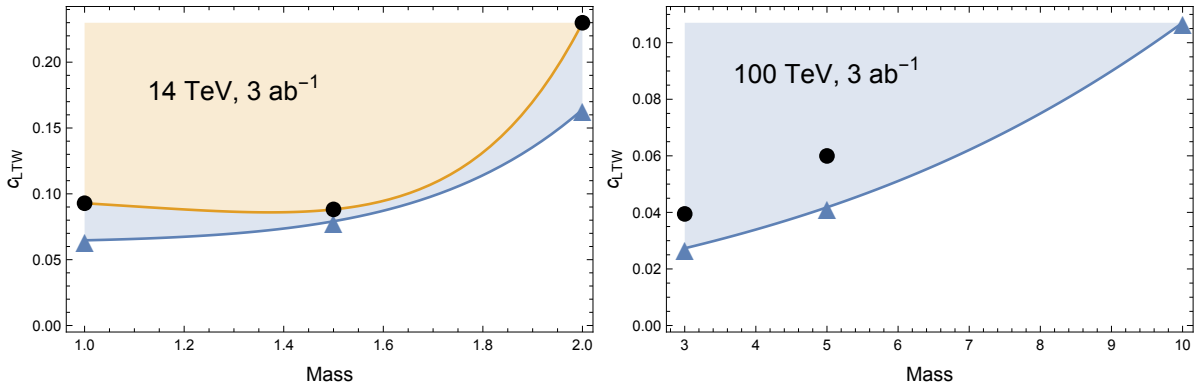

Fig. 29: Exclusion limits in the coupling-mass plane (mass expressed in TeV) at 14 TeV with $\mathcal{L} = 3\ ab^{-1}$ (left) and at 100 TeV with $\mathcal{L} = 3\ ab^{-1}$(right). In spite of a different notation, the plane is the same of Figure 26.

5.3 Supersymmetry

5.3.1 Outline

Supersymmetry offers an appealing solution to the naturalness problem of the SM Higgs mass, as discussed in Section 5.1. Unlike the models discussed in Section 5.2, which require a new dynamical scale associated to some new strong interactions, in this case the Higgs mass is protected by a special type of symmetry and the theory is weakly coupled. As such, it can be extrapolated up to the Planck scale, with a calculability and predictivity power whose appeal has been emphasized in Section 5.1.3.3.

In order to represent an efficient solution to the SM Higgs mass problem, the supersymmetry spectrum, and in particular stops, gluinos, and Higgsinos, must appear at a scale not too far from the EW scale. A realistic and updated estimate of the position of the latter scale is crucial in order to i) assess the significance of the present experimental bounds and the motivation of further searches and ii) assess the potential of future experimental options to reach and probe the scale of supersymmetric particles. In the above assessment, the choice of the model in the wide parameter space of theoretical options plays a crucial role.

Here, we will first of all consider the "quasi-natural" scenario defined and motivated in Section 5.1.3.3, in which the Higgs sector of the MSSM is augmented by a singlet (NMSSM) and the stops are allowed to be below a TeV. Such a scenario is both motivated by data (it does better than minimal supergravity, which prefers stops well below the experimental limit and a lower Higgs mass) and theoretically appealing (it mitigates the fine-tuning problem in a simple and effective way and is independently motivated). New physics can be sought through direct and indirect searches in the Higgs sector and through direct searches in the sfermion and chargino sectors. Such a "quasi-natural" scenario will be discussed in Sections 5.3.2– 5.3.5. In particular, Section 5.3.2 describes the set-up, Section 5.3.3 discusses the Higgs sector, and Sections 5.3.4 and 5.3.5 discuss the sfermion sector, comparing the expectation

on their masses following from the naturalness argument with the experimental prospects. As we will see, while the interpretation of experimental searches in terms of bounds on supersymmetric masses is not very different than in the MSSM (in fact, we will present the bounds in terms of simplified models, which can capture the qualitative features of the bounds in both the MSSM and NMSSM), the pressure that the bounds set on the model is significantly weaker than e.g. in msugra. In Section 5.3.6 we will then consider the possibility that the bounds themselves are weaker than what a simplified interpretation would suggest. This further weakens the pressure on supersymmetric models, sometimes at the price of selecting a special slice of the parameter space or of additional theoretical effort. In Section 5.3.7 we will discuss the searches of charginos and neutralinos ("electroweakinos"). Finally, in Section 5.3.8 we will consider the possibility that the naturalness argument is not relevant in the context of supersymmetric models.

5.3.2 A quasi-natural benchmark scenario

As mentioned in Section 5.1.3.3, the prototypical example of supersymmetric models, minimal supergravity, happens to maximise the fine-tuning necessary to reproduce the observed value of the Higgs mass. This is because i) the radiative corrections to the Higgs mass that need to be cancelled are proportional not only to the stop mass squared but also to a large, $\mathcal{O}(70)$ logarithm; and ii) the stop mass to which the corrections are proportional is bounded not only by the direct experimental bounds but also by the need to overcome the tree level bound on the Higgs mass, $m_H \leq M_Z$, and bring m_H within its experimental range.

On the other hand, the latter two unfortunate features of msugra are far from being shared by all supersymmetric models. The logarithm enhancing the radiative corrections to the Higgs mass can be significantly lower if the scale at which the sfermion masses originate is low, for example $\mathcal{O}(100\,\mathrm{TeV})$ in gauge mediated supersymmetry breaking models [236–243] or even lower if the supersymmetric masses arise at the tree level [244, 245, 283, 284]. Moreover, the indirect bound on the stop mass only holds in the presence of the very minimal field content required by a viable supersymmetric theory (MSSM). It suffices to add an extra singlet to the spectrum (NMSSM) [246, 285] to raise the tree-level prediction for the Higgs mass and avoid the indirect bound on the stop masses. Such a minimal and harmless extension of the very minimal field content was independently motivated by the solution to the μ-problem [246].

We will then consider as our "quasi-natural" standard supersymmetry benchmark model the NMSSM with sfermion mass terms generated at a relatively low scale $M \sim 100\,\mathrm{TeV}$. We will not assume flavour universality of the sfermion masses at the scale M, as that could lead to additional, indirect constraints on the stop masses. We will assume for the time being that R-parity is conserved.

The Higgs sector of the NMSSM includes one additional complex singlet scalar. The experimental opportunities offered by such an extended Higgs sector are richer than in the MSSM. They will be studied in Section 5.3.3, where a comparison of the potential of direct and indirect searches of CP-even scalars will be made.

Aside from the scalar sector, the collider phenomenology of our benchmark model is not drastically different than the MSSM one, the difference being mainly due to the presence of one extra neutralino and chargino (see Section 5.3.6.1). After reviewing in greater detail in Section 5.3.4 how their bounds translate into fine-tuning, we will then discuss in Section 5.3.5 the searches for sfermions, gauginos, and Higgsinos using standard supersymmetric signals in the context of simplified models. The two things together allow to assess the potential and motivation of future experiments in a currently representative supersymmetric scenario.

5.3.3 NMSSM Higgs sector: direct vs indirect searches

It is well known that the tree-level upper bound on the lightest Higgs boson in the MSSM, $m_h < m_Z$, can be lifted due to the top-stop correction to the Higgs quartic coupling, embodied in the Δ_t parameter

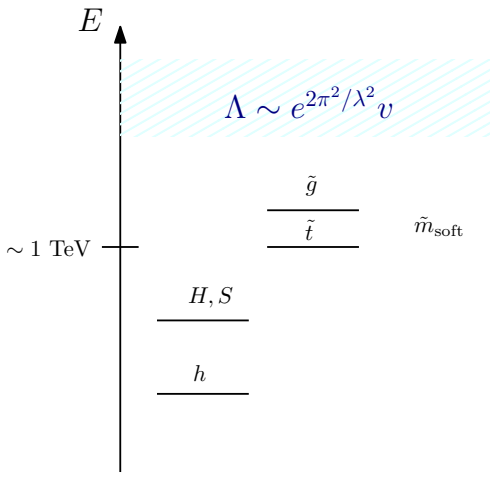

Fig. 30: Spectrum of the NMSSM scenario under consideration.

(see e.g. [286]),

$$m_h^2 \lesssim m_Z^2 c_{2\beta}^2 + \Delta_t^2. \tag{7}$$

However, the values of the stop masses needed to account for the measured Higgs mass are large enough to give rise to a significant fine-tuning (see Section 5.3.4). On the other hand, other contributions to the Higgs mass, besides the stop corrections, are possible, so that in their presence the stops are allowed to be lighter. The NMSSM is a paradigmatic example, in which a contribution to the Higgs quartic coupling is obtained at tree-level from the supersymmetric superpotential interaction

$$\mathcal{W} \supset \lambda S H_u H_d + f(S), \tag{8}$$

where S is a singlet superfield and $f(S)$ is a polynomial up to the third order in S. The Yukawa-like term contributes to the Higgs mass as

$$m_h^2 \lesssim \lambda^2 v^2 s_{2\beta}^2 + m_Z^2 c_{2\beta}^2 + \Delta_t^2. \tag{9}$$

The importance of the coupling λ is two-fold. First, it gives a large supersymmetric contribution to the Higgs mass (with a different dependence on $\tan\beta$ than the usual terms) that is sufficient to achieve 125 GeV at tree-level. Second, it modifies the dependence of the electro-weak vacuum expectation value (VEV) on the Lagrangian parameters, allowing for parametrically larger soft masses of stops and gluinos – by a factor of $\sim 2\lambda/g$ – than in the MSSM, for a given amount of tuning. While $\lambda \geq 1$ softens the tuning in the VEV, it increases the tuning in the Higgs mass as evident from (9). Moreover, the coupling is not asymptotically free and if $\lambda \gtrsim 0.7$ the theory undergoes a strong coupling regime at a scale lower than the GUT scale. We will consider both regimes in the following, as they both have been deeply studied in the literature.

5.3.3.1 Strategy

Aside from the fine-tuning issue, the NMSSM with a sizeable λ – which is the leading parameter also for phenomenology – opens the interesting possibility that the lightest new particles are the extra scalar bosons of its extended Higgs sector (with the possible exception of the LSP), see Fig. 30. These new degrees of freedom consist, in any particular NMSSM, of two extra CP-even neutral scalars, which we dub h_2 ("singlet-like") and h_3 ("doublet-like"), two CP-odd ones, A_1 and A_2, and the charged Higgs $H^\pm$.

This extended Higgs sector can be probed/constrained by means of two complementary approaches:

– Indirect searches: modification of the couplings of the 125 GeV Higgs boson.
– Direct searches: production and detection of the heavy scalars.

The phenomenology of the NMSSM is controlled by several parameters, so that its study is often performed via scans on some motivated ranges (see e.g. the recent [287] and [288]). In particular, [287] provides several benchmark points for which details of the phenomenology of *all* the new scalars at the 13 TeV LHC are given. While studies of this kind are certainly useful, they need the specification of a particular version of the NMSSM potential (i.e. the function $f(S)$ and all the soft terms). Also, they make it somehow difficult to compare the reaches of different searches or different models, given the proliferation of points and parameters. Here we prefer to keep a more general view, and to have at the same time an analytic understanding of the phenomenological properties of the extra Higgs bosons, focusing on the CP-even ones, in the spirit of [289, 290].

The physical eigenstates $h_{1,2,3}$ consist of an admixture of the states h, S, H, with $\langle h \rangle = v$; in particular $h_1 = c_\gamma(c_\delta h - s_\delta H) + s_\gamma S$ can be identified with the particle discovered at the LHC. Under the motivated assumptions of CP-conservation and negligible radiative corrections (apart from Δ_t), the CP-even scalar mass matrix in the basis (H, h, S) can be parametrized in full generality as

$$\mathcal{M}^2 = \begin{pmatrix} m_A^2 + s_{2\beta}^2(m_Z^2 - \lambda^2 v^2) + \frac{\Delta_t^2}{t_\beta^2} & \frac{s_{4\beta}}{2}(m_Z^2 - \lambda^2 v^2) - \frac{\Delta_t^2}{t_\beta} & \lambda v M_1 \\ \frac{s_{4\beta}}{2}(m_Z^2 - \lambda^2 v^2) - \frac{\Delta_t^2}{t_\beta} & m_Z^2 c_{2\beta}^2 + \lambda^2 v^2 c_{2\beta}^2 + \Delta_t^2 & \lambda v M_2 \\ \lambda v M_1 & \lambda v M_2 & M_3^2 \end{pmatrix} \tag{10}$$

where $v \simeq 174$ GeV, $m_A^2 = m_{H^\pm}^2 - \lambda^2 v^2$, and $M_{1,2,3}$ are parameters that depends on the supersymmetric and soft terms that involve the singlet S.

The actual expressions of the third column entries are almost irrelevant for the phenomenology of the CP-even Higgs bosons. As noted in [289], by diagonalization of the matrix (10) one can express the mixing angles δ, γ, σ among the three states as a function of the 6 independent parameters $m_{h_{2,3}}^2, m_{H^\pm}^2, \lambda, \tan\beta, \Delta_t$. This is crucial since it simplifies the study of the impact of the Higgs fit on the physical parameters, and it also keeps this study independent of the choice of a specific potential.

A fit of the Higgs signal strengths measured at the LHC results in the constraints displayed in Fig. 31, where the expected reach of LHC14 with 300 fb^{-1} is also displayed.

In the following, motivated by current Higgs coupling constraints, we choose to work in the simple limit where the second doublet H (or equivalently h_3) is completely decoupled. This turns out to be a good approximation of the full three-state mixing case when h_3 is reasonably heavier than $h_{1,2}$ (see Section 3 of [289]). The opposite situation, where the singlet-like state is decoupled, is more similar to the MSSM case, and has been discussed in [289].

The only relevant effect from the sparticles can safely be assumed to be the one of the top squark, with the possible exception of a light chargino contribution to $h_2 \to \gamma\gamma$. The model is then fully described by the following parameters:

– the mass of the singlet-like scalar m_{h_2},
– $\tan\beta$,
– the singlet-doublet coupling λ,
– the top-stop contribution to the Higgs potential Δ_t,
– the vacuum expectation value of the singlet v_S.

The vev v_S is the only parameter reminiscent of the explicit potential for the scalars, which we leave unspecified. However, while it plays an important role in all the triple couplings among Higgs bosons,

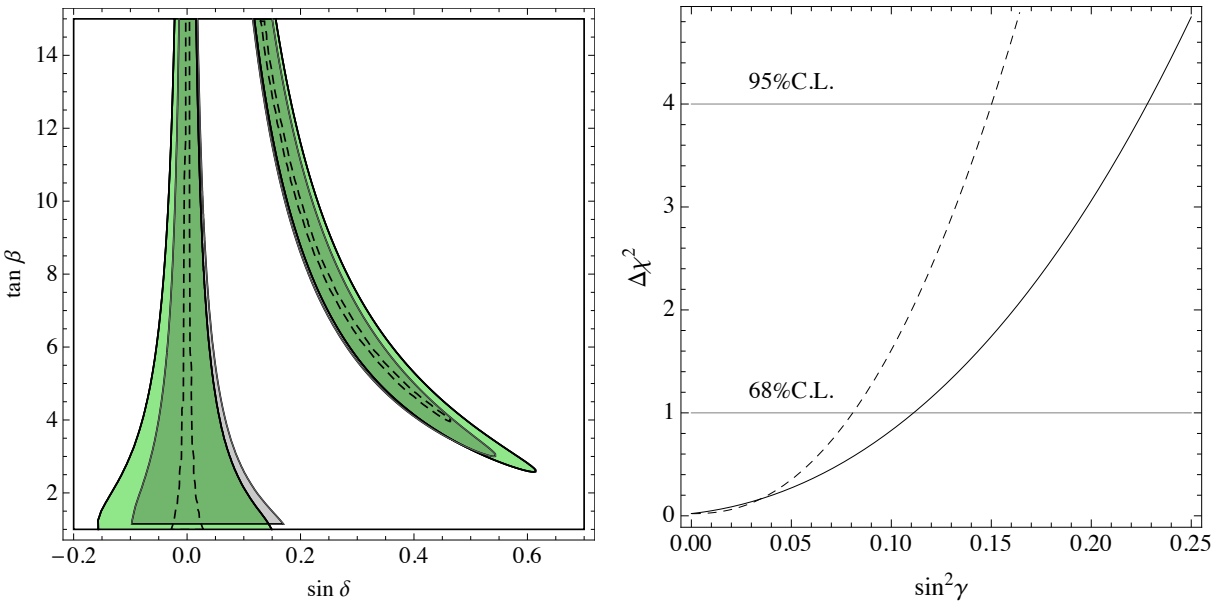

Fig. 31: Results of a fit to the Higgs signal strengths, for the angles δ and γ. Left: present constraints on s_δ for $s_\gamma^2 = 0$ (green) and $s_\gamma^2 = 0.15$ (grey), and projection at LHC14 for $s_\gamma^2 = 0$ (dashed). Right: present constraint (solid) and projection at LHC14 (dashed) on s_γ^2 for $s_\delta = 0$.

v_S does not influence deviations in the couplings of h_1 to fermions and vectors, nor the couplings of h_2 and h_3 to non-Higgs particles.

The mixing angle γ between the Higgs and the singlet is given by

$$\sin^2\gamma = \frac{m_Z^2\cos^2 2\beta + \lambda^2 v^2 \sin^2 2\beta + \Delta_t^2 - m_h^2}{m_{h_2}^2 - m_h^2}, \tag{11}$$

and is constrained to be $\sin^2\gamma < 0.23$ at 95% C.L. by a fit of the Higgs couplings. Notice that the above parameterisation is valid for any form of the NMSSM potential. As we are going to see, the small number of parameters in this limit allows us to compare the reaches of direct and indirect searches in a systematic way.

5.3.3.2 Current constraints and future reaches

We now discuss the current constraints on this picture, both from Higgs couplings measurements and from direct scalar searches at the LHC, together with the foreseen impact of the next runs at 14 TeV, for the benchmark luminosities of 300 fb^{-1} and 3 ab^{-1}. Concerning direct searches, we assume that there are no invisible decay channels of h_2, and that it is produced via gluon fusion (which actually dominates for $m_{h_2} \lesssim 1$ TeV , given the singlet-like nature of h_2). The explicit cross-sections and branching ratios of the Higgs states have been given in [289, 290] and we will not repeat them here.

In the following, we fix the value of Δ_t to 75 GeV, which is compatible with a lightest stop mass $m_{\tilde{t}} \simeq 700$ GeV or higher, and we take values of v_S of the order of v.[10] For each value of λ, the model is now completely described by m_{h_2} and $\tan\beta$, so that it is possible to visualise the relative phenomenology on a plane.

[10]For moderate values of $\Delta_t \lesssim 85$ GeV, motivated by naturalness, the results do not strongly depend on the actual value of Δ_t.

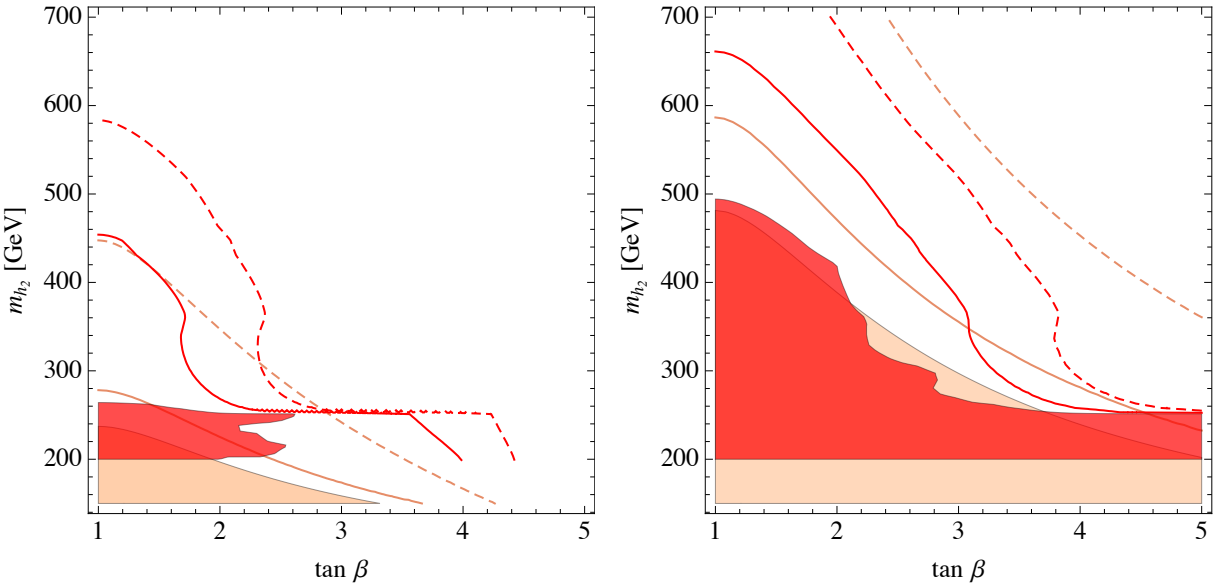

Fig. 32: Current and foreseen LHC reaches in the $h_2 \to ZZ$ channel for $\lambda = 0.8$ (left) and $\lambda = 1.4$ (right), and with $v_S = 2v$. The colored regions are excluded at 95% C.L., the solid (dashed) lines are the expected limits at LHC14 with 300 fb^{-1} (3 ab^{-1}).

The $h_2 \to ZZ$ channel

The dominant branching ratios of the heavy Higgs h_2 are into a pair of lighter Higgs particles – if kinematically allowed – and into vector bosons, WW or ZZ [289]. The ZZ channel, in particular, plays a dominant role because of the good experimental sensitivity.

In Fig. 32 we show in a single plot the current bounds (LHC8) and the foreseen LHC reaches with 300 fb^{-1} of luminosity (LHC14), for the two cases $\lambda = 0.8$ and $\lambda = 1.4$, and with $v_S = 2v$:

- LHC8: the colored regions are excluded at 95% C.L. The shaded orange region is excluded by the fit of the Higgs signal strengths ($\sin^2\gamma < 0.23$); the red region is excluded by CMS searches of a heavy scalar h_2 decaying into ZZ [291].
- LHC14: the colored solid (dashed) lines show the expected exclusions at 95% C.L. with 300 fb^{-1} (3 ab^{-1}). The orange lines are the foreseen reaches of the Higgs fit, assuming central values for the Higgs signal strengths like in the SM, with the projected uncertainties of [264,292]; the dashed red lines are the expected exclusions of a $h_2 \to ZZ$ search, taken from figure 7 of [293].

Triple Higgs coupling and $h_2 \to h_1 h_1$

Deviations in the Higgs-self couplings, as well as the partial width $\Gamma(h_2 \to h_1 h_1)$ are controlled also by v_S. Among the $h_2 \to h_1 h_1$ searches, the only one currently relevant is the one recently published by CMS [294] for $hh(\to b\bar{b}\gamma\gamma)$ (see also the ATLAS results [295]). As can be seen from the purple region in Fig. 33, it is relevant only for $\lambda = 1.4$, and in any case it is superseded by the Higgs fit and by the $h_2 \to ZZ$ searches for moderate values of v_S. Concerning future reaches, the only detailed study performed so far is the one for $hh \to 4b$ at the LHC14 [296], and its result is also shown in Fig. 33. Current searches in $hh \to 4b$ are not shown since they are not yet sensitive. Notice that the search in the $b\bar{b}\gamma\gamma$ channel, which still lacks a detailed analysis for LHC14, is expected to be more sensitive also in the future. However, performing a detailed study of its future reach goes beyond the purpose of this note.

From the point of view of indirect searches, it is interesting that large deviations from the SM value are possible in the triple Higgs coupling $g_{h_1^3}$, as shown in [289] and confirmed in a particular

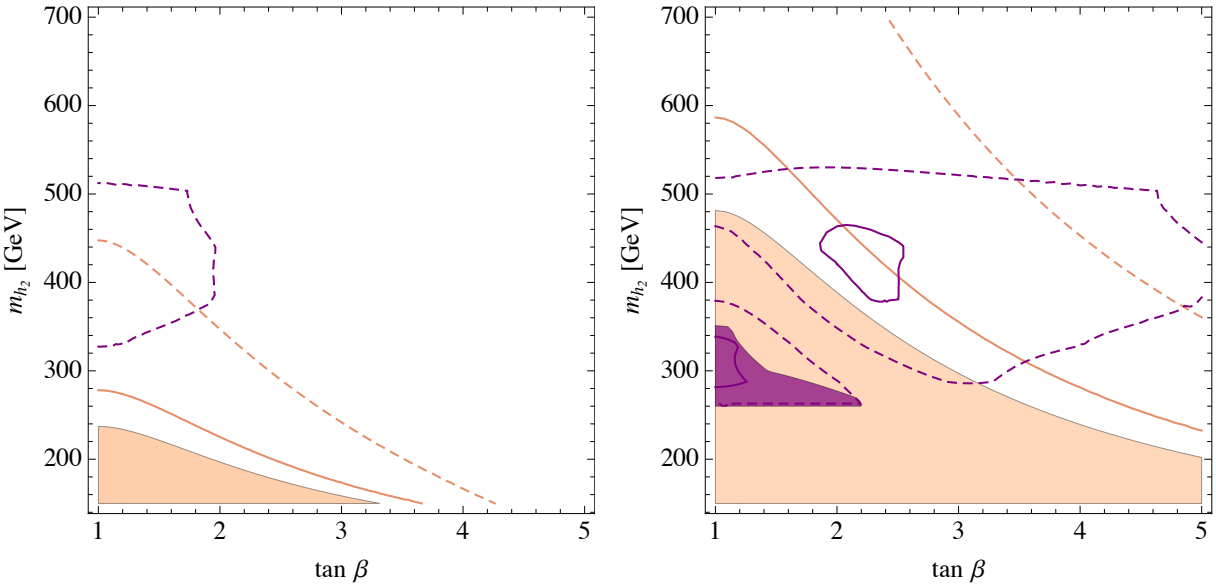

Fig. 33: Current and foreseen LHC reaches in the $h_2 \to h_1 h_1$ channels, for $\lambda = 0.8$ in the large v_S limit (left), and for $\lambda = 1.4$ and $v_S = 2v$ (right). The colored regions are excluded at 95% C.L., the solid (dashed) lines are the expected limits at LHC14 with 300 fb^{-1} (3 ab^{-1}). Purple corresponds to the indirect searches, while beige shows the limits for direct searches. The present direct exclusions come from the $b\bar{b}\gamma\gamma$ channel, while the projections are from the $b\bar{b}b\bar{b}$ channel.

model by [288], and contrary for example to the MSSM case. To illustrate this, we show in Fig. 34 the ratio $g_{h_1^3}/g_{h^3}^{\rm SM}$ [289]. The HL-LHC could probe the trilinear Higgs coupling at the indicative precision of 50% (see Section 1.3 of the report [46]), thus providing a powerful way of exploring the parameter space of our framework.

A singlet-like boson lighter than 125 GeV

The case $m_{h_2} < m_{h_{\rm LHC}}$ is still allowed by current constraints, and we believe an experimental effort is necessary to exclude such a possibility. The LEP direct searches play an important role in excluding some regions, however they are not sufficient to exclude a light h_2, as can be seen from Fig. 35.

The future reach of the HL-LHC looks capable of covering a relevant part of the allowed regions by means of Higgs couplings measurements. Direct searches appear to be challenging, although a new singlet-like scalar could be detectable in the $\gamma\gamma$ channel, for some particular values of the parameters [297]. We show in Fig. 35 the signal strength for $h_2 \to \gamma\gamma$ normalised to the one of a SM Higgs boson of the same mass, in a particular scenario with all three mixing angles non-zero. Such figures also provide an example of how our analytic approach can be used in the case where none of the Higgs bosons are decoupled.

5.3.3.3 Conclusions

Overall, keeping in mind the various simplifications of our approach, we have shown that natural extensions of the MSSM, such as the NMSSM with largish λ under consideration, can provide interesting signatures at the LHC14.

In particular we discussed how the LHC8 data constrain the scenario of a singlet-like CP-even scalar coupled to the SM Higgs boson. From the measurement of the Higgs signal strengths we cannot derive strong bounds on the picture. This leads to consider direct searches as an alternative to probe the unconstrained parameter space. Indeed we showed that direct searches for extra Higgs bosons can

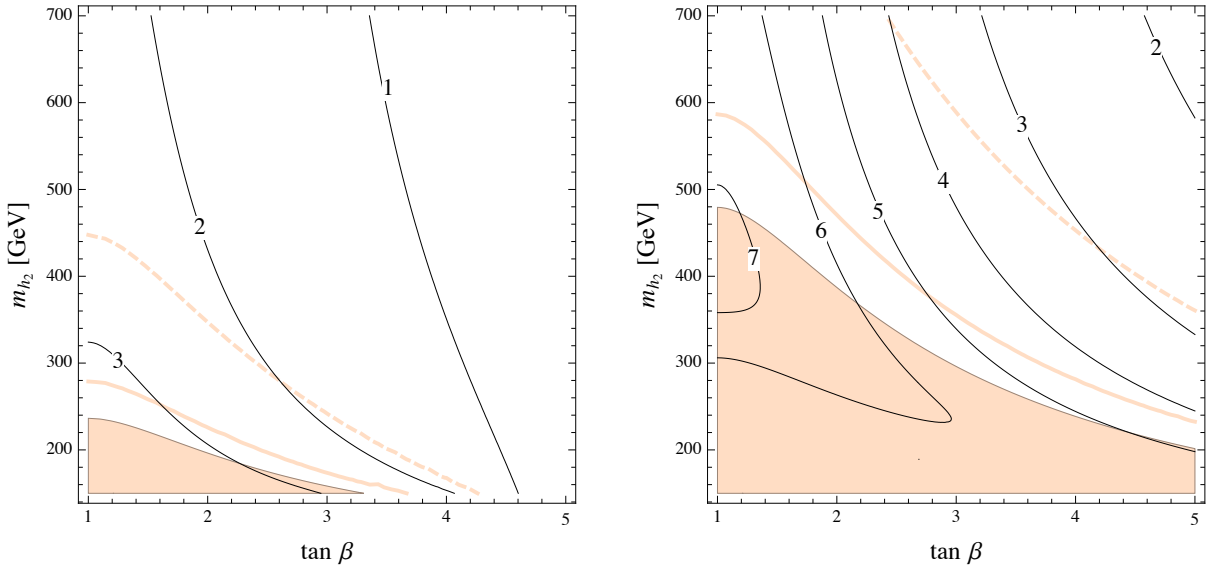

Fig. 34: Isolines of $g_{h_1^3}/g_{h^3}^{\rm SM}$. Left: $\lambda = 0.8$ and $v_S = 2v$. Right: $\lambda = 1.4$ and $v_S = v$. The coloured region is excluded at 95%C.L., the coloured solid (dashed) lines are the expected limits at LHC14 with 300 fb^{-1} (3 ab^{-1}).

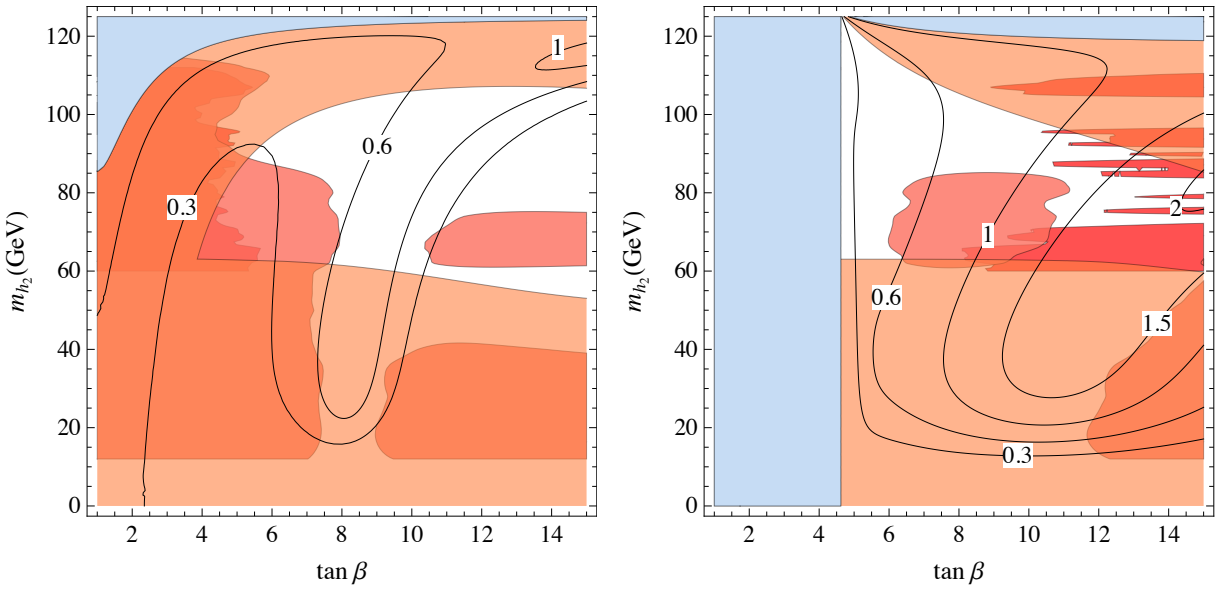

Fig. 35: Fully mixed situation with a light singlet. Isolines of the signal strength of $h_2 \to \gamma\gamma$ normalized to the SM. We take $m_{h_3} = 500$ GeV, $s_\sigma^2 = 0.001$ and $v_s = v$. Left: $\lambda = 0.1$, $\Delta_t = 85$ GeV. Right: $\lambda = 0.8$, $\Delta_t = 75$ GeV. The orange region is excluded by the Higgs fit, and the blue region is unphysical. The red and dark red regions are excluded by LEP direct searches for $h_2 \to b\bar{b}$ and $h_2 \to$ hadrons, respectively.

already set limits competitive with the Higgs coupling fit. In particular we emphasized the role of the reinterpretation of searches for a SM Higgs boson at high mass, in the $ZZ \to 4\ell$ channel. We also presented some projections of the 95% CL exclusion reach attainable at the LHC14 with 300/fb and 3000/fb, showing that direct searches for $h_2 \to VV$ will play a prominent role.

Another possible signature of this scenario is the hh channel. Current data on $hh \to \gamma\gamma b\bar{b}, b\bar{b}b\bar{b}$ are not sensitive yet to the interesting region, however when available we presented some projections for the next runs of the LHC. They turn out to be hardly competitive with $h_2 \to ZZ$ or Higgs coupling measurements, except in some corners of the parameter space. However, to better assess the potential of the hh channel, further studies of the future sensitivities are needed. Among indirect searches, the expected sensitivity of the HL-LHC to the trilinear Higgs coupling makes it, at such a collider, one of the strongest probes of this scenario.

We remark that the case of another singlet-like scalar lighter than 125 GeV is not yet excluded, and that a larger experimental effort should be dedicated to directly probe this possibility, already with the LHC8 dataset.

Finally, in case of a positive signal, direct or indirect, it may be important to try to interpret it in a fully mixed scheme, involving all the three CP-even states. To this end the analytic relations of the mixing angles to the physical masses given in [289, 290] offer a useful tool, as shown in the explicit example of a $h_2 \to \gamma\gamma$ signal in Fig. 35.

5.3.4 Fine tuning and the scale of supersymmetric particles

As anticipated, an estimate of the scale of supersymmetric particles, stops, gluinos and Higgsinos in particular, is needed in order to assess the significance of the present experimental bounds and the motivation of further searches. The estimate is based on the naturalness argument: the scale of supersymmetric particles (new physics in general) should not lead to fine-tuned, accidental cancellations in the determination of the Higgs mass. While the upper bound on the scale of new particles this argument sets depends on the amount of cancellation considered palatable, and is therefore to some extent subjective, the cancellation needed (if any) can definitely be precisely quantified, as we now briefly recall.

Let us consider the case of the a supersymmetric extension of the SM with the supersymmetry breaking mass terms originating at a scale $M \sim 100\,\mathrm{TeV}$. Let us also consider, for illustrative purposes, a (decoupling) limit in which a linear combination H of the two Higgs doublets H_u and H_d plays the role of the SM Higgs doublet, with a potential

$$V = m^2 H^2 + \lambda_H H^4, \tag{12}$$

and the VEVs of the two doublets are somewhat hierarchical, $v_u > v_d$. Then the SM-like Higgs mass is $m_H^2 \approx -2m^2$ and one has

$$\begin{aligned} m^2 &\approx |\mu^2| + m_{H_u}^2 = \\ &= |\mu^2| + m_{H_u}^2\big|_{\text{tree}} + \delta m_{H_u}^2\big|_{\text{loop}}\,, \end{aligned} \tag{13}$$

where μ is the (supersymmetric) mass term for the Higgsinos and $m_{H_u}^2$ is a (supersymmetry breaking) mass term for the H_u doublet. We have split $m_{H_u}^2$ in two contributions: $m_{H_u}^2\big|_{tree}$, which originates at the scale M, and $\delta m_{H_u}^2\big|_{\text{loop}}$, which arises due to renormalization group effects that intertwine $m_{H_u}^2$ to the other MSSM mass terms.

The terms in eq. (13) have different physical origin. In particular, the parameter μ is allowed by supersymmetry, whereas $m_{H_u}^2$ has to do with its breaking. In turn the tree level part of $m_{H_u}^2$ is fully controlled by the supersymmetry breaking and mediation mechanism. On the other hand, the loop contribution is largely driven by the gauge and Yukawa interactions of the MSSM and by other supersymmetry breaking masses. Given the very different nature of the contributions to m^2 in eq.(13),

the simple and natural way to obtain a realistic $m^2 \sim m_H^2/2$ is that *each* of the three terms be at most of order $m_H^2/2$. If one or more of them is much larger than $m_H^2/2$, eq.(13) implies a cancellation between at least two of them, so that the sum of the two terms is (much) smaller than each of the two. While this is not at all impossible, such a tight correlation among terms with different physical origin is considered unlikely and the model is said to be *fine-tuned* [298, 299].

The degree of tuning can be quantified by comparing the physical value of m^2 to the size of each of the contributions δm^2 entering its determination,

$$\Delta \equiv \frac{\delta m^2}{m^2} \,. \tag{14}$$

where δm^2 represents any of the contributions in eq. (13), for instance $\delta m_{H_u}|_{loop}$. A value $\Delta \lesssim 1$ corresponds to the absence of tuning. If instead, as it typically happens, $\delta m^2 \gg m^2$, then the determination of m^2 requires a cancellation of 1 part in Δ. For a given maximum value of Δ one is willing to tolerate, it is then possible to set an upper bound on the parameters entering eq. (13) and to the corresponding sparticle mass. For example in the case of the μ parameter, tightly related to the Higgsino masses, one has

$$\mu \leq 0.3\,\text{TeV} \cdot \left(\frac{\Delta}{10}\right)^{1/2} \,. \tag{15}$$

The radiative contribution $\delta m^2_{H_u}\big|_{\text{loop}}$ is dominated by loops of top squarks

$$\delta m^2_{H_u}\big|_{\text{stop}} \simeq -\frac{3y_t^2}{8\pi^2}\left(m^2_{Q_3} + m^2_{U_3} + |A_t|^2\right) \ln\left(\frac{M}{\text{TeV}}\right) \,, \tag{16}$$

where m_{Q_3}, m_{U_3} and A_t are supersymmetry-breaking parameters of the top squark sector. This allows to correlate those parameters, and thus the sum of the stop masses $m^2_{t_1} + m^2_{t_2} \approx m^2_{Q_3} + m^2_{U_3}$ to the fine-tuning Δ and to get the bound

$$\sqrt{m^2_{t_1} + m^2_{t_2}} \lesssim \frac{0.8\,\text{TeV}}{\sqrt{1+x^2}} \left(\frac{\Delta}{10}\right)^{1/2} \left(\frac{2}{\log_{10}(M/\,\text{TeV})}\right)^{1/2} \,, \tag{17}$$

where $x = A_t/\sqrt{m^2_{t_1} + m^2_{t_2}}$ is usually order unity and we have taken $\sin\beta = 1$. Note that the bound is less stringent for low scales of supersymmetry breaking mediation [300], as anticipated by eq. (5), which indeed for $x = 0$, $m_{\text{NP}} = \sqrt{m^2_{t_1} + m^2_{t_2}}$ approximately reproduces eq. (17). Similarly one can analyze the two loop contribution of the gluino mass M_3 and derive another limit from

$$\delta m^2_{H_u}\big|_{\text{gluino}} \simeq -\frac{y_t^2}{\pi^2}\left(\frac{\alpha_s}{\pi}\right)|M_3|^2 \ln^2\left(\frac{M}{\text{TeV}}\right) \,, \tag{18}$$

which implies

$$M_3 \lesssim 1.5\,\text{TeV} \cdot \left(\frac{\Delta}{10}\right)^{1/2} \left(\frac{2}{\log_{10}(M/\,\text{TeV})}\right) \,. \tag{19}$$

Eqs. (16,18) have been obtained by solving the corresponding RGEs in the leading log approximation. The resummation is actually important and has been taken into account in the numerical values quoted in eqs. (17,19). A more precise computation of the fine-tuning using the exact solution of the 1-loop RGEs is shown in the left panel of Fig. 36 in the stop/gluino mass plane, together with the indicative reach of future accelerator experiments. The plot shows that present data put a relatively weak pressure on the quasi-natural model we consider and shows that future searches can cover a relevant region of the fine-tuning space. There are two main reasons why the tension with data is loosened. The first is due

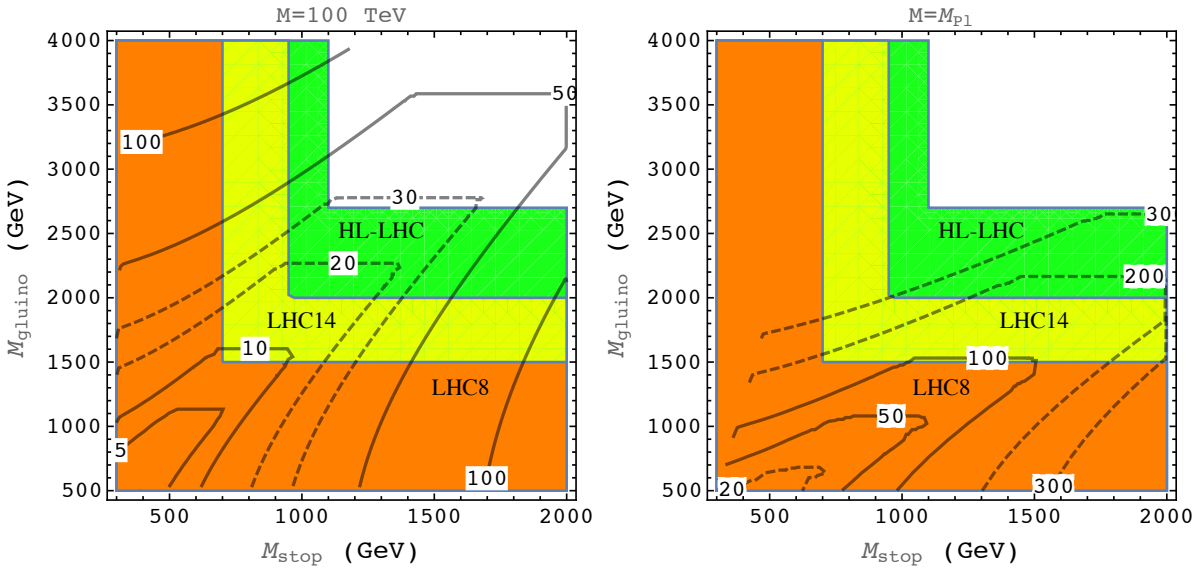

Fig. 36: Left panel: contour lines of fine-tuning in the stop/gluino mass plane for our benchmark supersymmetric scenario and indicative reach of future accelerator experiments. Right panel: example of fine-tuning in a supergravity scenario with soft terms generated at the Planck scale.

to the lower origin of the supersymmetry breaking terms, here chosen to be $M = 100\,\text{TeV}$. The impact on fine-tuning, encoded in eqs. (17,19), is apparent from the comparison with a typical supergravity model, right panel of Fig. 36, in which the supersymmetry breaking terms originate at the Planck scale, $M = M_{\text{Pl}}$. The second reason why the tension is loosened is that the presence of the extra NMSSM singlet loosens the indirect lower bound on the stop masses set by the Higgs mass measurement, as discussed in Section 5.3.3. In the MSSM, where no extra singlet can help with the Higgs mass, stops are forced, in the best case scenario (large A-terms), to be above about $1.5\,\text{TeV}$. Such an indirect bound would rule out a large part of the parameter space in Fig. 36 (both panels), hence implying a larger tension with present data. And it would of course rule out part of the parameter space accessible at future accelerators.

Let us discuss in greater detail and quantify the effect of evading the indirect bound on the Higgs mass. If the indirect limit can be evaded, the bound on the lightest stop mass is given by direct searches, $m_{\tilde{t}_1} \gtrsim 700\,\text{GeV}$ in its most stringent form (see below Section 5.3.5). Comparing with the qualitative estimate in eq. (17), we see that this corresponds to a fine-tuning of about $\Delta \gtrsim 15$ (for $M = 100\,\text{TeV}$). On the other hand, if the extra NMSSM singlet did not come to rescue, the Higgs mass measurement would require stops as heavy as $10\,\text{TeV}$ [301] for vanishing stop mixing, corresponding to a fine-tuning $\Delta \gtrsim 3 \cdot 10^3$, and as heavy as $1.5\,\text{TeV}$ [301] in the best case scenario with optimised stop mixing, corresponding to a fine-tuning $\Delta \gtrsim 70$. While stop mixing helps, the fine-tuning is much worse than what actually required by the stop direct experimental searches.

One can wonder if the presence of an extra scalar singlet in the NMSSM could modify the expression we used to quantify fine-tuning, eq. (14) [302]. In first approximation, this is not the case. In order to appreciate that, let us consider again a decoupling limit in which only a SM-like Higgs remains light, with the potential in eq. (12). In first approximation, the parameters of the potential are given by

$$\lambda_H = \frac{g^2 + g'^2}{8} \cos^2 2\beta + \frac{\lambda^2}{4} \sin^2 2\beta + \text{rad. corr.} \tag{20}$$

$$m^2 = m_{H_u}^2 \sin^2\beta + m_{H_d}^2 \cos^2\beta + |\mu|^2, \tag{21}$$

where λ is the coupling appearing in the NMSSM superpotential term $\lambda S H_u H_d$ (see Section 5.3.3). In

the MSSM, the same expressions hold with $\lambda = 0$. The two above equations are related to different aspects of the fine-tuning problem. The first equation determines the indirect bound on the stop masses. That is where the extra singlet plays a role, providing the extra term proportional to λ^2. The second equation determines the fine-tuning for given values of the stop and other sparticle masses (which enter for example through the radiative corrections to $m^2_{H_u}$). The extra singlet does not play a direct role in this equation, in the decoupling limit we are considering. As a consequence, the fine-tuning associated to the large radiative corrections $\delta m^2_{H_u}$ to $m^2_{H_u}$ is again given by

$$\Delta = \frac{\delta m^2_{H_u}}{m^2} \sin^2 \beta, \tag{22}$$

as in eq. (14), where we had set $\sin \beta = 1$. Here, however, the presence of the extra λ^2 term allows to avoid the need of sizeable radiative corrections $\propto \log m_{\tilde{t}}$ in eq. (20), which in turn allows to reduce the fine-tuning associated to the stop mass, $\delta m^2_{H_u} \propto m^2_{\tilde{t}}$, in eq. (22).

As explained, the indirect bound on the stop mass is evaded due to the λ^2 contribution in eq. (20). In order for that to be sizeable enough, we need λ not to be too small and $\tan \beta$ not to be too large. The required value of λ_H, $\lambda_H = m^2_H/(2v^2) \approx 0.13$ (about twice as large as the MSSM upper bound $(g^2 + g'^2)/8$), can be obtained at the tree level, without the need of any top-stop radiative corrections, for $\lambda \lesssim 1$ and $\tan \beta \sim$ 3–4. The extra singlet contribution in eq. (20) can even be larger than needed, for $\lambda > 1$ and moderate $\tan \beta$. This is unnecessary and unwelcome. The value of λ_H given by eq. (20) would be too large and a cancellation with extra corrections that become relevant when we depart from the decoupling limit we considered would be needed, possibly leading to extra fine-tuning [303]. Moreover, large values of $\tan \beta$ and λ may spoil the agreement of the electroweak precision tests with the NMSSM predictions [304].

In what above we focused on the stop contribution to fine-tuning. Gluinos also play an important role, as shown by equations (18,19) and in Fig. 36. The role of gluinos in the fine-tuning problem is in first approximation the same in the MSSM and in the NMSSM. On the other hand, lowering the scale M has a particularly strong impact, as the radiative contribution of gluinos to the Higgs squared mass is quadratic (not just linear) in $\log M$. A possible way to further relax the impact of gluino bounds on fine-tuning is provided by the possibility that gluinos be Dirac fermions [305]. The naturalness bound on Higgsinos does not depend (in first approximation) neither on having an extra singlet nor on the position of the messenger scale M, and is given in eq. (15).

5.3.5 Standard SUSY signals at hadron colliders

5.3.5.1 R-parity, dark matter, and missing energy

The simple requirement that the supersymmetric extension of the Standard Model is invariant under supersymmetry and gauge transformations allows in principle lepton and baryon number violating superpotential interactions,

$$W_{\rm RPV} = \lambda''_{ijk} u^c_i d^c_j d^c_k + \lambda'_{ijk} L_i Q_j d_k + \lambda_{ijk} L_i L_j e_k + \mu_i L_i H_u \,, \tag{23}$$

which go under the name of R-parity violating (RPV) interactions. Baryon and lepton number are accidental symmetries of the Standard Model and are measured to be conserved to very high accuracy, which implies very strong experimental bounds on the RPV couplings [306]. In order to avoid these stringent bounds these interactions are set to zero in the MSSM and its extensions. This is achieved by imposing a discrete symmetry, the R-parity, under which all the SM matter fields are even, whereas the supersymmetric partners are odd. Such a symmetry forces $W_{\rm RPV} = 0$ and makes baryon and lepton number accidental symmetries in supersymmetry as well.

One of the most relevant consequences of this symmetry is that the supersymmetric particles get a distinctive conserved quantum number, whose conservation prevents the Lightest Supersymmetric

Particle (LSP) from decaying into lighter Standard Model states, and hence makes it a stable particle. The LSP is often a gaugino, a Higgsino, or a sneutrino, as renormalization group effects tend to make the rest of the superpartners somewhat heavier due to their stronger gauge interactions. This means that a Weakly Interacting Massive Particle is likely to be the Lightest Supersymmetric Particle and, if R-Parity is an exact symmetry, to also be stable, which makes it an excellent candidate for thermal relic Dark Matter [307]. In the following we will generically denote such a particle as χ.

The presence of R-parity has also important consequences for collider searches, as it gives rise to the prototypical supersymmetry signal: missing energy. The decay of any supersymmetric particle produced must in fact give rise to at least one χ in the final state of a (possibly multi-step) decay chain. Furthermore, an even number of superpartners must be produced. These two facts are very consequential for the signal that we expect to observe from the productions of supersymmetric particles. The two χ will leave no trace in the detector, their momentum will not be measured, and an apparent imbalance of momentum will arise. That's why the generic signal of supersymmetry searched for at the LHC is in the form

$$pp \to jets + leptons + photons + \text{mET}\,. \tag{24}$$

where mET is the result of the missing momentum carried away by the weakly interacting particles χ.

Signals of this type are quite spectacular and relatively easy to identify over the Standard Model backgrounds. As a matter of fact the production of signals of this type in the Standard Model is quite rare, because the only source of mET are the neutrinos. Neutrinos can be produced at the LHC in QCD events in the decay of hadrons and in particular of heavy quarks b and t. However the mET generated in this way is typically only up to few hundreds of GeV, which is the typical overall mass scale of Standard Model processes. On the other hand supersymmetric particles are expected to have masses up to about 1 TeV and their decay would generically result in large mET $\gtrsim 100\,\mathrm{GeV}$, well observable above the SM background. In this subsection we present the current limits obtained from such standard searches at LHC Run-1, and the expected limits at the next run of the LHC and at future colliders. As we will see, there is a great potential to improve the current bounds. We also highlight the blind spots where current searches are giving weaker bounds and some discussion of the reach in these blind spots. The present and future limits will be presented in the context of "simplified" models, where only a limited number of supersymmetric particles is assumed to be involved in the analysis. While such analyses are certainly oversimplified when more degrees of freedom can take part to the relevant process, they still provide a simple and practical way to estimate the limits and allow an understanding of the relevant features of the searches.

5.3.5.2 Extrapolation of bounds on sparticles masses at hadronic machines up to 100 TeV

The results of the searches for supersymmetry at LHC 7 and 8 TeV runs and their connection to models of supersymmetry and dark matter have been the subject of several reviews [308–310]. Here we try to complement the statement of the current status with the available extrapolations to higher luminosity and higher energy colliders up to 100 TeV and few $1/ab$. In particular, we aim at giving an estimate of the mass reach and of the fine-tuning implications that follow from the discussion in Section 5.3.4.

The extrapolation of the bounds on sparticle masses at higher energy hadronic machines can be performed as described in Ref. [259]. In the absence of new backgrounds or dramatic changes in the signal definition, the reach of future hadron colliders can be estimated using the background yields of current searches by rescaling the parton luminosities for the initial state $(gg, qq, q\bar{q}, gq, ...)$ and the geometrical factors that enter in the hard cross-section for the scattering process that produces new heavy states. Ref. [311] provides a quick web-based computation of these *rescaled* collider reaches.

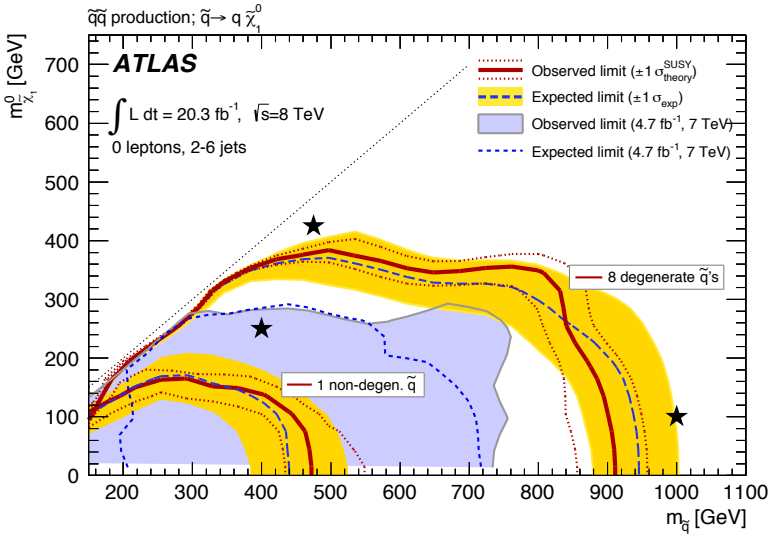

Fig. 37: LHC run 1 bounds [312] on the squark-χ simplified model.

5.3.5.3 squark-LSP

We now discuss the different experimental bounds and projections in the context of simplified models. In the squark-LSP simplified model only χ and a number of squark flavours are light enough to be produced at the given collider.

BSM particles	production	Decay
$\tilde{q} = \{\tilde{u}_{L,R}, \tilde{d}_{L,R}, \tilde{s}_{L,R}, \tilde{c}_{L,R}\}, \chi$	$pp \to \tilde{q}\tilde{q}^*$	$\tilde{q} \to q\chi$

The present bounds from Ref. [312] are shown in Fig. 37, which excludes a single flavour of squark in a region of mass that extends up to about 400 GeV for a massless χ. When more flavours are added the bounds get tighter and squark masses up to 900 GeV for a massless χ are excluded for 8 squark flavours (u, d, c, s flavours for both SU(2) singlets and doublets). It is important to stress that these bounds are usually weaker when χ becomes heavier. This is, as explained above, due to the fact that the energy stored in the mass of the primary supersymmetric particle, the squark in this case, is not released into decay product momenta, but into their masses, which, unlike momentum, does not get transferred to the detector. The softening of the final state momenta reduces the ability of discriminating the production of squarks from ordinary Standard Model scattering, and this is why the curve for a single flavour of squarks does not exclude regions where $m_{\tilde{q}} - m_\chi \lesssim 50\,\text{GeV}$. We remark that increasing the signal-cross-section by considering more squark species, the bound reaches the kinematic boundary $m_{\tilde{q}} = m_\chi$, at least for relatively small squark masses, signifying that the search strategy is suitable to cover the case of compressed spectra, provided that enough signal rate is available.

Ref. [313] has studied the reach of future machines for this simplified model. The result is reported in Fig. 38, which shows an exclusion up to 8 TeV squark masses for 3/ab at a 100 TeV pp collider. This is roughly a factor of 10 larger excluded mass than the current bounds from Run 1 of the LHC. The implication of such improved bounds for the fine-tuning of the theory, in light of the estimates given in 5.3.4, would be dramatic. Roughly speaking, the fine-tuning grows with the squared of the mass reach, which means that a improvement by a factor 10 in the mass reach corresponds to an improvement by a factor 100 in the fine-tuning.

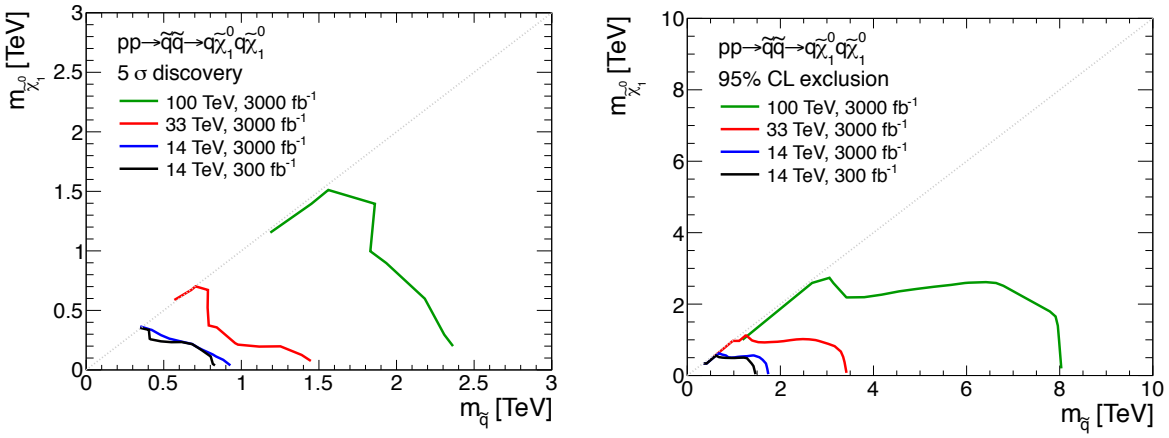

Fig. 38: Expected 5σ discovery (left) and 95%CL exclusion (right) reach for the squark-χ model for 8 squark species at future machines [313].

5.3.5.4 gluino-LSP

In this simplified model, also inspired by split-supersymmetry scenarios (see Section 5.3.8 below), only the χ and a the gluino are light enough to be produced at the given collider.

BSM particles	production	Decay
$\tilde{g}, \chi$	$pp \to \tilde{g}\tilde{g}$	$\tilde{g} \to \bar{q}q\chi$

The same search Ref. [312] considered above for the squark-χ simplified model can be used here. Limits are are shown in Fig. 39 and a gluino of mass 1.3 TeV is excluded for a massless χ. Increasing the mass of χ loosens the bound on the gluino. Coverage of the entire available m_χ range available for each $m_{\tilde{g}}$ is possible for gluino masses up to 600 GeV. The reach at future colliders up to a 100 TeV pp collider has been studied in Ref. [313]. Their result is reported in Fig. 40. In this case as well the reach is increased by a factor about 10 compared to the present bounds from LHC Run 1. The maximal mass that can be excluded at a 100 TeV collider at 95% CL is around 13 TeV.

For this simplified model Ref. [313] has also studied the impact on their estimated reach of changes in the search strategy, systematic uncertainties and effect of pile-up. The effect of pile-up has been found to be small and can be neglected. For the search strategy they find that using different optimization criteria for the event selection, for instance putting more or less importance on mET, the search discovery reach changes by about 5% in mass.

The effects of systematic uncertainties has been evaluated and, even in worse case scenario of 30% systematic uncertainties on backgrounds rates, they find that the mass reach drops only about 10% compared to the nominal result that they quote (which is for a conservative 20% systematic uncertainty). The issue of systematic uncertainties is particularly acute when the gluino becomes degenerate with the LSP. Ref. [313] has performed a dedicated study of the compressed region of this simplified model and they find that a model with a degenerate gluino and neutralino could be discovered up to about 600 GeV (1.1 TeV) for 30% (5%) systematic uncertainty.

5.3.5.5 gluino-squark-LSP

In this case both squarks (of the first two families) and gluinos can be produced and the experimental phenomenology is richer than in the previous two simplified models. Cross-sections are significantly larger due to the presence of several production modes including mixed gluino-squark production.

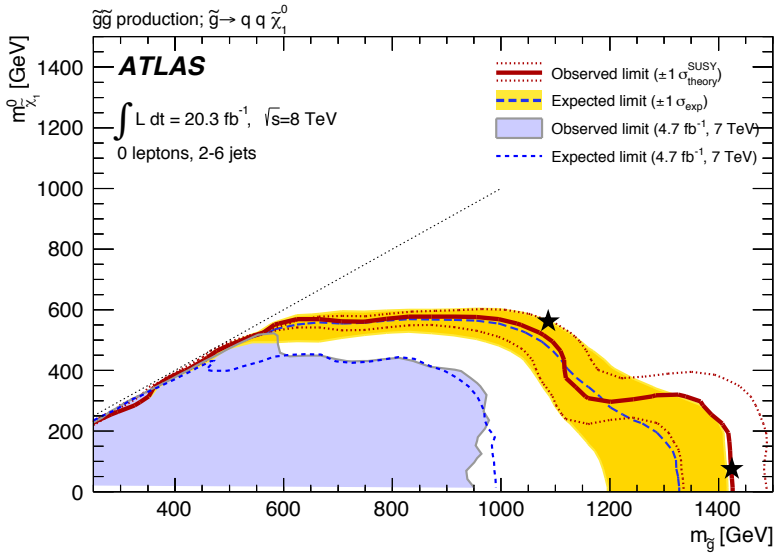

Fig. 39: LHC run 1 bounds [312] on the gluino-χ simplified model.

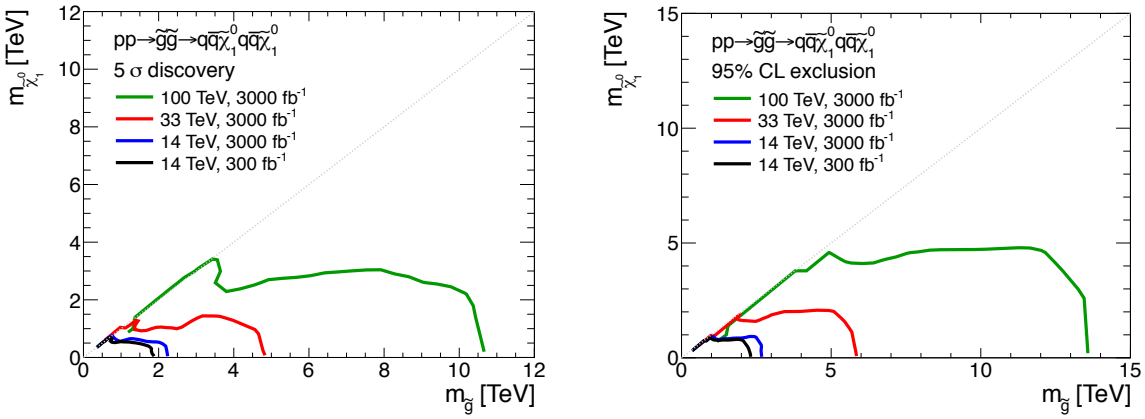

Fig. 40: Expected 5σ discovery (left) and 95%CL exclusion (right) reach for the gluino-χ model for 8 squark species at future machines [313].

BSM particles	production	Decay
$\tilde{g}, \tilde{q}, \chi$	$pp \to \tilde{g}\tilde{g}, \tilde{q}\bar{\tilde{q}}^*, \tilde{q}\tilde{q}, \tilde{q}\tilde{g}, \tilde{q}^*\tilde{g}$	$\tilde{q} \to q\chi$ $\tilde{g} \to \bar{q}q\chi$

The decay of the heavier between the gluino and the squark may proceed through a 2-body decay into the lightest of the two, for instance $\tilde{g} \to q\tilde{q}$ followed by $\tilde{q} \to q\chi$ or $\tilde{q} \to \tilde{g}q$ followed by $\tilde{g} \to q\bar{q}\chi$. In Fig. 41 we show the bounds obtained in Ref. [312]. The excluded gluino mass for massless χ is 1.3 TeV for decoupled squarks. These results depend on the mass of χ, but even for a mass as large as 700 GeV the bounds remain strong in the $m_{\tilde{g}} \sim m_{\tilde{q}}$ region.

Ref. [313] has studied the reach for this simplified model of future colliders up to a 100 TeV pp collider. The result is reported in Fig. 42, which shows a minimum exclusion above 15 TeV for both $m_{\tilde{q}}$ and $m_{\tilde{g}}$. The reach of a 100 TeV pp collider would in this case, as well as in the others shown in the previous sections, extend the reach in mass by a factor 10, which implies an improvement of a factor 100 in the level of fine-tuning probed.

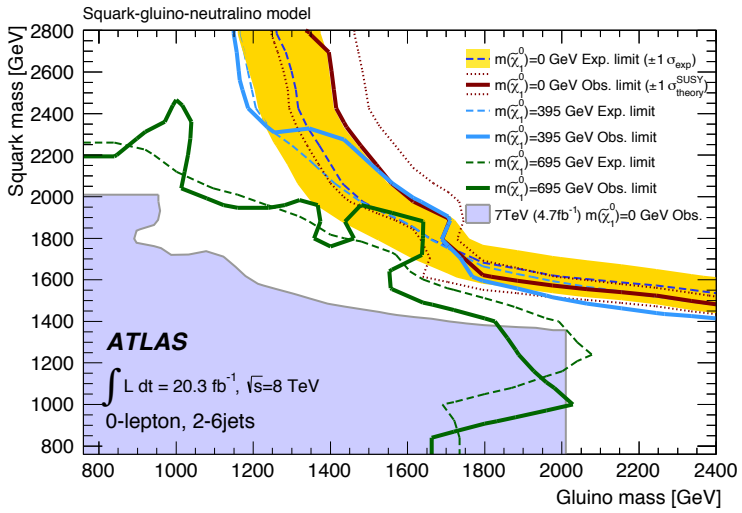

Fig. 41: LHC run 1 bounds [312] on the gluino-squark-χ simplified model.

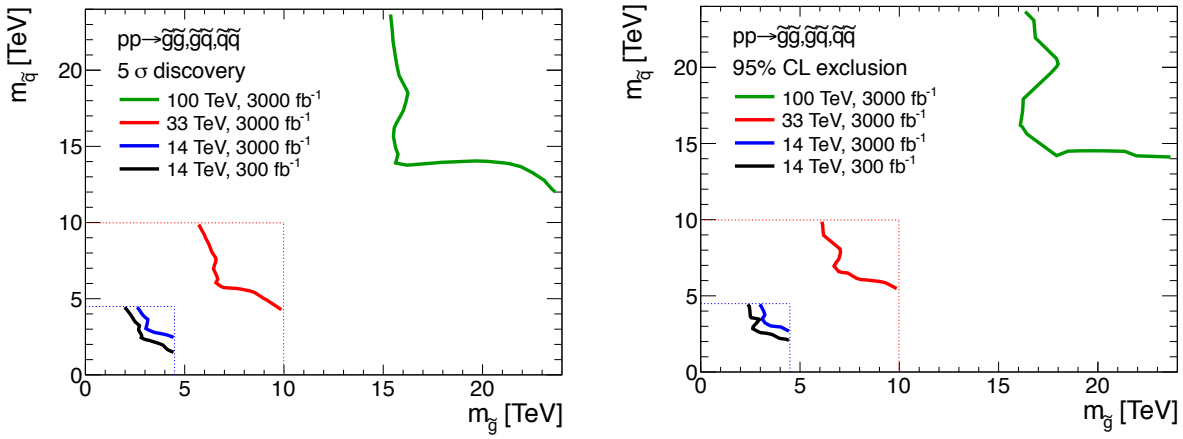

Fig. 42: Expected 5σ discovery (left) and 95%CL exclusion (right) reach for the gluino-squark-χ model at future machines [313].

5.3.5.6 sbottom-LSP

BSM particles	production	Decay
$\tilde{b}, \chi$	$pp \to \tilde{b}\tilde{b}^*$	$\tilde{b} \to b\chi$

A simplified model for sbottom and χ could naively be seen as a sub-case of the simplified model for squarks and χ discussed in Section 5.3.5.3. However the sbottom is expected to produce b-quark final states, which give a different, and in general more recognizable, experimental signal in detectors. For this reason there are specialized searches and dedicated interpretations for this type of simplified model. The present results from a CMS analysis of the Run 1 LHC data is presented in Fig. 43. For comparison the bound from the same search on the squark-χ model is also displayed, which shows the advantage of having a b-jet in the signal. For this simplified model, to the best of our knowledge, there are no available projections at future machines. However the lesson from the comparison of LHC results in the two panels of Fig. 43 should allow to say that the projections for the squarks-χ simplified models

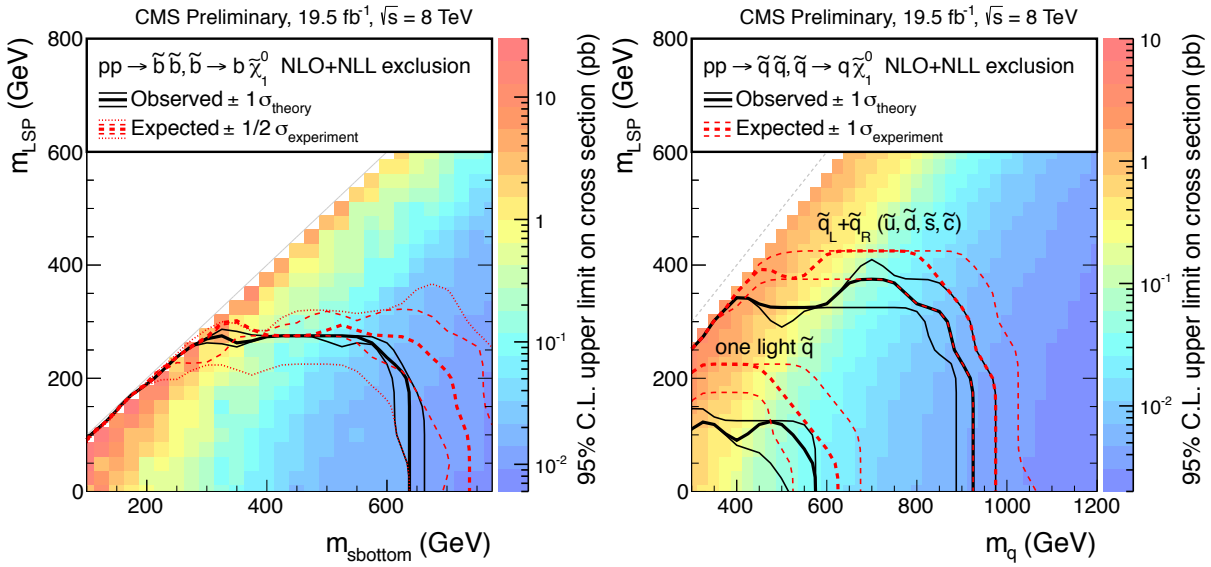

Fig. 43: LHC run 1 bounds [314] on the sbottom-χ simplified model (left) and on a light flavour squark-χ model (right).

discussed in Section 5.3.5.3 are a good estimate of the reach for the $\tilde{b}$-χ simplified model [11].

Another simplified model can be considered for sbottoms, which is not usually considered for squarks. In case both a chargino and a neutralino are light enough to be final states of the sbottom decay, one can have a richer final state, that includes a top quark final state and extra fermions.

BSM particles	production	Decay
$\tilde{b}, \chi^+, \chi$	$pp \to \tilde{b}\tilde{b}^*$	$\tilde{b} \to \chi^+ t, \chi^+ \to f f' \chi$

The most useful final states for the χ^+ decay usually involve leptons and for a decay into on-shell top quarks projections to future machines are available in Ref. [52].

5.3.5.7 stop-LSP

For this simplified model the only relevant light particles are the stop and the lightest supersymmetric particle χ. The phenomenology is very rich as the stop can decay into a $bff'\chi$ final state directly or through a number of possible on-shell intermediate states, for instance $\tilde{t} \to t\chi$ or $\tilde{t} \to bW\chi$. In some models decays induced by loops can be relevant and searches exist for the $\tilde{t} \to c\chi$ channel. The summary of the presently available searches is given in Fig. 45.

BSM particles	production	Decay
$\tilde{t}, \chi$	$pp \to \tilde{t}\tilde{t}^*$	$\tilde{t} \to c\chi, \tilde{t} \to bff'\chi$

The bounds in the region $m_{\tilde{t}} > m_t + m_\chi$ are rather strong and exclude stop masses up to 700 GeV. Larger masses cannot be probed at the LHC Run1 because of the limited production cross-section of such heavy stops. Lighter stops, on the other hand, are challenging, despite the larger production cross-sections, because of the little differences in the kinematical distributions with respect to the backgrounds. The leading background is usually $pp \to t\bar{t}$, therefore the challenge in the detection of light stops lies in differentiating a light stop decay from a Standard Model top quark decay.

[11] The actual improvement brought by having a b-quark final state is conditional to the performances of b-jet tagging at high energies.

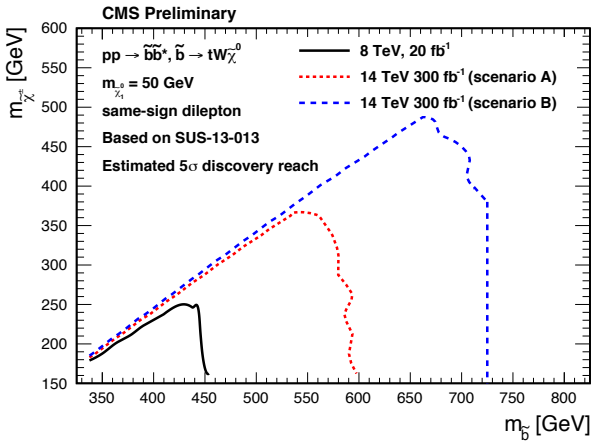

Fig. 44: Expected discovery reach at the LHC Run2 for a $\tilde{b}$-χ^+-χ simplified model. The two different lines consider different levels of uncertainties on the backgrounds, the blue one being more optimistic, the red one more conservative.

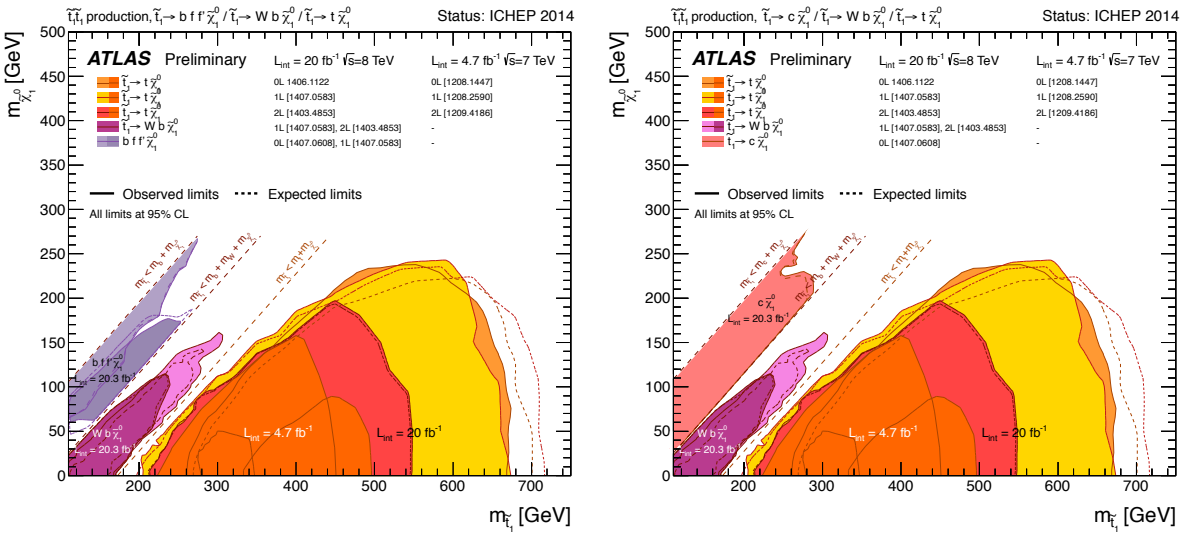

Fig. 45: Limits from [315] on the $\tilde{t}$-χ simplified model assuming $BR(\tilde{t} \to bff'\chi) = 1$ (left) or $BR(\tilde{t} \to c\chi) = 1$ (right) in the region $m_{\tilde{t}} - m_\chi < m_W + m_b$.

To address the light stop scenario it has been observed that it is possible to put direct bounds looking at *precision* measurements of the top quark properties such as the cross-section [316] or spin correlation effects [317]. These analyses of precision top observables are particularly powerful in the region at low m_χ, the so-called *stealth* region, where the amount of momentum carried by invisible particles, and therefore the mET, is expected to be very small.

In Fig. 46 we report the available projections for Run 2 of the LHC for $m_{\tilde{t}} - m_\chi > m_W + m_b$. The projections show the extended sensitivity at high stop mass, and stops up to almost 1 TeV might be discoverable [52]. The difficulty to have powerful searches for light stops at the Run1 of the LHC usually applies as well to higher energies colliders.

As discussed a light stop is copiously produced and the difficulty for its detection arises from its subtle decay final state. The most important element for the discovery in these difficult scenarios is the understanding of backgrounds. In Fig. 46 two different assumptions are made for the background uncertainties. The blue curve corresponds to an improved knowledge of the backgrounds, whose uncertainty

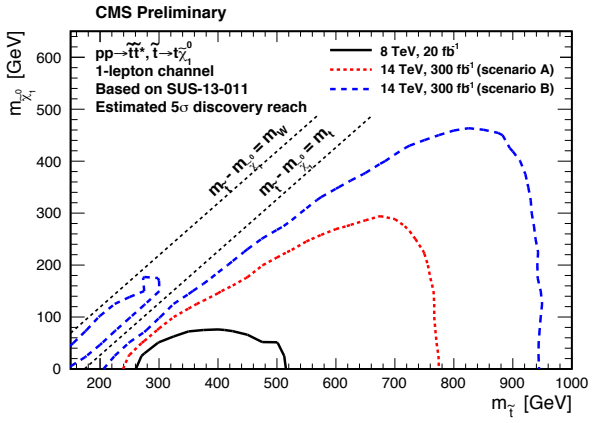

Fig. 46: Expected discovery reach at the LHC Run2 for the $\tilde{t}$-χ simplified model. The blue and the red lines correspond to different assumptions for the knowledge of the backgrounds, the blue one being more optimistic and the red one being more conservative (see text).

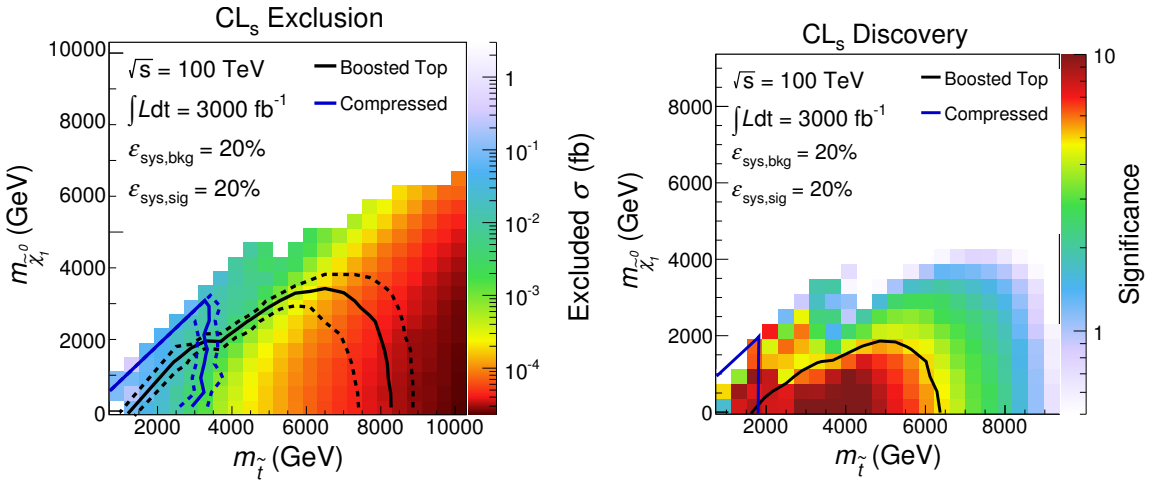

Fig. 47: The 95% CL expected exclusion (left) and discovery reach (right) for the $\tilde{t}$-χ simplified model [318]. The result for a boosted jet analysis strategy and for a search strategy optimized for spectra with small $m_{\tilde{t}} - m_{\chi}$ are shown.

is assumed to follow the expected statistical improvement, but is considered to be at best 10%. The red curve instead assumes the same relative uncertainty in the backgrounds as in the current searches. As apparent from the comparison, in order to be able to discover the light stop scenario it is very important to get improved background uncertainties.

The reach of a future 100 TeV machine for this simplified model has been investigated in Ref. [318]. The very high energy of the machine allows one to search for stops exploiting their large boost and jet substructure techniques to differentiate the signal from backgrounds. With this type of approach stop masses up to 8 TeV can be excluded for most values of m_{χ}, as shown in Fig. 47. For the difficult scenarios where $m_{\tilde{t}} - m_{\chi}$ is small, Ref. [318] also reports studies and an alternative search strategy, which is expected to exclude stop masses up to 3 TeV for any m_{χ}.

5.3.6 Experimentally difficult scenarios

We now turn to the discussion of scenarios in which sparticles might have escaped the present searches because their experimental detection turns out to be more challenging. Such scenarios can still allow

sparticle masses below the generic bounds shown in Section 5.3.5. Lowering the experimental bounds of course helps reducing the experimental pressure on supersymmetric models.

5.3.6.1 Reduced mET signals

As discussed above, the reach of searches for new supersymmetric states becomes much more difficult when the supersymmetric invisible particles do not carry large momentum. For this reason, deviations from the simplified models discussed above that result in less momentum being carried by the supersymmetric invisible particles can give looser bounds.

Higher multiplicity signals

A very simple option to reduce the mET of a signal is to increase the number of final state particles that share the mass of the original mother particle. Therefore when the decay $A \to b\chi$ becomes

$$A \to b\, c\, d\, ...\chi$$

we automatically get reduced momentum carried by χ, hence a smaller mET.

A situation of this sort can be achieved in models with an extended Higgs sector, such as the NMSSM, although the modification of the mass bounds in a generic point of the parameter space is only about 10-20% [319, 320]. In the NMSSM there is an extra complex scalar compared to the MSSM. If we denote by s a generic scalar of the Higgs sector and by χ_2 the second lightest neutralino we can have now decay chains

$$\tilde{q} \to q\chi_2 \to qs\chi \to qb\bar{b}\chi$$

where the last decay $s \to bb$ is just an example for the sake of concreteness, as the generic scalar s might decay in several different ways. The nature of χ_2 and χ depends on the choice of parameters of the NMSSM, however it is possible that these states contain a significant fraction of the fermionic partner of the new gauge singlet scalar. If χ is very close to be a gauge singlet, it evades the LEP limits on neutralino searches, because of its suppressed interactions with the gauge bosons. Similarly, s can be below the LEP kinematic reach if it is almost a gauge singlet. Such a scenario can have a reduced mET.

An example of reduced mET distribution is shown in Fig. 48 [319] (blue line) and compared to the corresponding MSSM scenario (red line). In both cases the signal is associated to the production of a $870\,\mathrm{GeV}$ squark. In the NMSSM case, $m_s = 83\,\mathrm{GeV}$ and $m_\chi = 5.3\,\mathrm{GeV}$ are the masses of the singlet-like scalar and its fermionic partner (absent in the MSSM case), and $m_{\chi_2} = 89\,\mathrm{GeV}$ is the mass of the bino-like second lightest neutralino. As apparent from the figure, the reduction can be substantial and the number of events that pass the selections of a typical search for supersymmetry can be a factor 10 lower than in the MSSM. This is however mainly due here to the closeness to the kinematical threshold for the $\chi_2 \to \chi s$ decay, a sort of fine-tuning, which almost completely suppresses the mET carried away by the LSP χ (the blue distribution in figure originates from the neutrinos from the decay chain of s).

Stealth spectra

A reduction in the mET can arise even in the absence of higher multiplicities, due to kinematical properties of decays. For instance in a two-body decay

$$A \to b\, c$$

a significant reduction takes place close to the kinematical threshold $m_A \approx m_b + m_c$, especially if A is almost degenerate to b (c is then significantly lighter). The momenta have then to be boosted to the laboratory frame. If the proximity to the threshold is due to the approximate degeneracy of A and b, $m_A = m_b + \epsilon$, in the center of mass frame we have

$$(E_b, p_b) \sim (m_A, \epsilon), \quad (E_c, p_c) \sim (\epsilon, \epsilon)\,,$$

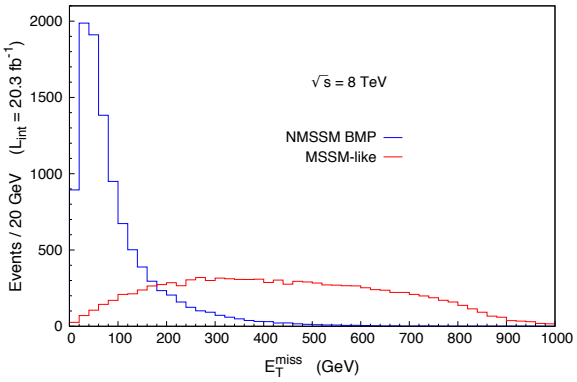

Fig. 48: mET spectrum for a MSSM-like choice of parameters of the NMSSM (red) and for a specific NMSSM spectrum that gives rise to small mET [319, 320].

which means that the momentum of the light particle is small even after the boost. This causes a dramatic reduction of the mET, one example of which is shown in Fig. 48 for a NMSSM realization of the so called "stealth" SUSY spectrum.

Compressed spectra

In the case of a compressed spectrum, a reduction of mET is obtained again because of the proximity to a decay kinematical threshold, but none of the decay products is assumed to be light. For example, for $\tilde{t} \to t\chi$ the spectrum is compressed when $m_{\tilde{t}} \simeq m_t + m_\chi$. In this case the momenta of the decay products, small in the rest frame, are not small anymore when boosted to the laboratory frame. On the other hand, the stop are pair produced,

$$pp \to \tilde{t}\tilde{t}^*,$$

and, as a consequence of the compression of the spectrum, the momenta of the two χ from stop decays turn out to be very correlated. In particular, when no radiation affects the kinematics, the two stops and the two χ turn out to have opposite transverse momenta, so that the total mET is still small, which in turn reduces the observability of the signal.

The anti-alignment that results from a compressed spectrum can be spoiled by higher order production mechanisms such as

$$pp \to \tilde{t}\tilde{t}^* + \text{jets}$$

In a process with an extra *hard* jet with $p_{T,j} \sim m_{\tilde{t}}$ the anti-alignment of the two χ is much reduced, because of the three-body final state. The theoretical modelling of the extra radiation is not easy. The leading order process is in fact $pp \to \tilde{t}\tilde{t} + 1jet$ and needs to be computed at next-to-leading order in perturbation theory to have a reliable prediction of the high-$p_{T,j}$ region of the phase-space where the supersymmetric process develops a large mET. Progress in the improvement of these calculations is steady (see Refs. [321, 322] for recent results) and the complete automatization of the computation of higher-order QCD corrections to supersymmetric production is underway [323].

Reach

While we do not expect that a significant reduction of the mET in the signature would completely kill the sensitivity of searches for light flavour squarks and gluinos, the situation is different for heavy flavour quarks such as stops. In fact stops usually give rise to even higher multiplicity and in general more complex final states. The additional structure of stop events makes them more affected by the reduction of mET. One example is the drop of sensitivity in the searches in the 4-body decay region of the stop

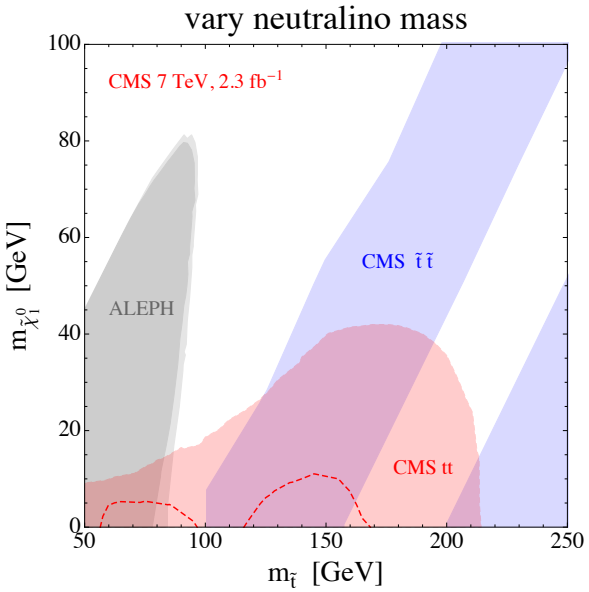

Fig. 49: Sensitivity of top quark cross-section analysis to supersymmetric spectra with light stops [316].

$\tilde{t} \to bff'\chi$ where both the ATLAS monojet search [324] and the ATLAS single lepton search [325] currently fail to put a bound for $m_\chi < 60\,\text{GeV}$. As discussed in Section 5.3.5.7 this difficult region can be addressed searching for deviations of precisely measured quantities from the SM predictions, *e.g.,* the $t\bar{t}$ production cross section [120, 316, 317].

In Fig. 46 we report the available projections for Run 2 of the LHC for $m_{\tilde{t}} - m_\chi > m_W + m_b$. The higher energy of the LHC Run2 clearly will help to collect more data and understand better the backgrounds, hence improving the reach of the searches. In particular, the region of compressed spectra will be more thoroughly probed and the exclusion will reach lower m_χ. At the same time improvements of top quark measurements such as those considered in Refs. [120, 316, 317] will start closing the gap at low χ mass. For illustration we report in Fig. 49 the bounds from 7 TeV measurements at the LHC. The study of Ref. [316] shows some sensitivity for light stops and m_χ up to 40 GeV. Improved measurements of the top cross-section and other top quark properties will be able to further probe the difficult "stealth" scenarios [326].

5.3.6.2 Searches for resonances and R-parity violation

The presence of a stable invisible particle at the bottom of each decay chain of supersymmetric particles is the very reason for the large mET signals expected in supersymmetric models. The large mET is usually a powerful discriminator to reject backgrounds. On the other hand, alternative strategies, not based on the presence of large mET, can be helpful as well. A classic example is the search of Breit-Wigner resonances, which can be effectively searched over a smoothly falling background. This has been the case for instance of the observation of the Higgs boson decay into two photons [12].

Resonance searches are unfortunately not very effective in the presence of stable invisible particles, because they carry away momentum and it is not possible to use them in the reconstruction of the resonance. In presence of stable invisible particles, it is still possible to exploit features of multi-particles invariant masses [327–329] or single particle properties [330, 331]. However such methods are useful only for searches for specific scenarios [332, 333] and are in general more suited to probe the mass spectrum of the model rather than to isolate a signal from the backgrounds. An effective use of resonant searches in supersymmetric models requires the absence of a stable invisible LSP in the final state.

[12] Up to the fact that due to resolution effects the shape is actually closer to a gaussian than to a Breit-Wigner.

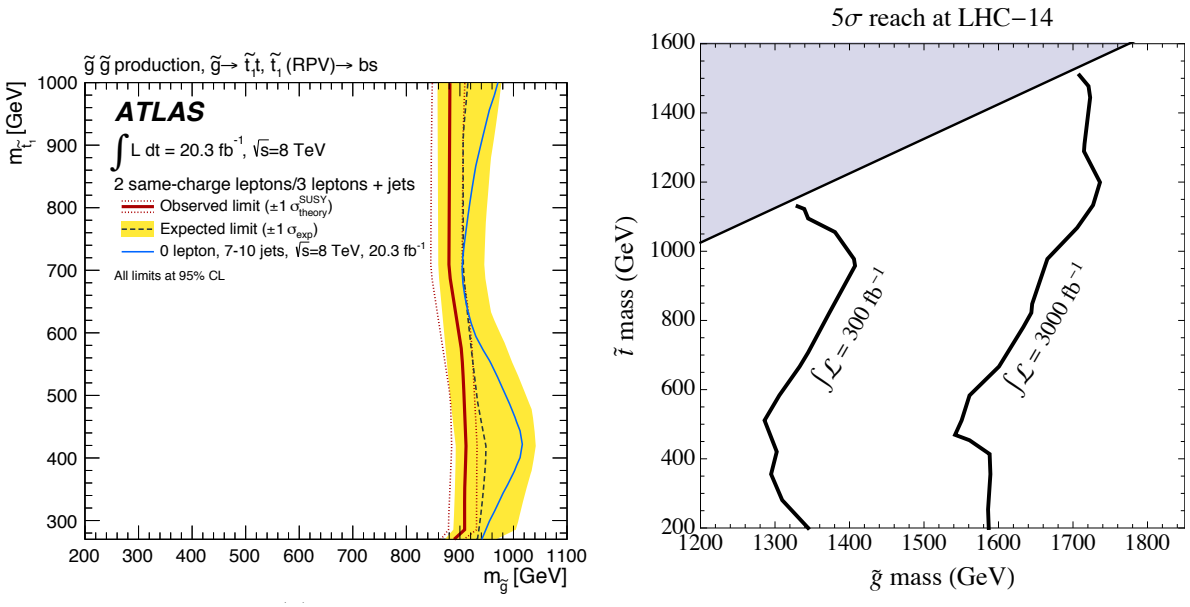

Fig. 50: Exclusion from the LHC 8 TeV run (left) [335] and expected discovery reach (right) [337] for the RPV gluino simplified model decaying into heavy flavours in the same-sign di-lepton channel.

R-parity violation

As discussed in Section 5.3.5.1, the LSP is stable only as a consequence of having imposed R-parity. If R-parity is not conserved, the superpotential interactions in eq. (23) are allowed and eventually lead to the decay of any sparticle, in particular the LSP, into a set of possibly observable SM particles, for example

$$\tilde{q} \to jj \text{ or } \tilde{g} \to q\tilde{q} \to q\bar{q}q.$$

If this is the case, and the decay is prompt, the event will not have mET. Most of the RPV couplings have to be small as they can give rise to baryon number or lepton number violating process such as proton decay, neutron-antineutron oscillations, large neutrino masses, or because they mediate flavour changing neutral current processes. Despite their smallness, they can be sufficient to avoid the mET signature. For example, an R-parity violating (RPV) coupling of order 10^{-5} would still be large enough to give a decay $\chi \to q\bar{q}q$ with average decay path below 10^{-6} meters.

The lack of mET relaxes to some extent the bounds on supersymmetric particles and moderately alleviates the fine-tuning problem. From this point of view, the most relevant result is the bound on the gluino shown in Fig. 50. The strongest bound on the gluino mass in RPV scenarios comes indeed from the fact that for a Majorana gluino decaying into heavy flavours can give rise to a signal with two hard leptons with the same electric charge [334]. The limits from the $8\,\mathrm{TeV}$ run of the LHC exclude masses up to $900\,\mathrm{GeV}$ [335]. Compared to the most optimistic bound in R_P conserving scenarios, the bound is about 30% lower, which improves the FT by a factor 2, at some theoretical price [336]. Estimates for the 14 TeV LHC have been presented in [337] and are also reported in Fig. 50. According to this analysis, the High Luminosity LHC should be able to discover a gluino of mass up to $1.6\,\mathrm{TeV}$.

Many other R-parity violating simplified models giving rise to resonances have been considered. Baryonic RPV signals have been more extensively studied, as leptonic RPV is tightly bounded by the presence of hard leptons in the final states [338, 339] [13].

Bound on simplified models in which the gluino can only decay into three fermions have been set by ATLAS and CMS in [341–343] and range between $350\,\mathrm{GeV}$ and $1\,\mathrm{TeV}$, depending also on the

[13] Scenarios of leptonic RPV where this may not be the case have been studied in Ref. [340].

assumption on the flavour of the three decay products.

Simplified models for the RPV decay of a squark into two jets have been constrained by CDF [344] and ATLAS [345]. The bounds are weak because of the large QCD background, they exclude masses up to $100\,\mathrm{GeV}$ only. Future projections range from $300\,\mathrm{GeV}$ to about $1\,\mathrm{TeV}$ for the exclusion at the end of a High Luminosity Run [346], see also [347]. If the squark is a stop or a sbottom, the presence of bottom or top quarks in the final state provides a useful handle, allowing a discovery up to about $200\,\mathrm{GeV}$ using LHC Run1 data [348].

Simple and motivated variations on the simplified model theme give several jets in the final states, allowing to achieve higher sensitivities. For example the presence of a light neutralino could help constraining the stop simplified model. The stop would now decay via R_P-conserving couplings into the neutralino, which would then have a RPV decay into three jets. As a consequence, a stop mass exclusion up to $1.5\,\mathrm{TeV}$ and a discovery up to $1\,\mathrm{TeV}$ will be possible in the HL-LHC [349]. The general case of a complete spectrum with several sparticles involved in the decay chains can lead to larger multiplicities. Searches have been conducted up 8 jet final states [350] at CMS and up to 7 jets at ATLAS [343]. For higher multiplicities the typical search for non-perturbative phenomena such as black-hole formation [351] is able to capture signals from complex RPV spectra. The result of this recast of [343] and [351] gives exclusions of gluino masses up to $1\,\mathrm{TeV}$ [349]. In ref. [346] the extrapolation to pp colliders up to $33\,\mathrm{TeV}$ has also been considered. The background predictions for events with many jets are less reliable, also due to the difficulty to resolve each parton jet and to the uncertainties in the theoretical prediction for the cross-sections. The use of jet substructure techniques [352–354] can help [355].

5.3.7 Electroweak simplified models

The above simplified models all used colored particles, most copiously produced at hadron colliders, as the primary source of supersymmetric states. In this subsection we will consider simplified models for purely weakly interacting sparticles, where a chargino and an extra (degenerate) neutralino, and possibly lighter sleptons are considered together with the LSP χ. The search for electroweakinos is of course relevant per se, but also because of the link of Higgsinos with the naturalness of the Higgs mass, eq. (15), and because the weakly interacting sparticles might represent the solution of the Dark Matter puzzle.

The main disadvantage in the search for purely electroweak states is that their production is suppressed by powers of the weak coupling constant, which gives at least one order of magnitude of suppression in the hard cross-section compared to QCD interactions. Further suppression arises from initial state luminosities, as for instance the gluon-gluon initial state and colored combination of quarks tend to not contribute to the production of electroweak states.

Nevertheless, electroweak states can be observed because of the tendency of the heavier ones to radiate or decay into electroweak bosons and energetic charged leptons. A collection of the bounds from ATLAS on final states with leptons is showed in Fig. 51 for the case in which the extra states are Wino-like. In the less favorable scenarios, where there are no lighter sleptons, the bound on the mass of the charginos is up to $400\,\mathrm{GeV}$ for light χ. For heavier charginos, the production rates at the 8 TeV LHC are too small to be probed. These bounds degrade for spectra where there is a small mass splitting and the chargino tends to be degenerate with χ. In fact, for χ closer than 20 GeV to the chargino the present searches do not extend the limits from LEP.

The difficulty that arises when the heavier electroweakinos are close in mass to the LSP is that the charged leptons that are used to trigger and to isolate the signals from backgrounds become too soft to be cleanly identified and measured in the busy LHC events. In this case a more promising strategy is to exploit the production of electroweak states in association with a hard jet, for instance

$$pp \to \chi\chi + \text{jets}\,. \tag{25}$$

In this process the jet, if sufficiently hard, can be used to trigger the event and automatically opens the

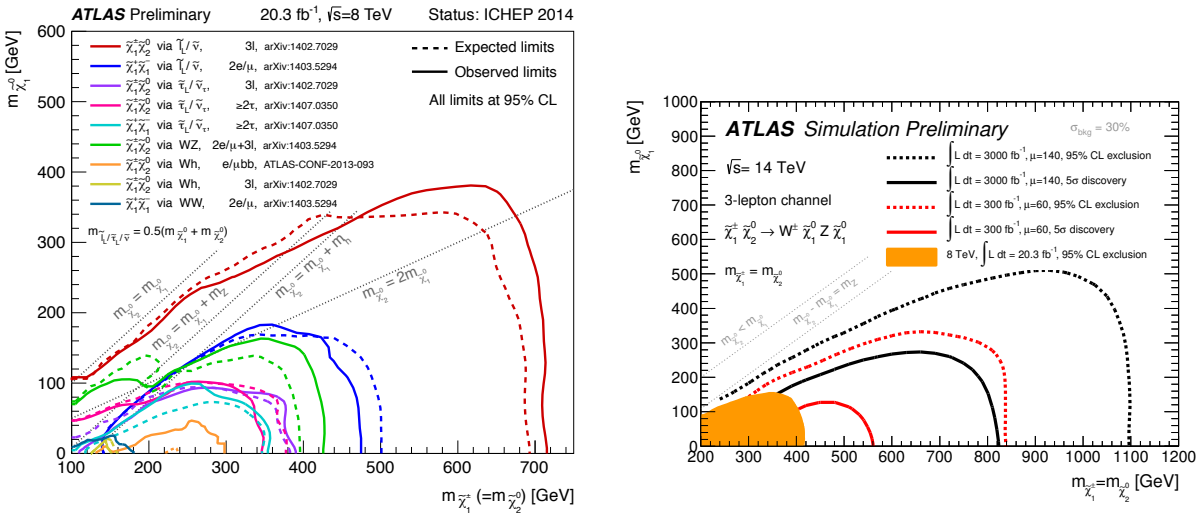

Fig. 51: (left) Summary of the searches for electroweak SUSY states at ATLAS [356]. (right) Expected exclusion and discovery reach at the 14 TeV run in the 3 leptons channel [357].

possibility to have large mET in the events. Similar production mechanisms can be used for electrically charged particles, so that final states with sufficiently hard leptons, jets and mET can be obtained.

5.3.7.1 Pure Winos or Higgsinos

We now discuss the detection reach on electroweakinos in the extreme case in which only Winos or Higgsinos are produced. The spectrum is thus made of a charged and a neutral state (Majorana in the Wino case, Dirac in the Higgsino case). The two are degenerate at the tree level but they are split by radiative corrections. Given the smallness of the mass difference, the search strategy must be based on eq. (25) or, if the degeneracy is strong enough to make the charged particle sufficiently long-lived, on disappearing tracks.

Let us first neglect disappearing tracks. Limits can be set at the 14 TeV run of the LHC, where the production rate is sufficiently large. In Fig. 52 we report the estimates for the exclusions achievable for a Wino-like and a Higgsino-like neutralino at the High Luminosity LHC 14 [358]. Wino masses up to 200-300 GeV and Higgsino masses up to 100-200 GeV can be probed. The uncertainty of the exclusion reach reflects the expected knowledge of the backgrounds, usually dominated by $pp \to (Z \to \nu\nu) + \text{jets}$.

The above mass reaches, though interesting, are far from the values for which Winos or Higgsinos can play the role of the Dark Matter particle (about $1\,\text{TeV}$ for Higgsinos and $3\,\text{TeV}$ for Winos thermally saturating the relic density). On the other hand, it is possible to get much closer to those ranges at higher energy colliders [358–361]. The larger energy available makes it possible to produce hard radiation more easily and the process in eq. (25) acquires a sizeable cross-section even for large mass of the electroweak sparticle. The expected performance of a $100\,\text{TeV}$ machine is also shown in Fig. 52, from which we can see that Wino masses up to $1.4\,\text{TeV}$ and Higgsino masses up to about $900\,\text{GeV}$ can be probed.

As mentioned, another search strategy that can be exploited for nearly degenerate weak multiplets is the lifetime of the heavier states in the multiplet. At tree-level the states in the weak multiplets are degenerate, however EW symmetry breaking loop effects give rise to a mass splitting of order $\alpha_W m_W \sim 100\,\text{MeV}$ which is know to two loops accuracy [362] and is equal to $164.6\,\text{MeV}$ for a Wino and about twice as much for the Higgsino. The lifetime is in the range of $c\tau \sim 10\,\text{cm}$, so that it becomes possible to observe the chargino track in the tracker of the LHC experiments. Such a track would suddenly disappear somewhere in the tracker region. Despite the many backgrounds (from instrumental defects, to coincidences of tracks, and irreducible backgrounds from QCD long-lived hadrons), the AT-

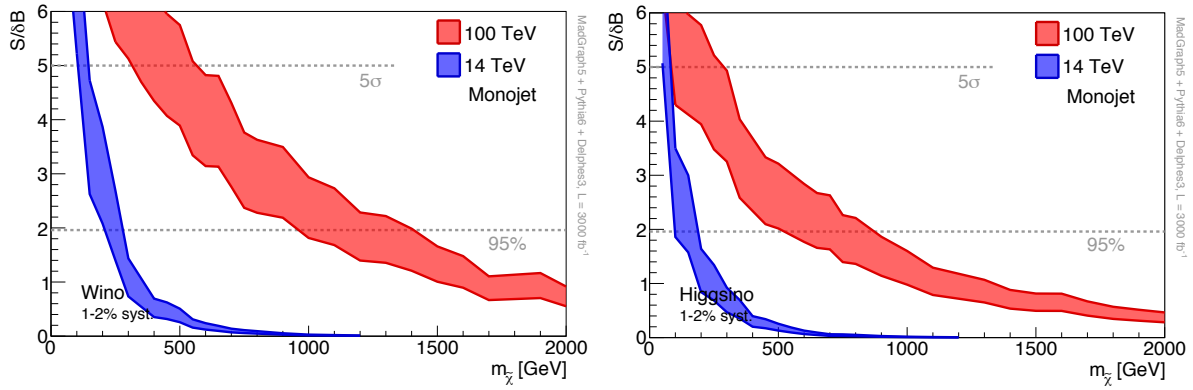

Fig. 52: Reach of the monojet analysis for a pure Wino (left) or Higgsino (right) in the monojet channel with $3000\,\text{fb}^{-1}$ at the 14 TeV LHC (blue) and a 100 TeV proton-proton collider (red) [358]. The bands represent different hypothesis on the knowledge of the backgrounds.

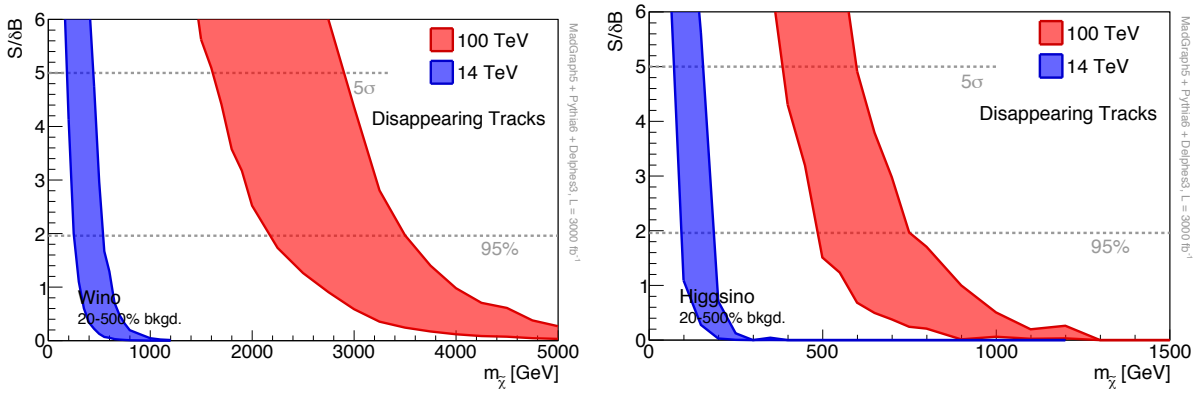

Fig. 53: Reach of the disappearing track analysis for a pure Wino (left) or Higgsino (right) with $3000\,\text{fb}^{-1}$ at the 14 TeV LHC (blue) and a 100 TeV proton-proton collider (red) [358]. The bands represent different hypothesis on the knowledge of the backgrounds.

LAS experiment has been able to probe Wino masses up to about 270 GeV [363]. This limit is expected to improve dramatically at higher energy colliders, thanks to the larger boost that can be imparted to the chargino, as a recoil against harder radiation from the $q\bar{q}$ initial state. In fact with a larger boost one has longer tracks and tighter bounds are expected. The bounds at the High Luminosity LHC and at a 100 TeV collider are shown in Fig. 53. They turn out to be far stronger than those from the monojet analysis. Wino masses up to about 3 TeV and Higgsino masses up to 900 GeV can be excluded at a 100 TeV machine. The larger mass splitting of the Higgsino makes the track disappear faster in the core of the detectors, and leads to worse limits. The difference of the reach for Wino and Higgsinos shows well how much the disappearing tracks search can depend on details of the spectrum.

While the discovery reach of the disappearing track search can be higher, the monojet analysis can be considered as safety net, in case the challenging disappearing track analysis will turn out to be too difficult at the High Luminosity LHC or at a 100 TeV machine. In this case a large portion of the both the Wino and the Higgsino type thermal relic Dark Matter hypothesis will be tested at a 100 TeV machine, and it is not excluded that future refinements might lead to a full coverage. On the other hand, only a partial coverage will be possible at the High Luminosity LHC. For comparison of the two analyses we summarize the expected performance in Fig. 54.

channel	systematics/ normalization	14 TeV		100 TeV	
		95% limit	5σ discovery	95% limit	5σ discovery
monojet	1%	280 GeV	140 GeV	1.4 TeV	560 GeV
	2%	205 GeV	100 GeV	960 GeV	310 GeV
disappearing tracks	500%	250 GeV	180 GeV	2.1 TeV	1.6 TeV
	100%	385 GeV	295 GeV	2.9 TeV	2.2 TeV
	20%	535 GeV	440 GeV	3.5 TeV	2.9 TeV

channel	systematics/ normalization	14 TeV		100 TeV	
		95% limit	5σ discovery	95% limit	5σ discovery
monojet	1%	185 GeV	80 GeV	870 GeV	285 GeV
	2%	95 GeV	50 GeV	580 GeV	80 GeV
disappearing tracks	20%	185 GeV	155 GeV	750 GeV	595 GeV
	100%	140 GeV	95 GeV	615 GeV	485 GeV
	500%	90 GeV	70 GeV	485 GeV	380 GeV

Fig. 54: Reach of the monojet and disappearing track analysis for different hypothesis on the knowledge of the backgrounds for a pure Wino (top) and for a pure Higgsino (bottom) [358].

5.3.7.2 Mixed spectra

Let us now consider the case in which the LSP is a superposition of Binos and Higgsinos or Winos. This allows to obtain the correct thermal relic abundance for a range of masses (depending on the size of the mixing), lower than the value needed in the case of pure Wino or Higgsino. This is because the geometrical rescaling of the dark matter annihilation cross-section associated to a variation of the Dark Matter mass can be compensated by the variations of its couplings associated to the mixing. As a matter of fact, there exists a number of possible mixing patterns that satisfy all the constraints on Dark Matter abundance and scattering cross-section in direct searches of Dark Matter. The hyperspace of the relevant mass parameters that realize viable Dark Matter candidates is visualized in Fig. 55, with their Spin-Independent cross-section on nucleon reported reported using the color code.

For these mixed states a large portion of the viable Dark Matter scenarios have a small mass splitting between the lowest lying multiplet of states. The actual mass splitting is shown in Fig. 55 for points that give the measured relic abundance of Dark Matter from a thermal freeze-out calculation. When the mass splitting is too small to generate hard leptons one has to rely on the monojet searches or, if the mass splitting allows, the disappearing track search strategy discussed for the pure states in Section 5.3.7.1 above. However, there is a sizable fraction of the parameter space where mass splittings above 20 GeV are compatible with the Dark Matter hypothesis. In this case it is possible to search for relatively soft leptons, in any case harder than about 10 GeV, coming out from the decay of the second lightest neutralino or of the chargino. This is in complete parallel to current searches carried out at the LHC such as those in Refs. [365, 366]. The reach of this type of searches at the High Luminosity LHC and a future 100 TeV pp collider are shown in Fig. 56. From the figure we see that at the LHC only masses up to 400 GeV can be excluded by combining several searches. On the other hand at a pp 100 TeV collider the exclusion reach extends above 1 TeV.

5.3.7.3 Cascade decays

Finally one can consider the case in which both (almost) pure Winos and Higgsinos take part in the event and they have a significant separation in mass [359, 361]. The latter can give rise to a large boost

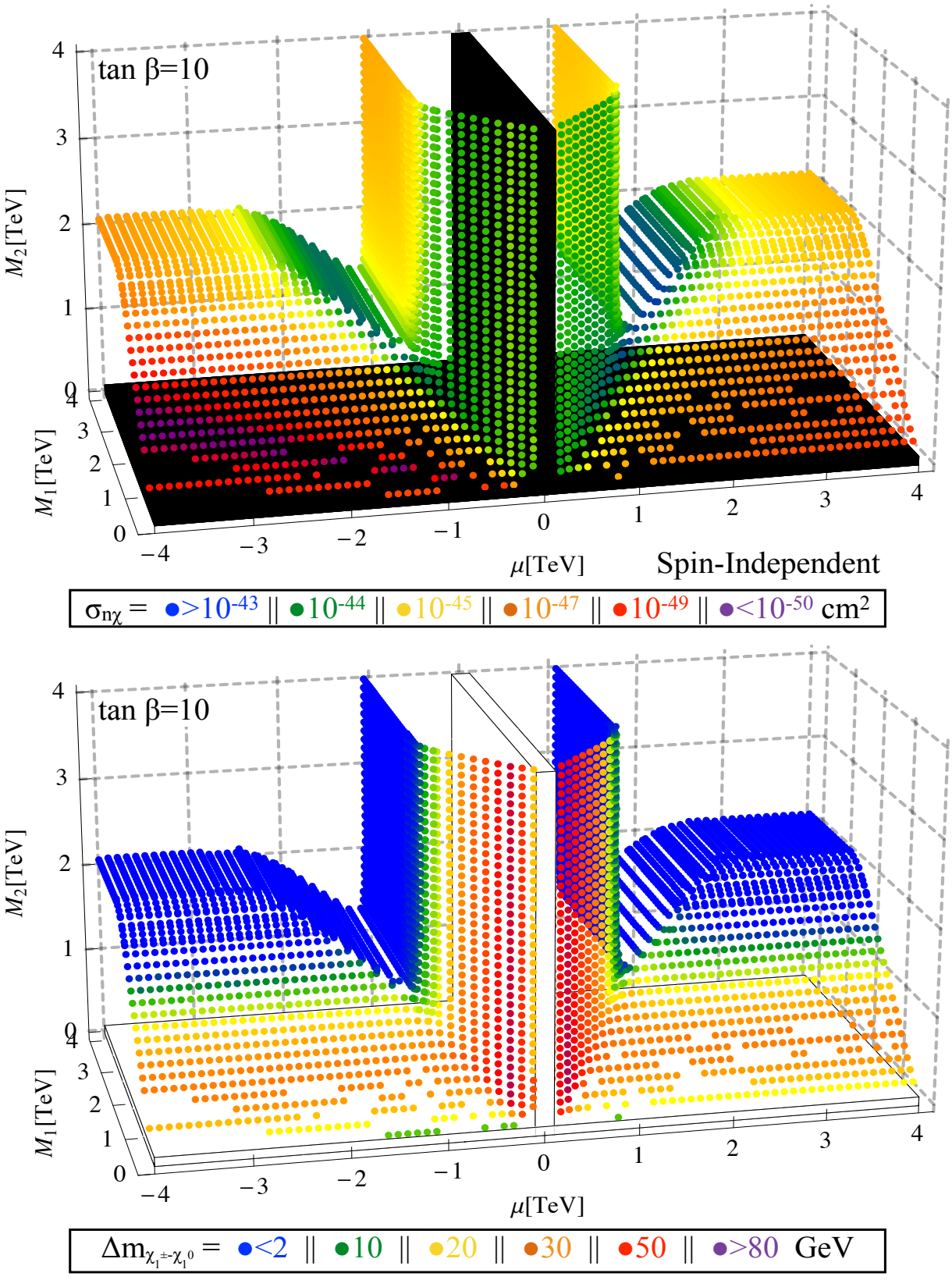

Fig. 55: (top) Spin-Independent nucleon-Dark Matter cross-section for mixed Dark Matter candidates in the MSSM [364] (bottom) mass splitting between the Chargino and the lightest Neutralino [364].

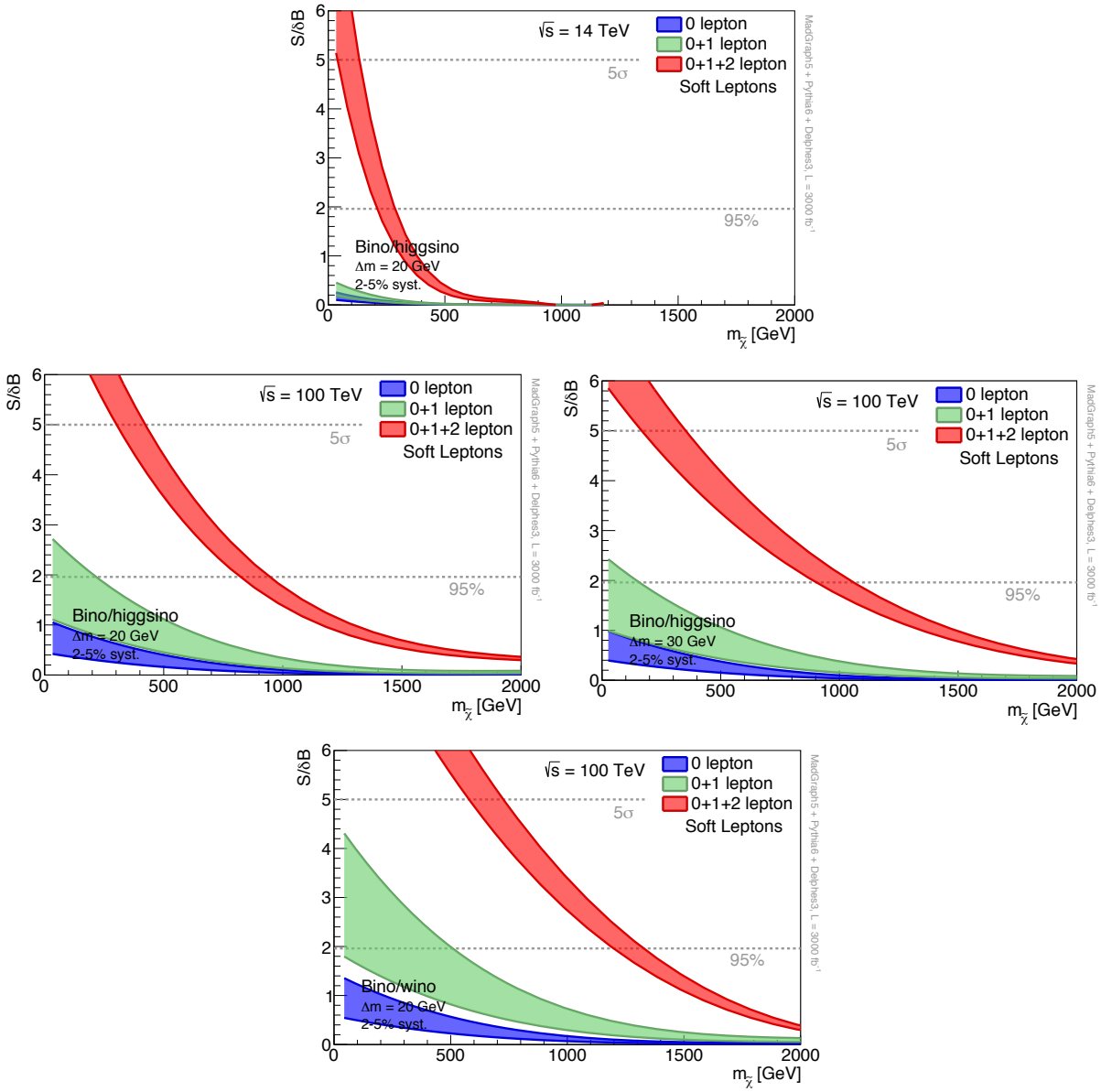

Fig. 56: Reach of soft leptons searches for a Bino-Higgsino mixture and 20 GeV mass splitting between the chargino and the lightest neutralino at the 14 TeV High Luminosity LHC (top) for a 20 GeV and 30 GeV mass splitting at a 100 TeV pp collider (middle) and a Bino-Wino mixture for 20 GeV mass splitting at a 100 TeV pp collider (bottom) [358]. The bands represent different hypothesis on the knowledge of the backgrounds.

of the lighter states when produced by the decay of the heavier, leading to harder and more collimated decay products. For instance one could consider a case with a heavy Wino-like multiplet, so that $m_{\chi_2^+} \simeq m_{\chi_3} \simeq M_2$, and a light Higgsino-like multiplet, so that $m_\chi \simeq m_{\chi^+} \simeq m_{\chi_2} \simeq \mu$. The production of heavy wino like states

$$pp \to \chi_2^+ \chi_3 \to \chi^+ \chi_2 ZW \to \text{leptons} + \chi\chi \tag{26}$$

results into harder leptons than that which one would get from the more copious direct production of the Higgsino-like states $pp \to \chi^+ \chi_2 \to 3\ell\chi\chi$. Given the low cross-section of heavy electroweakinos, this strategy can only be applied to a future 100 TeV pp collider, as the rates at the LHC are too small. In Fig. 57 we report the reach that Ref. [359] has found by combining searches with a number of lepton multiplicities and charges for processes of the type in eq. (26) for different combinations of gauge eigen-

(NLSP, LSP)	5σ discovery	95% CL exclusion
$(\tilde{W}, \tilde{H})$	(2.2, 0.8) TeV	(3.3, 1.3) TeV
$(\tilde{H}, \tilde{W})$	(1.5, 0.6) TeV	(2.6, 1.0) TeV
$(\tilde{H}, \tilde{B})$	(1.8, 0.7) TeV	(2.9, 1.1) TeV
$(\tilde{W}, \tilde{B})$	(3.2, 1.4) TeV	(4.2, 2.2) TeV

Fig. 57: Highest exclusion achievable for different combination of NLSP and LSP quantum numbers for a 3/ab luminosity at a pp 100 TeV collider [359].

states at the bottom and at the top of the spectrum. It is remarkable that this search strategy would be able to exclude a LSP up to 1 TeV for NLSP masses up to 2-4 TeV, depending on the gauge quantum numbers of the NLSP.

5.3.8 Fine-tuned scenarios

As discussed in Section 5.1, the argument underlying the expectation that new physics should appear somewhere near the electroweak scale is based on the assumption that extremely fine-tuned cancellations in the determination of the Higgs mass (in terms of alleged superheavy fundamental parameters) should be ruled out because extremely unlikely.

On the other hand, an apparently fine-tuned cancellation can take place because forced by an unknown dynamical mechanism or because of "environmental selection" arguments. The latter possibility arises in the so called "multiverse" scenario, in which Nature possesses a huge enough number of local vacua (not so unlikely in string theory [367–370]) with randomly distributed values of certain parameters entering the determination of the Higgs mass, populated by a proper cosmological evolution. Each vacuum then corresponds to a universe with given values of those parameters. In such a scenario, the number of universes in which an extremely fine-tuned cancellation takes place, allowing the Higgs mass and the electroweak scale to be as small as measured, is tiny but non zero. On the other hand, here is the intriguing hint supporting the whole idea [371], those few universes are the only ones in which life as we know it could have developed (and ended up wondering why the Higgs mass looks so fine-tuned). It is therefore no surprise that we live in one of those extremely rare universes, as it is no surprise that we live on a planet whose distance from the sun is fine-tuned to allow life to develop. Such an anthropic argument had been first proposed by Weinberg as a possible explanation for the smallness of the cosmological constant [372], before the latter would be measured to lie in the range predicted by the anthropic argument. Weinberg's argument remains perhaps the only concrete explanation of the smallness of the cosmological constant.

The above explanation of the naturalness problem of the Higgs mass belongs to the class of "naturalness independent" scenarios discussed in Section 5.4. Here we discuss its implementation in supersymmetry, which turns out to be particularly interesting. Indeed, it leads to specific scenarios such as split [247–249] and mini-split [249, 373–375] supersymmetry, with definite, testable predictions; it allows retention of the appealing ideas about quantum number unification and neutrino physics discussed in Section 5.1.2 and the success of supersymmetry with gauge coupling unification and dark matter; it is free of most problematic aspects of supersymmetry, such as the flavour and CP problem; it explains why supersymmetric particles have not been found so far (as it not constrained by the naturalness argument); it explains why the Higgs mass turned out to be heavier than that expected in natural supersymmetric scenarios.

What is in this case the scale of the extra degrees of freedom provided by supersymmetry? When

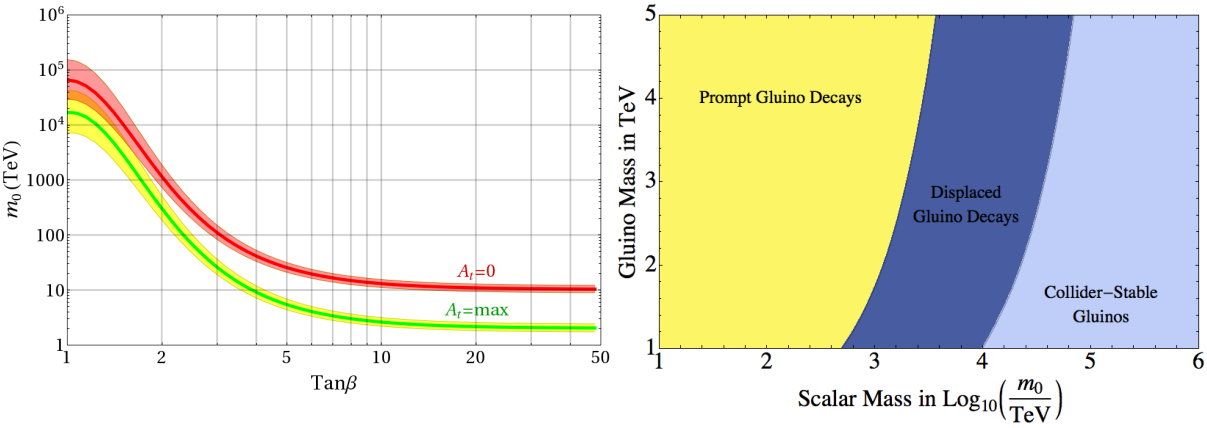

Fig. 58: Left: prediction for the scale of the scalar degrees of freedom in split supersymmetry as a function of $\tan\beta$ [375]. The two curves correspond to no and maximal stop mixing. The error bands correspond to the (dominating) 1σ error on the top mass. Right: gluino lifetime and corresponding collider behaviour as a function of the scalar mass scale in split supersymmetry.

the requirement of a natural determination of the Higgs mass is given up, the extra bosons can lie several orders of magnitude above the electroweak scale and therefore be unobservable. Assuming the minimal field content necessary to supersymmetrize the Standard Model, their mass (the stop masses in particular) is constrained by the Higgs mass measurement as shown in Fig. 58 (left) [375]. Raising the scale of those extra bosons does not affect gauge coupling unification too much, as long as the extra fermions, gauginos and higgsinos, remain pinned to the electroweak scale. In such a case, a linear combination of the extra neutral fermions can still play the role of dark matter particle and account for the observed relic abundance, without conflicting with direct detection bounds. In such a minimal scenario, the scale of gauginos and Higgsinos can be restricted by gauge coupling unification and the relic density.

The scale of supersymmetric particles is subject not only to the above phenomenological constraints, but also to theoretical considerations. A particularly appealing scenario, from the theoretical point of view, is the "mini-split" one, in which the gaugino and sfermion masses are parametrically separated by a loop factor with, roughly speaking, gauginos around the TeV scale and sfermions within an order of magnitude from the 100 TeV scale [249, 283, 373–375]. Depending on the model, the Higginos can live at either scales.

From the experimental point of view, the most promising signal is the decay of the gluino to the lightest neutralino state. The latter takes place through heavy scalars. If the scalar mass scale is within 100–1000 TeV, as suggested by the Higgs mass measurement for $\tan\beta \gtrsim 2$ (Fig. 58, left) and by the loop factor theoretical argument, the gluino decay is still prompt (Fig. 58, right). The current exclusion bounds and the prospects for future searches are therefore well described by Figs. 39 and 40 respectively.

Also important from the experimental point of view are the constraints and prospects on gauginos and Higgsinos, described from a general point of view in Section 5.3.7. For definiteness, let us consider here the case in which the parameter space is bound by the dark matter constraint. Namely, let us assume that the lightest supersymmetric particle (LSP) is stable and contributes through thermal production to the relic abundance. If the LSP *saturates* the relic density, that gives a precise constraint on the mass of the LSP. If an additional dark matter component is present (e.g. an axion), the latter constraint becomes an upper bound on the scale of the LSP. It should be emphasized that such constraints can be evaded, for example in the presence of a dilution mechanism, such as the decay into a lighter gravitino. Still, they represent a useful guideline to compare the experimental prospects with the theoretical expectations. General prospects for detection of electrowinos have been studied in [376–381].

The dark matter constraint depends on the nature of the LSP. As the sfermions are heavy, the LSP must be a neutralino, i.e. a linear combination of Bino, neutral Wino, and neutral Higgsinos. In the simplest case, the LSP is an almost pure state. Under our assumptions, it must be a Higgsino or a Wino (a Bino would overclose the universe). If the LSP is a mixed state, it can be either a Bino-Higgsino or a Bino-Wino or a Wino-Higgsino superposition. Let us briefly investigate the two pure cases and the Bino-Higgsino case (as a representative of the mixed case – a sufficiently large Bino-Wino mixing requires an approximate degeneracy of M_1 and M_2, which can be considered as an additional fine-tuning; the Wino-Higgsino case is not particularly illuminating).

5.3.8.1 Bino-Higgsino LSP

In such a case, the three mass eigenstates (the LSP and the two orthogonal linear combinations of Bino and the two Higgsino components) are below the Higgsino bound of $1\,\mathrm{TeV}$. This is a favourable case for experimental searches, especially at very high energy colliders. Assuming gaugino mass unification, for example, the Wino and gluino masses are forced to be below about $2\,\mathrm{TeV}$ and $6\,\mathrm{TeV}$ respectively. The LHC will cover in this case almost half of the gluino parameter space, while a $100\,\mathrm{TeV}$ collider would comfortably cover all of it (Figs. 39 and 40). The prospects for the electroweakinos are shown in Fig. 56.

5.3.8.2 Mostly Higgsino LSP

In such a case, the Higgsino mass is about $1\,\mathrm{TeV}$ [382], or lower if there is an additional contribution to the relic density. All gauginos are necessarily heavier than that. Gluinos can be within the reach of a $100\,\mathrm{TeV}$ collider, but that is not guaranteed. In the worst case, the Higgsino might be the only new particle within experimental reach. The experimental prospects at LHC14 and at a $100\,\mathrm{TeV}$ machine are illustrated in Fig. 52 and 53 (right). As discussed in Section 5.3.7, the search possibly involves the identification of disappearing tracks. The latter are due to the small splitting between charged and neutral Higgsinos, which can be as small as $\sim 350\,\mathrm{MeV}$, thus making the lifetime for the charged Higgsino decay into the LSP and soft pions correspondingly large.

Note that such a mostly Higgsino dark matter candidate is out of the reach of current and future direct detection experiments [383].

5.3.8.3 Mostly Wino LSP

In such a case, the Wino mass is about $3\,\mathrm{TeV}$ [382] (which is possibly above indirect detection constraints [384]), or lower. The Higgsino is heavier, possibly out of reach at foreseeable colliders. The Bino must also be heavier, $|M_1| > |M_2|$. This needs a non-standard relation among gaugino masses, such as the one provided by anomaly mediation, where $|M_2| < |M_1| < |M_3|$. In the case of anomaly mediation, the gluino mass upper limit would be above $20\,\mathrm{TeV}$. If the Wino thermal production saturates the relic density, the gluino would be forced to its upper limit, a challenge even for a $100\,\mathrm{TeV}$ collider, but in the presence of extra dark matter components the gluino could be lighter. As in the case of Higgsino detection, the Wino detection can exploit disappearing tracks, here due to a splitting between the charged and neutral Winos that can be as small as $\sim 170\,\mathrm{MeV}$. The experimental prospects at LHC14 and at a $100\,\mathrm{TeV}$ machine are illustrated in Fig. 52 and 53 (left). A $100\,\mathrm{TeV}$ machine has the potential to cover most of the parameter space.

Note that such a mostly Wino dark matter candidate is also out of the reach of current and future direct detection experiments [383].

5.4 Naturalness-independent scenarios

In the previous Sections we outlined the conceptual importance of the Naturalness argument but we also remarked that it does not guarantee the discovery of new physics. The EWSB scale might turn out to be Unnatural, in which case Naturalness would remain as an open theoretical issue but it would have

failed as a guideline to formulate BSM theories and consequently to organize our experimental efforts in the search of new physics. It is thus interesting to consider alternative paradigms for BSM physics, independently of any Naturalness or Unnaturalness consideration. Several approaches exist and some of those will be described below, classified as "Minimal Models" and "Dark Sector" scenarios. For the purpose of this document we will mainly focus on the models which might be tested by experimental programs of interest for CSN1, and for which dedicated experiments are being proposed.

5.4.1 Minimal models

The "Minimality Principle" is the idea that we should extend the SM with the smallest possible set of fields and renormalisable interactions which are sufficient to account for the experimental evidences. This could lead to a renormalisable and thus completely calculable and self-sufficient description of Nature below the Planck scale. Minimality is a well motivated criterion and it is indubitably the guideline we would adopt if a clear discovery of a BSM particle occurred: we would simply add it to the spectrum without worrying too much if it fits or not with our theoretical prejudices based on Naturalness or on other considerations. Moreover we do have experimental evidence of BSM physics, namely neutrino mass, Dark Matter (DM) and Dark Energy. Furthermore the observed Baryon Asymmetry of the Universe seems to require a dedicated "Baryogenesis" mechanism and the need of Cosmic Inflation also appears as an established fact. Clearly none of these experimental facts is as sharp as a new particle discovery and any of them could be accounted for by a number of radically different mechanisms. Nevertheless we can try to account for some or all of them by the Minimality Principle.

For instance, the existence of DM can be explained in a minimal scenario [385] which extends the SM with only one multiplet of the EW group. This easily explains the correct DM abundance thanks to the WIMP Miracle with a DM mass in the multi–TeV range. In this scenario the concept of Minimality is extended in the sense that not only the particle but also the symmetry content of the theory is minimal: the DM stability is due to an accidental discrete symmetry which need not be imposed on the theory. Another example is the "New Minimal SM" [386], which explains DM by introducing one new scalar degree of freedom and neutrino masses by two right–handed neutrinos. The latter are also responsible for Baryogenesis via Leptogenesis. One scalar Inflaton provides Cosmic inflation and Dark Energy is introduced as a cosmological constant term. This explains all the currently observed phenomena including classical Gravity in terms of a model which remains weakly–coupled up to the Planck scale, where new unspecified ingredients will be needed for a quantum theory of Gravity.

Along similar lines, another option is the "ν Minimal SM" (νMSM) [387, 388]. The model, its experimental signatures and the perspectives of testing it with future experiments are described in detail below.

5.4.2 νMSM

5.4.2.1 Motivation

The νMSM is a Minimal model that accounts for neutrino masses, for the evidence of dark matter (DM) and of the baryon asymmetry of the Universe.

The simplest and most popular option to account for neutrino masses is adding right-handed singlet neutrinos ("sterile neutrinos" (SN) in the following) to the SM field content (at least two, most often three, one for each family of SM fermions). Their introduction is also motivated by several gauge extensions of the SM group (LR symmetric groups, Pati-Salam, SO(10)): they make the SM fermion content more symmetrical. By means of those three additional SN only, with appropriate Majorana masses and couplings, the νMSM can account not only for neutrino masses, but also for the evidence of dark matter and for the baryon asymmetry in the universe — a remarkable result.

The three SN generate Majorana masses for the three SM neutrinos through the see-saw mechanism [389–392]. While in most see-saw models the SN live much above the electroweak scale, in the

νMSM they are lighter. The lightest state (N_1 in what follows) is in the $\mathcal{O}(1\text{–}10)\,\mathrm{keV}$ range, while the two heaver ones ($N_{2,3}$) have a mass that can be as low as (0.2–2) GeV (depending on assumptions) and as large as the EW scale.

The scale of the SN affects our understanding of the anomalous smallness of neutrino masses. The special feature of singlet neutrinos is that their masses do not arise from EWSB and are therefore allowed to be arbitrarily large. Superheavy SN then allow to account for the smallness of neutrino masses while keeping their Yukawa couplings of the same order as the SM ones, $\mathcal{O}(10^{-5}\text{–}1)$. The scale of the SN in the νMSM requires Yukawa couplings in the $\mathcal{O}(10^{-11}\text{–}10^{-6})$ range. Very small Yukawa couplings are of course also viable.

On the other hand, the fact that all its degrees of freedom lie at a scale not larger than the Higgs mass provides a further motivation for the νMSM, as it allows to speculate on possible unorthodox solutions of the naturalness problem of the Higgs mass. In fact, as discussed above, the latter problem is physically meaningful only in the presence of superheavy degrees of freedom. Of course, as also discussed above, such speculations have to address the existence of the Planck scale and imply giving up not only lepton number breaking at superheavy scales but also our understanding of the structure of the SM gauge quantum numbers in Grand Unified Theories (although the hypercharge quantum numbers can still be accounted for by anomaly cancellation [393, 394]).

In any case, the existence of new physics below the EW scale, so far undetected because of their small couplings to the SM fields, is complementary to the standard setup in which new physics is undetected, despite its sizeable coupling to the SM fields, because significantly heavier than the EW scale.

5.4.2.2 Discussion and structure of the allowed parameter space

The constraints from the observed dark matter relic density, baryon asymmetry, and neutrino masses and mixings and consistency with the known cosmological, astrophysical, and experimental bounds lead to quite a specific spectrum. The constraints on the parameter space depend on the assumptions made on the model and the cosmological evolution.

In the minimal (or "constrained") version of the νMSM no extra fields (such as extra scalars, or an inflaton) or interactions (such as higher order operators) are added to the νMSM lagrangian, except possibly Planck suppressed higher order operators. The νMSM therefore holds, as it is, up to the Planck scale. At temperatures well above the EW scale, the N_1 density, accounting for DM, and the baryon asymmetry vanish [387, 388, 395]. The dark matter abundance, the baryon asymmetry, and neutrino masses are all generated within the νMSM dynamics (the baryon asymmetry around or above the EW scale, the dark matter abundance and neutrino masses below it; dark matter production occurs due to the lepton asymmetry generated during the freeze out or non-equilibrium decays of $N_{2,3}$ at temperatures around few GeV). This is of course quite an appealing set-up because of its predictivity and self-sufficiency, but is strongly constrained and the possibility to test its parameter space with SHiP is not obvious, while FCC-ee accelerator experiments can probe part of it, as discussed in the next Section. This parameter space can be constrained by further development of the theory of the early Universe and by new cosmological data.

Extended versions of the νMSM can include inflation scenarios, most notably by introducing non-minimal coupling between the Higgs field of the SM and gravity. Alternatively, they assume that either neutrino masses or the dark matter abundance or the Baryon asymmetry involve extra ingredients, such as higher dimensional operators below the Planck scale (for neutrino masses [396] or to get the correct DM abundance and baryon asymmetry [397]) or additional fields or interactions (e.g. for the DM abundance [398, 399]). The advantage of such extended versions of the νMSM over the SM may be reduced (neutrino masses and the baryon asymmetry, for example, could be accounted for by analogous non-minimal extensions of the SM, without light singlets [397]), but the parameter space of this extended class of models is significantly less constrained, giving rise to additional possibilities of experimental

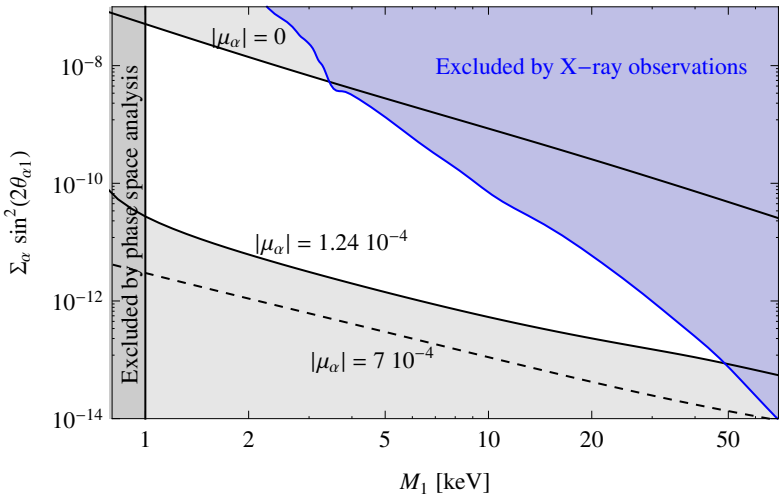

Fig. 59: Allowed parameter space for the lighter singlet neutrino N_1 [404] (see text).

tests by future experiments, as discussed in the next sections. Moreover, the extra ingredients involved, *e.g.,* inflaton, can give rise to new experimental signatures and can be possibly detected in those experiments.

Let us briefly illustrate the constraints on the parameter space mentioned above. As mentioned, the three sterile neutrinos split in two sets, a lighter one, N_1, and two heavier ones, N_2 and N_3.

The lighter SN constitutes the dark matter (it is unstable, but its lifetime is much longer than the age of the universe). Its mixing with the other two neutrinos and its contribution to the light neutrino masses through the see-saw formula are negligible. Its mass is in the $\mathcal{O}(1\text{–}10)\,\mathrm{keV}$ range. The constraints on its relevant parameter space are summarized in Fig. 59 [400]. On the two axes are the N_1 mass M_1 and a combination of its mixings $\theta_{\alpha 1}$ with the SM neutrinos ν_α. The νMSM allowed parameter space corresponds to the unshaded region. In non-minimal versions, the region below the lower solid line (labelled by the lepton asymmetry attainable within the νMSM) are also allowed. The angles $\theta_{\alpha 1}$ are determined by its $\mathcal{O}\left(10^{-11}\right)$ Yukawa couplings. The recent weak line found in the X-ray spectra of galaxies and galaxy clusters [401, 402] and the Milky Way center [403] represents an intriguing hint for a dark matter particle with mass and couplings in the very range shown in Fig. 59 [400].

Since N_1 does not contribute significantly to the see-saw, the lightest active neutrino mass turns out to be negligible. As a consequence, the absolute scale of neutrino masses is predicted to be the lowest possible, and the two heavier neutrinos are predicted to have masses $m_2 \approx 0.9 \cdot 10^{-2}\,\mathrm{eV}$ and $m_3 \approx 0.5 \cdot 10^{-1}\,\mathrm{eV}$ (normal hierarchy) or $m_1 \approx m_2 \approx 0.5 \cdot 10^{-1}\,\mathrm{eV}$ (inverted hierarchy) [387]. The effective Majorana mass m_{ee} entering neutrinoless double β decay (the "11" entry of the neutrino mass matrix in the flavour basis) is also predicted to be $1.3\,\mathrm{meV} < |m_{ee}| < 3.4\,\mathrm{meV}$ (normal hierarchy) and $13\,\mathrm{meV} < |m_{ee}| < 50\,\mathrm{meV}$ (inverted hierarchy) [405].

The two heavier SN are associated to the generation of the baryon asymmetry. Their masses must be i) degenerate and ii) not much lighter than a GeV. In the minimal νMSM defined above, the two latter constraints may challenge the possibility of a natural and testable simultaneous explanation of neutrino masses, dark matter, and baryon asymmetry. Let us then quantify those two constraints in turn, assuming first that everything is accounted for by the low-energy νMSM dynamics.

The mass difference $\Delta M_{23} = |M_2 - M_3|$ must be in this case $(10^{-9}\text{–}10^{-7})\,\mathrm{eV}$ or $(10^{-14}\text{–}10^{-10})\,\mathrm{eV}$ [396, 406], [14] The challenge here is that ΔM_{23} gets a contribution Δm_ν from the

[14] To provide a dark matter candidate (N_1) which does not contradict X-ray and Lyman-α constraints, it is sufficient to have

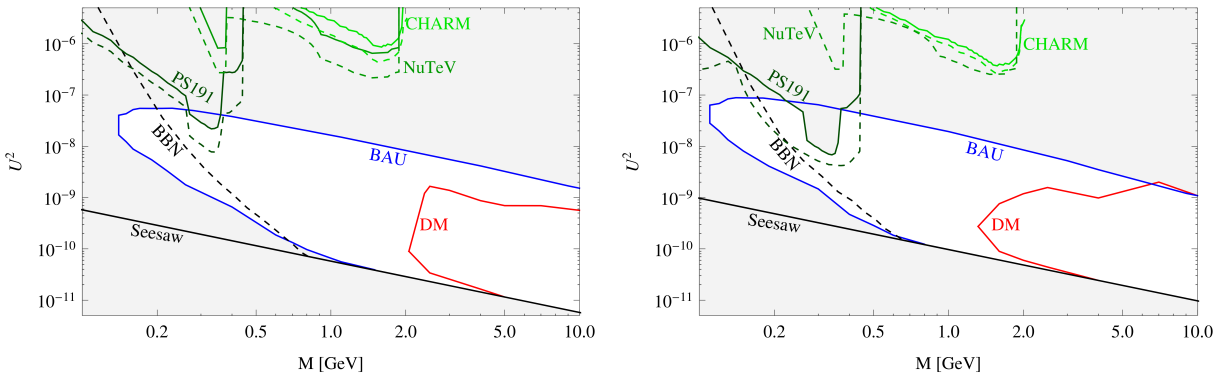

Fig. 60: Constraints on the common $N_{2,3}$ mass M and total mixing U^2 for the case of normal (left panel) and inverted (right panel) neutrino mass hierarchy.

seesaw that turns out to be given by the much larger difference of the two heavier SM neutrino masses, $\Delta m_\nu = 0.04\,\text{eV}$ (normal hierarchy) or $\Delta m_\nu = 0.8 \cdot 10^{-3}\,\text{eV}$ (inverse hierarchy). This can be cancelled by other contributions, but at a price of a tuning of at least one part out of 10^4–10^6. Otherwise, a non-minimal ingredient is needed. For example, one way to avoid the above cancellation is to give up the assumption that the νMSM alone accounts for light neutrino masses [396]. In such a case, physics beyond the νMSM is required to account for neutrino masses, but the νMSM can still account for dark matter and the baryon asymmetry. Alternatively, relaxing the hypotheses on the dark matter production, the parameter space opens up and both the baryon asymmetry and neutrino masses can be explained without fine-tuning [407].

Let us now consider the allowed range for the heavier degenerate SN (again within the scenario of low temperature lepton asymmetry generation). The relevant parameter space is shown in Fig. 60 [404]. The region within the blue line allows to account for the baryon asymmetry (for proper values of the free parameters of the model) within the νMSM. The part of the parameter space in which the DM abundance is also accounted for by the νMSM dynamics, as discussed in the definition of "minimal" νMSM above, is the one within the red line. This part is barely accessible by the experiments discussed in the next Sections, but it should be said that those lines are affected by theoretical uncertainties (up to $\mathcal{O}(1\text{–}2)$) and, again, not so drastic extensions of the νMSM (involving *e.g.,* an inflaton or other non-minimal interactions) can avoid the dark matter constraint [397–399, 408]. The common mass of $N_{2,3}$ is on the horizontal axis, while the vertical axis shows the (squared) total mixing with the three active neutrinos $U^2 = \sum_{\alpha=e,\mu,\tau} |U_\alpha|^2$. The mixings with the active neutrinos U_α are determined by the corresponding Yukawa couplings, are related to active neutrino masses and mixings, and are experimentally relevant as they enter the amplitude for $N_{2,3}$ production and decay. Also shown in the plot are the bounds from accelerator experiments and big-bang nucleosynthesis. Below the "seesaw" line, the mixing is too small to give rise to light neutrino masses sizeable enough.

Let us finally comment on the size of the parameter space that can be accessed by future experimental searches. We focus here on non-minimal versions, for which the entire region within the blue line in Fig. 60 (and not excluded by BBN or other experiments) can be considered as a conservative benchmark scenario for future searches.

a ΔM_{23} larger than Δm_ν, which does not require fine-tuning. The extra constraints follow from the requirement that the necessary abundance is produced by the νMSM interactions. Astrophysical and cosmological (structure formation) data seem to imply that a non-zero lepton asymmetry is required at the moment of DM production, although the systematic uncertainties on those data might challenge this conclusion. If that is the case, and the resonant production of dark matter N_1 occurs due to the lepton asymmetry that was generated during the freeze out or non-equilibrium decays of $N_{2,3}$ around a few GeV, the much smaller values of ΔM_{23} quoted above are required.

The region along the horizontal axis covered by production through charm or B meson decays lies of course below their masses (see Fig. 61) and is therefore only a portion of the allowed range, which extends up to the EW scale. On the other hand, symmetry arguments can be invoked to motivate a mass M not far from the GeV range [409].

The region along the vertical axis within the reach of foreseen experiments is not very close to the "seesaw" line in Fig. 60 The meaning of the "seesaw" line is the following. If only one of the two SN $N_{2,3}$ took part to the see-saw, the corresponding Yukawa, and thus the total mixing U^2, would be determined (for a given value of M) by the see-saw formula in terms of the atmospheric neutrino mass scale, $m_{\rm ATM} = (\Delta m^2_{23})^{1/2} \approx 0.05\,{\rm eV}$, to lie on that line. The parameter space below or above that line would not be allowed. On the other hand, as both neutrinos contribute (through the seesaw) to the light neutrino masses, a cancellation between their two contributions can take place. This allows their Yukawas to be larger than in the previous case and U^2 to lie above the "seesaw" line. Clearly, the further away a point in Fig. 60 is from the seesaw line, the stronger is the cancellation required. On the other hand, such a cancellation is not necessarily accidental, as it could be enforced by a slightly broken symmetry [406, 409], already suggested by the necessary approximate degeneracy of $N_{2,3}$.

5.4.2.3 Signal characteristics

The minimal model discussed above has a well defined phenomenology which can be explored with accelerator experiments. This phenomenology is common to a larger class of models incorporating SN. In this section the status and perspective of experimental searches will be described in a generic scenario. The considerations in Section 5.4.2.2 about the limitations in parameter space provided by the benchmark minimal model can be further applied to the generic analyses discussed in the following. Depending on the SN mass value, one could expect for the SN a few different signatures. At low masses, $\mathcal{O}(MeV)$, the SN may lead to observable effects in short-medium baseline oscillation experiments. Indeed, some departure from the expected behavior of the standard three family oscillation scenario has been recently observed [410–417], hinting, though with a tension among the different measurements, towards a fourth neutrino.

At intermediate masses, from MeV to the Z^0 mass, the SN can be produced in the decay of mesons or gauge bosons (actually, whenever an active neutrino is present in the decay diagram) and may decay into standard model particles [418–427].

Since the SN mixes with the active neutrinos with a probability U^2, in experiments where on-shell SN production is searched for, one has to account for a factor U^2 at the production and another U^2 at the decay. Both production and decay occur in Feynman diagrams that include a neutrino, such as the semi-leptonic $D \to X + M_N$ or $W \to \mu\nu$ decays, and the $M_N \to \pi\mu$ at masses below a few GeV (this decay being just the inverse process of the pion decay) or $M_N \to q\bar{q}\nu$ decays at larger masses.

The lifetime of the SN is therefore also proportional to U^2 and, for relatively small masses, below a few GeV, is very long, leading to decay paths of the order of several km, for U^2 values that are not already excluded by past experiments.

Two types of experiments are in principle possible: at masses below a few GeV, if one wants to observe the SN decay in the detector (e.g. like in the past PS191, CHARM or NuTeV [428, 429]), since the detector for practical reasons is much shorter than the SN mean decay length, the number of expected events is proportional to U^4 and therefore, to maximise the sensitivity, as long as a possible detector is needed; at larger masses the lifetime shortens considerably and therefore the dependence becomes U^2. The other possibility is to make a kink search, allowing for a U^2 dependence no matter what the lifetime is, though this approach requires a full control of the event kinematics, which is only possible in a very limited set of experiments like electron-proton colliders.

Excluded ranges in the U^2 vs Majorana mass m plane from theoretical considerations depend on the details of the model, and have been discussed above. The studies discussed in this section focus on

the region allowed by the Baryon Asymmetry of the Universe (BAU) and by the seesaw mechanism.

As said above, three guidelines in designing experiments are important: maximizing the signal yields, maximizing the detector acceptance and suppressing the backgrounds, the latter coming both from other decay modes of the parent particle and from the other particles in the event. In general, this background suppression requirement is the toughest to be achieved.

SHiP at SPS

The proposed SHiP experiment [430, 431] is a beam dump experiment, performed with the maximum possible intensity of the CERN-SPS 400 GeV proton beam, aiming at detecting beyond-the-SM long-lived sterile or weakly interacting particles, that decay into SM particles. The beam and particle backgrounds are suppressed to negligible levels by adding a particle filter downstream of the target, allowing only the new particles (plus some residual muons and the active neutrinos) to reach a long evacuated decay tunnel equipped with detectors. The particle filter, the decay tunnel and the position of the detectors are designed to optimize the sensitivity to new physics, for the given proton beam. The residual muon and active neutrino induced backgrounds can be effectively suppressed by kinematics and particle identification cuts.

The experiment is designed such that a significant evidence, above the expected backgrounds, for decays inside the decay tunnel can be directly interpreted as physics beyond the SM: interesting signals include e^+e^-, $\mu^+\mu^-$, $\pi^+\pi^-$, $\pi^+\mu^-$, π^+e^-, $\rho^+\mu^-$, ρ^+e^- pairs originating from a single vertex located in the decay tunnel.
To quantify the sensitivity and compare it to existing or planned experiments, interpretation in the context of the different portals is given. In the context of the neutrino portal, SHiP aims at improving by 2 orders of magnitude the U^2 sensitivity reach of past experiments, as shown in Fig. 61 for different values of the model parameters, exploiting SN's from D and B decays. The design of this experiment is still in an

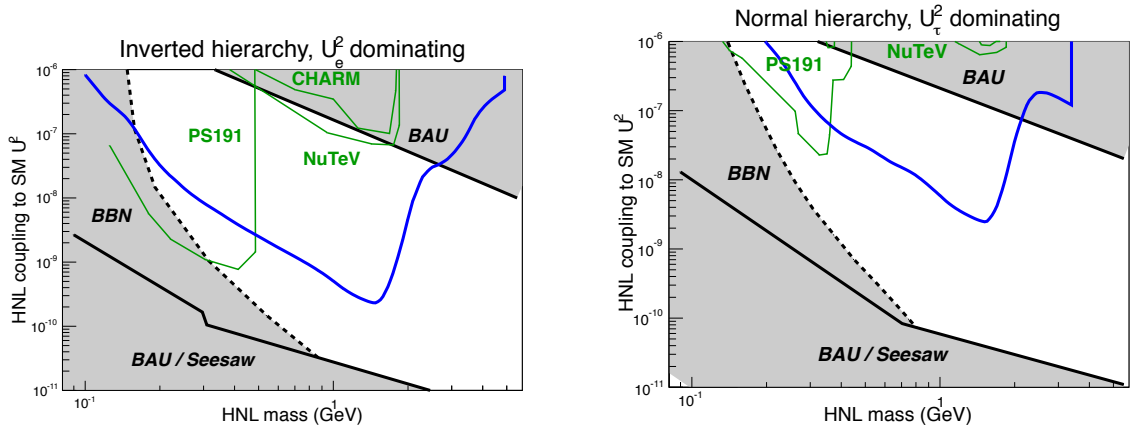

Fig. 61: Past and future of neutrino portal: in blue the SHIP sensitivity (expressed at 95% C.L. expected upper limit assuming 0 observed events in $2 \cdot 10^{20}$ p.o.t.), in grey the excluded regions from cosmological considerations in the model of [388]. The two plots correspond to the possibility that the parameter U^2 defined in Section 5.4.2 is dominated by the mixing with the electron or the tau lepton respectively.

optimization phase so that the results on sensitivity shown here have to be considered as preliminary.

NA62 at SPS

NA62 is an experiment devoted to the search for rare K decays at the CERN SPS scheduled to take data from this year. Designed to operate with a high intensity hadron beam, it has a high-acceptance

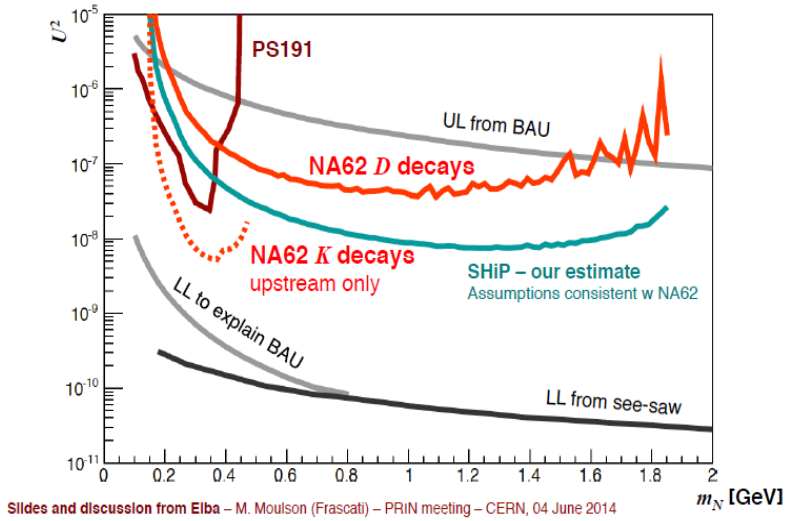

Fig. 62: Sensitivity of the NA62 experiment to a Majorana Neutrino. The assumed statistics is 5 years of data at SHiP intensity: 4.5×10^{13} protons per spill (ppp). The continuous (dashed) red lines show the NA62 sensitivity respectively for D (K) decay. The light blue line shows an estimate of the SHiP sensitivity calculated under the same assumptions.

spectrometer and a 65 m decay region. Both K and D decays can be used in the search of a SN. A preliminary study was performed [432] from which the results shown in Fig. 62 is extracted. The main conclusion, based on the simulation of an existing detector is that with the same beam assumed for the SHIP experiment, a sensitivity can be expected which is approximately one order of magnitude lower than the ultimate SHIP sensitivity.

High energy hadronic and leptonic colliders

Sterile neutrinos below the W/Z mass can be searched for in the decays of the W and Z bosons, which are very abundantly produced at the high-luminosity LHC and at the proposed FCC, both in its ee and hh configurations. The signature for the decay $Z \to \nu\mathrm{SN}$ is the decay of the SN into a lepton or a hadron pair inside the sensitive volume of the detector. For the case of leptonic decays away from the primary vertex, this signature is dubbed 'lepton jets'. The ATLAS collaboration [433] has e.g. published an analysis on existing data showing that 'lepton jets' can be detected with acceptable efficiency and separated from backgrounds in a fiducial volume between approximately 1 cm and 1 m from the interaction vertex. The number of SN decays detectable for a given experimental configuration can be simply calculated from the number of leptonic decays of Z or W bosons once the mixings of the SN and the size of the fiducial volume have been specified. An example is given in the study from Reference [434] for FCC-ee, where the coverage in parameter space for different assumed integrated luminosities and assumptions on the fiducial volume is given. An example is given in Fig. 63, where one can observe that with a sufficient number of Z decays, and separation from signal and background, the FCC-ee should be able to cover at least a part of the area for masses above 2 GeV favored by DM constraints in the minimal model.

Similar considerations are valid for high-luminosity LHC, which with 3 ab^{-1} would produce approximately 2×10^{11} Z bosons, and 6×10^{11} W bosons. A 100 GeV FCC-hh with 1 ab^{-1} would produce approximately 4×10^{11} Z bosons and 10^{12} W bosons. Detailed studies would be needed to assess the actual potential, but the vector boson decays seem to be the best chance to cover the mass region up to a few tens of GeV. For the W and a decay of the MN into a lepton and a π, it would yield a signature

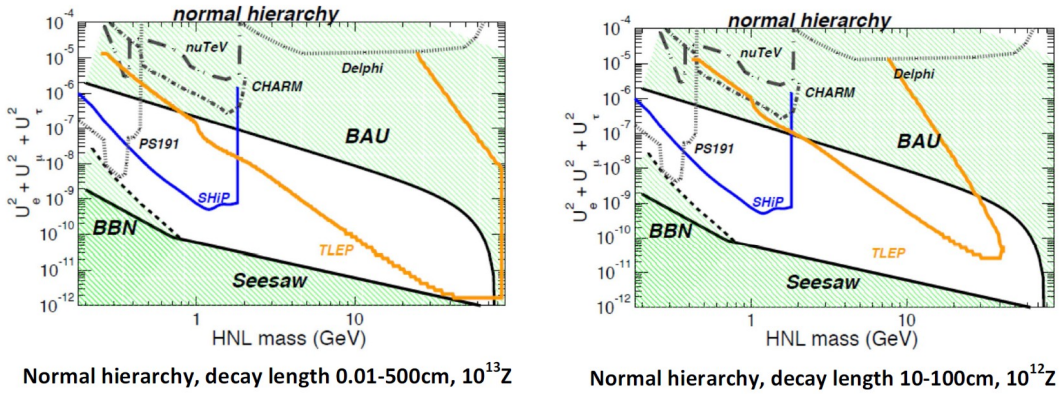

Fig. 63: Sensitivity of experimentation at FCC-ee to a Majorana Neutrino. the TLEP lines correspond to 3 decays produced in the decay interval shown below the figure.

with two leptons and a π with p_T in excess of 20 GeV with invariant mass of 80 GeV, and one of the leptons and the π will have an invariant mass corresponding to the MN mass. Such a signature should allow detection of a signal over a broad range of parameters.

5.4.2.4 Summary

- The νMSM is a simple and minimal model aiming at addressing the main experimental shortcomings of the SM: non vanishing neutrino masses, dark matter, and the baryon asymmetry.
- Its self-sufficient form, in which nothing but its dynamics below the EW scale (in particular a lepton asymmetry produced by decays and freeze out of $N_{2,3}$) accounts for the above anomalies, requires a fine-tuned cancellation and is barely testable by the SHiP experiment, but may be accessible to an experiment at FCC-ee, and partially accessible at a high-luminosity LHC or an FCC-hh experiment.
- Non minimal versions or additional cosmological mechanisms, on the other hand, are natural and have a larger parameter space, whose lower mass, larger mixing part can be tested by the SHiP, HL-LHC and FCC-ee or hh experiments.
- As all Majorana neutrino mass models, the νMSM can be falsified if the light neutrinos are found to be inversely hierarchical and neutrinoless double beta decay experiments exclude the $|m_{ee}| > 10^{-2}\,\mathrm{eV}$ region, or if a partially degenerate neutrino mass spectrum (i.e. a non negligible lightest neutrino mass) is found.

5.4.3 Dark sectors

The Dark Sector paradigm is a way to organize new physics searches based on the following observation. For several reasons we tend to believe that new physics will show up at short distances, *i.e.* at high energies, in the form of particles which are heavy enough to have escaped detection so far. This pushes us towards the exploration of the Energy Frontier. However new physics might have escaped detection not because it is heavy but because it is feebly coupled to the SM particles, which leads to small production rates and negligible indirect effects. We should thus also explore the "High Intensity" frontier, searching for new light weakly–coupled particles which form part of some new Dark Sector. The reader is referred to the dedicated Snowmass report in Ref. [435] for a comprehensive review of the subject.

The Dark Sectors are classified in terms of the operators which mediate their interactions with the SM particles. These interactions are the "Portals" to the Dark Sector, some of which are listed below

Portal	Particles	Operator(s)
"Vector"	Dark photons	$-\frac{\epsilon}{2\cos\theta_W} B_{\mu\nu} F'^{\mu\nu}$
"Axion"	Pseudoscalars	$\frac{a}{f_a} F_{\mu\nu}\widetilde{F}^{\mu\nu}$, $\frac{a}{f_a} G_{i\mu\nu}\widetilde{G}_i^{\mu\nu}$, $\frac{\partial_\mu a}{f_a}\overline{\psi}\gamma^\mu\gamma^5\psi$
"Higgs"	Dark scalars	$(\mu S + \lambda S^2) H^\dagger H$
"Neutrino"	Sterile neutrinos	$y_N L H N$

Each portal is representative of a class of theories and in each class one can find representative and motivated models. For instance the sterile neutrinos discussed in detail in the previous section fit in the "Neutrino" Portal. Models solving the strong–CP problem involve Axions and provide one example of the "Axion" Portal. Furthermore Axions might be valid DM candidates, providing one further motivation for this Portal.

Generically for this kind of model the Hidden particles are produced by mixing with ordinary particles, such as photons, neutral pions and active neutrinos, and can be looked for in the decays of heavy flavour hadrons or gauge and higgs bosons, or in their direct production. Given the large range of masses and couplings considered for these models, searches with accelerators will benefit from complementary approaches, including high intensity fixed target experiments with both electron and proton beams, with both thin and thick ("beam dump") targets, and high luminosity and high energy collider experiments. In particular for masses below a few GeV there is a window of opportunity for fixed target in the exploration of very low couplings to the hidden sector which may imply very high intensity and the possibility to measure decays lengths in excess of a few meters, both of which can be difficult or impossible to achieve in high energy colliders.

The next sections will concentrate on two Portals, namely the Vector and the Higgs Portals. In order to avoid repetition with Ref. [435], the existing limits, and the proposals described for Snowmass will only be briefly treated, giving more emphasis on more recent work which has become available in the last year or so.

5.4.3.1 Vector portal

The "Dark Photon" (DP) is the simplest and most studied benchmark for the Vector Portal. It is a new Abelian gauge field A' associated to a new $U(1)_D$ "Dark" symmetry that we add to the SM group. The SM fields are neutral under $U(1)_D$ and thus their interactions with the DP (as in Table 5.4.3) can only emerge from kinetic mixing, the one with the SM Hypercharge B being the only one allowed by symmetries. This mixing reads

$$-\frac{\epsilon}{2\cos\theta_W} B_{\mu\nu} F'^{\mu\nu}\,, \tag{27}$$

where θ_W is the Weinberg angle and ϵ is an arbitrarily small parameter. Giving a mass to the DP requires the $U(1)_D$ group being spontaneously broken by one further "Dark Higgs" new physics sector which we take to be completely neutral under the SM group. In this hypothesis it cannot not participate to EWSB and thus it delivers a mass only for the A' boson

$$\frac{1}{2} m_{A'}^2 A'^\mu A'_\mu\,. \tag{28}$$

The DP mass is also a completely free parameter from the theoretical viewpoint. In principle, the Dark Higgs sector could deliver a more general mass–matrix, including a Z–A' mixings, but only if it is charged under the EW group and breaks the EW symmetry. This possibility is however disfavored by the strong lower limit on the scale of new EW–charged particles combined with the upper one on new contributions to EW boson masses. The combined diagonalization of the kinetic mixing and of the mass–matrix (including of course the SM Z mass term) gives an order ϵ A' component to the physical Photon, leading to an A' coupling to the EW current

$$\epsilon e A'_\mu J^\mu_{\rm EM}\,. \tag{29}$$

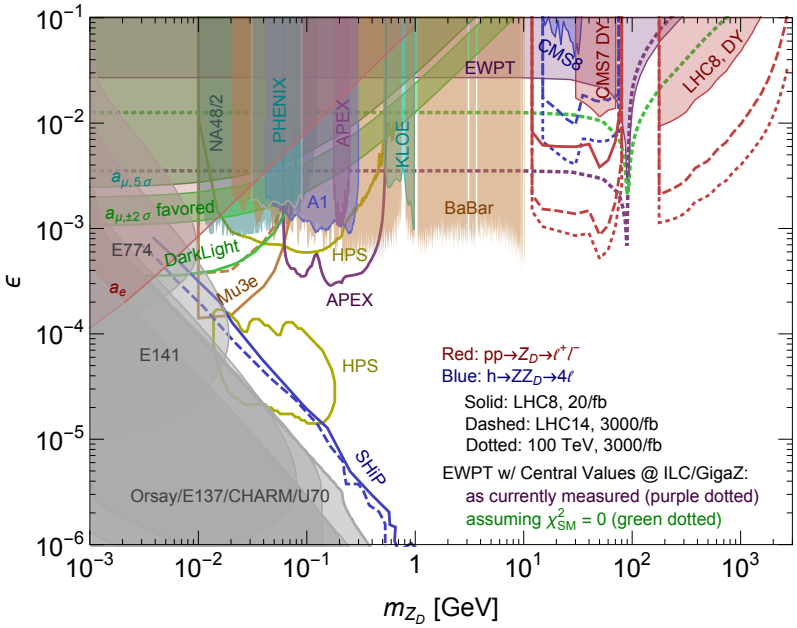

Fig. 64: Summary of dark photon constrains and prospects in the $\epsilon - m(Z_D)$ plane ($Z_D \equiv A'$ in the text) based on in visible $Z_D \equiv A'$ decays, and on precision EW observables.

The A' component of the physical Z boson is instead of order $\epsilon m_{A'}^2/m_Z^2$ which is completely negligible in most of the parameter space.

The DP phenomenology is extremely simple. It is produced in the same way as a Photon, but with ϵ^2 suppressed rate. It decays, if kinematically allowed, to all the possible charged particle/anti–particle pairs with relative Branching Ratios dictated by the electric charge. This includes decay to charged leptons or to hadrons. If these are the only decay channels, the DP decay length is

$$\gamma c\tau \simeq \frac{0.8\text{cm}}{N_{\text{eff}}} \left(\frac{E_0}{10\text{ GeV}}\right)\left(\frac{10^{-4}}{\epsilon}\right)^2\left(\frac{100\,\text{MeV}}{m_{A'}}\right)^2 \tag{30}$$

where N_{eff} counts the number of kinematically allowed decay channels and E_0 is the A' energy. The current experimental situation and future prospects in the $\epsilon - m_{A'}$ plane (from Ref. [435]) are summarized in Fig 64. All the direct search limits in the figure assume the absence of additional decay channels for the DP, namely unit Branching Fraction to visible objects is assumed.

Below we discuss two experiments that might make progresses in this plane and might be of interest for CSN1.

SHiP

In the proton beam dump experiment, three production mechanisms of the Dark photon were considered: meson decays, proton bremsstrahlung, and QCD production [436–438], which provides valid formulae up to masses of about 3 GeV. The reach of the SHiP experiment has been the object of a recent theoretical study, [438], and a detailed study from the Collaboration [439]. Assuming no background, and the ability to detect with 100% efficiency all decay channels of the dark photon, both leptonic and hadronic, a 90% C.L. sensitivity area is obtained, in the $\epsilon^2 - m_{A'}$ plane, shown in in Fig. 65.

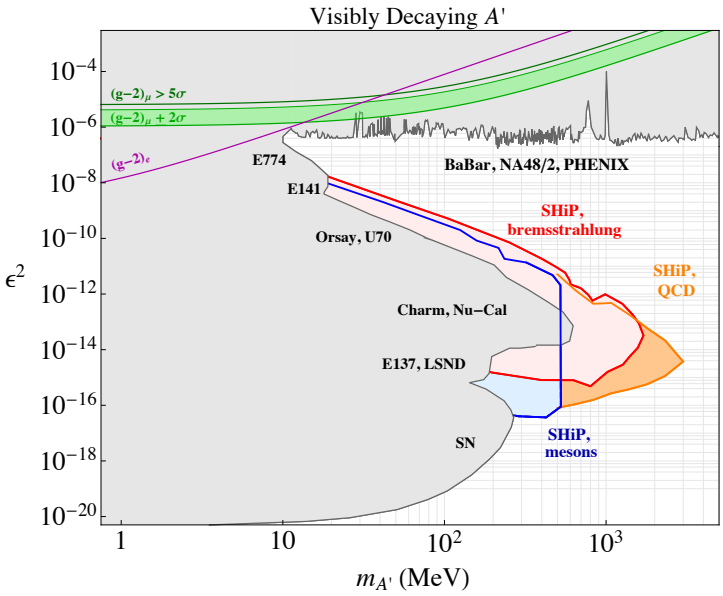

Fig. 65: Constraints on the dark photon model. The projected SHiP sensitivity contour is derived using three modes of production: mesons, bremsstrahlung, and QCD production.

PADME

The DP searches performed so far were based on the hypothesis that the dark sector does not contain any particle of mass lower than that of the A' and therefore it decays to Standard Model lepton or meson pairs. In the most general scenario the dark sector may contain particles lighter than the dark photon itself, thus allowing the so called "invisible" decays. The decay products are non-Standard Model particles which escape detection. Given the small coupling of the DP to visible objects, which makes the visible rates suppressed by ϵ^2, it is not hard to imagine a situation where the invisible decay dominate, the visible rate is small and the previous searches are ineffective. There are studies on the searches of a A' decaying into dark sector particles. However, the sensitivities sometimes rely on the assumption that the dark decay products constitute the dark matter, and are anyway model dependent [440].

The Positron Annihilation into Dark Matter Experiment (PADME) [441] aims at a model-independent search for the production of a dark photon using the 550 MeV positron beam provided by the LNF DAϕNE linac impinging on a thin target. The process of interest is

$$e^+e^- \to A'\gamma, \tag{31}$$

where the positrons are the beam particles and e^- are the electrons in the target. The accompanying SM photon 4-momentum is measured by a calorimeter regardless of the A' decay products. A single kinematic variable characterizing the process, the missing mass, is computed using the formula:

$$M^2_{miss} = (P_{e^-} + P_{beam} - P_\gamma)^2. \tag{32}$$

Its distribution should peak at $M^2_{A'}$ for DP decays, at zero for the concurrent $e^+e^- \to \gamma\gamma$ process, and should be smooth for the remaining background. The experiment is composed of a diamond target, to measure the average position and intensity of the beam during a single bunch, a spectrometer immersed in field of a dipole magnet, to deflect the positron beam and to measure the charged particle momenta, and an electromagnetic calorimeter to measure/veto final state photons. The apparatus is inserted into a vacuum chamber, to minimize the unwanted interactions of primary and secondary particles.

The possible DP production mechanisms accessible in e^+-on-target collisions are $e^+e^- \to A'\gamma$ and $e^+N \to e^+NA'$, the so called annihilation and A'-strahlung production. Both processes are similar

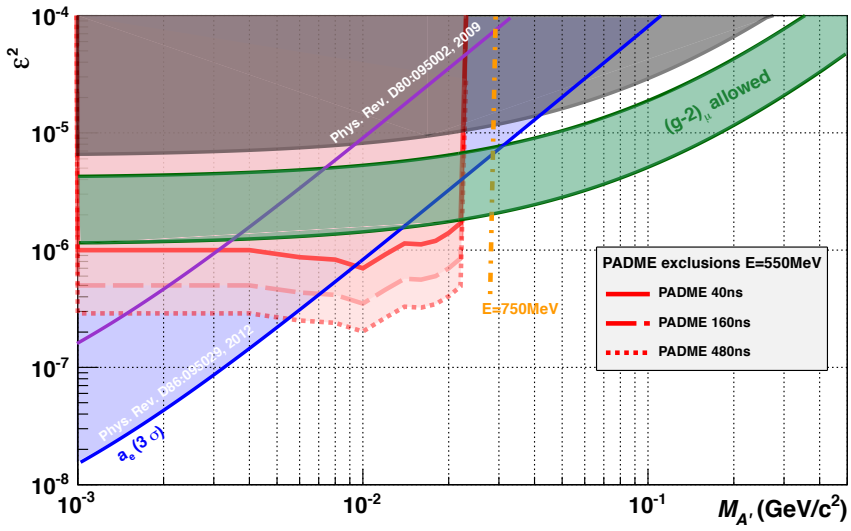

Fig. 66: *Expected exclusion in the invisible channel compared with the band of values preferred by current $g_\mu - 2$ discrepancies. [441]*

to the ones for ordinary photons, and their cross section scales with ϵ^2. Four different types of dark photon searches are in principle accessible by combining production processes and decay final states: annihilation produced DP decaying into dark sector particles or into $\ell^+\ell^-$ pairs, bremsstrahlung produced dark photons decaying into dark sector particles or into $\ell^+\ell^-$ pairs. The present linac maximum positron energy of 550 MeV allows the production of dark photons through annihilation up to a mass of 23.7 MeV, while an upgrade to 750 MeV would allow to reach 27.7 MeV. Masses up to 600 MeV can be reached by DP produced by A'-strahlung using 800 MeV electrons. At present detailed studies have been performed only for annihilation production to asses the sensitivity to invisible decays. Studies on the other final states are ongoing.

The sensitivity of the experiment was estimated assuming one year of running with 60% efficiency, a constant positron flux and different bunch lengths, as indicated in Fig. 66, corresponding to about $1 \cdot 10^{13}$, $3 \cdot 10^{13}$, and $1 \cdot 10^{14}$ positrons on target respectively. Under the assumption of no signal, an upper limit on the DP coupling ϵ can be set, using the statistical uncertainty on the simulated background. The result shown in Fig. 66 applies to both visible and invisible dark photon decays, since the selection includes both cases. The Figure also shows the region excluded (grey) and favoured (green) by the $g_\mu - 2$ measurement, and the region excluded by the $g_e - 2$ measurement (blue) [442]. PADME sensitivity to visible decays of DP generated by bremsstrahlung is under investigation together with the possibility of performing a dedicated beam dump experiment with 10^{20} electrons on target (EOT) [443]. The PADME search for new low mass mediators is completely general, in particular in the "invisible" case. Therefore the experiment will be sensitive to any new small mass particle, like low mass dark Higgs [444] or leptonic gauge bosons [445], produced in e^+e^- collisions.

ATLAS and CMS

The search for dark photons is a very active field of analysis at the LHC, and search results have been published by ATLAS and CMS. The published results mostly focus on the search for “lepton jets” in the decay of a Dark Higgs in the FRVZ [446, 447] model. The latest result from ATLAS is shown in Fig. 67, where the excluded area in the mass-coupling plane is shown. The result is of course only valid in the assumed FRVZ model, but it gives a feeling on real data of the interval of couplings which can be

covered at the LHC in this kind of search.

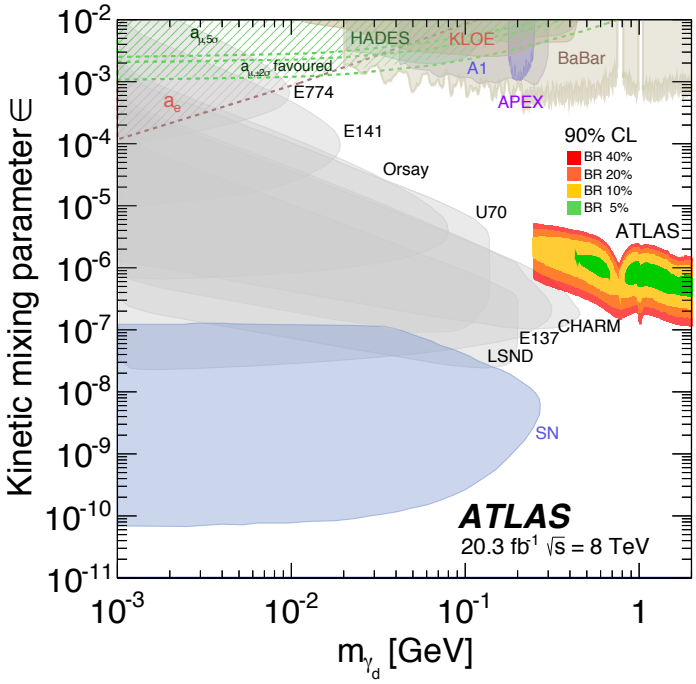

Fig. 67: ATLAS limit in the $\epsilon - m_{A'}$ plane for the model in [446, 447].

Additional possibilities in literature are reviewed in chapter 8 of [448], which identifies three main venues for DP searches at the LHC:

- Direct production of Dark Photons [449, 450];
- Rare Z decays into the dark sector [449, 450];
- Ewkino decays into the dark sector [451].

The number of Dark Photon decays available for detection depends of on the model. For the direct production of the Dark Photon, for instance, the number of prompt photons at a high luminosity LHC with 3 ab^{-1} would be 0.5×10^{12}.

5.4.3.2 Higgs portal

As a last example we consider one specific Higgs portal model where the new dark sector merely consists of a light scalar h (not to be confused with the Higgs H) with mass m_h in the 100 MeV to 10 GeV to be relevant for the SHiP experiment, whose only coupling with the SM is a mixing with the Higgs boson [452]. Because of this assumption, all the h vertices with SM particles are just equal to those of the Higgs scaled down by a factor $\sin\rho$, where ρ is the mixing angle of h with the Higgs. Aside from the mass, the phenomenology is thus entirely characterised by $\sin^2\rho$ that controls the production rate and the lifetime of h

$$c\tau = \frac{c\tau_{SM}}{\sin^2\rho}, \tag{33}$$

where $c\tau_{SM}$ is the mean decay length of a scalar of mass m_h with exactly SM Higgs couplings. There are large uncertainty in the lifetime of h above the $\pi\pi$ threshold, the model of Ref. [453] is assumed here.

As for the case of a dark photon, bounds in the $\sin^2\rho$ vs m_h plane could be set by LEP, meson decays and fixed target experiments. The limits from B-factories and from the CHARM experiment are

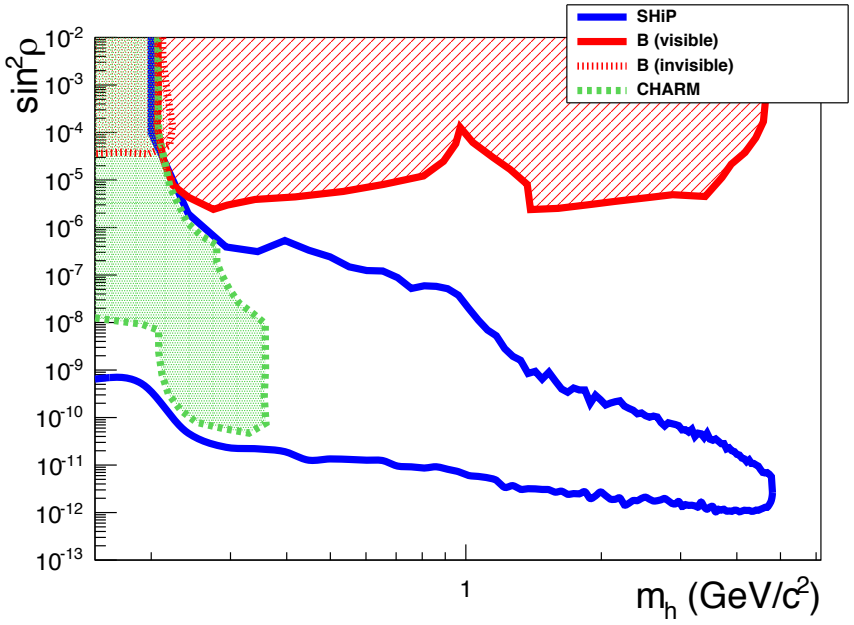

Fig. 68: SHiP exclusion limit at 90 % C.L. for a light scalar particle of mass m_S coupling to the Higgs with $\sin^2\rho$ mixing parameter and decaying in e^+e, $\mu^+\mu^-$, $\pi^+\pi^-$, K^+K^- final states (solid blue line). Red dashed area is the excluded region from B-factories in the visible modes, red dotted area is the excluded region from B-factories in the invisible modes and green shaded area in the exclusion region from the CHARM experiment.

reported in Figure 68, together with an estimate of the SHiP 90% C.L. upper limits in the no–background hypothesis. Only B production was considered since beam dump absorbs most of the kaons.

5.5 Collider friendly dark matter

Interactions of DM with SM quarks are extremely important from a phenomenological point of view since they open the possibility of studying, at the same time, DM production at the LHC and DM elastic scattering on nuclei (direct detection). The simultaneous study of these two processes – usually performed using the effective field theory approach in which the interactions between DM and SM quarks are described by a set of higher-dimensional operators – leads to strong constraints on the characteristic parameter space of the analyzed theoretical framework. On a general ground, it turns out that bounds from direct detection, in particular in the presence of a spin-independent DM-nucleon interactions, are particularly stringent, and they can be alleviated by limiting the analysis to motivated cases in which the corresponding operators are suppressed. In the following we focus on two relevant cases that are consistent with this view:

1. DM is a self-conjugate Majorana particle, $\Psi_{\rm M} = \Psi_{\rm M}^{\rm C}$, singlet under the SM gauge group; in this case the characteristic pseudo-vector bilinear $\overline{\Psi}_{\rm M}\gamma^\mu\gamma^5\Psi_{\rm M}$ has suppressed spin-independent interactions with SM quarks [454], thus leading to a scenario in which direct detection limits do not lead to strong constraints.
2. DM is made of two slightly degenerate states (see also Section 5.3.8); the light state is stable and constitutes the DM of the Universe, while constraints from direct detection – if the mass splitting is larger than the typical $\mathcal{O}(100$ keV) momentum transfer in DM-nucleon scatterings – are avoided since DM cannot scatter elastically [455,456]. In a typical LHC scenario, the slightly heavier state can decay to the light one and produce SM particles [457].

These scenarios represent two ideal paradigms to motivate collider searches of DM. In the absence of direct detection bounds it is crucial to understand the constraining power – or, equivalently, the detection capabilities – of the LHC in the near future.

5.5.1 Majorana dark matter

A self-conjugate Majorana particle $\Psi_{\rm M} = \Psi_{\rm M}^{\rm C}$ is characterized by vanishing vector and tensor structures, $\overline{\Psi}_{\rm M}\gamma^\mu\Psi_{\rm M} = \overline{\Psi}_{\rm M}\sigma^{\mu\nu}\Psi_{\rm M} = 0$, with $\sigma^{\mu\nu} \equiv i[\gamma^\mu, \gamma^\nu]/2$. As a consequence, the only dimension-six operators involving DM and the SM quarks have the following scalar and pseudo-vector structures

$$\mathcal{O}_{\rm S}^q \equiv \frac{m_q}{\Lambda^2}\,\overline{\Psi}_{\rm M}\Psi_{\rm M}\,\left[c_{\rm S}^{(q)}\,\overline{q}q + c_{\rm S_5}^{(q)}\,\overline{q}\gamma^5 q\right]\,, \tag{34}$$

$$\mathcal{O}_{\rm PV}^q \equiv \frac{1}{\Lambda^2}\,\overline{\Psi}_{\rm M}\gamma^\mu\gamma^5\Psi_{\rm M}\,\left[c_{\rm PV}^{(q)}\,\overline{q}\gamma_\mu q + c_{\rm PV_5}^{(q)}\,\overline{q}\gamma_\mu\gamma^5 q\right]\,. \tag{35}$$

In eq. (34) we have assumed that the scalar operators $\mathcal{O}_{\rm S}^q$ scale with the fermion mass m_q, as is often the case. Despite its simplicity, this scenario leads to an interesting phenomenological picture. As far as direct detection properties are concerned, a straightforward analysis of these operators in the non-relativistic limit [454] reveals that the two operators in eq. (34) have, respectively, un-suppressed spin-independent and spin-dependent interactions with nuclei. From the point of view of collider physics, on the other hand, the operators in eq. (34) are usually unconstrained – at least considering DM production via light quarks and typical $\mathcal{O}(1)$ couplings – because of the parametric suppression due to the small value of the quark mass. In this case, therefore, collider physics can not compete with present and future direct detection sensitivities. The two operators in eq. (35), on the contrary, feature opposite properties. In particular, the vector-like interaction with SM quarks, $\overline{q}\gamma_\mu q$, leads to suppressed spin-independent (due to the small value of DM velocity) and spin-dependent (due to the small value of transferred momentum) interactions with nuclei. Finally, the interaction with the pseudo-vector quark current, $\overline{q}\gamma_\mu\gamma^5 q$, has vanishing spin-independent interactions but unsuppressed spin-dependent ones.

All in all, the dimension-six operator in eq. (35) can not be constrained by the strong bound on the spin-independent elastic cross-section on nuclei currently measured by the LUX [458] and XENON100 [459] experiments, and is expected to be out of the reach of forthcoming upgrades on sensitivities. As a benchmark, we focus in more detail on the phenomenology of this effective operator in the context of astroparticle and collider physics. The following discussion does not pretend to be exhaustive; on the contrary, its aim is solely to present a practical example in which collider searches at the LHC play the role of a fundamental cross-channel in dark matter physics. Three observables define the phenomenological scenario we are interested in: *i)* the dark matter relic density, *ii)* the spin-dependent dark matter-nucleon cross-section, and *iii)* the mono-jet searches at the LHC.

The evolution of dark matter density, according to the standard freeze-out paradigm, is driven by the expansion of the Universe and the interactions of dark matter with SM particles; in the presence of weakly-interacting particles an annihilation rate of the order of $\langle\sigma v\rangle \approx 3\times 10^{-26}$ cm^{3}s^{-1} is required. Considering the Taylor expansion in velocity $\langle\sigma v\rangle = a + bv^2 + \mathcal{O}(v^4)$, the only contribution to the s-wave a comes from the operator $(\overline{\Psi}_{\rm M}\gamma^\mu\gamma^5\Psi_{\rm M})(\overline{q}\gamma_\mu q)$ but it features a mass suppression due to a chirality flip in the final state [460]. In order to strengthen the connection with LHC physics, we consider in this discussion only interactions with light quarks $q = u, d, s$; the s-wave contribution, as a consequence, can be neglected and the relic abundance is entirely set by the p-wave term.

The pseudo-vector operator $(\overline{\Psi}_{\rm M}\gamma^\mu\gamma^5\Psi_{\rm M})(\overline{q}\gamma_\mu\gamma^5 q)$ induces a dark matter-nucleon (either proton or neutron) coupling proportional to the fraction of the spin carried by the quark q inside the nucleon, thus resulting in a net spin-dependent dark matter-nucleon cross-section. In order to allow for a direct comparison with the limit found in refs. [461, 462], we focus on this specific interaction and we set $c_{\rm PV}^{(q)} = 0$ in eq. (35).

At the LHC, both ATLAS and CMS are searching for dark matter particles using events containing a jet plus missing transverse momentum [463, 464]. Good agreement is observed between the number of events in data and the SM predictions; as a result, these searches are translated in terms of exclusion limits on dark matter properties.

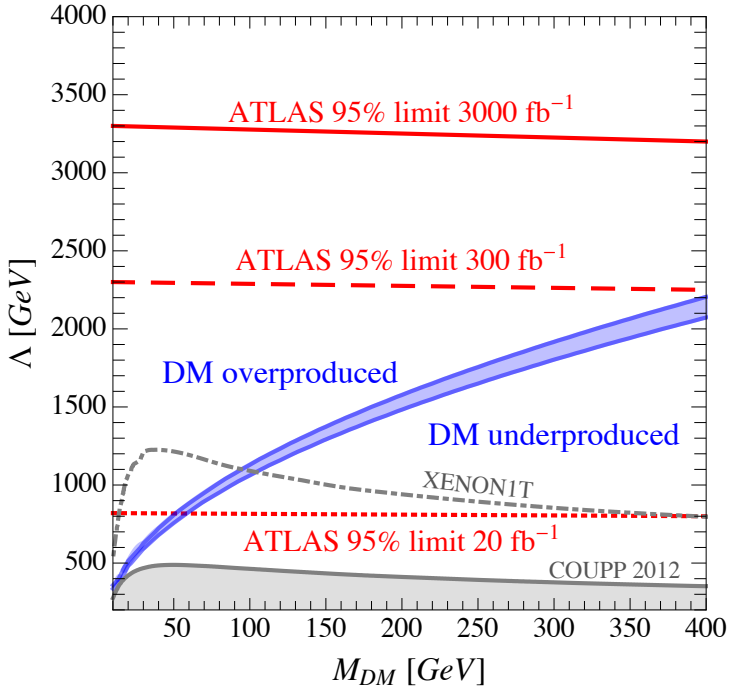

Fig. 69: *Prospective bounds on the effective pseudo-vector operator* $(\overline{\Psi}_{\rm M}\gamma^\mu\gamma^5\Psi_{\rm M})(\bar{q}\gamma_\mu\gamma^5 q)/\Lambda^2$ *in the case of Majorana dark matter. In the blue region the effective operator reproduces the observed value of relic abundance. The limits in red are extracted from ref. [465] for different values of luminosity. The dotted and dashed lines correspond to the 95% C.L. limit with, respectively,* $\sqrt{s} = 8$ *TeV and 20 fb*$^{-1}$ *of luminosity and* $\sqrt{s} = 14$ *TeV and 300 fb*$^{-1}$ *of luminosity; these limits were obtained from the simulation in ref. [465] considering a signal region defined by* $E_{\rm T}^{\rm miss} > 800$ *GeV, and a total background systematic uncertainty equal to 5%. The red solid line represents an optimistic limit with* $\sqrt{s} = 14$ *TeV, 3000 fb*$^{-1}$ *of luminosity, a signal region defined by* $E_{\rm T}^{\rm miss} > 800$ *GeV, and a total background systematic uncertainty equals to 1%. The region shaded in gray is the 90% C.L. limit on the spin-dependent dark matter-proton elastic cross-section derived in ref. [461]; the dot-dashed line represents the XENON1T prospective limit on the same observable.*

In fig. 69, we show prospective ATLAS 95% exclusion limits for different values of luminosities in the plane dark matter mass versus effective scale Λ (see also ref. [466] for a recent analysis in this direction). We assume democratic interactions with light quarks, and we set for simplicity $c_{\rm PV_5}^{(q=u,d,s)} = 1$. The blue region represents the 5-σ region in which it is possible to correctly reproduce the value of dark matter relic density observed by the Planck collaboration [467]. Remarkably, the model exhibits an interesting interplay between relic density and collider prospects at the LHC. With 300 fb^{-1} of luminosity it will be possible to completely cover the region of parameter space in which the model is able to reproduce the correct value of abundance up to $M_{\rm DM} \approx 400$ GeV. More importantly, this region is out of reach of present and future direct detection experiments. For definiteness, in fig. 69 we show the 90% C.L. exclusion limit on the spin-dependent dark matter-proton cross-section derived by the COUPP experiment [461]. This bound is usually much weaker than the corresponding bound imposed on the spin-independent dark matter-nucleon cross section since the total spin-dependent scattering amplitude is determined only by the spins of the unpaired nucleons in a given nucleus. Future prospects of XENON1T (dot-dashed gray line in fig. 69) will be able to test the region reproducing the correct dark matter relic

abundance only for $M_{\rm DM} \lesssim 100$ GeV. As a final comment, we note that the toy scenario outlined in this section can not be constrained by indirect dark matter detection (in particular using the antiproton flux measured by the PAMELA experiment [468] and the gamma-ray observations of the Fermi-LAT [469]) since the annihilation cross-section of dark matter particles into SM particles in today's halos is suppressed by the small value of the dark matter velocity.

5.5.2 Pseudo-Dirac dark matter

This scenario is for example realised by the almost pure Higgsino case considered in Section 5.3.8. In order to study it in full generality, the starting point is the Lagrangian describing a generic four-component fermion Ψ with both Dirac and Majorana masses

$$\mathcal{L}_0 = \bar{\Psi}(i\partial\!\!\!/ - M_{\rm D})\Psi - \frac{m_{\rm L}}{2}\left[\overline{\Psi_{\rm L}^{\rm C}}\Psi_{\rm L} + \overline{\Psi_{\rm L}}\Psi_{\rm L}^{\rm C}\right] - \frac{m_{\rm R}}{2}\left[\overline{\Psi_{\rm R}^{\rm C}}\Psi_{\rm R} + \overline{\Psi_{\rm R}}\Psi_{\rm R}^{\rm C}\right] \,, \tag{36}$$

in which we consider the pseudo-Dirac limit of the mass matrix, $M_D \gg m_{\rm L}$, $m_{\rm R}$ and for simplicity we assume all masses to be real. We denote the mass eigenstates as $\chi_{1,2}$, with eigenvalues $m_{1,2} = M_{\rm D} \pm (m_{\rm L} + m_{\rm R})/2$. From here, we can construct the Majorana fields $\Psi_1^{\rm M} \equiv \chi_1 + \chi_1^{\rm C}$, $\Psi_2^{\rm M} \equiv \chi_2 + \chi_2^{\rm C}$. The lightest state, $\Psi_2^{\rm M}$, plays the role of DM. At dimension-six, we have the following effective vector interactions with SM quarks [457]

$$\mathcal{L}_{\rm int}^{f} = \frac{1}{\Lambda^2}\left[\bar{\Psi}\gamma^\mu(c_{\rm L}P_{\rm L} + c_{\rm R}P_{\rm R})\Psi\right] \times \left[\bar{q}\gamma_\mu(c_{\rm L}^{(q)}P_{\rm L} + c_{\rm R}^{(q)}P_{\rm R})q\right] \,, \tag{37}$$

with $P_{\rm R,L} = (1 \pm \gamma^5)/2$. In terms of the Majorana fields previously introduced, the interactions in eq. (37) can be recast in the following effective operators involving Ψ_2^M

$$\mathcal{O}_{\rm A}^q \equiv \frac{1}{\Lambda^2}\left(\frac{c_{\rm R} - c_{\rm L}}{4}\right)(\overline{\Psi_2^{\rm M}}\gamma^\mu\gamma^5\Psi_2^{\rm M}) \times \underbrace{\left[\left(\frac{c_{\rm L}^{(q)} + c_{\rm R}^{(q)}}{2}\right)\bar{q}\gamma_\mu q\right]}_{\text{both SD and SI suppressed}} + \underbrace{\left(\frac{c_{\rm R}^{(q)} - c_{\rm L}^{(q)}}{2}\right)\bar{q}\gamma_\mu\gamma^5 q\Bigg]}_{\text{unsuppressed SD interaction}} \,, \tag{38}$$

$$\mathcal{O}_{\rm B}^q \equiv \frac{-i}{\Lambda^2}\left(\frac{c_{\rm R} + c_{\rm L}}{2}\right)(\overline{\Psi_1^{\rm M}}\gamma^\mu\Psi_2^{\rm M}) \times \left[\left(\frac{c_{\rm L}^{(q)} + c_{\rm R}^{(q)}}{2}\right)\bar{q}\gamma_\mu q + \left(\frac{c_{\rm R}^{(q)} - c_{\rm L}^{(q)}}{2}\right)\bar{q}\gamma_\mu\gamma^5 q\right] \,, \tag{39}$$

where, as discussed in section 5.5.1, we highlighted the direct detection properties of each structures. The only unsuppressed structure is the spin-dependent operator $(\overline{\Psi_2^{\rm M}}\gamma^\mu\gamma^5\Psi_2^{\rm M})(\bar{q}\gamma_\mu\gamma^5 q)$ in eq. (38). In eq. (39), direct detection constraints can be evaded by having a large enough splitting. A further difference with respect to the Majorana case discussed in Section 5.5.1 is that the relic density is set by the co-annihilation channel described by the effective operator proportional to the mixed structure $\overline{\Psi_1^{\rm M}}\gamma^\mu\Psi_2^{\rm M}$. The first term in eq. (39), in fact, features an unsuppressed s-wave that – supposing a mass splitting not too large – dominates, even at the freeze-out epoch, over the p-waves discussed in Section 5.5.1.

5.6 Physics Beyond Standard Model: Summary and Outlook

The results of the LHC running at 8 TeV, including the discovery of a low mass scalar, and no sign of new physics below the TeV scale have generated a tension on the naturalness principle.

In order to understand what is the present status of naturalness, and what are the perspectives for exploring this issue with foreseeable accelerator-based experiments we have focused on two representative classes of model, which have constituted a benchmark for new physics in the past and will be in the foreseeable future, Supersymmetry and Composite Higgs.

An alternative route is the study of minimal models, which concentrate on incorporating features which would solve the outstanding problems of fundamental physics such as Dark Matter and Baryon Asymmetry in the universe, ignoring the issue of Naturalness. To this class, to some extent, belong also the so-called portal models which provide an interesting phenomenology which could be studied also in fixed target experiments.

- **Composite Higgs Models.**
  - Figures (21,25,26) quantify the LHC reach on CH models. With 100 or 300 fb^{-1} Top Partners might be robustly bounded to be above around 1.4 TeV, corresponding to a level of tuning $\Delta \gtrsim 10$. The tuning bound would almost double for large values, $c \sim 1$, of the single production couplings, for which the mass limit is pushed above 2 TeV. From $\xi < 0.1$, expected from Higgs coupling measurements, a comparable bound on the tuning could be inferred at the end of the LHC program. On a time scale, Top Partner searches will be the first one in testing the scenario, though in a more model-dependent way, as discussed above.
  - The High–Luminosity LHC program will have a significant impact on the study of the CH scenario. This is shown in Figs. (22,25,26), where the expected limits are shown on mass–coupling planes. Paying attention to the fact that the g_ρ parameter for the vectors is actually the inverse of the physical coupling to fermions which controls the production rate, the common message is that High–Luminosity is not very effective in pushing the reach to high masses but it dramatically improves it in the weak–coupling direction.
  - An 100 TeV collider could extend the reach on CH particles above 10 TeV, which means exploring, through Top Partner searches, a level of tuning well above 2 orders of magnitude. Comparable performance is expected for precise leptonic machines. In Section 5.2.1 we considered CLIC, the best performing of such leptonic options, and compared its reach with the one of 100 TeV direct searches. The result is that the 100 TeV reach overcomes indirect CLIC limits for moderately small g_ρ, below 4, while above that value the coupling to fermions of the resonance is too small and the indirect limits dominate.
- **Supersymmetry.**
  - The lack of NP signals at LHC put pressure on supersymmetric models. The amount of pressure is highly model-dependent. Minimal SUGRA, for example, is under strong pressure and can be considered disfavoured by data (barring unknown dynamical or environmental selection mechanisms). On the other hand, models with low scale of mediation and minimal extensions of the field content (our benchmark, on which the conclusions below are based) feel a weaker pressure.
  - The first LHC phase forces a fine-tuning of about $1/10$. This is mild enough not to motivate further searches. A qualitative indication of the reach of LHC14 with 300/fb and the high-luminosity program both in terms of masses and fine-tuning is provided in Fig. 36. An ultimate 100 TeV collider would increase the reach on colored sparticles by an order O(10) and the reach in fine-tuning space by O(100), up to $\sim 1/1000$.
  - In case of no discovery at a $100\,\mathrm{TeV}$ collider, a fine-tuning of order 1/1000 would be strong evidence that a dramatic change of paradigm in the understanding of the Higgs mass in terms

of higher scales would be necessary.

  - The high luminosity LHC program would be most effective in probing "electrowinos" (charginos and neutralinos) and the Higgs sector. The range of EWino masses probed depends on the details of the spectrum, but can double the reach of LHC 14 by up to a factor of ~ 2. This allows one to probe a significant part of the DM-relevant parameter space, but does not necessarily cover all of it. A 100 TeV machine, on the other hand, would get closer to fully cover the parameter space of a thermal relic. For an LSP DM candidate with mass below 250 GeV an ILC should be able to cover the parameter space not accessible to a HL-LHC, or in case of discovery, to perform measurements on the observed signal.
  - As for the (NMSSM) Higgs sector, the high-luminosity run would allow to probe its structure both indirectly, through the measurement of deviations from the SM couplings, and in direct searches in the $h_2 \to h_1 h_1$ channel. It would also allow one to probe potentially large deviations (unlike in the MSSM) of the SM-like Higgs trilinear couplings. Direct searches are more powerful at lower luminosities, with indirect searches catching up at higher luminosities.

- **Naturalness independent scenarios**
  - The option of a minimal model, the νMSM, has been examined in detail. The Heavy Majorana neutrinos present in the theory can be detected in the decay of mesons or gauge bosons. High statistics beam dump experiments, such as SHiP, can cover a part of the range of mixing required by the model, but their mass reach is limited by the mass of the mesons of which they study the decay. The very minimal version of the model is barely testable by the SHiP experiment, as the relevant mass of the heavy neutrinos, although somewhat uncertain, goes from $\sim$2 GeV to a few tens of GeV. The most likely experimental venue is in this case the observation of displaced decays of Z and W bosons: on the order of 10^{12}-10^{13} W and Z bosons are needed. For the Z decay this signal would provide a strong motivation for a high luminosity FCC-ee machine. For the W decay HL-LHC and FCC-hh could cover part of the parameter space through clean leptonic signatures, but the required number of decays is at the limit of the present projections for high luminosity colliders.
    Non minimal versions or additional cosmological mechanisms, on the other hand, are natural and have a larger parameter space, whose lower mass, larger mixing can in part be tested by the SHiP, HL-LHC and FCC-ee or -hh experiments.
  - The Dark Sector, which assumes the presence of new BSM particles feebly coupled to the SM model, has been considered as an additional benchmark, in particular the case with a vector mediator, which gives rise to a Dark Photon (DP). Such a model has a large parameter space, with couplings varying over more than 10 orders of magnitude, and masses ranging from zero to multi-GeV. To cover such a large space different kinds of experimental approaches, are required, including searches for the decay of the DP into SM particles inside the detectors and disappearance searches, due because DP decays outside of the detector.
    Collider and fixed target experiments cover complementary regions in the mass-coupling parameter space determined by the number of DP decays and by the decay length interval to which the detector is sensitive. It is conceivable that in the next 10–20 years the combination of the proposed experiments will cover most of the space for a DP lighter than 1 GeV down to couplings of 10^{-7} of the DP.
    For models where the mediator is a scalar the main venue is the detection in the decay of the discovered Higgs boson, but the possibility of low mass higgs-like particles gives a chance to fixed target experiments, with a coverage similar to the one for Dark Photons.

- **Collider friendly dark matter**
  - Direct and Indirect DM detection experiments place limits which in some cases are orders of

magnitude above what is testable at colliders. Though not performed in a clean laboratory environment and thus harder to interpret, they must be taken into account, leading sometimes to pessimistic statements on the collider perspectives on DM searches.

– We outline that the situation can actually be reversed in certain classes of DM models where collider searches are by far the most powerful, also in comparison with upgraded versions of Direct detection limits which could be available in the near future. Interestingly enough, the case of Majorana DM, which is a very well motivated and minimal possibility (being DM an eminently neutral object), falls in this category. Notice however that we restricted our analysis to vector operators, while scalar ones are also expected. Though suppressed by quark masses they could still be considerably bounded by Direct searches because they produce spin–independent cross–sections. An assessment of this latter point is currently in progress.

6 Flavour Physics

6.1 Introduction

The state of the art in particle physics can be very briefly summarized as follows. On one side the triumph of the Higgs discovery and the absence of any clear signal of new physics at the LHC give strong support to the Standard Model (SM) as it is now. On the opposite side the three weaknesses of the SM stand up more than ever: i) its inability to account for Dark Matter or the B-asymmetry in the universe; ii) the sensitivity of the Higgs mass to any short distance physics, including gravity, kept under control by an unacceptable tuning of the Higgs mass parameter itself; iii) the plethora of parameters that account, in one-to-one correspondence, for the observed masses and mixings of quarks and leptons. It is difficult to overestimate the importance of the experimental program in particle physics to try to overcome this sort of "unstable equilibrium" between two different ways of judging the status of the SM. In particular the possible discovery of new particles at LHC in the first phase of its operation at higher energies, due to start in 2015, would certainly give a decisive orientation. This may or may not happen. In either case, however, the role of flavour physics experiments remains intact.

As customary, there are at least two different ways to try to assess the impact that flavour measurements can have as a whole on the medium term future of particle physics. One way is to consider the highest energies that flavour measurements can explore by assuming no structure of flavour physics. The most important probes are well known: $\Delta F = 2$ transitions, where F is S or C or B, $\mu \to e$ transitions, normally more sensitive than $\tau \to \mu$, or the Electric Dipole Moments, either of the electron or of the neutron. Although specific statements can be made in specific cases only, energies up to $10^{4\div5}$ TeV can be indirectly probed in this way, not easily achievable otherwise. Alternative or complementary to this is the view that new flavour physics phenomena may be related to Beyond the Standard Model (BSM) physics in the TeV range, if there is any, compatible with current or even achievable bounds from LHC.

As an example, carrying out a general analysis of $\Delta F = 2$ processes [470–482] it is possible to translate the experimental constraints into allowed ranges for the Wilson coefficients, parameterized as

$$C_i(\Lambda) = \frac{F_i L_i}{\Lambda^2}, \tag{40}$$

where F_i is a function of the new physics flavour couplings, L_i is a loop factor, and Λ is the scale of new physics [476]. Fig. 70 reports the lower bounds on new physics scale at 95% probability, assuming strongly coupled new physics ($F_i L_i \sim 1$) with no flavour suppression, derived from mixing and CP violation results in the neutral K, D, B_d and B_s meson systems. These bounds can then be translated into (less stringent) constraints on the NP scale for models featuring weak interactions and/or some kind of flavour suppression, until the extreme case of Minimal Flavour Violation (MFV) [483–485], which, if combined with the absence of flavour-changing strong interactions, allows NP to be very close to the weak scale.

To illustrate instead the view that new flavour physics phenomena may be related to NP in the TeV range, we may follow Ref. [487], where it is recalled that current flavour measurements still allow BSM contributions to the Cabibbo-Kobayashi-Maskawa (CKM) picture of flavour physics at about 20 to 30% level [15]. While this level of precision, attained through the last fifteen years of experiments, does not compare with the standards in other areas of particle physics — *and clearly motivates per se that one keeps improving on it* — it is nevertheless already significant enough to require that some mechanism be active to keep any flavour violation at the TeV scale under control. Several such mechanisms can in fact be conceived, relying on suitable dynamical assumptions, that cannot be recalled here for reasons of brevity. Rather it is of interest to know what is possible to achieve in an effective picture close enough to the CKM one, based on symmetries and on their possible breaking pattern only, i.e. without referring to specific models or to appropriately chosen dynamical assumptions. This goal can be accomplished in the quark sector in two different "effective" ways, based on either $U(3)_q \times U(3)_u \times U(3)_d \equiv U(3)^3$,

[15] see also the discussion in Section 6.8

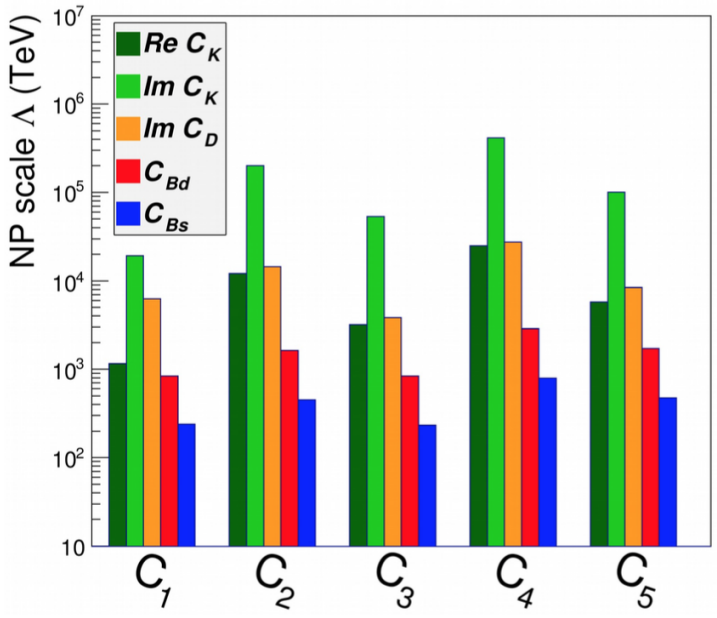

Fig. 70: Lower bounds on new physics scale at 95% probability, assuming strongly coupled new physics, from $\Delta F = 2$ processes in the neutral K, D, B_d and B_s meson systems [486].

or $U(2)_q \times U(2)_u \times U(2)_d \equiv U(2)^3$, with the symmetry-breaking pattern described in [487]. While the origin of these patterns is unknown at a fundamental level, we may nevertheless take them as a low energy property of some basic theory at an effective Lagrangian level.

Whatever extension of the SM, respecting either of these symmetries leads to a CKM-like picture of flavour physics. From an effective field theory point of view this amounts to the dominance of the same set of flavour breaking operators that operate in the SM, with a flavour dependence accounted for by the same specific combinations of matrix elements $\xi_{ij} = V_{tj}V_{ti}^*$ of the CKM matrix V. $U(2)^3$ relative to $U(3)^3$ allows more freedom in the relative weights of these operators and on their phases. Every other symmetry and symmetry breaking inside $U(3)^3$ either leads to one of these two patterns or deviates from the CKM-like picture because of the occurrence of different operators and/or of operators with a flavour dependence not controlled by the ξ_{ij} only.

As an example, Fig. 71 illustrates the current allowed regions by $U(2)^3$ or $U(3)^3$ on some of the most constrained flavour observables at 65% or 95% C.L. Still as an example, these constraints in the case of *Natural Supersymmetry* are both competitive with and complementary to the direct s-particle searches at LHC.

The experimental progress of the last fifteen years has turned the flavour sector of the SM from a hypothetical piece of theory into an empirically based description of flavour physics. Yet both the still relatively moderate precision achieved so far, as already remarked, and the competitive character of flavour measurements with searches of new physics in direct production experiments, current and foreseeable in the medium term future, motivate on the same time scale a strong program of flavour physics experiments.

Confining the attention to the quark sector, it is useful to make a few comments of a general nature on the impact/limitation of QCD uncertainties on such program. There already exists a series of relevant experimental observables not limited by theoretical uncertainties. A partial list of them includes: $B \to \tau\nu/\mu\nu$, $B \to K^{(*)}\bar{\nu}\nu$, $B \to X_s l^+ l^-$ $B_{s,d} \to l^+ l^-$, $\phi_{s,d}^{\Delta}$ (CPV in $\Delta B_{s,d} = 2$), the determination of the angle γ from tree level decays (like $B \to DK$, etc) and of the angle α from the isospin analysis, $K^+ \to \pi\bar{\nu}\nu$, $K_L \to \pi\bar{\nu}\nu$, CP violation in $B \to X_{s+d}\gamma$ and in D–$\bar{D}$ mixing.

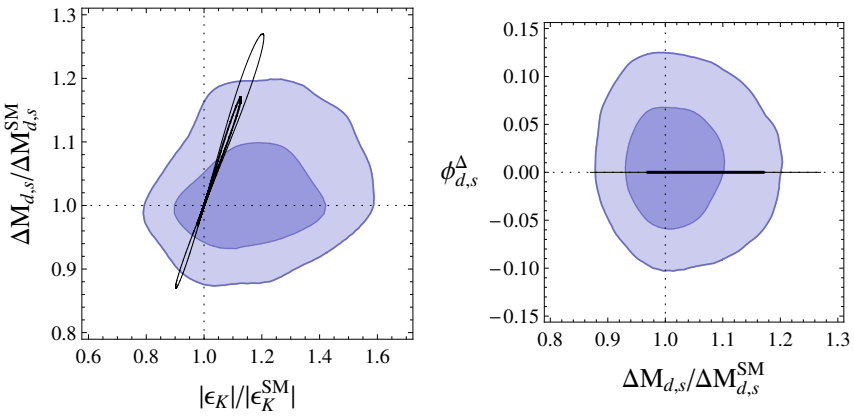

Fig. 71: Allowed deviations from the SM of some $\Delta F = 2$ observables in $U(2)^3$ (the pancake shapes) or in $U(3)^3/MFV$ (the thin shapes) at 68% and 95% probability.

The experimental status and progress expected in this sector in the next decade is discussed in Sections 6.2 for kaon, 6.3 for charm, 6.4 and 6.5 for beauty hadrons, respectively. The resulting experimental program, together with the foreseen reduction on the uncertainties of several QCD parameters, to near the percent level by lattice QCD in a decade or so, as discussed in Section B.2, can lead, for example, to a significant shrinkage of the pancake shapes in Figure 71 or to a test, at the 5% level, of the CKM picture. At the same time, however, it would be wrong to neglect the possibility to reduce the theoretical uncertainties in other areas, for example involving charm, by a cooperation of precision measurements of several different decay channels, thus orienting the phenomenological/theoretical analyses of the corresponding physical systems.

Similar considerations can be made in the lepton sector and for EDMs, which are discussed in Sections 6.6 and 6.7, respectively.

Section 6.8 presents initial thoughts of an *eXtreme Flavour eXperiment (XFX)* aimed at exploiting the full luminosity of the HL-LHC to increase the precision on flavour observables by at least one order of magnitude with respect to the reach of the currently planned facilities.

In summary we can restate what was said at the beginning. The search for the production of new particles, as expected in BSM at the TeV scale, is a primary task of the next LHC phase. The exploration of most part of the sensitive region of parameter space in motivated theories is actually likely to take place in the relatively early stage of the new LHC phase. After that, whatever the findings of this exploration will be, precision measurements in flavour physics (and not only in flavour physics) will play a leading role for a sufficiently long period of time. In the light of what has been said above, the potential of a strong flavour program appears highly significant.

6.2 Kaon Physics

For the past 70 years, experimental studies of kaons have played a singular role in propelling the development of the Standard Model. As in other branches of flavour physics, the continuing experimental interest in the kaon sector derives from the possibility of conducting precision measurements, particularly of suppressed or rare processes, that may reveal the effects of new physics with mass-scale sensitivity exceeding that which can be explored directly, e.g., at the LHC, or even at a next-generation hadron collider. The small number of kaon decay modes and simplicity of the final states, together with the possibility of producing intense kaon beams, make kaon decay experiments in many ways the quintessential intensity-frontier experiments.

In the following Sections, we review the areas currently of interest in kaon physics. We then

overview current experimental programs, and present perspectives on some initiatives for future experiments.

6.2.1 Areas of interest in kaon physics

6.2.1.1 The $K_S K_L$ system; CP and CPT observables

ε, Δm_K

The $\Delta S = 2$ $K^0 \leftrightarrow \bar{K}^0$ transition is a FCNC process that can be used to directly probe the Standard Model (SM). In particular, the value of ε, which parametrizes CP violation in $K^0 - \overline{K}^0$ mixing, can be related to the CKM matrix elements, and together with the neutral kaon oscillation frequency Δm_K, provides constraints on new physics. From fits to experimental data on K_L and K_S decays, $|\varepsilon| = 2.228(11) \times 10^{-3}$ [488], while in the SM, $|\varepsilon| = 1.81(28) \times 10^{-3}$ [489]. Of the total uncertainty on the SM value, the part due to the limited knowledge of external parameters accounts for 0.23×10^{-3}, and should decrease in the future. Uncertainties from higher-order corrections to the charm amplitudes contribute 0.14×10^{-3}, while the uncertainty arising from the hadronic matrix element $\hat{B}_K$ contributes less than 0.05×10^{-3}. In fact, new lattice results have reduced the uncertainty on $\hat{B}_K$ to 1.3% [490] since the SM evaluation of $|\varepsilon|$ of Ref. [489], and there are prospects for reducing the uncertainty on $\hat{B}_K$ even further, perhaps to below 0.5%, as discussed in Section B.2. However, even with these improved calculations of $\hat{B}_K$, the measured value of ε will not provide a useful probe of the SM until further progress can be made on the higher-order corrections for charm. This progress might be obtained on the lattice, if certain theoretical and technical issues can be kept under control [491].

$\mathrm{Re}\,\varepsilon'/\varepsilon$

The existence of direct CP violation was confirmed and the CKM paradigm for CP violation validated by the measurement of $\mathrm{Re}\,\varepsilon'/\varepsilon$. The average of the final results from NA48 [492] and KTeV [493] gives $\mathrm{Re}\,\varepsilon'/\varepsilon = 1.64(19) \times 10^{-3}$ [81, 494]. Because of the delicate balance between the amplitudes for the two isospin contributions, it is difficult to perform a reliable calculation of $\mathrm{Re}\,\varepsilon'/\varepsilon$ in the SM. It has recently become possible to generate lattice ensembles at physical quark masses. Because of this and other technical advances, it may be possible to evaluate $\mathrm{Re}\,\varepsilon'/\varepsilon$ on the lattice to within ∼20% within a few years [495]. In principle, the value of $\mathrm{Re}\,\varepsilon'/\varepsilon$ is sensitive to new physics in the same manner as the exceptionally sensitive observable $\mathrm{BR}(K_L \to \pi^0\nu\bar{\nu})$ discussed in Section 6.2.1.3. It is unlikely that the experimental value of $\mathrm{Re}\,\varepsilon'/\varepsilon$ will be useful for precision tests in the near term, but it may provide constraints on some models of NP before precise measurements of $\mathrm{BR}(K_L \to \pi^0\nu\bar{\nu})$ become available.

CPT tests

The Bell-Steinberger relation [496] links the value of $\mathrm{Re}\,\varepsilon$ to $\mathrm{Im}\,\delta$, which parameterizes CPT violation, via a unitarity sum of terms bilinear in the complex amplitudes for K_L and K_S decays to the same final state. In the $K_S K_L$ system, only a few final states give significant contributions to the sum, so the Bell-Steinberger relation can provide a powerful CPT test. An analysis of this type in the Particle Data Group review is regularly updated as new measurements become available [488]. At present, the results of this analysis give the most stringent test of CPT: $|m_{K^0} - m_{\overline{K}^0}| < 4 \times 10^{-19}$ GeV at 95% CL. The dominant uncertainty is from the experimental value of ϕ_{+-}, the phase of the amplitude ratio for K_L and K_S decays to $\pi^+\pi^-$. The $\pi^+\pi^-$ channel is the largest contribution to the unitarity sum.

T violation

Kaon decays can also be used to probe the violation of T independently of CP or CPT. An example is the transverse muon polarization in $K^+ \to \pi^0\mu^+\nu_\mu$ ($K^+_{\mu 3}$) decays: finite polarization of the muon along the axis orthogonal to the decay plane would violate T. In the SM, P_T is expected to be on the order of 10^{-7}; spurious effects from final-state interactions may give rise to values of $P_T < 10^{-5}$. The current experimental limit is from the E246 experiment at KEK: $P_T < 0.0050$ at 90% CL [497]. Time-reversal violation has been observed in the neutral B meson system [498].

6.2.1.2 *Precision observables in $K_{\ell 2}$ and $K_{\ell 3}$ decays*

$R_K = \Gamma(K \to e\nu)/\Gamma(K \to \mu\nu)$

In the SM, $K \to \ell\nu$ decays are helicity suppressed, but BSM contributions (such as, e.g., scalar exchange of an H^+) would not be. In the R-parity conserving MSSM, the width for the decay $K \to e\nu$ may receive a contribution from lepton-flavour violation in the effective coupling at one loop, leading to the presence of a ν_τ in the final state [499]. For large $\tan\beta$, this could result in percent-level changes in the value of R_K. The SM prediction for the ratio, $R_K = \Gamma(K \to e\nu)/\Gamma(K \to \mu\nu) = 2.477(1) \times 10^{-5}$, involves only radiative corrections and is known to better than 0.04% [500], making R_K an interesting observable. NA62 has obtained the result $R_K = 2.488(10) \times 10^{-5}$, i.e., with an uncertainty of 0.4% [501]. Further progress is possible, although interest in the measurement has declined somewhat due to the failure to observe other evidence of large-$\tan\beta$ supersymmetry at the LHC.

First-row CKM unitarity tests

The most precise test of CKM unitary comes from the first-row condition $V_{ud}^2 + V_{us}^2 + V_{ub}^2 = 1$. From nearly 200 measurements of $0^+ \to 0^+$ nuclear beta decays, $V_{ud} = 0.97417(21)$ [502]. The most precise measurements of V_{us} come from kaon decays. $K_{\ell 3}$ rates give V_{us}; $K_{\ell 2}$ and $\pi_{\ell 2}$ decays give the ratio V_{us}/V_{ud}. Hadronic matrix elements are needed and can be obtained from the lattice: the form factor $f_+(0)$ in the former case, and the ratio of decay constants f_K/f_π in the latter. After ten years of progress both in kaon decay measurements [503, 504] and in lattice evaluation of the hadronic quantities [490], uncertainties on V_{us} and V_{ud} now contribute about equally to the unitarity sum (V_{ub}^2 is an insignificant contribution). From experimental data on $K_{\ell 3}$ decays, $V_{us}\, f_+(0) = 0.2165(4)$. With the $N_f = 2+1+1$ lattice[16] result $f_+(0) = 0.9704(32)$ [505], $V_{us} = 0.2232(9)$ is obtained. Similarly, from experimental data on $K_{\mu 2}$ decays, $V_{us}/V_{ud} \times f_K/f_\pi = 0.2760(4)$, which gives $V_{us}/V_{ud} = 0.2312(10)$ with the $N_f = 2+1+1$ lattice result $f_K/f_\pi = 1.194(5)$ [490]. In either case, the dominating uncertainties are from the lattice constants rather than experiment, but not by much ($\sim$0.3% vs $\sim$0.2% in the case of $K_{\ell 3}$). Combining all of the above information with a fit as in [504] gives $V_{ud} = 0.97416(21)$, $V_{us} = 0.2240(7)$, and $\Delta_{\rm CKM} = V_{ud}^2 + V_{us}^2 + V_{ub}^2 - 1 = -0.0008(5)$ (-1.6σ). The agreement is somewhat better if $N_f = 2+1$ lattice results are used (-1.0σ), but the facade of previously perfect agreement with unitarity has developed some cracks, particularly for $K_{\ell 3}$ decays [504]. In the future, alternative determinations of V_{ud} may become competitive in precision to that from nuclear beta decays. In particular, the determination of V_{ud} from pion beta decay does not require nuclear-structure dependent radiative or isospin-breaking corrections. However, the value of V_{ud} from the current best result from the PIBETA experiment has an uncertainty ten times larger than that from nuclear beta decays [506]. For V_{us}, the uncertainties on the lattice determinations of $f_+(0)$ and f_K/f_π may be decreased to the 0.1% level within the next decade [507]. If this can be achieved, there will be a demand for BR and lifetime measurements for K_L, K_S, and $K^\pm$ with matching precision. New evaluations of the radiative corrections (and for $K^\pm$, isospin-breaking effects) will also be needed [508].

6.2.1.3 *FCNC decays as clean short-distance probes*

Four rare kaon decays provide information on the unitarity triangle, as illustrated in Fig. 72. These are flavour-changing neutral current processes that probe the $s \to d\nu\bar{\nu}$ or $s \to d\ell^+\ell^-$ transitions. They are highly GIM suppressed and their Standard Model rates are very small. Complications from long-distance physics affect the modes unevenly. The $K \to \pi\nu\bar{\nu}$ decays are the least affected and therefore provide the cleanest probes of short-distance physics in the kaon sector.

$K_L \to \pi^0\nu\bar{\nu}$ and $K^+ \to \pi^+\nu\bar{\nu}$

The $K \to \pi\nu\bar{\nu}$ decays probe the $s \to d\nu\bar{\nu}$ transition via the Z-penguin and box diagrams shown

[16] As discussed in Section B.2, an important aspect of lattice simulations is the number of dynamical quark flavours. $N_f = 2+1$ simulations include virtual quark loops for degenerate up and down quarks and for strange quarks, while $N_f = 2+1+1$ simulations also include charm quarks.

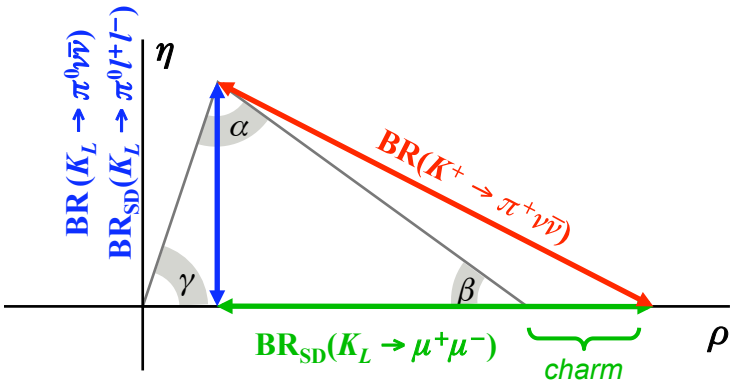

Fig. 72: Determination of the unitarity triangle with rare kaon decays.

in Figure 73. For several reasons, the SM calculation for their branching ratios (BRs) is particularly clean

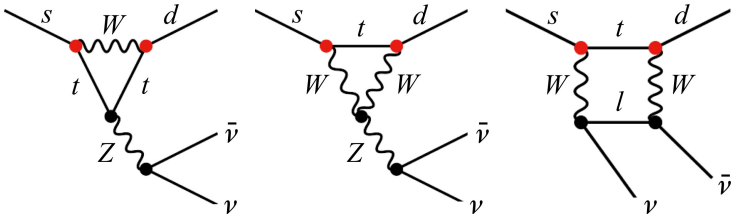

Fig. 73: Diagrams contributing to the process $K \to \pi\nu\bar{\nu}$.

(see [509] for a recent review):

- The loop amplitudes are dominated by the top-quark contributions. The neutral decay violates CP; its amplitude involves the top-quark contribution only. In fact, $\mathrm{BR}(K_L \to \pi^0\nu\bar{\nu})$ gives a direct measurement of the height (and therefore twice the area, J) of the unitarity triangle. Small corrections to the amplitudes from the lighter quarks come into play for the charged channel.
- The hadronic matrix elements for these decays can be obtained from the precise experimental measurement of the K_{e3} rate.
- There are no long-distance contributions from processes with intermediate photons. This point in particular distinguishes the $K \to \pi\nu\bar{\nu}$ decays from the other modes appearing in Fig. 72.

In the SM [510],

$$\mathrm{BR}(K_L \to \pi^0\nu\bar{\nu}) = 2.43(0.39)(0.06) \times 10^{-11}; \tag{41}$$

$$\mathrm{BR}(K^+ \to \pi^+\nu\bar{\nu}) = 7.81(0.75)(0.29) \times 10^{-11}. \tag{42}$$

The uncertainties listed first derive from the input parameters. The smaller uncertainties listed second demonstrate the size of the intrinsic theoretical uncertainties. Because of the corrections from lighter-quark contributions, these are slightly larger for the charged channel.

Because the SM rates are small and predicted very precisely, the BRs for these decays are sensitive probes for new physics. In evaluating the rates for the different FCNC kaon decays, the different terms of the operator product expansion are differently sensitive to modifications from a given new-physics scenario. If $\mathrm{BR}(K_L \to \pi^0\nu\bar{\nu})$ and $\mathrm{BR}(K^+ \to \pi^+\nu\bar{\nu})$ are ultimately both measured, and one or both BRs is found to differ from its SM value, it may be possible to characterize the physical mechanism responsible, e.g., a mechanism with minimal flavour violation [511], manifestations of supersymmetry [512], a fourth generation of fermions [513], a realization of Higgs compositeness by spontaneous symmetry breaking,

as in the littlest Higgs model [514], or an extra-dimensional mechanism such as in the Randall-Sundrum model [515].

$\mathrm{BR}(K_L \to \pi^0\nu\bar{\nu})$ has never been measured. $\mathrm{BR}(K^+ \to \pi^+\nu\bar{\nu})$ was measured by Brookhaven experiment E787 and its successor, E949. The combined result from the two generations of the experiment, obtained with seven candidate events, is $\mathrm{BR}(K^+ \to \pi^+\nu\bar{\nu}) = 1.73^{+1.15}_{-1.05} \times 10^{-10}$ [516].

$K_L \to \pi^0\ell^+\ell^-$

Like $K_L \to \pi^0\nu\bar{\nu}$, the short-distance part of this decay gives information on $|V_{ts}^*V_{td}|$ and thus measures the height of the unitarity triangle. To the extent that there is little constraint on the CP-violating phase of the $s \to d\ell^+\ell^-$ transition, measurement of the $K_L \to \pi^0\ell^+\ell^-$ BRs may reveal the effects of new physics [517]. However, there are long-distance contributions of the same order of magnitude as the short-distance component. First, there is an indirect-CP-violating contribution of the type $K_L \to K_S \to \pi^+\ell^+\ell^-$, the magnitude of which can be obtained from the measured BR for the corresponding K_S decay. Second, for $K_L \to \pi^0\mu^+\mu^-$, there is a CP-conserving long-distance contribution mediated by $K_L \to \pi^0\gamma\gamma$ (this is helicity suppressed for the e^+e^- mode). In the SM, $\mathrm{BR}(K_L \to \pi^0e^+e^-) = 3.2(^{+8}_{-9}) \times 10^{-11}$ and $\mathrm{BR}(K_L \to \pi^0\mu^+\mu^-) = 1.29(24) \times 10^{-11}$ [518]. The best experimental limits are from KTeV: $\mathrm{BR}(K_L \to \pi^0e^+e^-) < 28 \times 10^{-11}$ [519] and $\mathrm{BR}(K_L \to \pi^0\mu^+\mu^-) < 38 \times 10^{-11}$ [520] at 90% CL.

The indirect-CP-violating contribution to the total width for either decay is of the same order as the short-distance contribution, so significant progress on the BR measurements for $K_S \to \pi^0e^+e^-$ and $K_S \to \pi^0\mu^+\mu^-$ is required. Both have been measured by NA48 [521, 522]. For $\mu^+\mu^-$, NA48 has $\mathrm{BR} = (2.9^{+1.5}_{-1.2} \pm 0.2) \times 10^{-9}$; for e^+e^- there are complications from photon-conversion background from $K_S \to \pi^0\pi^0$, but the level of precision is similar to that for $\mu^+\mu^-$. The physics of the decay $K^+ \to \pi^+\ell^+\ell^-$ is similar to that for $K_S \to \pi^0\ell^+\ell^-$. For the K^+ decay, interference with the long-distance amplitude from $K^+ \to \pi^+\gamma^*$ leads to a CP-violating charge asymmetry for the e^+e^- channel, but the rate asymmetry in the SM is too small to be observed [523].

$K_L \to \mu^+\mu^-$

Of the FCNC processes discussed here, $K_L \to \mu^+\mu^-$ is the one for which experimental knowledge of the BR is most precise, but for which the SM calculation of the decay rate is most severely affected by complications from long-distance physics [524, 525]. The dispersive short-distance amplitude arises from processes analogous to the diagrams in Fig. 73, where the top-quark contribution is dominant and there are small QCD corrections. There is also a dispersive long-distance contribution from $K_L \to \gamma^*\gamma^*$, which is the dominant source of theoretical uncertainty. The long- and short-distance dispersive amplitudes destructively interfere, and the vast majority of the width is from the absorptive amplitude arising from $K_L \to \gamma\gamma$ (with real photons). Experimentally, $\mathrm{BR}(K_L \to \mu^+\mu^-) = 6.84(11) \times 10^{-9}$ [526], but this leads to only weak constraints on the short-distance component and hence ρ.

In the case of $K_S \to \mu^+\mu^-$, the short distance component is absorptive, while the dispersive long-distance amplitude is determined unambiguously at lowest order in the chiral expansion. In the SM, $BR(K_S \to \mu^+\mu^-) = (5.1 \pm 0.2) \times 10^{-12}$ [527]; about one-third of this is from the short-distance component. Since the CP-violating phase of the $s \to d\ell^+\ell^-$ transition is poorly determined, there is room for new physics to manifest itself in an unexpectedly high value of $BR(K_S \to \mu^+\mu^-)$. Contributions to the BR of up to an order of magnitude above the SM expectation are allowed, while enhancements to BR values above 10^{-10} are less likely [528]. In addition, limits on $BR(K_S \to \mu^+\mu^-)$ at the level of 10^{-11} would help to discriminate among new physics scenarios, if measurements of other modes were to indicate an enhancement of the amplitude for the $s \to d\ell^+\ell^-$ transition [528]. The limit from LHCb, $BR(K_S \to \mu^+\mu^-) < 9 \times 10^{-9}$ at 90% CL [529], which improves upon the previous limit by a factor 30, demonstrates the potential of collider experiments in this field. About 10^{13} K_S mesons are produced per fb^{-1} at the LHC (see Section 6.2.3.2), so a future flavour experiment exploiting the full luminosity of the HL-LHC (see Section 6.8) would have potential sensitivity to new physics in this channel.

6.2.1.4 *Kaon decays with explicit lepton flavour or number violation*

Many SM extensions introduce new interactions that may give rise to violation of lepton flavour and/or number conservation in specific processes. Experiments with neutral kaons have reached sensitivities to LFNV branching ratios as low as 10^{-12}, which, by simple dimensional arguments, can provide access to mass scales upwards of 100 TeV in the search for new physics at tree level (e.g., a new gauge boson mediating the tree-level $s \to d\mu e$ transition) [530], while limits from experiments with charged kaons are generally about an order of magnitude higher. Precisely because the results from searches for LFNV kaon decays up through the '90s posed such stringent constraints on models such as technicolor, for the past decade or so, it appears to have been tacitly assumed that it would be difficult to make any further progress with kaon decays [531]. However, interest in searches for LFNV in charged lepton decays has remained robust, as witness the interest in experiments such as MEG and Mu2e as well as in searches for $\tau \to \mu\gamma$, for example, at next-generation flavour factories [532]. In this context, next-generation rare kaon decay experiments represent opportunities to push down the limits on decays such as $K_{S,L} \to (\pi^0)\mu e$ (LFV), $K^+ \to \pi^+\mu^\pm e^\mp$ (LFV), $K^+ \to \pi^-\ell^+\ell^+$ (LNV), and $K^+ \to \pi^-\mu^+e^+$ (LFNV).

6.2.1.5 *Searches for heavy neutral leptons and secluded-gauge bosons*

Searches for heavy neutral leptons [533] and secluded-gauge bosons [534] require experiments featuring intense beams and exclusive reconstruction of the decay products with high-efficiency particle identification. These features are shared with experiments to search for rare kaon decays. Heavy neutral leptons of mass up to m_K may be observed directly in rare kaon decay experiments, either by exclusive reconstruction of the decays of these particles, or by the missing momentum they carry, e.g., as small peaks in the tails of the missing-mass distribution for $K \to \mu\nu$ decays. Secluded-gauge bosons can be searched for exclusively, among the decays of kaons to final states with $\ell^+\ell^-$ pairs, or inclusively, for decay channels with an unreconstructed photon (virtual or real). It should be noted in this regard that rare K^+ experiments observe copious quantities of tagged π^0 decays, which are ideal for use in the search for a light secluded-gauge boson.

Heavy neutral leptons and secluded-gauge bosons are discussed in Secs. 5.4.2 and 5.4.3, respectively. Although these are not strictly speaking topics of interest in kaon physics, it should be kept in mind that some rare kaon decay experiments may be able to perform sensitive searches in these areas while carrying out their main programs.

6.2.2 *Tests of chiral perturbation theory*

Chiral perturbation theory (ChPT) [535, 536] is the effective theory of the Standard Model at the pion and kaon mass scales, so naturally, there has been a close interplay in the kaon sector between advances in experiment and the development of ChPT. There is an active ChPT community for which new measurements, such as of the branching ratios and form factors for $K_{\ell 4}$, $K_{\ell 3}$, and radiative decays such as $K_{\mu 3\gamma}$, $K_{\pi 2\gamma}$, and $K \to \pi\gamma\gamma$, provide valuable tests of ChPT, as well as inputs needed to refine the theory further [509]. Virtually all of the experiments discussed here can perform important tests of ChPT as a by-product of the programs for which they were designed.

6.2.3 *Experimental programs: Present and near-future*

6.2.3.1 *KLOE-2*

KLOE-2 continues the experimental program of the KLOE experiment at DAΦNE, the Frascati ϕ factory. The KLOE experiment was based on the abundant production of ϕ mesons in e^+e^- collisions at $\sqrt{s} = m_\phi$. More than 80% of the time, the ϕ decays into a $K\bar{K}$ pair (K^+K^- or K_SK_L) in a well-defined quantum state with $J^{PC} = 1^{--}$. As a result, the observation of a K_S can be used to tag the presence of a K_L and vice versa; the same is true of K^+ and K^- decays. This is particularly useful for the

precision measurement of the principal charged and neutral kaon branching ratios. Moreover, because for $K_S K_L$ events, the K_S and K_L are produced in a coherent quantum state, interference patterns can be observed in the differential decay-time distribution, allowing various phase differences and amplitude ratios that describe the $K_S K_L$ system to be measured. These measurements additionally provide tests of the persistence of quantum coherence that can probe the basic tenets of quantum mechanics [537].

Due to issues with DAΦNE performance, all KLOE-2 activity to date in the kaon sector has focused on completing the analysis of the original KLOE data set. Upgrades to the KLOE detector recently completed include a new GEM-based inner tracker and new small-angle calorimeters. If the machine performance issues can be addressed, KLOE-2 should be able to obtain original results within the next three years.

6.2.3.2 LHCb

While it may seem surprising to find LHCb among the list of kaon experiments, the new limit from LHCb for $K_S \to \mu^+\mu^-$, $\mathrm{BR} < 9 \times 10^{-9}$ at 90% CL [529], evinces the potential of LHCb to compete with dedicated kaon experiments, at least for the measurement of rare K_S decays, in particular those with $\mu\mu$ pairs. Only $1/3$ of the available data has been analyzed, so this limit could be further decreased. Moreover, estimates of the potential sensitivity after the LHCb upgrade taking into account the uncertainty on the background estimate indicate that a limit in the 10^{-10} range could be obtained. Of the other K_S decays with dimuons that LHCb might be able to measure, $K_S \to \pi^0\mu^+\mu^-$ is particularly interesting because of its importance in the understanding of $K_L \to \pi^0\mu^+\mu^-$. Reconstruction of the π^0 is challenging for LHCb, but studies indicate that a few events may be found in the 3 fb^{-1} collected so far. A measurement may be possible with Run 2 data, or in any event, after the upgrade [538].

Estimated SM BRs for the decays $K_S \to 4e$, $K_S \to ee\mu\mu$, and $K_S \to 4\mu$ are at the levels of 10^{-10}, 10^{-11}, and 10^{-14}, respectively [539]. LHCb may be able to observe the first two decays. Measurement of these BRs could help in the evaluation of the long-distance contributions to $K_L \to \mu\mu$.

LHCb may also be able to use K^+ decays to $\pi^+\mu^+\mu^-$ final states with displaced vertices to search for secluded-gauge bosons ($\mu^+\mu^-$ displaced) or heavy neutral leptons ($\pi^+\mu^-$ displaced).

Other kaon physics topics that might be addressed with LHCb at an upgraded LHC with $L > 10^{34}$ $\mathrm{cm}^{-2}\mathrm{s}^{-1}$ are discussed in Section 6.8.2.4.

6.2.3.3 NA62

The NA62 experiment at the CERN SPS will measure $\mathrm{BR}(K^+ \to \pi^+\nu\bar{\nu})$ with a precision of about 10% during the next few years. NA62 is the only experiment (planned, proposed, or running) pursuing this measurement.

Observation of $\sim$100 signal events will require a sample of 10^{13} K^+ decays within the geometrical acceptance of the experiment, for which the signal detection efficiency must be at least 10%. An overall background rejection factor of 10^{12} is required against abundant decays such as $K^+ \to \mu^+\nu$ and $K^+ \to \pi^+\pi^0$ (together representing about 84% of the total K^+ width). The experiment makes use of a 75-GeV unseparated positive secondary beam with a total rate of 750 MHz, of which about 6% is K^+s. About 10% of these decay in the fiducial volume of the experiment. The experimental signature is a K^+ coming into the experiment and decaying to a π^+, with no other particles present. Precise reconstruction of the primary and secondary tracks allows the abundant two-body decays to be rejected on the basis of the missing mass. The remainder of the experiment's rejection power (in particular, for decays without closed kinematics) must come from redundant particle identification systems and highly-efficient, hermetic photon veto detectors. The NA62 apparatus, schematically illustrated in Fig. 74, was designed around these principles.

NA62's first run started in October 2014. The detector has been fully commissioned and is ready to take data in 2015. With 200 days of data taking at 50% uptime during the period 2015–2017 and a

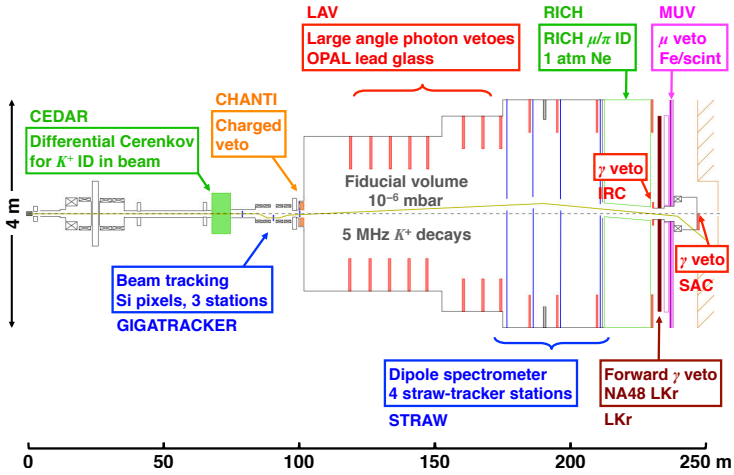

Fig. 74: Schematic diagram of the NA62 experiment.

signal acceptance of about 10%, NA62 will collect a sample of 10^{13} K^+ decays in the FV, containing about 100 $K^+ \to \pi^+\nu\bar{\nu}$ events.

The same characteristics necessary for NA62's measurement of $\mathrm{BR}(K^+ \to \pi^+\nu\bar{\nu})$ allow exploration of a wide variety of topics in kaon physics, among which the following.

R_K In 2007, the nascent NA62 collaboration used a subset of detectors from the unmodified NA48/2 experiment to measure R_K [501]. With the precision tracking and redundant particle identification of the new NA62 detector, as well as the abundant statistics of the expected data set, the uncertainty on R_K can be reduced from the present 0.4%, perhaps to 0.2%.

Measurements related to V_{us} NA48/2 has presented preliminary results on K^+_{e3} and $K^+_{\mu 3}$ form-factor parameters that are of higher precision than any other published measurements [540]. NA62 should be able to improve on the NA48/2 results. NA62 could also provide precise new measurements of the dominant BRs for K^+ decays, providing new direct inputs for the evaluation of V_{us}.

Tests of chiral perturbation theory NA48/2 and NA62 (in the preliminary R_K phase) have performed various measurements that provide tests of ChPT, including kinematic distributions and BRs for K_{e4} [541] and $K^+ \to \pi^+\gamma\gamma$ [542, 543] decays. This slate of measurements will be extended and improved when NA62 becomes fully operational with the new detector.

Decays violating lepton flavour or number Preliminary estimates of NA62's single-event sensitivities[17] (SES) for K^+ decays to states such as $\pi^+\mu^\pm e^\mp$ (LFV), $\pi^-\mu^+e^+$ (LFNV), and $\pi^-e^+e^+$ or $\pi^-\mu^+\mu^+$ (LNV) give results at the level of 10^{-12} [544].

Rare π^0 decays The NA62 kaon data set will contain 2×10^{12} π^0 decays from $K \to \pi\pi^0$ (BR = 21%). The SES will be at the level of 10^{-11} for LFV π^0 decays such as $\pi^0 \to \mu^\pm e^\mp$. Besides the LFV processes, rare or forbidden π^0 decays to which NA62 has potential sensitivity include $\pi^0 \to 3\gamma$, $\pi^0 \to 4\gamma$, and $\pi^0 \to e^+e^-e^+e^-$. NA62 would have the potential to set a limit on $\mathrm{BR}(\pi^0 \to \mathrm{invisible})$ at the level of $\sim 10^{-9}$, which is about 100 times better than present limits [545].

Heavy neutral leptons NA62 can perform exclusive searches [546] for heavy neutral leptons N decaying to channels such as $e\pi$ or $\mu\pi$, where the Ns are produced either at the target in K or D decays, as in the proposed SHiP experiment [547], or in K decays along the first 100 m of the beamline. The latter possibility is unique to NA62. With 5 years of data at the nominal beam intensity, NA62 could confirm and extend existing limits [548] for Ns from K decays, and for $m_K < m_N < m_D$,

[17] Single-event sensitivity is defined as the reciprocal of the number of decays in an experiment's acceptance. It is the BR for which a single detected event would be expected in the absence of background.

begin to probe values of the N's coupling to the active neutrinos that lie in the range expected from observations of the baryon asymmetry of the universe [549].

Secluded gauge bosons $\pi^0 \to e^+e^-\gamma$ decays can be used to search for a secluded-sector vector boson ("dark photon", or U-boson). A U boson with a mass of less than $m_{\pi^0}/2$ might be directly observable in $\pi^0 \to U\gamma$ decays with $U \to e^+e^-$ [550]

6.2.3.4 KOTO

The KOTO experiment at J-PARC is the only experiment (planned, proposed, or running) to pursue the measurement of the decay $K_L \to \pi^0\nu\bar{\nu}$. KOTO continues in the tradition of the KEK experiment E391a in technique. The primary challenge is the rejection of background from the decay $K_L \to \pi^0\pi^0$ in which two photons are lost. The salient features of KOTO are the use of a highly collimated, low-energy "pencil" beam and very high performance hermetic calorimetry and photon vetoing. K_Ls in the secondary beam have a mean momentum of 2.1 GeV, so the KOTO experiment is much more compact than NA62: the decay chamber is 2 m in diameter and 5.5 m long. A schematic of the experiment is shown in Fig. 75.

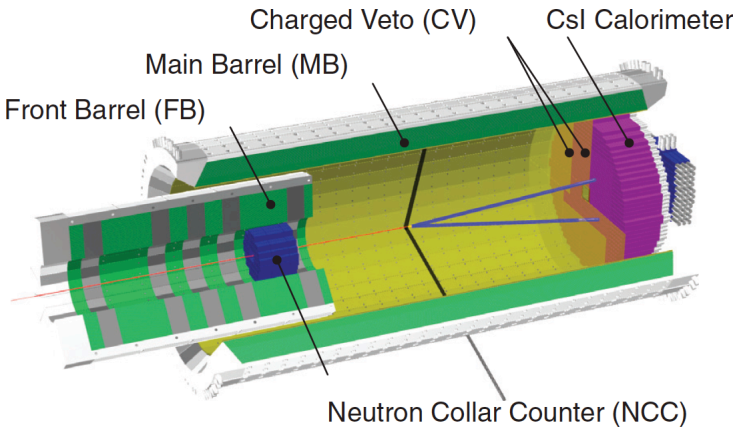

Fig. 75: Schematic diagram of the KOTO experiment.

The design intensity for the primary beam is 2×10^{14} p per 3.3 s spill, or 300 kW. In three years of data taking at the design intensity (with 10^7 s/yr), KOTO's SES is 8×10^{-12}, corresponding to 3.5 SM events. The expected S/B ratio is 1.4, with the dominant background from $K_L \to \pi^0\pi^0$ decays. With these parameters, KOTO would stand a good chance of being the first experiment to observe the $K_L \to \pi^0\nu\bar{\nu}$ decay.

The experiment started taking data in May 2013 with a beam power of 25 kW, corresponding to 10% of the design intensity, but was halted due to a radiation accident in the J-PARC Hadron Hall after about 100 hours of running. Preliminary results from the 100-hour run were presented in September 2014 [551]. An SES of 1.3×10^{-8} was reached. Signal candidates are defined by cuts on the FV (a 1.7-m region in z) and $p_\perp(\pi^0)$ (the "π^0" from $K_L \to \pi^0\pi^0$ events with two lost photons, for which the photons may be incorrectly paired, is reconstructed with $p_\perp < 150$ MeV). One event was observed in the signal box, against an expected background of 0.36 ± 0.16 events. Data taking is expected to resume in 2015 at a beam power of 25 kW. There is an upgrade path to increase the beam power to 100 kW over the course of the next few years. This is still considerably less than the original design intensity of 300 kW. On the other hand, the K_L component of the beam has been measured to be larger than expected by a factor of 2.4, so there are prospects for approaching the planned sensitivity of the experiment.

6.2.3.5 TREK

The TREK (E06) experiment at J-PARC is based on the upgrade of the E246 detector, which was used at KEK in the '90s to study T-violating muon polarization in $K_{\mu 3}$ decay [497]. The main goal of the experiment is to extend limits on P_T to 10^{-4} or below, with potential sensitivity to new physics. 270 kW of primary beam power (at 30 GeV) is required to produce the 2 MHz of K^+ necessary for the measurement. Since beam power of 100 kW or greater is not expected to become available at J-PARC until 2018 or later, in early-stage running as the E36 experiment, the TREK upgrades will be put to use for the precision measurement of R_K, with an overall uncertainty of 0.25% [552]. E36 will also perform an inclusive search for $K^+ \to \mu^+ N$ decays, where N is a heavy neutrino, as well as a search for secluded gauge bosons, by examining the e^+e^- invariant mass spectra in $K^+ \to \mu^+\nu e^+e^-$ decays. These aspects of the E36 physics program can be carried out with the beam power expected in 2015.

6.2.4 Experimental programs: Longer-term future

6.2.4.1 J-PARC

The KOTO experiment was proposed as a continuation of the experimental program of E391a, and the intention to upgrade KOTO to perform a 100-event measurement of $\mathrm{BR}(K_L \to \pi^0\nu\bar{\nu})$ was part of the multigenerational program set forth in the original proposal [553]. The basic elements of the Step-2 upgrade are as follows [554]:

- An increase in the primary intensity to 3×10^{14} p per spill (beam power ∼450 kW).
- A new neutral beamline at 5° instead of 16°, with the mean K_L momentum increased to 5.2 GeV. The harder K_L spectrum makes for easier photon vetoing. The beamline must be lengthened to allow hyperons to decay before reaching the experiment.
- Lengthening of the vacuum tank from ∼6 m to 15 m to provide lengthening of the FV from 2 m to 11 m. The diameter of the vacuum tank and of the CsI calorimeter will also be increased from 2 m to 3 m.

Studies performed for the original proposal indicated that these upgrades could allow the experiment to collect more than 100 events in three years of data taking (at 10^7 s/yr) with $S/B \sim 5$. The upgrade is ambitious, in the sense that the detector must be almost entirely rebuilt; extension of the J-PARC Hadron Hall will also be necessary to house the upgraded experiment. Ultimately, the primary beam intensity may prove to be a significant limitation: it is expected to be difficult to increase the beam power beyond 100 kW. At 100 kW, the Step-2 sensitivity would be 10 SM events per 10^7-s year.

The KOTO Collaboration intends to gain experience with the Step-1 experiment before making a formal proposal. If Step-2 construction were to begin in 2020, the experiment could be taking data by 2025, but this is merely a statement of possibility, not a schedule.

6.2.4.2 CERN

The schedule for fixed-target running at the SPS depends on the LHC schedule, Fixed-target runs corresponding to LHC runs 2, 3, and 4 are thus foreseen for the periods from fall 2014 to mid 2018, from early 2020 to the end of 2023, and from early 2025 to the end of 2028.

NA62 has just started to take data, and although its initial request was for 200 days of data taking, it seems likely that the experiment will run throughout Run 2. In terms of a standard data-taking year of 10^7 s, NA62's sensitivity is about 100 SM events per year. Especially if the sensitivity of the experiment were to be upgraded by a small factor (2–3), additional running in Run 3 could make possible a 5% measurement of $\mathrm{BR}(K^+ \to \pi^+\nu\bar{\nu})$. If that can be accomplished, interest will likely shift to the K_L decay, for which prospects for even a 10% measurement are considerably less certain.

A subset of the Italian NA62 groups have obtained a PRIN grant to conduct feasibility studies for an experiment based on the NA62 infrastructure to measure $\mathrm{BR}(K_L \to \pi^0\nu\bar{\nu})$ (KLEVER, PRIN call

2010-2011). In contrast to KOTO, this experiment would use a high-energy beam. This makes photon vetoing significantly easier, but increases considerably the size of the detector, and in particular, the volume to be covered with photon vetoes.

The possibility of a neutral beam at NA62 was foreseen in the Technical Design Document [555]. A neutral beam extracted at 2.4 mrad (to reduce the neutron flux) would have a mean momentum of 97 GeV, with full width at half maximum spanning the range 40–140 GeV. However, a substantial increase in the primary beam intensity would be required. The PRIN studies assume an increase from the current 3×10^{12} to to 2.4×10^{13} p per 16.8 s spill, providing 3×10^{12} K_L decays per year in the FV.

The baseline design for the $K_L \to \pi^0 \nu\bar{\nu}$ experiment uses roughly the same vacuum tank layout as NA62. The FV starts about 100 m downstream of the target to allow short-lived components of the beam to decay and is about 60 m long, since 80 m between the edge of the FV and the LKr calorimeter are helpful for background rejection. The FV acceptance is 2.7%. The 140-m long vacuum tank is lined by 26 new, ring-shaped photon veto stations which provide hermetic coverage out to 100 mrad for photons with energies down to 20 MeV. The existing lead-glass NA62 large-angle vetoes do not have sufficiently high efficiency for photons with $E < 100$ MeV for use in a K_L experiment, but scintillator/tile detectors can provide the needed sensitivity [556]. The NA48 LKr calorimeter is used both to reconstruct π^0s and to reject events with extra photons; its efficiency for the detection of photons with $E > 1$ GeV appears to be sufficient. High-energy photons escaping down the beamline are intercepted by a new in-beam veto (IBV), which must have excellent timing resolution and be relatively insensitive to hadronic interactions, since the beam consists of ∼800 MHz of neutrons. In order for this detector to work at all, upstream filters made of a high-Z material must also reduce the ∼2000 MHz of beam photons from the primary interaction by an order of magnitude or more. Charged-particle vetoes will be needed but have yet to be incorporated into the design.

The sensitivity estimates for the baseline experiment are preliminary. In particular, the only background source to have been seriously studied yet is $K_L \to \pi^0\pi^0$. Signal candidates are defined as having two hits on the LKr and no activity elsewhere in the detector, with the z-coordinate of the π^0 decay vertex reconstructed in the FV and $p_\perp(\pi^0) < 100$ MeV. At the beam intensity assumed, the experiment could collect 10 SM signal events per data-taking year of 10^7 s, with a $S/B \sim 1$. This sensitivity is about the same as for KOTO Step 2 at a beam power of 100 kW, although the background rejection needs further improvement. However, for the long development time and significant costs of the project to be justified, it would be desirable to have a sensitivity of at least 30 SM events/year, which would allow for a true 100-event measurement. A variety of modifications to the baseline experiment to increase the sensitivity are under study, including varying the beam energy and solid angle acceptance and the dimensions of the fiducial volume and replacing the NA48 LKr calorimeter with a larger device that is more efficient for low energy photons ($E \sim 1$ GeV).

The most pressing limitation is from the beam intensity. To handle the assumed intensity of 2.4×10^{13} p spill, major infrastructural upgrades to the primary beamline and cavern would be required; these upgrades may turn out to be impractical for the existing cavern. However, preliminary design studies and cost estimates for a high-intensity fixed target infrastructure for the SHiP experiment have been carried out by the CERN EN division [557]. A flux of 4×10^{19} p on target per year could be delivered at this facility, which is 4 times greater than the assumed flux for the PRIN project. Although the cost of such a facility would be high (CHF 113M), the project demonstrates what fluxes can be obtained in the North Area without upgrades to the PS-SPS complex. A next-generation K_L experiment could be envisioned as a centerpiece of a new high-intensity North Area facility.

While a $K_L \to \pi^0 \nu\bar{\nu}$ experiment would require substantial modifications to the basic layout of the NA62 experiment, measurements of the BRs for the $K_L \to \pi^0 \ell^+ \ell^-$ decays might be attempted with relatively minor modifications to the existing NA62 apparatus. Some beamline elements, as well as the CEDAR and Gigatracker detectors, would have to be removed, and other detectors, such as the straw chambers and RICH would have to be modified to allow the neutral beam to pass without interception.

Simulations to assess the sensitivity and background levels are underway as part of the PRIN project. In the meantime, studies performed for NA48 [558] can be extrapolated on the basis of the K_L flux assumed. The results seem initially to be discouraging, with a few counts in each channel, $\pi^0 e^+ e^-$ and $\pi^0 \mu^+ \mu^-$, and predicted backgrounds several times more abundant than the signal, with a significant complication for the $K_L \to \pi^0 e^+ e^-$ channel from background from $K_L \to e^+ e^- \gamma\gamma$ events (BR $\sim 10^{-7}$) [559]. However, these results do not account for improvements to the NA48 apparatus made for NA62. Moreover, they are based on a simple cut-and-count analysis, whereas gains are expected from kinematic fitting and other more refined analysis techniques. In any event, design and construction of a $K_L \to \pi^0 \nu\bar{\nu}$ experiment would take many years and require realistic testing of critical elements such as the in-beam veto detector. As such, a $K_L \to \pi^0 \nu\bar{\nu}$ experiment would likely run in Run 4. Run 3 data-taking with a neutral beam and a minimally modified NA62 apparatus would push down the limits on the BRs for the $K_L \to \pi^0 \ell^+ \ell^-$ decays, and as well would provide a platform for detector R&D for the $K_L \to \pi^0 \nu\bar{\nu}$ measurement. Significant progress might also be made in the neutral-channel analogues for many of the secondary topics in NA62's physics program discussed above, and in particular, in searches for heavy neutral leptons and K_L decays with explicit LFV.

6.3 Charm physics

6.3.1 Introduction

The charm quark is the only up-type quark whose hadronization and subsequent weak decay can be studied. Charm physics offers the unique possibility to probe for new physics in the up-type quark sector and extends the search to an energy scale that goes beyond the LHC center-of-mass (CM) energy. The study of charm physics provides other interesting opportunities, such as the test of non-perturbative QCD and lattice QCD calculations and the study quarkonia and exotic states. It is also part of a wider flavour physics program that requires precision measurements of charm decays, as for example the measurement of the CKM angle γ in $B^\pm \to DK^\pm$ decays.

The discovery potential of charm physics has been discussed in a dedicated a workshop organized in Milano [560]. Three main topics were identified as the most relevant for new physics searches:

1. $D^0 - \overline{D}^0$ oscillations and CP violation in mixing: The relatively high rate of $D^0 - \overline{D}^0$ oscillations is intriguing and could be due to Standard Model (SM) or to new physics, though theoretical calculations are affected by large uncertainties. Evidence of CP violation in mixing would be a clear signature of new physics.
2. CP violation in the decay: CP violation in $\Delta C = 1$ transitions is expected to be small, at most at the level of $\mathcal{O}(V_{ub}V_{cb}^*/V_{us}V_{cs}^*) \sim 10^{-3}$ in the SM. A CP-violating signal in excess of this prediction can provide a *smoking gun* signature of new physics.
3. Rare decays: FCNC transitions directly probe new physics models. SM contributions are small but long distance effects are usually dominant. The decay $D^0 \to \mu^+ \mu^-$ is a very useful probe of new physics, provided that the long distance contribution mediated by $D^0 \to \gamma\gamma$ is experimentally determined. Among the *charm* rare decays we can include also the B_c^+ meson, the lightest particle with two heavy quarks of different flavour.

The experimental facilities that have contributed (and continue to do so) to the study of charm physics can be divided in three main categories. The first is represented by the fixed target experiments at Fermilab, such as E687, E791 and FOCUS that pioneered the study of charm decays. Second are the experiments at e^+e^- colliders such as CLEO, BaBar and Belle running at the $\Upsilon(4S)$ resonance peak, where the charm signal is produced from the $e^+e^- \to c\bar{c}$ reactions, and CLEO-c and BES-III running on and near the $\psi(3770)$ peak. The first evidence of $D^0 - \overline{D}^0$ oscillations was obtained in 2007 by BaBar and Belle [561, 562], and a wide range of CP violation measurements were accomplished. In this category, CLEO-c and BESIII experiments are notable since running mostly at the $\psi(3770)$ resonance peak can

exploit the coherent production of $D^0 - \overline{D}^0$ pairs. In this case the environment is very clean with no additional fragmentation particles produced. The third category can be identified by the experiments at hadron colliders such as CDF at the Tevatron and LHCb at the LHC, where large charm production cross-sections and efficient triggers give rise to enormous statistics. LHCb has recently produced the world best measurements for $D^0 - \overline{D}^0$ mixing and CP violation [563, 564].

Intense experimental activity in the charm sector is foreseen for the future. In 2017 the BelleII experiment will start the data taking and is expected to accumulate a data sample corresponding to an integrated luminosity of 50 ab^{-1} at the CM energy of 10.58 GeV, corresponding to about 40 times the statistics of the current B-factory dataset. The LHCb upgrade is foreseen in 2018 and will accumulate an integrated luminosity of 50fb^{-1} in 10 years of data taking at a CM energy of 14 TeV, with improved trigger efficiency and twice the cross-section with respect to the run at 7 TeV. Recently, an interesting proposal for an High Intensity Electron Positron Accelerator (HIEPA) to be built in China was advanced [565]. The facility would operate mainly at the CM energy of 4 GeV for charm and τ physics, providing a peak luminosity of 10^{35} cm^{-2}s^{-1} and aiming to collect a data sample of 1 ab^{-1}. In addition, a new fixed-target experiment (SHiP) at the CERN SPS accelerator has been proposed and will use decays of charm mesons to search for heavy neutral leptons which are right-handed partners of the SM neutrinos [430].

6.3.2 $D^0 - \overline{D}^0$ oscillations and CP violation in mixing

Flavour-changing neutral currents (FCNC) are much suppressed in the SM due to a very effective Glashow-Iliopoulos-Maiani (GIM) mechanism for charm. However, a relatively large $D^0 - \overline{D}^0$ mixing has been observed experimentally and the mixing parameters

$$x = \frac{m_1 - m_2}{\Gamma}, \qquad y = \frac{\Gamma_1 - \Gamma_2}{2\Gamma}, \tag{43}$$

have been determined to be $x = (0.41^{+0.14}_{-0.15})\%$ and $y = (0.63^{+0.07}_{-0.08})\%$ [566], where $m_{1,2}$ and $\Gamma_{1,2}$ are the masses and the widths of the Hamiltonian eigenstates, respectively, and $\Gamma = (\Gamma_1 + \Gamma_2)/2$. This is a quite intriguing result that could be explained by the SM long-distance contributions or by new physics effects. However long-distance contributions cannot be reliably computed at present, therefore SM predictions for x and y are poorly known. Conversely, CP violation in the SM is expected to be well below the future experimental sensitivity, so evidence for CP violation would point to New Physics. In Fig. 76 are reported the average results for mixing (x, y) and CP violation parameters ($|q/p|$, $\arg(q/p) = \varphi$) obtained from the combination of the relevant experimental measurements [566]. From the relation that holds between the mixing and CP violation parameters [567, 568],

$$\tan\varphi = \frac{1 - |q/p|^2}{(1 + |q/p|^2)}\frac{x}{y} \sim (1 - |q/p|)\frac{x}{y}, \tag{44}$$

and from the experimental results, i.e. $x/y = \mathcal{O}(1)$, we should expect $1 - |q/p| \sim \varphi$. As shown in Fig. 70, a general analysis of $\Delta F = 2$ processes in the case of strongly-coupled new physics with no flavour suppression, demonstrates that the experimental results from the neutral D meson system provide the best limits on the scale of new physics after the kaon system.

In Table 15, the expected sensitivites for the measurements of mixing and CP violation parameters at LHCb and BelleII are compared with present results in the golden channels $D^0 \to K^0_S\pi^+\pi^-$, $D^0 \to K^+K^-, \pi^+\pi^-$ and $D^0 \to K^+\pi^-$ wrong-sign decays. The estimates of the sensitivities for the $D^0 \to K^0_S\pi^+\pi^-$ decay assume a precise knowledge of the Dalitz plot amplitudes, or a model-independent approach [569], in order to avoid amplitude-dependent systematic uncertainties. The analysis of BESIII data would provide crucial information on the relative amplitudes and phases $A(\overline{D}^0 \to f)/A(D^0 \to f) = -re^{-i\delta_f}$ between D^0 and $\overline{D}^0$, by exploiting the coherent production of $D^0 - \overline{D}^0$ pairs [570]. The

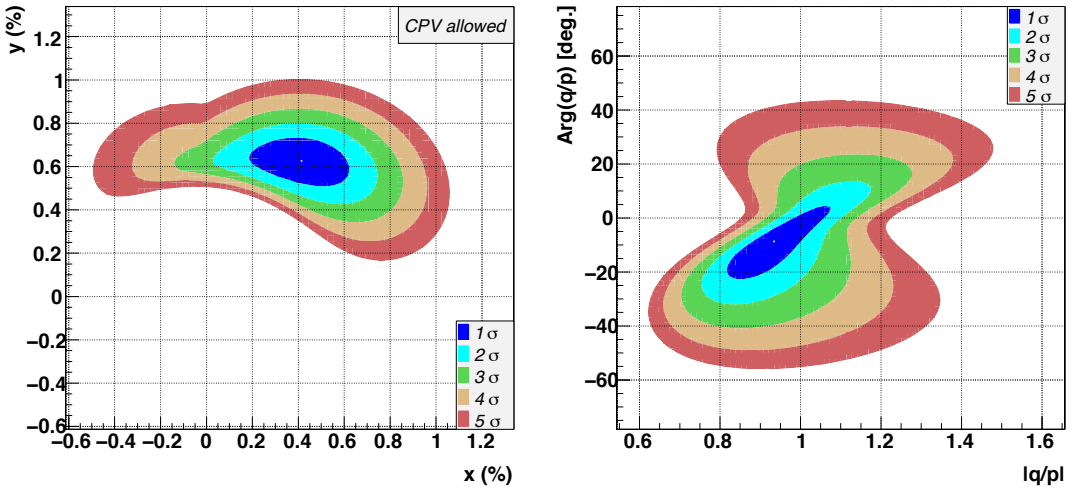

Fig. 76: Global fit results for $D^0 - \overline{D}^0$ mixing with CP violation allowed: (left) contour plot for 1-5 σ regions for x and y mixing parameters; (right) contour plot for 1-5 σ regions for $|q/p|$ and $\arg(q/p)$ CP violation parameters.

mixing parameter y_{CP} and the CP violation parameter A_Γ can be measured from the lifetime ratio of the CP-even decays $D^0 \to h^+h^-$ ($h = K, \pi$) with respect to the CP-mixed state $D^0 \to K^+\pi^-$, and from the lifetime difference of $D^0 \to h^+h^-$ and $\overline{D}^0 \to h^+h^-$ decays, respectively. The time-dependent analysis of wrong-sign $D^0 \to K^+\pi^-$ decays allows the measurement of the mixing parameters x'^2, y' and the CP violation parameters $|q/p|$, A_D and φ. In particular A_D is sensitive to CP violation in the decay while $|q/p|$ and φ are sensitive to CP violation in mixing.

6.3.3 CP violation in decay

In general CP violation in charm decays is very small in the SM allowing for a significant *null test* of the theory. However, asymmetries at a few times 10^{-3} within the SM cannot be excluded according to recent calculations. In any case, at the level of few 10^{-4}, one hits the largely uncalculable SM suppressed amplitudes which spoil the potential sensitivity to new contributions in strong penguin and chromomagnetic dipole operators [571].

Nevertheless, it is important to search for CP violation in many decay modes since this may allow for data-driven methods to estimate the SM uncertainty, such as SU(3)-flavour analyses [572]. Some examples of interesting decay modes to study are $D^+ \to \pi^+\pi^0$ (no CP violation is expected in the SM), $D^0 \to K^0_S K^0_S$ (possible CP violation enhancement due to the suppressed production rate), $D^0 \to V\gamma$ (possible enhanced CP violation effects related to gluonic penguin contributions). In addition, the study of 3-body and 4-body decays allows localised CP violation in different regions of phase space to be probed. This approach enhances the sensitivity due to several interfering amplitudes with different relative strong phases contributing to the decay. In 4-body decays it is relevant to note that the search for CP violation using T-odd correlations, e.g. defined as the triple product of final state particle momenta $C_\pm = \text{sign}[p_1 \cdot (p_2 \times p_3)]$, is characterised by a different sensitivity to CP violation with respect to the

Analysis	Obs.	LHCb (3 fb^{-1})	LHCb (50 fb^{-1})	Belle (1 ab^{-1})	BelleII (50 ab^{-1})
$K^0_S\pi^+\pi^-$	x	2×10^{-3}	4×10^{-4}	1.9×10^{-3}	8×10^{-4}
	y	2×10^{-3}	4×10^{-4}	1.5×10^{-3}	5×10^{-4}
	$\|q/p\|$	0.2	0.04	0.16	0.06
	φ	15°	3°	11°	4°
K^+K^-,	y_{CP}	3×10^{-4}	2×10^{-5}	2.2×10^{-3}	4×10^{-4}
$\pi^+\pi^-$	A_Γ	3×10^{-4}	2×10^{-5}	2.0×10^{-3}	3×10^{-4}
$K^+\pi^-$	x'^2	5×10^{-5}	1×10^{-5}	2.2×10^{-4}	3×10^{-5}
	y'	1×10^{-3}	2×10^{-4}	3.4×10^{-3}	4×10^{-4}
	$\|q/p\|$	0.25	0.05	0.6	0.06
	A_D	0.02	4×10^{-3}	-	-
	φ	-	-	25°	2.3°

Table 15: Expected sensitivities to mixing and CP violation parameters foreseen at LHCb upgrade and BelleII are compared with the present uncertainties. LHCb and BelleII use different variables in the fit for CP violation parameters of wrong-sign $D^0 \to K^+\pi^-$ decays. See the text for a discussion of theoretical uncertainties.

rate asymmetry and is affected by very small systematic uncertainties [573]. Table 16 summarizes these channels with their expected experimental sensitivities.

Decay	LHCb (50 fb^{-1})	BelleII (50 ab^{-1})
$D^0 \to K^+K^-$	1.0×10^{-4}	3×10^{-4}
$D^0 \to \pi^+\pi^-$	1.5×10^{-4}	5×10^{-4}
$D^0 \to \pi^0\pi^0$	-	9×10^{-4}
$D^+ \to K^0_S K^+$	1.0×10^{-4}	5×10^{-4}
$D^+ \to \phi\pi^+$	8.0×10^{-5}	4×10^{-4}
$D^+ \to \pi^+\pi^-\pi^+$	8.0×10^{-5}	-
$D^0 \to K^+K^-\pi^+\pi^-$	2.5×10^{-4}	-

Table 16: Expected sensitivities to CP-violating asymmetries for different charm decay modes. For the decay $D^0 \to K^+K^-\pi^+\pi^-$ the reported sensitivity is relative to the CP-violating asymmetry based on T-odd correlations. The - sign indicates that no sensitivity prediction is available. See the text for a discussion of theoretical uncertainties.

6.3.4 Rare Decays

In the charm sector the GIM cancellation in loop processes is very effective. Branching ratios that are mediated by FCNC are not expected to exceed $\mathcal{O}(10^{-10})$ in the SM. However, contributions from beyond SM physics could enhance the values by several order of magnitudes with respect to SM expectations. Among the most interesting signals, the rare decay $D^0 \to \mu^+\mu^-$ is dominated in the SM by *long distance* contributions. The largest contribution comes from the two-photon unitarity component. In particular, we can write the relation $\mathcal{B}(D^0 \to \mu^+\mu^-) \simeq 2.7 \times 10^{-5} \cdot \mathcal{B}(D^0 \to \gamma\gamma)$ [574]. The expected branching ratio for $D^0 \to \gamma\gamma$ is at the level of 10^{-8} in the SM, therefore we anticipate a branching ratio $\mathcal{B}(D^0 \to \mu^+\mu^-) \simeq 3 \times 10^{-13}$. The values can be dramatically enhanced in R-parity violating SUSY, which allows for branching ratios for $(D^0 \to \mu^+\mu^-)$ up to the level of 10^{-6} [574]. The present limit is $\mathcal{B}(D^0 \to \mu^+\mu^-) < 7.6 \times 10^{-9}$ at 95% C.L. [575] — it is expected to improve by about a factor 10 with the LHCb upgrade (50 fb^{-1}). Other interesting rare decays include $D^+ \to \pi^+\mu^+\mu^-$, $D^+_s \to \pi^+\mu^+\mu^-$ and $D^0 \to \pi^+\pi^-\mu^+\mu^-$. The present upper limits at 95% C.L. from LHCb are at the level of 8.3×10^{-8},

4.8×10^{-7}, and 6.7×10^{-7}, respectively [576, 577], and can improve by about a factor 10 with the LHCb upgrade. It is almost certain that the long-distance contributions are often completely dominant, and absolute values of branching ratios are not useful indicators of presence of new physics. The study of kinematical variables such as the dilepton invariant mass, or the forward-backward asymmetry can discriminate between SM and new physics.

6.3.5 The $B_c^\pm$ laboratory

The pseudoscalar B_c^+ meson, the ground state of the $\bar{b}c$ system, is the lightest particle containing two heavy quarks of different flavours and thus represents a unique laboratory in which to study heavy-quark dynamics. The investigation of the $B_c^\pm$ meson properties is of special interest compared to the flavour symmetric heavy-quarkonium ($b\bar{b}$, $c\bar{c}$) states, and provides a new testing ground for predictions in the context of effective models inspired by quantum chromodynamics [578]. The decay processes of the $B_c^\pm$ meson can be generically divided into three classes: those involving the decay of the b quark, the decay of the c quark, and the annihilation of the b and c quarks [578–580].

The advent of the CERN LHC has opened a new era for $B_c^\pm$ investigations; a rich program of measurements involving new decay modes is being carried out mainly by the LHCb experiment with some contributions from CMS and ATLAS as well.

New attention has emerged to this particle and it is natural to ask to what extent it is interesting for testing the SM and, in particular, for the study of CP violation [581]. Pure tree decays $B_c^\pm \to D_s^\pm D$ are particularly well suited to extract the CKM angle γ through amplitude relations. In contrast to conceptually similar strategies using $B^\pm \to DK^\pm$ or $B_d \to DK^{*0}$ decays, the advantage of the $B_c^\pm$ approach is that the corresponding triangles have three sides of comparable length and do not involve small amplitudes. Decays of the type $B_c^\pm \to D^\pm D$, the U-spin counterparts of $B_c^\pm \to D_s^\pm D$, can be added to the analysis, as well as channels where the $D_s^\pm$ and $D^\pm$ mesons are replaced by higher resonances.

Statistics is still the main obstacle to pursue these studies, and thus, the topic is relevant in the discussion for a possible *Extreme Flavour* project. Reliable measurements of the $B_c^\pm$ branching fractions and cross-section are needed to quantify the luminosity required to perform CP studies. In general, accurate investigation of the $B_c^\pm$ meson will allow to deepen our knowledge of the heavy flavour field and carry out consistency checks in a system where b and c quark live together.

6.4 B Physics at hadron colliders

Flavour physics involving b-quark hadrons is extensively studied in two experimental environments: e^+e^- B Factories, running on the $\Upsilon(4S)$ mass, and proton colliders. The former offer the advantages of an initial state with well defined energy-momentum and quantum numbers, and low multiplicity events. The two B Factory experiments Babar and Belle showed that full event reconstruction is achievable, the decay products of both B mesons from the $\Upsilon(4S)$ decay can be disentangled, particle identification is excellent, reconstruction of neutral hadrons is efficient, and neutrinos can be indirectly detected by missing mass. Hadron colliders offer much higher production rates and the possibility to produce all flavoured mesons and baryons. However, high background rates require selective triggers and the acceptance is restricted. The LHCb experiment at the LHC exploits the long decay paths of B hadrons produced at the LHC and, due to very precise charged particle tracking and identification, is able to discriminate B decays from background and search for the rare decays most sensitive to new physics.

In the following sections, which are partly adapted from Refs. [582,583], key results on B physics are briefly reviewed, and the continuation of these studies with upgraded LHC detectors is motivated, together with the precision on key observables that would be obtained on a timescale of ten years. For further details, the reader is encouraged to consult already existing extensive reports [584–586].

6.4.1 Introduction

The first run of the LHC machine demonstrated definitively that it is possible to impact significantly on the flavour physics landscape by collecting unprecedented samples of heavy flavoured hadrons with the LHCb detector.

The core of the LHCb physics programme in rare decays and CP violation will continue in the next few years during the LHC Run2. In many channels, the LHCb results are already the world's most precise, and begin to reach the sensitivity where small deviations from SM predictions may be observed. In several areas hints of large anomalies from previous measurements have not been confirmed: the branching fraction of $B_s^0 \to \mu^+\mu^-$ [587], the forward-backward lepton asymmetry of $B^0 \to K^{*0}\mu^+\mu^-$ [588] and the CP-violation phase in B_s^0 oscillations [589] are all found to be consistent with the SM, within current uncertainties. Nevertheless, in all these cases more precise measurements are mandatory. In addition, other channels exhibit strengthened, or new, hints of unexpected effects: for example, the anomalous isospin asymmetry in $B \to K\mu^+\mu^-$ decays [590], a local 3.7σ effect in the distribution of an optimized observable in $B \to K^*\mu^+\mu^-$ decays [591], a hint of lepton universality violation in $B \to K^+\ell^+\ell^-$ decays [592]. Other anomalies still persist in data samples collected at the B Factories, for instance in $B \to D^{(*)}\tau\nu$ decays [593], in the discrepancy of the determination of the CKM matrix elements $|V_{ub}|$ and $|V_{cb}|$ with inclusive and exclusive decays [81].

All these effects demand to be followed up with more data, and with studies of complementary decay channels. More generally speaking, the need to exploit fully the flavour physics potential of the LHC motivates the upgrade of the LHCb experiment in light of the latest results. This upgrade will take place during the second shut-down of the LHC in 2018-2019 (LS2), such that an upgraded detector can accumulate in ten years an integrated luminosity one order of magnitude larger than that foreseen in Run1+Run2.

6.4.2 Highlights of measurements and their implications

6.4.2.1 Rare decays

Among rare decays, both CMS and LHCb have established evidence for the decay $B_s^0 \to \mu^+\mu^-$ [587, 594] , placing stringent limits on NP models that enhance the branching fraction. A recent combination of the CMS and LHCb analyses [595] shown in Fig. 77, allows to establish a measurement of $B_s^0 \to \mu^+\mu^-$ well above 5σ, as well as obtain evidence for the $B \to \mu^+\mu^-$ decay:

$$\begin{aligned} \mathcal{B}(B_s^0 \to \mu^+\mu^-) &= (2.8^{+0.7}_{-0.6}) \times 10^{-9}\,, \\ \mathcal{B}(B^0 \to \mu^+\mu^-) &= (3.9^{+1.6}_{-1.4}) \times 10^{-10}\,. \end{aligned}$$

The above branching fraction can be compared to the SM predictions: $\mathcal{B}(B_s^0 \to \mu^+\mu^-)_{\rm SM} = (3.65 \pm 0.23) \times 10^{-9}$, $\mathcal{B}(B^0 \to \mu^+\mu^-)_{\rm SM} = (1.06 \pm 0.09) \times 10^{-10}$ [596]. This result puts severe constraints on NP models [597].

A full analysis of the $B^0 \to K^{*0}\mu^+\mu^-$ decays [598] allows the determination of numerous optimized NP-sensitive observables (see, for example, Refs. [599, 600]). The measurements obtained from such an analysis, as well as similar studies of related channels, such as $B_s^0 \to \phi\mu^+\mu^-$ [601], allow model-independent constraints on NP, manifested as limits on the operators of the effective Hamiltonian (see, for example, Refs. [602,603]). LHCb has measured the zero crossing point of the forward-backward asymmetry, finding it in agreement with the SM prediction [598]. Moreover, other optimized observables have been measured [591]. General agreement with respect to the SM is found, except for a local 3.7σ discrepancy for one of the observables, as shown in Fig. 78. The significance of this deviation is under debate as the SM prediction might have larger uncertainties than those shown in Fig. 78 [604–606]. Given the integrated luminosity collected at LHCb, it is now possible to perform the measurement of the photon polarization in radiative decays, which is predominantly left-handed in the SM. The photon polarization is inferred by measuring the up-down asymmetry with respect to the hadronic decay

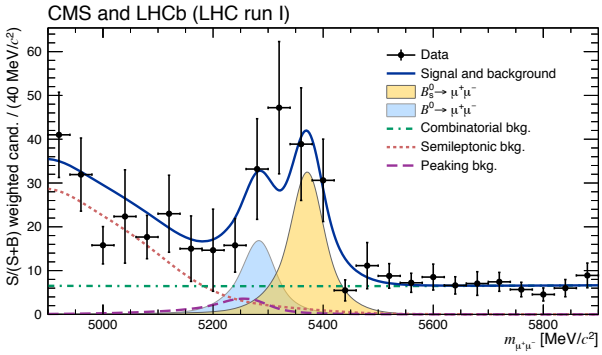

Fig. 77: Weighted distribution of the dimuon invariant mass for all categories. Superimposed on the data points in black are the combined fit (solid blue) and its components: the B_s^0 (yellow shaded) and B^0 (light-blue shaded) signal components; the combinatorial background (dash-dotted green); the sum of the semileptonic backgrounds (dotted salmon); and the peaking backgrounds (dashed violet). From [595].

plane in $B^+ \to K_{res}\gamma$, where K_{res} is an intermediate strange resonance decaying in $K^+\pi^+\pi^-$. LHCb measured [607] an up-down asymmetry, on a sample of 8000 decays into a mixture of K resonances, $A_{ud} = 0.085 \pm 0.019_{(stat)} \pm 0.004_{(syst)}$, giving evidence for photon polarization in $b \to s\gamma$ decays. However, due to multiple overlapping resonances, it is difficult to measure the photon polarization for each single decay. More theoretical studies are needed in order to progress further. Similarly, studies of observables such as isospin asymmetries [590] are important since they allow to pin down in which operators the NP effects occur. A recent measurement of the relative ratio of decays involving electron and muons in the final state is challenging lepton universality [592]. More data are needed in order to clarify if this is the case.

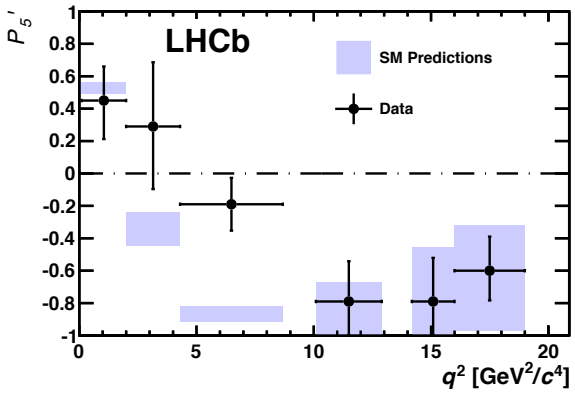

Fig. 78: Measured values (black points), compared with SM prediction, of $P_5^{'}$, a theoretically clean observable in $B^0 \to K^{*0}\mu^+\mu^-$ decays. From Ref. [591].

6.4.2.2 CP violation in the B sector

Measurements of the neutral B meson mixing parameters provide an excellent method to search for NP effects, due to the low theoretical uncertainties associated to several observables. The LHCb measurements of the CP-violating phase, ϕ_s, and the width difference, $\Delta\Gamma_s$, in the B_s^0 system [608] significantly reduce the phase space for NP:

$$\phi_s = 0.058 \pm 0.049\,(\text{stat}) \pm 0.006\,(\text{syst})\,\text{rad}\,, \quad \Delta\Gamma_s = 0.0805 \pm 0.0091\,(\text{stat}) \pm 0.0032\,(\text{syst})\,\text{ps}^{-1}\,. \tag{45}$$

Fig. 79 shows visually the agreement with the SM predictions. Deviations of $\mathcal{O}(0.1)$ are still possible, and are typically due to some well-motivated NP models that survive the present experimental bounds (such as in Ref. [609]).

The indirect determination of ϕ_s within the SM is very precise [610, 611], calling for an order-of-magnitude improvement of the direct measurement. However, the theoretical uncertainty in the extraction of ϕ_s from $B_s \to J/\psi X$ decays has to be carefully controlled using data-driven methods. For such methods, the theoretical uncertainty is expected to scale with the statistics, however detailed studies are needed to show that the theoretical error remains negligible [612–615].

In addition, to understand the origin of the anomalous dimuon asymmetry seen by D0 [616], improved measurements of semileptonic asymmetries in both B_s^0 and B^0 systems are needed. LHCb has released measurements of the B_s^0 and B^0 asymmetries [617, 618], finding agreement with the SM and demonstrating the potential to perform more precise measurements with increased statistics. The semileptonic asymmetry for the B^0 system has also been successfully measured at the B Factories, see e.g. Ref. [619]; improved precision will be achieved at Belle-II.

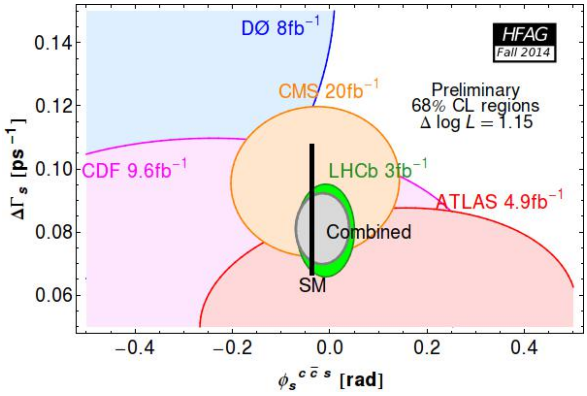

Fig. 79: HFAG world combination of ϕ_s and $\Delta\Gamma_s$ measurements. The green ellipse in the center represents the LHCb result and the grey ellipse shows the world average. The result of the first ϕ_s measurement in the $B_s^0 \to D_s^+ D_s^-$ decays $\phi_s = +0.02 \pm 0.17 \pm 0.02\ rad$ is also included in the LHCb combination.

Among the B^0 mixing parameters, improved measurements of both ϕ_d (i.e., $\sin 2\beta$) and $\Delta\Gamma_d$ are needed. Reducing the uncertainty on the former will help to improve the global fits to the CKM matrix [610, 611], and may clarify the current situation regarding the tension between various inputs to the fits (see, for example, Ref. [620]).

Another crucial observable is the angle γ, which, when measured in the tree-dominated $B \to DK$ processes, provides a benchmark measurement of CP violation. LHCb has made impressive progress on the determination of γ, by exploiting a large variety of decays modes and analysis techniques and combining the resulting measurements [621]. The current knowledge of this CKM parameter is dominated by LHCb, with the uncertainty foreseen to reach the 7° level after exploiting the full power of the Run 1 dataset.

Knowledge of γ from tree-dominated processes is also essential to test the consistency with measurements from loop-dominated processes. In particular, the study of $B_s^0 \to K^+K^-$ and $B^0 \to \pi^+\pi^-$ decays [622], which are related by U-spin, allows a powerful test of the consistency of the observables with the SM [623, 624]. Similarly, the U-spin partners $B_s^0 \to K^{*0}\overline{K}^{*0}$ [622] and $B^0 \to K^{*0}\overline{K}^{*0}$ are among the golden channels to search for NP contributions in $b \to sq\bar{q}$ penguin amplitudes [625]. Another important channel in this respect is $B_s^0 \to \phi\phi$ [626], for which the CP violating observables are predicted with low theoretical uncertainty in the SM. Studies of CP violation in multibody b hadron decays [627, 628] offer additional possibilities to search for both the existence and features of NP.

6.4.3 Sensitivity of the upgraded LHCb experiment to key observables

Given the strong motivation to exploit fully the flavour physics potential of the LHC, the estimated sensitivities for various key observables have been determined, based on the results to date. A detailed description of the upgraded LHCb experiment can be found in the Letter of Intent (LoI) [586], complemented by the framework technical design report (FTDR) [585], which sets out the timeline and costing for the project, and by Technical Design Reports (TDR) for the individual subsystems [629–632]. The upgrade is necessary to progress beyond the limitations imposed by the current hardware trigger that, due to its maximum output rate of $1\,\mathrm{MHz}$, restricts the instantaneous luminosity at which data can most effectively be collected. To overcome this, the upgraded detector will be read out at the maximum LHC bunch-crossing frequency of $40\,\mathrm{MHz}$ so that the trigger can be fully implemented in software. With such a flexible trigger strategy, the upgraded LHCb experiment can be considered as a general purpose detector in the forward region. The upgraded detector will be installed during the long shutdown of the LHC planned for 2018-2019.

Several important improvements compared to the current detector performance can be expected in the upgrade era, as detailed in the LoI and FTDR. However, the sensitivity studies that have been performed assume detector performance as achieved during the Run 1 data taking. The exception is in the trigger efficiency, where channels selected at hardware trigger level by hadron, photon or electron triggers are expected to have their efficiencies doubled (channels selected by muon triggers are expected to have marginal gains, that have not been included in the extrapolations). Several other assumptions are made:

- LHC collisions will be at $\sqrt{s} = 14\,\mathrm{TeV}$, with heavy flavour production cross-sections scaling linearly with $\sqrt{s}$;
- the instantaneous luminosity in LHCb will be $\mathcal{L}_{\mathrm{inst}} = 10^{33}\,\mathrm{cm}^{-2}\,\mathrm{sec}^{-1}$: this will be achieved with $25\,\mathrm{ns}$ bunch crossings and an average number of visible interactions per crossing $\mu = 2$;
- LHCb will change the polarity of its dipole magnet with similar frequency as in 2011/12 data taking, to approximately equalise the amount of data taken with each polarity for better control of certain potential systematic biases;
- the integrated luminosity will be $\mathcal{L}_{\mathrm{int}} = 5\,\mathrm{fb}^{-1}$ per year, and the experiment will run for 10 years to give a total sample of $50\,\mathrm{fb}^{-1}$.

The sensitivity to various flavour observables is summarised in Table 17, which is taken from Ref. [633] and represents an update of previous studies documented in the FTDR [585] and in the LoI [586]. The measurements considered include CP-violating observables, rare decays and fundamental parameters of the CKM Unitarity Triangle. More details about these observables are given below. The current precision, taken from LHCb measurements on Run 1 data, is given and compared to the estimated sensitivity with the upgrade. As an intermediate step, the estimated precision that can be achieved prior to the upgrade is also given for each observable. For this, a total integrated luminosity of $5.0\,\mathrm{fb}^{-1}$ at pp centre-of-mass collision energies $\sqrt{s} = 13\,\mathrm{TeV}$ recorded in 2015–17 is assumed. Another assumption is that the current efficiency of the muon hardware trigger can be maintained at higher $\sqrt{s}$, but that higher thresholds will be necessary for other triggers, reducing the efficiency for the relevant channels by a factor of 2 at $\sqrt{s} = 13\,\mathrm{TeV}$.

In LHCb measurements to date, the CP-violating phase in B_s^0 mixing, measured in both $J/\psi\,\phi$ and $J/\psi\,f_0(980)$ final states, has been denoted ϕ_s. In the upgrade era it will be necessary to remove some of the assumptions that have been made in the analyses to date, related to possible penguin amplitude contributions, and therefore the observables in $b \to c\bar{c}s$ transitions are denoted by $2\beta_s = -\phi_s$, while in $b \to q\bar{q}s$ ($q = u, d, s$) transitions the notation $2\beta_s^{\mathrm{eff}}$ is used. This parallels the established notation used in the B^0 system (α, β, γ convention for the CKM Unitarity Triangle angles is used). While penguin contributions in $b \to c\bar{c}s$ transitions are expected to be small, a detailed estimate of the theoretical uncertainty can only be provided by data-driven methods which require channels still to be measured [615]. The

Table 17: From Ref. [633] – Statistical sensitivities of the LHCb upgrade to key observables. For each observable the expected sensitivity is given for the integrated luminosity accumulated by the end of LHC Run 1, by 2018 (assuming $5\,\text{fb}^{-1}$ recorded during Run 2) and for the LHCb Upgrade ($50\,\text{fb}^{-1}$). An estimate of the theoretical uncertainty is also given – this and the potential sources of systematic uncertainty are discussed in the text.

Type	Observable	LHC Run1	LHCb 2018	**Upgrade** ($50\,\text{fb}^{-1}$)	Theory uncertainty
B_s^0 mixing	$2\beta_s\,(B_s^0 \to J/\psi\,\phi)$	0.05 [608]	0.025	0.009	~ 0.003
	$2\beta_s\,(B_s^0 \to J/\psi\,f_0(980))$	0.068 [634]	0.035	0.012	~ 0.01
	a_{sl}^s	2.8×10^{-3} [617]	1.4×10^{-3}	0.5×10^{-3}	0.03×10^{-3}
Gluonic penguins	$2\beta_s^{\text{eff}}(B_s^0 \to \phi\phi)$	0.15 [626]	0.10	0.023	0.02
	$2\beta_s^{\text{eff}}(B_s^0 \to K^{*0}\bar{K}^{*0})$	0.19 [635]	0.13	0.029	< 0.02
	$2\beta^{\text{eff}}(B^0 \to \phi K_S^0)$	0.30 [636]	0.20	0.04	0.02
Right-handed currents	$2\phi^{\text{eff}}(B_s^0 \to \phi\gamma)$	0.20 [637]	0.13	0.03	< 0.01
	$\tau^{\text{eff}}(B_s^0 \to \phi\gamma)/\tau_{B_s^0}$	5 %	3.2 %	0.8 %	0.2 %
Electroweak penguins	$S_3(B^0 \to K^{*0}\mu^+\mu^-; 1 < q^2 < 6\,\text{GeV}^2/c^4)$	0.04 [598]	0.020	0.007	0.02
	$q_0^2\,A_{\text{FB}}(B^0 \to K^{*0}\mu^+\mu^-)$	10 % [598]	5 %	1.9 %	7 %
	$A_{\text{I}}(K\mu^+\mu^-; 1 < q^2 < 6\,\text{GeV}^2/c^4)$	0.09 [590]	0.05	0.017	~ 0.02
	$\mathcal{B}(B^+ \to \pi^+\mu^+\mu^-)/\mathcal{B}(B^+ \to K^+\mu^+\mu^-)$	14 % [638]	7 %	2.4 %	~ 10 %
Higgs penguins	$\mathcal{B}(B_s^0 \to \mu^+\mu^-)$	1.0×10^{-9} [595]	0.5×10^{-9}	0.19×10^{-9}	0.3×10^{-9}
	$\mathcal{B}(B^0 \to \mu^+\mu^-)/\mathcal{B}(B_s^0 \to \mu^+\mu^-)$	~ 220 %	~ 110 %	~ 40 %	~ 5 %
Unitarity triangle angles	$\gamma\,(B \to D^{(*)}K^{(*)})$	$\sim 7^\circ$ [621]	4°	1.1°	negligible
	$\gamma\,(B_s^0 \to D_s K)$	17° [639]	11°	2.4°	negligible
	$\beta\,(B^0 \to J/\psi\,K_{\text{S}}^0)$	1.7° [640]	0.8°	0.31°	negligible
Charm *CP* violation	A_Γ	3.4×10^{-4} [564]	2.2×10^{-4}	0.5×10^{-4}	–
	$\Delta\mathcal{A}_{CP}$	0.8×10^{-3} [641]	0.5×10^{-3}	0.12×10^{-3}	–

flavour-specific asymmetry in the B_s^0 system, $a_{\rm sl}^s$ in Table 17, probes CP violating in mixing. The "sl" subscript is used because the measurement uses semileptonic decays. The largest sources of systematic uncertainty in the current result are all determined with data-driven techniques, providing confidence that they can be controlled at better than 10^{-4}. Detailed further studies will be necessary to ensure that the measurement is sensitive to possible small deviations from the SM prediction, which is itself $\mathcal{O}(10^{-4})$.

Sensitivity to the emitted photon polarisation is encoded in the effective lifetime, $\tau^{\rm eff}$ of $B_s^0 \to \phi\gamma$ decays, together with the effective CP-violation parameter $2\beta_s^{\rm eff}$. Two of the most interesting of the full set of angular observables in $B^0 \to K^{*0}\mu^+\mu^-$ decays [642], are S_3, which is related to the transverse polarisation asymmetry [643], and the zero-crossing point (q_0^2) of the forward-backward asymmetry. As discussed above, isospin asymmetries, denoted A_I, are also of great interest.

In the charm sector, already discussed earlier, it is important to improve the precision of ΔA_{CP}, described above, and related measurements of direct CP violation. One of the key observables related to indirect CP violation is the difference in inverse effective lifetimes of $D^0 \to K^+K^-$ and $\bar{D}^0 \to K^+K^-$ decays, A_Γ.

The extrapolations in Table 17 assume the central values of the current measurements, or the SM where no measurement is available. While the sensitivities given include statistical uncertainties only, preliminary studies of systematic effects suggest that these will not affect the conclusions significantly, except in the most precise measurements, such as those of $a_{\rm sl}^s$, A_Γ and ΔA_{CP}. Branching fraction measurements of B_s^0 mesons require knowledge of the ratio of fragmentation fractions f_s/f_d for normalisation [644]. The uncertainty on this quantity is limited by knowledge of the branching fraction of $D_s^+ \to K^+K^-\pi^+$, and improved measurements of this quantity will be necessary to avoid a limiting uncertainty on, for example, $\mathcal{B}(B_s^0 \to \mu^+\mu^-)$. The systematic uncertainty in the current analysis of $2\beta_s$ from $B_s^0 \to J/\psi\,\phi$ is at the level of 0.01 rad, and is expected to be reduced further as larger data samples are accumulated.

6.4.4 Importance of LHC upgrades for flavour physics

Although other experiments will study flavour-physics observables in a similar timeframe to the LHCb upgrade, the sample sizes in most exclusive B and D final states will be far larger than those that will be collected elsewhere, for example at the upgraded e^+e^- B factories. The LHCb upgrade will have no serious competition in most of its studies of B_s^0 decays, b-baryon decays, charm mixing and CP violation. Similarly the yields in charmed-particle decays to final states consisting of only charged tracks cannot be matched by any other experiment.

The general-purpose experiments at the LHC are also well-suited to study rare decays with muons in the final states, e.g. $B_{(s)} \to \mu^+\mu^-$. As an example, Section B.1 presents a case study of this decay channel by using the graded Phase-1 and Phase-2 CMS detector. The expected yields, shown in Fig. 80, would result in an expected precision on the ratio of branching fractions between B^0 and B_s^0 decays with two muons in the final state at the 20% level, about half of the expectation for the LHCb upgrade.

After the LHCb upgrade era, the only road to improve beyond the sensitivity expectations listed in Table 17 will be a new specialized experiment (XFX) capable of exploiting the full luminosity of the HL-LHC for flavour physics, yielding samples two orders of magnitude above the LHCb upgrade (see Section 6.8).

In conclusion, the study of deviations from the SM in quark flavour physics provides key information about any extension of the SM. Hopefully, ATLAS and CMS will detect new particles, but the couplings of the theory and, in particular, its flavour structure, cannot be determined only using high-$p_{\rm T}$ data. Therefore, the LHCb upgrade and the possibility to perform studies in flavour physics in Phase 2 of the LHC, both with the existing general purpose detectors and new dedicated detectors, will play a vital role in any of these new physics scenarios, including the possibility of covering phase space regions which *a priori* cannot be exploited by high energy searches.

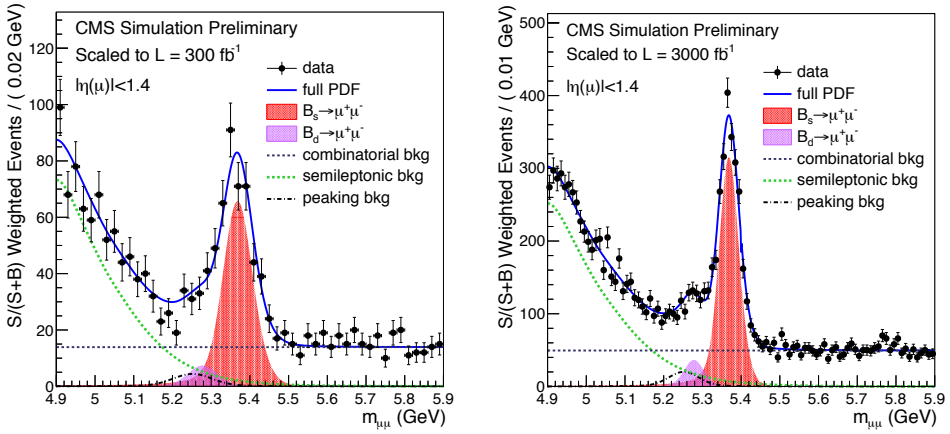

Fig. 80: Projections of the mass fits of muon pairs expected in 300 fb^{-1} (left) and 3000 fb^{-1} (right) of integrated luminosity, respectively assuming the expected performances of Phase-1 and Phase-2 CMS detector. Left plot is for barrel plus endcaps, while right plot is for barrel only.

6.5 B Physics at e^+e^- colliders

The primary scientific goal of the Belle-II experiment will be to perform detailed and comprehensive studies of flavour observables in B, and D mesons and τ lepton decays, to detect a signal of New Physics (NP). The detector will be installed at the interaction point of the electron and positron beams at the SuperKEKB collider, under commissioning at the moment of writing this report. The beam centre-of-mass energies are around the Υ resonances. Most of the data will be collected at the $\Upsilon(4S)$ resonance, which is just above threshold for B-meson pair production, so that exactly two mesons of opposite flavour are produced. SuperKEKB has a design instantaneous luminosity of $8 \times 10^{35}\text{cm}^{-2}\text{s}^{-1}$, about 40 times larger than the luminosity of its predecessor KEKB. Data taking for physics analyses is expected to begin in late 2017 and the total data sample of 5×10^{10} b, c and τ pairs is anticipated to be analyzed by the end of the experiment. The beam energies are asymmetric to provide a boost to the centre-of-mass system and allow time-dependent CP violation measurements. To maximize luminosity, the boost is slightly less than that at KEKB, which improves the hermeticity of the detector. The impact of smaller boost on time dependent CP measurements is compensated by an improved vertex detector.

6.5.1 SuperKEKB and Belle II unique capabilities

Several key characteristics make SuperKEKB and Belle II a unique facility to perform a systematic exploitation of the flavour physics discovery potential with B, D and τ decays. $B^0\bar{B}^0$ pairs in $\Upsilon(4S)$ decays are produced in a quantum correlated 1^{--} state, with no additional particles in the final state. Therefore, detection of the decay products of one B allows the flavour of the other B to be tagged and time dependent CP violation measurements to be performed. The clean sample of B pairs produced, together with the low background environment, allow the reconstruction of final states with multiple photons from the decays of π^0 and higher mass resonances. Among neutrals also the K_L^0 hadron can be detected by its interaction in the electromagnetic calorimeter and in a dedicated muon and K_L^0 detector. The e^+e^- environment permits precise luminosity measurement with Bhabha scattering, to be used for absolute branching ratio measurements. Thanks to the fact that the initial state is known, missing mass and inclusive analyses are possible. In particular, full event reconstruction, extensively used and refined at the B-factory experiments BaBar and Belle, will be an extremely powerful tool to observe and study rare decays with neutrinos in the final state or fully inclusive analyses with minimal model dependence. Finally, in addition to producing large samples of B and D decays, an e^+e^- machine produces large

samples of τ leptons allowing for measurements of rare τ decays and searches for lepton flavour and lepton number violating τ decays in a very low background environment.

6.5.2 NP-sensitivity at Belle II

Belle II will have unprecedented sensitivity to the presence of NP effects, being capable to cover a broad set of measurements in $B^{0(\pm)}$ and $B_s^{(*)}$ meson decays, charm physics, τ lepton physics, spectroscopy, and electroweak measurements. A large number of planned measurements will over-constrain the SM as well as its extensions and will shed light on the nature of NP. In the following, expectations on the reachable accuracy on several golden modes are shown. Most of those expectations are based on extrapolation of Belle results, estimating improvements on reducible systematic uncertainties that can scale with the luminosity. There is an on-going initiative among theorists and experimentalists to build the Belle II Physics Program, select golden observables and understand in detail the physics reach of the experiment [18].

6.5.2.1 CKM matrix elements and UT measurements

Belle II can improve on all the measurements of the Unitarity Triangle (UT) angles, α, β, γ to a precision of about 1°, 0.3° and 1.5°, respectively. While the impact of theory uncertainties on the determinations of β and γ will be negligible, the measurement of α will be theory limited and achieving high precision requires a set of measurements to determine strong phases. Also the measurement of γ will be performed using a range of methods using $B \to D^{(*)}K^{(*)}$ decays. The angle γ and $|V_{ub}|$ determinations, being driven by tree-level processes where NP is not expected, can play the particular role of setting the SM baseline to detect discrepancies in UT fits due to NP processes. Analyses of the full dataset of BaBar and Belle for determination of $|V_{ub}|$ from exclusive and inclusive decays show a tension that must resolved for precision tests of the SM. To a lesser extent a similar puzzle also afflicts the $|V_{cb}|$ determination. The Belle II physics program on semileptonic B decays includes systematic measurements of rates and form factors of many $b \to cl\nu$ and $b \to ul\nu$ exclusive modes and of inclusive analyses. Thanks to the expected improvements on theory and on reducible experimental uncertainties, the total uncertainty on the $|V_{ub}|$ determination from exclusive $B \to \pi\ell\nu$ can be reduced to the 2% level, and on the determination from inclusive $B \to X_u\ell\nu$ to the 3% level.

6.5.2.2 Leptonic B decays

The leptonic B decay $B \to \tau\nu$, resulting in the SM from a W-exchange diagram with an expected branching fraction of $(0.74^{+0.09}_{-0.07}) \times 10^{-4}$ [610], is sensitive to models that predict the existence of a charged Higgs (H^+). The effect of a H^+ on the partial leptonic decay width of B mesons is given by $\Gamma(B^+ \to \tau^+\nu) = \Gamma_{\rm SM}(B^+ \to \tau^+\nu)[1 - (m_B^2/m_H^2)\tan^2\beta]^2$, where $\tan\beta$ denotes the ratio of the vacuum expectation values of the two Higgs fields. The final state contains multiple neutrinos and is measurable only in an e^+e^- experiment. Experimentally, the leptonic branching fraction measurement consists of reconstruction of the accompanying B meson in the event, called the tagging B meson ($B_{\rm tag}$). The $B_{\rm tag}$ can be fully reconstructed in a number of hadronic decays or partially reconstructed in semileptonic decays. The remaining particles in the event are assigned to the signal B meson ($B_{\rm sig}$); if they are consistent with a possible τ decay, the undetected part of the event consists of one or more neutrinos from (semi-)leptonic decays. The signature of such event is thus a little or no residual energy detected in the EM calorimeter, after removing the contributions from the particles used in the reconstruction of $B_{\rm tag}$ and the τ from $B_{\rm sig} \to \tau\nu$. The current average branching fraction from Belle [645, 646] and BaBar [647,648] is $(1.14 \pm 0.22) \times 10^{-4}$, slightly higher than the SM expectation. Belle II should reduce this uncertainty to around 3%. The related channel $B \to \mu\nu$ will be measured to about 6% precision and can be used to constrain lepton flavour universality.

[18] https://belle2.cc.kek.jp/ twiki/bin/view/Public/B2TIP

6.5.2.3 *Semileptonic decays with tau leptons*

Semileptonic B decays with an electron or a muon in the final state were used at present B-factories to determine the CKM parameters$|V_{ub}|$ and $|V_{cb}|$. The τ lepton in the final state makes the process also very sensitive to physics beyond the standard model (the large τ mass, for example, allowing for coupling to a charged Higgs). Analysis of the full data set of BaBar and Belle measured an excess with respect to SM expectation of more than 3σ. The statistics that will be accumulated with Belle II will permit an early confirmation of the effect and an extensive study of $b \to q\tau\nu$ decays to determine the details of NP contributions.

6.5.2.4 *Electroweak and radiative penguins*

The clean environment at SuperKEKB will allow an exhaustive study of electroweak penguin $b \to s$ decays in all the lepton species final states (e, μ ,τ and ν pairs), performing both a sum-of-exclusive-states analysis and a fully inclusive approach. Among those the $B \to K^{(*)}\nu\bar{\nu}$ decay is theoretically very clean, and Belle II will be able to reach the level expected within the SM. Many interesting measurements in $b \to s\gamma$ and $b \to s\ell^+\ell^-$ will be possible exploiting the unique capability of full event reconstruction: exclusive and inclusive (with respect to the X_s hadronic system in the final state) analyses for the measurement of rates, CP asymmetries, isospin asymmetries, angular distributions, triple product correlations. Inclusive measurements will be possible only at Belle II, while in exclusive analyses Belle II can complement measurements of muon modes at LHCb, by precise measurements of electron final states, and search for the as-yet-unseen tau final state.

6.5.2.5 B_s *physics at* $\Upsilon(5S)$

Belle II is expected to collect data of order of 5 ab^{-1} at the $\Upsilon(5S)$ resonance. While the largest data sample of B_s will be studied at LHCb, there are key NP sensitive modes that can be observed only with Belle II. These are $B_s \to \gamma\gamma$, thanks to the clean e^+e^- environment and the excellent electromagnetic calorimeter, and $B_s \to \tau\tau$, possible only with a full reconstruction of the event. In addition, the analyses of decay final states not covered at LHC will be performed.

6.5.2.6 *Direct searches for NP*

Direct searches of new particles at or below the GeV scale are possible at Belle II. Theory models predict a rich sector of particles that were hidden because of their small couplings with ordinary matter, that includes Weakly (and non-Weakly) Interacting Massive Particles, dark matter candidates, dark photons and dark Higgs. Those candidates can be searched studying for example the decays of $\Upsilon(3S) \to \pi^+\pi^- invisible$, or Υ or B reactions that include lepton pairs.

6.5.3 Comparison with and LHC and LHCb

Table 18 summarizes the expected sensitivities of selected flavour observables at early (5 ab^{-1}) and nominal full dataset (50 ab^{-1}). The physics goals are complementary to the ones at LHC, since if, hopefully, NP is observed at LHC, precision measurements will reveal the structure the flavour structure of the NP. In the unfortunate scenario of no evidence of NP, indirect measurements will provide a unique tool to detect NP physics beyond the TeV scale. Belle II and LHCb share the same role and objective described above, but they will be complementary. LHCb will collect the largest data sample of both B_s and B mesons and clearly dominate in all-charged final states. Belle II, instead, will dominate measurements of final states with missing energy and neutrals, and τ lepton physics.

Table 18: Expected errors on several selected flavour observables with an integrated luminosity of 5 ab^{-1} and 50 ab^{-1} of Belle II data. The current results from Belle, or from BaBar where relevant (denoted with a †) are also given. Items marked with a ‡ are estimates based on similar measurements.

	Observables	Belle	Belle II	
		(2014)	5 ab^{-1}	50 ab^{-1}
UT angles	$\sin 2\beta$	$0.667 \pm 0.023 \pm 0.012$ [649]	0.012	0.008
	α [°]	85 ± 4 (Belle+BaBar) [610]	2	1
	γ [°]	68 ± 14 [650]	6	1.5
Gluon. peng.	$S(B \to \phi K^0)$	$0.90^{+0.09}_{-0.19}$ [651]	0.053	0.018
	$S(B \to \eta' K^0)$	$0.68 \pm 0.07 \pm 0.03$ [652]	0.028	0.011
	$S(B \to K^0_S K^0_S K^0_S)$	$0.30 \pm 0.32 \pm 0.08$ [653]	0.100	0.033
	$\mathcal{A}(B \to K^0 \pi^0)$	$-0.05 \pm 0.14 \pm 0.05$ [654]	0.07	0.04
UT sides	$\lvert V_{cb}\rvert$ incl.	$41.6 \cdot 10^{-3}(1 \pm 1.8\%)$ [655]	1.2%	
	$\lvert V_{cb}\rvert$ excl.	$37.5 \cdot 10^{-3}(1 \pm 4.0\%)$ [656]	1.8%	1.4%
	$\lvert V_{ub}\rvert$ incl.	$4.47 \cdot 10^{-3}(1 \pm 6.5\%)$ [657]	3.4%	3.0%
	$\lvert V_{ub}\rvert$ excl. (had. tag.)	$3.52 \cdot 10^{-3}(1 \pm 9.5\%)$ [658]	4.4%	2.3%
Missing E	$\mathcal{B}(B \to \tau\nu)$ [10^{-6}]	$96(1 \pm 27\%)$ [646]	10%	5%
	$\mathcal{B}(B \to \mu\nu)$ [10^{-6}]	< 1.7 [659]	20%	7%
	$R(B \to D\tau\nu)$	$0.440(1 \pm 16.5\%)$ [593]†	5.2%	3.4%
	$R(B \to D^*\tau\nu)^\dagger$	$0.332(1 \pm 9.0\%)$ [593]†	2.9%	2.1%
	$\mathcal{B}(B \to K^{*+}\nu\overline{\nu})$ [10^{-6}]	< 40 [660]	< 15	20%
	$\mathcal{B}(B \to K^{+}\nu\overline{\nu})$ [10^{-6}]	< 55 [660]	< 21	30%
Rad. & EW	$\mathcal{B}(B \to X_s\gamma)$	$3.45 \cdot 10^{-4}(1 \pm 12.4\%)$	7%	6%
	$A_{CP}(B \to X_{s,d}\gamma)$ [10^{-2}]	$2.2 \pm 4.0 \pm 0.8$ [661]	1	0.5
	$S(B \to K^0_S \pi^0 \gamma)$	$-0.10 \pm 0.31 \pm 0.07$ [662]	0.11	0.035
	$S(B \to \rho\gamma)$	$-0.83 \pm 0.65 \pm 0.18$ [663]	0.23	0.07
	C_7/C_9 $(B \to X_s\ell\ell)$	∼20% [664]	10%	5%
	$\mathcal{B}(B_s \to \gamma\gamma)$ [10^{-6}]	< 8.7 [665]	0.3	–
	$\mathcal{B}(B_s \to \tau\tau)$ [10^{-3}]	–	< 2 [666]‡	–

6.6 Lepton Flavour Violation

6.6.1 Introduction

In the Standard Model hadronic flavour transitions arise from the misalignment between the kinetic and the Yukawa terms in the Lagrangian, which give rise to the unitary CKM matrix whose elements represent how likely a quark from a specific family is expected to turn into a different quark of a possibly different family.

In the lepton sector, on the other hand, since SM neutrinos are massless, it is possible to rotate independently the fields in the kinetic and in the Yukawa part of the Lagrangian without having to introduce a CKM-like matrix. As a consequence, in this picture, transitions between charged and neutral leptons preserve flavour, as is observed in Nature.

Flavour transitions between neutral leptons have nevertheless been observed in the phenomenon of neutrino oscillations [81] which imply the non conservation of lepton flavour number. It is natural to assume that lepton flavour is not conserved also in transitions involving charged leptons, even though the SM contribution due to neutrino mixing is negligible. As can be seen from Fig. 81, to contribute to the $\mu \to e\gamma$ amplitude the muon neutrino has to oscillate into an electron neutrino within a W's lifetime, and

Table 19: Expected sensitivities of key observables at Belle II. Continuation of Table 18.

	Observables	Belle	Belle II	
		(2014)	5 ab^{-1}	50 ab^{-1}
Charm Rare	$\mathcal{B}(D_s \to \mu\nu)$	$5.31 \cdot 10^{-3}(1 \pm 6.5\%)$ [667]	2.9%	0.9%
	$\mathcal{B}(D_s \to \tau\nu)$	$5.70 \cdot 10^{-3}(1 \pm 6.5\%)$ [667]	3.5%	3.6%
	$\mathcal{B}(D^0 \to \gamma\gamma)$ [10^{-6}]	< 1.5 [668]	30%	25%
Charm CP	$A_{CP}(D^0 \to K^+K^-)$ [10^{-2}]	$-0.32 \pm 0.21 \pm 0.09$ [669]	0.11	0.06
	$A_{CP}(D^0 \to \pi^0\pi^0)$ [10^{-2}]	$-0.03 \pm 0.64 \pm 0.10$ [670]	0.29	0.09
	$A_{CP}(D^0 \to K^0_S\pi^0)$ [10^{-2}]	$-0.21 \pm 0.16 \pm 0.09$ [670]	0.08	0.03
Charm Mix.	$x(D^0 \to K^0_S\pi^+\pi^-)$ [10^{-2}]	$0.56 \pm 0.19 \pm {}^{0.07}_{0.13}$ [671]	0.14	0.11
	$y(D^0 \to K^0_S\pi^+\pi^-)$ [10^{-2}]	$0.30 \pm 0.15 \pm {}^{0.05}_{0.08}$ [671]	0.08	0.05
	$\lvert q/p\rvert(D^0 \to K^0_S\pi^+\pi^-)$	$0.90 \pm {}^{0.16}_{0.15} \pm {}^{0.08}_{0.06}$ [671]	0.10	0.07
	$\phi(D^0 \to K^0_S\pi^+\pi^-)$ [°]	$-6 \pm 11 \pm {}^{4}_{5}$ [671]	6	4
Tau	$\tau \to \mu\gamma$ [10^{-9}]	< 45 [672]	< 14.7	< 4.7
	$\tau \to e\gamma$ [10^{-9}]	< 120 [672]	< 39	< 12
	$\tau \to \mu\mu\mu$ [10^{-9}]	< 21.0 [673]	< 3.0	< 0.3

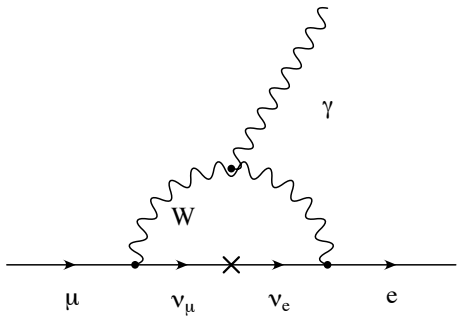

Fig. 81: Feynman diagram of the $\mu \to e\gamma$ decay induced by neutrino oscillations. Its amplitude is very extremely tiny, since neutrinos have to oscillate within a W boson's lifetime.

this results in a probability of the process at the 10^{-52} level [674].

Theories beyond the Standard Model predict additional particles and interactions that can enhance such processes up to a measurable level (for a recent review of both theory and experiment see [675]).

Charged lepton flavour violation (CLFV) searches are of particular interest because of the possibility to carry out clean measurements which are at the same time free of theoretical background. In the case of observation they would give a clear piece of evidence of physics beyond the standard model, but even in case of non observation they pose strong limits on the development of new theories.

On the other hand such searches are difficult to be carried out at general-purpose machines and detectors, so dedicated detectors, and even dedicated accelerators or storage rings, have to be designed.

As we will see in the following, the search for lepton flavour violation is expected to make a significant step forward in the next few years. An international program of CLFV searches exists, with experiments recently completed, currently running, and soon to be constructed in the United States, Japan, and Europe. These include the completion of the MEG experiment at PSI, its upgrade MEG-II, the proposed *Mu3e* search at PSI, new searches of muon to electron conversion (Mu2e at Fermilab, COMET at J-PARC), studies of τ decay at SuperKEKB, and over the longer term, experiments exploiting

megawatt proton sources such as PIP-2.

6.6.2 Theory and Phenomenology

Independently of the specific theory and model, CLFV transitions are related to new lepton-lepton couplings and effective operators that give rise to processes like the ones depicted in Fig. 82. These processes

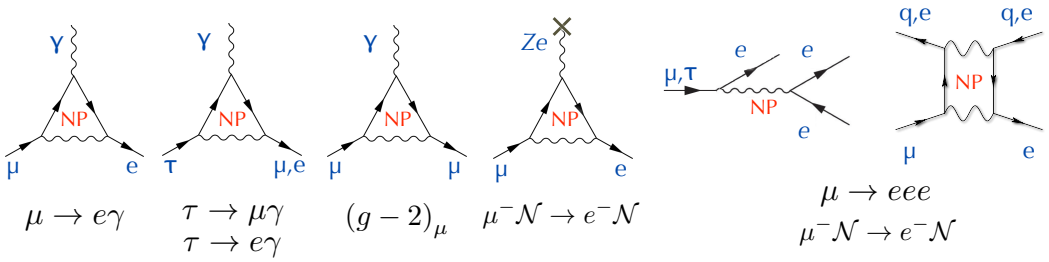

Fig. 82: Schematic representation of vertices and interactions of some of CLFV processes in which new physics (NP) contribution could be measurable.

can be divided in dipole amplitudes, described by dimension-5 operators, and four-fermion dimension-6 operators (compare the first four diagrams in Fig. 82 and the last two). It is customary to parametrize the interplay between the two effects by means of two parameters [676]: Λ, which sets the scale of the four fermion amplitude, and κ, which governs the ratio of the four fermion amplitude to the dipole amplitude.

For $\kappa \ll 1 (\gg 1)$ the dipole-type (four-fermion) operator dominates CLFV phenomena. Fig. 83 summarizes the power of different searches to explore this parameter space. A scale $\Lambda < 1000$ TeV is already excluded by present limits, posing serious constraints on Standard Model extensions, supersymmetry especially. Nonetheless Λ is only an effective scale and is not immediately comparable to the mass M of new particles accessible by direct search. For the magnetic moment type of interaction, M is related to Λ via a loop factor and the new BSM coupling g_{bsm} as follows: $1/\Lambda^2 \sim g^2_{bsm} e^2/(16\pi^2 M^2)$. For the four fermion operators, Λ is more directly related to the mass of new particles, $1/\Lambda^2 \sim g^2_{bsm}/M^2$. In both cases, the real mass M tested by CLFV processes is significantly above that accessible at the LHC.

CLFV importance is therefore independent from what the LHC can find in the next several years when the direct searches will keep testing the TeV scale.

On the other hand, the interpretation of a direct observation of new physics at LHC will have to take into account precise measurements (or constraints) from MEG and Mu2e: the comparison between these determinations will help pin down the underlying theory.

An example is shown for the Scalar Leptoquark searches. In Fig. 84a, the reach for the new coupling λ, as defined from eq. 14 of [677], is reported for a range of Scalar Leptoquark masses for both MEG upgrade and conversion experiments. The compilation is extracted from the Mu2e TDR. It is clear that while not excluding the Leptoquark existence at few TeV masses, the CLFV coverage extends up to masses of O(100 TeV).

Another example is shown for the Left-Right symmetric models that is a BSM theory useful to restore parity at short-distances. A recent study [678] predicts the CLFV rates in this environment assuming a new mass breaking scale at around 5 TeV. The correlation between the BR for the MEG upgrade and $R_{\mu e}$ for the conversion experiments are shown in Fig. 84b. It is clear that the two experiments can cover the expectations for the full phase space of this theory. The ratio of the two measurements will help constrain it.

It is clear how CLFV searches complement the searches of new particles, and, among them, muon measurements have the best sensitivity over the largest range of parameter space of many models of new physics. We summarize in Table 20 the present and near future status of muon-based experiments.

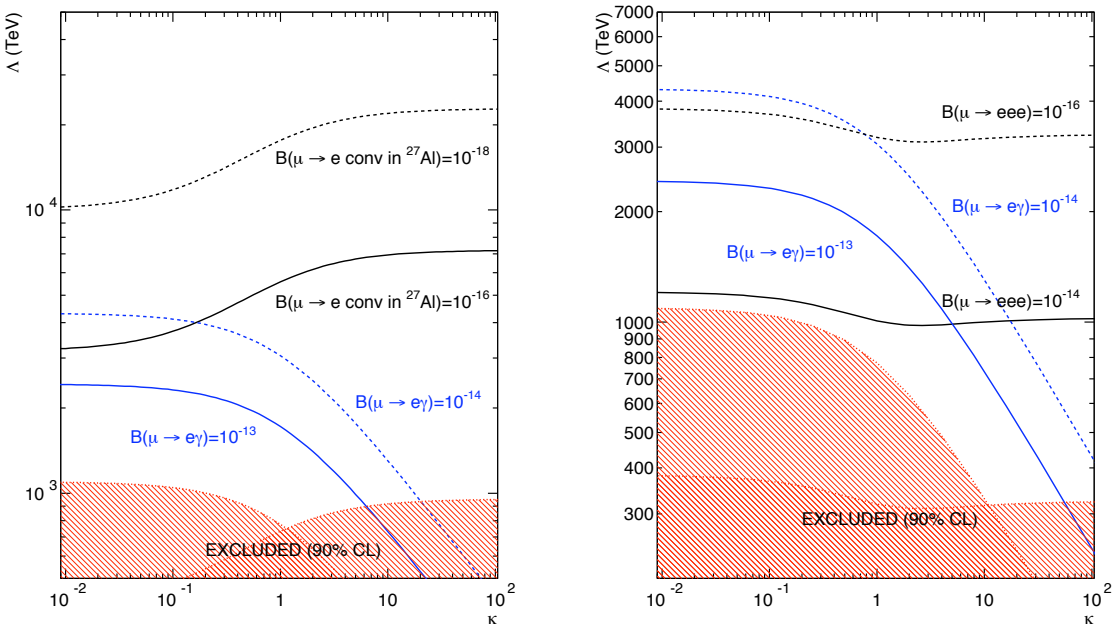

Fig. 83: Sensitivity of $\mu \to e\gamma$, $\mu \to e$ transition and $\mu \to 3e$ to the scale of new physics Λ as described in the text, as a function of the parameter κ that defines the proportion of dipole versus four-fermion amplitude. Note that $\mu \to e\gamma$ is sensitive mainly in the dipole dominating region, while $\mu \to e$ and $\mu \to 3e$ receive contributions also from the four-fermion interactions. The shaded areas are excluded by present limits. The left plot focuses on the relation between $\mu \to e\gamma$ and $\mu \to e$ conversion, the right one on the relation between $\mu \to e\gamma$ and $\mu \to eee$.

Table 20: Comparison of muon CLFV experiments.

Process	$\mu^+ \to e^+\gamma$	Muon Conversion	$\mu^+ \to e^+e^-e^+$
Kinematics	2-body decay monoenergetic e^+ and γ back-to-back	Quasi 2-body decay monoenergetic e^- single particle detected	3-body decay invariant mass constraint zero total momentum
Background	Accidental background	Decay in orbit beam-related π and $\bar{p}$ Cosmics	Radiative decay with internal conversion Accidental Background
Preferred beam	Continuous	Pulsed	Continuous
Best limit	5.7×10^{-13} MEG 2013 [679]	7×10^{-13} (Gold) SINDRUM II 2006 [680]	1×10^{-12} SINDRUM 1988 [681]
Planned experiments	MEG-II at PSI [682]	Mu2e at FERMILAB [683, 684] DeeMe [686] and COMET [687] at J-PARC	Mu3e at PSI [685]
Planned single event sensitivity	2×10^{-14}	Mu2e: 5.6×10^{-17} DeeMe: 1×10^{-14} COMET: 4×10^{-17}	7×10^{-17}

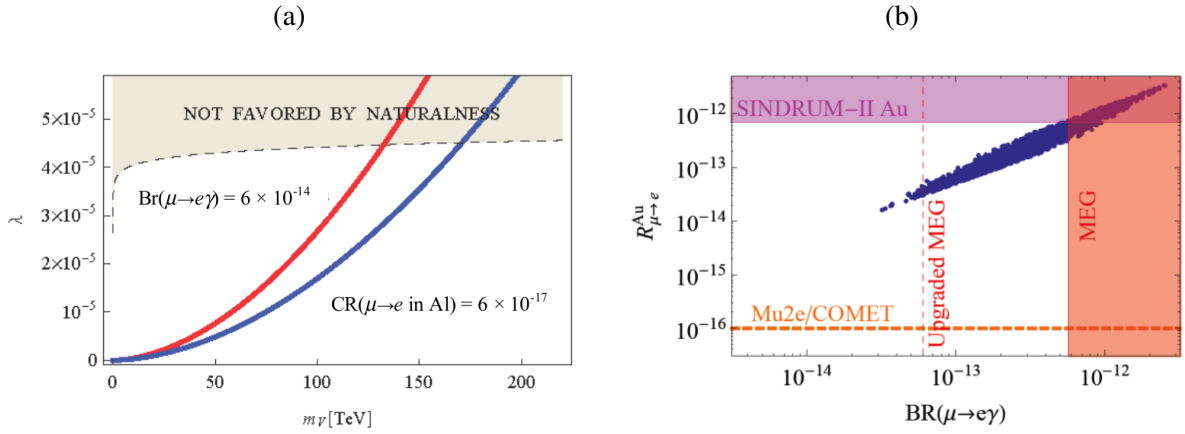

Fig. 84: (a) Reach achievable in the Scalar Leptoquark search for the MEG upgrade and Mu2e as a function of the coupling λ and the Scalar Leptoquark mass. (b) Expected BR and $R_{\mu e}$ for Left-Right symmetric models for the MEG upgrade and the muon conversion experiments.

6.6.3 Search for $\mu \to e\gamma$

The current limit on $\mu \to e\gamma$ comes from the MEG experiment at PSI [688], whose analysis of the 2009-2011 data resulted in $BR(\mu \to e\gamma) < 5.7 \times 10^{-13}$ at 90% confidence level [679]. The MEG experiment has finished its data taking and the collaboration is finalizing the analysis of the data taken in the years 2012-2013, doubling the dataset, with the result expected at the beginning of 2015.

The sensitivity to the $\mu \to e\gamma$ decay is given by the capability of the experimental apparatus to distinguish two monochromatic, time coincident, back-to-back particles from the background composed of (1) muon radiative decays or (2) accidental coincidences between a high-energy photon and a positron from a normal muon decay. The regime in which the two kinds of background are dominant is different: radiative decays emit four time coincident particles: $e\gamma\nu\bar{\nu}$ and mimic the two body decay at the very end of the kinematic edge where the two neutrinos share almost zero energy. It can be shown [689] that the number of radiative decays that emit a photon and a positron within 1% of the two-body decay energy is of the order of 10^{-15} and therefore this background can be neglected for MEG whose sensitivity is at the 10^{-13} level. In Fig. 85, taken from [689], we see the fraction of radiative decays mimicking a $\mu \to e\gamma$ transition as a function of the experimental resolutions on positron and photon energies (δx and δy respectively). The number of accidental coincidences is on the other hand dominant, scales with the square of the muon rate R_μ and it is proportional to the energy, time and relative direction resolutions of the experiment [689]:

$$N_{\rm acc} \propto R_\mu^2 \times {\rm Totaltime} \times \Delta t_{e\gamma} \times \Delta E_e \times \Delta E_\gamma^2 \times \Delta \Phi_{e\gamma}^2 \tag{46}$$

It is for this reason that the optimum muon beam for a $\mu \to e\gamma$ decay search is a continuous beam, which minimizes, for the same number of delivered muons, the number of accidental coincidences.

The sensitivity of MEG is limited by its resolutions on the kinematic variables of the two particles. For this reason an upgrade is under way, called MEG-II [682], in which the positron tracker will be completely replaced by a single-volume, homogeneous drift chamber coupled to a new highly-segmented timing counter. The liquid xenon photon detector will be refurbished with new photosensors to improve its energy and position reconstruction. In this way the expected improvement in detector resolutions (see Table 21 for a comparison of the MEG and MEG-II resolutions) allows for a larger muon stopping rate. The accidental background will still be the dominant one since the expected sensitivity is at the level of 5×10^{-14}.

The MEG-II detector is presently under construction and it is expected to have its first engineering

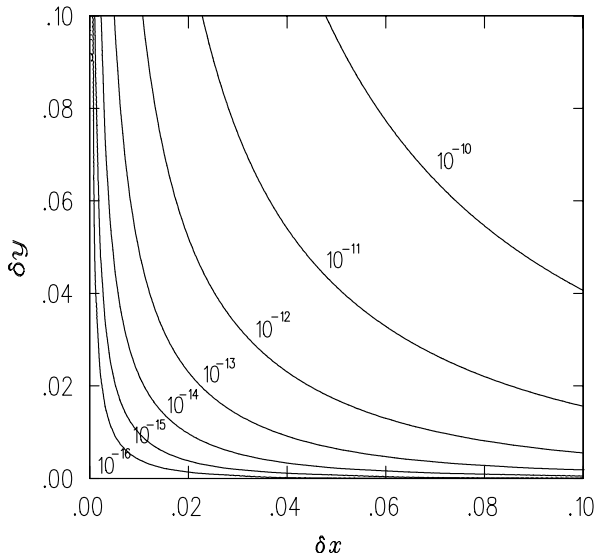

Fig. 85: Branching ratio of the physics background from the muon radiative decay as a function of the relative e^+ (δx) and photon (δy) energy resolutions. After [689].

Table 21: Resolution and efficiencies of the MEG experiment vs. MEG-II

PDF parameters	Present MEG	Expected MEG-II
Positron Energy Resolution (keV)	380	110
Positron angular resolution (θ, ϕ) (mrad)	9,11	5,5
Positron position resolution on target(y, z) (mm)	2.0/1.0	1.2/0.7
Photon energy resolution (%, deep events)	1.6	1.0
Photon position resolution (mm)	4	2
Positron-Photon relative timing (ps)	120	80
Efficiency (%)		
trigger	≈ 99	≈ 99
γ reconstruction	60	60
e^+ reconstruction	40	95
event selection	80	85

run in 2015 with data taking in the years 2016-2018.

6.6.3.1 Future developments

To reach sensitivities below the 10^{-14} level new approaches must be studied. Some strong points of the previous experiments are thought to be mandatory (*e.g.* the need for a surface or sub-surface muon beam[19], which permits a sub-mm stopping target to minimize multiple scattering) but there are new ideas that could help to overcome the present limitations induced by the accidental background to reach the ultimate limit posed by the radiative decay.

As apparent from Equation 46 an increase of muon flux together with an improvement in experi-

[19] Surface muon beams are muons decaying from pions at rest on the surface of the production target, having a well defined momentum of ≈ 29 MeV/c. Sub-surface muons are muons produced in the same way but in a skin of finite thickness just below the target surface.

mental resolutions is mandatory:

- To improve the energy resolution on the photon leg at the percent level one could follow the approach to convert the photon and measure the resulting e^+e^- pair. The advantage of better resolutions on the charged particles is partly spoiled by the addition of the converting material that increases multiple scattering;
- The usage of conversion pairs allows to track the photon back to the target, permitting a vertex constraint that is absent in present and planned experiments. A pointing calorimeter with a degree resolution could play the same role;
- An active target pinpointing the parent muon decay position could also help in reducing the number of accidentals, without the need to improve the energy resolutions;
- Spreading the muon beam decay points to several targets, and identifying the starting target of both positron and photon, reduces the accidental rate linearly with the number of targets, without the need of improving experimental resolutions.

These are just a few of the ideas discussed within the working group that could be the starting point for a baseline design of an "ultimate" $\mu \to e\gamma$ decay search.

A factual application of the aforementioned ideas is carried out in the so-called CIRCE conceptual design [690] in which a significant increase in $\mu \to e\gamma$ sensitivity can be obtained by turning the calorimetric photon energy measurement into a momentum measurement, through the conversion of the photon into an electron pair.

In this approach, a low mass cylindrical drift chamber occupying the volume of a large volume solenoid magnet (*e.g.* the KLOE coil, 2.5 m radius, 3.8 m length, with a field of 0.6 T) may provide more than 200 layers of tracking, utilizing small cells (of order 0.5 cm drift length) for a number of sense wires approaching 105. Beyond the radius corresponding to the full containment of the 53 MeV/c electron track (about 60 cm) the drift chamber volume is divided in several cylindrical shells, separated by thin converter foils and having a sufficient number of measuring layers to precisely reconstruct the electron pair momenta. Excellent photon mass resolution could be obtained, thanks also to the large number of kinematical constraints available.

It has been estimated [690] that relative improvements with respect to the latest MEG results of up to two orders of magnitude in sensitivity with a two orders of magnitude background reduction may be within reach with this novel approach.

An inner detector made of a few layers of HV-MAPS, similar to the one proposed by the Mu3e experiment, around the stopping target and layers of scintillating fibers placed next to the conversion foils may provide the necessary redundancy and enhance the signal to background ratio.

6.6.4 Search for $\mu \to eee$

The $\mu \to 3e$ decay is sensitive to new physics present both in the dipole term (with a tree-diagram contribution which is roughly a factor α with respect to the $\mu \to e\gamma$ term) and in the contact term through the virtual loop (see Fig. 82). The current experimental limit dates back to the SINDRUM experiment at PSI and is $BR(\mu^+ \to e^+e^-e^+) < 1 \times 10^{-12}$ [681].

The kinematic of this decay is peculiar since one has to search for three charged particles coming from a muon decay at rest, with the correct charges and lying on the same plane. The drawback is that positron and electron of such a low energy (30 MeV on average) suffer very much from multiple scattering. The possibility to track and constrain to a common vertex three charged particles is very effective in reducing the accidental background. Nevertheless the fraction of normal decays $\mu \to 3e\nu\bar{\nu}$ for which the energy of the two neutrinos is less than 1 MeV is $\approx 2 \times 10^{-17}$ [691] which sets an upper limit on the sensitivity achievable.

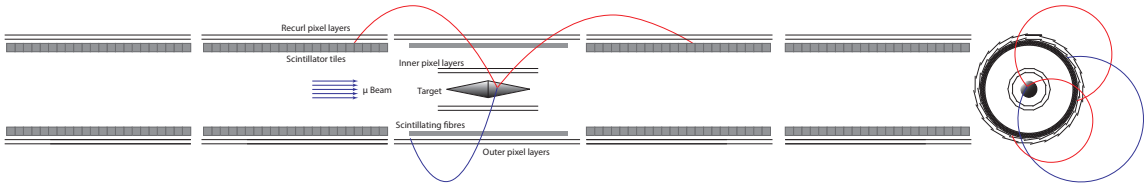

Fig. 86: Schematic view of the *mu3e* experiment detector geometry as it should appear in the third stage, *i.e.* with all tracking stations and tile timing counters in place. An initial stage is planned in which only the central portion of the detector will be operating to reach a sensitivity of 10^{-14}.

The Mu3e experiment [685] has been proposed at PSI to improve the present experimental bound by four orders of magnitude in a three-stage approach. At present, there is no involvement of INFN groups in the project. A beam of surface muons (29 MeV/c muons originating from pions decaying at rest, the same as the MEG experiment) is stopped in a hollow double-cone target made of thin aluminum (see Fig. 86). The experiment should be sensitive to positrons of transverse momentum > 12 MeV/c and to reduce multiple scattering a tracker based on 50 μm high-voltage monolithic active pixel sensors (HV-MAPS) is envisaged. A double set of timing counters, one based on 250 μm scintillating-fibers in the central part followed by a 0.5 cm thick plastic scintillator, are placed in the so-called recurling stations.

The experiment is thought to follow a three-stage approach: a first stage (called IA) making usage of the central portion of the detector to reach 10^{-14} followed by a second stage (called IB) down to 10^{-15} in which the recurling stations (*i.e.* the outer detectors) are added. A third stage (called phase II) to reach 10^{-16} sensitivity needs a new, higher intensity ($2 \times 10^9 \mu$/s) continuous muon beam which was originally planned at PSI but it is not clear now if it can be built. There are presently no other proposals for a competing $\mu \to 3e$ project.

6.6.5 Search for μ to e conversion

The measurement of the neutrinoless μ^- to e^- conversion rate, in presence of a nucleus, is defined relatively to the ordinary capture of the muon on the nucleus as follows:

$$R_{\mu e} = \frac{R(\mu^- + A(Z,N) \to e^- + A(Z,N))}{R(\mu^- + A(Z,N) \to \nu_\mu + A(Z-1,N)}. \quad (47)$$

The best limit on $R_{\mu e}$ is 7×10^{-13} as obtained by Sindrum-II [680] at PSI, where a negative muon beam of 55 MeV/c momentum and intensity of 1.2×10^7 μ^-/sec was stopped on a gold target.

The *conversion signal*, CE, consists of a monoenergetic electron close to the muon mass, once corrected for binding energy and nuclear recoil, that has to be separated by means of high momentum resolution from the spectrum of the electrons produced in the *muon decay in orbit* process, DIO. The stopped muons have a large chance of decaying when orbiting around the nucleus and their spectrum is substantially modified from the free decay by the presence of a large recoil tail that falls rapidly as the energy approaches the kinematical endpoint.

However, in Sindrum-II additional background sources were dominating. In particular, after rejection of cosmics, a prompt background coming from *radiative pion capture*, RPC, $\pi + N \to \gamma^* + N'$, was found to be the most resistant background. In this process, the electron positron pair, produced either by internal or external conversion, becomes a source of CE candidate when the e^- momentum falls in the right selection window.

These observations have driven the design strategy of the new generation of experiments for muon to electron conversion: Mu2e [683,684] at FNAL, USA and COMET [687] at JPARC, Japan. Their goal is achieving a single CE event sensitivity of $2-3\times10^{-17}$ (or BR limit of $6-7\times10^{-17}$ at 90% C.L.), which is four orders of magnitude better than the previous best limit.

There are four needed ingredients to do so:

1. *An high intensity muon beam*. The goal is to increase by at least four orders of magnitude to 10^{11}/sec the muon intensity on target from today's limit of 10^{7}/sec. This can be done at a dedicated machine by means of muon production on targets and curved solenoidal systems to allow for charge and momentum selection. The usage of solenoids allows to create a very selective muon transport line that increases intensity while reducing the associated needs for beam power (compare 1 MW at PSI for Sindrum-II and 8 kW for Mu2e and 56 kW for COMET-phase 2).
2. *The beam structure has to be pulsed* in order to reject the prompt background. The target has to be selected in a way that the muon lifetime, τ_μ, in the bound system is smaller than the bunch period. Both for Mu2e and COMET, the selected target is aluminum where τ_μ is 864 ns that matches well with the bunch period (1684 ns at FNAL, 1100 ns at JPARC). In both experiments, the plan is to wait for the *beam-flash* of particles travelling with the transported beam to disappear as well as waiting for the most relevant prompt backgrounds to decay. The data acquisition start is typically set at $\sim$ 700 ns after the bunch arrival time.
3. The out of time particles travelling with the beam have to be negligible. This is referred to as the *proton extinction requirement*. Calculation by full simulation showed that to suppress prompt backgrounds coming from beam electrons, muon and pion decays-in-flight and RPC requires a pulsed beam where the ratio of beam between pulses to the beam contained in a pulse is less than 10^{-10}.
4. *A redundant high-precision detector* has to analyze the capture products to separate CE and DIO spectra and reduce to negligible contribution the additional background sources. A very similar technique is used in both experiments, where a high precision low-mass straw tube tracker (with a core momentum resolution of $\approx$ 200 keV) is followed by a crystal based calorimeter for triggering and particle identification purposes.

6.6.5.1 Mu2e

The Mu2e experiment is shown in Fig. 87. An array of superconducting solenoids forms a graded magnetic system constituted by a Production Solenoid, PS, a Transport Solenoid, TS, and a Detector Solenoid, DS.

The PS contains the production target that intercepts an 8 GeV pulsed proton beam brought by means of a dedicated beam-line coming from the delivery ring. The gradient field in the PS works as a magnetic lens to focus low energy particles into the transport channel. The focused beam is comprised of muons, pions and a small number of protons and antiprotons. The S-shaped Transport Solenoid efficiently transfers low energy negatively charged particles to the end of the beam-line while allowing for a large fraction of the pions to decay to muons. A collimator in the middle section attenuates nearly all positively charged particles. The DS presents a graded field from 2 to 1 Tesla in the upstream region where the stopping target resides. This lens increases the acceptance for CE while helps rejecting beam-related backgrounds. A uniform magnetic field of 1 Tesla resides in the region of the tracker and calorimeter systems. The DS is covered externally by a Cosmic Ray Veto system.

When muons stop in the aluminum target, they are captured in an atomic excited state. They promptly fall to the ground state. 39% decay in orbit while 61% are captured on the nucleus. Low energy photons, neutrons and protons are emitted in the nuclear capture process and constitute an environmental background that produces a ionization dose and a neutron fluence on the detection systems as well as an

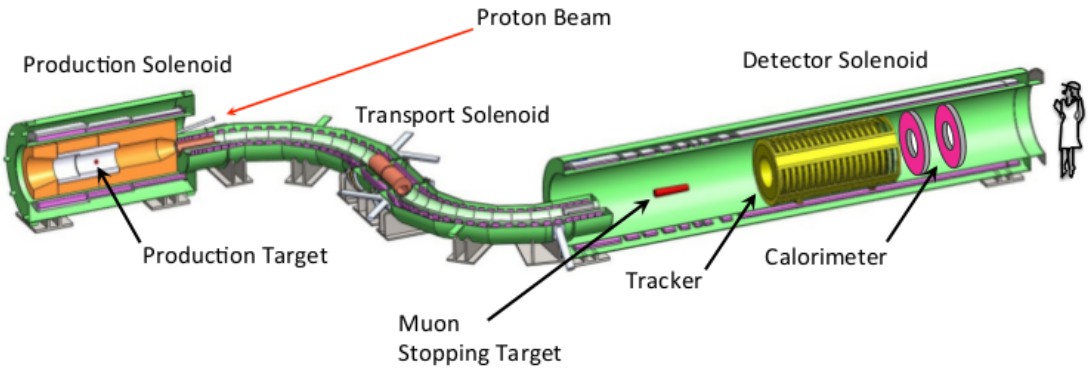

Fig. 87: Layout of the Mu2e experiment.

accidental occupancy for the reconstruction program. This background is fully simulated in overlap with the signals coming from the apparatus.

The tracking detector, made from low mass straw tubes, constitutes the high resolution spectrometer to separate DIO from CE events. After maximizing signal over background, selecting tracks with momentum between 103.75 and 105 MeV/c corresponds to a DIO contribution of 0.22 events and a CE S.E.S. of 2.6 $\times 10^{-17}$. The calorimeter system is composed of two BaF_2 disks and provides powerful Particle Identification, an independent trigger system and a seed for tracking in the complicated reconstruction environment.

At the moment of writing, the Mu2e experiment has successfully completed the CD-2 review for all systems and the CD-3 reviews for the superconducting cables, the civil construction and the Transport Solenoids. Completion of CD-3 will start the construction for the apparatus and for the solenoids. This is expected to happen in 2016. The schedule foresees a completion of the installation and a start of the data taking with beam in autumn 2020.

Apart from the measurement of the muon conversion to electron, there is also the possibility to measure the similar process with $\Delta L = 2$: $\mu^- A(Z,N) \rightarrow e^+ A(Z-2,N)$. This decay violates both the conservation of the total lepton number and the lepton flavour numbers, L_e and L_μ and is closely related to the neutrinoless double β-decay. Theoretical models find $R_{\mu e^+}$ from 10^{-12} to 10^{-14}. The best existing limit is 3.6×10^{-11} and has been obtained by the Sindrum II collaboration in the process $\mu^- + \mathrm{Ti} \rightarrow e^+ + \mathrm{Ca}$ [692].

6.6.5.2 Mu2e-II and future planning

For the long term future (after 2023), we note that the sensitivity reach for conversion experiments is not intrinsically limited. Their reach can be improved assuming to have higher beam intensity and to control the accidental activity coming from muon capture. In this context, only the option to improve by a factor of 10 the beam intensity [683] has been explored. This possibility has become more realistic after the P5 panel decision to support the development phase of a proton driver at FNAL [693]. This new accelerator, PIP-2, is no longer as flexible as the Project-X [694] but grants an increase by a factor of 10 of the muon beamline intensity using a 1 or 3 GeV proton beam on a production target while delivering the neutrino beam to LBNF. In this environment, a Mu2e-II experiment that reuses a large fraction of the Mu2e apparatus can provide a factor of 10 improved sensitivity.

Another relevant point is the dependence of the $R_{\mu e}$ rate on the stopping target, especially for high-Z nuclei, where the relative number of protons and neutrons plays a significant role since photons couple predominantly to protons while Z bosons couple to neutrons. In Fig. 88, the dependence of the

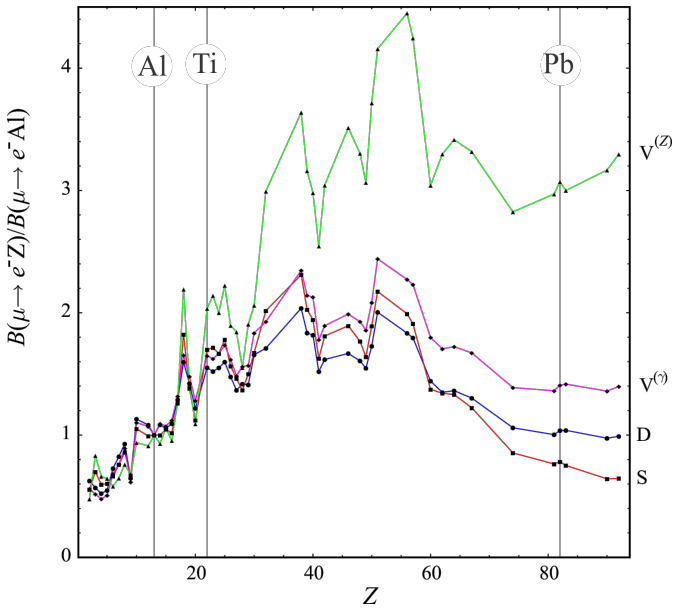

Fig. 88: Target dependence of $R_{\mu e}$ for different single operator dominance models.

$R_{\mu e}$ as a function of the target Z is reported for different possible theories [695]. Assuming to have an observation with the aluminum target a consistent program of running with different targets can allow to discriminate among models.

6.6.5.3 COMET phase-1 and phase-2

The COMET (COherent Muon to Electron Transition) experiment is planned at JPARC and, differently from Mu2e, follows a stage-based approach. The COMET solenoidal system has a C-shape geometry instead of the Mu2e S-shape design as shown in Fig. 89. The first C-section constitutes the muon selection and transport channel to the stopping target. The second C-section, *electron spectrometer*, not present in Mu2e, allows to transport the produced electrons from the target to the detection system while introducing a cut on their momentum ($p > 60$ MeV) that reduces the DIO rate and eliminates most of the protons produced in the nuclear capture. It also eliminates a good fraction of low energy events (neutrons and photons) coming from the target thus making the detection system relatively quiet from target noise.

The *electron spectrometer* constitutes the main difference from the Mu2e design and is obtained at the price of a longer length of the solenoidal system (+10 meters) and a much larger beam power (56 kW). The related background improvements are reduced by a shorter microbunch structure (1.1 μsec), which implies a smaller prompt beam rejection in the experiment. The detector concept is similar to Mu2e.

Although the full experiment has not been approved, a COMET phase-1 has already been funded. This staging consists on designing, constructing and running only $\sim$ one half of the first C-section in such a way that the number of muon/proton pulse will be identical to the final case. The intensity of the proton beam is reduced to 3.2 kW power and a beam of 6 $\times 10^9$ μ^-/sec reaches the aluminum stopping target. In 20 days of running (end of 2016) a sample of 10^{16} stopped muons will be collected to set a limit on the BR of 7×10^{-15}, i.e. one hundred times better than Sindrum-II. Two other interesting features for the physics search are:

– In phase-1, they can detect both positive and negative particles and look also for the charge changing reaction for neutrinoless muon conversion process: $\mu^- A(Z,N) \rightarrow e^+ A(Z-2,N)$. As stated above Mu2e can do that for the full statistical sample.

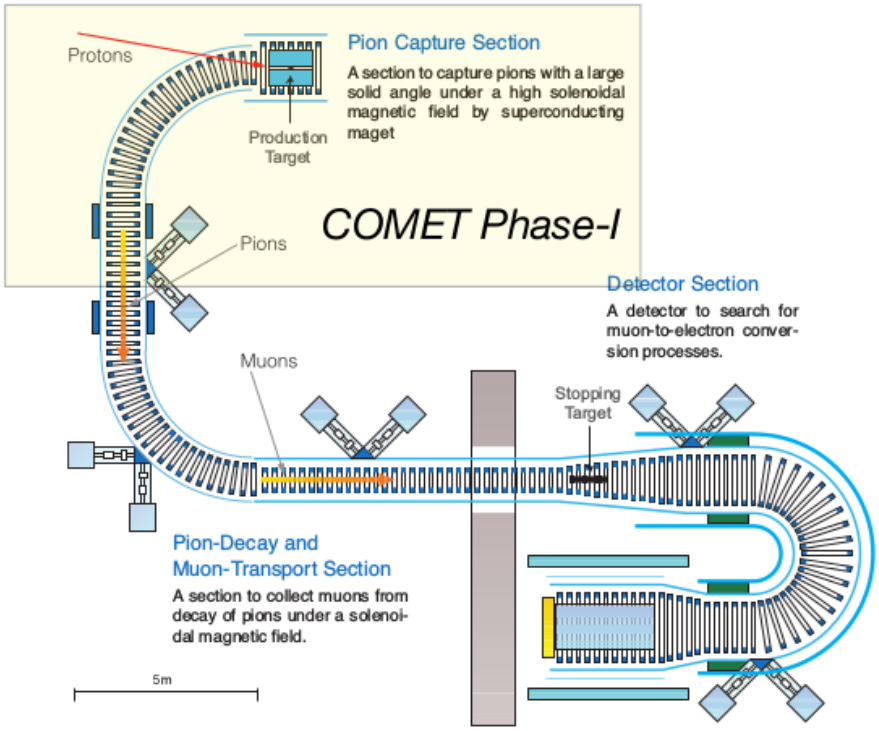

Fig. 89: COMET layouts: (left) Phase-1, (right) Phase-2.

– They can also search for $\mu^- e^- \to e^- e^-$, which is a process very similar to $\mu \to 3e$. The advantage is the clear two body kinematics. The disadvantage is the small probability of overlap between the e^- and μ^- wave functions. For comparison, in the case of conversion on nucleus the rate is proportional to Z^3. No experimental measurement exists on this process.

6.6.5.4 The DeeMe experiment

DeeMe [686] is a single-target experiment to search for $\mu \to e$ conversion in nuclei to be conducted at the H-line of J-PARC MLF facility, with a reduced sensitivity but a tighter time schedule when compared to both Mu2e and COMET.

Its main difference is the presence of a single silicon carbide (SiC) target where muons are produced and captured. When the 3 GeV pulsed proton beam hits the target, pions will be produced. Though negative pions stopping inside the target will be absorbed, pions in flight will decay into muons with a lifetime of approximately 26 ns, and some of the negative muons will stop in the target to form muonic atoms.

Electrons from possible $\mu \to e$ conversions may be emitted from muonic atoms formed at the target surface with small momentum loss.

The experiment will start physics runs in 2015 and its sensitivity is expected to be 2×10^{-14} in two years of data taking, therefore starting to bridge the four orders-of-magnitude gap between the Sindrum II result and the expected limits from Mu2e and COMET.

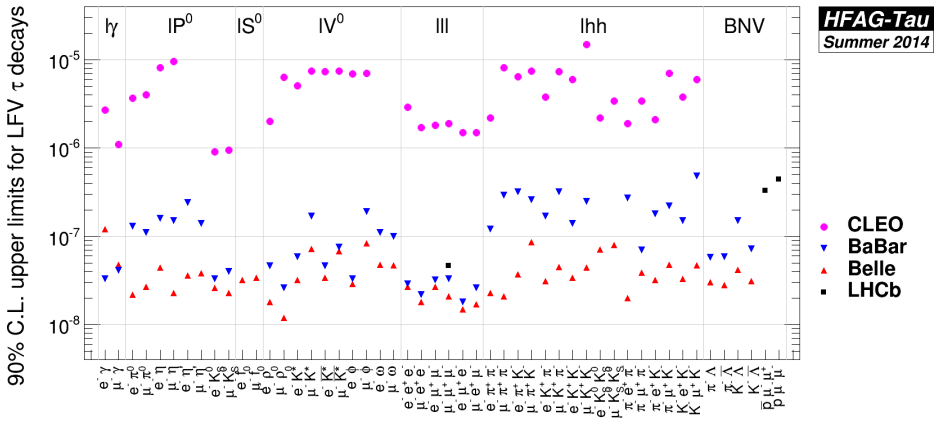

Fig. 90: Summary of the $B-$factories searches for LFV τ lepton decay modes.

6.6.6 LFV in the τ sector

6.6.6.1 Present status from B-factories

Searches for lepton-flavour violating tau decays are among the cleanest probes of new physics at past, present and future high luminosity flavour factories. Moreover the large τ mass implies many possible final states besides the natural $\tau \to e\gamma, \mu\gamma$ or $\tau \to 3e, 3\mu$. The branching ratio for LFV τ decays is generally predicted to be larger (usually by a power of m_τ/m_μ) compared to those of the muon. Conversely the number of produced taus and the experimental backgrounds partially spoils this advantage, with the result that the experimental reach in both τ and μ LFV decays probe comparable regions of the parameter space of new theories.

The present best experimental limits on LFV τ decays come from measurements at the $B-$factories Belle and BaBar and are reported in Fig. 90. These experiments and their successor Belle II can probe an entire range of decays. This is particularly interesting since different new physics scenarios predict very different patterns of τ LFV.

LFV tau decays are searched for by tagging one of the taus in the $e^+e^- \to \tau^+\tau^-$ event, dividing the event in two hemispheres and considering each hemisphere as a possible candidate for the LFV decay under consideration. Despite all cuts and kinematical constraints there remains generally a background which is irreducible, as, for instance, the initial state radiation $\tau^+\tau^-\gamma$ in the case of $\tau \to \mu\gamma$ searches.

The results presented in Fig. 90 come from a sample of $\approx 5 \times 10^8$ (BaBar) and $\approx 9 \times 10^8$ (Belle) $\tau\bar{\tau}$ pairs.

6.6.6.2 Future facilities

With a data sample of 50 ab^{-1} accumulated at SuperKEKB, the number of $\tau^+\tau^-$ events will increase to $\approx 5 \times 10^{10}$. Limits on background-free decay modes such as $\tau \to \mu\mu\mu$ should reach the 10^{-9} level, while the presence of irreducible background in $\tau \to e\gamma, \mu\gamma$ should worsen this number by a factor of 5. By the end of Belle II in 2022 it is expected to collect a sample of about 50 billion τ pairs to prove branching ratios at the 10^{-9} level.

Further improvements, at least on a restricted sample of decays, could come from running at lower center-of-mass energy (such as envisaged for τ/charm factories) since the initial state radiation photon spectrum is suppressed for the typical photon energies of the LFV processes [696]. Further gains are possible by exploiting beam polarization effects in the case of polarized factories: *e.g.* the helicity angles of the τ pair decay products can be used to significantly suppress the background when one τ decays to $\mu\gamma$ and the other one to $\pi\nu$ [697].

6.6.7 LFV at high energy colliders

LFV signatures might be observed at the LHC if e.g. supersymmetric particles are discovered, which naturally generate LFV couplings in slepton mass mixing. Consequently, if sleptons are light enough to be produced in pairs, different lepton flavours might show up in decay chains such as: $\tilde{\ell}^+\tilde{\ell}^- \rightarrow \ell^+\ell^{-\prime}\chi^0\chi^0$.

Known and new scalar or vector particles could also have lepton violating tree couplings and might be directly reconstructed from resonance peaks: $H \rightarrow \ell\ell'$ or $Z' \rightarrow \ell\ell'$. Due to the existing bounds on flavour changing processes, these LFV decays are small and difficult to detect above the large background from WW-production with subsequent leptonic decays. It seems however that with high enough luminosities, the LHC can e.g. go beyond the LEP bounds [698–701] on LFV Z decays [702], while waiting for ultimate limits from the $\approx 10^{13} Z$ bosons expected at future e^+e^- circular colliders.

If new particles exist at the TeV mass scale, i.e. in the discovery reach of the LHC, it is very likely that precision experiments will discover lepton flavour violation via radiative loops. Dedicated LFV search experiments like the proposed $\mu \rightarrow e$ experiments would then allow one to measure the LFV couplings of the new particles, complementary to the $\sim$TeV scale experiments at the LHC.

Conversely, in the case that no new physics were discovered at the LHC, the discovery of CLFV in precision experiments is not excluded as e.g. rare muon decays are testing mass scales that are much higher than LHC energy.

6.7 Search for the electron EDM in an electrostatic storage ring

6.7.1 Introduction

This section presents new ideas on a search for the electric dipole moments of the electron in an electrostatic storage ring. A comprehensive overview of the theoretical and experimental developments in the search for lepton EDMs can be found in Ref. [703].

Permanent EDMs (Electric Dipole Moments) of fundamental particles violate both time invariance and parity and, assuming the CPT theorem, this implies CP violation. This feature inserts EDMs among the most sensitive probes of CP violation. The standard model predicts non vanishing EDMs; however, their magnitudes are expected to be unobservably small. Hence, the discovery of a non-zero EDM would be a direct signal for "new physics" [704]. Until now, EDM searches have been limited to trapped neutral systems. Searches for EDMs of charged fundamental particles have hitherto been impossible because of the absence of the required new class of primarily electrostatic storage rings. Presently, two Collaborations are proposing the search for EDM of hadrons in a Storage Ring at BNL or FNAL [705] and at FZJ [706]. Interest for the measurement of the EDM of the electron has been expressed at Cornell University [707].

In supersymmetric theories, the radiative corrections due to heavy states could leave their footprints in the flavour structure of the supersymmetry breaking masses. Present and future searches for the muon and electron EDMs could be sensitive to the CP violation and flavour misalignment induced on slepton masses by the radiative corrections due to the right-handed neutrinos of the seesaw model and to the heavy Higgs triplets of SU(5) GUT. In particular, the experimental limit on the electron electric dipole moment strongly constrains the pattern of supersymmetric grand-unified theories with right-handed neutrinos: such constraints are already competing with the well-known ones derived by the limit on the proton lifetime [708]. Table 22 displays current and anticipated limits on the EDMs of fundamental particles.

6.7.2 Technique

The method for identifying an electric dipole moment (EDM) in these searches is to observe the rotation of the spin axis or polarization under the influence of a strong electric field. The best procedure begins

Particle	Adopted System	Current Limit	Future goal	SM prediction
Baryons				
Neutron	–	3.0×10^{-26}	10^{-28}	10^{-32}
Proton	^{199}Hg	7.9×10^{25}	10^{-29}	10^{-32}
Deuteron	–	–	–	10^{-29}
Leptons				
Electron	ThO	8.9×10^{-29}	10^{-29}	10^{-38}
Muon	–	1.9×10^{-19}	–	10^{-38}
Tau	$e^+e^- \to \tau^+\tau^-$	1.0×10^{-16}		

Table 22: Present status of EDM of various particles. No direct measurements on charged hadrons have ever been performed yet. The only direct measurements on leptons refers to the muon, its improvement is limited by the finite lifetime of the muon itself. At this stage of the development, the future goal for the limit on the electron EDM is purely speculative and in line with the other EDM searches in storage rings. A precise evaluation will be possible once the polarimeter issue, mentioned in the text, is addressed.

with the alignment of the beam polarization along the velocity of the beam, followed by the observation of any slow rotation of that polarization into the vertical direction caused by the torque induced on the EDM by a strong radial electric field. This imposes several feasibility requirements. First of all, the ring must utilize a special combination of electric (and possibly magnetic) fields in order to ensure that the usually unstable polarization along the direction of the velocity remains stable for long enough times (up to 1000 s) to allow any EDM effect to accumulate to a measurable level (*frozen-spin* condition). In addition, a dedicated polarimeter system has to be conceived and developed capable of detecting the emerging component of vertical polarization. It is estimated that an EDM at the $10^{-29} e \times cm$ causes an overall precession of the polarization of the order of 10^{-5} rad during the imposed observation time.

6.7.3 Statistical precision

An educated guess for the achievable statistical error is around $10^{-27} e \times cm$ for one month of data taking depending on the reachable Spin-Coherence Time (defined in the following Section). As mentioned before, a reasonable estimation is conditional on the polarimeter development. It should also be pointed out that an estimate of the statistical error on a real lattice has not been performed yet and should be the subject of a detailed investigation.

6.7.4 Design and realization of a magic ring *for electrons*

The energy corresponding to the frozen-spin condition for an electron storage ring ("magic-energy") is E = 14.5 MeV (γ =29.4). A state-of-the-art electric field of 6 MV/m acting on an electron of this energy determines a bending of R = 2.5 m, corresponding to a total perimeter of 20 m. There is no necessity to push the electric gradients at the mentioned level. Relaxing the demand, and adopting an electric field gradient of 2 MV/m, a machine with a total length of 50 m can be considered. Such a compactness, makes an electron-EDM experiment appealing, besides for its physics potential, also for its technological impact in the field of accelerator research and development. An electron EDM ring constitutes an ideal pioneering machine for a new generation of electrostatic storage rings and represents a first step towards a novel research line of physics beyond the SM by means of precision measurements in accelerators.

The design, commissioning and operation of a storage ring EDM experiment poses a series of experimental challenges and demands for innovative technological developments, some of which are briefly outlined in the following

6.7.4.1 *Design of the electrostatic lattice*

All-electric accelerator rings are rare. The ring most nearly resembling the one required for the electron (and proton) EDM experiment is the "Electron Analogue" ring successfully built and operated in Brookhaven in 1955 in connection with the AGS proton ring, mainly to investigate particle loss in passing through transition. The lattice design has to be supported by full beam-dynamics and spin-tracking simulations. The study of subtle effects and the simulation the particle and spin-dynamics during the build-up of the EDM signal, requires fast trackers capable of following up to several 109 turns samples of up to 107 particles. The addition of the spin-degree of freedom substantially enhances the required computing power.

6.7.4.2 *Production of high electric fields*

In the last twenty years there has been tremendous progress towards the development of the highest possible E-field strength on metallic surfaces. It was mainly driven by the linear collider R&D as well as work on energy recovery LINACs. As the experiment will make use of large area surfaces with high electric fields, dedicated competence will be demanded to investigate and control parameters like electric field strength applicable between the plates and induced dark current.

6.7.4.3 *Control of systematic uncertainties*

Most of the sources of systematic error can be identified by changing the polarization direction and storing beams in both clock-wise (CW) and counter-clock-wise (CCW) directions. There is a source of error that persists despite this procedure: a possible spurious net radial B-field around the ring. This field, acting on the electron magnetic moment, mimics the effect of the EDM. Besides the implementation of both passive and active shielding, monitoring and controlling the radial B-field at the required level (0.3 pG) will be one of the main challenges of the experiment.

6.7.4.4 *Spin-coherence time*

One of the problems connected with the requirement of maintaining a large horizontal polarization for the 20 minutes needed for the EDM effect to accumulate, arises from spin-decoherence effects. Normally, momentum spread among the beam particles leads to differences in the precession rates and the particle spins will decohere by spreading in the horizontal plane. The linear part of this effect may be canceled by using an RF cavity to bunch the beam, thereby imposing the same average cyclotron frequency on each particle. However, a lengthening of the orbital path that depends quadratically on the size of horizontal and vertical betatron oscillations while maintaining the cyclotron frequency will generate a smaller spread in spin precession rates that will lead to decoherence over a longer time. One of the goals of the EDM ring development program is to understand how to reduce or correct for such quadratic or higher order effects by, for example, adjusting the ring sextupole field components or by cooling the beam. Dedicated studies performed at COSY to examine the use of higher-order (6-pole) fields in the storage ring confirm that in the design of the ring, space has to be allocated for the installation of 6-pole fields [709].

6.7.4.5 *Polarimetry*

Polarimetry represents at this stage a not yet solved issue for an electron-EDM experiment. The establishment of a dedicated study group to define a working concept deserves high-priority for the project development. From the principle point of view, not neglecting the promising developments in scattering polarimetry [710], other options can be investigated as the use of resonators [707], or the exploitation of frequency measurements using SQUIDS [711].

6.7.4.6 *Magnetic shielding*

The whole ring needs to be shielded from magnetic fields: e.g. the earth's magnetic field must be reduced by a factor of 3×10^8. Being common to all of EDM projects, this problem can be addressed with a coordinated effort among the different Collaborations. Dedicated experience in magnetic shielding exists e.g. at PTB in Berlin [712], where highly sensitive magnetometers are adopted to measure the magnetic fields produced by a patient's inner organs (i.e. heart, brain, etc). In that environment the shielding is realized by means of an active outer shield, and a passive shield. The scheme adopted in the proton EDM project foresees the introduction, in addition, of an inner active shield, which, of course, cannot be used in the medical application [705].

6.7.5 Timeline and perspectives

The design and realization of the storage ring will take about 5 years (2 years for the design, and 3 years for the construction). It should be noticed the project has to be considered at the level of one of a kind project, but that after the realization of this first prototype ring, updated versions of the experiment are to be foreseen. As an example, in a second stage the possible implementation in the ring of also vertical magnetic-fields can be investigated. In the reference system of the moving particle such fields are effectively seen as radial electric fields much more intense than the ones practically achievable.

6.8 Extreme Flavour

A study of the possibility to exploit the full luminosity which will be provided by the HL-LHC for flavour physics studies has started very recently. The following summarizes the status of this study, as resulting from several "brainstorming" meetings which were attended by theorists and experimentalists. After a review of the theoretical motivations behind these studies, early thoughts on the design of a possible dedicated detector, with emphasis on trigger and data acquisition, are presented.

6.8.1 Introduction and Scope

The Large Hadron Collider (LHC) is an enormous source of heavy-flavoured hadrons, that will continue for many years in the future with growing intensity. In the High-Luminosity phase planned for 2025 and beyond, at instantaneous luminosities of about $10^{35}/cm^2/s$, the LHC will produce of order of 10^{14} beauty hadrons and 10^{15} charm hadrons per year, within comfortably accessible acceptance regions (two units of rapidity).

In spite of the recommendation of the European strategy group to perform "full exploitation of the LHC", no plans currently exist to take full advantage of this potential. This is not without a good reason, as processing and storing of order of 10^{14} LHC collisions is a huge technological challenge, even if projected a decade into the future. This would require an improvement of a factor $10^4 - 10^5$ both in permanent storage capacity and computing power with respect to the current state of the art, while Moore's law improvements might give us only a factor of 100 in the most optimistic view.

However, the physics opportunities offered by such unprecedented samples call for a serious study of the feasibility of such an "extreme" flavour experiment. The purpose of this Section is to discuss some preliminary ideas on how such an experiment could be performed, what the physics returns could be, and which feasibility studies need to be performed. Given the above-mentioned limitations on data-processing, the key to an extreme-flavour experiment (XFX) seems to be to perform the data analysis in real time, rather than off-line.

Beam crossings at the LHC will occur at a frequency of 40 MHz, for each beam crossing many elementary p-p collisions occur (typically around 150-200 at the HL-LHC), for each collision tens of charged particles are produced resulting in thousands of tracks traversing tracking detectors for each beam crossing (every 25 ns). However, not all the collisions in a crossing are interesting for the processes we want to study, and, more importantly not all the tracks in a collision event. If we can identify the

heavy-flavour decays of interest in real time and record only what is relevant to the study of that particular process, we will achieve a large reduction in the amount of data to be transmitted and stored permanently. If we can do that, we will gain several orders of magnitude in the number of decays collected per unit time with respect to what could be done with a traditional approach and we will alleviate the size of the data storage and the amount of computing power required for the final analysis to a point to make the experiment feasible.

In view of the future development of a FCC collider, the technologies developed in this context will become even more crucial to the performing of experiments in that context, where even the heaviest known quark, the top, will reach an impressive production rate of 3 kHz.

In rest of this Section, we will discuss in order the physics potential, and the technological ingredients needed for the design of an XFX.

6.8.2 Physics Targets

6.8.2.1 Unitarity Triangle Analysis in the SM and beyond

At present, the Unitarity Triangle Analysis (UTA) allows to determine the CKM parameters with an error of few percent (see Table 23) [610, 611]. The redundancy of the SM UTA also allows to constrain NP contributions to $\Delta F = 2$ amplitudes. This is achieved by generalizing the UTA to allow for NP loop-mediated contributions, determining simultaneously the CKM parameters and the possible NP contributions in all loop-mediated processes [470–482]. Obviously, the generalized UTA determines the CKM parameters less accurately than the SM one, leaving at present room for NP contributions in the $\Delta F = 2$ sector at the level of $20 - 30\%$ of the SM one (at 95% probability, see Table 24). In this sense, we can say that we are presently testing the CKM paradigm at the $20 - 30\%$ level. This already corresponds to very stringent bounds on the scale of NP (see Figure 70), unless the flavour structure of NP is identical (or very similar) to the SM one, which is the case of MFV [483–485].

Parameter	Output	Parameter	Output
λ	0.22534 ± 0.00065	A	0.821 ± 0.012
$\overline{\rho}$	0.132 ± 0.023	$\overline{\eta}$	0.352 ± 0.014
$\alpha[^\circ]$	88.6 ± 3.3	$\beta[^\circ]$	22.03 ± 0.86
$\gamma[^\circ]$	69.2 ± 3.4	$\beta_s[^\circ]$	1.071 ± 0.0041

Table 23: Determination of CKM parameters from the SM UTA (from ref. [611]).

Parameter	Output	Parameter	Output
C_{B_d}	1.07 ± 0.17	$\phi_{B_d}[^\circ]$	-2.0 ± 3.2
C_{B_s}	1.052 ± 0.084	$\phi_{B_s}[^\circ]$	0.7 ± 2.1
C_{ϵ_K}	1.05 ± 0.16		
λ	0.22535 ± 0.00065	A	0.802 ± 0.020
$\overline{\rho}$	0.159 ± 0.045	$\overline{\eta}$	0.363 ± 0.049

Table 24: Determination of UT and NP parameters from the UT fit. See ref. [611] for details.

As discussed in Section 6.1, improving the accuracy of the generalized UTA is of crucial importance to i) indirectly probe higher scales of NP and ii) to test the flavour structure of any NP within the reach of direct searches at present and future hadron colliders. A first, major step forward in this direction is represented by Belle II and the LHCb upgrade, which will considerably improve the experimental

accuracy on a large number of UTA-related and/or NP-sensitive observables in the quark sector. The NP reach however depends not only on experimental improvements, but also on the theoretical accuracy in the estimation of the relevant observables, both in the SM and beyond. Thus, assessing the impact of future experimental facilities is a nontrivial task, which requires dedicated studies, including an extrapolation of the accuracy of Lattice QCD. Detailed analyses of the impact of SuperB, Belle II and LHCb upgrade have been performed, leading to the conclusion that the UTA accuracy can be improved by a factor of 5–10, both for the SM and the generalized analysis, including the bounds on NP contributions (see for example ref. [713]).

While a detailed study of the impact of XFX on the UTA is beyond the scope of this work, a rough estimate can be provided on the basis of the expected experimental and Lattice QCD improvements described in the remainder of this Section. A first, preliminary and incomplete list of foreseen uncertainties in the inputs to the UTA is reported in Table 25. Based on these uncertainties, a preliminary extrapolation of the UTA indicates that present errors can be improved by up to two orders of magnitude. However, more detailed estimates of a few crucial inputs, such as semileptonic B decays or CP asymmetries in $B_{d,s} \to J/\psi P(V)$ decays, are needed before a these indications can be put on firm ground. Nevertheless, this very preliminary estimate displays the huge potential impact of XFX on testing the CKM picture of flavour and CP violation.

Parameter	Error	Comments
$\alpha_s(M_Z)$	$2 \cdot 10^{-4}$	
m_t	250 MeV	theory limited
m_b	10 MeV	$\times 3$ better
V_{us}	$1 \cdot 10^{-4}$	$\times 10$ better
V_{cb}	1%	Belle II / XFX
V_{ub}	1%	XFX
ϵ_K	5%	long distance + dim. 8
B_K^i		$\times 10$ better
F_{B_s}	1 MeV	
F_{B_s}/F_{B_d}	0.5%	
B_{B_s}	6%	
B_{B_s}/B_{B_d}	0.5%	
ΔM_d	0.06%	
ΔM_s	0.01%	
$\sin 2\beta$	0.06%	(see caption)
γ	0.09°	
ϕ_{B_s}	0.0004°	(see caption)

Table 25: Foreseen uncertainties for the generalized UTA. For $\sin 2\beta$ and ϕ_{B_s}, we assume that a sufficient number of $SU(3)$-related control channels can be measured (see refs. [612–615] for details).

6.8.2.2 Rare decays of beauty hadrons

We mainly focus on exclusive B and B_s rare decay modes with charged leptons and light hadrons (including η and η') in the final state. Other interesting processes involve $b-$baryons. The B_c meson can allow us to access other important rare transitions.

The FCNC modes $B_{s,d} \to \mu^+\mu^-$ are among the theoretically cleanest and most NP-sensitive rare

B decays. For $B_s \to \mu^+\mu^-$, the effective weak Hamiltonian reads:

$$H^{eff} = -\frac{4G_F}{\sqrt{2}} V_{tb}V_{ts}^* \sum_{i=10,P,S} \left[C_i O_i + C_i' O_i'\right] \ , \tag{48}$$

where $O_{10} = \frac{e^2}{16\pi^2}(\bar{s}_{L\alpha}\gamma^\mu b_{L\alpha})\ \bar{\mu}\gamma_\mu\gamma_5\mu$, the scalar and pseudoscalar operators $O_{S,P}$ can be neglected in the SM, and the primed operators involve right-handed fermions, and are zero in the SM. The current measurement $BR(B_s \to \mu^+\mu^-)|_{exp} = (2.8^{+0.7}_{-0.6}) \times 10^{-9}$ [714] must be compared to the SM prediction $BR(B_s \to \mu^+\mu^-)|_{SM} = (3.66 \pm 0.23) \times 10^{-9}$ [596]; this excludes NP models predicting a large enhancement of contributions from $O_{S,P}$.

For the mode $B_d \to \mu^+\mu^-$ the current experimental result $BR(B_d \to \mu^+\mu^-)|_{exp} = (3.9^{+1.6}_{-1.4}) \times 10^{-10}$ [714] must be compared to the SM expectation $BR(B_d \to \mu^+\mu^-)|_{SM} = (1.06 \pm 0.09) \times 10^{-10}$ [596]. It is clear that much more statistics is needed to measure with any precision the ratio $BR(B_d \to \mu^+\mu^-)/BR(B_s \to \mu^+\mu^-)$ which is of paramount importance as a probe of NP. Indeed, many theoretical uncertainties drop in the ratio, leaving us with $(f_{B_d}/f_{B_s} \times |V_{td}/V_{ts}|)^2$. From the extrapolated uncertainties of the UTA and of Lattice QCD, we expect to be able to predict this ratio at the percent level. From Table 17 [633] it is apparent that even at the end of the LHCb upgrade run, the expected resolution is no better than 40%, while CMS expects to measure the ratio to 20% at the HL-LHC (see Appendix B.1). The only way to measure precisely this quantity, for as far as we can see in the future, appears to be a flavour experiment at the HL-LHC as discussed in this Section, where a resolution comparable with the current theory uncertainty of 5% can be expected.

Other observables can also be considered besides branching fractions, in particular the mixing-induced CP asymmetry $S^{\mu^+\mu^-}$, and the quantity $\mathcal{A}_{\Delta\Gamma}^{\mu^+\mu^-}$ that enters in the expression of the time-dependent CP asymmetry when the width difference $\Delta\Gamma$ between the CP-conjugate states is sizable, as for $B_s - \bar{B}_s$.

Another very interesting class of rare B decays is represented by $b \to (s,d)\ell^+\ell^-$ transitions. The theoretical calculation of the exclusive decay $B_d \to K^*\mu^+\mu^-$ is however much more challenging, since factorization only holds in the infinite mass limit and power corrections can play an important role [715, 716]. Thus, improvements in the predictions require both a more precise knowledge of the hadronic form factors in the full range of the dilepton mass squared, and a better control of the neglected operators and of the non-factorizable contributions. The variety of experimental observables, on the other hand, provides a large amount of information to be used to identify deviations from the SM.

An important role is played by the angular distributions. Starting from these quantities, several observables can be introduced, namely:

- the lepton forward-backward asymmetry A_{FB};
- the longitudinal K^* polarization fraction F_L;
- binned observables, with their numerators and denominators separately integrated over q^2 bins.

The position of the zero of the forward-backward asymmetry has a high discriminating power among the SM and several NP scenarios. Other observables [717] are also modified with respect to the SM predictions if the weak Hamiltonian gets additional contributions from NP phenomena. Moreover, it is worth pointing out that: (i) $\tau^+\tau^-$ final state leptons provide new observables connected to the lepton polarization; (ii) the measurement of B_s vs B_d modes can be used to reduce the hadronic uncertainties; (iii) the separate measurement of μ and e final states gives access to the issue of lepton universality; (iv) the measurements of both CKM favoured and suppressed modes provide the ratio $|V_{td}/V_{ts}|$. An overview is presented in Table 26.

The main CKM suppressed rare semileptonic modes to investigate are $B \to (\pi,\rho)\ell^+\ell^-$ and $B_s \to K^{*0}(\to K\pi)\ell^+\ell^-$, for which only $BR(B^+ \to \pi^+\mu^+\mu^-)$ has been measured. Although in

$b \to s\ell^+\ell^-$	observable	PDG 2014 [81]	SM
$B \to K^*(\to K\pi)\ell^+\ell^-$	BR	$(9.9^{+1.2}_{-1.1}) \times 10^{-7}$ (n)	$(1.34 \pm 0.62) \times 10^{-7}\vert_{q^2 \in [16,\,19]\mathrm{GeV}^2}$
$(\ell = e, \mu)$		$(12.9 \pm 2.1) \times 10^{-7}$ (c)	
	$d\Gamma/dq^2$	✓	⋆
	$F_L(q^2)$	✓	⋆
	$A_{FB}(q^2)$	✓	⋆
	angular distributions	✓	⋆
	scalar $K\pi$ contribution		⋆
	$e - \mu$ universality		
$B \to K^*(\to K\pi)\tau^+\tau^-$	BR		$[0.4 - 1.2] \times 10^{-7}$
	τ pol. asymmetries		⋆
$B_s \to \phi(\to K\bar{K})\ell^+\ell^-$	BR	$(7.6 \pm 1.5) \times 10^{-7}(\mu)$	$[14.5 - 19.2] \times 10^{-7}$
	$d\Gamma/dq^2$	✓	⋆
	$F_L(q^2)$		
	$A_{FB}(q^2)$		⋆
	angular distributions		
	$e - \mu$ universality		
$B_s \to \phi(\to K\bar{K})\tau^+\tau^-$	BR		
	τ pol. asymmetries		
$B \to K\ell^+\ell^-$	BR	$(3.1^{+0.8}_{-0.7}) \times 10^{-7}$ (n)	$(0.86 \pm 0.20) \times 10^{-7}\vert_{q^2 \in [16,\,22.9]\mathrm{GeV}^2}$
$(\ell = e, \mu)$		$(4.51 \pm 0.23) \times 10^{-7}$ (c)	
	$d\Gamma/dq^2$	✓	⋆
	$e - \mu$ universality	✓	
$B \to K\tau^+\tau^-$	BR		$[0.6 - 1.6] \times 10^{-7}$
$\Lambda_b \to \Lambda(\to N\pi)\ell^+\ell^-$	BR	$(10.8 \pm 2.8) \times 10^{-7}(\mu)$	$(4.5 \pm 1.2) \times 10^{-7}\vert_{q^2 \in [15,\,20.28]\mathrm{GeV}^2}$
	$d\Gamma/dq^2$	✓	⋆
	$A_{FB}(q^2)$		⋆
	angular distributions		⋆
	Λ, Λ_b polarization asym.		
	$e - \mu$ universality		
$\Lambda_b \to \Lambda\tau^+\tau^-$	BR		⋆
$B_s \to (\eta,\, \eta')\ell^+\ell^-$	BR		$(2.6 \pm 0.7) \times 10^{-7}$ (η) [718]
			$(2.2 \pm 0.6) \times 10^{-7}$ (η')
	$d\Gamma/dq^2$		⋆
	$e - \mu$ universality		
$B_s \to (\eta,\, \eta')\tau^+\tau^-$	BR		$(8 \pm 1.5) \times 10^{-8}$ (η)
	BR		$(3.9 \pm 0.8) \times 10^{-8}$ (η')
$B_s \to f_0(980)\ell^+\ell^-$	BR		$(9.5 \pm 3.1) \times 10^{-8}$ [719]
	$d\Gamma/dq^2$		
	$e - \mu$ universality		
$B_s \to f_0(980)\tau^+\tau^-$	BR		$(1.1 \pm 0.4) \times 10^{-8}$
$b \to d\ell^+\ell^-$	observable	exp [638]	SM
$B \to \pi\ell^+\ell^-$	BR	$(2.3 \pm 0.6 \pm 0.1) \times 10^{-8}$ (c)	$(1.88^{+0.32}_{-0.21}) \times 10^{-8}$ [720]
	$d\Gamma/dq^2$		⋆
	$e - \mu$ universality		
$B \to \pi\tau^+\tau^-$	BR		

Table 26: FCNC semileptonic decays: main observables, 2014 status (c=charged mode, n=neutral), predictions (the quoted ranges are mainly due to the form factor uncertainties). The symbol ✓ indicates measured observables or ongoing experimental analyses (end of 2014). The symbol ⋆ indicates observables with updated theoretical analyses in the literature. The predicted branching fractions of $B \to K^{(*)}\ell^+\ell^-$ [721] and $\Lambda_b \to \Lambda\ell^+\ell^-$ [722] are quoted for selected ranges of q^2.

the SM the rates are suppressed by a factor $|V_{td}/V_{ts}|^2$ with respect to the CKM favoured modes, with $|V_{td}/V_{ts}| = 0.261 \pm 0.011$ [81], such processes are accessible at the hadron facility under discussion, with the variety of their observables.

6.8.2.3 *Charm Physics*

The very large statistics available at an Extreme Flavour Experiment would allow for use of high-purity selections that would be beneficial for rare decays and for precision measurements. A factor 10 improvement is foreseen in sensitivities to physics observables and between a factor 10 and 100 for upper limits on rare decays, depending on the level of irreducible background affecting the specific decay modes.

From a naive extrapolation obtained by scaling LHCb upgrade estimates for the $D^0 \to K^0_S\pi^+\pi^-$ decay mode, we obtain sensitivities for the mixing parameters x and y at the level of 10^{-5}, and for the CP-violating parameters $|q/p|$ and φ, at the level of 10^{-3} and 0.3°, respectively. We could reach statistical precision at the level of 10^{-5} or below in searches for CP violation in singly-Cabibbo suppressed charm meson decays. The search for $D^0 \to \mu^+\mu^-$ could improve by a factor 10 with respect to the LHCb upgrade, assuming no separation from the peaking background of $D^0 \to \pi^+\pi^-$ with π decaying in flight, reaching a level of sensitivity for the upper limit of about 10^{-11}. The reconstructed $D^0 \to \pi^+\pi^-$ peak actually appears shifted from the $D^0 \to \mu^+\mu^-$ by about 10 MeV, due the incorrect muon mass assignment to the decay products. This means that this background can actually be separated out, and the ultimate sensitivity to $D^0 \to \mu^+\mu^-$ be pushed towards 10^{-12}, provided a mass resolution of the experiment below ≈ 5 MeV can be attained (for reference, the resolution of the current LHCb detector for this decay is ≈ 9 MeV).

Given the extremely large sample of D decays available, the impact on lepton flavour violating interactions and on Majorana neutrino mass bounds from D decays should also be investigated. The initial studies of the possible experimental ways to search for sterile neutrinos (discussed at length in Section 5.4.2 of this document) determined that there were two main pathways: "The search of singlet fermions in the mass interval 2-5 GeV would require a considerable increase of the intensity of proton accelerators or the detailed analysis of kinematics of more than 10^{10} B-meson decays" [418]. The same argument can be made in reference to charm decays, as well. The second possibility, of collecting enormous samples of heavy quark decays was dismissed at the time (2007) as technologically unfeasible—in this Section we are revisiting that possibility with more modern eyes, and we are considering as realistic the possibility of even larger samples. In this approach, it is not necessary to see the decay of the sterile neutrino itself, but its presence is inferred by the distortion of the D or B decay kinematics (which is significant, due to the expected mass being around a GeV). From Fig. 91 showing the production cross-section as a function of the mass, one can see that the production rates would be significant at the proposed experiment.

These are strong motivations for the "Extreme Flavour" project and also calls for a theoretical reassessment of the SM contributions in charm decays.

Certainly, it would be an experimental challenge for the understanding of the systematic uncertainties at that level of precision. However, most of the systematic uncertainties can be estimated by using dedicated data control samples. The interpretation of the results for distinguishing new physics effects from the SM would be very challenging and would require a major advancement of the theory. Lattice developments that are foreseen in the near future and the large variety of available measurements might help in this respect (see Section B.2).

6.8.2.4 *Kaon physics*

An incomplete list of important Kaon decays that could be addressed by a high-intensity flavour experiment is given in Table 27.

This Section addresses the case for kaon physics studies at an XFX. We discuss first the decays $K_{S,L} \to \mu^+\mu^-$, then we turn the attention to $K \to \pi\pi l^+l^-$, charge asymmetry in $K^+ \to \pi^+l^+l^-$ and forward backward asymmetry.

– $K_{S,L} \to l^+l^-$, $K_{S,L} \to l^+l^-l^+l^-$ [81, 528, 723] The recent LHCb limit on $K_S \to \mu^+\mu^-$ [81] is testament to the potential of collider experiments in this field (see table). A high precision

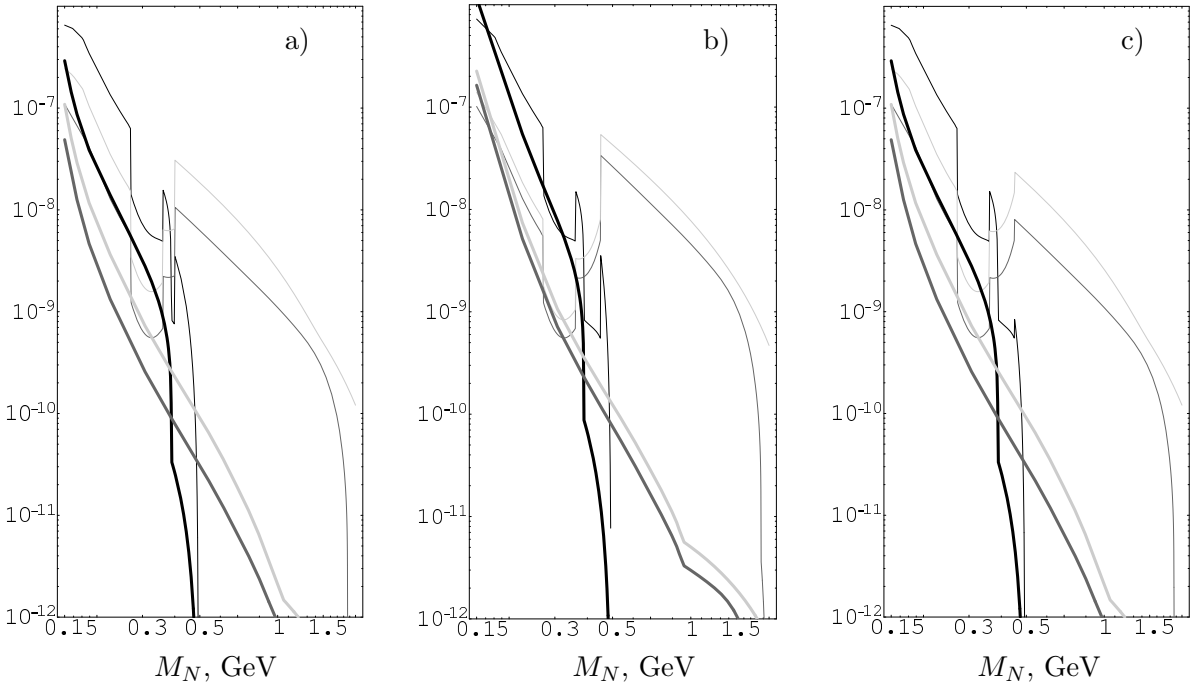

Fig. 91: Inclusive heavy neutral lepton production by strange (black lines), charm (dark gray lines) and beauty (light gray lines) hadrons in various models within νMSM (from ref. [418], Fig. 16). The interesting rates are between corresponding thin and thick lines which show upper and lower limits on couplings.

Table 27: Selected kaon decays for study at an Extreme Flavour experiment. The K_L mode is not expected to be studied at hadron colliders, however the interpretation of its measurement made elsewhere is affected by K_S studies. See text for more detail.

	PDG	Prospects
$K_S \to \mu\mu$	$< 9 \times 10^{-9}$ at 90% CL	(LD)$(5.0 \pm 1.5) \times 10^{-12}$ NP $< 10^{-11}$
$K_L \to \mu\mu$	$(6.84 \pm 0.11) \times 10^{-9}$	difficult: SD $\ll$ LD
$K_S \to \mu\mu\mu\mu$	–	SM LD $\sim 2 \times 10^{-14}$
$K_S \to ee\mu\mu$	–	$\sim 10^{-11}$
$K_S \to eeee$	–	$\sim 10^{-10}$
$K_S \to \pi^+\pi^-\mu^+\mu^-$	–	SM LD $\sim 10^{-14}$

measurement can test the short distance (SD) SM contribution provided the long distance (LD) prediction [528, 724] is improved with auxiliary channels [723]. A Flavour experiment at the HL-LHC is the only foreseeable possibility to measure the $\mathcal{B}(K_S \to \mu^+\mu^-)$ in the interesting physics range ($< 10^{-10}$, as extrapolated from the LHCb result with 1 fb^{-1}). Additional opportunities for reducing the background further are offered by the huge charm production that will be available (O(10^{15})/year)—this could allow performing some measurements on clean "D-tagged" kaon samples, e.g. kaons from $D^+ \to K_s\pi^+$ decays.

In the decay $K_L \to \mu\mu$, the smallness of the ratio SD/LD $\sim \frac{1}{30}$ may obscure an experimental improvement on the measurement of the branching fraction made at dedicated kaon experiments [528]. The situation would be a bit ameliorated if the sign of $A(K_L \to \gamma\gamma)$ were known. Information on this sign ambiguity could come from the experimental study of $K_{S,L} \to l^+l^-l^+l^-$ [723]. As seen in the table, the K_S channel is within reach of a high-intensity hadronic experiment, and

it may also yield the LD distance info needed for a better control of $K_L \to \mu\mu$. These four body decays have a peculiar feature: similarly to $K_{S,L} \to \pi^+\pi^- e^+ e^-$, the two different helicity amplitudes interfere; then one can measure the sign of $K_L \to\to \gamma^*\gamma^* \to l^+l^-l^+l^-$ by studying the time interference of $K_S\ K_L$ which has a decay length $2\Gamma_S$ [723].

- $K_S \to \pi^+\pi^- l^+ l^-$
  Only $K^+ \to \pi^+\pi^0 e^+ e^-$ has been studied so far [725]; $K_S \to \pi^+\pi^-\mu^+\mu^-$ appears more feasible experimentally even if it has less than 10 MeV phase space; from table I in Ref. [725] we can extract also that the expected branching fraction is $\mathcal{O}(10^{-14})$ and that the novel purely electric and magnetic contribution are enhanced with respect to the less interesting bremsstrahlung component.
- $K^+ \to \pi^+\mu^+\mu^-$ *charge asymmetry* NA48 has measured this asymmetry to be less than $2.1 \cdot 10^{-2}$ at 90% CL (e) and $2.9 \cdot 10^{-2}$ (μ) [81], SM is $\sim 10^{-6}$ [726] but in some regions of the phase space $\sim 10^{-4}$; NP models may reach $\sim 10^{-3}$
- *The* $K^+ \to \pi^+\mu^+\mu^-$ *forward-backward asymmetry* At the moment $A_{FB} < 2.3 \cdot 10^{-2}$ at 90% CL [81], limiting NP contributions generated by scalar tensor coupling [727] while SM contributions are $\sim 10^{-3}$ [728]. A_{FB} should be improved.
- *Lepton Flavour Violation* A tight constraint from $BR(K_L \to \mu e) < 5 \times 10^{-12}$ implies $BR(K_S \to \mu e) < 10^{-14}$ [81] so this channel is difficult to improve
- $K_{L,S} \to \pi^0 ll$ These interesting channels (latest Refs [729, 730]) are discussed in Section 6.2.

In conclusion, all channels reported in the table appear interesting for this program of extreme flavour, particularly the four body decays, and also $K^+ \to \pi^+\mu^+\mu^-$ asymmetries.

6.8.3 Detector Geometry

The best detector geometry for an XFX experiment cannot determined without a detailed study. Some initial considerations are however possible.

- A strong tracking capability seems to be the most important need, and at the same time the greatest challenge in the envisioned operating conditions. The next priorities are, in order: muon identification, hadron PID, calorimetry.
- The detector does not need to be hermetic. Since it is anticipated that the experiment will work only on a part of the collision data, it is not expected that global event variables, like the missing E_T, could play a useful role in this experiment, or be usefully determined.
- A tracking volume sufficient for good containment of K_S decays is considered by many a very desirable feature.
- Both "forward" and "central" configurations are possible. It seems that both a geometry "a la LHCb" or General-Purpose-like are in principle feasible for this experiment. There are however some clear trade-offs that should be worked out with a targeted study. A forward configuration has the advantage of an easier access to the detector, easier cabling etc. and allows room for large detectors, like those that may be required for PID purposes (see later). It is likely to require a smaller number of channels and be therefore less expensive. It may however suffer from larger radiation-resistance issues, and the high track density may be a hurdle to pattern recognition. Also, resolving tracks originating from separate primary vertexes along the Z-direction requires better impact parameter resolution than in the central configuration.
- Following the approach of ignoring the reconstruction of individual primary collisions, there is no need to separate primary vertexes from each other. It is assumed that the mode of operation will be to identify a few tracks of interest, and then analyze all remaining tracks that have a value of the z-intercept compatible with having originated from a common vertex. It is therefore advantageous to have a longer luminous region. If necessary, time-dependent measurements could be performed in the transverse plane.

– The readout can be conveniently organized according to the z_0 (z-position at closest approach to the z-axis) of the track. It is in fact envisioned that the tracks will be locally reconstructed "on-detector", and presented to the readout system sorted in separate channels, each representing a separate z_0 range.

6.8.4 Tracking

6.8.4.1 Radiation tolerance of future inner tracking detectors

Radiation damage in silicon detectors has been extensively studied and detailed parameterizations such as the so-called “Hamburg Model” describe quite well the behavior of silicon detectors at LHC. The damage is understood in terms of the creation of new energy levels between the valence and conduction bands, globally called defects, which have strong impact on the device performance after irradiation.

Assuming that LHC is going to accumulate 3000 fb^{-1}, the requirement on radiation damage for the inner pixel layers of the general-purpose detectors is $2-3\times10^{16}n_{eq}/cm^2$, while for the inner strip layers it is $\approx 10^{15}n_{eq}/cm^2$. The VELO system of the upgraded LHCb detector is expected to accumulate, after 50 fb^{-1} of integrated luminosity, a maximum integrated flux of up to $\approx 8\times10^{15}n_{eq}/cm^2$. Silicon remains the only material that has the capability of reaching this goal within the timescale of the LHC upgrade, with the possible exception of diamond for the innermost pixel layer and/or specialized detectors. For very irradiated silicon its impossible to reach full depletion voltage, so only a part of the sensor is active. The key parameters are therefore the amount of trapping and the drift voltage extension at a given bias voltage. A beneficial effect that counterbalances charge trapping in heavily irradiated detectors is the onset of charge multiplication, due to the presence of localized, very high electric fields.

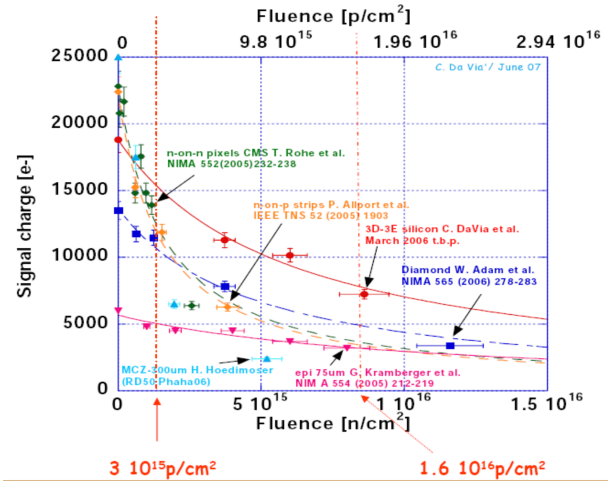

Fig. 92: Signal charge collected in various devices as a function of fluence.

Figure 92 shows the collected signal charge from a MIP as a function of fluence for values up to $2-3\times10^{16}neq/cm^2$. The decrease in signal amplitude is quite dramatic for thick sensors, while it’s less pronounced for thinner one, as the drift path is shorter. The expected fluence at an extreme flavour experiment will depend on the detailed detector geometry and configuration. Naively, in the case of a forward spectrometer, one can extrapolate the expected flux for the LHCb VELO upgrade by a couple of orders of magnitudes. At these much higher fluences, $10^{17}-10^{18}n_{eq}/cm^2$, the signal charge decreases further: the silicon bulk becomes heavily doped and it can be depleted only for a small part, making the number of initial e/h pairs very small. Moreover trapping will prevent charges from drifting any reasonable distance. These fundamental problems can be overcome only with the introduction of new technologies that will be able to work with small signals and short drift paths. HVCMOS, or a similar

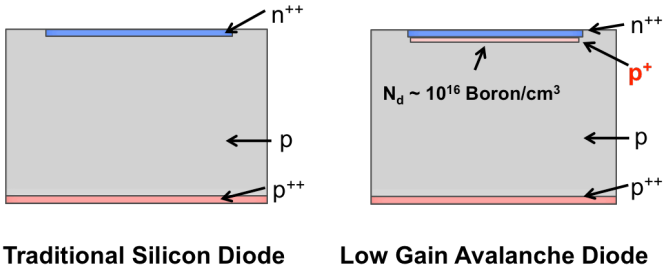

Fig. 93: Schematic of a traditional silicon diode (left) and of a Low-Gain Avalanche Diode (right).

technology where the readout electronics is embedded in the sensor itself, might compensate for these effects.

6.8.4.2 On line momentum determination

The online measurement of charged particle momenta could be performed using the so-called pt-modules [731], employed for the upgrade of the CMS detector Silicon Tracker. These modules consist of two silicon sensors (either strips or macro-pixels), separated by a few mm, which measure the local flight direction of the particle, by correlating the cluster positions in both sensors. The sensor spacing and the strip/pixel pitch determine the accuracy of the direction measurement: for 4 mm spacing and 80 μm pitch the angular resolution is about 8 mrad. These modules can measure the momenta of the particles outside of the dipole magnet with an accuracy of about $\delta p_T/p_T^2 \approx 3\%$.

6.8.4.3 On line impact parameter determination

A useful extension of the concept could be realized with a triplet of sensors which find all combinations of triplets in a single chip, similar to the concept of the Tiny Triplet Finder (TTF) of the BTeV experiment [732]. The idea is to form a sandwich of three pixelated sensors: the logic should sit in the middle sensor together with the one that performs the triplet finder. Studies need to be performed to see whether this triplet readout could be realized in custom ASIC, for instance in 65 nm technology.

Alternatively, this trigger could be implemented by taking pairs of doublets that are then matched in special boards in the collision hall.

6.8.4.4 Design Optimization of Ultra-Fast Silicon Detectors

The design of ultra-fast silicon detectors [733] (UFSD) exploits the effect of charge multiplication in silicon to obtain detectors that can concurrently measure with high accuracy time and space. Figure 93 shows on the left a schematic of a traditional silicon diode, while on the right the $n^{++} - p^{+} - p - p^{++}$ structure of a UFSD. The extra deep p^{+} layer creates a strong electric field that generates charge multiplication.

The time resolution σ_t can be expressed as the sum of three terms [734]: (i) Time Walk, (ii) Jitter, and (iii) TDC binning:

$$\sigma_t^2 = ([\frac{V_{th}}{S/t_r}]_{RMS})^2 + (\frac{N}{S/t_r})^2 + (\frac{TDC_{bin}}{\sqrt{12}})^2, \tag{49}$$

where S is the signal amplitude, t_r the signal rise time, N the noise, and V_{th} is the comparator threshold used to set the time of arrival of the particle ($V_{th} \sim 10 * N$). Equation (49) shows the main set of requirements to obtain excellent timing resolution: (i) low noise, (ii) large signals and (iii) a short rise time. These requirements are complemented by the additional requirement of having signals that are

very uniform: if the signal shape varies significantly on an event-to event basis, then the timing accuracy is severely degraded.

The ultimate performance of UFSD depends critically on the combination of the sensors with the read-out electronics. A highly pixelated UFSD requires a full custom ASIC read-out, bump bonded to the sensor. The design of UFSD requires the optimization of many intertwined parameters. We are considering two distinct options for the realization of a highly pixelated UFSD system, Figure 94: (i) Left: a single read-out chip, able to measure position and time, or (ii) Right: a split design, where we use double-sided readout to separate the position measurement from the time determination. This second design is mechanically more challenging, however reduces the complexity of each read-out chip. Both designs assure (i) excellent timing capability, due to the enhanced signal and reduced collection time, and (ii) accurate position determination, due to the pixelated electrodes.

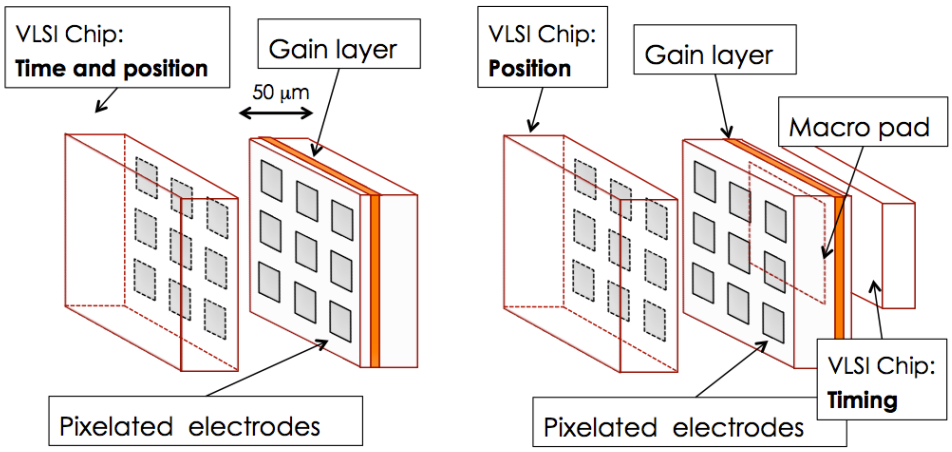

Fig. 94: Sketch of a UFSD sensor and associated VLSI electronics. Left side: single read-out chip, right side: split read-out.

Our simulations and laboratory results indicates that thin sensors of small capacitance will give the best results. A resolution of 10-20 ps seems to be reachable with dedicated VLSI electronics.

6.8.5 Particle Identification

6.8.5.1 Muon identification

The performance of muon identification in an XFX depends crucially on the hit rates expected in the different muon detector regions and on the detector geometry. As an example, a naive extrapolation of the rates foreseen in the LHCb upgraded detector gives rates of the order of a few tens of MHz per cm^2 in the most busy regions, rapidly decreasing in the MHz/cm^2 range and less in the outer regions. These very high rates could be mitigated by e.g. adding more passive material and shielding, and/or reducing the detector coverage in the very forward region. Clearly, the impact of these choices on the efficiency in key signal modes should be carefully studied. Regarding detector technology, micro-pattern gaseous detectors offer excellent timing and spatial resolution, and tracking and triggering efficiencies. High-rate capability of Gas Electron Multipliers (GEMs) has also been demonstrated, while resistive micro-megas might achieve comparable rates in the future. Due to the high currents expected, power distribution needs to be carefully studied. Finely segmented scintillators would also be suitable as the active material, with scintillation light collected by fibers, which guide the light to photodetectors, such as Silicon Photomultipliers, which in case of a forward spectrometer could be properly shielded and housed in a region of reasonably low background radiation. Aging effects might be more severe for plastic scintillators with respect to gaseous detectors. In any case, the effects due to radiation damage

of all the sensitive detector components and associated electronics remains a critical issue and must be studied in a detailed R& D program.

6.8.5.2 Hadronic PID

The issue of the PID capabilities needed for an XFX have been discussed. The ability to distinguish hadrons in this environment is hard to achieve, but, according to some, it is not really crucial to the experiment's mission, and it may be given up in favor of concentrating on other issues. Anyhow, there is a wide consensus that the topic deserves a sizeable investment of resources in feasibility studies.

The track density seem to represent a big hurdle to solutions based on the Cherenkov effect. An alternative possibility is the use of thick (2-3 meters) Transition-Radiation Detectors. These detectors allow separation of hadrons up to very high momenta, and a thick prototype of this kind has actually been designed, built and tested many years ago ([FERMILAB-CONF-89-170E]). It seems possible to have good threshold discrimination of pions from kaons/protons, up to energies of several hundred GeV. It is also possible to integrate tracking capabilities within the TRD detector. The subject needs to be studied anew, considering the implementation possibilities allowed by newer materials, and the issues of signal timing, pileup, and synchronization.

6.8.6 Data acquisition

In the following we assume that the detector will produce an aggregate output data of the order of 0.5 PB/s. This estimate comes from scaling the foreseen 40 Tb/s output of the upgraded LHCb detectors (taken as a reasonable example of the detector size needed for meaningful coverage of interesting physics volume) by a factor of 100 for luminosity.

A first challenge arises from the fact that, with current technologies, the resulting number of serial data links needed to read out of the whole detector would be prohibitively huge. The fastest radiation-hard serialiser/deserialiser devices are the GigaBit Transceivers (GBTs), which are designed and built by the CERN micro-electronics team for the upgrades of the LHC experiments. These GBT devices operate at a transmission rate of 4.8 Gb/s[20]. Thus the number of GBT links that would be required to read out the whole detector if running at 1 PB/s would be of order of 2×10^6. Just for comparison, the readout system foreseen for the LHCb upgrade will require something like 9×10^3 optical data links, whose cost is estimated to be about 1.5 MCHF.

This highlights the fact that this experiments needs real-time processing of the raw data at the lowest possible level ("on-detector") in order to reduce the data flow, based on more complex data primitives than simple zero-suppressed hits. Also, a new radiation-hard serialiser chip featuring higher bandwidth than the GBT would be needed for data readout from the detector. The serialiser could be driven by a dedicated redundant logic circuitry, implemented on a suitable radiation-hard FPGA. The GBTs could be used to distribute clock signals and fast commands to all sub-detectors. The feasibility of such a new generation of high-speed radiation-hard devices for data transmission needs to be investigated.

Assuming one were able to reduce the aggregate output rate by an order of magnitude, e.g. by means of dedicated on-detector processing, down to, say, 1 Pb/s, the number of data links would still be as high as 2.5×10^5, assuming the same speed of the GBT in reading the data output from the on-detector reconstruction system. Present state-of-the-art FPGAs provide serial I/O link components covering a range between 10 Gb/s to 40 Gb/s. However, commercial-grade FPGAs cannot be exploited for transmission purposes from the detector, considering the failure rates due to both single event effects and total absorption dose. The radiation-hardened FPGAs, which could be used for the implementation of the control logic, are generally equipped with transceivers of limited bandwidth (of the order of few Gb/s). The importance of this issue depends on how far from the detector it will be possible to position

[20]The GBT transmits a 120-bit frame, with 32 bits reserved for the FEC code and 4 for a header. The link efficiency is therefore about 70%.

the real-time reconstruction electronics.

Assuming a device providing a transfer rate of 25 Gb/s per channel could be made available to work in these conditions, then the scale of the DAQ system would be manageable. For an output rate of 1 Pb/s, for the read out it would require order of 4×10^4 data links.

These data streams must enter the real-time analyzer, which identifies the presence of secondary decays of interest, and isolates the specific region in Z along the beam, and the associated tracks of relevance (see next Sections for more details). It is envisioned that the "event size" associated to this partial sampling, will not exceed 10 kB (for comparison, the full raw event size of LHCb is of order 100 kB). This leads to a rate of less than 10 Tb/s, to be transferred to permanent storage, which is less than that envisioned for the LHCb upgrade in 2020. It will therefore be possible to handle it with the same architecture, but with a more modest cost due to Moore's Law gains in the extra 5 years of lead time.

The data streams could be downloaded by plugging the data links directly into a computing farm built of commercial PCs, similarly to what is planned for the LHCb upgrade. The interface to each event-building server (the readout board) would transfer data to the PC's RAM using DMA over PCI express bus. The scale of the event-builder farm can be estimated by knowing the sustainable I/O through a single server. It has been recently demonstrated that a modern PC can safely sustain an input rate of about 100 Gb/s, corresponding to an aggregate I/O data rate of 400 Gb/s, by using two FDR InfiniBand network cards with 4x link aggregation, operating in full duplex mode[21].

The first EDR InfiniBand network cards and switches, with doubled data rates with respect to FDR cards, are now starting to appear on the market. According to the roadmap provided by the InfiniBand Trade Association, the data rate is expected to double again in a few years, with HDR cards, and grow further in the course of 2020's with the NDR cards.

6.8.7 Real-time track and vertex reconstruction at $\mathcal{L} = 10^{35}$

The reconstruction of tracks in real time has been a distinctive feature of the more advanced trigger systems of the pre-LHC generation of experiments. However, the challenges to be overcome for the first LHC run have forced the experiments to concentrate on other aspects of the TDAQ system, most notably increase in dimensions and standardization, and specialized track reconstruction systems have disappeared. Track-based trigger selections in LHC run I have indeed been in use, and in some cases very important, but only after a full offline-like reconstruction of the entire event, occurring at the HLT level.

The development of an experiment capable of flavour data processing in the future high-luminosity LHC runs requires a sophisticated tracking capability at the earliest possible processing level. This trend is already apparent in GP-experiments, and indeed both CMS and ATLAS are performing studies for bringing the track reconstruction from the HLT down to the L1 in the phase-2 upgrade, aimed at LHC phase-2 (from year 2025 on). A vigorous R&D program based on updated and improved Associative Memory ASICs is ongoing already in the INFN CSN1 (within "RD_FASE2") for this purpose, and its results will certainly be an important input in the design of the XFX.

It must however be noted that the requirements of XFX are even harsher than those of the GP experiments. First, a reconstruction of the majority of tracks is required, down to the lowest p_T of interest, and including all charged tracks, not just leptons or pre-determined regions of interest. Second, the reconstruction must be of sufficient quality to allow it to be used for full physics analysis, allowing the raw data to be discarded.

These elements require some additional developments.

A promising line of development is the R&D for a tracking (and vertexing) "vision-like" algorithm

[21] Note that an incoming flux from the detector of 100 Gb/s corresponds to 400 Gb/s, since the event-building implies four data fluxes through a single server.

that is very strongly parallel, and connectivity-based. It relies heavily on the availability of a high internal bandwidth in the new generation of electronic devices developed for the needs of telecommunication industry. and can be implemented in commercial programmable electronics, without the need for custom silicon structures. This new methodology has been demonstrated to provide offline-like performance with very low latency and high throughput, albeit in the specific geometry configuration of LHCb, and is being targeted by a specific R&D in CSN5 ("RETINA").

By extrapolating current studies to 2025, it appears that a combination of the results of the above two lines of research, together with an appropriately designed detector geometry, will be able to provide the necessary performance for the XFX both in terms of throughput and track quality, provided sufficient resources are devoted to this specific goal.

The recent arrival on the market of more advanced, 3D silicon structures, is likely to positively affect the above lines of development, strongly increasing the potential performance that can be obtained.

Regarding vertexing, a second level of processing based on the same parallel processing approaches is expected to be doable, and less resource-demanding than the tracking process. Following the approach outlined above, the reconstructed tracks will be sorted according to the Z-position of closest approach to the beam, and delivered to identical, but independent parallel processors, each dedicated to a specific Z-slice. In this way, secondary vertex finding can be performed in parallel in each slice, decays of interest identified, and only the selected slice of information transmitted to the further levels of processing/storage. Each slice will therefore have a manageable rate, and produce independent "partial events" of about 10 kB size.

6.8.8 Analysis Model

The huge size of data samples involved and the required level of precision mean that an extreme flavour experiment requires a different model of data analysis from the traditional paradigm in use in HEP.

It will likely still be possible to use the traditional method for rare processes, and in any case it will be necessary for the initial stage, and for some "control and calibration samples" that will be necessary to support the measurements made on the main samples. But the high-statistics samples at regime will require a different methodology from the usual sequence of "trigger, storage, calibration, offline analysis".

First of all, there is no way to store the entire event information for so many events—and it is not even necessary. Most of the event information is about other primary vertexes, and has no relevance for the interaction being selected—most of the time, just a single secondary weak vertex is the relevant information. While identifying a single vertex may be complicated, the strategy outlined in the previous Section, selecting only a specific Z region, is an easy way to identify a small sub-sample of relevant information within the collision data. In this way, a quantity of data of $O(10kB)$ can be extracted from each event, containing the relevant information for the decay of interest. Even so, for the highest statistic samples, this may imply something of the order of 1 EB of data to be stored (and analyzed) each year.

It will be important to explore the possibility of performing analysis via data summaries, that is, data structures that do not scale linearly with the number of candidates, such as simple histograms, or more sophisticated data structures.

Another important issue is how to perform the necessary detector calibrations. In this experiment, there is no way to redo the calibrations from the main data sample off-line, so there is a need for a different approach that can still guarantee the needed high precision. This can in principle be achieved in two ways: 1) by dedicated calibration samples, collected in parallel with physics data; 2) by building a real-time calibration system inside the DAQ system itself. The second way is possibly harder, but certainly more in line with the general philosophy of the approach, more general, and promises a much higher level of precision because it has access to many orders of magnitudes more data than what is permanently stored. The availability of detector-embedded track reconstruction, and the continuing improvement in

CPU computing power per unit cost, are crucial assets for this purpose.

In order to advance the design of an extreme flavour experiment, it will be crucial to perform the studies needed to demonstrate that a system for high-precision calibration in real time is indeed possible, and has the reliability required of a system for which there is no way to perform a second pass. If the calibration for a certain quantity of data is diagnosed to be defective, there is probably no way to recover, and that data will simply have to be discarded.

A natural handle to help achieve this goal comes from having built an on-detector reconstruction system, that will naturally have a strongly parallel architecture and large distributed computing power. This opens the door to designing an embedded calibration system, that makes extensive use of local information to determine the needed constants, and performs corrections on the fly.

A substantial development effort will be needed to produce a detailed design. The availability of large samples of data from past LHC data taking runs may be of great help in this process, allowing to perform extensive realistic tests.

Finally, we will have to discuss systematics control, and evaluation.

6.9 Flavour Physics: Summary and Outlook

Flavour physics has played a key role in the development of our knowledge of fundamental interactions, leading to several remarkable "New Physics" predictions, ranging from the existence of the charm quark to the presence of a third generation of quarks, as well as to very stringent constraints on new interactions, at the level of 10^5 TeV for $\mathcal{O}(1)$ New Physics (NP) flavour couplings. It is therefore of fundamental importance for the future development of the field of elementary particle physics to continue improving the theoretical and experimental tools needed to study flavour physics. These improvements should guarantee the achievement of a twofold goal: on one hand, increasing the reach of indirect searches for new physics, in order to be able to probe higher scales in the event that no NP is discovered by direct detection; on the other hand, providing a precise determination of the NP Lagrangian if any new particle is produced in direct search experiments.

From a theoretical point of view, particle physics is confronted with what can be called the "flavour paradox". On one side, the Higgs discovery and the related measurements are showing the physical reality of the relation $m_i = \lambda_i v$ between the fermion masses and their couplings to the Higgs boson. On the other side we have no clue whatsoever on the pattern of the λ_i themselves. The consideration of this "paradox" makes the program of testing BSM contributions to the CKM picture from the $20-30\%$ level, as it is now, down to $1-0.1\%$ precision a fundamental goal of all particle physics. This goal might be achieved in the next 10-15 years if appropriate steps are taken to put together a comprehensive program of flavour physics experiments and theory.

Considering the goals outlined above, the flavour physics What Next GdL has investigated future theoretical and experimental prospects, with particular emphasis on new experimental ideas that could represent a breakthrough in the development of this field, and in which INFN could play a key role.

- **Kaon Physics** In the very near future, the NA62 and KOTO experiments are expected to probe NP through the $K^+ \to \pi^+\nu\bar{\nu}$ and $K_L \to \pi^0\nu\bar{\nu}$ decays respectively. The expected data samples for the two experiments correspond to $\sim$ 100 events for the charged kaon decay and to a few events for the neutral kaon. While these results will already considerably improve our knowledge of the effective $\bar{s}d\nu\bar{\nu}$ interaction, the ultimate experimental goal should be a precise measurement of BR$(K_L \to \pi^0\nu\bar{\nu})$, since the theoretical uncertainty in this mode is much smaller than the one for the charged kaon decay. This goal might be achieved either by an upgrade of the KOTO experiment or by a K_L experiment based on the NA62 infrastructure at CERN. In both cases, one aims at obtaining a sample of $\sim$ 100 SM events. It is worth mentioning that even LHCb or an extreme flavour experiment (see below) could contribute to experimental progress in K physics by providing precise measurements of rare K_S decays.
- **Charm physics** Given the very small rate of CP violation in charm mixing expected in the SM, the recent experimental improvements in the measurement of mixing-related observables has lead the NP-constraining power of charm physics very close to the one of kaon physics. Belle II and LHCb upgrade will provide more precise data, probing CP violation in charm mixing to the degree level. SM theoretical uncertainties might start playing a role at this level of accuracy, and new ideas are being put forward on how to reduce them with data-driven methods. More precise experimental data, as well as data-driven theoretical improvements, will shed light on the amount of CP violation in singly Cabibbo-suppressed D decays and on its compatibility with the SM. Improved data on very rare decays will probe NP contributions that might produce large enhancements of the very suppressed SM short-distance contributions. A further order-of-magnitude experimental improvement of several key observables might come from an extreme flavour experiment (see below).
- B **physics, CP violation and the Unitarity triangle** The next decade will witness substantial improvements in the study of B physics, both from the experimental point of view (with Belle-II and the LHCb upgrade) and from the theoretical one (with the expected progress in Lattice

calculations of matrix elements and with the calculation of higher-order corrections to several interesting observables). With these improvements, a determination of the CKM parameters with 1% accuracy will become feasible, as well as an improvement of the bounds on NP contributions and a clarification of a few tensions between theory and experiment, in particular in rare $B_{(s)}$ decays.

– **flavour and CP violation in the lepton sector** Searching for flavour- and CP-violating processes involving charged leptons is an excellent probe of NP, since an observation of these processes would constitute a clean signal of NP. The complementarity of measurements of τ and μ FCNC transitions in decays to different final states and in conversions calls for an experimental improvement in all sectors. While Belle II, the MEG upgrade, Mu2e and COMET will be the players in the next decade, it is certainly worth exploring the possibility of further improvements by new techniques. Concerning CP violation, the feasibility study of a magic ring for electrons could open up the interesting possibility of performing electron EDM measurements at accelerators.

– **an extreme flavour experiment** In order to push to the extreme the intensity frontier, the very interesting possibility of exploiting the full luminosity provided by the HL-LHC (or by any future hadron collider) for flavour physics has been considered. This poses severe experimental and theoretical challenges: can a sample of 10^{14} bottom and 10^{15} charm mesons be fully exploited? Can theoretical uncertainties be kept below the projected experimental ones for a large number of interesting observables? While a full answer to these questions requires a much more detailed study than what was possibly achievable in the What Next WG, at present the necessary technical developments do not seem unfeasible. From the experimental point of view, storing and processing such data samples is a huge technological challenge, even if projected a decade into the future, thus requiring a paradigm shift by which data analysis will be performed in real time, rather than off-line. A detector with strong tracking capability at high luminosity seems technologically within reach, while a readout at 40MHz will be doable thanks to the foreseen progress of telecom technology. Specialized processors are needed to perform real-time event reconstruction and get tracks and other complex primitives straight out of the detector. The expected progress in CPU processing power would allow offline-grade reconstruction and calibration in real-time. Physics analysis *in real time* requires the ability to do precision measurements from reduced-size stored samples, the need to overcome the *event* concept by saving statistical summaries only, the usage of well-chosen control samples and special methods to control systematic effects. The resulting physics potential is impressive, leading to a determination of the angles of the unitarity triangle at the 0.1° level and of the CKM parameters at the 0.1% level, corresponding for example to a theoretical uncertainty on $BR(B_d \to \mu^+\mu^-)/BR(B_s \to \mu^+\mu^-)$ below 2%, to be compared with the expected experimental uncertainty of $\sim 4\%$; CP violation in charm mixing will be probed at the 0.1° level, comparable to the expected SM uncertainty. These are just a few examples of an extremely rich physics program that is still under investigation.

7 Hadron Physics and non-perturbative QCD

7.1 Introduction

There is overwhelming theoretical and experimental evidence that QCD is the theory of strong interactions. Yet, QCD is to a large extent unsolved. In particular, standard perturbation theory becomes completely unreliable in the infrared regime, where QCD is strongly coupled. Experimentally, there is a large number of facts that lack a detailed qualitative and quantitative explanation.

The most spectacular manifestation of our lack of theoretical understanding of QCD is the failure to observe the elementary degrees of freedom, quarks and gluons, as free asymptotic states (color confinement) and the occurrence, instead, of families of massive mesons and baryons (hadrons) that form approximately linear Regge trajectories in the mass squared. The internal, partonic structure of hadrons, and nucleons in particular, is still largely mysterious. Since protons and neutrons form almost all the visible matter of the Universe, it is of basic importance to explore their static and dynamical properties in terms of quarks and gluons interacting according to QCD dynamics. All issues discussed in this Chapter share this common motivation.

Several theoretical models have been developed through the years to describe the hadronic interactions starting from very basic principles. QCD has a remarkable success in describing the high energy and large momentum transfer processes, where the quarks in the hadrons behave, to some extent, as free particles and a perturbative approach can therefore be used. In this simple approach a fast moving nucleon is essentially considered as a collection of free partons, all moving parallel to the parent nucleon (collinear configuration). Nevertheless, the largest fraction of hadronic interactions involve low momentum transfer processes in which the effective strong coupling constant is large and a description with a perturbative approach is not adequate. Even at large momentum transfer, the simple collinear picture is not supported by experiments and fails badly in explaining many spin-dependent effects.

In most interactions involving hadrons, the dynamical properties and degrees of freedom of quarks and gluons combine with some non-perturbative QCD aspects, to give measured physical quantities. The description of the attempts to understand such processes is the purpose of the “Hadron physics and non-perturbative QCD" Chapter, which is then structured into several main issues, according to the following scheme.

In Section **7.2** a concise description of the theoretical framework underlying the non-perturbative approach to QCD is presented. Some of the issues are mentioned for consistency, although they will not be further discussed in the following Sections.

In Section **7.3** the most recent progress on the study, both theoretical and experimental, of the nucleon partonic structure is presented. Particular emphasis is given to the 3-dimensional structure, both in momentum and coordinate space: it represents a new phase in our image of the nucleon, which goes beyond the traditional and simple 1-dimensional picture of a fast moving nucleon as a bunch of collinearly moving partons.

Section **7.4** reports on hadron spectroscopy, which looks at the total quantum numbers of bound states of quarks and gluons. It shows that more and more precise experimental data are not yet well understood, while more unconventional, although possible, bound states are still not observed.

Section **7.5** deals with the study of the proton–proton total and elastic cross sections, and of the diffractive dissociation processes; these are of fundamental importance to understand the mechanisms of hadronic interactions and their evolution with respect to the center of mass energy and momentum transfer. The dynamical QCD properties of partons become crucial when processes involving hadrons at large energies take place and the role of multi parton interactions, rather than a single elementary interaction, has to be explored and understood. The latter issue is discussed in Section **7.6**.

A precise knowledge of the cross sections and of the properties of particle production in hadronic collisions is crucial in order to reduce the systematic errors in several measurements of great astrophysical interest. This issue is discussed in Section **7.7**.

For each of the above topics the prospects for new measurements at existing and future experimental facilities are considered and discussed. Emphasis is given to the phenomenological aspects of QCD and its application, to the understanding of the hadronic structure and its non-perturbative features and to the related experiments. An executive summary is given in Section **7.8**.

7.2 Confinement and non-perturbative QCD

The first challenge for any theoretical understanding of QCD is to describe the mechanism underlying color confinement and to reproduce qualitatively and quantitatively the spectrum of mesons and baryons, as opposed to the spectrum of quarks and of massless gluons that occur in perturbation theory. One would also like to take properly into account non-perturbative contributions to various Standard Model amplitudes and to predict the properties of strong interactions in extreme conditions, such as high temperature and density, i.e. to map the QCD phase diagram.

In absence of a systematic perturbative approach, a theoretical tool based on first principles is provided by lattice QCD simulations [735]. The theory, in its path integral formulation, is discretised on a space-time lattice and then computed numerically via Monte-Carlo algorithms. Nowadays, thanks to technological and theoretical advancements, lattice QCD is a mature field, which, however, requires a continuous effort to sustain the computational requirements and the algorithmic developments.

Another promising theoretical tool is large-N QCD [736], that allows us to describe QCD as a theory of an infinite number of mesons and glueballs weakly-coupled at all energy scales, as opposed to quarks and gluons that occur in perturbation theory.

Both large-N and lattice QCD predict the existence of glueballs, experimentally not clearly identified yet. Spectral properties are particularly accessible to lattice simulations: the accuracy for glueball and meson masses in QCD with physical quark masses [737] or in large-N computations [738–740] are not presently satisfactory yet, but it is conceivable that the accuracy will improve over the next 10 years. The systematic search for glueballs, and more generally of mesons and baryons, is one of the experimental challenges in the near future, in the reach of dedicated experiments such as BESIII (Beijing) and JLab (Newport News). Other experimental facilities able to explore the glueball and hadron spectrum are COMPASS, J-PARC (Japan), LHCb (CERN), and FAIR (Darmstadt) (to start in 2018).

On the theoretical side, recent developments go in the direction of the computation of the large-N QCD S-matrix [741], which is likely to remain inaccessible to Lattice QCD except for some interesting special cases [742]. This opens the way to a direct comparison with data provided by past (BaBar) and future experiments, such as FAIR (Darmstadt 2018) and JLab about meson form factors.

Moreover, glueball production, together with other interesting non-perturbative aspects of QCD are in the experimental reach of diffractive phenomenology, like high-energy p-p exclusive forward scattering, that allows to get a very accurate measure of the much smaller energy and momentum of the resonances produced in the central region (see Section 7.5.3). It is indubitable that this is a field where high precision experimental measurements can meet theoretical predictions from the lattice or from large-N QCD and possibly lead to a better understanding of strong interactions.

Another interesting experimental direction is the exploration of the QCD phase diagram by heavy-ion collision experiments, in particular regarding the detection of the transition to a Quark-Gluon Plasma phase, that may allow a comparison with lattice measurements. One should stress the investigation of collective and transport properties of the strongly coupled medium produced in such collisions, the search for a possible critical endpoint in the phase diagram at high baryon density and the possible rich phenomenology of strong interactions in the presence of strong magnetic fields [743], which are expected in the early stages of non-central heavy ion collisions. All that is relevant to many experiments at LHC (ALICE, ATLAS, CMS), at RHIC and FAIR. Lattice simulations are already providing precision results regarding QCD thermodynamics with and without external background fields, while new algorithms are needed to properly deal with the complex nature of the path integral measure in the presence of a finite

baryon density. The achievement of accurate results on transport properties is less trivial, since lattice simulations deal intrinsically with equilibrium physics.

There is one final issue, somehow at the intersection between the understanding of QCD and the search for new physics, that involves the computation of the QCD corrections to the muon anomalous magnetic moment, that is likely to be affected both by theoretical developments in computation of light-by-light scattering [741, 744] and by direct experimental measures of the relevant form factors [744].

7.3 The nucleon structure

From the perspective of hadron physics the main new recent interest in the nucleon structure is focused on its 3-dimensional partonic configuration, describing the spatial distribution and the intrinsic motion of quarks and gluons inside protons and neutrons. However, the usual integrated partonic distributions, depending only on the longitudinal momentum fraction of the parent nucleon carried by the parton, play a crucial role in many high energy processes and still have large uncertainties which affect the theoretical calculations. A short assessment of the actual situation is given as a starting point.

7.3.1 Parton distribution functions

Parton distribution functions, henceforth referred to as PDFs, are an essential ingredient of any computation of cross sections at hadron colliders, based on QCD [745]. According to the collinear factorisation of the cross section into short- and long-distance components, delimited by a factorization scale μ_F, the cross section for the production of a final state X in the hard scattering initiated by two hadrons h and h', with four-momenta P and P' and squared center-of-mass energy $s = (P + P')^2$, can be expressed as the convolution of PDFs and parton cross sections:

$$\sigma_{hh' \to X} = \sum_{i,j} \int_0^1 \mathrm{d}x_1 \, \mathrm{d}x_2 \, f_i^h(x_1, \mu_F^2) \, f_j^{h'}(x_2, \mu_F^2) \times \hat{\sigma}_{ij \to X}(x_1, x_2, s, \alpha_s(\mu_R^2)) \tag{50}$$

where f_i^h are the PDFs for the hadron h, the indices i, j run over all parton types, $\hat{\sigma}_{ij \to X}$ is the parton cross section for incoming partons with momenta $p_1 = x_1 P$ and $p_2 = x_2 P'$, and $\alpha_s(\mu_R^2)$ is the strong-coupling constant evaluated at the renormalisation scale μ_R.

Once the functional form of a PDF at a given starting scale Q_0^2 is fixed, its evolution at any given scale $Q^2 > Q_0^2$ can be described in perturbative QCD with the Dokshitzer, Gribov, Lipatov, Altarelli and Parisi (DGLAP) equations [746–748]. The PDF at the starting scale Q_0^2 needs to be determined from fits to experimental data. In the current determination of PDFs from the global QCD analysis of experimental data [749–753], measurements of deep inelastic scattering (DIS, $\ell N \to \ell X$) at lepton-nucleon colliders provide crucial information. Additional constraints are provided by fixed target experiments, neutrino data, and data from proton-antiproton and proton-proton collisions.

A precise knowledge of the PDFs is a fundamental prerequisite for the physics program at hadron colliders, including the measurement of cross sections, the determination of the fundamental parameters of the SM, and the search for physics beyond the SM. In Run II of the LHC collider, several fundamental measurements, including Higgs boson production via gluon-fusion processes, the measurement of the mass of the W boson, and the extraction of the weak-mixing angle from the Z boson forward-backward asymmetry, are likely to be dominated by the PDFs uncertainty, as discussed in Section 4.2.1 and Appendix A.1. Therefore, it is of fundamental importance to invest effort on both experimental and theoretical aspects of the PDFs determination.

Moderate discrepancies, at the level of one to two standard deviations, are observed in the comparison of predicted cross sections for the production of Higgs bosons at the LHC, based on different PDF sets [754, 755]. Since the origin of such differences in the Higgs prediction between the various PDF sets is not yet understood, it should be considered as an additional PDF uncertainty, according to the

PDF4LHC convention [756]. The total PDF uncertainty on gluon-fusion Higgs production cross section in proton-proton collisions at a center-of-mass energy of 8 TeV and 14 TeV is estimated at the level of 5%; if such a PDF uncertainty is not reduced, it will be one of the limiting factors in the accuracy for the determination of the Higgs boson couplings from the LHC data.

The QCD analysis of the full LHC data set collected in Run I, and of the future Run II measurements, will provide further constraints on the extraction of the PDFs, and significant reduction of the PDF uncertainties. However, a much improved determination of the PDFs can be achieved by measurements of DIS in $e\,p$ collisions at higher energies and higher luminosities, as those achievable by the LHeC collider [97].

7.3.2 The 3-dimensional picture of the nucleon: theory

For sufficiently inclusive processes, at leading order, the PDFs describe a fast-moving hadron as a collection of fast-moving collinear partons, each one sharing a fraction x of the parent hadron momentum. Many past experiments on DIS of lepton beams off nucleons exposed how partons share this momentum [749–753]. However, this one-dimensional view provides only limited information on the nucleon structure. For example, it does not answer the question of how partons share the nucleon's spin. Worldwide experimental measurements in the last two decades have shown that the spin of quarks and antiquarks contribute about 30% to the nucleon spin, and that the total spin carried by the gluons is non-zero but not sufficient to account for the missing 70% [757]. Therefore, the orbital angular momentum (OAM) of partons needs also to be addressed; understanding (and estimating) this contribution requires a description of the nucleon structure that goes beyond a simple one-dimensional view [758–760].

The most direct generalisation of PDFs is a new class of objects denoted as Transverse Momentum Dependent PDFs (TMD PDFs; for brevity, TMDs), that describe the joint distributions in x and in the parton transverse momentum $\boldsymbol{k}_\perp$ (transverse with respect to the parent nucleon's momentum) [761–765]. A similar generalisation holds for the fragmentation functions (TMD FFs). The TMDs are encoded in the cross section for semi-inclusive DIS (SIDIS, $\ell\,N \to \ell\,h\,X$) [765]. SIDIS has two natural scales: the lepton large momentum transfer, Q, and the transverse momentum, P_T, of the final hadron. If $P_T \ll Q$, a suitable factorisation theorem allows to isolate TMDs in the SIDIS cross section [766–768], which can be expressed as a convolutions of TMDs and perturbative elementary interactions: thus, measuring the $\boldsymbol{P}_T$ distribution reveals details of the transverse motion of the initial parton inside the target.

At leading twist, eight independent TMDs can be defined, each one appearing in a specific SIDIS (spin) asymmetry with its own peculiar dependence on the nucleon transverse spin and final hadron angles [765]. Three of them survive after integrating upon the parton $\boldsymbol{k}_\perp$, recovering the three collinear PDFs that are needed to describe the spin structure of a fast-moving nucleon in the collinear framework: the unpolarised, the helicity, and the transverse polarisation (transversity) distributions. The transversity distribution is the least known of the three, although it has been shown to be different from zero in a series of SIDIS measurements by HERMES [769] and COMPASS [770–772]. It is related to the tensor charge of the nucleon and its difference from the helicity distribution quantifies the relativistic effects in the hadronic structure. Among the other five TMDs, two of them have received particular attention since they depend on fundamental properties of QCD such as its color gauge invariance. For example, the so-called Sivers function [773] describes how the $\boldsymbol{k}_\perp$ distribution of an unpolarised quark is distorted by the transverse polarisation, $\boldsymbol{S}_T$, of its parent nucleon. As a consequence, in a SIDIS process off a transversely polarised nucleon, the $\boldsymbol{P}_T$ distribution of the final detected hadron is asymmetric with respect to flipping $\boldsymbol{S}_T$. The Sivers effect is thought to arise due to the residual color interactions between the struck parton and the target remnants [774–776]. It can happen also in Drell-Yan processes with a transversely polarised nucleon. In this case, however, the color gauge invariance is realised through initial state interactions between the nucleon's annihilating quark and the remnants of the other colliding hadron [777]. The net result is that the Sivers effect would have an opposite sign in Drell-Yan with respect to SIDIS [778,779]. This process dependence (or non-universality) of the Sivers function is a fun-

damental prediction based on the color gauge invariance of QCD. Therefore, an experimental verification of this sign change is of crucial importance in hadronic spin physics and is currently under investigation by the COMPASS collaboration, using for the first time a high energy beam of pions scattering off a transversely polarised fixed nucleon target [780].

Experimental evidence of the Sivers effect in SIDIS, and of different "QCD spin-orbit" effects involving other TMDs, will be described in the next subsection, together with an account of running and planned dedicated future experiments.

In this new scenario, multi-dimensional imaging of hadrons can be alternatively approached through hard exclusive processes like Deeply-Virtual Compton Scattering (DVCS, $\ell N \to \ell N \gamma$) [781]. For a lepton momentum transfer Q^2 much larger than the squared change in the nucleon target momentum [$Q^2 \gg -t = -(P - P')^2$], the so called Generalised Parton Distributions (GPDs) can be factorised in the cross section [781, 782]. They depend on t, x, and on the change ξ in the longitudinal parton momentum. For $\xi = 0$, the two-dimensional Fourier transform of the t dependence converts the GPDs into a spatial distribution of partons in the transverse plane at a given x [783, 784]. This may be regarded as a tomography of the nucleon, where two-dimensional spatial images are taken for different "slices" of the parton momentum x. Thus, the GPDs encompass in a unique framework the information on spatial densities (form factors) and on longitudinal momentum densities (PDFs).

For DVCS on a transversely polarised nucleon, the nucleon helicity-flip GPD E describes a distorted spatial distribution. It is the analogue in position space of the Sivers effect [785]. Indeed, a dynamical connection between the two phenomena can be formulated, although in a model dependent way since it is based on the non-perturbative description of color interactions between struck and spectator partons [786]. The GPD E is linked to the problem of calculating the parton OAM [787]. In fact, both the GPD E and its nucleon helicity-non-flipping partner H enter the so-called Ji's sum rule [788], where in the forward limit ($\xi = 0, t = 0$) the sum of their second Mellin moments gives the total angular momentum carried by partons. However, separating for each flavour the orbital contribution from the helicity is still a matter of debate, because it involves several conceptual aspects at the core of non-abelian gauge theories (for a recent review, see Ref. [789] and references therein).

A direct experimental access to the whole kinematic dependence of GPDs is not possible: the x dependence is integrated over in the scattering amplitude. To unravel GPDs requires dedicated, long-term measurements of a variety of observables like cross sections, beam and target spin asymmetries for both longitudinally and transversely polarised targets, as well as using different channels [790, 791]. Factorisation theorems for GPDs exist not only for DVCS but also, *e.g.*, for Deeply-Virtual Meson Production (DVMP, $\ell N \to \ell N M$) [792]. While DVCS or DVMP for neutral vector mesons involve GPDs of gluons or of sea quarks in particular flavour combinations [793], the DVMP for pseudoscalar mesons provides access to different flavour combinations of GPDs for longitudinally polarised quarks and anti-quarks [794].

We remark that TMDs and GPDs give independent and complementary information on the dynamics of partons confined inside hadrons. In fact, the spatial distributions obtained from GPDs are not correlated to the momentum distributions from TMDs [764]. While from GPDs we get "spatial" tomographies of the nucleon, from TMDs we can get independent "momentum" tomographies. Combining the two pictures will represent a new landmark in the process of understanding QCD confinement.

7.3.3 The 3-dimensional picture of the nucleon: experiments

As described in the previous subsections Deep Inelastic Scattering experiments provide the standard tool to investigate the structure of the nucleon. More recently, the importance of semi-inclusive DIS (SIDIS) experiments, that is DIS experiments in which at least one hadron from the current jet is detected, has increased considerably, in particular to obtain information on the new Transverse Momentum Dependent partonic distributions (TMD PDFs). In SIDIS the investigations of TMDs cannot be decoupled from the

measurements of the fragmentation functions, which also may depend on the transverse motion of the final hadron with respect to the fragmenting parton (TMD FFs). Then, complementary information must be gathered from e^+e^- and $p\,p$ colliders.

DIS and SIDIS experiments are being performed at CERN (COMPASS) and at JLab (CLAS); e^+e^- data have been collected at SLAC (BaBar) and KEK (Belle), while polarised $p\,p$ processes are studied at BNL (RHIC). Several important conclusions may be drawn from a huge amount of activities over the past 20 years:

- The decomposition of the spin of the nucleon in terms of its constituent partons is a highly non-trivial theoretical problem, still unsettled to-day
- The spin of the constituent partons cannot account for the whole nucleon spin; there must be a sizeable contribution from the orbital angular momentum (OAM) of the partons, still unmeasured and still incalculable.
- The standard (collinear) QCD description of a nucleon in terms of two PDFs, $f_1(x)$ and $g_1(x)$, has to be complemented by a third function, the so-called transversity distributions, $h_1(x)$ [795]. The measurements of HERMES and COMPASSS [769–772] have shown that h_1 is different from zero. First extractions of transversity from SIDIS and e^+e^- data have already been performed [796–801].
- The discovery of h_1 is not the only consequence of a renewed attention to transverse spin effects: the description of the nucleon in terms of 1-D PDFs has been generalised to include two more dimensions, defined either by the parton intrinsic momentum $\boldsymbol{k}_\perp$ (in momentum space) or by the impact parameter $\boldsymbol{b}_T$ (in coordinate space). In the first case one talks of TMDs, in the second of Generalized Parton Distributions (GPDs).
- The TMDs and the GPDs give a 3-D image of the nucleon which is much more detailed than the 1-D image given by the three collinear PDFs. Most important, they provide tools to access the missing contribution to the nucleon spin, namely the parton OAMs.

As described above, to access information on the TMDs one needs to perform SIDIS experiments; a complete 3-D description of the nucleon requires, at leading-twist, the knowledge of 8 TMD PDFs. So far the most important results have been obtained by the HERMES and COMPASS Collaborations by scattering high energy leptons off transversely polarised nucleons; such results regard essentially the Sivers function which has definitely been shown to be different from zero [802–804]. This TMD is particularly important because it quantifies a correlation between the intrinsic quark momentum and the spin of a transversely polarised nucleon and, due to parity invariance, must be related to the parton orbital angular momentum. The $\boldsymbol{P}_T$ dependence of the final hadron, as measured in the unpolarised cross sections or multiplicities [805, 806], has given information on the unpolarised TMD and demands the presence of the quark intrinsic motion, with a $\boldsymbol{k}_\perp$ dependence which seems to be well described by Gaussian distributions [807].

So far, some knowledge has been obtained on the unpolarised distribution $f_1(x, \boldsymbol{k}_\perp)$, the helicity distribution $g_1(x, \boldsymbol{k}_\perp)$, the transversity distribution $h_1(x, \boldsymbol{k}_\perp)$ and the Sivers distribution $f_1^\perp(x, \boldsymbol{k}_\perp)$, while the other four are essentially unknown. In particular very little is known on the so-called Boer-Mulders TMD, which gives the interesting correlation between the quark's transverse motion and its spin, which, again, must involve the quark orbital angular momentum. A non-vanishing Boer-Mulders function would allow subtle spin effects even in processes involving unpolarised protons, which seems to be the case with the azimuthal dependence measured in Drell-Yan processes.

In the TMD sector basically all the existing information has come from the HERMES and COMPASS Collaborations, but HERMES has now stopped operating and in the near future of COMPASS only SIDIS measurements on a liquid hydrogen target [780] are foreseen, in the years 2016 and 2017, which hopefully will provide information on the Boer-Mulders function. On the contrary, JLab experiments at the upgraded energy of 12 GeV (JLab 12) should provide a wealth of SIDIS data on transversely

polarised targets, albeit at lower energy, *i.e.* mainly at large x values [808].

It should be added that the investigation of transverse spin effects and the introduction of TMDs has finally allowed an understanding of the huge and mysterious single spin effects known for decades and measured in proton-proton interactions over a very large energy range [809].

Turning to the 3-D picture of the nucleon in coordinate space, as stated above, the GPDs encode such information. The GPDs can be extracted from measurements of exclusive reactions, like deeply virtual Compton scattering (DVCS) or deeply virtual meson production (DVMP), in which a high energy lepton scatters off a nucleon and the final state consists of only the scattered lepton, the nucleon and a photon or a produced meson. The extraction of GPDs from experimental results needs a large amount of data on hard exclusive processes over a broad kinematic range. So far information in the high energy regime at low x was provided by H1 [810, 811] and ZEUS [812] at DESY and, in the low energy regime at high x by HERMES [813] and JLab [814]. The COMPASS measurements will provide a connection between these measurements by covering the kinematic regime of $x \simeq 0.1$, where both sea and valence quarks are equally important. Some DVMP measurements have already been performed by COMPASS [815] on a transversely polarised proton target, in parallel to the transverse single spin effects in SIDIS, and future measurements of DVCS and DVMP on a liquid hydrogen target [780] are already planned for the years 2016 and 2017. On a longer time scale, measurements of DVCS on a transversely polarised proton target are also planned, to access the GPD E and possibly exploit Ji's sum rule to get the total angular momentum of a quark inside a polarised nucleon. Very much as for the SIDIS measurement, JLab 12 will be a major player in this field in the next decade, in the complementary large x-value range.

On the horizon, the best facility to pursue the investigation of the spin structure of the nucleon is a polarised electron–polarised proton (or ion) collider (EIC). An international study group has been working for at least 10 years on two parallel projects [816]; one to be realised at Brookhaven National Laboratory (BNL), which would exploit the existing high energy (up to 250 GeV) polarised proton beam of RHIC, adding an electron machine, and one to be realised at JLab, which would exploit the 12 GeV polarised electron beam, adding a polarised proton machine. Both proposals are attractive, in both cases there are several options with different values of the center of mass energy ($\sqrt{s}$ = 45–175 GeV for BNL, 12–140 GeV for JLab), and most likely the decision of which one (if any) to choose will be a political one. The scientific programme is impressive and one indeed expects that a 3-D imaging of the nucleon could be achieved. The spin program will not be the only goal of the project: the exploration of the gluon content of the nucleon, the assessment of the conditions which lead to the saturation of the gluon density and the modifications induced by the nuclear environment are also very important goals. A European team has tried to see whether a polarized electron-proton collider could be built at FAIR [817], possibly using for the proton ring the antiproton storage ring HESR foreseen for the PANDA experiment, but the chances of such a project being pushed forward are probably very small. Most recently, a proposal for a similar EIC project in China has been presented [818], which seems to have reached some level of approval and clearly deserves full attention.

From a different perspective, one finds another project of interest for the QCD structure of the nucleon, namely a Large Hadron Electron Collider at CERN (LHeC@CERN) [97]. The project sits at the high energy frontier ($\sqrt{s}$ = 800–1300 GeV), and utilises a high energy proton beam from LHC, colliding with a newly built electron beam of 60 GeV (or possibly 140 GeV). The physics programme complements the LHC and its discovery potential for physics beyond the Standard Model with high precision deep inelastic scattering measurements. The LHeC would continue the path of deep inelastic scattering (DIS) into unknown areas of physics and kinematics. With a design luminosity of 10^{33} cm^{-2} s^{-1} the LHeC is projected to exceed the integrated HERA luminosity by two orders of magnitude, which means that the parton distributions can be determined with unprecedented accuracy. No polarisation of the proton beam is envisaged, thus the issues of the QCD spin structure of the nucleon cannot be addressed by this machine, whose scopes are clearly different.

7.4 Hadron spectroscopy

Until the end of the previous century, all known hadrons could be described by Quantum Chromodynamics (QCD) as bound states of either a quark and an antiquark (integer spin particles known as "mesons"), or three quarks (half integer spin objects called baryons). In principle, QCD can predict the existence of a larger variety of hadrons, made of two quarks and two antiquarks (tetraquarks or meson molecules), or four quarks and an antiquark (pentaquarks), six quarks (exaquarks), or even no quarks (glueballs). For more than forty years such exotic states have been searched for without success. A notable exception is represented by the long-standing problem of identification of the light scalar mesons, which are hardly explainable as simple $q\bar{q}$ systems, but are more successfully accommodated to form a nonet with inverted mass hierarchy, as suggested in references [819], using the tetraquark model. With the advent of B-factories [820], together with the discovery of many missing pieces of the standard spectra, a plethora of 'exotic' candidates have been claimed by the experiments. Heavy-light diquark-antidiquark mesons have been proposed for the first time in [821] where, together with the interpretation of the X(3872) as a compact tetraquark meson, a complete scheme for the description of similar expected states was proposed. The picture was updated in [822] in view of the most recent experimental findings.

This review will first focus on the relatively simple pattern describing all heavy-light pseudoscalar and vector mesons, and the heavy baryons, whose spectroscopy have benefited not just from B-factories, but also from the Tevatron and LHC in the recent past. Then we will review the recent progress in heavy quarkonium spectroscopy [823], which has experienced a second renaissance [824] in the last decade, with the unexpected discoveries of states above or across open flavour thresholds, which have opened new pathways to the missing narrow states, solving old puzzles, but raising intriguing new questions.

7.4.1 Heavy Mesons and Baryons

In spite of the recent achievements of lattice QCD (summarised in Fig.95) we are still lacking a full understanding of the spectroscopy of light hadrons starting from the QCD Lagrangian [825]. Only 1.2 percent of the nucleon mass (and therefore of the visible mass of the Universe) is due to the Higgs coupling: the hadron masses are mostly due to the dynamics of the strong force.

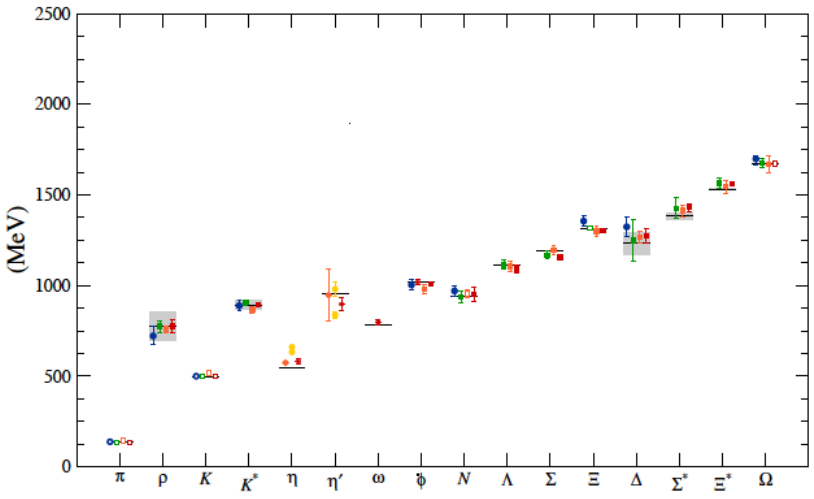

Fig. 95: Summary of most recent lattice results on u,d,s mesons and baryons, from Ref. [826]

The bare masses of the u and d quarks are approximately 3 and 5 MeV, and all the rest comes from the gluonic field which binds together the three quarks in the nucleon, in relativistic motion around the common center of mass. It must be noticed that the mass difference between the down and up quarks

has a crucial role in determining the mass difference between the neutron and the proton: if only QED effects were present, protons would decay to neutrons.

In order to decouple the mass effects from the dynamics of relativistic, non-perturbative QCD, we can study systems with one or more heavy quarks (strange, charm, bottom), and compare them with systems made only of light quarks.

A large contribution to baryon and meson masses comes from spin-dependent forces, which are inversely proportional to quark masses. The large mass difference between the π (135 MeV, quark spin antiparallel to the spin of the antiquark) and the ρ meson (770 MeV, parallel spins), progressively gets smaller when we replace the u, d quarks with s, c, b quarks.

The mass of ground state hadrons can be described quite well by the following formula:

$$M(q\bar{q}; qqq) = \Sigma_i \, m_i + \Sigma_{i>j} \, \frac{\vec{\sigma_i} \cdot \vec{\sigma_j}}{m_i \, m_j} \, v_{ij}^{hyp} \tag{51}$$

where m_i are the so called constituent quark masses, larger than the bare masses, and v_{ij}^{hyp} is a hyperfine interaction with different strengths, but the same flavour dependence. The success of the constituent quark model is not fully understood by theory [827].

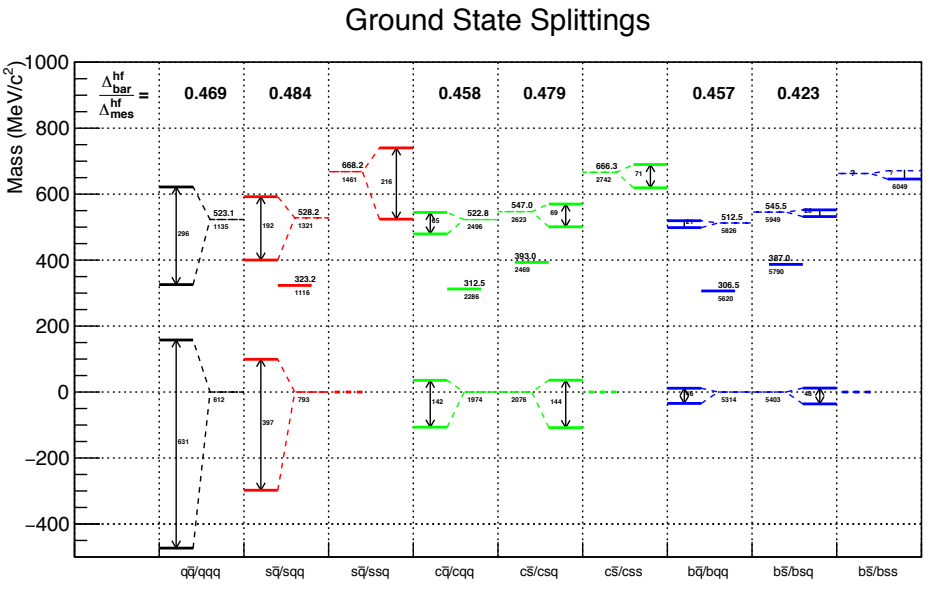

Fig. 96: S-wave meson and baryon mass splittings

Figure 96 summarises the current understanding of most S-wave mesons and baryons. For these hadrons, the measured mass depends only on the mass of the valence quarks and their spin alignment. For baryons, we can sort them assuming that the two lighter quarks are either in a spin singlet state (scalar diquark) or in a spin triplet state (vector diquark). In this second case, the diquark spin can either be antiparallel ($J = 1/2^+$) or parallel ($J = 3/2^+$) to the quark spin. Figure 96 shows baryon-meson mass splittings, calculated relative to the spin-weighted average of the S-wave mesons. A remarkable scale invariance can be observed after averaging out spin effects. HQET predicts that the hyperfine splittings in mesons scale with $1/m_Q$. The same happens with baryons, and the ratio is constant within 10 percent, as we span from strange to bottom [828].

If we average out spin effects, all baryons can be modeled within a few percent as diquark-quark systems. The exchange of a $\bar{u}, \bar{d}$ antiquark with an antisymmetric ud diquark shifts the energy up by about 315 MeV, independent of the heavy quark (s, c, b). This shift is about 75 MeV higher if the light

antiquark is replaced by an antisymmetric sq diquark. If the light antiquark is replaced by a vector diquark, the shift is 520 MeV (547 for a vector qs diquark). The scale independence is even more impressive when a $\bar{s}$ is replaced by a ss diquark: the spin averaged splitting is 668 MeV when the third quark is a u, d type, and 666 when it is a charm quark. In the bottom strange system, the $J^P = 3/2^+$ partner of Ω_b' has not yet been observed, while the Ξ_b' doublet has recently been observed by LHCb [829]. The doubly heavy baryons ccq, bbq have not been observed yet. An early claim by experiment SELEX at Fermilab [830, 831] has not been confirmed by the B factories [832, 833] or hadron [834] colliders. But the search is not over, as suggested by the unexpectedly large rate of production of double charmonium at Belle [835] and Babar [836]. In the coming years, LHCb and Belle-II are likely to discover the doubly heavy baryons.

Both for mesons and baryons, the analysis of P-wave excitation spectra is made difficult by the large width of many states, both in the light and heavy-light systems. The quantum numbers of spin triplet (singlet) P-wave $q\bar{q}$ states are $0, 1, 2^{++}(1^{+-})$. The identification of the multiplet of scalar mesons that can be formed by u, d, s quarks has been a problem for theory since a long time: a recent paper [837] confirms the resonant nature of the broad σ and κ states, that can form a nonet with inverted mass hierarchy, with the $a_0(980)$ and $f_0(980)$ states, as suggested in reference [821], using the tetraquark model.

P-wave D mesons can be modelled by grouping the four state in two doublets, the lightest (heaviest) with the u, d type quark with total angular momentum $j_q = s + l_q = 1/2\ (3/2)$. We expect then two broad states with quantum numbers $J^P = 0^+, 1^+$, and two narrow states with quantum numbers $J^P = 1^+, 2^+$, whose single pion decay to D^* is suppressed by the angular momentum barrier, as the pion is emitted in d-wave. This pattern is observed in the D mesons, but is not observed in the D_s mesons, as the 0^+ and 1^+ members, discovered by Babar [838] and CLEO [839], are below the DK and DK^* thresholds, and their hadronic decay is therefore forbidden. We have then a set of four narrow states. A similar pattern should be observed with B_s mesons.

7.4.2 Heavy Quarkonium: Charmonium, Bottomonium and B_c

In the literature, heavy quarkonia are described as mesons with a $c\bar{c}$, a $b\bar{c}$, or a $b\bar{b}$ pair . While charmonium was discovered in 1974 (the November revolution), and bottomonium in 1977, the discovery of the ground state B_c is quite recent [840], and the study of the spectroscopy of its excited states has just started. Among all mesons, charmonium and bottomonium have the richest spectrum of states.

The known spectrum of charmonium and bottomonium is shown in Fig. 97, in comparison with the D_s and B_s meson spectra. While all S and P-wave states below the open charm threshold have been discovered, the D-wave states are now a very active field of research. The most recent progress in the spectrum of narrow charmonia is the discovery of the long sought $\psi(1^3D_2)$, the $J = 2$ partner of the $\psi(3770)$ in the D-wave triplet, which decays into $\gamma\,\chi_c$, observed by Belle in B decays [841]. This state is very narrow even if it is above the $D\bar{D}$ threshold, as its quantum numbers (2^{--}) forbid its decay to $D\bar{D}$.

The two D-wave states with quantum numbers 2^{-+} and 3^{--} are the last missing pieces of the $c\bar{c}$ spectrum below the open charm threshold.

Besides many states with total widths below 1 MeV, it is quite noticeable to observe that the broadest charmonium state below threshold is actually the η_c(1S), i.e. the ground state of the whole system, which has a total width of (32.2 ± 0.9) MeV [81].

The bottomonium spectrum is shown in Fig. 97: we expect to have 3 S-wave and 3 P-wave multiplets below the open flavour threshold. A major breakthrough in our understanding of bottomonium spectrum occurred in the last decade: all spin singlet states were discovered after 2007, starting from the $\eta_b(1S)$, found by BaBar [842, 843]. In 2010, the simultaneous observation by Belle of $\eta_b(1, 2S)$ [844] and $h_b(1, 2P)$ [845] was made possible only by the experimental observation of a new pathway from

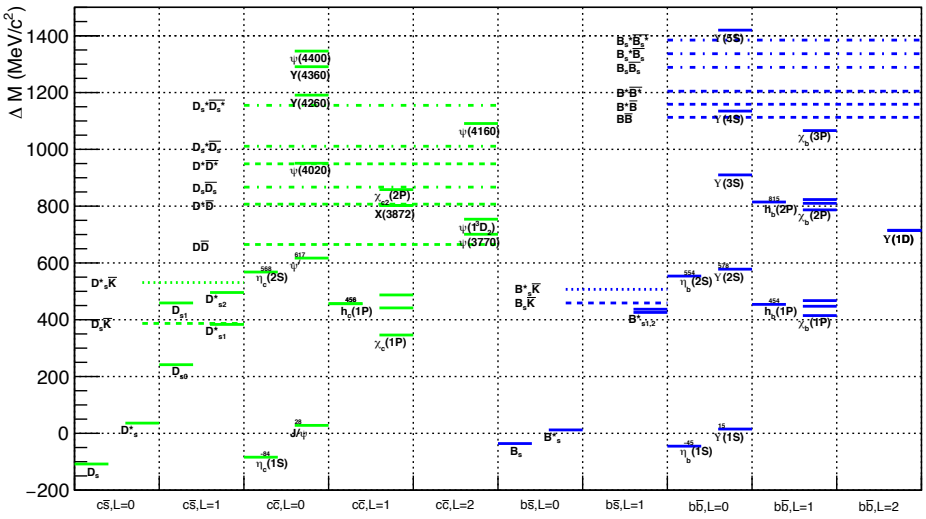

Fig. 97: Spectra of charmonium and bottomonium (S, P, D-wave), compared with D_s and B_s mesons (S, P-wave)

the $\Upsilon(5S)$ state, via two charged bottomonia, which will be described in the next subsection. More recently, Belle discovered that the largest transition from the $\Upsilon(4S)$ to narrow bottomonia is actually an η transition to $h_b(1P)$: this is the first ever observed S-wave η transition, and is by far much stronger than the $\eta\Upsilon(1S)$ and the $\pi\pi\Upsilon(1S)$ transitions. The quantitative understanding of the strength of these transitions remains a challenge for theorists.

After this series of discoveries, we can calculate the hyperfine splittings in bottomonium for $1S, 2S$ and $1P, 2P$ states: the results are summarised in Table 28.

ΔM_{hf}	n=1	n=2
S-wave: $M(\Upsilon) - M(\eta_b)$	62.3 ± 3.2	24 ± 4
P-wave: $M(\chi_{cog}) - M(h_b)$	0.7 ± 1.1	0.2 ± 1.3

Table 28: Hyperfine splittings in bottomonium (MeV).

The P-wave splittings are calculated using $M(\chi_{cog})$, the spin weighted average of the χ_b states, and are consistent with zero, as we expect from the one gluon exchange potential. The S-wave splitting is quite a challenge for theorists. For the ground state, the experimental result is consistent with lattice predictions [846], and in slight tension with the pNRQCD prediction [847].

The hyperfine splitting ratio $r_{hf} = \Delta M_{hf}(2S)/\Delta M_{hf}(1S)$ is 0.412 ± 0.012 in charmonium and 0.38 ± 0.07 in bottomonium. A lattice prediction of $r_{hf}(b\bar{b})$ is consistent with the existing result. We can then compare the spin averaged $1P - 1S$ splitting for $c\bar{c}$ and $b\bar{b}$ and we obtain 457.5 ± 0.3 for charmonium and 453.3 ± 1.3 for bottomonium. Remarkably, also these splittings are independent of the hard scale.

Also in bottomonium the D-wave multiplet is still unresolved, and the spin singlet state $\eta_{b2}(1D)$ has not yet been found. CLEO discovered a mixture of spin triplet $\Upsilon(1D)$ states in 2003 [848], and further confirmations came from Babar and Belle. $\Upsilon(1D)$ can be reached from both $3S$ and $4, 5S$ states. The $\chi_b(3P)$ multiplet was discovered recently by ATLAS [849] and is also being studied by its LHC competitors, CMS and LHCb [850]; the production of $\chi_b(3P)$ in radiative or hadronic transitions from the $\Upsilon(4, 5S)$ is currently being studied by Belle at KEKB.

Many missing states are close to the open bottom thresholds: $\eta_b(3S)$, $h_b(3P)$, all $\Upsilon(2D)$ states, and even the $\Upsilon(1F)$ multiplet, expected around 10350 MeV/c^2.

The last frontier of heavy quarkonium studies is the spectrum of B_c mesons, discovered in 1998 by CDF [840]. More recently, thorough studies on these states are being performed by LHC experiments:

- ATLAS observed a combination of the two S wave radial excitations. In the meantime, the vector B_c^* state, which is dominantly expected to decay to B_c and one $M1$ photon, is still unobserved.
- LHCb has performed state-of-the-art measurements of the mass of the ground state, using a variety of new channels.

The spectrum of excitations of the B_c meson is completely unexplored and it will be a challenging task for the collider experiments at LHC.

7.4.3 Multiquark systems

The discovery of X(3872) in B decays at Belle [851] came quite unexpectedly, and its confirmation by CDF in prompt production at the Tevatron attracted a large amount of theoretical interest on this state. Some authors believe that strong interaction analogs of Van der Waals forces could generate potentials binding hadron molecules. However, several issues about their production mechanism at hadron colliders have been studied [852,853]. After more than a decade from this discovery, we know that the X(3872) has quantum numbers $J^{PC} = 1^{++}$, and its width is narrower than 1.2 MeV, but its nature is still uncertain. It could either be a mixture of a charmonium state (the $\chi_{c1}(2P)$) and a $D\bar{D}^*$ molecule, or a tetraquark.

One year after, Babar observed another exotic state [854] with vector quantum numbers, the $Y(4260)$, decaying to $J/\psi\pi\pi$ in exact correspondence with a steep drop of the $c\bar{c}$ cross section. Soon after, Belle discovered two more vectors at $E_{cm} = 4.36$ and 4.66 GeV, decaying to $\psi'\pi\pi$. Recently, BES-III has reported the observation of radiative transitions between the $Y(4260)$ and the $X(3872)$, a discovery that may hint at a common nature of these two states.

After the discovery of the $Y(4260)$, Belle started a massive campaign of studies to search for the bottomonium counterpart of this state, triggered by the observation of very large yields of dipion transitions to $\Upsilon(1,2,3S)$ from the proximity of the peak of the $\Upsilon(5S)$ resonance. This study yielded the discovery of the two spin singlet P wave states, $h_b(1,2P)$ described in the previous chapter, but, most important, it also represented the first observation of two charged bottomonium states, dubbed $Z_b(10610)$ and $Z_b(10650)$, in close proximity to the $B\bar{B}^*$ and $B^*\bar{B}^*$ thresholds. Charged states were explicitly predicted by compact tetraquark models [855] and have a clear role in the picture proposed in [822]. The discovery of heavy charged multiquark systems has further ignited a renewed theoretical interest in the field of hadron spectroscopy [856, 857].

Soon after, Belle and BES-III discovered the charged charmonium states $Z_c(3900)$ and $Z_c(4020)$, in the proximity of the $D\bar{D}^*$ and $D^*\bar{D}^*$ thresholds. As in the case of the Z_b states, which are reachable via single pion transitions from the $\Upsilon(5S)$, the Z_c states can be reached via single pion transitions from the $Y(4260)$ and the $Y(4360)$. A difference between Z_c's and Z_b's can be found in the decay patterns: While both Z_b's decay with comparable BR's to all 1^{--} and 1^{+-} narrow bottomonia, the $Z_c(3900)$ decays preferentially to $\pi J/\psi$ and the $Z_c(4020)$ prefers $h_c\pi$.

A thorough program of studies is underway at BES-III to investigate the nature of the charged charmonia, and the exotic charmonium-like states. Future prospects of studies at Belle-II will include the search for the doubly charmed meson T_{cc}, with quark content $cc\bar{u}\bar{d}$.

7.4.4 Hybrids

Hybrids, i.e states containing both quark and gluon excitations, have been studied in various models [858–863], but recent lattice simulations [864–869] have generated greater expectations [869]. More-

over, on the experimental side, in recent years (see the previous subsection) several new states, in particular in the charmonium spectrum, have been discovered. These probably include a hybrid resonance, the $Y(4260)$, discovered by Babar [854].

Conventional heavy quarkonia are well described by non-relativistic QCD, so that one can expect that hybrids containing heavy quarks could be treated in a similar way, i.e. by considering gluon excitations in the presence of slow quarks. Moreover, in the physical gauge, the dynamical gluons can be separated from the instantaneous Coulomb-type forces that act between color charges; thus, while the non-abelian Coulomb potential is expected to be responsible for binding and confinement, the remaining, transverse gluon excitations could contribute to the spectrum. In non-relativistic, physical gauge QCD, the lowest mass charmonium hybrid multiplet has been predicted to be composed by the states with quantum numbers $J^{PC} = 1^{--}$; $(0;\, 1;\, 2)^{-+}$ [870]. This four-state hybrid multiplet identified in physical gauge calculations, has been recently identified also in lattice simulations [867–869], both in the heavy [867, 868] and light quark sectors [869]; moreover, it includes an exotic state (a state with exotic quantum numbers) with $J^{PC} = 1^{-+}$.

In the non-relativistic, physical gauge QCD the lowest mass charmonium hybrid multiplet can be explained as due to a color-octet $c\bar{c}$ pair with ${J_q}^{P_q C_q} = 0^{-+}$ or 1^{--} corresponding to the total quark-antiquark spin with $S_q = 0$ and $S_q = 1$, respectively, coupled to a single physical, transverse gluon with predicted quantum numbers $J_g^{P_g C_g} = 1^{+-}$ [870, 871]; the unusual positive parity of the physical gluon originates from the non-abelian nature of the Coulomb interactions as explained in Refs. [870, 871]. It will be important to study both experimentally and theoretically all their possible decays that distinguish them from ordinary quark antiquark states [872].

Meson Spectroscopy is a powerful tool to answer fundamental questions in QCD, like the origin of color confinement and the role of gluons inside hadrons. Mesons are the simplest quark bound system and, therefore, the ideal laboratory to study the strong force at the non-perturbative energy scale of a few GeV. In particular, unconventional mesons would be the best experimental evidence of the active role of gluons in hadron dynamics. In this respect, from an experimental side there will be dedicated experiments at CERN, as well as at Jlab, FAIR, BES and Belle. New high-statistics and precise data need an adequate analysis [872, 873]. Beyond providing a deeper understanding of the inner workings of non-perturbative QCD, theoretical control over hadronic final-state interactions is also essential for the hunt of physics beyond the Standard Model.

7.5 Total, elastic and diffractive cross sections

When two hadrons collide, inelastic processes contribute to around 50% of the cross section. The remaining almost-half of the total cross section is due to elastic (around 25%) and (mainly soft) diffractive processes. The latter ones are characterised by the exchange of a color-singlet object (historically known as Pomeron) resulting in the dissociation of one (single diffraction) or both (double diffraction) of the incoming hadrons, which are scattered at very small angles and carry most of the initial energy. Investigating the region very close to the outgoing beams is therefore mandatory for a measurement of the total cross section and complementary to studying the central region surrounding the collision point.

Because it involves the detection of the elastically or diffractively scattered protons, measurements of the total and of the elastic cross sections, as well as that of diffractive processes, require full rapidity coverage and special engineering solutions to access the primary vacuum of the machine. For the first issue, trackers and calorimeters have to be placed in the "forward" regions surrounding the beam pipe; for the second one, special insertions of the beam pipe (roman pots) are utilised to host detectors to track the scattered protons. At the LHC, only TOTEM and ATLAS-ALFA are at the moment equipped with detectors insertable with roman pots.

In the case of elastic and inelastic interactions, since the cross sections of the involved processes are large, the statistics is usually not a problem. The main uncertainties originate from systematic ef-

fects. For the measurements which require a precise knowledge of the luminosity, the uncertainty on the luminosity itself is the largest error source. It has in fact been proven difficult for the experiments to keep this uncertainty at the level of one percent. Another systematics is related to the incomplete rapidity coverage in the forward region. Usually the experiments are not instrumented at rapidities higher (lower) than about $+5$ (-5), losing the possibility of catching diffractive events at low masses, whose amount has to be extrapolated, introducing therefore a sizeable systematic error. Other systematic effects in the measurement of the elastic and diffractive scattering are related to the machine optics. The kinematics of the scattered protons must in fact be reconstructed from the angle and position of protons which have passed through several machine elements and which are eventually detected in the roman pots, hundreds of meters away from the IP.

7.5.1 Total cross section in pp collisions

The first experimental results on cross sections at hadron colliders date back to the early 1970's with the CERN Intersecting Storage Rings (ISR) which provided $\bar{p}p$ and pp collisions with a center of mass energy of 20 to 50 GeV. During the 1980's and 1990's the experiments at the new accelerators SPS at CERN and Tevatron at Fermilab accumulated data on $\bar{p}p$ scattering at energies from 0.5 to 1.8 TeV. The start of the LHC and its operations at $\sqrt{s} = 7$ and 8 TeV have provided plenty of data which are still being thoroughly analysed. In terms of proton-proton cross sections, the results extend to an unprecedented energy domain. Moreover, the LHC energies begin to overlap with the range of cosmic ray showers, as discussed in Section 7.7.

The measurement of the total cross section can be achieved by measuring the inelastic and elastic rate or, exploiting the optical theorem, the elastic scattering only, provided that the differential distribution is measured at angles small enough (at the LHC it means four-momentum transfer $|t| < 0.5$ GeV^2). It has to be noted that the former measurement can be luminosity independent, while for the second one a measurement of the luminosity is mandatory. All the available measurements of the total, elastic and inelastic cross sections are summarised in Fig. 98.

Concerning the total cross section, the rise with the centre of mass energy has been confirmed by the LHC data. This evidence can be interpreted as a proton becoming larger and blacker as the energy increases. Moreover the data, fitted by several authors, favor a $\ln^{\gamma} s$ behavior, with γ compatible with 2, which can be seen as a qualitative saturation of the Froissart-Martin bound, since it corresponds to the maximum rate of rise with energy which is allowed by analiticity and unitarity; numerically, the actual data lie well below the bound itself. In particular, the measurements of the total cross section at $\sqrt{s} = 7$ and 8 TeV definitely indicate consistency with a $\ln^2 s$ dependence, as predicted several years ago by the COMPETE Collaboration [874].

Several theoretical models have been developed during the last decades to interpret the experimental results. Unfortunately, the perturbative QCD approach cannot be used in this context since most of the processes contributing to the total cross section are characterised by low momentum transfer. Some of the models are still based on Regge theory, while others prefer using optical or eikonal approaches. Moreover, so-called QCD-inspired models are trying to connect the concepts of Pomeron trajectories and proton opacity to the QCD description of elementary interactions between quarks and gluons. At the moment, no model manages to describe qualitatively and quantitatively the large amount of data available; they all have merits and shortcomings. Typically, they successfully describe the experimental results in a certain kinematic range but completely fail in other ones.

7.5.2 Elastic scattering

The distribution of the four momentum transfer t in elastic scattering (Fig. 99) exhibits a pronounced forward peak which is well described, at first approximation, by an exponential of the form $e^{-B(s)t}$. In general, the overall forward peak ($|t| \lesssim 0.5$ GeV^2) does not follow a simple exponential shape,

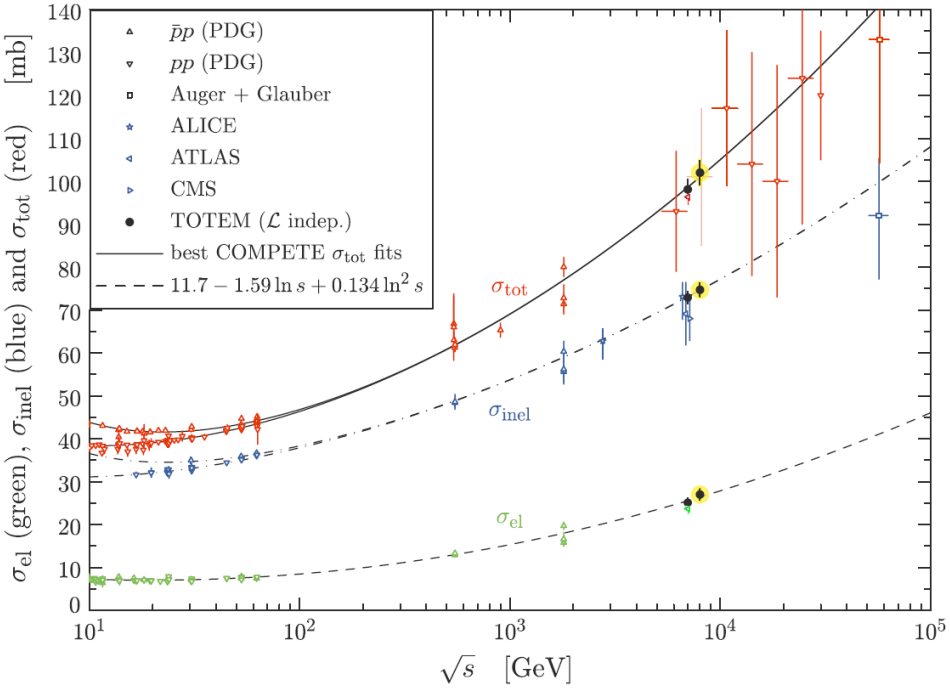

Fig. 98: The dependence of total, inelastic and elastic cross sections on the center of mass energy $\sqrt{s}$. The continuous black lines (lower for pp, upper for $\bar{p}p$) represent the best fits of the total cross section data by the COMPETE collaboration [874]. The dashed line results from a fit of the elastic scattering data. The dash-dotted curves correspond to the inelastic cross section and have been obtained as the difference between the continuous and dashed fits.

which has important implications in the understanding of the hadronic interactions and of the interference between the hadronic and electromagnetic ones. This aspect is being investigated by TOTEM, whose latest measurements allowed to access the kinematical region where the Coulomb interaction becomes visible.

At larger momentum transfers a diffraction-like structure is observed, followed by a smooth behaviour. The dip appears to recede towards zero with increasing energy at a value of t roughly proportional to σ_{tot}^{-1}, as suggested by the geometrical picture. Data from pp and $\bar{p}p$ scattering differ considerably in the region where the diffractive structure appears: the former shows a pronounced dip, while the latter actually shows more of a shoulder than a dip.

7.5.3 Diffraction

In diffractive processes in proton-proton collisions, the final state contains one ($pp \to pX$) or both ($pp \to pXp$) of the incoming proton(s) and a hadronic system X. Because no quantum numbers are exchanged between X and p, one (two) region(s) in rapidity devoid of particles (large rapidity gap, LRG) is (are) the signature of such processes in addition to the scattered proton(s). Diffraction is also observed in the interaction of point-like probes with hadrons, and it has been extensively studied in Deep-Inelastic ep Scattering (DIS) at the HERA collider [875], where, by changing the virtuality of the photon, the size of the probe can be varied at will, spanning the transition from the soft regime, typical of diffractive reactions in hadron physics, to the hard regime, where pQCD becomes applicable. This is the reason why the understanding of diffraction in QCD has received a great boost from the HERA results.

In the pre-LHC era, at HERA, Tevatron (and also at RHIC), tagging the LRG or the outgoing proton(s) provided complementary results (high statistics with the LRG technique, conversely well un-

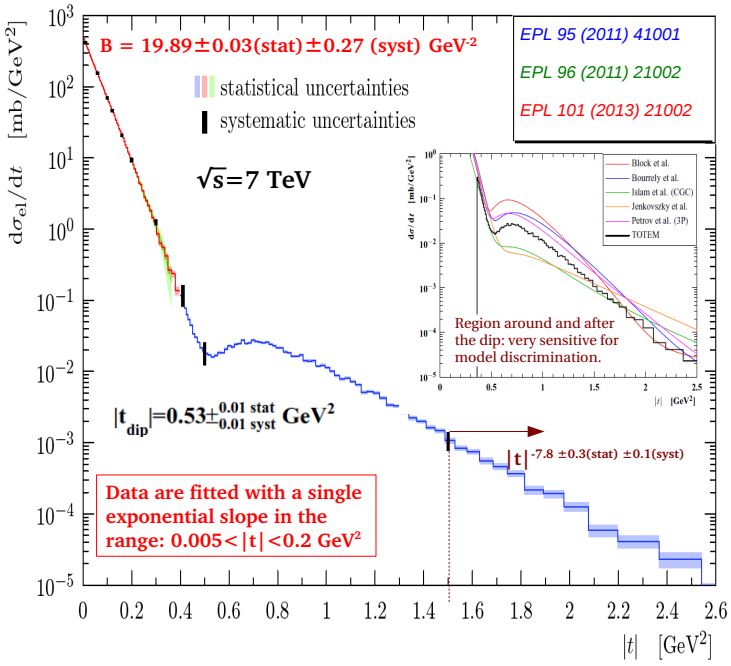

Fig. 99: A summary of the TOTEM results for the single differential elastic cross section, $d\sigma_{el}/dt$, at $\sqrt{s} = 7$ TeV.

derstood systematics with the proton taggers). At the LHC, and notably in the case of ATLAS and CMS, the presence of pileup spoils the rapidity gap signature. This made the LRG technique already a challenge with the Run I data (see e.g. [876–878]). LRG measurements will be possible with the forthcoming Run II data in special running conditions [879] or with the LHCb detector, which operates in low-pileup scenario due to special settings and offset leveling techniques. Conversely, measuring diffractive interactions at high luminosity with ATLAS and CMS will be possible only with proton taggers. Both experiments have a program for instrumenting the forward region. In the CMS case, the TOTEM detector, conceptually designed for forward physics as illustrated above, shares the same interaction point. Exploiting the synergy between the two experiments, which started already in 2012 when CMS and TOTEM successfully took common data (the runs were synchronised and the data merged offline), is the heart of the CMS-TOTEM Precision Proton Spectrometer (CT-PPS) project [880], recently approved by the LHCC. It consists of a pixel silicon tracking system to measure the position and direction of the protons, and a set of timing Cherenkov quartz counters to measure their arrival time. The ATLAS Forward Proton (AFP) detector [881] consists of similar devices. They will allow the reconstruction of the mass and momentum of the system X resulting in central exclusive production (CEP) processes, $pp \to pXp$. The mass of the system X depends on the longitudinal momentum losses, ξ, of the scattered protons; the acceptance in ξ of the proton taggers in turn depends on the machine optics: protons with any ξ can be detected in TOTEM and ATLAS-ALFA roman pots in special low-luminosity runs (betatron function at the interaction point β^*=90 m)[22] in which the mass coverage in CEP reactions extends to any M_X as long as $|t|$ of both scattered protons is larger than 0.04 GeV^2. This is complementary to the range $M_X \geq 300$ GeV in normal high-luminosity runs. Furthermore, the CEP via a double diffractive channel, with constrained kinematics, provides a unique method to access a variety of physics topics at the LHC, such as new physics via anomalous production of W and Z boson pairs, high$-p_T$ jet production, and possibly the production of new resonances, including a thorough spin analysis and a study of the decay

[22] In terms of the accelerator optics, the value of the betatron function β at a point is the distance from this point to the one at which the beam is twice as wide. The lower is the value of β^*, the smaller is the beam size and thus the larger is the luminosity. In standard LHC runs β^* = 0.5 m

modes of glueball candidates, like the $f_0(1710)$, in high-β^* runs [879].

A key physics issue in diffractive processes is whether the Diffractive Parton Distributions Functions (DPDFs), introduced as a class of parton distribution functions or fracture functions [882–884]—describing the usual proton PDFs conditional to having a diffractive scattering—are or are not universal, i.e. whether collinear factorisation [885] holds. DPDFs were extracted from high-precision HERA data by performing perturbative QCD fits at next-to-leading order accuracy and including full experimental and theoretical error estimations [875, 886–888]. Support of factorisation was provided by analyses of diffractive di-jet cross sections in DIS which, despite large theoretical errors, are well described by next-to-leading order predictions based on DPDFs extracted from the inclusive diffractive DIS data [889]. However, hard scattering factorisation was proven to fail in $p\bar{p}$ collisions at the Tevatron [890, 891], where single diffractive production cross sections of di-jet and electro-weak bosons are overestimated by an order of magnitude by predictions based on HERA DPDFs.

The factorisation theorem is at the heart of modern QCD phenomenology at hadron colliders. It provides crucial predictivity to the theory and, so far, has been tested and verified by all phenomenological analyses. Understanding the mechanism, still unknown, responsible for the striking breaking of factorisation in hard diffraction would unveil the non-perturbative phenomena behind it. There are other processes at the LHC which may substantially improve our knowledge, namely the single diffractive Drell-Yan process. A measurement of the dependence of the cross section on the invariant mass of the di-lepton pair would be very informative. This analysis would reveal if the factorisation breaking mechanism depends on Q^2, and appropriate ratios to the inclusive Drell-Yan cross sections could spot this eventual dependence in a model independent way. In the simplest scenario in which the single diffractive cross section is scaled by a common factor, independent of Q^2, it would be extremely interesting to estimate to what extent the partonic structure of the diffractive exchange (encoded in the DPDFs) is altered in hadronic collisions with respect to diffractive DIS. For this purpose, it will be mandatory to select kinematic ranges of the proton energy loss ξ and of the lepton-pair rapidity (and therefore of the DPDFs fractional momentum β) corresponding to regions in which the DPDFs have been determined in diffractive DIS with sufficient precision. Since the Drell-Yan process is essentially a quark-dominated process, this measurement should be complemented by the study of other processes sensitive to the (dominant) gluon DPDF, such as single diffractive prompt photon and di-jet production.

High transverse momentum production of jets and/or photons in photon-Pomeron interactions can be measured if the full kinematics of final state protons can be reconstructed, since photon and Pomeron emissions from protons are expected to populate different regions of the t spectrum. If this measurement turns out to be feasible, the LHC machine could possibly offer the answer to the unsolved question raised in diffractive di-jet photo-production at HERA. To conclude, the hard diffraction program at LHC can address fundamental issues in our understanding of non-perturbative phenomena in high energy hadron interactions and investigate in detail the only case in which factorisation, at the heart of QCD phenomenology, is strikingly broken.

7.6 Multi-parton interactions

In collisions with large momentum transfer exchange, the interaction between hadronic constituents is localised in regions in transverse space much smaller than the hadronic dimension. On the other hand, at high energies and relatively low p_t, hard collisions contribute to a finite fraction of the total inelastic cross section. In such a regime, the hard component of the interaction may be disconnected in transverse space. The process is thus given by the incoherent sum of weakly correlated hard and semi-hard subprocesses and is called Multiple Parton Interaction (MPI).

When the hard component of the interaction is disconnected, the hard process is initiated by several pairs of partons. The cross section is hence characterised by a much stronger dependence on the incoming parton flux, as compared with the familiar case of hard processes originated by just a single pair of partons. MPI become therefore more and more important when increasing the centre of mass energy of

the colliding hadrons, where partons with smaller and smaller fractional momenta play an active role. Another general feature is that MPI are characterised by at least one non-perturbative scale, related to the typical transverse distance between the hard interaction regions. A direct consequence is that MPI cross sections decrease much faster, as a function of transverse energy, as compared with usual large p_t single scattering parton interactions. MPI are further characterized by peculiar correlations. Final state partons generated by a connected hard interaction are in fact highly correlated in transverse momenta and rapidities. Disconnected hard interactions produce various groups of highly correlated partons in the final state, while correlations between partons belonging to different groups are weak.

All state-of-the-art Monte Carlo event generators need in fact to include MPI in order to be able to reproduce the global features of inelastic events (final state multiplicities, energy densities, etc.). In almost all cases MPI are implemented by assuming a Poissonian distribution of elementary partonic interactions, with average number depending on the impact parameter of the hadronic collision [892]. Specific conjectures, concerning in particular the actual distribution of initial state partons in transverse space, the regularisation of the elementary partonic interaction at low transverse momenta and hadronisation, depend on the specific assumptions in the different Monte Carlo codes. The non-perturbative component of MPI combined with the contribution to the final state due to soft radiation and to the fragmentation of initial state remnants, cannot be completely separated from each other, in such a way that the resulting quantitative information on MPI is unavoidably rather uncertain even if several decompositions have been attempted based on topological constraints and specific selections of final states [893–895].

In this respect, a cleaner understanding of the different dynamical mechanisms, taking place in the relatively low p_t region, can be obtained by direct observation of MPI processes. In the simplest case, Double Parton Interaction (DPI), the general features characterising MPI are summarized in the 'pocket formula' of the corresponding inclusive cross section [896]:

$$\sigma_{double}^{(A,B)} = \frac{m}{2}\frac{\sigma_A \sigma_B}{\sigma_{eff}}\,, \tag{52}$$

where A and B label the two elementary partonic processes, localised in two different disconnected regions, m is a symmetry factor ($m = 1$ if A and B are identical processes and $m = 2$ if A and B are different), σ_A and σ_B are the two cross sections to observe inclusively either the process A or the process B in the same hadronic collision. All unknowns in the process converge into the value of a single quantity with the dimensions of a cross section, σ_{eff}. Actually, when hard interactions are rare, the probability to have the process B in an inelastic interaction is given by the ratio σ_B/σ_{inel}. Once the process A takes place, the probability to have the process B in the same inelastic interaction is different. It can anyway be always written as σ_B/σ_{eff}, where σ_{eff} plays *effectively* the role, which was of the inelastic cross section in the unbiased case.

Double-PDFs encode information on the correlations between two partons inside a target and represent the non-perturbative contribution to the hadron structure, not accessible in a single-scattering large-p_t interaction [897]. One may thus expect σ_{eff} to depend on all the different observables characterising the process. Conversely, it is remarkable that, although more precise measurements are expected to reveal some dependence of σ_{eff} on the reaction channel and on the kinematical regime, Eq.(52) has shown to be able to describe the experimental results of the direct search for DPI in rather different kinematical regimes [898–902] with a value of σ_{eff} compatible with a universal constant (see Fig. 52). Even though the value of σ_{eff} is still rather uncertain, the actual experimental evidence is that its value is much smaller than σ_{inel} (roughly by a factor 4), which represents a rather clear indication of the presence of important correlations in the hadronic structure. On the other hand, the experimental study of DPI in pp collisions can only provide limited information. In particular it cannot provide a suitable understanding of the small observed value of σ_{eff}.

A handle to obtain additional information is provided by DPI in pA collisions [903]. The dynamics of DPI is in fact different in pp and in pA collisions. In addition to the process where DPIs take place between the projectile proton and a given target nucleon, in pA DPIs can in fact also occur between the

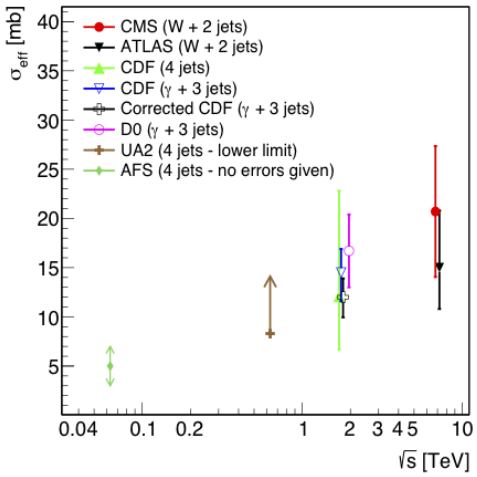

Fig. 100: Different experimental results on the value of σ_{eff}

projectile and two different target nucleons. While the first contribution to the cross section is proportional to A and is very similar to DPI in a pp collision, the second contribution is proportional to $1/R^2$, where R is the nuclear radius, and grows with A as $A^{4/3}$. The second contribution therefore introduces a rather strong anti-shadowing correction to the first one, which may be of the order of 200-300% in the case of $p-Pb$ collisions. Moreover, while the first contribution, linear with A, is proportional to $1/\sigma_{eff}$ and it is therefore related to the typical transverse region, where the two elementary hard interactions take place, the second contribution, being proportional to the inverse nuclear radius squared, is practically independent, in the case of heavy nuclei, of the distance between partons in transverse space. Its contribution to the cross section is therefore directly proportional to the multiplicity of pairs of partons in the projectile, which can thus be estimated by measuring the amount of anti-shadowing in DPI in pA collisions. DPI in pA collisions can therefore provide valuable indications on the multiplicities of parton pairs in the hadron at different fractional momenta. By comparing with the measured value of σ_{eff} in pp collisions one therefore obtains indications on the corresponding typical transverse distances between the interacting parton pairs. One should also emphasise that, in this way, one has access to unprecedented information on the three dimensional partonic structure of the hadron.

Reducing substantially the experimental errors in the measurement of σ_{eff} is required as well as measuring the dependence of σ_{eff} on Q^2 and on fractional momenta in different reaction channels and different kinematics, while quantifying the amount of anti-shadowing in DPI in pA collisions in the same reaction channels and regimes. Both high luminosities, in order to significantly increase statistics, and high centre of mass collisions energies, to increase the parton flux and thus the relative rate of MPI, are key issues. From the theory side further efforts are needed to unravel features of DPI, which are still a matter of debate (the relevance of the contribution of the interplay region between connected and disconnected hard interactions [904], the role of spin and color [905]).

A clear indication on the dependence of σ_{eff} on transverse momenta will provide valuable indications on the deviations from the Poissonian distribution of elementary partonic interactions to be included in the Monte Carlo event generators, improving in this way the physics content and reducing the space to phenomenological assumptions, affecting in particular the relative importance of radiation with respect to MPI in the description of the inelastic event.

A relevant point is finally that an accurate determination of the value of σ_{eff}, for different processes and kinematics, will allow accurate estimates of the backgrounds due to DPI in various processes of interest in the search for new physics. The contribution of MPI is in fact expected to become signifi-

cant, when looking at various processes that are absent, at leading order, in the Standard Model [906].

7.7 Cosmic rays and the impact of collider experiments

A precise modeling of the properties of hadronic interactions is mandatory to understand and interpret correctly the showers generated by cosmic rays in the Earth's atmosphere and in other astrophysical environments related to dark matter searches or neutrino physics. Uncertainties on cross sections and on the properties of particle production in hadronic collisions are indeed in several cases the main source of systematic error in measurements of great interest. An appropriate program of measurements with accelerators beams could provide the information to reduce the systematic errors to a level that would significantly enhance the scientific value of existing and future observation programs.

7.7.1 High Energy Cosmic Rays

The energy spectrum of cosmic rays (CR) covers a very broad energy range, at least up to $E \simeq 10^{20}$ eV, with an intensity that decreases rapidly with energy, approximately as a power law ($\phi(E) \propto E^{-\alpha}$) with an exponent α between 2.7 and 3.3. CR direct observations with detectors placed above the Earth's atmosphere on balloons or satellites are only possible in the low energy region, where sufficient statistics can be collected. Above an energy of order $E \simeq 10^{14}$–10^{15} eV, the CR spectrum and mass composition can only be estimated by indirect methods, from the observation of the extensive air showers generated in the atmosphere by the primary particles (most of the high energy particles are protons of fully ionised nuclei).

The reconstruction of the energy and identity (mass number) of the primary particle from the shower observables requires a sufficiently precise description of the relevant properties of hadronic interactions, and uncertainties in their modeling are the main source of systematic error. An example is given in Fig. 101, where data obtained by the Auger detector [907] on $X_{\max}$ (the column density of air where the longitudinal development of a shower has its maximum) are shown. The different lines in the figure illustrate, as a function of energy, the theoretical predictions on $\langle X_{\max}(E)\rangle_{p,\mathrm{Fe}}$ for proton and iron showers, obtained with different Monte Carlo models. The spread among the lines gives a rough indication of the present uncertainties on the modeling of the shower development, and of their impact in the interpretation of the data. The reduction of such theoretical systematics would allow a better determination of the CR average mass (as a function of energy), with important consequences on the understanding of their origin and propagation. Similar considerations apply also to the low energy range ($E \simeq 10^{15}$–10^{18} eV), where the energy spectrum shows features (the most prominent being the so called "knee") that should be better described and understood.

The laboratory-frame energy range 10^{15}–10^{20} eV corresponds, for a proton primary particle, to nucleon–nucleon interactions with centre-of-mass energy in the interval $\sqrt{s} = 1.4$–430 TeV, that extends far beyond the maximum energy available at LHC. The study of the highest energy CR requires therefore an extrapolation of the results obtained in accelerator experiments. Detailed studies performed at the highest energy available at LHC play a crucial role in reducing the uncertainties associated with this extrapolation.

CR showers develop in air, where the target is formed by nuclei (Nitrogen, Oxygen and Argon) with mass numbers $A = 14$–18, while the primary cosmic rays consist of protons and fully ionized nuclei, with a mass number distribution that extends up to elements in the iron group ($A \lesssim 56$). The shower modeling therefore requires a good understanding of hadron-nucleus and nucleus-nucleus collisions with the mass number of the target and projectile nucleus in the quoted intervals.

One infers from the discussion above that measuring hadronic interaction properties in pp and $\bar{p}p$ collisions is fundamental. The recent results on the total and elastic cross sections by TOTEM, ALICE, ATLAS and CMS at $\sqrt{s} = 7$ and 8 TeV, discussed in Section 7.5, are very informative as they cover an unprecedented energy range, and even more so will be the future Run II measurements. With the caveat

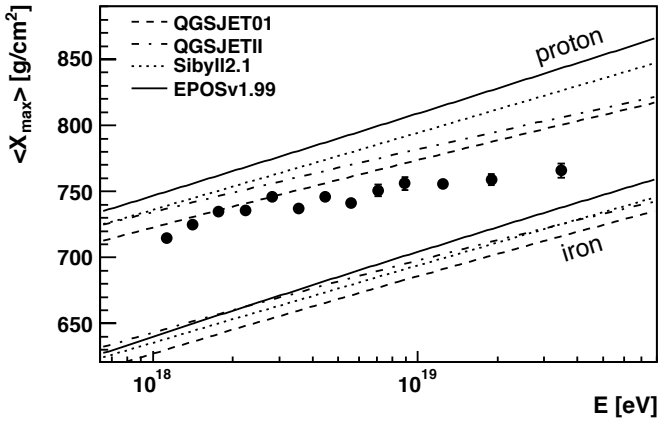

Fig. 101: Average $X_{\max}$ measured by the Auger experiment [907] compared with air shower simulations using different hadronic interaction models.

that to use such results for the modeling of CR showers one needs to apply corrections based on a good understanding of nuclear effects. Obtaining measurements for p-nucleus and nucleus-nucleus scattering would be highly desirable. The properties of meson-nucleus collisions are also important because high energy $\pi^{\pm}$ and kaons produced in the cascades have a small decay probability, and interact.

The development of CR air showers is driven by the interaction lengths of the particles and by average properties of particle production, such as inclusive energy spectra and multiplicity distributions. Therefore, in most CR studies the rare, hard processes that are the main interest and motivation in accelerator experiments are of little importance. The secondary particles generated in the collisions that are most important for the shower development are those carrying large energy in the laboratory frame and control the energy flow. These particles correspond to the projectile fragmentation region ($x_F \gtrsim 0.1$), and are unfortunately very difficult to measure in collider experiments because they emerge at very small angle with respect to the beam direction. At LHC the beam fragmentation regions, i.e. those at large pseudorapidity $|\eta|$, are studied by detectors such as TOTEM, CASTOR and LHCf. The LHCf experiment has a short-medium term plan which foresees to repeat at 13 TeV the Run I measurements on neutral-particle (neutral pions, gammas and nucleons) production cross sections in the very forward region of proton-proton and nucleus-nucleus interactions. A plan has been presented to perform similar studies at RHIC with 500 GeV pp collisions [908] and with proton-nucleus collisions [909].

The study of collisions using the extracted LHC beam on a fixed target could also be very valuable. A possible scheme for beam extraction is the technique of crystal channeling [910], proposed in the CRYSBEAM project (ERC CoG, funded), where the strategy is to direct the LHC beam on an instrumented absorber made of light materials (carbon, nitrogen, oxygen,..) emulating the Earth atmosphere composition. Also studies at lower energy (for example with a beam extracted from the SPS accelerator) would allow measurements useful for a reduction of the systematic uncertainties on shower development. In this context it seems very interesting to have an experimental program associated to an extraction of the LHC proton beam [911] (using perhaps techniques such as those discussed in [912]).

7.7.2 Galactic cosmic rays and cosmic antimatter

As discussed in the previous subsection the galactic cosmic rays observed with direct measurements span an energy range from about tens of MeV up to hundreds of TeV, and include protons, iron and nickel nuclei, antiprotons, leptons and γ-rays. The interpretation of galactic cosmic ray data requires, as well as the correct modeling of their sources and of the turbulence spectrum of the galactic magnetic

field, also the knowledge of the cross sections that regulate the production and destruction of cosmic rays interacting with the interstellar medium. For many production and inelastic cross sections, data are scarce or completely missing.

In particular, the *antiprotons* in the Galaxy are of secondary origin and are produced by the scattering of cosmic protons and helium nuclei off the hydrogen and helium in the interstellar medium. The only measured production cross section is the proton-proton one, while all the reactions involving helium have no laboratory data in the useful antiproton energy range ($\sim$ 0.1-100 GeV) [913, 914]. The empirical modeling of those cross sections induces an uncertainty in the antiproton flux of about 30-40%. This should be compared with the $\sim 10\%$ accuracy expected for the forthcoming AMS-02 data on the antiproton flux. The interpretation of the data collected in space will be likely limited by the lack of laboratory measurements!

Accurate knowledge of the cosmic antiproton flux is not only useful to the understanding of the origin and propagation of galactic cosmic rays, but also to the indirect dark matter searches, as will be discussed in the next subsection. The secondary antiproton flux acts as a background when looking for a dark matter signal in the observed antiproton flux.

We emphasise here the need for a dedicated experiment aimed at measuring the exclusive cross section $p + \mathrm{He}$, with particular interest for the channel $p + \mathrm{He} \rightarrow \bar{p} + X$. This measure would also reduce the uncertainties in the predictions of cosmic *antideuterons*. Having the higher signal-to-background ratio, antideuterons are considered at present the most favoured indirect dark matter channel.

As for the scattering $p + \mathrm{He}$, we stress the importance of the measurement of the exclusive cross section. We notice that the knowledge of the cross section for $\gamma - rays$ from the neutral pions produced in $p + \mathrm{He}$ scattering is of relevance for the modeling of the galactic emission [915] and therefore the interpretation of the plethora of data taken by the Large Area Telescope (LAT) on the Fermi Gamma-ray Space Telescope (Fermi). A better modeling of the γ-rays from hadronic reactions, and in particular the ones involving scattering on helium, would improve the power of the indirect dark matter searches through γ-rays and the study of the origin of cosmic rays.

A dedicated experiment with a beam of protons accelerated at CERN to energies of a few GeVs and scattering off a helium target would therefore be of the utmost importance in the effort to understand the mystery of dark matter in the Universe and the origin and propagation of cosmic rays in the Milky Way. More generally, an extensive laboratory campaign aimed at measuring the missing production and destruction cross sections is envisaged for a large number of nuclei, isotopes, anti-nuclei and positrons, in the perspective of a reliable interpretation of the direct measurements on galactic cosmic rays.

7.7.3 Dark Matter searches

Dark Matter (DM) in the form of Weakly Interactive Massive Particles (WIMPs) can be detected observing the particles produced in the annihilation (or in some models in the decay) of the DM particles forming the invisible halo of our galaxy. The charged particles produced in the annihilations or decay remain partially confined by the galactic magnetic field and can be observed as an excess over the expected fluxes generated by known mechanisms. The best sensitivity is obtained measuring the flux of anti–particles such as positrons and anti–protons, which have a smaller background from known processes. The dominant known source of anti–protons in cosmic radiation is due to the interactions of cosmic rays with the interstellar medium gas (in reactions such as $pp \rightarrow ppp\bar{p} + X$). Uncertainty in the production of anti–nucleons in pp and $p\mathrm{He}$ interactions in the interesting energy range $E \lesssim M$ (with $M \sim$ 10–1000 GeV the mass of the DM particles) can be as large as 50% at the highest energies. This energy range is accessible with accelerator experiments. The interest of these studies is discussed in [913].

7.7.4 Atmospheric neutrinos

Another field of research where a program of measurements of hadronic interaction properties could reduce systematic errors is the study of neutrino oscillations using atmospheric neutrinos. New large mass Cherenkov neutrino telescopes (PINGU [916] and ORCA [917]) have been proposed with the main goal to determine the neutrino mass hierarchy (normal or inverted) from a precision measurement of the energy and zenith angle distributions of atmospheric neutrinos. Extensions of this program could also be sensitive to the phase δ in the PMNS neutrino mixing matrix. Precision measurements of proton interactions on an air target would allow a more precise prediction of the no-oscillation flux.

7.8 Hadron Physics and non-perturbative QCD: Summary and Outlook

The internal, partonic structure of nucleons, and hadrons in general, is still largely mysterious. As protons and neutrons form almost all of the visible matter of the Universe, it is certainly worth exploring their content in terms of quarks and gluons interacting according to QCD dynamics. All issues discussed in the "Hadron physics and non-perturbative QCD" Chapter share this motivation.

The 3-dimensional nucleon structure, both in momentum and coordinate space, represents a new phase in our imaging of the nucleon, which goes beyond the traditional and simple 1-dimensional picture of a fast moving nucleon as a bunch of co-linearly moving partons. Hadron spectroscopy, dealing with the total quantum numbers of bound states of quarks and gluons, shows that more and more precise experimental data are not well understood, while unconventional, although possible, bound states are still not observed. The dynamical QCD properties of partons should be able to explain diffractive and elastic cross sections in proton nucleon interactions at high energies; the role of multi-parton interactions, rather than a single elementary interaction, has to be explored and understood. A precise knowledge of the cross sections and of the properties of particle production in hadronic collisions is crucial in order to reduce the systematic errors in several measurements of great astrophysical interest. For each of these themes the prospects for new measurements at existing and future experimental facilities have been considered.

- **Confinement and large distance QCD.**
  The first challenge towards a complete understanding of QCD is to describe the confinement mechanism and the spectrum of mesons and baryons. Both large-N and lattice QCD predict the existence of glueballs of any integer spin, experimentally not clearly identified yet.
  In particular, the slope of glueball Regge trajectories with respect to the meson trajectories has a fundamental theoretical meaning. Experimentally, there are presently no candidates for the odd-spin glueballs. The measurement of their slope in relation to the slope of even-spin glueballs is even more important theoretically.
  The systematic search for glueballs is one of the experimental challenges in the next 10 years, in the reach of dedicated experiments such as BESIII, JLab, FAIR, J-PARK and LHCb. Glueball production, together with other interesting non-perturbative aspects of QCD, are in the reach of diffractive phenomenology, like high-energy p-p exclusive forward scattering. A most interesting experiment at CERN along this line is the joint collaboration TOTEM+CMS at LHC.
  Another interesting experimental direction is the exploration of the QCD phase diagram by heavy-ion collision experiments, in particular regarding the detection of the transition to a Quark-Gluon Plasma phase, which may allow a comparison with lattice QCD simulations. All that is relevant to many experiments at LHC (ALICE, ATLAS, CMS), at RHIC and FAIR.
- **3-dimensional nucleon structure**
  The quarks and gluons inside a proton (which is a gigantic object, compared to their size) must have some intrinsic motion and space distribution. In particular, one expects partons to have some orbital angular momentum, which contributes to the total nucleon spin. This 3-dimensional information on the nucleon structure has been encoded in the so-called Transverse Momentum Dependent partonic distributions (TMDs, concerning the momentum distribution) and the Generalised Partonic Distributions (GPDs, concerning the spatial distribution).
  Information on TMDs can be obtained in semi-inclusive processes, like SIDIS ($\ell\, N \rightarrow \ell\, h\, X$) and Drell-Yan (D-Y, $h\, N \rightarrow \ell^+\ell^- X$); information on GPDs come from exclusive processes like $\ell\, p \rightarrow \ell\, p\, \gamma$ or $\ell\, p \rightarrow \ell\, p\, \pi$. So far, data on TMDs and GPDs have been collected by the HERMES and COMPASS Collaborations and at RHIC-BNL. Some related information on the transverse momentum dependent fragmentation functions have been obtained by the Belle and BaBar Collaborations. A genuine 3-dimensional imaging of the proton is emerging, but more data are necessary. These will be available from COMPASS and JLab (at 12 GeV) experiments. Great expectations are related to the planned Electron Ion Collider (EIC).

Of very special interest is the measurement of one of the spin-dependent TMDs, the so-called Sivers function. This is known from SIDIS data, but the current QCD understanding of its origin predicts that this same function, when observed in D-Y processes, should have the opposite sign. Such a measurement will be soon performed by COMPASS at CERN, in the D-Y process $\pi\, p \to \ell^+\ell^- X$.

– **Spectroscopy**
Hadron spectroscopy has been living a second renaissance since the advent of the B-factories. Spectra of heavy quarkonia, heavy light mesons, and heavy baryons allow precise tests of QCD at various scales, from the perturbative domain to the confinement region. In addition to the discovery of known and long sought states (e.g. parabottomonia), many new and unexpectedly narrow states (such as D_{s0} and D_{s1} mesons, the X(3872), Y(4260), Z(4430) and so on) are challenging phenomenologists. A large fraction of these states are close to thresholds, and their dynamics is significantly affected by light quark degrees of freedom. Most future efforts will focus on casting light on this abundance of new states.
In the meantime, the overall pattern of narrow quarkonia is approaching completion, and precise experimental mass measurements show that, after having averaged out spin effects, the mass splittings are independent of the mass scale, in spite of the large variation of α_s in the 1 to 10 GeV energy range. A similar scale independence is emerging, when we compare heavy baryons with heavy mesons. For the color interaction, an antiquark is equivalent to a diquark: can we use diquarks as building blocks of this new spectroscopy? In addition, hyperfine and fine splittings can be explained with a relatively naive constituent quark model. An explanation of this success starting from the first principles of QCD is still missing. Are we overlooking some deeper symmetries? What are the actual degrees of freedom of hadronic bound states?

– **Total pp cross section, elastic scattering, diffraction**
One way of studying the inner properties of protons is to observe how they interact with each other, i.e. to measure the total proton-proton cross section. Run I TOTEM, ATLAS, CMS and ALICE data have confirmed that the proton behaves as if it becomes larger at the unprecedented energies of 7 and 8 TeV.
Among the several theoretical models developed during the last decades, a global and quantitative description of the experimental results has not yet emerged. Perturbative QCD techniques cannot be applied since most of the processes contributing to the total cross section are characterised by low momentum transfer. The new data at 13 TeV not only will take the energy domain to new territory, but also will begin to overlap with the energy range of cosmic ray showers, therefore providing input to the understanding of shower developments in the atmosphere and of the cosmic ray energy spectrum and particle composition.
Elastic and diffractive processes, in which one or both of the incoming hadrons are scattered elastically or carry most of the initial energy and scatter at very small angles, contributes roughly half of the total proton-proton cross section; investigating the region very close to the outgoing beams is therefore complementary to studying the central region surrounding the interaction point. It requires as much rapidity coverage as possible and possibly appropriate detectors capable of operating in close proximity to the beams.
In addition to TOTEM, which was designed for elastic and diffractive physics, LHCb, ATLAS, ALICE and CMS have made an effort during the present shutdown to reinforce their forward physics programs. A key physics issue in diffractive processes is whether the diffractive Parton Distributions Functions (the usual proton PDFs conditional to having a diffractive scattering) are or are not universal, i.e. whether the (Collins) collinear factorisation holds. It was proven to be broken when going from diffractive ep scattering at HERA to $p\bar{p}$ collisions at the Tevatron, but the mechanism and its onset are not yet understood. Single-diffractive production processes (Drell-Yan, W and Z, di-jet) have the potential to shed light on the underlying non-perturbative phenomena. Experimentally, one critical point of diffractive measurements at high luminosity is

that the large number of pileup interactions in a bunch crossing spoils the diffractive rapidity gap signature, leaving proton tagging as the only possible strategy. It is being pursued by both CMS and ATLAS. In the former case, TOTEM proton taggers will be used in 2015 in conjunction with the CMS central detector (already at the end of Run I the two experiments took data jointly).
This is a first step towards the realisation of the CMS-TOTEM Precision Proton Spectrometer, consisting in new precision tracking and timing stations allocated in TOTEM roman pots. This device will allow studying central exclusive production, $pp \to pXp$, a unique method (also pursued by ATLAS, LHCb and RHIC experiments) to access a variety of physics topics, such as new physics via anomalous production of W and Z boson pairs, high-p_T jet production, and possibly the production of new resonances.

– **MPI and underlying events**
Multi-Parton Interactions play an increasingly important role in hadronic interactions at high energies. A deeper understanding of the phenomenon is thus necessary to improve the actual implementations of MPI in Monte Carlo event generators and for a correct evaluation of the backgrounds of various processes of interest for the search for new physics. MPI represent also a research topic of interest by itself, since the non-perturbative input to MPI contains information on correlations between partons, not accessible in single-scattering large-p_t experiments.
The simplest case of MPI, Double Parton Interaction, was successfully observed and studied by most high energy experiments at hadron colliders. The available experimental information on DPI is however still limited and the experimental errors rather large. Higher luminosities at LHC will produced increased statistics and higher c.m. collision energies will boost the parton flux and thus the relative rate of MPI. Present experimental errors in the measured DPI cross sections can thus be reduced, while differential measurements of the cross section, as a function of the incoming fractional momenta and of the produced transverse energy, may become feasible. Differential measurements together with experimental studies of correlations in rapidities, at different azimuthal configurations of the produced states, would increase significantly the efficiency in disentangling the contribution of DPI from background processes, providing also indications on possible correlations between initial state partons. Information on the dependence of correlations on flavour can be obtained by comparing DPI in different reaction channels.
Additional information can be gained by measuring DPI in pp and in pA collisions, in the same kinematical conditions. The DPI mechanism is in fact different in pp and in pA. Actually, in the case of heavy nuclei, DPI are dominated by the contribution where two different target nucleons take part in the process. By comparing the effects of the two different DPI mechanisms, one will be able to learn on correlations in the transverse distances and in the distributions in multiplicity of parton pairs of the incoming proton.

– **Hadronic interactions and cosmic ray studies**
The precise modeling of the properties of hadronic interactions is needed for a sufficiently accurate description of the showers generated by cosmic rays in the Earth's atmosphere and in astrophysical environments. Observed air showers must be interpreted to estimate the energy and mass of the primary particles. Showers in astrophysical environments generate secondaries such as anti–protons, positrons and photons that can be used to study the properties of the sites of cosmic ray acceleration and propagation, and constitute the background for the indirect search for Dark Matter in the form of Weakly Interacting Massive Particles.
Measurements at LHC and at lower energy accelerators with appropriate coverage of phase space (with the very forward fragmentation region playing a crucial role) can significantly reduce the existing uncertainties and enhance the science reach of existing and future programs in these lines of research. Of particular interest appears to be an accurate measurement of the cross section for the production of antiprotons in $p + \mathrm{He}$ interactions.
Experimental studies of the total and elastic cross sections and of the properties of particle production over the entire phase space would also help and stimulate the extension of theoretical QCD

studies toward bridging the gap between between hard and soft hadronic physics.

8 Conclusions and *recommendations*

This report describes in detail the huge potential for physics achievable with current and future accelerators. First and foremost it shows the importance of a detailed understanding of the EW symmetry breaking sector of the SM and of direct searches for new physics covering a broad range of possible theories. This is complemented by precision measurements and searches for highly suppressed processes which test the structure of the SM and provide tight constraints on models of new phenomena. Moreover, current and future experiments at accelerators complement direct dark matter searches and provide key measurements needed to unfold results in neighboring fields, such as astrophysics.

The strategy to pursue the physics drivers mentioned above will be influenced by the evolution of present and future machines, the available acceleration and detection technologies, the level of financial support and the human resources available. Our current understanding of the major trends of these constraints is key to the formulation of a realistic strategy for INFN.

- **Present and future accelerators**
  The most important accelerators, where HEP experiments involving INFN researchers are either running or in preparation, are as follows. In the area of hadron colliders LHC at CERN (Switzerland) explores the energy frontier with proton-proton collisions at the highest available energy, while SuperKEKB in Tsukuba (Japan), BEPC in Beijing (China), DAFNE in Frascati (Italy) provide electron-positron collisions in the 1 to 10 GeV range. Extracted beams for fixed target experiments are provided by the SPS at CERN, featuring high energy hadron and meson beams, and PSI in Zurich (Switzerland), Fermilab and JLAB in the USA, J-PARC in Tokai (Japan), featuring high intensity proton beams mostly used to produce secondary neutrino or muon beams. More details can be found in Section 2.
  The lifespan of these machines is approximately the next five to ten years, then they lose much of their usefulness unless substantial upgrades are implemented. Currently, significant improvements in beam intensity are planned for LHC, Fermilab and J-PARC on these time scales; CERN is also considering the implementation of extracted beams of much higher intensity from the SPS. The technology and basic infrastructure needed for these upgrades are all essentially available at affordable costs. We expect therefore that their implementation will actually occur according to plans, thus extending their usefulness for an additional $\sim$ 10 years taking us to around the mid 2030's.
  New major accelerators might become operational on that time scale: a superconducting electron-positron linear collider (ILC) with the potential to deliver e^+e^- collisions from 250 up to 1000 GeV with successive upgrades, and/or an enlarged version of the LHC with about 100 km circumference (FCC-hh in Europe or SppC in China) and high field magnets capable of 100 TeV proton-proton collisions; an e^+e^- version (FCC-ee in Europe or CEPC in China) could be built in the same tunnel with less demanding magnets.
- **Technology context**
  Completely new acceleration techniques, such as those based on plasma wake-field acceleration for instance (see discussion in Section 2.3), are unlikely to become capable to produce the high energy and high intensity beams needed for HEP on the time scale of twenty years from now, so the new machines will need to be based on more conventional technologies.
  The superconducting cavity technology developed for the ILC in the last twenty years has reached a high level of maturity. It is already operational at the FLASH facility in DESY and a much larger implementation is already under construction for the XFEL in Germany. Assuming availability of funds and a clear commitment to its construction, a 250 GeV Linear Collider can most likely be built within ten years of the decision to start the project.
  The high field magnet technology based on Nb_3Sn and/or high temperature superconductors has been developing for many years and a few magnets of the Nb_3Sn type are planned for installation in the new LHC interaction regions scheduled for the mid-2020's. The development of cost ef-

fective methods to mass produce such magnets by industry, as needed for a future proton-proton collider, will likely take additional time after this very limited production. The actual speed at which this technology develops has a strong impact on the choice of potential future accelerators. For instance, increasing the LHC energy to $\sim$30 TeV by replacing the existing magnets with high field ones is likely to become a viable option only after the completion of the HL-LHC program. If additional time is needed for the magnet technology to mature, it will affect the decisions on the construction of the FCC's and the choice between hadron and electron beams for its initial operation.

Recommendation #1:
CSN1 urges INFN to continue and strengthen its support of R&D for the development of new high field magnets and conventional or un-conventional accelerator structures.

Currently available detector technologies can mostly cope with the needs of the future experiments with fairly straightforward improvements, although significant engineering efforts must be made to make the existing technologies cheaper and easier to produce to prepare for the needs of future large experiments. Further detector developments can significantly improve performance and physics reach, or open new experimental scenarios, for example with some specific technologies: pico-second timing in counters and tracking devices, extremely radiation resistant trackers, high jet energy resolution calorimeters, DAQ/trigger systems capable of handling huge data flows, smart detectors with distributed processing capabilities.

Recommendation #2:
CSN1 recommends a closer cooperation with CSN5 to boost the development of the most needed technologies.

We note that computing needs for the experiments at HL-LHC are estimated to be significantly larger than the expected technology will be able to provide at a constant cost from now. While ways to increase the computing power are currently under study, there is still no obvious solution.

Recommendation #3:
We urge the experiments planned for HL-LHC to develop plans to deal with the computing issue. In particular efficient ways to reduce the data flow to storage should be studied by means of appropriate enhancements of their trigger and DAQ systems.

- **Financial context**
  It is very difficult to reliably predict the future funding situation of INFN and more specifically CSN1 over the next ten years. We assume a scenario of constant funding with no inflation adjustments. We note that since the future new projects have not yet defined a clear funding profile, the effect of variations of the baseline scenario is hard to assess at this moment.
  While all currently approved programs can be completed in this assumption, major new programs will not be possible without additional project specific funding from within INFN and/or other external sources such as EU or Italian Education and Research Ministry grants.
  We note that even small variations of the baseline funding of CSN1 have considerable impact on its activities; for instance a 5% overall increase has a $\sim$25% effect on the funds that can be used for the construction of new detector components. Consequently even a small budget increase can significantly expand the potential for new projects.

8.1 Future new projects

Before addressing the potential future projects, it is worth remarking that CSN1 is currently supporting a strong program, including several experiments, addressing all the physics drivers described in this report and extending until approximately the middle of the next decade.

Recommendation #4:
It is a top priority of the CSN1 to continue funding of all approved experiments and their approved upgrades until their planned completion.

We note that for most of them construction funding will be complete by the end of 2017 with only the LHCb upgrade and possibly Mu2E continuing constructions until the end of 2019.

In the next few years the LHC will deliver data at twice the energy of the previous run, thus increasing significantly the reach for new physics. Two very different scientific scenarios will develop depending on whether evidence of new phenomena is or is not observed. As a result our recommendations may need to be revised a few years from now. We note however that the implications of these different scenarios mainly affect the future large machines.

In the following we give a list potential future new programs with our comments and recommendations. All of them have yet to consolidate a funding plan and to complete significant R&D.

Recommendation #5:
It is of great importance that well defined proposals be ready by mid-2017 to allow a realistic plan of how experiments at HL-LHC and other new CSN1 activities can coexist.

1. **ATLAS and CMS upgrades for HL-LHC**
   There is a compelling physics case for precision studies of the EW breaking sector of the Standard model (see Section 4), and to search for new physics (see Section 5) or study it if observed. Additional precision measurements provide additional constraints (or details) on models of new physics. Calibration of the PDF's and Montecarlo programs set the groundwork for physics at future accelerators.
   The high luminosity upgrade of LHC is already part of the CERN program and can be funded within its standard budget. There are no major technical hurdles to overcome in order to have HL-LHC operating in 2025 as scheduled.

   Recommendation #6:
   The ATLAS an CMS detector upgrades for HL-LHC are the highest priority of CSN1.

   We note, however, that the costs currently estimated by the ATLAS and CMS collaborations are quite large. Even assuming realistic reductions of scope and a very strong compression of all other activities, an adequate funding of these upgrades will require a substantial additional contribution to the CSN1 budget to supplement the standard baseline.
2. **Future Colliders**
   The case for future circular colliders in the leptonic and hadronic flavours has been made very strongly both in Europe and China during 2014 and global collaborations to study these machines are forming. The case for ILC has been on the table for some time. Japan has offered to host the project and is working on getting international partners. Apart from the technical issues previously discussed, these machines represent an enormous investment and require time and strong motivations to secure funding. In any case the final strategy for the next particle accelerator will appear more clearly when results from the 13 TeV pp collision data from LHC is available. In the absence of new physics observations at LHC (including its high-luminosity upgrade), it will be crucial to develop first a detailed examination of the electroweak sector, in particular for precision measurements of the recently discovered Higgs boson; this could be achieved with a new electron-positron machine, possibly complemented at a later stage with a very high-energy hadron collider, for direct searches for new physics. On the other hand if LHC provides solid indications of new physics, a specific strategy has to be developed, depending on the nature of the new phenomena.

   Recommendation #7:

CSN1 supports INFN participation in studies and R&D related to the future colliders. Our community must be part of the planning of the future.

We note that, at this stage, this work involves mostly human resources. While no significant funds are involved here, manpower can become a problem in case of conflicts with the many other ongoing projects. Adequate priorities must be assigned in these cases. Additional R&D work on magnet and cavity technology is currently supported by INFN outside of CSN1.

3. **Other direct searches for new physics**
New physics can appear in a wide range of possible models, as discussed in Section 5. While experiments at the energy frontier colliders explore a broad spectrum of models and parameter space, in some cases dedicated experiments with specialized detectors at lower energy can provide complementary sensitivity. If no new phenomena are observed at LHC, the case for these experiments gets even stronger as we will want to explore new physics models more broadly. Potential new experiments of this type are being considered for high intensity electron or proton beams. We note that, if extracted beams from the LHC become available at some point in the future, the possibilities in the area could be even richer.

Recommendation #8:
CSN1 supports the development of experimental proposals for new physics searches with fixed target experiments covering signatures not easily accessible by colliders. The priority of these experiments will depend on the theoretical relevance and parameter space coverage for the models being addressed, and the LHC indications from Run2.

4. **Flavour physics**
Flavour physics measurements are sensitive indirect probes of new physics. They are of great importance to understand the flavour structure of the SM and of new phenomena, if observed, as described in Section 6. A substantial program of flavour physics is ongoing and is well supported by CSN1 at CERN with the NA62 and LHCb experiments, at KEK with Belle II, at BEPC with BES III and at DAFNE with KLOE. Other experiments in the charged lepton sector are in various stages of preparation for new data taking periods both in Europe at PSI and at Fermilab in the US. In about ten years from now, final results from all of these experiments will be available, improving the precision of key measurements on CP violation and rare decays in the quark flavour sector by an order of magnitude, and extending the searches for charged lepton-number-violating processes by one to four orders of magnitude, depending on the channel. Owing to these achievements, significantly larger mass scales will be probed, depending on new physics models, than those explored by direct searches. If new physics is observed in direct searches, clear indications on the structure of the interactions can be obtained from flavour physics.
In order to achieve significant improvements in the reach of flavour physics, some relevant challenges must be tackled, as the required sensitivities often scale with the inverse of the fourth power of the mass scale probed. For this reason, a gain of orders of magnitude in statistics will be needed to make a real difference. Such large data samples could be obtained by exploiting the full HL-LHC luminosity and/or extracted beams of very high intensity that will be available worldwide. These explorations require new developments in detector design; some ideas are outlined in Section 6.8.

Recommendation #9:
CSN1 encourages further studies and R&D for a new generation of flavour physics experiments, which can provide notable improvements over current and forthcoming programs.

5. **Non-perturbative phenomena**
The major challenge for QCD, as described in Section 7, is the explanation of processes that cannot be treated with perturbation theory. Unfortunately many very common phenomena fall

in this category, in particular the internal structure of the hadron, elastic and diffractive proton interactions, and hadron spectroscopy. In addition many cross-sections important to interpret astro-particle experiment results are also poorly known. Present and future work at LHC will improve our knowledge of the PDF's, hadron spectroscopy, global proton properties and cross-sections for astro-particle. Additional detailed spectroscopy results are coming or will come from studies at BES III and Belle II.
The three dimensional structure of the proton is currently studied mainly at CERN by the COMPASS experiment and at J-Lab in the US. With the increase of the instantaneous luminosity at LHC multiple parton interactions could provide an additional probe. We note that additional facilities like FAIR and maybe EIC in the US or China may come into play at some point in time to address this area of work.

Recommendation #10:
A common plan from all the INFN communities currently working on the 3D structure of the nucleon should be prepared on the time scale of a year.

This report will be updated by mid-2017. By then it will be clear if new physics is observed at LHC and most potential new experiments will have consolidated their proposals. This timing will also allow us to give our input to the update of the European strategy on particle physics planned for 2018.

Additional Material

A Standard Model Physics: in-depth analyses and additional contributions

A.1 Prospects for a precise W mass measurement at LHC

A.1.1 Introduction

A.1.1.1 The experimental method

At hadron colliders, the W boson mass is extracted from the study of the charged-current (CC) Drell-Yan (DY) process, $p\overset{(-)}{p} \rightarrow l^+\nu_l + X$ (and also $p\overset{(-)}{p} \rightarrow l^-\bar{\nu}_l + X$). In the leptonic final state the neutrino is not measured, so that the invariant mass of the lepton pair can not be reconstructed. The value of m_W is determined from the study of the lepton transverse momentum, of the missing transverse energy and of the lepton-pair transverse mass distributions. These observables have an enhanced sensitivity to m_W because of their jacobian peak at the W resonance. More precisely, it is the study of their shape, rather than the study of their absolute value, which provides information about m_W These observables are defined in terms of the components of the lepton momenta in the transverse plane. The main experimental uncertainties are related to the determination of the charged lepton energy and momentum on one side, and, on the other side, to the reconstruction of the missing transverse energy distribution, so that the neutrino transverse momentum can be inferred in an accurate way. The modeling of the lepton-pair transverse momentum distribution also plays a major role in the determination of the neutrino components. A systematic description of the size of the experimental uncertainties affecting the measurement and of their impact on the m_W measurement can be found in [918–921].

A.1.1.2 Sensitivity to m_W of different observables

The sensitivity of the observables to the precise m_W value can be assessed with a numerical study of their variation under a given shift of this input parameter. In Fig. A.1 we show the ratio of two distributions obtained with $m_{W0} = 80.398$ GeV and with $m_{W,i} = m_{W0} + \Delta m_W$. The distortion of the shapes amounts to one to few parts per mill, depending if one considers the lepton transverse momentum or the lepton-pair transverse mass. We can rephrase this remark by saying that a measurement of m_W at the 10 MeV level requires the control of the shape of the relevant distributions at the per mill level. The codes used to derive the results in Fig. A.1 do not include the detector simulation; the conclusions about the sensitivity to m_W should be considered as an upper value, which can be reduced by additional experimental smearing effects.

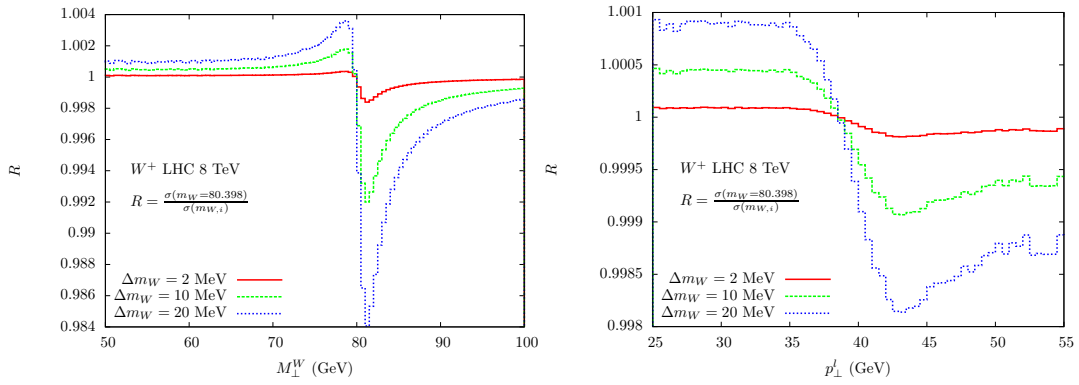

Fig. A.1: Ratio of lepton-pair transverse mass (left) and lepton transverse momentum (right) distributions which have been generated with different W boson masses.

The W boson mass is measured by means of a template fit approach: the distributions are computed with Montecarlo simulation codes for different values of m_W and are compared with the corresponding data; the value which maximizes the agreement is chosen as the preferred value. The templates are theoretical objects, computed with some assumptions about input parameters, proton PDF choices

and perturbative accuracy. The uncertainties affecting the templates, missing higher orders, PDF and input parameters uncertainties, have an impact on the result of the fit and should be treated as a theoretical systematic error.

A.1.2 Available tools and sources of uncertainty

The DY reaction in LO is a purely EW process, which receives perturbative corrections due to the EW and to the QCD interactions; in higher orders also mixed QCDxEW contributions appear and are of phenomenological relevance. The observables under study have a different behaviour with respect to the perturbative corrections, so that in some cases a fixed-order prediction is not sufficient and the resummation to all orders of logarithmically enhanced contributions becomes necessary. With the resummation, three different kinds of entangled ambiguities appear in the preparation of the templates: 1) missing higher-order logarithmically enhanced terms in the resummed expression, 2) ambiguities of the matching between fixed-order and all-order results, 3) the interplay, in the region of low lepton-pair transverse momenta, of perturbative and non-perturbative QCD corrections. This latter source of uncertainty is also related to the non-perturbative effects parametrized, in the collinear limit, in the proton PDFs.

The m_W value follows from the precise study of the shape of the observables; for this reason, the use of distributions normalized to their respective integrated cross sections removes an important class of uncertainties associated to the DY total rate determination.

A.1.2.1 EW radiative corrections

EW radiative corrections to CC and neutral-current (NC) DY are available with NLO-EW accuracy and are implemented in several public codes: `WZGRAD` [922,923], `RADY` [924], `SANC` [925], `HORACE` [926,927]. The effect of multiple photon emissions is accounted for in `HORACE` by a QED Parton Shower (PS), properly matched with the fixed-order calculation; higher-order universal effects, that can be reabsorbed in a redefinition of the tree-level couplings, are also available in the above codes and play an important role in the description of the NC invariant mass distribution.

Real-photon emissions from the final state leptons greatly modify the value of the measured lepton energies and momenta. The distortion of the jacobian peak is at the level of 5-18%, depending on the observable, on the kind of lepton and on the procedure that recombines QED radiation that surrounds the lepton into an effective calorimetric object. The impact at $\mathcal{O}(\alpha)$ of this radiation can be estimated to yield a shift of m_W of $\mathcal{O}(150\,\text{MeV})$ [918]. Additional radiation induces a further change in the result of $\mathcal{O}(10\%)$ of the $\mathcal{O}(\alpha)$ effect.

Subleading terms, i.e. not enhanced by a final state lepton mass logarithm, are exactly available as part of the $\mathcal{O}(\alpha)$ calculation and are partially available at $\mathcal{O}(\alpha^2)$ thanks to the matching procedure between QED PS and exact $\mathcal{O}(\alpha)$ matrix elements. Their impact amounts to a few contributions, each yielding a shift of $\mathcal{O}(5\,\text{MeV})$. The residual uncertainty due to missing higher orders has been estimated to be smaller than 5 MeV, in the framework of a purely EW analysis; it should be however kept in mind that the interplay of EW and QCD corrections leads, for some observables like e.g. the lepton transverse momentum distribution, to an increase of the purely EW estimate.

A.1.2.2 QCD radiative corrections

QCD corrections to lepton-pair production are available at fully differential level through $\mathcal{O}(\alpha_s^2)$ and are implemented in the Montecarlo integrators `FEWZ` [928], `DYNNLO` [929] and `SHERPA` [222]. The gauge boson transverse momentum distribution is known with NNLL+NLO accuracy (and with NNLO accuracy on the total cross section) and is implemented in the Montecarlo integrator `DYqT` [930], without the description of the decay into leptons [23]. The NNLL resummation, without the NNLO accuracy on the total

[23] The β-version of the code that includes the gauge boson decay is available from the authors of the code.

cross section, is available in the integrator ResBos [931, 932]. The effects on the total cross section and on the gauge boson rapidity distribution of the logarithmic threshold corrections have been included up to N^{3}LO+NNLL accuracy [933, 934]. Standard tools of the experimental analyses are the Shower Montecarlo (SMC) event generators with NLO-QCD accuracy, like MC@NLO [169] or POWHEG [935] (more recently HERWIG [936] or SHERPA [937]). They have NLO-QCD accuracy on the total cross section, but only LO-QCD accuracy in the description of the lepton-pair transverse momentum. Recently, progresses have been made in the direction of a merging of NNLO-QCD matrix elements with a QCD PS, in SHERPA [222] or in NNLOPS [221] or in GENEVA [216].

The QCD corrections have important effects on the DY observables in terms of absolute normalization and in terms of shapes. The former can be mitigated by considering normalized distributions, while the latter are the most critical ingredient in the theoretical framework. Among the observables relevant for the m_W measurement, the lepton transverse momentum distribution is a paradigmatic example: its prediction in fixed order is affected by the very large logarithmic corrections for small lepton-pair transverse momenta and only after their resummation a sensible description becomes possible. In this case, the evaluation of the QCD uncertainty on m_W is possible with a joint systematic study of matching ambiguities, renormalization/factorization scale variations, of the effect of subleading logarithmic terms and of the modeling of the non-perturbative effects at very low transverse momenta [930, 938]. A very naive estimate of the combination of all these effects, in a simplified setup, might be translated into a shift of the measured m_W by $\mathcal{O}(50 - 100)$ MeV, which would clearly be a dramatic conclusion of the uncertainty analysis. It has been proposed in [939] to consider ratios of W and Z observables, with an evident reduction of the scale uncertainties both in size and in shape. A study of the residual uncertainty on m_W in this approach is in progress [940]. The published Tevatron results [918, 919] do not quote a comprehensive QCD uncertainty that includes perturbative effects; they rather use the generator ResBos with a fixed choice of the perturbative scales and of the proton PDF to describe the Z boson transverse momentum distribution; this analysis allows to fit the parameters of a model describing the non-perturbative low-transverse-momentum components of QCD radiation, which are then used to simulate the CC DY process; this approach assumes universality of these parameters and their independence on the process energy scale. In the Tevatron analyses the error assigned to the $p_\perp^W$ modeling is due to a variation only of the non-perturbative parameters in the range allowed by the fit of the Z boson data.

The impact of the different QCD uncertainties mentioned above is milder in the case of the lepton-pair transverse mass, because this observable is more stable with respect to the inclusion of higher-order QCD corrections. The shape distortion observed when comparing its NLO- and NNLO-QCD determinations is minimal; the scale variations do not significantly modify the shape around the jacobian peak, and so the impact on the m_W determination is limited.

A.1.2.3 Proton PDF uncertainty

The proton PDFs enter in the m_W determination because they are needed to compute the templates used in the fit of the data. Different PDF set choices, or different replica choices within the same set, imply a change of the templates shape and in turn of the preferred m_W value. The propagation of the PDF error is computed according to the prescription of each PDF collaboration, and eventually the different results can be combined with the PDF4LHC recipe [756].

Neglecting all detector effects, which have an important impact on the acceptance determination, the PDF uncertainty on the m_W extracted from the study of the normalized lepton-pair transverse mass distribution remains below the 10 MeV level [85, 941], whereas the spread in the case of the lepton transverse momentum distribution, again estimated at generator level, ranges between 6 and 18 MeV, depending on the chosen PDF set, collider energy and final state [942], as shown in Fig. A.2. A crucial role is played by the acceptance cuts, on the leptons but also an the lepton pair. At higher collider energies, the PDF uncertainty associated to the lepton-pair transverse mass remains stable, whereas the one on m_W extracted from the lepton transverse momentum distribution increases for proton-proton

collider energies between 8 and 100 TeV (cfr. table A.1); the application of a cut $p_\perp^W < 15$ GeV on the lepton-pair transverse momentum keeps the estimated uncertainty to remain below the 15 MeV level [942].

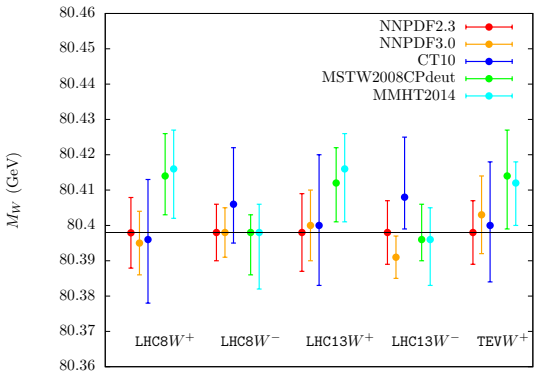

Fig. A.2: Summary of PDF uncertainty on m_W computed with different PDF sets, colliders and final states, for a measurement based on the lepton transverse momentum. A cut $p_\perp^W < 15$ GeV on the lepton-pair transverse momentum has been applied.

A.1.2.4 Mixed QCDxEW radiative corrections

QCD corrections, via initial state radiation, modify the kinematics of the DY events, whereas the leading EW effects are due to a variation of the leptonic spectra due to final state radiation. The interplay between these two groups of corrections is not trivial and strongly depends on the observable under study. The first perturbative order at which these mixed corrections appear is $\mathcal{O}(\alpha\alpha_s)$, but there is not an exact calculation available, so that one has to rely on some approximations. The NLO-QCD and NLO-EW exact matrix elements have been implemented in POWHEG and have been consistently matched with both QCD-PS and QED-PS for CC [185, 943] and NC [184] DY. In this approach all the QCD-LL (initial state collinear logarithms) and all the QED-LL (final state mass logarithms) corrections, in all possible combinations, are taken into account, including the leading $\mathcal{O}(\alpha\alpha_s)$ terms. The first terms that are beyond the accuracy of the code are of $\mathcal{O}(\alpha\alpha_s)$ and subleading in the expansion with respect to the EW logarithms. The role of the mixed corrections is particularly relevant in the prediction of the lepton transverse momentum distribution [184, 185]. For this quantity, as discussed in [944, 945], a naive factorization recipe to combine QCD and EW corrections, fails. The POWHEG implementation of the QCDxEW combination misses, on one hand, subleading effects of $\mathcal{O}(\alpha\alpha_s)$; it provides, on the other hand, an exact treatment of the kinematics of each radiated parton and thus gives the correct convolution of QCD and EW corrections including those effect that break the factorization *Ansatz*. The study of the impact of different combinations of QCD and EW effects, with and without NLO accuracy, is in progress [946].

A.1.3 Prospects of improvement

Let us briefly discuss the prospects for a high-precision measurement of m_W at a high- energy/luminosity proton-proton collider in the next 10-20 years, under the assumption that progresses that today can be wished, or expected in the long term, will be available.

A.1.3.1 Montecarlo generators

1. Definition of a matching procedure that allows a Montecarlo event generator to reach NNLO-QCD accuracy on the DY total cross section and NNLL-QCD accuracy in the resummation of

the logarithms of the lepton-pair transverse momentum (partial results are already available, by different groups).

2. Evaluation of the N^{3}LO-QCD corrections to the DY processes, as the first step towards the construction of an integrator code that reaches N^{3}LO accuracy on the total cross section and N^{3}LL accuracy in the resummation of the logarithms of the lepton-pair transverse momentum (the results in the soft limit are already available, by different groups).
   The formulation of an integrator with this accuracy on the lepton-pair transverse momentum is intertwined with the consistent definition of the non-perturbative contributions to the same observable. With a similar tool, and with the event generator of item 1), the evaluation of the ratio of W to Z observables should be sufficiently stable from the QCD point of view and the residual corresponding uncertainty on m_W could fall down to the 5 MeV level; this estimate is, at the moment, a guess that can become more sound after the estimate with the presently available tools of the QCD uncertainty on m_W extracted from ratios of W over Z observables.
3. Completion of the full calculation of the corrections at $\mathcal{O}(\alpha\alpha_s)$ to the DY processes, to fix the ambiguity affecting the combination of QCDxEW corrections at the first non trivial order (partial results in the W pole approximation are already available, matrix elements for different subprocesses that contribute at this order are available). The analysis of the purely EW effects on the m_W determination indicates a residual uncertainty at the 5 MeV level, but suffers from being a LO-QCD study; the inclusion of the $\mathcal{O}(\alpha\alpha_s)$ corrections will make the conclusion more stable against QCD-scale variations.
4. Determination of proton PDFs which can be consistently matched with an $\mathcal{O}(\alpha\alpha_s)$ calculation (NLO accuracy mixed QCDxEW).
5. Completion of the calculation of the full set of $\mathcal{O}(\alpha^2)$ corrections, to reduce the uncertainties in the calibration phase (Z mass determination and precise understanding of the absolute lepton energy scale).

A.1.3.2 Error reduction with higher energy/luminosity

We compare the perspective at future colliders for a measurement of m_W from the lepton transverse momentum and from the lepton-pair transverse mass. With the high luminosity projected at a high-energy (13, 33 or 100 TeV) hadron collider, and in particular with the high-luminosity programs planned at 13 TeV, the number of events useful for an accurate m_W measurement will be extremely large, making the error of statistical nature negligible, compared to those of systematic origin (theoretical and experimental).

Higher energy and PDFs. The energy scale of the DY processes, relevant for the W mass measurement, is given by the masses of the W and Z gauge bosons. An increase of the center-of-mass energy of a hadron collider reduces the values of the partonic-x, the fraction of the hadron momenta carried by the colliding partons, relevant to produce a final state of given invariant mass, and modifies the so called parton-parton luminosity, i.e. the effective number of colliding partons, and eventually the cross section. The change of collider energies has thus an impact on the PDF uncertainty, because of the different partonic-x range probed. The PDF uncertainty on m_W measured from the lepton-pair transverse mass distribution is already today at the 10 MeV level and is improving as long as LHC data become available, with some realistic chances that a contribution to the error on m_W will become soon of the order of 5 MeV [84, 941]. A preliminary estimate, at generator level, of the PDF uncertainty associated to the lepton transverse momentum distribution, using only the PDF set `NNPDF3.0`, can be found in Table A.1. These results assume the possibility of a cut on the lepton-pair transverse momentum; in the case that such an assumption could not be verified, a steeper growth of the uncertainty, up to $\mathcal{O}(25)$ MeV at 100 TeV, would be observed.

It will require a global effort to reduce the present $\mathcal{O}(20)$ MeV uncertainty down below the 10

MeV level, because of the contribution to the error of all the parton densities in a wide range of partonic x. The use of ratios of W over Z observables should partially reduce the PDF uncertainty, especially the one associated to gluon-induced subprocesses.

normalized distribution, additional cut $p_\perp^W < 15$ GeV				
	8 TeV	13 TeV	33 TeV	100 TeV
W^+	80.395 ± 0.009	80.400 ± 0.010	80.402 ± 0.010	80.404 ± 0.013
W^-	80.398 ± 0.007	80.391 ± 0.006	80.385 ± 0.007	80.398 ± 0.011

Table A.1: Estimate of the central values and of the PDF uncertainty on m_W, extracted from the normalized lepton transverse momentum distributions simulated with the `NNPDF3.0_nlo_as_0118` PDF set and with the `POWHEG` NLO-QCD event generator matched with the `PYTHIA 6.4.26` QCD Parton Shower. The fit interval is $p_\perp^l \in [29, 49]$ GeV.

Higher luminosity and neutrino momentum determination. The very large number of collisions occurring at each bunch crossing in the collider will make the so called pile-up phenomenon more and more pronounced with higher collider luminosity: the latter increases the hadronic activity in the transverse plane, making the reconstruction of the missing transverse momentum (and eventually of the neutrino transverse momentum) problematic. As a consequence, the uncertainty on the shape of the lepton-pair transverse mass will limit the possibility of a high-precision measurement.

A.1.4 Conclusions

- The progress in the calculation of higher order QCD and EW corrections seems to offer some chances that adequate theoretical tools will become available to perform a m_W measurement at the 10 MeV level.
- The lepton transverse momentum distribution has a very clean experimental definition and does not suffer of the pile-up problems that show-up with high-luminosity conditions. On the other hand it is extremely sensitive to any detail of the QCD description, both in the perturbative regime and for what concerns the PDF uncertainties, which could forbid any hope of measuring m_W at the 10 MeV level. The definition of W over Z ratios could be the clue to sensibly reduce all common theoretical systematics, as it has been demonstrated in [939]; this same approach could also help to mitigate the PDF problem. The availability of predictions with N^{3}LO+N^{3}LL accuracy should make it possible to reduce the QCD systematic error below the 10 MeV level.
- The lepton-pair transverse mass distribution has a very mild dependence on the details of QCD corrections, so that it should be possible to make its theoretical prediction accurate enough, to contribute with a systematic error at the 10 MeV level. The PDF uncertainty on this observable is moderate and will benefit of the inclusion of more LHC data in the global PDF fit. On the other hand, the accuracy of the measurement will deteriorate in presence of higher luminosity conditions, mostly because of increasing pile-up effects that disturb the identification of the hard scattering process.

A.2 Monte Carlo tools for electroweak physics

In this section we give a brief overview on the state of the art of the tools for precision electroweak physics, in view of the forthcoming experiments at the LHC run-II and the prospects of developments for future experiments at very high energy colliders, like the FCC-hh and FCC-ee. Some emphasis will be put on codes for hadronic collisions, while for e^+e^- colliders we will refer to the state of the art at the end of the LEP data analysis, discussing some issues and prospects relevant for future high luminosity/energy machines.

A.2.1 Hadron colliders

As already noted in Section 4.4, the experimental precision foreseen for LHC run-II will require the inclusion of the complete SM, both the QCD and the electroweak part, in the evaluation of quantum corrections for reliable simulations. The most accurately measured processes, where the inclusion of electroweak radiative corrections is already mandatory, are charged and neutral Drell-Yan, in addition to Higgs channels for the precise determination of its properties. In the past, i.e. at Tevatron and LHC run-I, the simulations and analysis have been performed by exploiting the dominance of QED LL photonic emission from external leptons and the relative suppression of QED radiation from quarks with respect to gluon radiation. In practice this was achieved by describing final state leptonic QED radiation by means of process-independent codes such as PHOTOS [947] or internal algorithms provided by the shower MC itself, as for instance in HERWIG++ [175, 948–950], PYTHIA(8) [172, 173, 951] and SHERPA [182, 952] . With the ultimate precision reached at Tevatron measurements, in particular the combined CDF and D0 W-boson mass measurements [953], a more precise theoretical description of Drell-Yan processes became necessary, at least for the estimate of the systematic uncertainties induced by the approximate factorized QCD$\otimes$QEDPS approach of the simulation tools. In fact, several complete fully differential electroweak NLO calculations are available in the literature and implemented in corresponding simulation codes, such as HORACE [926, 927], RADY [924, 954, 955] SANC [925, 956], WGRAD [922], WINHAC [957, 958] and ZGRAD [923]. These codes share the common feature of LO QCD and NLO electroweak accuracy. Several detailed comparisons exist in the literature [959–962], which allow to understand the level of technical as well as physical precision reached on the electroweak side of the calculations. Among the fixed order codes, it is worth mentioning that SANC can calculate the NLO contributions of $\mathcal{O}(\alpha_s)$ and $\mathcal{O}(\alpha)$, while the code FEWZ [963] adds up the EW NLO corrections to the QCD NNLO corrections for the neutral Drell-Yan process. The HORACE generator includes also the effect of all order photonic effects, consistently matched to the NLO calculation without double counting, in analogy with the QCD NLOPS codes such as MC@NLO and POWHEG. Only recently a consistent merging of NLO EW and QCD NLO corrections within a single event generator, matched with higher order QED and QCD emissions has been achieved within the POWHEG framework [185, 964] [24]. In this way also terms of $\mathcal{O}(\alpha\alpha_s)$ are included. In particular, terms of $\mathcal{O}(\alpha)$ dressed with soft/collinear QCD radiation and terms of $\mathcal{O}(\alpha_s)$ dressed with soft/collinear QED radiation are correctly accounted for. The remaining $\mathcal{O}(\alpha\alpha_s)$ terms are source of theoretical uncertainty which can be fixed by comparison with a complete two-loop $\mathcal{O}(\alpha\alpha_s)$ calculation. At present such a calculation has been carried out in pole approximation for the charged and neutral Drell-Yan processes [944]. A solid estimate of these and NNLO EW perturbative contributions will be crucial for future precision measurements of the W-boson mass at the LHC A.1. The complete NNLO calculation, beyond pole approximation, will be a challenge for future theoretical advances.

Besides the Drell-Yan processes, exact NLO EW calculations exist for a limited number of final states, such as dijets, $V + 1$ jet, $t\bar{t}$, single-top, $V(= W, Z, \gamma) + 3$ jets, $V + H$. The recent progress in the automation of NLO QCD calculations, described in section 4.4 is being extended to include also the calculation of NLO EW corrections. There are in principle no obstacles to this, even if the EW corrections are more involved due to the presence of different mass scales circulating in the loops, together with the presence of unstable particles and chiral interactions. Several groups are working in this direction: GoSaM [177, 965], HELAC-NLO [966], MadLoop [176, 967], OpenLoops [179] and Recola [178]. First complete results obtained with automated tools appeared in Refs. [968–971]. During the 2013 edition of the Les Houches Workshop on Physics at TeV Colliders a "High Precision Wish List" has been proposed [754], which can be considered as the goal of the high precision calculations for the next coming years. By inspection of Tables [1-3] of Ref. [754], we can see that the NLO EW corrections, consistently added to the (N)NLO QCD ones and matched with higher order QCD/QED PS contributions are required

[24] An independent implementation has been presented in Ref. [943], where the higher order shower corrections are given by the QCD shower only.

for all the processes in the tables. This list of processes will allow to fully exploit the LHC data at 14 TeV in understanding the Standard Model to such an extent that any possible evidence for new physics will be unambiguous. It is worth noticing that, in addition to the already discussed Drell-Yan processes, the consistent matching of NLO EW corrections with higher order QED PS is only available for Higgs decay to four leptons [972].

Usually the size of the "genuine" EW corrections (i.e. excluding the leading terms of electromagnetic origin) is moderate, at the few % level. However, when the scales involved in the considered scattering process become large with respect to M_W, the NLO EW corrections can be particularly enhanced, because of the presence of logarithmic terms of the form $\alpha \ln^2(Q^2/M_W^2)$ and $\alpha \ln(Q^2/M_W^2)$, where Q^2 is a typical energy scale of the process. These terms are known as Sudakov logarithms and correspond to the soft and collinear singularities of QCD and QED, induced by the presence of massless particles. In the case of the EW corrections, however, the W boson mass acts as a physical cutoff so that the virtual corrections can be considered separately from the real contributions [25], giving rise to large negative corrections in the phase space regions where $Q^2 \gg M_W^2$. Moreover, on pure theoretical grounds, the cancellation of Sudakov logarithms in the EW sector can only be partial, due to the incomplete summation of the contribution of $SU(2)$ doublets in the initial state. The Sudakov logarithmic structure of the electroweak corrections has been studied in detail in the literature [973–975, 975–979] and a general algorithm able to extract, in a process-independent way, the coefficients of the double and single logarithms has been presented in Refs. [980, 981]. Such an algorithm has been recently implemented in the ALPGEN event generator, with first phenomenological results for the processes $Z/\gamma+$ multi-jets [982], particularly important backgrounds for the search of New physics in the extreme kinematical regime at the LHC. Further studies at the energies of 33 TeV and 100 TeV, typical reference energies for future hadronic colliders, have been carried out within the 2013 Snowmass Community Summer Study. For example, for few selected processes, as dijet production, inclusive vector boson production, V + jets, vector boson pair production, it has been shown that, in the extreme regions probed at the LHC with $\sqrt{s} = 8$ TeV, the electroweak effects on the tails of some distributions become of the same order of magnitude of the experimental accuracy. This means that with the future run-II of the LHC we will enter the Sudakov zone, where the EW corrections are relevant for data analysis and will be even more important for higher energies, as shown in Table A.2, where the size of the corrections can reach several tens of percent. With such large effects also the issue of the resummation of EW corrections should be addressed, as suggested in Refs. [978, 983–986].

Process	$\sqrt{s} = 8$ TeV	$\sqrt{s} = 14$ TeV	$\sqrt{s} = 33, 100$ TeV
Inclusive jet, dijet	Yes	Yes	Yes
Inclusive W/Z tail	$\sim$ Yes	Yes	Yes
Wγ, Zγ tail ($\ell\nu\gamma, \ell\ell\gamma$)	No	$\sim$ Yes	Yes
W/Z+jets tail	$\sim$ Yes	Yes	Yes
WW leptonic	Close	$\sim$ Yes	Yes
WZ, ZZ leptonic	No	No	Yes
WW, WZ, ZZ semileptonic	$\sim$ Yes	Yes	Yes

Table A.2: Are we in the Sudakov zone yet? Taken from Ref. [987].

A.2.2 Lepton colliders

The simulation tools for lepton colliders can be grouped in two different classes, according to the physics purpose: generators for the precision luminosity determination on the one side and programs for the

[25] The real corrections produce different final states, which usually in the experimental analysis are considered as different processes with respect to the one under consideration.

analysis of the large angle data. These two kinds of theoretical tools allow for the completion of the high precision physics program of an e^+e^- collider.

A.2.2.1 Event generators for luminosity

The luminosity can be determined through a counting measurement of a process which has a large cross section and is theoretically precisely known, such as the small angle Bhabha scattering. This process is in fact largely dominated by QED t-channel photon exchange and its cross section can be calculated perturbatively with a high level of precision. During LEP1 and LEP2 era the reference generator for small angle Bhabha scattering was BHLUMI [988, 989], which was based on QED NLO corrections to t-channel scattering supplemented with higher order corrections in the Yennie-Frautschi-Suura exponentiation approach. The physical precision of BHLUMI was scrutinized by means of independent calculations, such as for instance SABSPV [990], mainly based on QED NLO precision plus higher orders photonic corrections in the QED structure function approach. The final theoretical accuracy on Bhabha scattering at LEP1 was at the level of 0.05%.

The experience gained at LEP has been fruitful for the development of Monte Carlo tools for the luminosity determination at the low-energy flavour factories by means of large angle Bhabha scattering, cross-checked with $e^+e^- \to \gamma\gamma$. In this context the first QED parton shower matched to the NLO fixed order calculation for the QED processes $e^+e^- \to e^+e^-$, $e^+e^- \to \mu^+\mu^-$ and $e^+e^- \to \gamma\gamma$ has been realized [991–993]. In parallel, an impressive effort has been devoted to the calculation of the exact NNLO QED corrections to Bhabha scattering (see for example Ref. [994] and references therein). A future consistent inclusion of these results into Monte Carlo generators could push the accuracy at the level of a few 0.01%, at least as far as QED corrections are concerned.

A source of theoretical uncertainty (driven by experimental errors) is the hadronic contribution to the vacuum polarisation $\Delta\alpha_{had}(M_Z)$, which is derived from low energy data through dispersion relations. In this context, the present measurements at low energy machines are extremely important to reduce one of the uncertainties which were dominant at LEP.

It is worth mentioning that an alternative process to Bhabha scattering for luminometry is $e^+e^- \to \gamma\gamma$, which is not affected, at least up to NNLO order, by the error on $\Delta\alpha_{had}$ and thus, in principle, it could be calculated with higher theoretical precision.

A.2.2.2 Simulation tools for Z and W bosons at FCC-ee

Given the available statistics at LEP1, a 0.1% precision level was reached for most of the observables. With such a level of precision, the necessary ingredients for the simulation tools (event generators and semi-analytical programs, such as for instance KORALZ [995, 996], TOPAZ0 [997–1000] and ZFITTER [1001–1004]) were the exact NLO EW corrections to the $e^+e^- \to f\bar{f}$ hard scattering, convoluted with QED final and initial state radiation. Since around the Z resonance the latter contribution is very large, of the order of 30%, higher order effects were included through the Yennie-Frautschi-Suura formalism or the QED structure function approach. In order to match the target accuracy, also higher order effects of weak and QCD origin, contributing for instance to the ρ and Δr parameters, had to be included in the computational tools. It is clear that a future GigaZ run of an e^+e^- collider will require complete EW NNLO calculations, supplemented with improved higher order QED corrections. While the theoretical framework of the Standard Model two-loop renormalization has been set in Refs. [1005–1007], the calculation of observables at NNLO accuracy for the processes $e^+e^- \to f\bar{f}$ is still a challenge for the future.

The high luminosity run of a future e^+e^- collider at energies close and above the WW, ZZ and ZH thresholds will be very challenging for the development of Monte Carlo codes able to provide precise theoretical predictions. In fact, at LEP2 most of the tree-level predictions for four-fermion final states were based on tree-level matrix element, supplemented with convolution with initial state radiation

effects and leading electroweak corrections in the form of running couplings, together with a scheme for the treatment of the unstable virtual bosons (see Ref. [1008–1010] for a review). Complete NLO predictions for $e^+e^- \to 4$ fermions final states appeared only after the end of LEP2 operations [1011–1014]. Most probably the required theoretical precision at FCC-ee will be NNLO EW corrections to $e^+e^- \to 4$ fermion final states, interfaced with algorithms for the treatment of QED higher order initial state radiation, a very challenging task for the present available theoretical knowledge.

B Flavour Physics: in-depth analyses and additional contributions

B.1 A case study at CMS

The excellent B physics performance of the current CMS detector shows that it is possible to produce competitive results in this field also for a non-dedicated hadron collider experiment. The LHC luminosity upgrade will open new possibilities for B physics measurements, especially for what concerns the observation and study of rare processes like the $B^0_{(s)} \to \mu^+\mu^-$ decays. On the other hand, the high instantaneous luminosity and increased pileup will create demanding conditions for the trigger and offline reconstruction of B production and decay.

In this paragraph, the B-physics potential of the upgraded CMS detector is illustrated by presenting a study of the $B^0 \to \mu^+\mu^-$ and $B_s \to \mu^+\mu^-$ decays. This work is based on the $\mathcal{B}(B_s \to \mu^+\mu^-)$ measurement published by the CMS collaboration with the LHC Run 1 data [1015], and focuses on the implementation of a prototype L1-trigger algorithm and on the estimate of the final analysis sensitivity. The only way to build a Level 1 trigger for the B^0 and B_s signal at the HL-LHC is exploiting the Track Trigger architecture of the upgraded CMS detector, as the Muon chambers information only has no sufficient resolution and could not distinguish muons coming from the huge (about 140) pileup events.

The Level 1 B candidate is built from two muons, which satisfy selection criteria based on transverse momentum, pseudorapidity, invariant mass and origin from a common primary vertex, and is required to have $p_{\mathrm{T}}^{\mu\mu} > 4\,\mathrm{GeV}$, $|\eta^{\mu\mu}| < 2$, and $3.9 < M^{\mu\mu} < 6.9\,\mathrm{GeV}$.

The invariant mass distributions of the Level 1 B candidates for $B^0 \to \mu^+\mu^-$ and $B_s \to \mu^+\mu^-$ signal events are shown in Fig. B.1 for an integrated luminosity of 3000 fb^{-1}. The invariant mass resolution at L1 is about 70 MeV for both resonances. The rate of the L1 trigger on Minimum Bias events is a few hundreds Hz, which is only a small fraction of the total di-muon L1 trigger rate.

The offline signal reconstruction is performed by requiring two opposite-charge muons, each having $p_{\mathrm{T}}^{\mu} > 4\,\mathrm{GeV}$. The B candidate is built from the two muons and is required to have $p_{\mathrm{T}}^{\mu\mu} > 5\,\mathrm{GeV}$ and $4.9 < M^{\mu\mu} < 5.9\,\mathrm{GeV}$.

Three different scenarios have been considered: the 2019 Phase-1 detector with no aging and with an aging corresponding to 1000 fb^{-1} of integrated luminosity, and the Phase-2 upgraded detector. For the first two scenarios, both barrel and endcaps are taken into account ($|\eta^{\mu}| < 2.5$), while for the Phase-2 scenario only barrel is considered ($|\eta^{\mu}| < 1.4$), trading the loss in efficiency with an increase in overall resolution. All the resolutions do not show significant changes between the two aging conditions of the 2019 detector, thus only the latter is used in the following.

The invariant mass resolutions measured in the barrel, extracted from the widths of Gaussian fits to the mass peaks found with the full detector simulation, are 42 MeV for the Phase-1 scenario and 27 MeV for the Phase-2 scenario. The Phase-1 resolutions are comparable to those of the Run 1 measurement, while the Phase-2 gives an improvement of a factor 1.5. In general, no significant differences between the resolutions of the two peaks are seen.

Figure 80 shows toy-MonteCarlo projections of the B^0 and B_s analysis results for the two different scenarios. Left plot corresponds to barrel events and a total integrated luminosity of 300 fb^{-1}, while right plot corresponds to barrel events and a total integrated luminosity of 3000 fb^{-1}. In both cases, the $\sigma \times \mathcal{B}$ predicted by the SM is assumed for B^0 and B_s. The background models are taken from the $\mathcal{B}(B_s \to \mu^+\mu^-)$ measurement published by CMS with the LHC Run 1 data. Conservatively, a

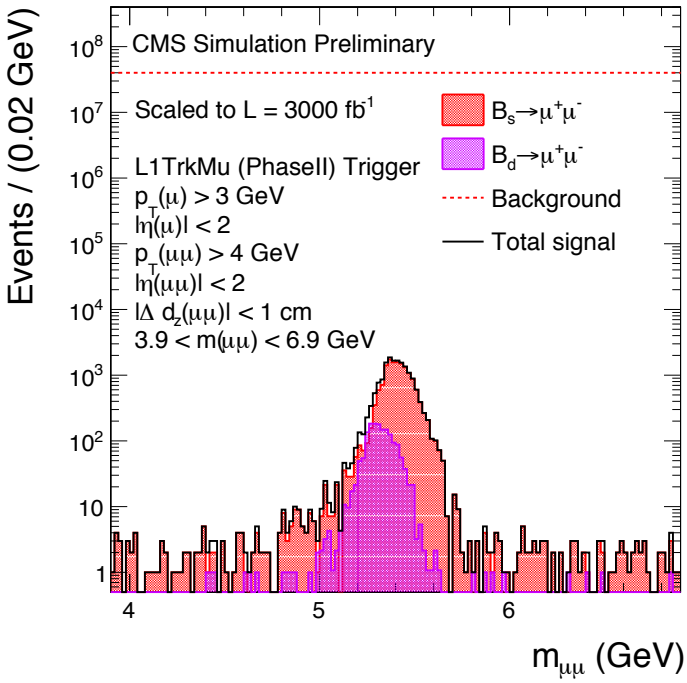

Fig. B.1: The di-muon invariant mass distributions at Level 1 trigger for $B^0 \to \mu^+\mu^-$ (purple) and $B_s \to \mu^+\mu^-$ (red) events for a total integrated luminosity of 3000 fb^{-1}. The red dashed line shows the expected background level.

loss of efficiency equal to 35% for the signal and 30% for the backgrounds is assumed for the Phase-2 projections with respect to the Run 1 results. More details on the model used in the toy-MC estimates can be found in [1016]. These results show that while in the 2019 scenario the B^0 peak is covered by the long resolution tail of the B_s resonance, in the 2023 scenario the two peaks can be resolved due to the improved invariant mass resolution.

The analysis performance is estimated for the Phase-2 scenario under the assumptions outlined above for a total integrated luminosity of 3000 fb^{-1}. The expected number of $B^0 \to \mu^+\mu^-$ and $B_s \to \mu^+\mu^-$ events after all the analysis cuts is respectively $\sim$ 260 and $\sim$ 2200. The sensitivity for the observation of the $B^0 \to \mu^+\mu^-$ decay is expected to be $\approx 6.8\,\sigma$, while the branching fractions $\mathcal{B}(B^0 \to \mu^+\mu^-)$ and $\mathcal{B}(B_s \to \mu^+\mu^-)$ can be measured with a precision of 18% and 11% respectively. Their ratio $\frac{\mathcal{B}(B^0\to\mu^+\mu^-)}{\mathcal{B}(B_s\to\mu^+\mu^-)}$ can be measured with a 21% uncertainty, to be compared with the 40% expected in LHCb with 50 fb^{-1}.

B.2 Predicting the accuracy of Flavour Lattice QCD

B.2.1 Recent progresses in Lattice QCD

A significant progress in the search for New Physics (NP) requires a combined improvement of the experimental and theoretical accuracies. A crucial ingredient from the theory side is the capability to determine the hadronic matrix elements with the same level of accuracy of the experimental measurements.

Lattice QCD has a primary role in the computation of long-distance QCD contributions and thus of the hadronic matrix elements. Lattice QCD is a non-perturbative approach based on first principles, as it does not introduce additional free parameters besides the QCD fundamental couplings. Moreover,

all systematic uncertainties affecting the results of lattice QCD calculations can be reduced with the increasing availability of computational power.

Lattice QCD has witnessed a very important progress in the last ten-fifteen years, mainly for two reasons. The first one is the increase of the computational power that has allowed the overtaking of quenched simulations by unquenched simulations, i.e. the inclusion of the contribution of loops of quarks. Nowadays essentially all lattice Collaborations perform unquenched simulations with either $N_f = 2$ (up and down), $2 + 1$ (up, down and strange) or $2 + 1 + 1$ (up, down, strange and charm) dynamical fermions. The second important reason is the algorithmic improvement that has led to lattice simulations with light quark masses close to the physical value. This has been possible thanks to new algorithms that have enormously reduced the dependence of the computational cost on the simulated quark mass.

A sketch of the progress achieved in the last decade by lattice QCD is provided in Table B.1 where, for some hadronic parameters of interest for Flavour Physics, the 2002 and 2013 lattice accuracies are compared. The progress achieved in lattice QCD in the last decade makes us optimistic on the improvement that we can expect in the next decade.

Hadronic Parameter	2002 [1017]	2013 [1018]
$f_+^{K\pi}(0)$	-	0.4%
B_K	17%	1.3%
f_{B_s}	13%	2%
f_{B_s}/f_B	6%	1.7%
B_{B_s}	9%	7%
B_{B_s}/B_B	3%	10%
$F_{D^*}(1)$	3%	2%
$B \to \pi$	20%	10%

Table B.1: *Accuracy on some hadronic parameters (decay constants, form factors and bag-parameters) of interest for Flavour Physics.*

B.2.2 Basic idea of the predicting analysis

In the following we tempt to predict the accuracy that we can expect in 2025 (in the *What Next Era*) from lattice QCD for the hadronic parameters of interest for Flavour Physics, in particular for the parameters collected in Table B.1. We closely follow the study performed by Vittorio Lubicz in the appendix of the SuperB-factory conceptual design report [713], where the extrapolation in time was from 2007 to 2015. Predictions of this kind are necessarily based on somehow educated guesses and their reliability decreases the more one attempts to go further in time.

The last decade teaches us that important progresses can come from a theoretical breakthrough, as for the recent algorithmic improvements, which is difficult or impossible to be predicted. In this study of the expected increase of precision in lattice QCD only the increase of computational power is taken into account. We are not able, in fact, to account for the unpredictable impact of possible algorithmic improvements and developments of new theoretical techniques. For these reasons, the predictions we are going to quote have to be taken with caution.

In order to predict the precision expected from lattice QCD we proceed in the following way. We consider three benchmark levels of accuracy, namely 1%, 0.5% and 0.1% and we estimate the values of the parameters (number of configurations N_{conf}, lattice spacing a, light quark mass m_ℓ, size L) of the lattice simulation that allows to achieve that level of accuracy. For each of these simulations we estimate the computational cost. Finally we compare the required computational cost with the computational power expected in 2025. Such a comparison tells us what level of accuracy we should achieve in 2025.

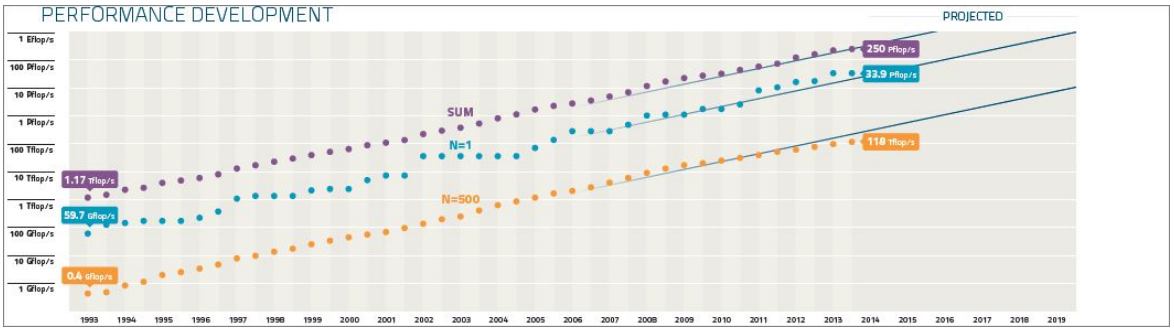

Fig. B.2: *Performance development of the most powerful computer systems in the world as a function of the year [1019]. The top (violet) points correspond to the sum of the* 500 *fastest computer systems, the middle (light blue) points to the fastest in the world, the bottom (yellow) points to the number* 500 *in the list.*

This study will distinguish between light (π and K), charm and beauty sectors, because they are affected in a different way by systematic uncertainties. Moreover, one has to take into account that some hadronic parameters present additional difficulties w.r.t to others.

B.2.3 Expected increase of the computational power

Let's first discuss the expected increase with time of the available computational power. At variance with other ingredients in the present analysis, the computational power can be predicted with rather good reliability, since it is found to follow a simple scaling law. This is the Moore's Law, formulated by Gordon Moore in 1965 from the observation that the number of transistors on integrated circuits doubles approximately every two years, thanks to miniaturization. It turns out out into a performance improvement of $\mathcal{O}(10^3)$ every 10 years.

This is illustrated in Fig. B.2, which shows the performance of the 500 most powerful computer systems in the world as a function of the year [1019]. The top (violet) points correspond to the sum of the 500 fastest computer systems, the middle (light blue) points to the fastest in the world, the bottom (yellow) points to the number 500 in the list. At present the most powerful computer system in the world is the National Super Computer Center in Guangzhou (China) with a sustained speed of 33.86 PFlops, while the 500th in the list has a speed of about 0.13 PFlops. Typical computer systems that are available today for lattice QCD simulations have performances in the range $0.1 - 0.5$ PFlops, that is within the lower part of the top-500 list. By extrapolating the bottom (yellow) points one can estimate the available computer power for 2025 lattice QCD simulations to be in the range $100 - 500$ PFlops, i.e. three orders of magnitude faster than what we have today.

In performing predictions one may worry about the ultimate limits of the Moore's Law. Already in 2005 Gordon Moore himself said in an interview: *In terms of size you can see that we are approaching the size of atoms, which is a fundamental barrier, but it'll be two or there generations before we get that...We have another 10 to 20 years before we reach a fundamental limit*. The same concern was raised several times and every time it was concluded that the Moore's law would have lasted at least another decade. Nowadays there exist different estimates for the ultimate limit of the Moore's law. For the present study, we just observe that there is general consensus on the fact that 2025 will be in the validity range of the Moore's law.

B.2.4 Lattice parameters for benchmark simulations

We now want to estimate the parameter values that have to be required in a lattice simulation in order to achieve the benchmark levels of accuracy of 1%, 0.5%, 0.1%. To this purpose we will ask all the statistical and systematic uncertainties to be under control at the considered level of accuracy.

In typical lattice computations the dominant systematic uncertainties are due to: discretization effects, heavy quark extrapolation, chiral extrapolation, finite size effects, renormalization. The latter source of uncertainty is, at present, already well under control, at the level of 1% or better and is expected to further improve in the future, without representing a limiting factor in improving the future precision of lattice results. We briefly discuss the other sources of uncertainty in order to estimate the values for the simulation parameters that allow to achieve the desired accuracy.

Statistical error

As the statistical error scales as $1/\sqrt{N_{conf}}$, it can be reduced by increasing the number of configurations N_{conf}. Lattice studies based on $\mathcal{O}(10^2)$ independent configurations have typically a $\sim 1\%$ statistical error. It follows that reducing it to 0.5% or 0.1% would be possible by generating ~ 400 and $\mathcal{O}(10^4)$ independent configurations, respectively.

Discretization effects

Numerical simulations are performed on lattices with finite lattice spacing a, and a continuum extrapolation ($a \to 0$) is required to get the physical result. The control of this extrapolation strongly depends on the values of the simulated lattice spacing, which should be as fine as possible. In order to estimate the value of the minimum simulated lattice spacing required to reduce the discretization error at the 1, 0.5 or 0.1% level, we will consider an heuristic argument [713, 1020], which is simple and expected to provide a conservative estimate.

The argument assumes that lattice simulations are performed at two values of the lattice spacing, namely a_{min} and $\sqrt{2}a_{min}$ and the lattice data (Q_{latt}) are extrapolated linearly in a^2 to get a determination of the physical observable (Q_{cont}).[26]

The relation between Q_{latt} and Q_{cont}, however, also contains higher order terms in the a-expansion. It can be schematically written as

$$Q_{latt} = Q_{cont}\, \left[1 + (a\Lambda_2)^2 + (a\Lambda_n)^n + \dots\right] , \tag{B.1}$$

where the parameters Λ_2,Λ_n, $\dots$ are of the order of Λ_{QCD} for observables involving only light quark, and of order of the heavy quark mass m_H in the presence of heavy quarks. The power n of the sub-leading correction in Eq. (B.1) depends on the action. For instance, it is $n = 3$ for $\mathcal{O}(a)$-improved Wilson quarks and $n = 4$ for maximally twisted, staggered and Ginsparg-Wilson fermions.

The performed continuum extrapolation including only the $\mathcal{O}(a^2)$ term introduces an error, ε_{discr}, that can be easily estimated comparing the so obtained result to the result that one would obtain for Q_{cont} from Eq. (B.1), that is

$$\varepsilon_{discr} \equiv \delta Q_{cont}/Q_{cont} \simeq (2^{n/2} - 2)(a_{min}\Lambda_n)^n \, . \tag{B.2}$$

By taking $\varepsilon_{discr} = \{1, 0.5, 0.1\}\%$ one can extract the three values to be chosen in the benchmark simulations for the minimum lattice spacing a_{min} .

For observables involving the quark beauty, we consider simulations performed with the heavy quark mass at the physical point ($m_H \simeq m_b$) or closer to the charm quark mass m_c, for instance in the range $m_c \div 2m_c$. In the first case $\Lambda_n = m_b$ in Eq. (B.2), while in the second case $\Lambda_n = 2m_c$ and an extrapolation in the heavy quark mass is needed to get the physical result. The latter extrapolation introduces a systematic error that has to be taken into account.

[26] We have assumed that the fermionic action chosen in the simulation is $\mathcal{O}(a)$-improved, implying the absence of the leading discretization effect of $\mathcal{O}(a)$ in the expansion.

Heavy quark mass extrapolation

In order to estimate the systematic error due to the heavy quark mass extrapolation we compare the approximated result of a linear fit in $1/m_H$ with the result including the sub-leading term of $\mathcal{O}(1/m_H^2)$. The argument assumes that lattice simulations are performed at two values of the heavy quark mass, namely m_H^{max} and $m_H^{max}/\sqrt{2}$. As mentioned before, this kind of procedure produces a conservative estimate. This is particularly true for the heavy quark mass extrapolation since we are not considering nor quantifying the impact of already existing smart methods to treat the beauty quark on the lattice (like effective actions, ratio methods,...), which play a crucial role in keeping the systematic uncertainty under control.

Chiral extrapolation

In order to estimate the light quark mass value to be adopted in the benchmark simulations we follow a procedure similar to the estimate of the minimum value for the lattice spacing. The dependence of physical quantities on light quark masses, in QCD, is predicted by Chiral perturbation theory (ChPT). ChPT expansions involve both analytic (local) and non-analytic (due to pion loops) terms. For simplicity we estimate the uncertainty due to the chiral extrapolation neglecting the non-analytic contribution, i.e. assuming a ChPT expansion of the following form

$$Q_{latt} = Q_{phys}\ \left[1 + c_1(m_{PS}/m_V)^2 + c_2(m_{PS}/m_V)^4 + \dots\right]\ , \tag{B.3}$$

where m_{PS} and m_V are the simulated pseudoscalar and vector meson masses (at the physical point $m_{PS} = m_\pi$ and $m_V = m_\rho$) and the coefficients c_1 and c_2 are expected to be of $\mathcal{O}(1)$. We observe that m_{PS}^2 is proportional to the light quark masses and that $m_V \sim m_\rho$ provides the typical scale entering the chiral expansion.

By assuming that lattice simulations are performed at two values of the light quark masses, corresponding to $(m_{PS}/m_V)_{min}$ and $\sqrt{2}(m_{PS}/m_V)_{min}$, and that the lattice data are extrapolated linearly in $(m_{PS}/m_V)^2$, according to Eq. (B.3) the error in determination of the physical result is given by

$$\varepsilon_{chir} \equiv \delta Q_{phys}/Q_{phys} \simeq 2c_2(m_{PS}/m_V)^4_{min}\,. \tag{B.4}$$

By taking $\varepsilon_{chir} = \{1, 0.5, 0.1\}\%$ one can extract the three benchmark values for $(m_{PS}/m_V)_{min}$ or, equivalently by using the ChPT relation between the two ratios, for $(m_l/m_s)_{min}$.

Finite size effects

Finite size effects (FSE) are related to the infrared behavior of the theory and in QCD they can be estimated by using ChPT. They turn out to be exponentially suppressed for correlation functions that are free of physical singularities (thus, in particular, for all matrix elements involving at most one stable state in the initial and final states). The dominant contribution comes from the propagation of virtual pions and can be expressed as

$$\varepsilon_{FSE} \equiv \delta Q_{phys}/Q_{phys} \sim C_Q(m_\pi, L)\exp\left(-m_\pi L\right), \tag{B.5}$$

where L is the one-dimensional size of the lattice and the function C_Q, which depends on the observable Q, can be computed in ChPT and it is typically of $\mathcal{O}(1)$. By taking $C_Q = 1$ and requiring $\varepsilon_{FSE} = \{1, 0.5, 0.1\}\%$, on can estimate the values for the product $m_\pi L$ to be adopted in the benchmark simulations. By simultaneously requiring the same level of accuracy in the chiral extrapolation, which implies a value for the simulated $(m_l/m_s)_{min}$ or equivalently for $(m_\pi)_{min}$, one gets the lattice extension for the benchmark simulations.

Following the procedure outlined above we get for the benchmark simulation parameters the values collected in Tables B.2-B.5.

Looking at Table B.2 we observe that the two blank spaces in correspondence of $\Lambda_n = 2m_c$ and of the 0.5 and 0.1% accuracies mean that the uncertainty due to the heavy quark mass extrapolation

Λ_n	$\varepsilon_{discr} = 1\%$	$\varepsilon_{discr} = 0.5\%$	$\varepsilon_{discr} = 0.1\%$
$\Lambda_{QCD} \sim 0.8$ GeV	0.065	0.055	0.037
$m_c \sim 1.5$ GeV	0.035	0.029	0.020
$2m_c \sim 3.0$ GeV	0.018	-	-
$m_b \sim 4.5$ GeV	0.012	0.010	0.005

Table B.2: *Benchmark simulated values for the lattice spacing (a_{min}), in fermi units.*

$\varepsilon_{chir} = 1\%$	$\varepsilon_{chir} = 0.5\%$	$\varepsilon_{chir} = 0.1\%$
0.08	0.05	0.02

Table B.3: *Benchmark simulated values for the quark mass ratio $(m_l/m_s)_{min}$.*

$\varepsilon_{FSE} = 1\%$	$\varepsilon_{FSE} = 0.5\%$	$\varepsilon_{FSE} = 0.1\%$
4.6	5.3	6.9

Table B.4: *Benchmark simulated values for the product $m_\pi L$.*

$\varepsilon_{FSE} = 1\%$	$\varepsilon_{FSE} = 0.5\%$	$\varepsilon_{FSE} = 0.1\%$
6.5	7.5	9.7

Table B.5: *Benchmark simulated values for the lattice size, in fermi units, in a simulation at the light physical point $m_\pi = m_\pi^{phys}$.*

dominates over the discretization error, so that the target levels of 0.5 and 0.1% cannot be achieved by simulating heavy quark masses in the physical charm region. We notice that in present π/K (i.e. with $\Lambda_n = \Lambda_{QCD}$) simulations the typical finest lattice spacing is ~ 0.05 fm, allowing for a level of accuracy of about 0.5%.

It is interesting to observe that in Table B.3 the value $(m_l/m_s)_{min} = 0.05$ corresponding to the 0.5% accuracy is very close to the physical value $(m_l/m_s)^{phys} = 0.04$. This means that in order to reduce the chiral uncertainty to the 0.5% level or better, simulations at light physical point are needed and, indeed, some collaborations have already performed them and other collaborations are working in that direction (see [1018] for a recent review).

In order to compare the values of the product $m_\pi L$ in Table B.4 with the state of the art of present simulations we notice that the FLAG13 [1018] color code for FSE is such that the green star is assigned if $m_\pi L > 4$.

Finally, Table B.5 shows the benchmark values of the lattice size for light physics simulations performed at the physical point, that is with $m_\pi = m_\pi^{phys}$.

B.2.5 Computational cost of the benchmark simulations

Having determined the parameter values of the benchmark simulations we want to estimate the corresponding computational cost and to compare it to the computational power expected in 2025.

There is an empirical formula that expresses the computational cost of a numerical simulation with present algorithms as a function of the parameters: number of independent gauge configurations (N_{conf}), space-time extension of the lattice ($L^3 \times T$), value of the average up/down quark mass (m_l) or equivalently value of the ratio m_l/m_s, and value of the lattice spacing (a). For Wilson-like fermions

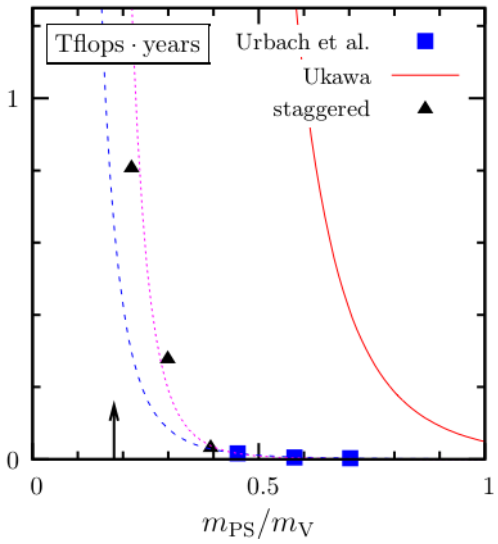

Fig. B.3: *Plot taken from [1022] for the computational cost to generate* 1000 *independent gauge configurations for some different fermionic actions and algorithms as a function of the ratio* m_{PS}/m_V*. The cost estimate presented by Ukawa at the Lattice 2001 conference (Berlin wall) is also shown.*

with $N_f = 2$ flavours of dynamical quarks, this formula reads [1021][27]

$$TFlops - years \simeq 0.03 \left(\frac{N_{conf}}{100}\right) \left(\frac{L}{3fm}\right)^5 \left(\frac{T}{2L}\right) \left(\frac{0.2}{m_l/m_s}\right) \left(\frac{0.1fm}{a}\right)^6 , \qquad \text{(B.6)}$$

where the cost is expressed in TFlops-years, representing the number of years of run required to perform the simulation on a 1-TFlop machine.

The linear dependence on the inverse light quark mass is an important example of how unpredictable theoretical and algorithmic developments can have a significant impact in the progress of numerical simulations. Until about ten years ago, in fact, that dependence was cubic that is much steeper, as shown in Fig. B.3. The latter steep dependence was named *the Berlin wall* at the Lattice 2001 conference in Berlin, meaning that simulations at the physical point seemed to be forbidden with the available algorithms.

The factor 0.03 in Eq. (B.6) turns out to be increased by a factor 3 for simulations with $N_f = 2 + 1$ instead of $N_f = 2$ and by a factor 1.5 in case of $\mathcal{O}(a)$-improved actions. Moreover, one has to take into account an overhead that can be estimated as a multiplicative factor $2 - 3$, to include the cost of simulations at coarsest lattice spacings to perform the continuum extrapolation. Therefore, we multiply the estimate of the computational cost provided by Eq. (B.6) by a factor ten. We observe that we are not considering simulations with Ginsparg-Wilson fermions, which are significantly (one order of magnitude) more expensive.

We collect in Table B.6 the estimates of the computational cost, in PFlops-years, of the benchmark simulations. They are given separately for the π/K, D, D_s, B and B_s sectors, which are affected in a different way by systematic uncertainties, thus requiring different values for the simulation parameters.

We recall that from the Moore's law the available computational power in 2025 should be of about 100-500 PFlops-years. Therefore, Table B.6 tells us that the accuracy in lattice calculations is expected to achieve the 0.1% level for D_s observables, the 0.5% level for π/K, D and B_s and the 1% level for B-physics.

[27] Eq. (B.6) is based on the study of the domain-decomposition-Hybrid-Monte-Carlo (DD-HMC) algorithm. Other recent algorithms provide similar performances.

Sector	$\varepsilon = 1\%$	$\varepsilon = 0.5\%$	$\varepsilon = 0.1\%$
π/K	0.5	15	$4 \cdot 10^4$
D	20	$7 \cdot 10^2$	$2 \cdot 10^6$
D_s	0.2	2	$5 \cdot 10^2$
B	10^3	-	-
B_s	20	$4 \cdot 10^2$	$3 \cdot 10^5$

Table B.6: *Estimated computational cost, in PFlops-years, of the benchmark simulations. Two predictions for the B-sector, that in the present analysis could be estimated only in a very naif way, are omitted.*

As mentioned before, for B and B_s lattice studies we are not taking into account the important role of approaches like effective actions and ratio methods in reducing the discretization and heavy quark extrapolation errors. For these sectors the computational cost quoted in Table B.6 represents a pessimistic estimate.

B.2.6 Predicted accuracy for Flavour Lattice QCD in 2025

Before providing the predictions for the lattice accuracy in 2025, we wish to advise the reader to take with caution estimates below 1%.

At that level of precision, in fact, small effects that are typically negligible have to be considered. This is true for isospin breaking and electromagnetic effects. They are of $\mathcal{O}((m_d - m_u)/\Lambda_{QCD}$ and of $\mathcal{O}(\alpha_{e.m.})$, respectively, and thus at the 1% level. First lattice studies of isospin breaking and electromagnetic effects have been performed in the last years leading to very promising results [1023–1029].

Other small effects that are at present well under control and can start contributing to the uncertainty in the future are, for instance, related to the suppression of the excited states and to the differences between determinations of the lattice spacing from different observables.

Finally, in providing the lattice predictions that are collected in Table B.7, we have considered that different hadronic quantities for a given sector present a different degree of complexity. The computational costs in Table B.6 essentially refer to the simplest hadronic matrix elements like decay constants and bag-parameters, which are determined from two-point correlators and ratios of correlators, respectively. Lattice calculations of form factors, which are extracted from more noisy three-point correlators and imply an extrapolation in the transferred momentum, are more expensive. For the semileptonic decays $K \to \pi\ell\nu$ and $B \to D/D^*\ell\nu$, however, one measures on the lattice the difference of the form factor from unity (that is the $SU(3)$ or heavy quark symmetric limit), so that the uncertainty on the form factor itself turns out to be smaller.

Hadronic Parameter	What Next Era (2025)
$f_+^{K\pi}(0)$	0.1%
B_K	$0.1 - 0.5\%$
f_{B_s}	0.5%
f_{B_s}/f_B	0.5%
B_{B_s}	$0.5 - 1\%$
B_{B_s}/B_B	$0.5 - 1\%$
$F_{D^*}(1)$	0.5%
$B \to \pi$	$\geq 1\%$

Table B.7: *Expectations for the Lattice accuracy in the What Next Era (2025).*

References

[1] J. Koutchouk, "Luminosity optimization and leveling". Proceedings of Chamonix 2010 workshop on LHC Performance, https://espace.cern.ch/acc-tec-sector/Chamonix/Chamx2010/papers/JPK_9_04.pdf.

[2] S. Fartoukh, "Pile up management at the high-luminosity LHC and introduction to the crab-kissing concept", *Phys.Rev.ST Accel.Beams* **17** (2014), no. 11, 111001, doi:10.1103/PhysRevSTAB.17.111001.

[3] "Proton Improvement Plan-II". https://http://projectx-docdb.fnal.gov/cgi-bin/ShowDocument?docid=1232.

[4] "The International Linear Collider Technical Design Report". arXiv:1306.6327 (vol.1), arXiv:1306.6352 (vol.2), arXiv:1306.6353 (vol.3), arXiv:1306.6328 (vol.4), arXiv:1306.6329 (vol.5).

[5] D. Asner et al., "ILC Higgs White Paper", arXiv:1310.0763.

[6] J. Brau, talk given at the International Workshop on Future Linear Colliders (LCWS14), 6-10 October 2014, Belgrade, Serbia, http://lcws14.vinca.rs/.

[7] W. Schnell, "A two stage RF linear collider using a superconducting drive LINAC", *Ettore Majorana Int.Sci.Ser.Phys.Sci.* **29** (1987) 67.

[8] M. Aicheler et al., "A Multi-TeV Linear Collider Based on CLIC Technology", doi:10.5170/CERN-2012-007.

[9] "Future Circular Collider Study Kickoff Meeting, Geneva, 12-15 February 2014". https://indico.cern.ch/event/282344/.

[10] "Future Circular Collider Study Hadron Collider Parameters - FCC-ACC-SPC-0001", Technical Report FCC-ACC-SPC-0001, FCC study group, Geneva, 2014.

[11] "Future Circular Collider Study Lepton Collider Parameters - FCC-ACC-SPC-0003", Technical Report FCC-ACC-SPC-0003, FCC study group, Geneva, 2014.

[12] "11^{th} ICFA Seminar, talk by Weiren Chou, Beijing, October 27, 2014". http://indico.ihep.ac.cn/conferenceDisplay.py?confId=3867.

[13] A. Blondel and F. Zimmermann, "A High Luminosity e^+e^- Collider in the LHC tunnel to study the Higgs Boson ", arXiv:1112.2518.

[14] "Future Circular Collider Study Kickoff Meeting, talk by Yifang Wang, Geneva, 12-15 February 2014". https://indico.cern.ch/event/282344/.

[15] R. J. England, R. J. Noble, Z. Wu, and M. Qi, "Dielectric Laser Acceleration", *Rev.Mod.Phys.* **86** (2014) 1337, doi:10.1103/RevModPhys.86.1337, arXiv:1309.7637.

[16] E. Esarey, C. Schroeder, and W. Leemans, "Physics of laser-driven plasma-based electron accelerators", *Rev.Mod.Phys.* **81** (2009) 1229–1285, doi:10.1103/RevModPhys.81.1229.

[17] D. Gordon et al., "Observation of Electron Energies Beyond the Linear Dephasing Limit from a Laser-Excited Relativistic Plasma Wave", *Phys.Rev.Lett.* **80** (1998) 2133–2136, doi:10.1103/PhysRevLett.80.2133.

[18] V. Malka, "Laser plasma accelerators", *Phys.Plasmas* **19** (2012) 055501, doi:10.1063/1.3695389.

[19] W. Leemans et al., "Multi-GeV Electron Beams from Capillary-Discharge-Guided Subpetawatt Laser Pulses in the Self-Trapping Regime", *Phys.Rev.Lett.* **113** (2014), no. 24, 245002, doi:10.1103/PhysRevLett.113.245002.

[20] M. Litos et al., "High-efficiency acceleration of an electron beam in a plasma wakefield accelerator", *Nature* **515** (2014), no. 7525, 92–95, doi:10.1038/nature13882.

[21] W. Leemans, "White paper of the ICFA-ICUIL joint task force: High power laser technology for accelerators", *ICFA Beam Dyn.Newslett.* **56** (2011) 10–88.

[22] G. Mourou et al., "Are fiber-based lasers the future of accelerators?", *Nucl.Instrum.Meth.* **A740** (2014) 17–20, doi:10.1016/j.nima.2013.10.041.

[23] A. Seryi, "Future prospects of accelerator science for particle physics", *Nucl.Instrum.Meth.* **A623** (2010) 23–28, doi:10.1016/j.nima.2010.02.145.

[24] J.-P. Delahaye et al., "A Beam Driven Plasma-wakefield Linear Collider from Higgs Factory to Multi-TeV". Proceedings of IPAC2014, Dresden, Germany.

[25] W. Barletta et al., "Future hadron colliders: From physics perspectives to technology R&D", *Nucl.Instrum.Meth.* **A764** (2014) 352–368, doi:10.1016/j.nima.2014.07.010.

[26] L. Rossi et al., "The EuCARD-2 Future Magnets European Collaboration for Accelerator-Quality HTS Magnets", *IEEE Transaction on Applied Superconductivity* **25** (2014) doi:10.1109/TASC.2014.2364215.

[27] D. B. Cline, "Physics potential of a few 100-GeV mu+ mu- collider", *Nucl.Instrum.Meth.* **A350** (1994) 24–26, doi:10.1016/0168-9002(94)91150-9.

[28] V. D. Barger, M. Berger, J. Gunion, and T. Han, "Higgs Boson physics in the s channel at mu+ mu- colliders", *Phys.Rept.* **286** (1997) 1–51, doi:10.1016/S0370-1573(96)00041-5, arXiv:hep-ph/9602415.

[29] C. Rubbia, "A complete demonstrator of a muon cooled Higgs factory", arXiv:1308.6612.

[30] MAP, MICE Collaboration, "Muon Colliders and Neutrino Factories", arXiv:1412.3487.

[31] D. Neuffer et al., "A muon collider as a Higgs factory", arXiv:1502.02042.

[32] H. Kirk et al., "4-MW Target Station for a Muon Collider or Neutrino Factory", *Conf.Proc.* **C100523** (2010) 3590–3592.

[33] Neutrino Factory and Muon Collider Collaboration, "Muon Capture, Phase Rotation, and Cooling in Pressurized RF Cavities", Technical Report FERMILAB-CONF-09-164-APC, PAC09-WE6PFP089, 2009.

[34] D. Neuffer, "Comments on Ionization Cooling Channel Characteristics", arXiv:1312.1266.

[35] MICE Collaboration, "Characterisation of the muon beams for the Muon Ionisation Cooling Experiment", *Eur.Phys.J.* **C73** (2013), no. 10, 2582, doi:10.1140/epjc/s10052-013-2582-8, arXiv:1306.1509.

[36] F. Forti, "Trends in detector R&D", *PoS* **EPS-HEP2013** (2013) 147.

[37] S. Cittolin, "The data acquisition and reduction challenge at the Large Hadron Collider", *Phil.Trans.Roy.Soc.Lond.* **A370** (2012) 950–964, doi:10.1098/rsta.2011.0464.

[38] B. Pietrzyk, "LEP asymmetries and fits of the standard model", arXiv:hep-ex/9406001.

[39] ALEPH Collaboration, DELPHI Collaboration, L3 Collaboration, OPAL Collaboration, "Updated Parameters of the Z^0 Resonance from Combined Preliminary Data of the LEP Experiments", Technical Report CERN-PPE-93-157, CERN, Geneva, Aug, 1993.

[40] CDF Collaboration, "Evidence for top quark production in $\bar{p}p$ collisions at $\sqrt{s} = 1.8$ TeV", *Phys.Rev.Lett.* **73** (1994) 225–231, doi:10.1103/PhysRevLett.73.225, arXiv:hep-ex/9405005.

[41] The ALEPH, DELPHI, L3, OPAL Collaborations, the LEP Electroweak Working Group, "Electroweak Measurements in Electron-Positron Collisions at W-Boson-Pair Energies at LEP", *Phys. Rept.* **532** (2013) 119, arXiv:1302.3415.

[42] ATLAS Collaboration, "Observation of a new particle in the search for the Standard Model Higgs boson with the ATLAS detector at the LHC", *Phys.Lett.* **B716** (2012) 1–29, doi:10.1016/j.physletb.2012.08.020, arXiv:1207.7214.

[43] CMS Collaboration, "Observation of a new boson at a mass of 125 GeV with the CMS experiment at the LHC", *Phys.Lett.* **B716** (2012) 30–61, doi:10.1016/j.physletb.2012.08.021, arXiv:1207.7235.

[44] LHC Higgs Cross Section Working Group Collaboration, "Handbook of LHC Higgs Cross Sections: 3. Higgs Properties", doi:10.5170/CERN-2013-004, arXiv:1307.1347.

[45] M. E. Peskin, "Estimation of LHC and ILC Capabilities for Precision Higgs Boson Coupling Measurements", arXiv:1312.4974.

[46] S. Dawson et al., "Working Group Report: Higgs Boson", arXiv:1310.8361.

[47] S. Forte et al., "The Standard Model from the LHC to future colliders: a contribution to the Workshop "What Next" of INFN", arXiv:1505.01279.

[48] https://twiki.cern.ch/twiki/bin/view/LHCPhysics/CrossSections.

[49] https://twiki.cern.ch/twiki/bin/view/LHCPhysics/HiggsEuropeanStrategy2012.

[50] C. Anastasiou et al., "Higgs boson gluon-fusion production in N3LO QCD", arXiv:1503.06056.

[51] https://atlas.web.cern.ch/Atlas/GROUPS/PHYSICS/PUBNOTES/ATL-PHYS-PUB-2014-016.

[52] CMS Collaboration, "Projected Performance of an Upgraded CMS Detector at the LHC and HL-LHC: Contribution to the Snowmass Process", arXiv:1307.7135.

[53] C. Adolphsen et al., "The International Linear Collider Technical Design Report - Volume 3.II: Accelerator Baseline Design", arXiv:1306.6328.

[54] International Workshop on Future Linear Colliders (LCWS14), 6-10 October 2014, Belgrade, Serbia, http://lcws14.vinca.rs/.

[55] http://indico.cern.ch/event/282344/timetable.

[56] M. E. Peskin, "Comparison of LHC and ILC Capabilities for Higgs Boson Coupling Measurements", arXiv:1207.2516.

[57] S. Dittmaier et al., "Handbook of LHC Higgs Cross Sections: 2. Differential Distributions", doi:10.5170/CERN-2012-002, arXiv:1201.3084.

[58] M. Gomez-Bock et al., "Concepts of Electroweak Symmetry Breaking and Higgs Physics", arXiv:0712.2419.

[59] A. Djouadi, "The Anatomy of electro-weak symmetry breaking. II. The Higgs bosons in the minimal supersymmetric model", *Phys.Rept.* **459** (2008) 1–241, doi:10.1016/j.physrep.2007.10.005, arXiv:hep-ph/0503173.

[60] J. Cao, L. Wu, P. Wu, and J. M. Yang, "The Z+photon and diphoton decays of the Higgs boson as a joint probe of low energy SUSY models", *JHEP* **1309** (2013) 043, doi:10.1007/JHEP09(2013)043, arXiv:1301.4641.

[61] ATLAS Collaboration, "Update of the prospects for the $H \to Z\gamma$ search at the High-Luminosity LHC", Technical Report ATL-PHYS-PUB-2014-006, CERN, Geneva, May, 2014.

[62] K. Agashe and R. Contino, "Composite Higgs-Mediated FCNC", *Phys.Rev.* **D80** (2009) 075016, doi:10.1103/PhysRevD.80.075016, arXiv:0906.1542.

[63] R. Harnik, J. Kopp, and J. Zupan, "Flavor Violating Higgs Decays", *JHEP* **1303** (2013) 026, doi:10.1007/JHEP03(2013)026, arXiv:1209.1397.

[64] CMS Collaboration, "Search for lepton-flavour-violating decays of the Higgs boson", arXiv:1502.07400.

[65] D.-N. Gao, "A note on Higgs decays into Z boson and $J/\psi(\Upsilon)$", *Phys.Lett.* **B737** (2014) 366–368, doi:10.1016/j.physletb.2014.09.019, arXiv:1406.7102.

[66] G. Isidori, A. V. Manohar, and M. Trott, "Probing the nature of the Higgs-like Boson via $h \to V\mathcal{F}$ decays", *Phys.Lett.* **B728** (2014) 131–135, doi:10.1016/j.physletb.2013.11.054, arXiv:1305.0663.

[67] D. Curtin et al., "Exotic decays of the 125 GeV Higgs boson", *Phys.Rev.* **D90** (2014), no. 7, 075004, doi:10.1103/PhysRevD.90.075004, arXiv:1312.4992.

[68] https://atlas.web.cern.ch/Atlas/GROUPS/PHYSICS/PUBNOTES/ATL-PHYS-PUB-2013-013/.

[69] L. J. Dixon and Y. Li, "Bounding the Higgs Boson Width Through Interferometry", *Phys.Rev.Lett.* **111** (2013) 111802, doi:10.1103/PhysRevLett.111.111802, arXiv:1305.3854.

[70] CMS Collaboration, "Constraints on the Higgs boson width from off-shell production and decay to Z-boson pairs", *Phys.Lett.* **B736** (2014) 64, doi:10.1016/j.physletb.2014.06.077, arXiv:1405.3455.

[71] ATLAS Collaboration, "Determination of the off-shell Higgs boson signal strength in the high-mass ZZ and WW final states with the ATLAS detector", arXiv:1503.01060.

[72] F. Caola and K. Melnikov, "Constraining the Higgs boson width with ZZ production at the LHC", *Phys.Rev.* **D88** (2013) 054024, doi:10.1103/PhysRevD.88.054024, arXiv:1307.4935.

[73] N. Kauer and G. Passarino, "Inadequacy of zero-width approximation for a light Higgs boson signal", *JHEP* **1208** (2012) 116, doi:10.1007/JHEP08(2012)116, arXiv:1206.4803.

[74] J. Baglio et al., "The measurement of the Higgs self-coupling at the LHC: theoretical status", *JHEP* **1304** (2013) 151, doi:10.1007/JHEP04(2013)151, arXiv:1212.5581.

[75] D. de Florian and J. Mazzitelli, "Higgs Boson Pair Production at Next-to-Next-to-Leading Order in QCD", *Phys. Rev. Lett. 111,* **201801** (2013) 201801, doi:10.1103/PhysRevLett.111.201801, arXiv:1309.6594.

[76] J. Grigo, K. Melnikov, and M. Steinhauser, "Virtual corrections to Higgs boson pair production in the large top quark mass limit", *Nucl.Phys.* **B888** (2014) 17–29, doi:10.1016/j.nuclphysb.2014.09.003, arXiv:1408.2422.

[77] https://twiki.cern.ch/twiki/pub/CMSPublic/PhysicsResultsFP/ECFA-CMSPublicResults.pdf.

[78] https://atlas.web.cern.ch/Atlas/GROUPS/PHYSICS/PUBNOTES/ATL-PHYS-PUB-2014-019.

[79] M. Baak et al., "The Electroweak Fit of the Standard Model after the Discovery of a New Boson at the LHC", *Eur.Phys.J.* **C72** (2012) 2205, doi:10.1140/epjc/s10052-012-2205-9, arXiv:1209.2716.

[80] ALEPH, DELPHI, L3, OPAL, LEP Electroweak Collaboration, "Electroweak Measurements in Electron-Positron Collisions at W-Boson-Pair Energies at LEP", *Phys.Rept.* **532** (2013) 119–244, doi:10.1016/j.physrep.2013.07.004, arXiv:1302.3415.

[81] Particle Data Group Collaboration, "Review of Particle Physics (RPP)", *Chin. Phys. C* **38** (2014) 090001.

[82] ALEPH Collaboration, DELPHI Collaboration, L3 Collaboration, OPAL Collaboration, SLD Collaboration, LEP Electroweak Working Group, SLD Electroweak Group, SLD Heavy Flavour Group Collaboration, "Precision electroweak measurements on the Z resonance", *Phys.Rept.* **427** (2006) 257–454, doi:10.1016/j.physrep.2005.12.006, arXiv:hep-ex/0509008.

[83] Gfitter Group Collaboration, "The global electroweak fit at NNLO and prospects for the LHC and ILC", *Eur.Phys.J.* **C74** (2014), no. 9, 3046, doi:10.1140/epjc/s10052-014-3046-5, arXiv:1407.3792.

[84] M. Baak et al., "Study of Electroweak Interactions at the Energy Frontier", arXiv:1310.6708.

[85] G. Bozzi, J. Rojo, and A. Vicini, "The Impact of PDF uncertainties on the measurement of the W boson mass at the Tevatron and the LHC", *Phys.Rev.* **D83** (2011) 113008, doi:10.1103/PhysRevD.83.113008, arXiv:1104.2056.

[86] H. Baer et al., "The International Linear Collider Technical Design Report - Volume 2: Physics", arXiv:1306.6352.

[87] M. Bicer et al., "First Look at the Physics Case of TLEP", *JHEP* **1401** (2014) 164, doi:10.1007/JHEP01(2014)164, arXiv:1308.6176.

[88] CDF Collaboration, "Indirect measurement of $\sin^2\theta_W$ (or M_W) using $\mu^+\mu^-$ pairs from γ^*/Z bosons produced in $p\bar{p}$ collisions at a center-of-momentum energy of 1.96 TeV", arXiv:1402.2239.

[89] ATLAS Collaboration, "Measurement of the forward-backward asymmetry of electron and muon pair-production in pp collisions at $\sqrt{s}$ = 7 TeV with the ATLAS detector", arXiv:1503.03709.

[90] J. Rojo, "PDF uncertainties in the determination of the W boson mass and of the effective lepton mixing angle at the LHC", *PoS* **DIS2013** (2013) 280.

[91] M. Beccaria, G. Macorini, G. Panizzo, and C. Verzegnassi, "New Physics signals from measurable polarization asymmetries at {LHC}", *Physics Letters B* **730** (2014), no. 0, 149 – 154, doi:http://dx.doi.org/10.1016/j.physletb.2014.01.010.

[92] A. Blondel, "A Scheme to Measure the Polarization Asymmetry at the Z Pole in LEP", *Phys.Lett.* **B202** (1988) 145, doi:10.1016/0370-2693(88)90869-6.

[93] D. Marzocca, "Prospects for bounds on electroweak and Higgs observables via scaling effects", arXiv:1405.3841.

[94] ATLAS Collaboration, "Studies of Vector Boson Scattering And Triboson Production with an Upgraded ATLAS Detector at a High-Luminosity LHC", Technical Report ATL-PHYS-PUB-2013-006, 2013.

[95] CMS Collaboration, "Vector Boson Scattering and Quartic Gauge Coupling Studies in WZ Production at 14 TeV", Technical Report CMS-PAS-FTR-13-006, 2013.

[96] S. Fichet et al., "Probing new physics in diphoton production with proton tagging at the Large Hadron Collider", arXiv:1312.5153.

[97] LHeC Study Group Collaboration, "A Large Hadron Electron Collider at CERN: Report on the Physics and Design Concepts for Machine and Detector", *J.Phys.* **G39** (2012) 075001, doi:10.1088/0954-3899/39/7/075001, arXiv:1206.2913.

[98] ILC Collaboration, "International Linear Collider Reference Design Report Volume 2: Physics at the ILC", arXiv:0709.1893.

[99] CDF Collaboration, "Observation of top quark production in $\bar{p}p$ collisions", *Phys.Rev.Lett.* **74** (1995) 2626–2631, doi:10.1103/PhysRevLett.74.2626, arXiv:hep-ex/9503002.

[100] D0 Collaboration, "Observation of the top quark", *Phys.Rev.Lett.* **74** (1995) 2632–2637, doi:10.1103/PhysRevLett.74.2632, arXiv:hep-ex/9503003.

[101] ATLAS Collaboration, CDF Collaboration, CMS Collaboration, D0 Collaboration, "First combination of Tevatron and LHC measurements of the top-quark mass", arXiv:1403.4427.

[102] G. Degrassi et al., "Higgs mass and vacuum stability in the Standard Model at NNLO", *JHEP* **1208** (2012) 098, doi:10.1007/JHEP08(2012)098, arXiv:1205.6497.

[103] V. Branchina, E. Messina, and A. Platania, "Top mass determination, Higgs inflation, and vacuum stability", *JHEP* **1409** (2014) 182, doi:10.1007/JHEP09(2014)182, arXiv:1407.4112.

[104] A. De Simone, M. P. Hertzberg, and F. Wilczek, "Running Inflation in the Standard Model", *Phys.Lett.* **B678** (2009) 1–8, doi:10.1016/j.physletb.2009.05.054, arXiv:0812.4946.

[105] A. Juste et al., "Determination of the top quark mass circa 2013: methods, subtleties, perspectives", arXiv:1310.0799.

[106] CMS Collaboration, "Measurement of masses in the $t\bar{t}$ system by kinematic endpoints in pp collisions at $\sqrt{s}$ = 7 TeV", *Eur.Phys.J.* **C73** (2013) 2494, doi:10.1140/epjc/s10052-013-2494-7, arXiv:1304.5783.

[107] CMS Collaboration, "Projected improvement of the accuracy of top-quark mass measurements at the upgraded LHC",. CMS-PAS-FTR-13-017.

[108] A. Kharchilava, "Top mass determination in leptonic final states with J/ψ", *Phys.Lett.* **B476** (2000) 73–78, doi:10.1016/S0370-2693(00)00120-9, arXiv:hep-ph/9912320.

[109] R. Chierici and A. Dierlamm, "Determination of the top mass with exclusive events $t \to Wb \to l\nu J/\psi X$", Technical Report CERN-CMS-NOTE-2006-058, 2006.

[110] CMS Collaboration, "Measurement of the top quark mass using the B-hadron lifetime technique", Technical Report CMS-PAS-TOP-12-030, 2013.

[111] S. Catani, B. Webber, and G. Marchesini, "QCD coherent branching and semiinclusive processes at large x", *Nucl.Phys.* **B349** (1991) 635–654, doi:10.1016/0550-3213(91)90390-J.

[112] B. Webber, "A QCD Model for Jet Fragmentation Including Soft Gluon Interference", *Nucl.Phys.* **B238** (1984) 492, doi:10.1016/0550-3213(84)90333-X.

[113] B. Andersson, G. Gustafson, G. Ingelman, and T. Sjostrand, "Parton Fragmentation and String Dynamics", *Phys.Rept.* **97** (1983) 31–145, doi:10.1016/0370-1573(83)90080-7.

[114] A. H. Hoang and I. W. Stewart, "Top Mass Measurements from Jets and the Tevatron Top-Quark Mass", *Nucl.Phys.Proc.Suppl.* **185** (2008) 220–226, doi:10.1016/j.nuclphysbps.2008.10.028, arXiv:0808.0222.

[115] G. Corcella, "Hadronization systematics and top mass reconstruction", arXiv:1409.8592.

[116] CMS Collaboration, "Study of the dependence of the top-quark mass measurement on event kinematics", Technical Report CMS-PAS-TOP-12-029, 2013.

[117] CMS Collaboration, "Measurement of the top-quark mass in t t-bar events with lepton+jets final states in pp collisions at sqrt(s)=8 TeV", Technical Report CMS-PAS-TOP-14-001, 2014.

[118] M. Czakon, P. Fiedler, and A. Mitov, "Total Top-Quark Pair-Production Cross Section at Hadron Colliders Through $\mathcal{O}(\alpha_S^4)$", *Phys.Rev.Lett.* **110** (2013) 252004, doi:10.1103/PhysRevLett.110.252004, arXiv:1303.6254.

[119] CMS Collaboration, "Determination of the top-quark pole mass and strong coupling constant from the t t-bar production cross section in pp collisions at $\sqrt{s}$ = 7 TeV", *Phys.Lett.* **B728** (2014) 496–517, doi:10.1016/j.physletb.2014.08.040,10.1016/j.physletb.2013.12.009, arXiv:1307.1907.

[120] ATLAS Collaboration, "Measurement of the $t\bar{t}$ production cross-section using $e\mu$ events with b -tagged jets in pp collisions at $\sqrt{s} = 7$ and 8 TeV with the ATLAS detector", *Eur.Phys.J.* **C74** (2014), no. 10, 3109, doi:10.1140/epjc/s10052-014-3109-7, arXiv:1406.5375.

[121] S. Alioli et al., "A new observable to measure the top-quark mass at hadron colliders", *Eur.Phys.J.* **C73** (2013) 2438, doi:10.1140/epjc/s10052-013-2438-2, arXiv:1303.6415.

[122] ATLAS Collaboration, "Determination of the top-quark pole mass using tt t+1-jet events collected with the ATLAS experiment in 7 TeV pp collisions", Technical Report ATLAS-CONF-2014-053, 2014.

[123] A. Hoang et al., "Top - anti-top pair production close to threshold: Synopsis of recent NNLO results", *Eur.Phys.J.direct* **C2** (2000) 1, arXiv:hep-ph/0001286.

[124] A. Hoang and T. Teubner, "Top quark pair production close to threshold: Top mass, width and momentum distribution", *Phys.Rev.* **D60** (1999) 114027, doi:10.1103/PhysRevD.60.114027, arXiv:hep-ph/9904468.

[125] M. Martinez and R. Miquel, "Multiparameter fits to the t anti-t threshold observables at a future e+ e- linear collider", *Eur.Phys.J.* **C27** (2003) 49–55, doi:10.1140/epjc/s2002-01094-1, arXiv:hep-ph/0207315.

[126] F. Simon, Presented at the 7th TLEP-FCCee workshop, 19-21 June 2014, CERN, URL

http://indico.cern.ch/event/313708/.

[127] K. Seidel, F. Simon, M. Tesar, and S. Poss, "Top quark mass measurements at and above threshold at CLIC", *Eur.Phys.J.* **C73** (2013) 2530, doi:10.1140/epjc/s10052-013-2530-7, arXiv:1303.3758.

[128] A. Hoang and T. Teubner, "Top quark pair production at threshold: Complete next-to-next-to-leading order relativistic corrections", *Phys.Rev.* **D58** (1998) 114023, doi:10.1103/PhysRevD.58.114023, arXiv:hep-ph/9801397.

[129] A. Czarnecki, J. G. Korner, and J. H. Piclum, "Helicity fractions of W bosons from top quark decays at NNLO in QCD", *Phys.Rev.* **D81** (2010) 111503, doi:10.1103/PhysRevD.81.111503, arXiv:1005.2625.

[130] CMS Collaboration, "Measurement of top quark-antiquark pair production in association with a W or Z boson in pp collisions at $\sqrt{s} = 8$ TeV", *Eur.Phys.J.* **C74** (2014), no. 9, 3060, doi:10.1140/epjc/s10052-014-3060-7, arXiv:1406.7830.

[131] ATLAS Collaboration, "Evidence for the associated production of a vector boson (W, Z) and top quark pair in the dilepton and trilepton channels in pp collision data at $\sqrt{s} = 8$ TeV collected by the ATLAS detector at the LHC", Technical Report ATLAS-CONF-2014-038, 2014.

[132] CMS Collaboration, "Measurement of the t-channel single-top-quark production cross section and of the $| V_{tb} |$ CKM matrix element in pp collisions at $\sqrt{s}$= 8 TeV", *JHEP* **1406** (2014) 090, doi:10.1007/JHEP06(2014)090, arXiv:1403.7366.

[133] ATLAS Collaboration, "Comprehensive measurements of t-channel single top-quark production cross sections at $\sqrt{s}$ = 7 TeV with the ATLAS detector", arXiv:1406.7844.

[134] B. Schoenrock, E. Drueke, B. A. Gonzalez, and R. Schwienhorst, "Single top quark cross section measurement in the t-channel at the high-luminosity LHC", arXiv:1308.6307.

[135] A. Juste et al., "Report of the 2005 Snowmass top/QCD working group", arXiv:hep-ph/0601112.

[136] E. Boos et al., "Single top production in e+ e-, e- e-, gamma e and gamma gamma collisions", *Eur.Phys.J.* **C21** (2001) 81–91, doi:10.1007/s100520100733, arXiv:hep-ph/0104279.

[137] S. Dutta, A. Goyal, M. Kumar, and B. Mellado, "Measuring anomalous Wtb couplings at $e^{-}p$ collider", arXiv:1307.1688.

[138] ATLAS Collaboration, "Measurement of the top quark charge in pp collisions at $\sqrt{s} = 7$ TeV with the ATLAS detector", *JHEP* **1311** (2013) 031, doi:10.1007/JHEP11(2013)031, arXiv:1307.4568.

[139] ATLAS Collaboration, "Measurement of the inclusive $t\bar{t}\gamma$ cross section with the ATLAS detector", Technical Report ATLAS-CONF-2011-153, 2011.

[140] K. Melnikov, M. Schulze, and A. Scharf, "QCD corrections to top quark pair production in association with a photon at hadron colliders", *Phys.Rev.* **D83** (2011) 074013, doi:10.1103/PhysRevD.83.074013, arXiv:1102.1967.

[141] J. Adelman, M. Baumgart, A. Garcia-Bellido, and A. Loginov, "Determining Top Quark Couplings at the LHC: Snowmass White Paper", arXiv:1308.5274.

[142] P. Janot, "Top-quark electroweak couplings at the FCC-ee", *JHEP* **1504** (2015) 182, doi:10.1007/JHEP04(2015)182, arXiv:1503.01325.

[143] F. Richard, "Present and future constraints on top EW couplings", arXiv:1403.2893.

[144] D. Barducci et al., "Exploring Drell-Yan signals from the 4D Composite Higgs Model at the LHC", *JHEP* **1304** (2013) 152, doi:10.1007/JHEP04(2013)152, arXiv:1210.2927.

[145] U. Baur, A. Juste, L. Orr, and D. Rainwater, "Probing electroweak top quark couplings at hadron colliders", *Phys.Rev.* **D71** (2005) 054013, doi:10.1103/PhysRevD.71.054013, arXiv:hep-ph/0412021.

[146] Top Quark Working Group Collaboration, "Working Group Report: Top Quark", arXiv:1311.2028.

[147] M. Amjad et al., "A precise determination of top quark electro-weak couplings at the ILC operating at $\sqrt{s} = 500$ GeV", arXiv:1307.8102.

[148] D. Barducci, S. De Curtis, S. Moretti, and G. M. Pruna, "Top pair production at a future e^+e^- machine in a composite Higgs scenario", arXiv:1504.05407.

[149] S. Redford, P. Roloff, and M. Vogel, "Physics potential of the top Yukawa coupling measurement at a 1.4 TeV Compact Linear Collider using the CLIC SiD detector", Technical Report CLICdp-Note-2014-001, 2014.

[150] CMS Collaboration, "Projections for Top FCNC Searches in 3000/fb at the LHC", Technical Report CMS-PAS-FTR-13-016, 2013.

[151] H. Khanpour, S. Khatibi, M. K. Yanehsari, and M. M. Najafabadi, "Single top quark production as a probe of anomalous $tq\gamma$ and tqZ couplings at the FCC-ee", arXiv:1408.2090.

[152] R. Martinez and J. A. Rodriguez, "The Anomalous chromomagnetic dipole moment of the top quark in the standard model and beyond", *Phys.Rev.* **D65** (2002) 057301, doi:10.1103/PhysRevD.65.057301, arXiv:hep-ph/0109109.

[153] CMS Collaboration, "Search for Anomalous Top Chromomagnetic Dipole Moments from angular distributions in $t\bar{t}$ Dileptonic events at $\sqrt{s} = 7$ TeV with the CMS detector.", Technical Report CMS-PAS-TOP-14-005, 2014.

[154] B. Fuks, "Opportunities with top quarks at future circular colliders", arXiv:1412.1685.

[155] A. Denner, S. Dittmaier, S. Kallweit, and S. Pozzorini, "NLO QCD corrections to off-shell top-antitop production with leptonic decays at hadron colliders", *JHEP* **1210** (2012) 110, doi:10.1007/JHEP10(2012)110, arXiv:1207.5018.

[156] G. Bevilacqua et al., "Complete off-shell effects in top quark pair hadroproduction with leptonic decay at next-to-leading order", *JHEP* **1102** (2011) 083, doi:10.1007/JHEP02(2011)083, arXiv:1012.4230.

[157] K. Melnikov and M. Schulze, "NLO QCD corrections to top quark pair production and decay at hadron colliders", *JHEP* **0908** (2009) 049, doi:10.1088/1126-6708/2009/08/049, arXiv:0907.3090.

[158] N. Kidonakis, "Next-to-next-to-leading soft-gluon corrections for the top quark cross section and transverse momentum distribution", *Phys.Rev.* **D82** (2010) 114030, doi:10.1103/PhysRevD.82.114030, arXiv:1009.4935.

[159] V. Ahrens et al., "RG-improved single-particle inclusive cross sections and forward-backward asymmetry in $t\bar{t}$ production at hadron colliders", *JHEP* **1109** (2011) 070, doi:10.1007/JHEP09(2011)070, arXiv:1103.0550.

[160] A. Jung, M. Schulze, and J. Shelton, "Kinematics of Top Quark Final States: A Snowmass White Paper", arXiv:1309.2889.

[161] J. M. Campbell and R. Ellis, "MCFM for the Tevatron and the LHC", *Nucl.Phys.Proc.Suppl.* **205-206** (2010) 10–15, doi:10.1016/j.nuclphysbps.2010.08.011, arXiv:1007.3492.

[162] CDF Collaboration, "Measurement of the inclusive leptonic asymmetry in top-quark pairs that decay to two charged leptons at CDF", *Phys.Rev.Lett.* **113** (2014) 042001, doi:10.1103/PhysRevLett.113.042001, arXiv:1404.3698.

[163] M. Czakon, P. Fiedler, and A. Mitov, "Resolving the Tevatron top quark forward-backward asymmetry puzzle", arXiv:1411.3007.

[164] D0 Collaboration, "Measurement of the forward-backward asymmetry in top quark-antiquark production in ppbar collisions using the lepton+jets channel", arXiv:1405.0421.

[165] CMS Collaboration, "Measurement of the charge asymmetry in top-quark pair production in

proton-proton collisions at $\sqrt{s} = 7$ TeV", *Phys.Lett.* **B709** (2012) 28–49, doi:10.1016/j.physletb.2012.01.078, arXiv:1112.5100.

[166] S. Berge and S. Westhoff, "Top-Quark Charge Asymmetry Goes Forward: Two New Observables for Hadron Colliders", *JHEP* **1307** (2013) 179, doi:10.1007/JHEP07(2013)179, arXiv:1305.3272.

[167] S. Catani, F. Krauss, R. Kuhn, and B. Webber, "QCD matrix elements + parton showers", *JHEP* **0111** (2001) 063, doi:10.1088/1126-6708/2001/11/063, arXiv:hep-ph/0109231.

[168] J. Alwall et al., "Comparative study of various algorithms for the merging of parton showers and matrix elements in hadronic collisions", *Eur.Phys.J.* **C53** (2008) 473–500, doi:10.1140/epjc/s10052-007-0490-5, arXiv:0706.2569.

[169] S. Frixione and B. R. Webber, "Matching NLO QCD computations and parton shower simulations", *JHEP* **0206** (2002) 029, doi:10.1088/1126-6708/2002/06/029, arXiv:hep-ph/0204244.

[170] P. Nason, "A New method for combining NLO QCD with shower Monte Carlo algorithms", *JHEP* **0411** (2004) 040, doi:10.1088/1126-6708/2004/11/040, arXiv:hep-ph/0409146.

[171] S. Frixione, P. Nason, and C. Oleari, "Matching NLO QCD computations with Parton Shower simulations: the POWHEG method", *JHEP* **0711** (2007) 070, doi:10.1088/1126-6708/2007/11/070, arXiv:0709.2092.

[172] T. Sjostrand, L. Lonnblad, S. Mrenna, and P. Z. Skands, "Pythia 6.3 physics and manual", arXiv:hep-ph/0308153.

[173] T. Sjostrand, S. Mrenna, and P. Z. Skands, "A Brief Introduction to PYTHIA 8.1", *Comput.Phys.Commun.* **178** (2008) 852–867, doi:10.1016/j.cpc.2008.01.036, arXiv:0710.3820.

[174] G. Corcella et al., "HERWIG 6: An Event generator for hadron emission reactions with interfering gluons (including supersymmetric processes)", *JHEP* **0101** (2001) 010, doi:10.1088/1126-6708/2001/01/010, arXiv:hep-ph/0011363.

[175] M. Bahr et al., "Herwig++ Physics and Manual", *Eur.Phys.J.* **C58** (2008) 639–707, doi:10.1140/epjc/s10052-008-0798-9, arXiv:0803.0883.

[176] J. Alwall et al., "The automated computation of tree-level and next-to-leading order differential cross sections, and their matching to parton shower simulations", *JHEP* **1407** (2014) 079, doi:10.1007/JHEP07(2014)079, arXiv:1405.0301.

[177] G. Cullen et al., "Automated One-Loop Calculations with GoSam", *Eur.Phys.J.* **C72** (2012) 1889, doi:10.1140/epjc/s10052-012-1889-1, arXiv:1111.2034.

[178] S. Actis et al., "Recursive generation of one-loop amplitudes in the Standard Model", *JHEP* **1304** (2013) 037, doi:10.1007/JHEP04(2013)037, arXiv:1211.6316.

[179] F. Cascioli, P. Maierhofer, and S. Pozzorini, "Scattering Amplitudes with Open Loops", *Phys.Rev.Lett.* **108** (2012) 111601, doi:10.1103/PhysRevLett.108.111601, arXiv:1111.5206.

[180] C. Berger et al., "An Automated Implementation of On-Shell Methods for One-Loop Amplitudes", *Phys.Rev.* **D78** (2008) 036003, doi:10.1103/PhysRevD.78.036003, arXiv:0803.4180.

[181] Z. Bern et al., "Next-to-Leading Order $W + 5$-Jet Production at the LHC", *Phys.Rev.* **D88** (2013), no. 1, 014025, doi:10.1103/PhysRevD.88.014025, arXiv:1304.1253.

[182] T. Gleisberg et al., "Event generation with SHERPA 1.1", *JHEP* **0902** (2009) 007, doi:10.1088/1126-6708/2009/02/007, arXiv:0811.4622.

[183] S. Platzer and S. Gieseke, "Dipole Showers and Automated NLO Matching in Herwig++", *Eur.Phys.J.* **C72** (2012) 2187, doi:10.1140/epjc/s10052-012-2187-7,

arXiv:1109.6256.

[184] L. Barze et al., "Neutral current Drell-Yan with combined QCD and electroweak corrections in the POWHEG BOX", *Eur.Phys.J.* **C73** (2013) 2474, doi:10.1140/epjc/s10052-013-2474-y, arXiv:1302.4606.

[185] L. Barze et al., "Implementation of electroweak corrections in the POWHEG BOX: single W production", *JHEP* **1204** (2012) 037, doi:10.1007/JHEP04(2012)037, arXiv:1202.0465.

[186] R. Hamberg, W. van Neerven, and T. Matsuura, "A Complete calculation of the order $\alpha - s^2$ correction to the Drell-Yan K factor", *Nucl.Phys.* **B359** (1991) 343–405, doi:10.1016/0550-3213(91)90064-5.

[187] R. V. Harlander and W. B. Kilgore, "Next-to-next-to-leading order Higgs production at hadron colliders", *Phys.Rev.Lett.* **88** (2002) 201801, doi:10.1103/PhysRevLett.88.201801, arXiv:hep-ph/0201206.

[188] C. Anastasiou and K. Melnikov, "Higgs boson production at hadron colliders in NNLO QCD", *Nucl.Phys.* **B646** (2002) 220–256, doi:10.1016/S0550-3213(02)00837-4, arXiv:hep-ph/0207004.

[189] V. Ravindran, J. Smith, and W. L. van Neerven, "NNLO corrections to the total cross-section for Higgs boson production in hadron hadron collisions", *Nucl.Phys.* **B665** (2003) 325–366, doi:10.1016/S0550-3213(03)00457-7, arXiv:hep-ph/0302135.

[190] C. Anastasiou, K. Melnikov, and F. Petriello, "Higgs boson production at hadron colliders: Differential cross sections through next-to-next-to-leading order", *Phys.Rev.Lett.* **93** (2004) 262002, doi:10.1103/PhysRevLett.93.262002, arXiv:hep-ph/0409088.

[191] S. Catani and M. Grazzini, "An NNLO subtraction formalism in hadron collisions and its application to Higgs boson production at the LHC", *Phys.Rev.Lett.* **98** (2007) 222002, doi:10.1103/PhysRevLett.98.222002, arXiv:hep-ph/0703012.

[192] A. Gehrmann-De Ridder, T. Gehrmann, E. Glover, and G. Heinrich, "NNLO corrections to event shapes in e+ e- annihilation", *JHEP* **0712** (2007) 094, doi:10.1088/1126-6708/2007/12/094, arXiv:0711.4711.

[193] O. Brein, A. Djouadi, and R. Harlander, "NNLO QCD corrections to the Higgs-strahlung processes at hadron colliders", *Phys.Lett.* **B579** (2004) 149–156, doi:10.1016/j.physletb.2003.10.112, arXiv:hep-ph/0307206.

[194] G. Ferrera, M. Grazzini, and F. Tramontano, "Associated WH production at hadron colliders: a fully exclusive QCD calculation at NNLO", *Phys.Rev.Lett.* **107** (2011) 152003, doi:10.1103/PhysRevLett.107.152003, arXiv:1107.1164.

[195] S. Catani et al., "Diphoton production at hadron colliders: a fully-differential QCD calculation at NNLO", *Phys.Rev.Lett.* **108** (2012) 072001, doi:10.1103/PhysRevLett.108.072001, arXiv:1110.2375.

[196] R. Boughezal et al., "Higgs boson production in association with a jet at next-to-next-to-leading order in perturbative QCD", *JHEP* **1306** (2013) 072, doi:10.1007/JHEP06(2013)072, arXiv:1302.6216.

[197] J. Currie, A. Gehrmann-De Ridder, E. Glover, and J. Pires, "NNLO QCD corrections to jet production at hadron colliders from gluon scattering", *JHEP* **1401** (2014) 110, doi:10.1007/JHEP01(2014)110, arXiv:1310.3993.

[198] M. Grazzini, S. Kallweit, D. Rathlev, and A. Torre, "$Z\gamma$ production at hadron colliders in NNLO QCD", *Phys.Lett.* **B731** (2014) 204–207, doi:10.1016/j.physletb.2014.02.037, arXiv:1309.7000.

[199] F. Cascioli et al., "ZZ production at hadron colliders in NNLO QCD", *Phys.Lett.* **B735** (2014) 311–313, doi:10.1016/j.physletb.2014.06.056, arXiv:1405.2219.

[200] T. Gehrmann et al., "W^+W^- production at hadron colliders in NNLO QCD", doi:10.1103/PhysRevLett.113.212001, arXiv:1408.5243.

[201] M. Brucherseifer, F. Caola, and K. Melnikov, "On the NNLO QCD corrections to single-top production at the LHC", *Phys.Lett.* **B736** (2014) 58–63, doi:10.1016/j.physletb.2014.06.075, arXiv:1404.7116.

[202] M. Brucherseifer, F. Caola, and K. Melnikov, "$\mathcal{O}(\alpha_s^2)$ corrections to fully-differential top quark decays", *JHEP* **1304** (2013) 059, doi:10.1007/JHEP04(2013)059, arXiv:1301.7133.

[203] A. Gehrmann-De Ridder, T. Gehrmann, and E. N. Glover, "Antenna subtraction at NNLO", *JHEP* **0509** (2005) 056, doi:10.1088/1126-6708/2005/09/056, arXiv:hep-ph/0505111.

[204] G. Abelof, A. Gehrmann-De Ridder, P. Maierhofer, and S. Pozzorini, "NNLO QCD subtraction for top-antitop production in the $q\bar{q}$ channel", *JHEP* **1408** (2014) 035, doi:10.1007/JHEP08(2014)035, arXiv:1404.6493.

[205] M. Czakon, "A novel subtraction scheme for double-real radiation at NNLO", *Phys.Lett.* **B693** (2010) 259–268, doi:10.1016/j.physletb.2010.08.036, arXiv:1005.0274.

[206] R. Boughezal, K. Melnikov, and F. Petriello, "A subtraction scheme for NNLO computations", *Phys.Rev.* **D85** (2012) 034025, doi:10.1103/PhysRevD.85.034025, arXiv:1111.7041.

[207] V. Del Duca, G. Somogyi, and Z. Trocsanyi, "Integration of collinear-type doubly unresolved counterterms in NNLO jet cross sections", *JHEP* **1306** (2013) 079, doi:10.1007/JHEP06(2013)079, arXiv:1301.3504.

[208] T. Gehrmann, A. von Manteuffel, L. Tancredi, and E. Weihs, "The two-loop master integrals for $q\bar{q} \to VV$", *JHEP* **1406** (2014) 032, doi:10.1007/JHEP06(2014)032, arXiv:1404.4853.

[209] F. Caola, J. M. Henn, K. Melnikov, and V. A. Smirnov, "Non-planar master integrals for the production of two off-shell vector bosons in collisions of massless partons", *JHEP* **1409** (2014) 043, doi:10.1007/JHEP09(2014)043, arXiv:1404.5590.

[210] F. Caola et al., "Two-loop helicity amplitudes for the production of two off-shell electroweak bosons in quark-antiquark collisions", *JHEP* **1411** (2014) 041, doi:10.1007/JHEP11(2014)041, arXiv:1408.6409.

[211] J. M. Henn and T. Huber, "The four-loop cusp anomalous dimension in $\mathcal{N} = 4$ super Yang-Mills and analytic integration techniques for Wilson line integrals", *JHEP* **1309** (2013) 147, doi:10.1007/JHEP09(2013)147, arXiv:1304.6418.

[212] S. Hoeche, F. Krauss, M. Schonherr, and F. Siegert, "QCD matrix elements + parton showers: The NLO case", *JHEP* **1304** (2013) 027, doi:10.1007/JHEP04(2013)027, arXiv:1207.5030.

[213] R. Frederix and S. Frixione, "Merging meets matching in MC@NLO", *JHEP* **1212** (2012) 061, doi:10.1007/JHEP12(2012)061, arXiv:1209.6215.

[214] S. Plätzer, "Controlling inclusive cross sections in parton shower + matrix element merging", *JHEP* **1308** (2013) 114, doi:10.1007/JHEP08(2013)114, arXiv:1211.5467.

[215] L. Lönnblad and S. Prestel, "Merging Multi-leg NLO Matrix Elements with Parton Showers", *JHEP* **1303** (2013) 166, doi:10.1007/JHEP03(2013)166, arXiv:1211.7278.

[216] S. Alioli et al., "Combining Higher-Order Resummation with Multiple NLO Calculations and Parton Showers in GENEVA", *JHEP* **1309** (2013) 120, doi:10.1007/JHEP09(2013)120, arXiv:1211.7049.

[217] L. Hartgring, E. Laenen, and P. Skands, "Antenna Showers with One-Loop Matrix Elements", *JHEP* **1310** (2013) 127, doi:10.1007/JHEP10(2013)127, arXiv:1303.4974.

[218] K. Hamilton, P. Nason, and G. Zanderighi, "MINLO: Multi-Scale Improved NLO", *JHEP* **1210** (2012) 155, doi:10.1007/JHEP10(2012)155, arXiv:1206.3572.

[219] K. Hamilton, P. Nason, C. Oleari, and G. Zanderighi, "Merging H/W/Z + 0 and 1 jet at NLO

with no merging scale: a path to parton shower + NNLO matching", *JHEP* **1305** (2013) 082, doi:10.1007/JHEP05(2013)082, arXiv:1212.4504.

[220] K. Hamilton, P. Nason, E. Re, and G. Zanderighi, "NNLOPS simulation of Higgs boson production", *JHEP* **1310** (2013) 222, doi:10.1007/JHEP10(2013)222, arXiv:1309.0017.

[221] A. Karlberg, E. Re, and G. Zanderighi, "NNLOPS accurate Drell-Yan production", *JHEP* **1409** (2014) 134, doi:10.1007/JHEP09(2014)134, arXiv:1407.2940.

[222] S. Hoeche, Y. Li, and S. Prestel, "Drell-Yan lepton pair production at NNLO QCD with parton showers", arXiv:1405.3607.

[223] S. Hoeche, Y. Li, and S. Prestel, "Higgs-boson production through gluon fusion at NNLO QCD with parton showers", arXiv:1407.3773.

[224] S. Alioli et al., "Matching Fully Differential NNLO Calculations and Parton Showers", *JHEP* **1406** (2014) 089, doi:10.1007/JHEP06(2014)089, arXiv:1311.0286.

[225] S. Alioli, talk presented at Parton Shower and resummation, 10-12 June 2014, Munster, Germany.

[226] L. Giusti, A. Romanino, and A. Strumia, "Natural ranges of supersymmetric signals", *Nucl.Phys.* **B550** (1999) 3–31, doi:10.1016/S0550-3213(99)00153-4, arXiv:hep-ph/9811386.

[227] A. Strumia, "Naturalness of supersymmetric models", arXiv:hep-ph/9904247.

[228] R. L. Arnowitt, P. Nath, and B. Zumino, "Superfield Densities and Action Principle in Curved Superspace", *Phys.Lett.* **B56** (1975) 81, doi:10.1016/0370-2693(75)90504-3.

[229] D. Z. Freedman, P. van Nieuwenhuizen, and S. Ferrara, "Progress Toward a Theory of Supergravity", *Phys.Rev.* **D13** (1976) 3214–3218, doi:10.1103/PhysRevD.13.3214.

[230] S. Deser and B. Zumino, "Consistent Supergravity", *Phys.Lett.* **B62** (1976) 335, doi:10.1016/0370-2693(76)90089-7.

[231] D. Z. Freedman and P. van Nieuwenhuizen, "Properties of Supergravity Theory", *Phys.Rev.* **D14** (1976) 912, doi:10.1103/PhysRevD.14.912.

[232] E. Cremmer et al., "Spontaneous Symmetry Breaking and Higgs Effect in Supergravity Without Cosmological Constant", *Nucl.Phys.* **B147** (1979) 105, doi:10.1016/0550-3213(79)90417-6.

[233] E. Cremmer, S. Ferrara, L. Girardello, and A. Van Proeyen, "Yang-Mills Theories with Local Supersymmetry: Lagrangian, Transformation Laws and SuperHiggs Effect", *Nucl.Phys.* **B212** (1983) 413, doi:10.1016/0550-3213(83)90679-X.

[234] A. H. Chamseddine, R. L. Arnowitt, and P. Nath, "Locally Supersymmetric Grand Unification", *Phys.Rev.Lett.* **49** (1982) 970, doi:10.1103/PhysRevLett.49.970.

[235] R. Barbieri, S. Ferrara, and C. A. Savoy, "Gauge Models with Spontaneously Broken Local Supersymmetry", *Phys.Lett.* **B119** (1982) 343, doi:10.1016/0370-2693(82)90685-2.

[236] M. Dine and W. Fischler, "A Phenomenological Model of Particle Physics Based on Supersymmetry", *Phys.Lett.* **B110** (1982) 227, doi:10.1016/0370-2693(82)91241-2.

[237] C. R. Nappi and B. A. Ovrut, "Supersymmetric Extension of the SU(3) x SU(2) x U(1) Model", *Phys.Lett.* **B113** (1982) 175, doi:10.1016/0370-2693(82)90418-X.

[238] L. Alvarez-Gaume, M. Claudson, and M. B. Wise, "Low-Energy Supersymmetry", *Nucl.Phys.* **B207** (1982) 96, doi:10.1016/0550-3213(82)90138-9.

[239] M. Dine and A. E. Nelson, "Dynamical supersymmetry breaking at low-energies", *Phys.Rev.* **D48** (1993) 1277–1287, doi:10.1103/PhysRevD.48.1277, arXiv:hep-ph/9303230.

[240] M. Dine, A. E. Nelson, and Y. Shirman, "Low-energy dynamical supersymmetry breaking simplified", *Phys.Rev.* **D51** (1995) 1362–1370, doi:10.1103/PhysRevD.51.1362, arXiv:hep-ph/9408384.

[241] M. Dine, A. E. Nelson, Y. Nir, and Y. Shirman, "New tools for low-energy dynamical supersymmetry breaking", *Phys.Rev.* **D53** (1996) 2658–2669, doi:10.1103/PhysRevD.53.2658, arXiv:hep-ph/9507378.

[242] S. Dimopoulos, G. Giudice, and A. Pomarol, "Dark matter in theories of gauge mediated supersymmetry breaking", *Phys.Lett.* **B389** (1996) 37–42, doi:10.1016/S0370-2693(96)01241-5, arXiv:hep-ph/9607225.

[243] G. Giudice and R. Rattazzi, "Theories with gauge mediated supersymmetry breaking", *Phys.Rept.* **322** (1999) 419–499, doi:10.1016/S0370-1573(99)00042-3, arXiv:hep-ph/9801271.

[244] M. Monaco, M. Nardecchia, A. Romanino, and R. Ziegler, "Extended Tree-Level Gauge Mediation", *JHEP* **1110** (2011) 022, doi:10.1007/JHEP10(2011)022, arXiv:1108.1706.

[245] F. Caracciolo and A. Romanino, "Simple and direct communication of dynamical supersymmetry breaking", *JHEP* **1212** (2012) 109, doi:10.1007/JHEP12(2012)109, arXiv:1207.5376.

[246] U. Ellwanger, C. Hugonie, and A. M. Teixeira, "The Next-to-Minimal Supersymmetric Standard Model", *Phys.Rept.* **496** (2010) 1–77, doi:10.1016/j.physrep.2010.07.001, arXiv:0910.1785.

[247] N. Arkani-Hamed and S. Dimopoulos, "Supersymmetric unification without low energy supersymmetry and signatures for fine-tuning at the LHC", *JHEP* **0506** (2005) 073, doi:10.1088/1126-6708/2005/06/073, arXiv:hep-th/0405159.

[248] G. Giudice and A. Romanino, "Split supersymmetry", *Nucl.Phys.* **B699** (2004) 65–89, doi:10.1016/j.nuclphysb.2004.11.048, arXiv:hep-ph/0406088.

[249] N. Arkani-Hamed, S. Dimopoulos, G. Giudice, and A. Romanino, "Aspects of split supersymmetry", *Nucl.Phys.* **B709** (2005) 3–46, doi:10.1016/j.nuclphysb.2004.12.026, arXiv:hep-ph/0409232.

[250] R. Barbieri, A. Pomarol, R. Rattazzi, and A. Strumia, "Electroweak symmetry breaking after LEP-1 and LEP-2", *Nucl.Phys.* **B703** (2004) 127–146, doi:10.1016/j.nuclphysb.2004.10.014, arXiv:hep-ph/0405040.

[251] G. Giudice, C. Grojean, A. Pomarol, and R. Rattazzi, "The Strongly-Interacting Light Higgs", *JHEP* **0706** (2007) 045, doi:10.1088/1126-6708/2007/06/045, arXiv:hep-ph/0703164.

[252] R. Contino, L. Da Rold, and A. Pomarol, "Light custodians in natural composite Higgs models", *Phys. Rev.* **D 75** (2007) 055014, doi:10.1103/PhysRevD.75.055014.

[253] K. Agashe et al., "LHC Signals for Warped Electroweak Neutral Gauge Bosons", *Phys. Rev.* **D 76** (2007) 115015, doi:10.1103/PhysRevD.76.115015, 0709.0007.

[254] K. Agashe et al., "LHC signals for warped electroweak charged gauge bosons", *Phys. Rev.* **D 80** (2009) 075007, doi:10.1103/PhysRevD.80.075007, 0810.1497.

[255] K. Agashe et al., "LHC Signals for Coset Electroweak Gauge Bosons in Warped/Composite PGB Higgs Models", *Phys. Rev.* **D 81** (2010) 096002, doi:10.1103/PhysRevD.81.096002.

[256] D. Pappadopulo, A. Thamm, R. Torre, and A. Wulzer, "Heavy Vector Triplets: Bridging Theory and Data", *JHEP* **1409** (2014) 060, doi:10.1007/JHEP09(2014)060, arXiv:1402.4431.

[257] K. Agashe, R. Contino, L. Da Rold, and A. Pomarol, "A Custodial symmetry for $Zb\bar{b}$", *Phys.Lett.* **B641** (2006) 62–66, doi:10.1016/j.physletb.2006.08.005, arXiv:hep-ph/0605341.

[258] C. Grojean, O. Matsedonskyi, and G. Panico, "Light top partners and precision physics", *JHEP* **1310** (2013) 160, doi:10.1007/JHEP10(2013)160, arXiv:1306.4655.

[259] A. Thamm, R. Torre, and A. Wulzer, "Future tests of Higgs compositeness: direct vs indirect", arXiv:1502.01701.

[260] CMS Collaboration, "Search for Resonances in the Dilepton Mass Distribution in pp Collisions at $\sqrt{s} = 8$ TeV", Technical Report CMS-PAS-EXO-12-061, 2013.

[261] CMS Collaboration, "Search for new resonances decaying via WZ to leptons in proton-proton collisions at $\sqrt{s} = 8$ TeV", *Phys.Lett.* **B740** (2015) 83–104, doi:10.1016/j.physletb.2014.11.026, arXiv:1407.3476.

[262] ATLAS Collaboration, "Search for high-mass dilepton resonances in pp collisions at $\sqrt{s} = 8$ TeV with the ATLAS detector", *Phys.Rev.* **D90** (2014), no. 5, 052005, doi:10.1103/PhysRevD.90.052005, arXiv:1405.4123.

[263] ATLAS Collaboration, "Search for WZ resonances in the fully leptonic channel using pp collisions at $\sqrt{s}$ = 8 TeV with the ATLAS detector", *Phys.Lett.* **B737** (2014) 223–243, doi:10.1016/j.physletb.2014.08.039, arXiv:1406.4456.

[264] CMS Collaboration, "CMS at the High-Energy Frontier. Contribution to the Update of the European Strategy for Particle Physics", Technical Report CMS-NOTE-2012-006. CERN-CMS-NOTE-2012-006, CERN, Geneva, Oct, 2012.

[265] ATLAS Collaboration, "Physics at a High-Luminosity LHC with ATLAS (Update)", Technical Report ATL-PHYS-PUB-2012-004, ATL-COM-PHYS-2012-1455, 2012.

[266] S. Dutta, K. Hagiwara, and Y. Matsumoto, "Measuring the Higgs-Vector boson Couplings at Linear e^+e^- Collider", *Phys.Rev.* **D78** (2008) 115016, doi:10.1103/PhysRevD.78.115016, arXiv:0808.0477.

[267] M. Klute et al., "Measuring Higgs Couplings at a Linear Collider", *Europhys.Lett.* **101** (2013) 51001, doi:10.1209/0295-5075/101/51001, arXiv:1301.1322.

[268] CLIC Detector and Physics Study Collaboration, "Physics at the CLIC e+e- Linear Collider – Input to the Snowmass process 2013", arXiv:1307.5288.

[269] CMS Collaboration, "Search for top-quark partners with charge 5/3 in the same-sign dilepton final state", *Phys.Rev.Lett.* **112** (2014) 171801, doi:10.1103/PhysRevLett.112.171801, arXiv:1312.2391.

[270] ATLAS Collaboration, "Search for pair and single production of new heavy quarks that decay to a Z boson and a third generation quark in pp collisions at $\sqrt{s} = 8$ TeV with the ATLAS detector", Technical Report ATLAS-CONF-2014-036, 2014.

[271] CMS Collaboration, "Inclusive search for a vector-like T quark with charge $\frac{2}{3}$ in pp collisions at $\sqrt{s}$ = 8 TeV", *Phys.Lett.* **B729** (2014) 149–171, doi:10.1016/j.physletb.2014.01.006, arXiv:1311.7667.

[272] O. Matsedonskyi, G. Panico, and A. Wulzer, "On the Interpretation of Top Partners Searches", arXiv:1409.0100.

[273] A. De Simone, O. Matsedonskyi, R. Rattazzi, and A. Wulzer, "A First Top Partner Hunter's Guide", *JHEP* **1304** (2013) 004, doi:10.1007/JHEP04(2013)004, arXiv:1211.5663.

[274] N. G. Ortiz, J. Ferrando, D. Kar, and M. Spannowsky, "Reconstructing singly produced top partners in decays to **Wb**", *Phys.Rev.* **D90** (2014) 075009, doi:10.1103/PhysRevD.90.075009, arXiv:1403.7490.

[275] J. Mrazek and A. Wulzer, "A Strong Sector at the LHC: Top Partners in Same-Sign Dileptons", *Phys.Rev.* **D81** (2010) 075006, doi:10.1103/PhysRevD.81.075006, arXiv:0909.3977.

[276] N. Vignaroli, "Early discovery of top partners and test of the Higgs nature", *Phys.Rev.* **D86** (2012) 075017, doi:10.1103/PhysRevD.86.075017, arXiv:1207.0830.

[277] J. Alwall et al., "MadGraph 5 : Going Beyond", *JHEP* **1106** (2011) 128, doi:10.1007/JHEP06(2011)128, arXiv:1106.0522.

[278] DELPHES 3 Collaboration, "DELPHES 3, A modular framework for fast simulation of a generic collider experiment", *JHEP* **1402** (2014) 057, doi:10.1007/JHEP02(2014)057,

arXiv:1307.6346.

[279] J. Anderson et al., "Snowmass Energy Frontier Simulations", arXiv:1309.1057.

[280] A. Avetisyan et al., "Methods and Results for Standard Model Event Generation at $\sqrt{s}$ = 14 TeV, 33 TeV and 100 TeV Proton Colliders (A Snowmass Whitepaper)", arXiv:1308.1636.

[281] A. Avetisyan et al., "Snowmass Energy Frontier Simulations using the Open Science Grid (A Snowmass 2013 whitepaper)", arXiv:1308.0843.

[282] A. Gennaro, "Study of the single production of a heavy top-quark partner at LHC and future hadronic colliders". M. Cobal (Supervisor), Università di Trieste, Laurea Magistrale in Fisica, 19 marzo 2015, http://thesis.units.it/store/handle/item/13898.

[283] M. Nardecchia, A. Romanino, and R. Ziegler, "Tree Level Gauge Mediation", *JHEP* **0911** (2009) 112, doi:10.1088/1126-6708/2009/11/112, arXiv:0909.3058.

[284] M. Nardecchia, A. Romanino, and R. Ziegler, "General Aspects of Tree Level Gauge Mediation", *JHEP* **1003** (2010) 024, doi:10.1007/JHEP03(2010)024, arXiv:0912.5482.

[285] P. Fayet, "Supergauge Invariant Extension of the Higgs Mechanism and a Model for the electron and Its Neutrino", *Nucl.Phys.* **B90** (1975) 104–124, doi:10.1016/0550-3213(75)90636-7.

[286] M. S. Carena, M. Quiros, and C. Wagner, "Effective potential methods and the Higgs mass spectrum in the MSSM", *Nucl.Phys.* **B461** (1996) 407–436, doi:10.1016/0550-3213(95)00665-6, arXiv:hep-ph/9508343.

[287] S. King, M. Muehlleitner, R. Nevzorov, and K. Walz, "Discovery Prospects for NMSSM Higgs Bosons at the High-Energy Large Hadron Collider", *Phys.Rev.* **D90** (2014), no. 9, 095014, doi:10.1103/PhysRevD.90.095014, arXiv:1408.1120.

[288] J. Cao et al., "Exploring the Higgs Sector of a Most Natural NMSSM and its Prediction on Higgs Pair Production at the LHC", arXiv:1409.8431.

[289] R. Barbieri et al., "Exploring the Higgs sector of a most natural NMSSM", *Phys.Rev.* **D87** (2013), no. 11, 115018, doi:10.1103/PhysRevD.87.115018, arXiv:1304.3670.

[290] R. Barbieri et al., "One or more Higgs bosons?", *Phys.Rev.* **D88** (2013) 055011, doi:10.1103/PhysRevD.88.055011, arXiv:1307.4937.

[291] CMS Collaboration, "Search for a standard model like Higgs boson in the decay channel H to ZZ to l+l- q qbar at CMS", Technical Report CMS-PAS-HIG-12-024, CERN, Geneva, 2013.

[292] T. ATLAS-collaboration, "Physics at a High-Luminosity LHC with ATLAS (Update)", Technical Report ATL-PHYS-PUB-2012-004, CERN, Geneva, Oct, 2012.

[293] E. Brownson et al., "Heavy Higgs Scalars at Future Hadron Colliders (A Snowmass Whitepaper)", arXiv:1308.6334.

[294] CMS Collaboration, "Search for resonant HH production in 2gamma+2b channel", Technical Report CMS-PAS-HIG-13-032, CERN, Geneva, 2014.

[295] ATLAS Collaboration, "Search For Higgs Boson Pair Production in the $\gamma\gamma b\bar{b}$ Final State using pp Collision Data at $\sqrt{s} = 8$ TeV from the ATLAS Detector", arXiv:1406.5053.

[296] M. Gouzevitch et al., "Scale-invariant resonance tagging in multijet events and new physics in Higgs pair production", *JHEP* **1307** (2013) 148, doi:10.1007/JHEP07(2013)148, arXiv:1303.6636.

[297] M. Badziak, M. Olechowski, and S. Pokorski, "New Regions in the NMSSM with a 125 GeV Higgs", *JHEP* **1306** (2013) 043, doi:10.1007/JHEP06(2013)043, arXiv:1304.5437.

[298] R. Barbieri and G. Giudice, "Upper Bounds on Supersymmetric Particle Masses", *Nucl.Phys.* **B306** (1988) 63, doi:10.1016/0550-3213(88)90171-X.

[299] G. F. Giudice, "Naturally Speaking: The Naturalness Criterion and Physics at the LHC", arXiv:0801.2562.

[300] R. Kitano and Y. Nomura, "Supersymmetry, naturalness, and signatures at the CERN LHC",

Phys. Rev. D **73** (May, 2006) 095004, doi:10.1103/PhysRevD.73.095004, arXiv:hep-ph/0602096.

[301] E. Bagnaschi, G. F. Giudice, P. Slavich, and A. Strumia, "Higgs Mass and Unnatural Supersymmetry", *JHEP* **1409** (2014) 092, doi:10.1007/JHEP09(2014)092, arXiv:1407.4081.

[302] E. Bertuzzo and C. Frugiuele, "A natural SM-like 126 GeV Higgs via non-decoupling D-terms", arXiv:1412.2765.

[303] T. Gherghetta, B. von Harling, A. D. Medina, and M. A. Schmidt, "The Scale-Invariant NMSSM and the 126 GeV Higgs Boson", *JHEP* **1302** (2013) 032, doi:10.1007/JHEP02(2013)032, arXiv:1212.5243.

[304] R. Barbieri, L. J. Hall, Y. Nomura, and V. S. Rychkov, "Supersymmetry without a Light Higgs Boson", *Phys.Rev.* **D75** (2007) 035007, doi:10.1103/PhysRevD.75.035007, arXiv:hep-ph/0607332.

[305] P. J. Fox, A. E. Nelson, and N. Weiner, "Dirac Gaugino Masses and Supersoft Supersymmetry Breaking", *Journal of High Energy Physics* **8** (August, 2002) 35, doi:10.1088/1126-6708/2002/08/035, arXiv:arXiv:hep-ph/0206096.

[306] R. Barbier et al., "R-Parity-violating supersymmetry", *Physics Reports* **420** (November, 2005) 1–195, doi:10.1016/j.physrep.2005.08.006, arXiv:arXiv:hep-ph/0406039.

[307] B. W. Lee and S. Weinberg, "Cosmological Lower Bound on Heavy Neutrino Masses", *Phys.Rev.Lett.* **39** (1977) 165–168, doi:10.1103/PhysRevLett.39.165.

[308] I. Melzer-Pellmann and P. Pralavorio, "Lessons for SUSY from the LHC after the first run", *European Physical Journal C* **74** (May, 2014) 2801, doi:10.1140/epjc/s10052-014-2801-y, arXiv:1404.7191.

[309] N. Craig, "The State of Supersymmetry after Run I of the LHC", arXiv:1309.0528.

[310] J. L. Feng, "Naturalness and the Status of Supersymmetry", *Ann.Rev.Nucl.Part.Sci.* **63** (2013) 351–382, doi:10.1146/annurev-nucl-102010-130447, arXiv:1302.6587.

[311] "Gavin Salam and Andreas Weiler - Collider Reach". http://collider-reach.web.cern.ch/collider-reach/.

[312] ATLAS Collaboration, "Search for squarks and gluinos with the ATLAS detector in final states with jets and missing transverse momentum using $\sqrt{s} = 8$ TeV proton–proton collision data", *JHEP* **1409** (2014) 176, doi:10.1007/JHEP09(2014)176, arXiv:1405.7875.

[313] T. Cohen et al., "SUSY Simplified Models at 14, 33, and 100 TeV Proton Colliders", arXiv:1311.6480.

[314] CMS Collaboration, "Search for supersymmetry in hadronic final states using MT2 with the CMS detector at sqrt(s) = 8 TeV", Technical Report CMS-PAS-SUS-13-019, CERN, Geneva, 2014.

[315] "ATLAS Stop Searches Summary". https://atlas.web.cern.ch/Atlas/GROUPS/PHYSICS/CombinedSummaryPlots/SUSY/index.html#ATLAS_SUSY_Stop_tLSP.

[316] M. Czakon et al., "Closing the stop gap", *Phys.Rev.Lett.* **113** (2014), no. 20, 201803, doi:10.1103/PhysRevLett.113.201803, arXiv:1407.1043.

[317] "Measurement of spin correlation in top–antitop quark events and search for top squark pair production in proton–proton collisions at $\sqrt{s}$=8 TeV using the ATLAS detector", Technical Report ATLAS-CONF-2014-056, CERN, Geneva, 2014.

[318] T. Cohen et al., "Boosting Stop Searches with a 100 TeV Proton Collider", arXiv:1406.4512v1.

[319] U. Ellwanger and A. M. Teixeira, "NMSSM with a singlino LSP: possible challenges for searches for supersymmetry at the LHC", arXiv:1406.7221.

[320] D. Das, U. Ellwanger, and A. M. Teixeira, "Modified signals for supersymmetry in the NMSSM with a singlino-like LSP", *Journal of High Energy Physics* **4** (April, 2012) 67, doi:10.1007/JHEP04(2012)067, arXiv:1202.5244.

[321] R. Gavin et al., "Squark Production and Decay matched with Parton Showers at NLO", arXiv:1407.7971.

[322] D. Goncalves, D. Lopez-Val, K. Mawatari, and T. Plehn, "Automated third generation squark production to next-to-leading order", arXiv:1407.4302.

[323] J. Alwall et al., "The automated computation of tree-level and next-to-leading order differential cross sections, and their matching to parton shower simulations", arXiv:1405.0301v1.

[324] ATLAS Collaboration, "Search for pair-produced third-generation squarks decaying via charm quarks or in compressed supersymmetric scenarios in pp collisions at $\sqrt{s} = 8$ TeV with the ATLAS detector", arXiv:1407.0608.

[325] ATLAS Collaboration, "Search for top squark pair production in final states with one isolated lepton, jets, and missing transverse momentum in $\sqrt{s} = 8$ TeV pp collisions with the ATLAS detector", arXiv:1407.0583.

[326] Z. Han and A. Katz, "Stealth Stops and Spin Correlation: A Snowmass White Paper", arXiv:1310.0356.

[327] I. Hinchliffe et al., "Precision SUSY measurements at CERN LHC", *Phys. Rev. D* **55** (May, 1997) 5520–5540, doi:10.1103/PhysRevD.55.5520, arXiv:arXiv:hep-ph/9610544.

[328] B. C. Allanach, C. Gorham Lester, M. A. Parker, and B. R. Webber, "Measuring sparticle masses in non-universal string inspired models at the LHC", *Journal of High Energy Physics* **9** (September, 2000) 4, doi:10.1088/1126-6708/2000/09/004, arXiv:arXiv:hep-ph/0007009.

[329] K. Kawagoe, M. M. Nojiri, and G. Polesello, "New supersymmetry mass reconstruction method at the CERN LHC", *Phys. Rev. D* **71** (February, 2005) 035008, doi:10.1103/PhysRevD.71.035008, arXiv:arXiv:hep-ph/0410160.

[330] F. W. Stecker, "Cosmic gamma rays", *NASA Special Publication* **249** (1971).

[331] K. Agashe, R. Franceschini, and D. Kim, "A simple, yet subtle 'invariance' of two-body decay kinematics", *Phys. Rev. D* **88** (September, 2013) 057701, doi:10.1103/PhysRevD.88.057701, arXiv:1209.0772.

[332] J. Eckel, W. Shepherd, and S. Su, "Slepton discovery in electroweak cascade decay", *Journal of High Energy Physics* **5** (May, 2012) 81, doi:10.1007/JHEP05(2012)081, arXiv:1111.2615.

[333] I. Low, "Polarized Charginos (and Tops) in Stop Decays", arXiv:1304.0491.

[334] H. Baer, C.-H. Chen, and X. Tata, "Impact of hadronic decays of the lightest neutralino on the reach of the CERN LHC", *Phys. Rev. D* **55** (February, 1997) 1466–1470, doi:10.1103/PhysRevD.55.1466, arXiv:hep-ph/9608221.

[335] ATLAS, "Search for supersymmetry at = 8 TeV in final states with jets and two same-sign leptons or three leptons with the ATLAS detector", *Journal of High Energy Physics* **6** (June, 2014) 35, doi:10.1007/JHEP06(2014)035, arXiv:1404.2500.

[336] A. Arvanitaki et al., "The Last Vestiges of Naturalness", *JHEP* **1403** (2014) 022, doi:10.1007/JHEP03(2014)022, arXiv:1309.3568.

[337] M. Saelim and M. Perelstein, "RPV SUSY with Same-Sign Dileptons at LHC-14", arXiv:1309.7707.

[338] ATLAS Collaboration, "Search for a heavy narrow resonance decaying to $e\mu$, $e\tau$, or $\mu\tau$ with the ATLAS detector in $\sqrt{s} = 7$ TeV pp collisions at the LHC", *Physics Letters B* **723** (June, 2013) 15–32, doi:10.1016/j.physletb.2013.04.035, arXiv:1212.1272.

[339] ATLAS Collaboration, "Search for supersymmetry in events with four or more leptons in $\sqrt{s}$ = 8 TeV pp collisions with the ATLAS detector", *Phys.Rev.* **D90** (2014), no. 5, 052001, doi:10.1103/PhysRevD.90.052001, arXiv:1405.5086.

[340] P. Graham, S. Rajendran, and P. Saraswat, "Supersymmetric Crevices: Missing Signatures of RPV at the LHC", arXiv:1403.7197.

[341] "Search for light- and heavy-flavor three-jet resonances in multijet final states at 8 TeV", Technical Report CMS-PAS-EXO-12-049, CERN, Geneva, 2013.

[342] ATLAS Collaboration, "Search for new phenomena in final states with large jet multiplicities and missing transverse momentum at sqrt(s)=8 TeV proton-proton collisions using the ATLAS experiment", arXiv:1308.1841.

[343] ATLAS Collaboration, "Search for massive particles in multijet signatures with the ATLAS detector in $\sqrt{s} = 8$ TeV pp collisions at the LHC", Technical Report ATLAS-CONF-2013-091, CERN, Geneva, Aug, 2013.

[344] CDF Collaboration, "Search for pair-production of strongly-interacting particles decaying to pairs of jets in $p\bar{p}$ collisions at $\sqrt{s} = 1.96$ TeV", arXiv:1303.2699.

[345] ATLAS Collaboration, "Search for massive colored scalars in four-jet final states in $\sqrt{s}$=7 TeV proton-proton collisions with the ATLAS detector", *European Physical Journal C* **71** (December, 2011) 1828, doi:10.1140/epjc/s10052-011-1828-6, arXiv:1110.2693.

[346] D. Duggan et al., "Sensitivity of an Upgraded LHC to R-Parity Violating Signatures of the MSSM", arXiv:1308.3903.

[347] Y. Bai, A. Katz, and B. Tweedie, "Pulling Out All the Stops: Searching for RPV SUSY with Stop-Jets", arXiv:1309.6631.

[348] R. Franceschini and R. Torre, "RPV stops bump off the background", arXiv:1212.3622.

[349] J. A. Evans, Y. Kats, D. Shih, and M. J. Strassler, "Toward full LHC coverage of natural supersymmetry", *Journal of High Energy Physics* **7** (July, 2014) 101, doi:10.1007/JHEP07(2014)101, arXiv:1310.5758.

[350] CMS Collaboration, "Search for Multijet Resonances in the 8-jet Final State", Technical Report CMS-PAS-EXO-11-075, 2012.

[351] S. Chatrchyan et al., "Search for microscopic black holes in pp collisions at TeV", *Journal of High Energy Physics* **7** (July, 2013) 178, doi:10.1007/JHEP07(2013)178, arXiv:1303.5338.

[352] T. Cohen, E. Izaguirre, M. Lisanti, and H. Keong Lou, "Jet Substructure by Accident", arXiv:1212.1456.

[353] T. Cohen et al., "Jet Substructure Templates: Data-driven QCD Backgrounds for Fat Jet Searches", arXiv:1402.0516.

[354] S. El Hedri, A. Hook, M. Jankowiak, and J. G. Wacker, "Learning How to Count: A High Multiplicity Search for the LHC", arXiv:1302.1870.

[355] ATLAS Collaboration, "Search for pair production of massive particles decaying into three quarks with the ATLAS detector in $\sqrt{(s)}$ = 7 TeV pp collisions at the LHC", arXiv:1210.4813.

[356] "ATLAS SUSY Electroweak Summary". https://atlas.web.cern.ch/Atlas/GROUPS/PHYSICS/CombinedSummaryPlots/SUSY/index.html#ATLAS_SUSY_EWSummary.

[357] "Search for Supersymmetry at the high luminosity LHC with the ATLAS experiment", Technical Report ATL-PHYS-PUB-2014-010, CERN, Geneva, 2014.

[358] M. Low and L.-T. Wang, "Neutralino Dark Matter at 100 TeV", arXiv:1404.0682v1.

[359] S. Gori, S. Jung, L.-T. Wang, and J. D. Wells, "Prospects for Electroweakino Discovery at a 100 TeV Hadron Collider", arXiv:1410.6287.

[360] M. Cirelli, F. Sala, and M. Taoso, "Wino-like Minimal Dark Matter and future colliders", arXiv:1407.7058.

[361] B. S. Acharya, K. Bozek, C. Pongkitivanichkul, and K. Sakurai, "Prospects for observing charginos and neutralinos at a 100 TeV proton-proton collider", arXiv:1410.1532.

[362] M. Ibe, S. Matsumoto, and R. Sato, "Mass splitting between charged and neutral winos at two-loop level", *Physics Letters B* **721** (April, 2013) 252–260, doi:10.1016/j.physletb.2013.03.015, arXiv:1212.5989.

[363] ATLAS Collaboration, "Search for charginos nearly mass-degenerate with the lightest neutralino based on a disappearing-track signature in pp collisions at $\sqrt{s}$ = 8 TeV with the ATLAS detector", arXiv:1310.3675.

[364] Bramante, J., Fox, P., Martin, A., Ostdiek, B., Plehn, T., Schell, T., and Takeuchi, M., "Supersymmetric Dark Matter and Mass Splitting Spectroscopy at the Nimatron", *To appear*.

[365] ATLAS Collaboration, "Search for direct production of charginos, neutralinos and sleptons in final states with two leptons and missing transverse momentum in pp collisions at = 8TeV with the ATLAS detector", *Journal of High Energy Physics* **5** (May, 2014) 71, doi:10.1007/JHEP05(2014)071, arXiv:1403.5294.

[366] ATLAS Collaboration, "Search for direct production of charginos and neutralinos in events with three leptons and missing transverse momentum in sqrt(s) = 8TeV pp collisions with the ATLAS detector", arXiv:1402.7029.

[367] R. Bousso and J. Polchinski, "Quantization of four form fluxes and dynamical neutralization of the cosmological constant", *JHEP* **0006** (2000) 006, doi:10.1088/1126-6708/2000/06/006, arXiv:hep-th/0004134.

[368] S. Kachru, R. Kallosh, A. D. Linde, and S. P. Trivedi, "De Sitter vacua in string theory", *Phys.Rev.* **D68** (2003) 046005, doi:10.1103/PhysRevD.68.046005, arXiv:hep-th/0301240.

[369] L. Susskind, "The Anthropic landscape of string theory", arXiv:hep-th/0302219.

[370] F. Denef and M. R. Douglas, "Distributions of nonsupersymmetric flux vacua", *JHEP* **0503** (2005) 061, doi:10.1088/1126-6708/2005/03/061, arXiv:hep-th/0411183.

[371] V. Agrawal, S. M. Barr, J. F. Donoghue, and D. Seckel, "The Anthropic principle and the mass scale of the standard model", *Phys.Rev.* **D57** (1998) 5480–5492, doi:10.1103/PhysRevD.57.5480, arXiv:hep-ph/9707380.

[372] S. Weinberg, "Anthropic Bound on the Cosmological Constant", *Phys.Rev.Lett.* **59** (1987) 2607, doi:10.1103/PhysRevLett.59.2607.

[373] J. D. Wells, "PeV-scale supersymmetry", *Phys.Rev.* **D71** (2005) 015013, doi:10.1103/PhysRevD.71.015013, arXiv:hep-ph/0411041.

[374] N. Arkani-Hamed, A. Delgado, and G. Giudice, "The Well-tempered neutralino", *Nucl.Phys.* **B741** (2006) 108–130, doi:10.1016/j.nuclphysb.2006.02.010, arXiv:hep-ph/0601041.

[375] A. Arvanitaki, N. Craig, S. Dimopoulos, and G. Villadoro, "Mini-Split", *JHEP* **1302** (2013) 126, doi:10.1007/JHEP02(2013)126, arXiv:1210.0555.

[376] T. Cohen et al., "SUSY Simplified Models at 14, 33, and 100 TeV Proton Colliders", *JHEP* **1404** (2014) 117, doi:10.1007/JHEP04(2014)117, arXiv:1311.6480.

[377] M. Low and L.-T. Wang, "Neutralino dark matter at 14 TeV and 100 TeV", *JHEP* **1408** (2014) 161, doi:10.1007/JHEP08(2014)161, arXiv:1404.0682.

[378] M. Cirelli, F. Sala, and M. Taoso, "Wino-like Minimal Dark Matter and future colliders", *JHEP* **1410** (2014) 033, doi:10.1007/JHEP10(2014)033, arXiv:1407.7058.

[379] S. Gori, S. Jung, L.-T. Wang, and J. D. Wells, "Prospects for Electroweakino Discovery at a 100

TeV Hadron Collider", *JHEP* **1412** (2014) 108, doi:10.1007/JHEP12(2014)108, arXiv:1410.6287.

[380] B. S. Acharya, K. Bozek, C. Pongkitivanichkul, and K. Sakurai, "Prospects for observing charginos and neutralinos at a 100 TeV proton-proton collider", arXiv:1410.1532.

[381] G. G. di Cortona, "Hunting electroweakinos at future hadron colliders and direct detection experiments", arXiv:1412.5952.

[382] J. Fan and M. Reece, "In Wino Veritas? Indirect Searches Shed Light on Neutralino Dark Matter", *JHEP* **1310** (2013) 124, doi:10.1007/JHEP10(2013)124, arXiv:1307.4400.

[383] P. Cushman et al., "Working Group Report: WIMP Dark Matter Direct Detection", arXiv:1310.8327.

[384] T. Cohen, M. Lisanti, A. Pierce, and T. R. Slatyer, "Wino Dark Matter Under Siege", *JCAP* **1310** (2013) 061, doi:10.1088/1475-7516/2013/10/061, arXiv:1307.4082.

[385] M. Cirelli, N. Fornengo, and A. Strumia, "Minimal dark matter", *Nucl.Phys.* **B753** (2006) 178–194, doi:10.1016/j.nuclphysb.2006.07.012, arXiv:hep-ph/0512090.

[386] H. Davoudiasl, R. Kitano, T. Li, and H. Murayama, "The New minimal standard model", *Phys.Lett.* **B609** (2005) 117–123, doi:10.1016/j.physletb.2005.01.026, arXiv:hep-ph/0405097.

[387] T. Asaka, S. Blanchet, and M. Shaposhnikov, "The nuMSM, dark matter and neutrino masses", *Phys.Lett.* **B631** (2005) 151–156, doi:10.1016/j.physletb.2005.09.070, arXiv:hep-ph/0503065.

[388] T. Asaka and M. Shaposhnikov, "The nuMSM, dark matter and baryon asymmetry of the universe", *Phys.Lett.* **B620** (2005) 17–26, doi:10.1016/j.physletb.2005.06.020, arXiv:hep-ph/0505013.

[389] P. Minkowski, "mu e gamma at a Rate of One Out of 1-Billion Muon Decays?", *Phys.Lett.* **B67** (1977) 421, doi:10.1016/0370-2693(77)90435-X.

[390] T. Yanagida, "Horizontal Symmetry and Masses of Neutrinos", *Prog.Theor.Phys.* **64** (1980) 1103, doi:10.1143/PTP.64.1103.

[391] M. Gell-Mann, P. Ramond, and R. Slansky, "Color Embeddings, Charge Assignments, and Proton Stability in Unified Gauge Theories", *Rev.Mod.Phys.* **50** (1978) 721, doi:10.1103/RevModPhys.50.721.

[392] R. N. Mohapatra and G. Senjanovic, "Neutrino Mass and Spontaneous Parity Violation", *Phys.Rev.Lett.* **44** (1980) 912, doi:10.1103/PhysRevLett.44.912.

[393] C. Geng and R. Marshak, "Uniqueness of Quark and Lepton Representations in the Standard Model From the Anomalies Viewpoint", *Phys.Rev.* **D39** (1989) 693, doi:10.1103/PhysRevD.39.693.

[394] K. Babu and R. Mohapatra, "Is There a Connection Between Quantization of Electric Charge and a Majorana Neutrino?", *Phys.Rev.Lett.* **63** (1989) 938, doi:10.1103/PhysRevLett.63.938.

[395] F. Bezrukov, D. Gorbunov, and M. Shaposhnikov, "On initial conditions for the Hot Big Bang", *JCAP* **0906** (2009) 029, doi:10.1088/1475-7516/2009/06/029, arXiv:0812.3622.

[396] A. Roy and M. Shaposhnikov, "Resonant production of the sterile neutrino dark matter and fine-tunings in the [nu]MSM", *Phys.Rev.* **D82** (2010) 056014, doi:10.1103/PhysRevD.82.056014, arXiv:1006.4008.

[397] F. Bezrukov, D. Gorbunov, and M. Shaposhnikov, "Late and early time phenomenology of Higgs-dependent cutoff", *JCAP* **1110** (2011) 001, doi:10.1088/1475-7516/2011/10/001, arXiv:1106.5019.

[398] M. Shaposhnikov and I. Tkachev, "The nuMSM, inflation, and dark matter", *Phys.Lett.* **B639**

(2006) 414–417, doi:10.1016/j.physletb.2006.06.063, arXiv:hep-ph/0604236.

[399] K. Petraki and A. Kusenko, "Dark-matter sterile neutrinos in models with a gauge singlet in the Higgs sector", *Phys.Rev.* **D77** (2008) 065014, doi:10.1103/PhysRevD.77.065014, arXiv:0711.4646.

[400] A. Boyarsky, D. Iakubovskyi, and O. Ruchayskiy, "Next decade of sterile neutrino studies", *Phys.Dark Univ.* **1** (2012) 136–154, doi:10.1016/j.dark.2012.11.001, arXiv:1306.4954.

[401] E. Bulbul et al., "Detection of An Unidentified Emission Line in the Stacked X-ray spectrum of Galaxy Clusters", *Astrophys.J.* **789** (2014) 13, doi:10.1088/0004-637X/789/1/13, arXiv:1402.2301.

[402] A. Boyarsky, O. Ruchayskiy, D. Iakubovskyi, and J. Franse, "An unidentified line in X-ray spectra of the Andromeda galaxy and Perseus galaxy cluster", arXiv:1402.4119.

[403] A. Boyarsky, J. Franse, D. Iakubovskyi, and O. Ruchayskiy, "Checking the dark matter origin of 3.53 keV line with the Milky Way center", arXiv:1408.2503.

[404] L. Canetti, M. Drewes, and M. Shaposhnikov, "Sterile Neutrinos as the Origin of Dark and Baryonic Matter", *Phys.Rev.Lett.* **110** (2013), no. 6, 061801, doi:10.1103/PhysRevLett.110.061801, arXiv:1204.3902.

[405] F. Bezrukov, "nu MSM-predictions for neutrinoless double beta decay", *Phys.Rev.* **D72** (2005) 071303, doi:10.1103/PhysRevD.72.071303, arXiv:hep-ph/0505247.

[406] M. Shaposhnikov, "The nuMSM, leptonic asymmetries, and properties of singlet fermions", *JHEP* **0808** (2008) 008, doi:10.1088/1126-6708/2008/08/008, arXiv:0804.4542.

[407] L. Canetti, M. Drewes, and B. Garbrecht, "Lab-to-Genesis", arXiv:1404.7114.

[408] A. Kusenko, "Sterile neutrinos, dark matter, and the pulsar velocities in models with a Higgs singlet", *Phys.Rev.Lett.* **97** (2006) 241301, doi:10.1103/PhysRevLett.97.241301, arXiv:hep-ph/0609081.

[409] M. Shaposhnikov, "A Possible symmetry of the nuMSM", *Nucl.Phys.* **B763** (2007) 49–59, doi:10.1016/j.nuclphysb.2006.11.003, arXiv:hep-ph/0605047.

[410] A. de Gouvea, "See-saw energy scale and the LSND anomaly", *Phys.Rev.* **D72** (2005) 033005, doi:10.1103/PhysRevD.72.033005, arXiv:hep-ph/0501039.

[411] LSND Collaboration, "Evidence for neutrino oscillations from the observation of anti-neutrino(electron) appearance in a anti-neutrino(muon) beam", *Phys.Rev.* **D64** (2001) 112007, doi:10.1103/PhysRevD.64.112007, arXiv:hep-ex/0104049.

[412] MiniBooNE Collaboration, "Improved Search for $\bar{\nu}_\mu \to \bar{\nu}_e$ Oscillations in the MiniBooNE Experiment", *Phys.Rev.Lett.* **110** (2013) 161801, doi:10.1103/PhysRevLett.110.161801, arXiv:1207.4809.

[413] G. Mention et al., "The Reactor Antineutrino Anomaly", *Phys.Rev.* **D83** (2011) 073006, doi:10.1103/PhysRevD.83.073006, arXiv:1101.2755.

[414] J. Abdurashitov et al., "Measurement of the response of a Ga solar neutrino experiment to neutrinos from an Ar-37 source", *Phys.Rev.* **C73** (2006) 045805, doi:10.1103/PhysRevC.73.045805, arXiv:nucl-ex/0512041.

[415] SAGE Collaboration, "Measurement of the response of the Russian-American gallium experiment to neutrinos from a Cr-51 source", *Phys.Rev.* **C59** (1999) 2246–2263, doi:10.1103/PhysRevC.59.2246, arXiv:hep-ph/9803418.

[416] GALLEX Collaboration, "Final results of the Cr-51 neutrino source experiments in GALLEX", *Phys.Lett.* **B420** (1998) 114–126, doi:10.1016/S0370-2693(97)01562-1.

[417] F. Kaether et al., "Reanalysis of the GALLEX solar neutrino flux and source experiments", *Phys.Lett.* **B685** (2010) 47–54, doi:10.1016/j.physletb.2010.01.030,

arXiv:1001.2731.

[418] D. Gorbunov and M. Shaposhnikov, "How to find neutral leptons of the νMSM?", *JHEP* **0710** (2007) 015, doi:10.1007/JHEP11(2013)101,10.1088/1126-6708/2007/10/015, arXiv:0705.1729.

[419] R. E. Shrock, "General Theory of Weak Leptonic and Semileptonic Decays. 1. Leptonic Pseudoscalar Meson Decays, with Associated Tests For, and Bounds on, Neutrino Masses and Lepton Mixing", *Phys.Rev.* **D24** (1981) 1232, doi:10.1103/PhysRevD.24.1232.

[420] R. E. Shrock, "General Theory of Weak Processes Involving Neutrinos. 2. Pure Leptonic Decays", *Phys.Rev.* **D24** (1981) 1275, doi:10.1103/PhysRevD.24.1275.

[421] R. Shrock, "New Tests For, and Bounds On, Neutrino Masses and Lepton Mixing", *Phys.Lett.* **B96** (1980) 159, doi:10.1016/0370-2693(80)90235-X.

[422] R. E. Shrock, "Pure Leptonic Decays With Massive Neutrinos and Arbitrary Lorentz Structure", *Phys.Lett.* **B112** (1982) 382, doi:10.1016/0370-2693(82)91074-7.

[423] D. Britton et al., "Measurement of the pi+ —> e+ neutrino branching ratio", *Phys.Rev.Lett.* **68** (1992) 3000–3003, doi:10.1103/PhysRevLett.68.3000.

[424] T. Yamazaki et al., "Search for Heavy Neutrinos in Kaon Decay", *Conf.Proc.* **C840719** (1984) I.262.

[425] D. Bryman and T. Numao, "Search for massive neutrinos in pi+ —>; mu+ neutrino decay", *Phys.Rev.* **D53** (1996) 558–559, doi:10.1103/PhysRevD.53.558.

[426] R. Abela et al., "Search for an Admixture of Heavy Neutrino in Pion Decay", *Phys.Lett.* **B105** (1981) 263–266, doi:10.1016/0370-2693(81)90884-4.

[427] R. Hayano et al., "HEAVY NEUTRINO SEARCH USING K(mu2) DECAY", *Phys.Rev.Lett.* **49** (1982) 1305, doi:10.1103/PhysRevLett.49.1305.

[428] G. Bernardi et al., "Search for Neutrino Decay", *Phys.Lett.* **B166** (1986) 479, doi:10.1016/0370-2693(86)91602-3.

[429] NuTeV, E815 Collaboration, "Search for neutral heavy leptons in a high-energy neutrino beam", *Phys.Rev.Lett.* **83** (1999) 4943–4946, doi:10.1103/PhysRevLett.83.4943, arXiv:hep-ex/9908011.

[430] W. Bonivento et al., "Proposal to Search for Heavy Neutral Leptons at the SPS", arXiv:1310.1762.

[431] W. Bonivento et al., "Answers to the questions from the SPSC concerning the SPSC-EOI-010", Technical Report CERN-SPSC-2013-024 / SPSC-EOI-010, CERN, Geneva, 2014.

[432] M. Moulson. Presentation at LTS1 2014: Workshop on the Long-Term Strategy of INFN-CSN1 (Elba, Italy, 22 May 2014).

[433] ATLAS Collaboration, "Search for long-lived neutral particles decaying into lepton jets in proton–proton collisions at $\sqrt{s} = 8$ TeV with the ATLAS detector", arXiv:1409.0746.

[434] team for the FCC-ee study Collaboration, "Search for Heavy Right Handed Neutrinos at the FCC-ee", arXiv:1411.5230.

[435] R. Essig et al., "Working Group Report: New Light Weakly Coupled Particles", arXiv:1311.0029.

[436] P. deNiverville, D. McKeen, and A. Ritz, "Signatures of sub-GeV dark matter beams at neutrino experiments", *Phys.Rev.* **D86** (2012) 035022, doi:10.1103/PhysRevD.86.035022, arXiv:1205.3499.

[437] J. Blümlein and J. Brunner, "New Exclusion Limits on Dark Gauge Forces from Proton Bremsstrahlung in Beam-Dump Data", *Phys.Lett.* **B731** (2014) 320–326, doi:10.1016/j.physletb.2014.02.029, arXiv:1311.3870.

[438] D. Gorbunov, A. Makarov, and I. Timiryasov, "Decaying light particles in the SHiP experiment:

Signal rate estimates for hidden photons", *Phys.Rev.* **D91** (2015), no. 3, 035027, doi:10.1103/PhysRevD.91.035027, arXiv:1411.4007.

[439] S. Alekhin et al., "A facility to Search for Hidden Particles at the CERN SPS: the SHiP physics case", arXiv:1504.04855.

[440] BDX Collaboration, "Dark matter search in a Beam-Dump eXperiment (BDX) at Jefferson Lab", arXiv:1406.3028.

[441] M. Raggi and V. Kozhuharov, "Proposal to Search for a Dark Photon in Positron on Target Collisions at DAΦNE Linac", *Adv.High Energy Phys.* **2014** (2014) 959802, doi:10.1155/2014/959802, arXiv:1403.3041.

[442] M. Pospelov, "Secluded U(1) below the weak scale", *Phys.Rev.* **D80** (2009) 095002, doi:10.1103/PhysRevD.80.095002, arXiv:0811.1030.

[443] M. Raggi, "PADME dump". https://agenda.infn.it/conferenceOtherViews.py?view=standardshort&confId=8563. What Next LNF, Frascati 10-11 November 2014.

[444] B. Batell, M. Pospelov, and A. Ritz, "Probing a Secluded U(1) at B-factories", *Phys.Rev.* **D79** (2009) 115008, doi:10.1103/PhysRevD.79.115008, arXiv:0903.0363.

[445] H.-S. Lee, "Muon g-2 Anomaly and Dark Leptonic Gauge Boson", *Phys.Rev.* **D90** (2014) 091702, doi:10.1103/PhysRevD.90.091702, arXiv:1408.4256.

[446] A. Falkowski, J. T. Ruderman, T. Volansky, and J. Zupan, "Hidden Higgs Decaying to Lepton Jets", *JHEP* **1005** (2010) 077, doi:10.1007/JHEP05(2010)077, arXiv:1002.2952.

[447] A. Falkowski, J. T. Ruderman, T. Volansky, and J. Zupan, "Discovering Higgs Decays to Lepton Jets at Hadron Colliders", *Phys.Rev.Lett.* **105** (2010) 241801, doi:10.1103/PhysRevLett.105.241801, arXiv:1007.3496.

[448] P. Nath et al., "The Hunt for New Physics at the Large Hadron Collider", *Nucl.Phys.Proc.Suppl.* **200-202** (2010) 185–417, doi:10.1016/j.nuclphysbps.2010.03.001, arXiv:1001.2693.

[449] M. Baumgart et al., "Non-Abelian Dark Sectors and Their Collider Signatures", *JHEP* **0904** (2009) 014, doi:10.1088/1126-6708/2009/04/014, arXiv:0901.0283.

[450] C. Cheung, J. T. Ruderman, L.-T. Wang, and I. Yavin, "Kinetic Mixing as the Origin of Light Dark Scales", *Phys.Rev.* **D80** (2009) 035008, doi:10.1103/PhysRevD.80.035008, arXiv:0902.3246.

[451] C. Cheung, J. T. Ruderman, L.-T. Wang, and I. Yavin, "Lepton Jets in (Supersymmetric) Electroweak Processes", *JHEP* **1004** (2010) 116, doi:10.1007/JHEP04(2010)116, arXiv:0909.0290.

[452] J. D. Clarke, R. Foot, and R. R. Volkas, "Phenomenology of a very light scalar (100 MeV $< m_h <$ 10 GeV) mixing with the SM Higgs", *JHEP* **1402** (2014) 123, doi:10.1007/JHEP02(2014)123, arXiv:1310.8042.

[453] J. F. Donoghue, J. Gasser, and H. Leutwyler, "The Decay of a Light Higgs Boson", *Nucl.Phys.* **B343** (1990) 341–368, doi:10.1016/0550-3213(90)90474-R.

[454] J. Fan, M. Reece, and L.-T. Wang, "Non-relativistic effective theory of dark matter direct detection", *JCAP* **1011** (2010) 042, doi:10.1088/1475-7516/2010/11/042, arXiv:1008.1591.

[455] L. J. Hall, T. Moroi, and H. Murayama, "Sneutrino cold dark matter with lepton number violation", *Phys.Lett.* **B424** (1998) 305–312, doi:10.1016/S0370-2693(98)00196-8, arXiv:hep-ph/9712515.

[456] D. Tucker-Smith and N. Weiner, "Inelastic dark matter", *Phys.Rev.* **D64** (2001) 043502, doi:10.1103/PhysRevD.64.043502, arXiv:hep-ph/0101138.

[457] A. De Simone, V. Sanz, and H. P. Sato, "Pseudo-Dirac Dark Matter Leaves a Trace",

Phys.Rev.Lett. **105** (2010) 121802, doi:10.1103/PhysRevLett.105.121802, arXiv:1004.1567.

[458] LUX Collaboration, "First results from the LUX dark matter experiment at the Sanford Underground Research Facility", *Phys.Rev.Lett.* **112** (2014), no. 9, 091303, doi:10.1103/PhysRevLett.112.091303, arXiv:1310.8214.

[459] XENON100 Collaboration, "Dark Matter Results from 225 Live Days of XENON100 Data", *Phys.Rev.Lett.* **109** (2012) 181301, doi:10.1103/PhysRevLett.109.181301, arXiv:1207.5988.

[460] W.-C. Huang, A. Urbano, and W. Xue, "Fermi Bubbles under Dark Matter Scrutiny Part II: Particle Physics Analysis", *JCAP* **1404** (2014) 020, doi:10.1088/1475-7516/2014/04/020, arXiv:1310.7609.

[461] COUPP Collaboration, "First Dark Matter Search Results from a 4-kg CF_3I Bubble Chamber Operated in a Deep Underground Site", *Phys.Rev.* **D86** (2012) 052001, doi:10.1103/PhysRevD.86.052001,10.1103/PhysRevD.90.079902, arXiv:1204.3094.

[462] M. Felizardo et al., "Final Analysis and Results of the Phase II SIMPLE Dark Matter Search", *Phys.Rev.Lett.* **108** (2012) 201302, doi:10.1103/PhysRevLett.108.201302, arXiv:1106.3014.

[463] ATLAS Collaboration, "Search for New Phenomena in Monojet plus Missing Transverse Momentum Final States using 10fb-1 of pp Collisions at sqrts=8 TeV with the ATLAS detector at the LHC",.

[464] CMS Collaboration, "Search for dark matter, extra dimensions, and unparticles in monojet events in proton-proton collisions at $\sqrt{s} = 8$ TeV", arXiv:1408.3583.

[465] **ATLAS** Collaboration, "Sensitivity to WIMP Dark Matter in the Final States Containing Jets and Missing Transverse Momentum with the ATLAS Detector at 14 TeV LHC", Technical Report ATL-PHYS-PUB-2014-007, CERN, Geneva, Jun, 2014.

[466] G. Busoni et al., "Making the Most of the Relic Density for Dark Matter Searches at the LHC 14 TeV Run", arXiv:1410.7409.

[467] Planck Collaboration, "Planck 2013 results. XVI. Cosmological parameters", *Astron.Astrophys.* **571** (2014) A16, doi:10.1051/0004-6361/201321591, arXiv:1303.5076.

[468] PAMELA Collaboration, "PAMELA results on the cosmic-ray antiproton flux from 60 MeV to 180 GeV in kinetic energy", *Phys.Rev.Lett.* **105** (2010) 121101, doi:10.1103/PhysRevLett.105.121101, arXiv:1007.0821.

[469] Fermi-LAT Collaboration, "Observations of Milky Way Dwarf Spheroidal galaxies with the Fermi-LAT detector and constraints on Dark Matter models", *Astrophys.J.* **712** (2010) 147–158, doi:10.1088/0004-637X/712/1/147, arXiv:1001.4531.

[470] M. Ciuchini et al., "Unitarity triangle analysis in the standard model and sensitivity to new physics", *eConf* **C0304052** (2003) WG306, arXiv:hep-ph/0307195.

[471] S. Laplace, Z. Ligeti, Y. Nir, and G. Perez, "Implications of the CP asymmetry in semileptonic B decay", *Phys.Rev.* **D65** (2002) 094040, doi:10.1103/PhysRevD.65.094040, arXiv:hep-ph/0202010.

[472] Z. Ligeti, "The CKM matrix and CP violation", *Int.J.Mod.Phys.* **A20** (2005) 5105–5118, doi:10.1142/S0217751X05028624, arXiv:hep-ph/0408267.

[473] F. Botella, G. Branco, M. Nebot, and M. Rebelo, "New physics and evidence for a complex CKM", *Nucl.Phys.* **B725** (2005) 155–172, doi:10.1016/j.nuclphysb.2005.07.006, arXiv:hep-ph/0502133.

[474] L. Silvestrini, "Rare decays and CP violation beyond the standard model", *Int.J.Mod.Phys.* **A21** (2006) 1738–1749, doi:10.1142/S0217751X06032721, arXiv:hep-ph/0510077.

[475] F. J. Botella, G. C. Branco, and M. Nebot, "CP violation and limits on New Physics including recent B_s measurements", *Nucl.Phys.* **B768** (2007) 1–20, doi:10.1016/j.nuclphysb.2006.12.022, arXiv:hep-ph/0608100.

[476] UTfit Collaboration, "Model-independent constraints on $\Delta F = 2$ operators and the scale of new physics", *JHEP* **0803** (2008) 049, doi:10.1088/1126-6708/2008/03/049, arXiv:0707.0636. updated results and plots available at: http://www.utfit.org/UTfit/.

[477] UTfit Collaboration, "First Evidence of New Physics in $b \longleftrightarrow s$ Transitions", *PMC Phys.* **A3** (2009) 6, doi:10.1186/1754-0410-3-6, arXiv:0803.0659. updated results and plots available at: http://www.utfit.org/UTfit/.

[478] A. Lenz et al., "Anatomy of New Physics in $B - \bar{B}$ mixing", *Phys.Rev.* **D83** (2011) 036004, doi:10.1103/PhysRevD.83.036004, arXiv:1008.1593.

[479] ETM Collaboration, "Kaon Mixing Beyond the SM from N$_f$=2 tmQCD and model independent constraints from the UTA", *JHEP* **1303** (2013) 089, doi:10.1007/JHEP07(2013)143,10.1007/JHEP03(2013)089, arXiv:1207.1287.

[480] ETM Collaboration, "B-physics from N_f = 2 tmQCD: the Standard Model and beyond", *JHEP* **1403** (2014) 016, doi:10.1007/JHEP03(2014)016, arXiv:1308.1851.

[481] F. Botella, G. Branco, M. Nebot, and A. Sanchez, "Mixing asymmetries in B meson systems, the D0 like-sign dimuon asymmetry and generic New Physics", *Phys.Rev.* **D91** (2015), no. 3, 035013, doi:10.1103/PhysRevD.91.035013, arXiv:1402.1181.

[482] N. Carrasco et al., "$D^0 - \bar{D}^0$ mixing in the standard model and beyond from N_f =2 twisted mass QCD", *Phys.Rev.* **D90** (2014), no. 1, 014502, doi:10.1103/PhysRevD.90.014502, arXiv:1403.7302.

[483] E. Gabrielli and G. Giudice, "Supersymmetric corrections to epsilon prime / epsilon at the leading order in QCD and QED", *Nucl.Phys.* **B433** (1995) 3–25, doi:10.1016/0550-3213(94)00400-9, arXiv:hep-lat/9407029.

[484] A. Buras et al., "Universal unitarity triangle and physics beyond the standard model", *Phys.Lett.* **B500** (2001) 161–167, doi:10.1016/S0370-2693(01)00061-2, arXiv:hep-ph/0007085.

[485] G. D'Ambrosio, G. Giudice, G. Isidori, and A. Strumia, "Minimal flavor violation: An Effective field theory approach", *Nucl.Phys.* **B645** (2002) 155–187, doi:10.1016/S0550-3213(02)00836-2, arXiv:hep-ph/0207036.

[486] L. Silvestrini, "$D^0 - \overline{D}^0$ mixing in the Standard Model", Presented at the CKM 2014 workshop, Vienna, Austria, 2014.

[487] R. Barbieri, D. Buttazzo, F. Sala, and D. M. Straub, "Flavour physics and flavour symmetries after the first LHC phase", *JHEP* **1405** (2014) 105, doi:10.1007/JHEP05(2014)105, arXiv:1402.6677.

[488] Particle Data Group Collaboration, "CPT invariance tests in neutral kaon decay", in *Chin. Phys. C* [81], p. 920.

[489] J. Brod and M. Gorbahn, "Next-to-Next-to-Leading-Order Charm-Quark Contribution to the CP Violation Parameter ϵ_K and ΔM_K", *Phys. Rev. Lett.* **108** (2012) 121801.

[490] S. Aoki and others (FLAG Working Group), "Review of lattice results concerning low-energy particle physics", *The European Physical Journal C* **74** (2014), no. 9, 2890, doi:10.1140/epjc/s10052-014-2890-7.

[491] RBC, UKQCD Collaboration, "Long distance contribution to the KL-KS mass difference", *Phys.Rev.* **D88** (2013) 014508, doi:10.1103/PhysRevD.88.014508, arXiv:1212.5931.

[492] NA48 Collaboration, "A Precision measurement of direct CP violation in the decay of neutral kaons into two pions", *Phys.Lett.* **B544** (2002) 97–112, doi:10.1016/S0370-2693(02)02476-0, arXiv:hep-ex/0208009.

[493] KTeV Collaboration, "Precise Measurements of Direct CP Violation, CPT Symmetry, and Other Parameters in the Neutral Kaon System", *Phys.Rev.* **D83** (2011) 092001, doi:10.1103/PhysRevD.83.092001, arXiv:1011.0127.

[494] M. Sozzi, "On the direct CP violation parameter epsilon-prime", *Eur.Phys.J.* **C36** (2004) 37–42, arXiv:hep-ph/0401176.

[495] N. Christ, "Nonleptonic Kaon Decays from Lattice QCD", *PoS* **KAON13** (2013) 029.

[496] J. Bell and J. Steinberger in *Proc. Oxford Int. Conf. on Elementary Particles*, p. 195. Oxford, UK, September, 1965. CERN-TH-605.

[497] KEK-E246 Collaboration, "A New limit of T-violating transverse muon polarization in the K+ —> pi0 mu+ nu decay", *Phys.Rev.Lett.* **93** (2004) 131601, doi:10.1103/PhysRevLett.93.131601, arXiv:hep-ex/0408042.

[498] BaBar Collaboration, "Observation of Time-Reversal Violation in the B^0 Meson System", *Phys. Rev. Lett.* **109** (Nov, 2012) 211801, doi:10.1103/PhysRevLett.109.211801.

[499] A. Masiero, P. Paradisi, and R. Petronzio, "Probing new physics through mu - e universality in K —> l nu", *Phys.Rev.* **D74** (2006) 011701, doi:10.1103/PhysRevD.74.011701, arXiv:hep-ph/0511289.

[500] V. Cirigliano and I. Rosell, "Two-loop effective theory analysis of pi (K) —> e anti-nu/e [gamma] branching ratios", *Phys.Rev.Lett.* **99** (2007) 231801, doi:10.1103/PhysRevLett.99.231801, arXiv:0707.3439.

[501] NA62 Collaboration, "Precision Measurement of the Ratio of the Charged Kaon Leptonic Decay Rates", *Phys.Lett.* **B719** (2013) 326–336, doi:10.1016/j.physletb.2013.01.037, arXiv:1212.4012.

[502] J. Hardy and I. Towner, "Superallowed $0^+ \to 0^+$ nuclear beta decays: 2014 critical survey, with precise results for Vud and CKM unitarity",.

[503] FlaviaNet Working Group on Kaon Decays Collaboration, "An Evaluation of |Vus| and precise tests of the Standard Model from world data on leptonic and semileptonic kaon decays", *Eur.Phys.J.* **C69** (2010) 399–424, doi:10.1140/epjc/s10052-010-1406-3, arXiv:1005.2323.

[504] in *Proc. 8th Int. Workshop on the CKM Unitarity Triangle (CKM 2014)*. Vienna, September, 2014. arXiv:1411.5252.

[505] A. Bazavov et al., "Determination of $|V_{us}|$ from a lattice-QCD calculation of the $K \to \pi\ell\nu$ semileptonic form factor with physical quark masses", *Phys.Rev.Lett.* **112** (2014), no. 11, 112001, doi:10.1103/PhysRevLett.112.112001, arXiv:1312.1228.

[506] I. Towner and J. Hardy, "The evaluation of V(ud) and its impact on the unitarity of the Cabibbo-Kobayashi-Maskawa quark-mixing matrix", *Rept.Prog.Phys.* **73** (2010) 046301, doi:10.1088/0034-4885/73/4/046301.

[507] C. Tarantino. Presentation at LTS1 2014: Workshop on the Long-Term Strategy of INFN-CSN1 (Elba, Italy, 22 May 2014).

[508] G. Martinelli. Presentation at the 11th Conf. on Quark Confinement and the Hadron Spectrum (St. Petersburg, Russia, 8 September 2014).

[509] V. Cirigliano et al., "Kaon Decays in the Standard Model", *Rev.Mod.Phys.* **84** (2012) 399, doi:10.1103/RevModPhys.84.399, arXiv:1107.6001.

[510] J. Brod, M. Gorbahn, and E. Stamou, "Two-Loop Electroweak Corrections for the $K- > \pi\nu\bar{n}u$ Decays", *Phys.Rev.* **D83** (2011) 034030, doi:10.1103/PhysRevD.83.034030, arXiv:1009.0947.

[511] T. Hurth, G. Isidori, J. F. Kamenik, and F. Mescia, "Constraints on New Physics in MFV models: A Model-independent analysis of Δ F = 1 processes", *Nucl.Phys.* **B808** (2009)

326–346, doi:10.1016/j.nuclphysb.2008.09.040, arXiv:0807.5039.

[512] G. Isidori et al., "Exploring the flavour structure of the MSSM with rare K decays", *JHEP* **0608** (2006) 064, doi:10.1088/1126-6708/2006/08/064, arXiv:hep-ph/0604074.

[513] A. J. Buras et al., "Lepton Flavour Violation in the Presence of a Fourth Generation of Quarks and Leptons", *JHEP* **1009** (2010) 104, doi:10.1007/JHEP09(2010)104, arXiv:1006.5356.

[514] M. Blanke et al., "FCNC Processes in the Littlest Higgs Model with T-Parity: a 2009 Look", *Acta Phys.Polon.* **B41** (2010) 657–683, arXiv:0906.5454.

[515] M. Blanke et al., "Rare K and B Decays in a Warped Extra Dimension with Custodial Protection", *JHEP* **0903** (2009) 108, doi:10.1088/1126-6708/2009/03/108, arXiv:0812.3803.

[516] BNL-E949 Collaboration, "Study of the decay K+ —> pi+ nu anti-nu in the momentum region 140 < P(pi) < 199-MeV/c", *Phys.Rev.* **D79** (2009) 092004, doi:10.1103/PhysRevD.79.092004, arXiv:0903.0030.

[517] C. Smith, "Rare K decays: Challenges and Perspectives", (2014). arXiv:1409.6162.

[518] P. Mertens and C. Smith, "The s —> d gamma decay in and beyond the Standard Model", *JHEP* **1108** (2011) 069, doi:10.1007/JHEP08(2011)069, arXiv:1103.5992.

[519] KTeV Collaboration, "Search for the rare decay K(L) —> pi0 e+ e-", *Phys.Rev.Lett.* **93** (2004) 021805, doi:10.1103/PhysRevLett.93.021805, arXiv:hep-ex/0309072.

[520] KTEV Collaboration, "Search for the Decay $K_L \to \pi^0\mu^+\mu^-$", *Phys.Rev.Lett.* **84** (2000) 5279–5282, doi:10.1103/PhysRevLett.84.5279, arXiv:hep-ex/0001006.

[521] NA48/1 Collaboration, "Observation of the rare decay K(S) —> pi0 e+ e-", *Phys.Lett.* **B576** (2003) 43–54, doi:10.1016/j.physletb.2003.10.001, arXiv:hep-ex/0309075.

[522] NA48/1 Collaboration, "Observation of the rare decay K(S) —> pi0 mu+ mu-", *Phys.Lett.* **B599** (2004) 197–211, doi:10.1016/j.physletb.2004.08.058, arXiv:hep-ex/0409011.

[523] G. D'Ambrosio, G. Ecker, G. Isidori, and J. Portoles, "The Decays K —> pi l+ l- beyond leading order in the chiral expansion", *JHEP* **9808** (1998) 004, doi:10.1088/1126-6708/1998/08/004, arXiv:hep-ph/9808289.

[524] G. Isidori and R. Unterdorfer, "On the short distance constraints from K(L,S) —> mu+ mu-", *JHEP* **0401** (2004) 009, doi:10.1088/1126-6708/2004/01/009, arXiv:hep-ph/0311084.

[525] M. Gorbahn and U. Haisch, "Charm Quark Contribution to K(L) —> mu+ mu- at Next-to-Next-to-Leading", *Phys.Rev.Lett.* **97** (2006) 122002, doi:10.1103/PhysRevLett.97.122002, arXiv:hep-ph/0605203.

[526] E871 Collaboration, "Improved branching ratio measurement for the decay K0(L) –> mu+ mu-", *Phys.Rev.Lett.* **84** (2000) 1389–1392, doi:10.1103/PhysRevLett.84.1389.

[527] G. Ecker and A. Pich, "The Longitudinal muon polarization in K(L) —> mu+ mu-", *Nucl.Phys.* **B366** (1991) 189–208, doi:10.1016/0550-3213(91)90056-4.

[528] G. Isidori and R. Unterdorfer, "On the short distance constraints from K(L,S) —> mu+ mu-", *JHEP* **0401** (2004) 009, doi:10.1088/1126-6708/2004/01/009, arXiv:hep-ph/0311084.

[529] LHCb Collaboration, "Search for the rare decay $K_S \to \mu^+\mu^-$", *JHEP* **1301** (2013) 090, doi:10.1007/JHEP01(2013)090, arXiv:1209.4029.

[530] R. N. Cahn and H. Harari, "Bounds on the Masses of Neutral Generation Changing Gauge Bosons", *Nucl.Phys.* **B176** (1980) 135, doi:10.1016/0550-3213(80)90067-X.

[531] L. Littenberg, "Rare kaon decays", arXiv:hep-ex/0512044.

[532] W. J. Marciano, T. Mori, and J. M. Roney, "Charged Lepton Flavor Violation Experiments", *Ann.Rev.Nucl.Part.Sci.* **58** (2008) 315–341, doi:10.1146/annurev.nucl.58.110707.171126.

[533] T. Asaka, S. Blanchet, and M. Shaposhnikov, "The nuMSM, dark matter and neutrino masses", *Phys.Lett.* **B631** (2005) 151–156, doi:10.1016/j.physletb.2005.09.070, arXiv:hep-ph/0503065.

[534] M. Pospelov, "Secluded U(1) below the weak scale", *Phys.Rev.* **D80** (2009) 095002, doi:10.1103/PhysRevD.80.095002, arXiv:0811.1030.

[535] S. Weinberg, "Phenomenological Lagrangians", *Physica* **A96** (1979) 327.

[536] J. Gasser and H. Leutwyler, "Chiral Perturbation Theory: Expansions in the Mass of the Strange Quark", *Nucl.Phys.* **B250** (1985) 465, doi:10.1016/0550-3213(85)90492-4.

[537] KLOE Collaboration, "First observation of quantum interference in the process phi —> K(S) K(L) —> pi+ pi- pi+ pi-: A Test of quantum mechanics and CPT symmetry", *Phys.Lett.* **B642** (2006) 315–321, doi:10.1016/j.physletb.2006.09.046, arXiv:hep-ex/0607027.

[538] C. Marin Benito for the LHCb Collaboration. Presentation at Les Rencontres de Physique de la Vallée d'Aoste (La Thuile, Italy, 25 February 2014).

[539] G. D'Ambrosio, D. Greynat, and G. Vulvert, "Standard Model and New Physics contributions to K_L and K_S into four leptons", *Eur.Phys.J.* **C73** (2013), no. 12, 2678, doi:10.1140/epjc/s10052-013-2678-1, arXiv:1309.5736.

[540] R. Wanke for the NA62 Collaboration in *Proc. 11th Int. Conf. on Heavy Quarks and Leptons (HQL 2012).* Prague, June, 2012. PoS(HQL2012)007.

[541] NA48/2 Collaboration, "Detailed study of the $\mathrm{K}^{\pm} \to \pi^0\pi^0\mathrm{e}^{\pm}\nu$ ($\mathrm{K}^{00}_{\mathrm{e}4}$) decay properties", *JHEP* **1408** (2014) 159, doi:10.1007/JHEP08(2014)159, arXiv:1406.4749.

[542] NA48/2 Collaboration, "A new measurement of the $K^{\pm} \to \pi^{\pm}\gamma\gamma$ decay at the NA48/2 experiment", *Phys.Lett.* **B730** (2014) 141–148, doi:10.1016/j.physletb.2014.01.038, arXiv:1310.5499.

[543] NA62 Collaboration, "Study of the $K^{\pm} \to \pi^{\pm}\gamma\gamma$ decay by the NA62 experiment", *Phys.Lett.* **B732** (2014) 65–74, doi:10.1016/j.physletb.2014.03.016, arXiv:1402.4334.

[544] M. Moulson for the NA62 Collaboration in *Proc. 2013 Kaon Int. Conf. (KAON '13).* Ann Arbor MI, USA, April, 2013. PoS(KAON13)013.

[545] T. Spadaro. Presentation at BLV 2013: 2013 Int. Workshop on Baryon and Lepton Number Violation: From the Cosmos to the LHC (Heidelberg, Germany, 10 April 2013).

[546] T. Spadaro. Presentation at PANIC 2014: Particles and Nuclei Int. Conf. (Hamburg, Germany, 25 August 2014).

[547] W. Bonivento et al., "Proposal to Search for Heavy Neutral Leptons at the SPS", (2013). CERN-SPSC-2013-024, arXiv:1310.1762.

[548] G. Bernardi et al., "FURTHER LIMITS ON HEAVY NEUTRINO COUPLINGS", *Phys.Lett.* **B203** (1988) 332, doi:10.1016/0370-2693(88)90563-1.

[549] L. Canetti, M. Drewes, T. Frossard, and M. Shaposhnikov, "Dark Matter, Baryogenesis and Neutrino Oscillations from Right Handed Neutrinos", *Phys.Rev.* **D87** (2013), no. 9, 093006, doi:10.1103/PhysRevD.87.093006, arXiv:1208.4607.

[550] E. Goudzovski. Presentation at 2014 MesonNet Workshop (Frascati, Italy, 29 September 2014).

[551] K. Shiomi for the KOTO Collaboration. Presentation at CKM 2014: 8th Int. Workshop on the CKM Unitarity Triangle (Vienna, Austria, 11 September 2014).

[552] C. Djalali, for the TREK Collaboration. Presentation at BEACH 2014: 11^{th} Int. Conf. on Hyperons, Charm and Beauty Hadrons (Birmingham, UK, 25 July 2014).

[553] J. Comfort et al. Technical Report Proposal P14, J-PARC, Tokai, Japan, 2006.

[554] M. Togawa in *Proc. 2013 Kaon Int. Conf. (KAON '13).* Ann Arbor MI, USA, April, 2013. PoS(KAON13)034.

[555] F. Hahn (ed.) et al., "NA62 Technical Design Document", (2010). NA62 Document 10-07,

http://cds.cern.ch/record/1404985.

[556] J. Comfort et al., "KOPIO Project: Conceptual Design Report", (2005).

[557] G. Arduini et al., "A New Experiment to Search for Hidden Particles (SHIP) at the SPS North Area: Preliminary Project and Cost Estimate", Technical Report CERN EN-DH-2014-007, CERN, Geneva, 2014.

[558] V. Martin, "Prospects for observing $K_L^0 \to \pi^0 e^+ e^-$", (1999). NA48 Note 99-12.

[559] H. Greenlee, "Background to $K_L^0 \to \pi^0 ee$ From $K_L^0 \to \gamma\gamma ee$", *Phys.Rev.* **D42** (1990) 3724–3731, doi:10.1103/PhysRevD.42.3724.

[560] "Workshop on charm physics, "What Next: Discovery Potential of Charm Physics", Milano, 7-8 October 2014". https://agenda.infn.it/event/whatnext_charm. Invited speakers: G. Casarosa, A. Di Canto, Y. Grossman, M. Jung, H. Li, M. Martinelli, A. Petrov, G. Punzi, A. Schwartz, N. Serra, L. Silvestrini.

[561] BaBar Collaboration, "Evidence for D^0 - $\overline{D}^0$ Mixing", *Phys.Rev.Lett.* **98** (2007) 211802, doi:10.1103/PhysRevLett.98.211802, arXiv:hep-ex/0703020.

[562] Belle Collaboration, "Evidence for D^0 - $\overline{D}^0$ Mixing", *Phys.Rev.Lett.* **98** (2007) 211803, doi:10.1103/PhysRevLett.98.211803, arXiv:hep-ex/0703036.

[563] LHCb Collaboration, "Measurement of $D^0 - \overline{D}^0$ mixing parameters and search for CP violation using $D^0 \to K^+\pi^-$ decays", *Phys.Rev.Lett.* **111** (2013) 251801, doi:10.1103/PhysRevLett.111.251801, arXiv:1309.6534.

[564] LHCb Collaboration, "Measurements of indirect CP asymmetries in $D^0 \to K^-K^+$ and $D^0 \to \pi^-\pi^+$ decays", *Phys.Rev.Lett.* **112** (2014), no. 4, 041801, doi:10.1103/PhysRevLett.112.041801, arXiv:1310.7201.

[565] "Workshop on Physics at Future High Intensity e^+e^- Collider @ 2-7 GeV in China". http://cicpi2011.lcg.ustc.edu.cn/hiepa2015/. Hefei, 13-17 January 2015.

[566] "Heavy Flavour Averaging Group". http://www.slac.stanford.edu/xorg/hfag/charm/index.html.

[567] M. Ciuchini et al., "D - $\overline{D}$ mixing and new physics: General considerations and constraints on the MSSM", *Phys.Lett.* **B655** (2007) 162–166, doi:10.1016/j.physletb.2007.08.055, arXiv:hep-ph/0703204.

[568] A. L. Kagan and M. D. Sokoloff, "On Indirect CP Violation and Implications for $D^0 - \overline{D}^0$ and $B_{(s)} - \overline{B}_{(s)}$ mixing", *Phys.Rev.* **D80** (2009) 076008, doi:10.1103/PhysRevD.80.076008, arXiv:0907.3917.

[569] A. Bondar, A. Poluektov, and V. Vorobiev, "Charm mixing in the model-independent analysis of correlated $D^0\overline{D}^0$ decays", *Phys.Rev.* **D82** (2010) 034033, doi:10.1103/PhysRevD.82.034033, arXiv:1004.2350.

[570] CLEO Collaboration, "First model-independent determination of the relative strong phase between D^0 and $\overline{D}^0 \to K^0_S\pi^+\pi^-$ and its impact on the CKM angle γ/ϕ_3 measurement", *Phys. Rev. D* **80** (Aug, 2009) 032002, doi:10.1103/PhysRevD.80.032002.

[571] Y. Grossman, A. L. Kagan, and Y. Nir, "New physics and CP violation in singly Cabibbo suppressed D decays", *Phys.Rev.* **D75** (2007) 036008, doi:10.1103/PhysRevD.75.036008, arXiv:hep-ph/0609178.

[572] G. Hiller, M. Jung, and S. Schacht, "SU(3)-Flavor Anatomy of Non-Leptonic Charm Decays", *Phys.Rev.* **D87** (2013) 014024, doi:10.1103/PhysRevD.87.014024, arXiv:1211.3734.

[573] LHCb Collaboration, "Search for CP violation using T-odd correlations in $D^0 \to K^+K^-\pi^+\pi^-$ decays", *JHEP* **1410** (2014) 5, doi:10.1007/JHEP10(2014)005, arXiv:1408.1299.

[574] G. Burdman, E. Golowich, J. Hewett, and S. Pakvasa, "Rare charm decays in the standard model

and beyond", *Phys. Rev. D* **66** (Jul, 2002) 014009, doi:10.1103/PhysRevD.66.014009.

[575] LHCb Collaboration, "Search for the rare decay $D^0 \to \mu^+\mu^-$", *Phys.Lett.* **B725** (2013) 15–24, doi:10.1016/j.physletb.2013.06.037, arXiv:1305.5059.

[576] LHCb Collaboration, "Search for $D^+_{(s)} \to \pi^+\mu^+\mu^-$ and $D^+_{(s)} \to \pi^-\mu^+\mu^+$ decays", *Phys.Lett.* **B724** (2013) 203–212, doi:10.1016/j.physletb.2013.06.010, arXiv:1304.6365.

[577] LHCb Collaboration, "Search for the decay $D^0 \to \pi^+\pi^-\mu^+\mu^-$", *Phys.Lett.* **B728** (2014) 234–243, doi:10.1016/j.physletb.2013.11.053, arXiv:1310.2535.

[578] Quarkonium Working Group Collaboration, "Heavy quarkonium physics", (2004). arXiv:hep-ph/0412158.

[579] I. Gouz et al., "Prospects for the B_c studies at LHCb", *Phys. Atom. Nucl* **67** (2004) 1559, doi:10.1134/1.1788046, arXiv:hep-ph/0211432.

[580] H.-M. Choi and C.-R. Ji, "Non leptonic two-body decays of the B_c meson in the light-front quark model and the QCD factorization approach", *Phys. Rev. D* **80** (2009) 114003, doi:10.1103/PhysRevD.80.114003, arXiv:0909.5028.

[581] F. Robert and W. Daniel, "Exploring CP violation with B_c decays", *Phys. Rev. D* **62** (2000) 057503, doi:10.1103/PhysRevD.62.057503, arXiv:0004010.

[582] LHCb Collaboration, "Implications of LHCb measurements and future prospects", Technical Report LHCb-PUB-2012-009. CERN-LHCb-PUB-2012-009, CERN, Geneva, Aug, 2012.

[583] LHCb Collaboration, "Updated sensitivity projections for the LHCb Upgrade", Technical Report LHCb-PUB-2013-015. CERN-LHCb-PUB-2013-015, CERN, Geneva, Sep, 2013.

[584] LHCb Collaboration, "Implications of LHCb measurements and future prospects", *Eur. Phys. J.* **C73** (2013) 2373, doi:10.1140/epjc/s10052-013-2373-2, arXiv:1208.3355.

[585] LHCb Collaboration, "Framework TDR for the LHCb Upgrade", Technical Report CERN-LHCC-2012-007. LHCB-TDR-012, CERN, Geneva, Apr, 2012.

[586] LHCb Collaboration, "Letter of Intent for the LHCb Upgrade", Technical Report CERN-LHCC-2011-001. LHCC-I-018, CERN, Geneva, Mar, 2011.

[587] LHCb Collaboration, "Strong constraints on the rare decays $B^0_s \to \mu^+\mu^-$ and $B^0 \to \mu^+\mu^-$", *Phys. Rev. Lett.* **108** (2012) 231801, doi:10.1103/PhysRevLett.108.231801, arXiv:1203.4493.

[588] LHCb Collaboration, "Differential branching fraction and angular analysis of the decay $B^0 \to K^{*0}\mu^+\mu^-$", *Phys. Rev. Lett.* **108** (2012) 181806, doi:10.1103/PhysRevLett.108.181806, arXiv:1112.3515.

[589] LHCb Collaboration, "Measurement of the CP-violating phase ϕ_s in the decay $B^0_s \to J/\psi\phi$", *Phys. Rev. Lett.* **108** (2012) 101803, doi:10.1103/PhysRevLett.108.101803, arXiv:1112.3183.

[590] LHCb Collaboration, "Measurement of the isospin asymmetry in $B \to K^{(*)}\mu^+\mu^-$ decays", *JHEP* **07** (2012) 133, doi:10.1007/JHEP07(2012)133, arXiv:1205.3422.

[591] LHCb Collaboration, "Measurement of form-factor-independent observables in the decay $B^0 \to K^{*0}\mu^+\mu^-$", *Phys. Rev. Lett.* **111** (2013) 191801, doi:10.1103/PhysRevLett.111.191801, arXiv:1308.1707.

[592] LHCb Collaboration, "Test of lepton universality using $B^+ \to K^+\ell^+\ell^-$ decays", arXiv:1406.6482. to appear in Phys. Rev. Lett.

[593] BaBar Collaboration, "Evidence for an excess of $\bar{B} \to D^{(*)}\tau^-\bar{\nu}_\tau$ decays", *Phys.Rev.Lett.* **109** (2012) 101802, doi:10.1103/PhysRevLett.109.101802, arXiv:1205.5442.

[594] CMS Collaboration, "Measurement of the $B_s \to \mu^+\mu^-$ branching fraction and search for $B^0 \to \mu^+\mu^-$ with the CMS Experiment", *Phys.Rev.Lett.* **111** (2013) 101804, doi:10.1103/PhysRevLett.111.101804, arXiv:1307.5025.

[595] CMS Collaboration and LHCb Collaboration, "Observation of the rare $B_s^0 \to \mu^+\mu^-$ from the combined analysis of CMS and LHCb data", arXiv:1411.4413. submitted to Nature.

[596] C. Bobeth et al., "$B_{s,d} \to \ell^+\ell^-$ in the Standard Model with Reduced Theoretical Uncertainty", *Phys.Rev.Lett.* **112** (2014) 101801, doi:10.1103/PhysRevLett.112.101801, arXiv:1311.0903.

[597] D. M. Straub, "Constraints on new physics from rare (semi-)leptonic B decays", arXiv:1305.5704.

[598] LHCb Collaboration, "Differential branching fraction and angular analysis of the decay $B^0 \to K^{*0}\mu^+\mu^-$", *JHEP* **08** (2013) 131, doi:10.1007/JHEP08(2013)131, arXiv:1304.6325.

[599] U. Egede et al., "New observables in the decay mode $\bar{B}_d \to \bar{K}^{*0}\ell^+\ell^-$", *JHEP* **11** (2008) 032, doi:10.1088/1126-6708/2008/11/032, arXiv:0807.2589.

[600] U. Egede et al., "New physics reach of the decay mode $\bar{B} \to \bar{K}^{*0}\ell^+\ell^-$", *JHEP* **10** (2010) 056, doi:10.1007/JHEP10(2010)056, arXiv:1005.0571.

[601] LHCb Collaboration, "Measurement of the ratio of branching fractions for $B_s^0 \to \phi\mu\mu$ and $B_s^0 \to J/\psi\phi$", Technical Report LHCb-CONF-2012-003, Mar, 2012.

[602] W. Altmannshofer and D. M. Straub, "Cornering new physics in $b \to s$ transitions", *JHEP* **08** (2012) 121, doi:10.1007/JHEP08(2012)121, arXiv:1206.0273.

[603] T. Hurth and F. Mahmoudi, "The minimal flavour violation benchmark in view of the latest LHCb data", *Nucl.Phys.* **B865** (2012) 461–485, doi:10.1016/j.nuclphysb.2012.08.004, arXiv:1207.0688.

[604] S. Jäger and J. Martin Camalich, "On $B \to Vll$ at small dilepton invariant mass, power corrections, and new physics", *JHEP* **1305** (2013) 043, doi:10.1007/JHEP05(2013)043, arXiv:1212.2263.

[605] S. Jäger and J. Martin Camalich, "Reassessing the discovery potential of the $B \to K^*\ell^+\ell^-$ decays in the large-recoil region: SM challenges and BSM opportunities", arXiv:1412.3183.

[606] J. Lyon and R. Zwicky, "Resonances gone topsy turvy - the charm of QCD or new physics in $b \to s\ell^+\ell^-$?", arXiv:1406.0566.

[607] LHCb Collaboration, "Observation of photon polarization in the $b \to s\gamma$ transition", *Phys. Rev. Lett.* **112** (2014) 161801, doi:10.1103/PhysRevLett.112.161801, arXiv:1402.6852.

[608] LHCb Collaboration, "Precision measurement of CP violation in $B_s^0 \to J/\psi K^+K^-$ decays", Technical Report arXiv:1411.3104. LHCB-PAPER-2014-059. CERN-PH-EP-2014-271, CERN, Geneva, Nov, 2014. Comments: 6 figures.

[609] R. Barbieri et al., "U(2) and minimal flavour violation in supersymmetry", *Eur.Phys.J.* **C71** (2011) 1725, doi:10.1140/epjc/s10052-011-1725-z, arXiv:1105.2296.

[610] CKMfitter group Collaboration, "CP violation and the CKM matrix: assessing the impact of the asymmetric B factories", *Eur.Phys.J.* **C41** (2005) 1–131, doi:10.1140/epjc/s2005-02169-1, arXiv:hep-ph/0406184. updated results and plots available at: http://ckmfitter.in2p3.fr.

[611] UTfit Collaboration, "The 2004 UTfit collaboration report on the status of the unitarity triangle in the standard model", *JHEP* **07** (2005) 028, doi:10.1088/1126-6708/2005/07/028, arXiv:hep-ph/0501199. updated results and plots available at: http://www.utfit.org/UTfit/.

[612] M. Ciuchini, M. Pierini, and L. Silvestrini, "The Effect of penguins in the $B_d \to J/\psi K_S$ CP asymmetry", *Phys.Rev.Lett.* **95** (2005) 221804, doi:10.1103/PhysRevLett.95.221804, arXiv:hep-ph/0507290.

[613] K. De Bruyn, R. Fleischer, and P. Koppenburg, "Extracting gamma and Penguin Topologies

through CP Violation in $B_s \to J/\psi K_S$", *Eur.Phys.J.* **C70** (2010) 1025–1035, doi:10.1140/epjc/s10052-010-1495-z, arXiv:1010.0089.

[614] M. Jung, "Determining weak phases from $B \to J/\psi P$ decays", *Phys.Rev.* **D86** (2012) 053008, doi:10.1103/PhysRevD.86.053008, arXiv:1206.2050.

[615] K. De Bruyn and R. Fleischer, "A Roadmap to Control Penguin Effects in $B_d^0 \to J/\psi K_{\rm S}^0$ and $B_s^0 \to J/\psi\phi$", arXiv:1412.6834.

[616] D0 Collaboration, "Measurement of the anomalous like-sign dimuon charge asymmetry with 9 fb^{-1} of $p\bar{p}$ collisions", *Phys.Rev.* **D84** (2011) 052007, doi:10.1103/PhysRevD.84.052007, arXiv:1106.6308.

[617] LHCb Collaboration, "Measurement of the flavour-specific CP-violating asymmetry $a_{\rm sl}^s$ in B_s^0 decays", *Phys. Lett.* **B728** (2014) 607, doi:10.1016/j.physletb.2013.12.030, arXiv:1308.1048.

[618] LHCb Collaboration, "Measurement of the Semileptonic CP Asymmetry in B^0-$\overline{B}^0$ Mixing", *Phys. Rev. Lett.* **114** (Jan, 2015) 041601, doi:10.1103/PhysRevLett.114.041601.

[619] BaBar Collaboration, "Study of CP Asymmetry in $B^0 - \bar{B}^0$ Mixing with Inclusive Dilepton Events", *Phys.Rev.Lett.* **114** (2015), no. 8, 081801, doi:10.1103/PhysRevLett.114.081801, arXiv:1411.1842.

[620] E. Lunghi and A. Soni, "Possible evidence for the breakdown of the CKM-paradigm of CP-violation", *Phys.Lett.* **B697** (2011) 323–328, doi:10.1016/j.physletb.2011.02.016, arXiv:1010.6069.

[621] LHCb Collaboration, "Improved constraints on γ: CKM2014 update", Technical Report LHCb-CONF-2014-004, Sep, 2014.

[622] LHCb Collaboration, "Determination of γ and $-2\beta_s$ from charmless two-body decays of beauty mesons", arXiv:1408.4368. submitted to PLB.

[623] R. Fleischer and R. Knegjens, "In pursuit of new physics with $B_s^0 \to K^+K^-$", *Eur.Phys.J.* **C71** (2011) 1532, doi:10.1140/epjc/s10052-010-1532-y, arXiv:1011.1096.

[624] M. Ciuchini, E. Franco, S. Mishima, and L. Silvestrini, "Testing the Standard Model and searching for new physics with $B_d \to \pi\pi$ and $B_s \to KK$ decays", *JHEP* **10** (2012) 029, doi:10.1007/JHEP10(2012)029, arXiv:1205.4948.

[625] M. Ciuchini, M. Pierini, and L. Silvestrini, "$B_s^0 \to K^{(*)0}\bar{K}^{(*)0}$ CP asymmetries: golden channels for new physics searches", *Phys.Rev.Lett.* **100** (2008) 031802, doi:10.1103/PhysRevLett.100.031802, arXiv:hep-ph/0703137.

[626] LHCb Collaboration, "Measurement of CP violation in $B_s^0 \to \phi\phi$ decays", arXiv:1407.2222. submitted to Phys. Rev. D.

[627] LHCb Collaboration, "Evidence for CP violation in $B \to K\pi\pi$ and $B \to KKK$ decays", Technical Report LHCb-CONF-2012-018, Jul, 2012.

[628] LHCb Collaboration, "Evidence for CP violation in $B \to KK\pi$ and $B \to \pi\pi\pi$ decays", Technical Report LHCb-CONF-2012-028, Oct, 2012.

[629] LHCb Collaboration, "LHCb VELO Upgrade Technical Design Report", Technical Report CERN-LHCC-2013-021. LHCB-TDR-013, CERN, Geneva, Nov, 2013.

[630] LHCb Collaboration, "LHCb PID Upgrade Technical Design Report", Technical Report CERN-LHCC-2013-022. LHCB-TDR-014, CERN, Geneva, Nov, 2013.

[631] LHCb Collaboration, "LHCb Tracker Upgrade Technical Design Report", Technical Report CERN-LHCC-2014-001. LHCB-TDR-015, CERN, Geneva, Feb, 2014.

[632] LHCb Collaboration, "LHCb Trigger and Online Upgrade Technical Design Report", Technical Report CERN-LHCC-2014-016. LHCB-TDR-016, CERN, Geneva, May, 2014.

[633] T. Gerson, "Updated sensitivity projections for the LHCb Upgrade", Technical Report

LHCb-PUB-2013-015. CERN-LHCb-PUB-2013-015, CERN, Geneva, Sep, 2013.

[634] LHCb Collaboration, "Measurement of resonant and CP components in $\bar{B}^0_s \to J/\psi\pi^+\pi^-$ decays", *Phys. Rev.* **D89** (2014) 092006, doi:10.1103/PhysRevD.89.092006, arXiv:1402.6248.

[635] LHCb Collaboration, "First observation of the decay $B^0_s \to K^{*0}\bar{K}^{*0}$", *Phys. Lett.* **B709** (2012) 50, doi:10.1016/j.physletb.2012.02.001, arXiv:1111.4183.

[636] LHCb Collaboration, "Study of $B^0_{(s)} \to K^0_S h^+ h'^-$ decays with first observation of $B^0_s \to K^0_S K^\pm \pi^\mp$ and $B^0_s \to K^0_S \pi^+\pi^-$", *JHEP* **10** (2013) 143, doi:10.1007/JHEP10(2013)143, arXiv:1307.7648.

[637] LHCb Collaboration, "Measurement of the ratio of branching fractions $\mathcal{B}(B^0 \to K^{*0}\gamma)/\mathcal{B}(B^0_s \to \phi\gamma)$ and the direct CP asymmetry in $B^0 \to K^{*0}\gamma$", *Nucl. Phys.* **B867** (2013) 1–18, doi:10.1016/j.nuclphysb.2012.09.013, arXiv:1209.0313.

[638] LHCb Collaboration, "First observation of the decay $B^+ \to \pi^+\mu^+\mu^-$", *JHEP* **1212** (2012) 125, doi:10.1007/JHEP12(2012)125, arXiv:1210.2645.

[639] LHCb Collaboration, "Measurement of CP asymmetry in $B^0_s \to D^\mp_s K^\pm$ decays", arXiv:1407.6127. submitted to JHEP.

[640] LHCb Collaboration, "Measurement of the time-dependent CP asymmetry in $B^0 \to J/\psi\, K^0_S$ decays", *Phys. Lett.* **B721** (2013) 24, doi:10.1016/j.physletb.2013.02.054, arXiv:1211.6093.

[641] LHCb Collaboration, "Measurement of CP asymmetry in $D^0 \to K^-K^+$ and $D^0 \to \pi^-\pi^+$ decays", *JHEP* **07** (2014) 041, doi:10.1007/JHEP07(2014)041, arXiv:1405.2797.

[642] W. Altmannshofer et al., "Symmetries and Asymmetries of $B \to K^*\mu^+\mu^-$ Decays in the Standard Model and Beyond", *JHEP* **0901** (2009) 019, doi:10.1088/1126-6708/2009/01/019, arXiv:0811.1214.

[643] F. Krüger and J. Matias, "Probing new physics via the transverse amplitudes of $B^0 \to K^{*0}(\to K^-\pi^+)\ell^+\ell^-$ at large recoil", *Phys.Rev.* **D71** (2005) 094009, doi:10.1103/PhysRevD.71.094009, arXiv:hep-ph/0502060.

[644] LHCb Collaboration, "Measurement of b hadron production fractions in 7 TeV pp collisions", *Phys. Rev.* **D85** (2012) 032008, doi:10.1103/PhysRevD.85.032008, arXiv:1111.2357.

[645] Belle Collaboration, "Evidence for $B^- \to \tau^-\bar{\nu}$ with a Semileptonic Tagging Method", *Phys.Rev.* **D82** (2010) 071101, doi:10.1103/PhysRevD.82.071101, arXiv:1006.4201.

[646] Belle Collaboration, "Evidence for $B^- \to \tau^-\bar{\nu}_\tau$ with a Hadronic Tagging Method Using the Full Data Sample of Belle", *Phys.Rev.Lett.* **110** (2013), no. 13, 131801, doi:10.1103/PhysRevLett.110.131801, arXiv:1208.4678.

[647] BaBar Collaboration, "Evidence of $B^+ \to \tau^+\nu$ decays with hadronic B tags", *Phys.Rev.* **D88** (2013), no. 3, 031102, doi:10.1103/PhysRevD.88.031102, arXiv:1207.0698.

[648] BaBar Collaboration, "A Search for $B^+ \to \ell^+\nu_\ell$ Recoiling Against $B^- \to D^0\ell^-\bar{\nu}X$", *Phys.Rev.* **D81** (2010) 051101, doi:10.1103/PhysRevD.81.051101, arXiv:0912.2453.

[649] I. Adachi et al., "Precise measurement of the CP violation parameter $\sin 2\phi_1$ in $B^0 \to (c\bar{c})K^0$ decays", *Phys.Rev.Lett.* **108** (2012) 171802, doi:10.1103/PhysRevLett.108.171802, arXiv:1201.4643.

[650] Belle Collaboration, "Study of direct CP in charmed B decays and measurement of the CKM angle gamma at Belle", arXiv:1301.2033.

[651] BELLE Collaboration, "Measurement of CP violating asymmetries in $B^0 \to K^+K^-K^0_S$ decays with a time-dependent Dalitz approach", *Phys.Rev.* **D82** (2010) 073011, doi:10.1103/PhysRevD.82.073011, arXiv:1007.3848.

[652] Belle Collaboration, "Time-dependent CP violation in B decays at Belle", *PoS* **EPS-HEP2013**

(2013) 369, arXiv:1312.5165.

[653] Belle Collaboration, "Observation of time-dependent CP violation in $B^0 \to \eta' K^0$ decays and improved measurements of CP asymmetries in $B^0 \to \phi K^0, K^0_s K^0_s K^0_s$ and $B^0 \to J/\psi K^0$ decays", *Phys.Rev.Lett.* **98** (2007) 031802, doi:10.1103/PhysRevLett.98.031802, arXiv:hep-ex/0608039.

[654] Belle Collaboration, "Measurements of time-dependent CP violation in $B^0 \to \omega K^0_S, f_0(980) K^0_S, K^0_S \pi^0$ and $K^+ K^- K^0_S$ decays", *Phys.Rev.* **D76** (2007) 091103, doi:10.1103/PhysRevD.76.091103, arXiv:hep-ex/0609006.

[655] Belle Collaboration, "Measurement of the Moments of the Photon Energy Spectrum in $B \to X_s \gamma$ Decays and Determination of $|V_{cb}|$ and m_b at Belle", *Phys.Rev.* **D78** (2008) 032016, doi:10.1103/PhysRevD.78.032016, arXiv:0803.2158.

[656] Belle Collaboration, "Measurement of the form factors of the decay $B0 \to D^{*-} \ell^+ \nu$ and determination of the CKM matrix element $|V_{cb}|$", *Phys.Rev.* **D82** (2010) 112007, doi:10.1103/PhysRevD.82.112007, arXiv:1010.5620.

[657] Belle Collaboration, "Measurement Of $|V_{ub}|$ From Inclusive Charmless Semileptonic B Decays", *Phys.Rev.Lett.* **104** (2010) 021801, doi:10.1103/PhysRevLett.104.021801, arXiv:0907.0379.

[658] Belle Collaboration, "Study of Exclusive $B \to X_u \ell \nu$ Decays and Extraction of $\|V_{ub}\|$ using Full Reconstruction Tagging at the Belle Experiment", *Phys.Rev.* **D88** (2013), no. 3, 032005, doi:10.1103/PhysRevD.88.032005, arXiv:1306.2781.

[659] Belle Collaboration, "A Search for the rare leptonic decays $B^+ \to \mu^+ \nu_\mu$ and $B^+ \to e^+ \nu_e$", *Phys.Lett.* **B647** (2007) 67–73, doi:10.1016/j.physletb.2007.01.068, arXiv:hep-ex/0611045.

[660] Belle Collaboration, "Search for $B \to h^{(*)} \nu \bar{\nu}$ with the full Belle $\Upsilon(4S)$ data sample", *Phys.Rev.* **D87** (2013), no. 11, 111103, doi:10.1103/PhysRevD.87.111103, arXiv:1303.3719.

[661] BELLE Collaboration, "Electroweak and radiative penguin processes in B decays at Belle", *PoS* **DIS2014** (2014) 196.

[662] Belle Collaboration, "Time-Dependent CP Asymmetries in $B^0 \to K^0_s \pi^0 \gamma$ transitions", *Phys.Rev.* **D74** (2006) 111104, doi:10.1103/PhysRevD.74.111104, arXiv:hep-ex/0608017.

[663] Belle Collaboration, "Measurement of branching fractions, isospin and CP-violating asymmetries for exclusive $b \to d\gamma$ modes", *Phys.Rev.Lett.* **101** (2008) 111801, doi:10.1103/PhysRevLett.101.111801, arXiv:0804.4770.

[664] Belle Collaboration, "Measurement of the Lepton Forward-Backward Asymmetry in Inclusive $B \to X_s \ell^+ \ell^-$ Decays", arXiv:1402.7134.

[665] Belle Collaboration, "Observation of $B^0_s \to \phi\gamma$ and Search for $B^0_s \to \gamma\gamma$ Decays at Belle", *Phys.Rev.Lett.* **100** (2008) 121801, doi:10.1103/PhysRevLett.100.121801, arXiv:0712.2659.

[666] BaBar Collaboration, "A search for the rare decay $B^0 \to \tau^+ \tau^-$ at BABAR", *Phys.Rev.Lett.* **96** (2006) 241802, doi:10.1103/PhysRevLett.96.241802, arXiv:hep-ex/0511015.

[667] Belle Collaboration, "Measurements of branching fractions of leptonic and hadronic D^+_s meson decays and extraction of the D^+_s meson decay constant", *JHEP* **1309** (2013) 139, doi:10.1007/JHEP09(2013)139, arXiv:1307.6240.

[668] BaBar Collaboration, "Search for the Decay $D^0 - > \gamma\gamma$ and Measurement of the Branching Fraction for $D^0 - > \pi^0 \pi^0$", *Phys.Rev.* **D85** (2012) 091107, doi:10.1103/PhysRevD.85.091107, arXiv:1110.6480.

[669] Belle Collaboration, "CP violation and mixing in the charm sector at Belle, and current HFAG averages", arXiv:1212.5320.

[670] Belle Collaboration, "Search for CP violation in $D^0 \to \pi^0 pi^0$ decays", *Phys.Rev.Lett.* **112** (2014) 211601, doi:10.1103/PhysRevLett.112.211601, arXiv:1404.1266.

[671] BELLE Collaboration, "Measurement of D0 - anti-D0 Mixing Parameters in D0 —> K(s)0 pi+ pi- decays", *Phys.Rev.Lett.* **99** (2007) 131803, doi:10.1103/PhysRevLett.99.131803, arXiv:0704.1000.

[672] Belle Collaboration, "New search for $\tau \to \mu\gamma$ and $tau \to e\gamma$ decays at Belle", *Phys.Lett.* **B666** (2008) 16–22, doi:10.1016/j.physletb.2008.06.056, arXiv:0705.0650.

[673] K. Hayasaka et al., "Search for Lepton Flavor Violating Tau Decays into Three Leptons with 719 Million Produced Tau+Tau- Pairs", *Phys.Lett.* **B687** (2010) 139–143, doi:10.1016/j.physletb.2010.03.037, arXiv:1001.3221.

[674] S. M. Bilenky, S. Petcov, and B. Pontecorvo, "Lepton Mixing, mu –>; e + gamma Decay and Neutrino Oscillations", *Phys.Lett.* **B67** (1977) 309, doi:10.1016/0370-2693(77)90379-3.

[675] F. Grancagnolo and M. Panareo, "Proceedings, 1st International Conference on Charged Lepton Flavor Violation (CLFV)", *Nucl.Phys.Proc.Suppl.* **248-250** (2014) pp.1–146.

[676] A. de Gouvea and P. Vogel, "Lepton Flavor and Number Conservation, and Physics Beyond the Standard Model", *Prog.Part.Nucl.Phys.* **71** (2013) 75–92, doi:10.1016/j.ppnp.2013.03.006, arXiv:1303.4097.

[677] J. M. Arnold, B. Fornal, and M. B. Wise, "Phenomenology of scalar leptoquarks", *Phys.Rev.* **D88** (2013) 035009, doi:10.1103/PhysRevD.88.035009, arXiv:1304.6119.

[678] C.-H. Lee, P. Bhupal Dev, and R. Mohapatra, "Natural TeV-scale left-right seesaw mechanism for neutrinos and experimental tests", *Phys.Rev.* **D88** (2013), no. 9, 093010, doi:10.1103/PhysRevD.88.093010, arXiv:1309.0774.

[679] MEG Collaboration, "New constraint on the existence of the $\mu^+ \to e^+\gamma$ decay", *Phys.Rev.Lett.* **110** (2013) 201801, doi:10.1103/PhysRevLett.110.201801, arXiv:1303.0754.

[680] SINDRUM II Collaboration, "A Search for muon to electron conversion in muonic gold", *Eur.Phys.J.* **C47** (2006) 337–346, doi:10.1140/epjc/s2006-02582-x.

[681] SINDRUM Collaboration, "Search for the Decay mu+ —>; e+ e+ e-", *Nucl.Phys.* **B299** (1988) 1, doi:10.1016/0550-3213(88)90462-2.

[682] A. Baldini et al., "MEG Upgrade Proposal", arXiv:1301.7225.

[683] mu2e Collaboration, "Feasibility Study for a Next-Generation Mu2e Experiment", arXiv:1307.1168.

[684] Mu2e Collaboration, "Mu2e Technical Design Report", arXiv:1501.05241.

[685] A. Blondel et al., "Research Proposal for an Experiment to Search for the Decay $\mu \to eee$", arXiv:1301.6113.

[686] DeeMe Collaboration, "DeeMe experiment - An experimental search for a mu-e conversion reaction at J-PARC MLF", *Nucl.Phys.Proc.Suppl.* **248-250** (2014) 52–57, doi:10.1016/j.nuclphysbps.2014.02.010.

[687] COMET Collaboration, "Experimental Proposal for Phase-I of the COMET Experiment at J-PARC", technical report, 2012.

[688] J. Adam et al., "The MEG detector for $\mu^+ \to e^+\gamma$ decay search", *Eur.Phys.J.* **C73** (2013) 2365, doi:10.1140/epjc/s10052-013-2365-2, arXiv:1303.2348.

[689] Y. Kuno and Y. Okada, "Muon decay and physics beyond the standard model", *Rev.Mod.Phys.* **73** (2001) 151–202, doi:10.1103/RevModPhys.73.151, arXiv:hep-ph/9909265.

[690] J. Albrecht, M. Artuso et al., "Charged Leptons", arXiv:1311.5278v2.

[691] R. M. Djilkibaev and R. V. Konoplich, "Rare Muon Decay mu+ —>; e+ e- e+ nu(e)

anti-nu(mu)", *Phys.Rev.* **D79** (2009) 073004, doi:10.1103/PhysRevD.79.073004, arXiv:0812.1355.

[692] SINDRUM II Collaboration, "Improved limit on the branching ratio of mu- –>; e+ conversion on titanium", *Phys.Lett.* **B422** (1998) 334–338, doi:10.1016/S0370-2693(97)01423-8.

[693] HEPAP Subcommittee Collaboration, "Building for Discovery: Strategic Plan for U.S. Particle Physics in the Global Context",.

[694] S. Holmes et al., "Project X: Accelerator Reference Design", arXiv:1306.5022.

[695] V. Cirigliano, R. Kitano, Y. Okada, and P. Tuzon, "On the model discriminating power of mu —>; e conversion in nuclei", *Phys.Rev.* **D80** (2009) 013002, doi:10.1103/PhysRevD.80.013002, arXiv:0904.0957.

[696] Charm-Tau Factory Collaboration, "Project of a Super Charm-Tau factory at the Budker Institute of Nuclear Physics in Novosibirsk", *Phys.Atom.Nucl.* **76** (2013), no. 9, 1072–1085, doi:10.1134/S1063778813090032.

[697] SuperB Collaboration, "SuperB Technical Design Report", arXiv:1306.5655.

[698] OPAL Collaboration, "A Search for lepton flavor violating Z0 decays", *Z.Phys.* **C67** (1995) 555–564, doi:10.1007/BF01553981.

[699] DELPHI Collaboration, "Search for lepton flavor number violating Z0 decays", *Z.Phys.* **C73** (1997) 243–251, doi:10.1007/s002880050313.

[700] L3 Collaboration, "Search for lepton flavor violation in Z decays", *Phys.Lett.* **B316** (1993) 427–434, doi:10.1016/0370-2693(93)90348-L.

[701] ALEPH Collaboration, "Searches for new particles in Z decays using the ALEPH detector", *Phys.Rept.* **216** (1992) 253–340, doi:10.1016/0370-1573(92)90177-2.

[702] S. L. S. Davidson and P. Verdier, "LHC sensitivity to lepton flavour violating Z boson decays", arXiv:1207.4894.

[703] B. Robert and W. J. Marciano, "Lepton Dipole Moments". World Scientific, Singapore, 2009.

[704] F. Wilczek, "Importance and Promise of Electric Dipole Moments". http://www.usparticlephysics.org/sites/default/files/webform/p5/electricDipole01.pdf.

[705] Sr EDM Collaboration, "A Proposal to Measure the Proton Electric Dipole Moment with $10^{-29} e \cdot cm$ Sensitivity". http://www.bnl.gov/edm/files/pdf/proton_EDM_proposal_20111027_final.pdf.

[706] JEDI Collaboration, "Search for Electric Dipole Moments at COSY". http://collaborations.fz-juelich.de/ikp/jedi/public_files/proposals/EDM-COSY-Proposal_cover_02.05.2012.pdf.

[707] R. Talman, "Measuring the Electric Dipole Moment of the Electron at Wilson Lab.". http://jclub.chess.cornell.edu/papers/TalmanWilsonElectronEDM-rev.pdf.

[708] I. Masina and C. A. Savoy, "Heavy triplets: Electric dipole moments versus proton decay", *Phys.Lett.* **B579** (2004) 99–108, doi:10.1016/j.physletb.2003.11.007, arXiv:hep-ph/0309067.

[709] P. Lenisa, "Search for Electric Dipole Moments with Polarized Beams in Storage Rings.", *PoS* **PSTP2013** (2013) 013.

[710] M. Steigerwald, "Mev Mott Polarimetry at Jefferson Lab". http://web.fe.infn.it/~lenisa/edm/files/MOT.pdf.

[711] JEDI Collaboration, "Search for EDM at COSY. Step 1: Spin-coherence and systematic error studies.". http://collaborations.fz-juelich.de/ikp/jedi/public_files/proposals/JEDI-COSY-PROPOSAL-FINAL_21.1.2014.pdf.

[712] F. T. et al., "Demagnetization of magnetically shielded rooms.", *Rev. Sci. Instr.* **78** (2007) 035106.

[713] SuperB Collaboration, "SuperB: A High-Luminosity Asymmetric e+ e- Super Flavor Factory. Conceptual Design Report", arXiv:0709.0451.

[714] F. Archilli, "$B_s^0 \to \mu^+\mu^-$ at LHC", arXiv:1411.4964.

[715] M. Beneke, T. Feldmann, and D. Seidel, "Systematic approach to exclusive B to V l+ l-, V gamma decays", *Nucl.Phys.* **B612** (2001) 25–58, doi:10.1016/S0550-3213(01)00366-2, arXiv:hep-ph/0106067.

[716] A. Khodjamirian, T. Mannel, and Y. Wang, "$B \to K\ell^+\ell^-$ decay at large hadronic recoil", *JHEP* **1302** (2013) 010, doi:10.1007/JHEP02(2013)010, arXiv:1211.0234.

[717] S. Descotes-Genon, J. Matias, M. Ramon, and J. Virto, "Implications from clean observables for the binned analysis of $B \to K^*\mu^+\mu^-$ at large recoil", *JHEP* **1301** (2013) 048, doi:10.1007/JHEP01(2013)048, arXiv:1207.2753.

[718] M. Carlucci, P. Colangelo, and F. De Fazio, "Rare B(s) decays to eta and eta-prime final states", *Phys.Rev.* **D80** (2009) 055023, doi:10.1103/PhysRevD.80.055023, arXiv:0907.2160.

[719] P. Colangelo, F. De Fazio, and W. Wang, "$B_s \to f_0(980)$ form factors and B_s decays into $f_0(980)$", *Phys.Rev.* **D81** (2010) 074001, doi:10.1103/PhysRevD.81.074001, arXiv:1002.2880.

[720] A. Ali, A. Y. Parkhomenko, and A. V. Rusov, "Precise Calculation of the Dilepton Invariant-Mass Spectrum and the Decay Rate in $B^\pm \to \pi^\pm\mu^+\mu^-$ in the SM", *Phys.Rev.* **D89** (2014) 094021, doi:10.1103/PhysRevD.89.094021, arXiv:1312.2523.

[721] W. Altmannshofer and D. M. Straub, "Cornering New Physics in $b \to s$ Transitions", *JHEP* **1208** (2012) 121, doi:10.1007/JHEP08(2012)121, arXiv:1206.0273.

[722] P. Boer, T. Feldmann, and D. van Dyk, "Angular Analysis of the Decay $\Lambda_b \to \Lambda(\to N\pi)\ell^+\ell^-$", arXiv:1410.2115.

[723] G. D'Ambrosio, D. Greynat, and G. Vulvert, "Standard Model and New Physics contributions to K_L and K_S into four leptons", *Eur.Phys.J.* **C73** (2013) 2678, doi:10.1140/epjc/s10052-013-2678-1, arXiv:1309.5736.

[724] G. Ecker and A. Pich, "The Longitudinal muon polarization in K(L) -> mu+ mu-", *Nucl.Phys.* **B366** (1991) 189–208, doi:10.1016/0550-3213(91)90056-4.

[725] L. Cappiello, O. Cata, G. D'Ambrosio, and D.-N. Gao, "$K^+ \to pi^+pi^0e^+e^-$: a novel short-distance probe", *Eur.Phys.J.* **C72** (2012) 1872, doi:10.1140/epjc/s10052-012-2208-6,10.1140/epjc/s10052-012-1872-x, arXiv:1112.5184.

[726] G. D'Ambrosio, G. Ecker, G. Isidori, and J. Portoles, "The Decays K to pi l+ l- beyond leading order in the chiral expansion", *JHEP* **9808** (1998) 004, doi:10.1088/1126-6708/1998/08/004, arXiv:hep-ph/9808289.

[727] C.-H. Chen, C. Geng, and I.-L. Ho, "Forward backward asymmetry in K+ to pi+ l+ l-", *Phys.Rev.* **D67** (2003) 074029, doi:10.1103/PhysRevD.67.074029, arXiv:hep-ph/0302207.

[728] D.-N. Gao, "Long distance contribution to the forward backward asymmetry in decays K+ to pi+ l+ l-", *Phys.Rev.* **D69** (2004) 094030, doi:10.1103/PhysRevD.69.094030, arXiv:hep-ph/0311253.

[729] G. Isidori, C. Smith, and R. Unterdorfer, "The Rare decay K(L) to pi0 mu+ mu- within the SM", *Eur.Phys.J.* **C36** (2004) 57–66, doi:10.1140/epjc/s2004-01880-7, arXiv:hep-ph/0404127.

[730] F. Mescia, C. Smith, and S. Trine, "K(L) -> pi0 e+ e- and K(L) -> pi0 mu+ mu-: A Binary star on the stage of flavor physics", *JHEP* **0608** (2006) 088, doi:10.1088/1126-6708/2006/08/088, arXiv:hep-ph/0606081.

[731] G. Broccolo et al., "Design and Studies of micro-strip Stacked Module Prototypes for Tracking at Super-LHC", *Physics Procedia* **37** (2012), no. 0, 1925 – 1932, doi:http://dx.doi.org/10.1016/j.phpro.2012.02.515. Proceedings of the 2nd International Conference on Technology and Instrumentation in Particle Physics (TIPP 2011).

[732] BTeV Collaboration, "The application of Tiny Triplet Finder (TTF) in BTeV pixel trigger", *IEEE Trans.Nucl.Sci.* **53** (2006) 671–676, doi:10.1109/TNS.2006.874144.

[733] H.-W. Sadrozinski et al., "Ultra-fast silicon detectors", *Nucl.Instrum.Meth.* **A730** (2013) 226–231, doi:10.1016/j.nima.2013.06.033.

[734] N. Cartiglia et al., "Performance of Ultra-Fast Silicon Detectors", *JINST* **9** (2014) C02001, doi:10.1088/1748-0221/9/02/C02001, arXiv:1312.1080.

[735] K. G. Wilson, "Confinement of Quarks", *Phys.Rev.* **D10** (1974) 2445–2459, doi:10.1103/PhysRevD.10.2445.

[736] G. 't Hooft, "A Planar Diagram Theory for Strong Interactions", *Nucl.Phys.* **B72** (1974) 461, doi:10.1016/0550-3213(74)90154-0.

[737] E. Gregory et al., "Towards the glueball spectrum from unquenched lattice QCD", *JHEP* **1210** (2012) 170, doi:10.1007/JHEP10(2012)170, arXiv:1208.1858.

[738] H. B. Meyer and M. J. Teper, "Glueball Regge trajectories and the pomeron: A Lattice study", *Phys.Lett.* **B605** (2005) 344–354, doi:10.1016/j.physletb.2004.11.036, arXiv:hep-ph/0409183.

[739] H. B. Meyer, "Glueball regge trajectories", arXiv:hep-lat/0508002.

[740] G. S. Bali et al., "Mesons in large-N QCD", *JHEP* **1306** (2013) 071, doi:10.1007/JHEP06(2013)071, arXiv:1304.4437.

[741] M. Bochicchio, "An asymptotic solution of large-N QCD", *EPJ Web Conf.* **80** (2014) 00010, doi:10.1051/epjconf/20148000010, arXiv:1409.5144.

[742] M. Luscher, "Two particle states on a torus and their relation to the scattering matrix", *Nucl.Phys.* **B354** (1991) 531–578, doi:10.1016/0550-3213(91)90366-6.

[743] D. Kharzeev, K. Landsteiner, A. Schmitt, and H.-U. Yee, "Strongly Interacting Matter in Magnetic Fields", *Lect.Notes Phys.* **871** (2013) 1–624, doi:10.1007/978-3-642-37305-3.

[744] G. Colangelo et al., "Towards a data-driven analysis of hadronic light-by-light scattering", *Phys.Lett.* **B738** (2014) 6–12, doi:10.1016/j.physletb.2014.09.021, arXiv:1408.2517.

[745] D. Gross and F. Wilczek, "Asymptotically Free Gauge Theories. 1", *Phys. Rev. D* **8** (1973) 3633–3652, doi:10.1103/PhysRevD.8.3633.

[746] V. Gribov and L. Lipatov, "Deep inelastic e p scattering in perturbation theory", *Sov. J. Nucl. Phys.* **15** (1972) 438–450.

[747] G. Altarelli and G. Parisi, "Asymptotic Freedom in Parton Language", *Nucl. Phys. B* **126** (1977) 298, doi:10.1016/0550-3213(77)90384-4.

[748] Y. L. Dokshitzer, "Calculation of the Structure Functions for Deep Inelastic Scattering and e+ e- Annihilation by Perturbation Theory in Quantum Chromodynamics.", *Sov. Phys. JETP* **46** (1977) 641–653.

[749] J. Gao et al., "CT10 next-to-next-to-leading order global analysis of QCD", *Phys.Rev.* **D89** (2014), no. 3, 033009, doi:10.1103/PhysRevD.89.033009, arXiv:1302.6246.

[750] R. D. Ball et al., "Parton distributions with LHC data", *Nucl.Phys.* **B867** (2013) 244–289, doi:10.1016/j.nuclphysb.2012.10.003, arXiv:1207.1303.

[751] A. Martin, W. Stirling, R. Thorne, and G. Watt, "Parton distributions for the LHC", *Eur.Phys.J.* **C63** (2009) 189–285, doi:10.1140/epjc/s10052-009-1072-5, arXiv:0901.0002.

[752] S. Alekhin, J. Bluemlein, and S. Moch, "The ABM parton distributions tuned to LHC data", *Phys. Rev. D* **89** (2014) 054028, doi:10.1103/PhysRevD.89.054028, arXiv:1310.3059.

[753] P. Jimenez-Delgado and E. Reya, "Delineating parton distributions and the strong coupling", *Phys. Rev. D* **89** (2014) 074049, doi:10.1103/PhysRevD.89.074049, arXiv:1403.1852.

[754] J. Butterworth et al., "Les Houches 2013: Physics at TeV Colliders: Standard Model Working Group Report", arXiv:1405.1067.

[755] R. D. Ball et al., "Parton Distribution Benchmarking with LHC Data", *JHEP* **1304** (2013) 125, doi:10.1007/JHEP04(2013)125, arXiv:1211.5142.

[756] M. Botje et al., "The PDF4LHC Working Group Interim Recommendations", arXiv:1101.0538.

[757] D. de Florian, R. Sassot, M. Stratmann, and W. Vogelsang, "Evidence for polarization of gluons in the proton", *Phys.Rev.Lett.* **113** (2014) 012001, doi:10.1103/PhysRevLett.113.012001, arXiv:1404.4293.

[758] M. Burkardt, C. Miller, and W. Nowak, "Spin-polarized high-energy scattering of charged leptons on nucleons", *Rept.Prog.Phys.* **73** (2010) 016201, doi:10.1088/0034-4885/73/1/016201, arXiv:0812.2208.

[759] V. Barone, F. Bradamante, and A. Martin, "Transverse-spin and transverse-momentum effects in high-energy processes", *Prog.Part.Nucl.Phys.* **65** (2010) 267–333, doi:10.1016/j.ppnp.2010.07.003, arXiv:1011.0909.

[760] C. A. Aidala, S. D. Bass, D. Hasch, and G. K. Mallot, "The Spin Structure of the Nucleon", *Rev.Mod.Phys.* **85** (2013) 655–691, doi:10.1103/RevModPhys.85.655, arXiv:1209.2803.

[761] P. J. Mulders and R. D. Tangerman, "The complete tree-level result up to order $1/Q$ for polarized deep-inelastic leptoproduction", *Nucl. Phys.* **B461** (1996) 197–237, hep-ph/9510301. Erratum-ibid. **B484** (1997) 538.

[762] D. Boer and P. J. Mulders, "Time-reversal odd distribution functions in leptoproduction", *Phys. Rev.* **D57** (1998) 5780–5786, hep-ph/9711485.

[763] P. J. Mulders and J. Rodrigues, "Transverse momentum dependence in gluon distribution and fragmentation functions", *Phys. Rev.* **D63** (2001) 094021, arXiv:hep-ph/0009343.

[764] A. V. Belitsky, X. Ji, and F. Yuan, "Quark imaging in the proton via quantum phase-space distributions", *Phys. Rev.* **D69** (2004) 074014, arXiv:hep-ph/0307383.

[765] A. Bacchetta et al., "Semi-inclusive deep inelastic scattering at small transverse momentum", *JHEP* **02** (2007) 093, arXiv:hep-ph/0611265.

[766] X. Ji, J.-P. Ma, and F. Yuan, "QCD factorization for semi-inclusive deep-inelastic scattering at low transverse momentum", *Phys. Rev.* **D71** (2005) 034005, arXiv:hep-ph/0404183.

[767] X. Ji, J.-P. Ma, and F. Yuan, "QCD factorization for spin-dependent cross sections in DIS and Drell-Yan processes at low transverse momentum", *Phys. Lett.* **B597** (2004) 299–308, arXiv:hep-ph/0405085.

[768] J. C. Collins and A. Metz, "Universality of soft and collinear factors in hard- scattering factorization", *Phys. Rev. Lett.* **93** (2004) 252001, arXiv:hep-ph/0408249.

[769] HERMES Collaboration, "Effects of transversity in deep-inelastic scattering by polarized protons", *Phys.Lett.* **B693** (2010) 11–16, doi:10.1016/j.physletb.2010.08.012, arXiv:1006.4221.

[770] COMPASS Collaboration, "Experimental investigation of transverse spin asymmetries in muon-p SIDIS processes: Collins asymmetries", *Phys.Lett.* **B717** (2012) 376–382, doi:10.1016/j.physletb.2012.09.055, arXiv:1205.5121.

[771] HERMES Collaboration, "Evidence for a Transverse Single-Spin Asymmetry in Leptoproduction of pi+pi- Pairs", *JHEP* **0806** (2008) 017, doi:10.1088/1126-6708/2008/06/017, arXiv:0803.2367.

[772] COMPASS Collaboration, "A high-statistics measurement of transverse spin effects in dihadron

production from muon-proton semi-inclusive deep-inelastic scattering", *Phys.Lett.* **B736** (2014) 124–131, doi:10.1016/j.physletb.2014.06.080, arXiv:1401.7873.

[773] D. W. Sivers, "Single spin production asymmetries from the hard scattering of pointlike constituents", *Phys. Rev.* **D41** (1990) 83.

[774] S. J. Brodsky, D. S. Hwang, and I. Schmidt, "Final-state interactions and single-spin asymmetries in semi-inclusive deep inelastic scattering", *Phys. Lett.* **B530** (2002) 99–107, hep-ph/0201296.

[775] X. Ji and F. Yuan, "Parton distributions in light-cone gauge: Where are the final-state interactions?", *Phys. Lett.* **B543** (2002) 66–72, arXiv:hep-ph/0206057.

[776] A. V. Belitsky, X. Ji, and F. Yuan, "Final state interactions and gauge invariant parton distributions", *Nucl. Phys.* **B656** (2003) 165–198, arXiv:hep-ph/0208038.

[777] S. J. Brodsky, D. S. Hwang, and I. Schmidt, "Initial-state interactions and single-spin asymmetries in Drell-Yan processes", *Nucl. Phys.* **B642** (2002) 344–356, arXiv:hep-ph/0206259.

[778] J. C. Collins, "Leading twist single transverse-spin asymmetries: Drell-Yan and deep inelastic scattering", *Phys.Lett.* **B536** (2002) 43–48, doi:10.1016/S0370-2693(02)01819-1, arXiv:hep-ph/0204004.

[779] D. Boer, P. J. Mulders, and F. Pijlman, "Universality of T-odd effects in single spin and azimuthal asymmetries", *Nucl. Phys.* **B667** (2003) 201–241, arXiv:hep-ph/0303034.

[780] COMPASS Collaboration, "COMPASS-II Proposal",. CERN-SPSC-2010, 014 SPSC-P-340.

[781] M. Diehl, "Generalized parton distributions", *Phys. Rept.* **388** (2003) 41–277, doi:10.1016/j.physrep.2003.08.002, arXiv:hep-ph/0307382.

[782] J. C. Collins and A. Freund, "Proof of factorization for deeply virtual Compton scattering in QCD", *Phys.Rev.* **D59** (1999) 074009, doi:10.1103/PhysRevD.59.074009, arXiv:hep-ph/9801262.

[783] M. Burkardt, "Impact parameter space interpretation for generalized parton distributions", *Int.J.Mod.Phys.* **A18** (2003) 173–208, doi:10.1142/S0217751X03012370, arXiv:hep-ph/0207047.

[784] M. Diehl, "Generalized parton distributions in impact parameter space", *Eur. Phys. J.* **C25** (2002) 223–232, arXiv:hep-ph/0205208.

[785] M. Burkardt and D. S. Hwang, "Sivers asymmetry and generalized parton distributions in impact parameter space", *Phys. Rev.* **D69** (2004) 074032, arXiv:hep-ph/0309072.

[786] M. Burkardt, "Chromodynamic lensing and transverse single spin asymmetries", *Nucl. Phys.* **A735** (2004) 185–199, arXiv:hep-ph/0302144.

[787] M. Burkardt, "Transverse deformation of parton distributions and transversity decomposition of angular momentum", *Phys.Rev.* **D72** (2005) 094020, doi:10.1103/PhysRevD.72.094020, arXiv:hep-ph/0505189.

[788] X. Ji, "Gauge invariant decomposition of nucleon spin", *Phys. Rev. Lett.* **78** (1997) 610–613, hep-ph/9603249.

[789] C. LorcÂŐ, "Spin structure of the nucleon on the light front", arXiv:1409.6228.

[790] A. V. Belitsky, D. Mueller, and A. Kirchner, "Theory of deeply virtual Compton scattering on the nucleon", *Nucl.Phys.* **B629** (2002) 323–392, doi:10.1016/S0550-3213(02)00144-X, arXiv:hep-ph/0112108.

[791] A. V. Belitsky, D. MÂ§ller, and Y. Ji, "Compton scattering: from deeply virtual to quasi-real", *Nucl.Phys.* **B878** (2014) 214–268, doi:10.1016/j.nuclphysb.2013.11.014, arXiv:1212.6674.

[792] P. Kroll, H. Moutarde, and F. Sabatie, "From hard exclusive meson electroproduction to deeply

virtual Compton scattering", *Eur.Phys.J.* **C73** (2013), no. 1, 2278, doi:10.1140/epjc/s10052-013-2278-0, arXiv:1210.6975.

[793] S. Goloskokov and P. Kroll, "The Role of the quark and gluon GPDs in hard vector-meson electroproduction", *Eur.Phys.J.* **C53** (2008) 367–384, doi:10.1140/epjc/s10052-007-0466-5, arXiv:0708.3569.

[794] S. Goloskokov and P. Kroll, "Transversity in hard exclusive electroproduction of pseudoscalar mesons", *Eur.Phys.J.* **A47** (2011) 112, doi:10.1140/epja/i2011-11112-6, arXiv:1106.4897.

[795] R. Jaffe and X.-D. Ji, "Chiral odd parton distributions and polarized Drell-Yan", *Phys.Rev.Lett.* **67** (1991) 552–555, doi:10.1103/PhysRevLett.67.552.

[796] M. Anselmino et al., "Transversity and Collins functions from SIDIS and e+ e- data", *Phys.Rev.* **D75** (2007) 054032, doi:10.1103/PhysRevD.75.054032, arXiv:hep-ph/0701006.

[797] M. Anselmino et al., "Update on transversity and Collins functions from SIDIS and e+ e- data", *Nucl.Phys.Proc.Suppl.* **191** (2009) 98–107, doi:10.1016/j.nuclphysbps.2009.03.117, arXiv:0812.4366.

[798] M. Anselmino et al., "Simultaneous extraction of transversity and Collins functions from new SIDIS and e+e- data", *Phys.Rev.* **D87** (2013) 094019, doi:10.1103/PhysRevD.87.094019, arXiv:1303.3822.

[799] A. Bacchetta, A. Courtoy, and M. Radici, "First glances at the transversity parton distribution through dihadron fragmentation functions", *Phys.Rev.Lett.* **107** (2011) 012001, doi:10.1103/PhysRevLett.107.012001, arXiv:1104.3855.

[800] A. Bacchetta, A. Courtoy, and M. Radici, "First extraction of valence transversities in a collinear framework", *JHEP* **1303** (2013) 119, doi:10.1007/JHEP03(2013)119, arXiv:1212.3568.

[801] A. Martin, F. Bradamante, and V. Barone, "Extracting the transversity distributions from single-hadron and dihadron production", arXiv:1412.5946. arXiv:1412.5946 [hep-ph], accepted for publication on Phys. Rev. D.

[802] HERMES Collaboration, "Observation of the Naive-T-odd Sivers Effect in Deep-Inelastic Scattering", *Phys.Rev.Lett.* **103** (2009) 152002, doi:10.1103/PhysRevLett.103.152002, arXiv:0906.3918.

[803] COMPASS Collaboration, "Measurement of the Collins and Sivers asymmetries on transversely polarised protons", *Phys.Lett.* **B692** (2010) 240–246, doi:10.1016/j.physletb.2010.08.001, arXiv:1005.5609.

[804] COMPASS Collaboration, "Experimental investigation of transverse spin asymmetries in muon-p SIDIS processes: Sivers asymmetries", *Phys.Lett.* **B717** (2012) 383–389, doi:10.1016/j.physletb.2012.09.056, arXiv:1205.5122.

[805] HERMES Collaboration, "Transverse momentum broadening of hadrons produced in semi-inclusive deep-inelastic scattering on nuclei", *Phys.Lett.* **B684** (2010) 114–118, doi:10.1016/j.physletb.2010.01.020, arXiv:0906.2478.

[806] COMPASS Collaboration, "Hadron Transverse Momentum Distributions in Muon Deep Inelastic Scattering at 160 GeV/*c*", *Eur.Phys.J.* **C73** (2013), no. 8, 2531, doi:10.1140/epjc/s10052-013-2531-6, arXiv:1305.7317.

[807] M. Anselmino et al., "Unpolarised Transverse Momentum Dependent Distribution and Fragmentation Functions from SIDIS Multiplicities", *JHEP* **1404** (2014) 005, doi:10.1007/JHEP04(2014)005, arXiv:1312.6261.

[808] V. D. Burkert, "The JLab 12GeV Upgrade and the Initial Science Program", doi:10.3254/978-1-61499-197-7-303, arXiv:1203.2373. arXiv:1203.2373 [nucl-ex].

[809] U. D'Alesio and F. Murgia, "Azimuthal and Single Spin Asymmetries in Hard Scattering

Processes", *Prog.Part.Nucl.Phys.* **61** (2008) 394–454, doi:10.1016/j.ppnp.2008.01.001, arXiv:0712.4328. and references therein.

[810] H1 Collaboration, "Measurement of deeply virtual Compton scattering and its t-dependence at HERA", *Phys.Lett.* **B659** (2008) 796–806, doi:10.1016/j.physletb.2007.11.093, arXiv:0709.4114.

[811] H1 Collaboration, "Measurement of deeply virtual compton scattering at HERA", *Eur.Phys.J.* **C44** (2005) 1–11, doi:10.1140/epjc/s2005-02345-3, arXiv:hep-ex/0505061.

[812] ZEUS Collaboration, "A Measurement of the Q**2, W and t dependences of deeply virtual Compton scattering at HERA", *JHEP* **0905** (2009) 108, doi:10.1088/1126-6708/2009/05/108, arXiv:0812.2517.

[813] HERMES Collaboration, "Spin density matrix elements in exclusive ω electroproduction on ^{1}H and ^{2}H targets at 27.5 GeV beam energy", *Eur.Phys.J.* **C74** (2014), no. 11, 3110, doi:10.1140/epjc/s10052-014-3110-1, arXiv:1407.2119.

[814] CLAS Collaboration, "Deeply virtual and exclusive electroproduction of omega mesons", *Eur.Phys.J.* **A24** (2005) 445–458, doi:10.1140/epja/i2005-10032-4, arXiv:hep-ex/0504057.

[815] COMPASS Collaboration, "Transverse target spin asymmetries in exclusive ρ^0 muoproduction", *Phys.Lett.* **B731** (2014) 19–26, doi:10.1016/j.physletb.2014.02.005, arXiv:1310.1454.

[816] A. Accardi et al., "Electron Ion Collider: The Next QCD Frontier - Understanding the glue that binds us all", arXiv:1212.1701. arXiv:1212.1701 [nucl-ex].

[817] A. Lehrach et al., "The polarized electron-nucleon collider project ENC at GSI/FAIR", *J.Phys.Conf.Ser.* **295** (2011) 012156, doi:10.1088/1742-6596/295/1/012156.

[818] X. Chen, "EIC/HIAF in China, proceedings of 21st International Symposium on Spin Physics (Spin2014), 19 - 24 October 2014, Beijing, China",.

[819] G. 't Hooft et al., "A Theory of Scalar Mesons", *Phys.Lett.* **B662** (2008) 424–430, doi:10.1016/j.physletb.2008.03.036, arXiv:0801.2288.

[820] BaBar Collaboration, Belle Collaboration, "The Physics of the B Factories", *Eur.Phys.J.* **C74** (2014), no. 11, 3026, doi:10.1140/epjc/s10052-014-3026-9, arXiv:1406.6311.

[821] L. Maiani, F. Piccinini, A. Polosa, and V. Riquer, "Diquark-antidiquarks with hidden or open charm and the nature of X(3872)", *Phys.Rev.* **D71** (2005) 014028, doi:10.1103/PhysRevD.71.014028, arXiv:hep-ph/0412098.

[822] L. Maiani, F. Piccinini, A. Polosa, and V. Riquer, "The Z(4430) and a New Paradigm for Spin Interactions in Tetraquarks", *Phys.Rev.* **D89** (2014), no. 11, 114010, doi:10.1103/PhysRevD.89.114010, arXiv:1405.1551.

[823] Quarkonium Working Group Collaboration, "Heavy quarkonium physics", arXiv:hep-ph/0412158.

[824] N. Brambilla et al., "Heavy quarkonium: progress, puzzles, and opportunities", *Eur.Phys.J.* **C71** (2011) 1534, doi:10.1140/epjc/s10052-010-1534-9, arXiv:1010.5827.

[825] N. Brambilla et al., "QCD and Strongly Coupled Gauge Theories: Challenges and Perspectives", *Eur.Phys.J.* **C74** (2014), no. 10, 2981, doi:10.1140/epjc/s10052-014-2981-5, arXiv:1404.3723.

[826] A. S. Kronfeld, "Lattice Gauge Theory and the Origin of Mass", doi:10.1142/9789814425810_0018, arXiv:1209.3468.

[827] M. Karliner and H. J. Lipkin, "The Constituent quark model revisited: Quark masses, new predictions for hadron masses and KN pentaquark", arXiv:hep-ph/0307243.

[828] R. Mussa, "Open and hidden charm spectroscopy and decays: An overview", *AIP Conf.Proc.*

618 (2002) 329–339, doi:10.1063/1.1478852.

[829] LHCb Collaboration, "Observation of two new Ξ_b^- baryon resonances", arXiv:1411.4849.

[830] SELEX Collaboration, "Confirmation of the double charm baryon Xi+(cc)(3520) via its decay to p D+ K-", *Phys.Lett.* **B628** (2005) 18–24, doi:10.1016/j.physletb.2005.09.043, arXiv:hep-ex/0406033.

[831] SELEX Collaboration, "First observation of the doubly charmed baryon Xi+(cc)", *Phys.Rev.Lett.* **89** (2002) 112001, doi:10.1103/PhysRevLett.89.112001, arXiv:hep-ex/0208014.

[832] BaBar Collaboration, "Search for doubly charmed baryons Xi(cc)+ and Xi(cc)++ in BABAR", *Phys.Rev.* **D74** (2006) 011103, doi:10.1103/PhysRevD.74.011103, arXiv:hep-ex/0605075.

[833] Belle Collaboration, "Search for doubly charmed baryons and study of charmed strange baryons at Belle", *Phys.Rev.* **D89** (2014), no. 5, 052003, doi:10.1103/PhysRevD.89.052003, arXiv:1312.1026.

[834] LHCb Collaboration, "Studies of charmed baryons at LHCb", arXiv:1312.1601.

[835] Belle Collaboration, "Observation of double c anti-c production in e+ e- annihilation at s**(1/2) approximately 10.6-GeV", *Phys.Rev.Lett.* **89** (2002) 142001, doi:10.1103/PhysRevLett.89.142001, arXiv:hep-ex/0205104.

[836] BaBar Collaboration, "Measurement of double charmonium production in e^+e^- annihilations at $\sqrt{s} = 10.6$ GeV", *Phys.Rev.* **D72** (2005) 031101, doi:10.1103/PhysRevD.72.031101, arXiv:hep-ex/0506062.

[837] I. Caprini, G. Colangelo, and H. Leutwyler, "Mass and width of the lowest resonance in QCD", *Phys.Rev.Lett.* **96** (2006) 132001, doi:10.1103/PhysRevLett.96.132001, arXiv:hep-ph/0512364.

[838] BaBar Collaboration, "Observation of a narrow meson decaying to $D_s^+\pi^0$ at a mass of 2.32-GeV/c^2", *Phys.Rev.Lett.* **90** (2003) 242001, doi:10.1103/PhysRevLett.90.242001, arXiv:hep-ex/0304021.

[839] CLEO Collaboration, "Observation of a narrow resonance of mass 2.46-GeV/c**2 in the D*(s)+ pi0 final state, and confirmation of the D*(sJ)(2317)", *AIP Conf.Proc.* **698** (2004) 497–502, doi:10.1063/1.1664286, arXiv:hep-ex/0305017.

[840] CDF Collaboration, "Observation of the B_c meson in $p\bar{p}$ collisions at $\sqrt{s} = 1.8$ TeV", *Phys.Rev.Lett.* **81** (1998) 2432–2437, doi:10.1103/PhysRevLett.81.2432, arXiv:hep-ex/9805034.

[841] Belle Collaboration, "Evidence of a new narrow resonance decaying to $\chi_{c1}\gamma$ in $B \to \chi_{c1}\gamma K$", *Phys.Rev.Lett.* **111** (2013), no. 3, 032001, doi:10.1103/PhysRevLett.111.032001, arXiv:1304.3975.

[842] BaBar Collaboration, "Observation of the bottomonium ground state in the decay $\upsilon_{3S} \to \gamma eta_b$", *Phys.Rev.Lett.* **101** (2008) 071801, doi:10.1103/PhysRevLett.101.071801, arXiv:0807.1086.

[843] BaBar Collaboration, "Evidence for the eta(b)(1S) Meson in Radiative Upsilon(2S) Decay", *Phys.Rev.Lett.* **103** (2009) 161801, doi:10.1103/PhysRevLett.103.161801, arXiv:0903.1124.

[844] Belle Collaboration, "Evidence for the $\eta_b(2S)$ and observation of $h_b(1P) \to \eta_b(1S)\gamma$ and $h_b(2P) \to \eta_b(1S)\gamma$", *Phys.Rev.Lett.* **109** (2012) 232002, doi:10.1103/PhysRevLett.109.232002, arXiv:1205.6351.

[845] Belle Collaboration, "First observation of the P-wave spin-singlet bottomonium states $h_b(1P)$ and $h_b(2P)$", *Phys.Rev.Lett.* **108** (2012) 032001, doi:10.1103/PhysRevLett.108.032001,

arXiv:1103.3419.

[846] S. Meinel, "Bottomonium spectrum at order v^6 from domain-wall lattice QCD: Precise results for hyperfine splittings", *Phys.Rev.* **D82** (2010) 114502, doi:10.1103/PhysRevD.82.114502, arXiv:1007.3966.

[847] B. A. Kniehl et al., "M(eta(b)) and alpha(s) from nonrelativistic renormalization group", *Phys.Rev.Lett.* **92** (2004) 242001, doi:10.1103/PhysRevLett.92.242001, arXiv:hep-ph/0312086.

[848] CLEO Collaboration, "First observation of a Upsilon(1D) state", *Phys.Rev.* **D70** (2004) 032001, doi:10.1103/PhysRevD.70.032001, arXiv:hep-ex/0404021.

[849] ATLAS Collaboration, "Observation of a new χ_b state in radiative transitions to $\Upsilon(1S)$ and $\Upsilon(2S)$ at ATLAS", *Phys.Rev.Lett.* **108** (2012) 152001, doi:10.1103/PhysRevLett.108.152001, arXiv:1112.5154.

[850] LHCb Collaboration, "Measurement of the $\chi_b(3P)$ mass and of the relative rate of $\chi_{b1}(1P)$ and $\chi_{b2}(1P)$ production", *JHEP* **1410** (2014) 88, doi:10.1007/JHEP10(2014)088, arXiv:1409.1408.

[851] Belle Collaboration, "Observation of a narrow charmonium - like state in exclusive $B^{\pm} \to K^{\pm}\pi^{+}\pi^{-}J/\psi$ decays", *Phys.Rev.Lett.* **91** (2003) 262001, doi:10.1103/PhysRevLett.91.262001, arXiv:hep-ex/0309032.

[852] C. Bignamini et al., "Is the X(3872) Production Cross Section at Tevatron Compatible with a Hadron Molecule Interpretation?", *Phys.Rev.Lett.* **103** (2009) 162001, doi:10.1103/PhysRevLett.103.162001, arXiv:0906.0882.

[853] P. Artoisenet and E. Braaten, "Production of the X(3872) at the Tevatron and the LHC", *Phys.Rev.* **D81** (2010) 114018, doi:10.1103/PhysRevD.81.114018, arXiv:0911.2016.

[854] BaBar Collaboration, "Observation of a broad structure in the $\pi^{+}\pi^{-}J/\psi$ mass spectrum around 4.26-GeV/c^2", *Phys.Rev.Lett.* **95** (2005) 142001, doi:10.1103/PhysRevLett.95.142001, arXiv:hep-ex/0506081.

[855] L. Maiani, A. Polosa, and V. Riquer, "The Charged Z(4433): Towards a new spectroscopy", arXiv:0708.3997.

[856] S. Weinberg, "Tetraquark Mesons in Large N Quantum Chromodynamics", *Phys.Rev.Lett.* **110** (2013) 261601, doi:10.1103/PhysRevLett.110.261601, arXiv:1303.0342.

[857] S. J. Brodsky, D. S. Hwang, and R. F. Lebed, "Dynamical Picture for the Formation and Decay of the Exotic XYZ Mesons", *Phys.Rev.Lett.* **113** (2014), no. 11, 112001, doi:10.1103/PhysRevLett.113.112001, arXiv:1406.7281.

[858] D. Horn and J. Mandula, "A Model of Mesons with Constituent Gluons", *Phys.Rev.* **D17** (1978) 898, doi:10.1103/PhysRevD.17.898.

[859] N. Isgur and J. E. Paton, "A Flux Tube Model for Hadrons in QCD", *Phys.Rev.* **D31** (1985) 2910, doi:10.1103/PhysRevD.31.2910.

[860] Y. Simonov, "Gluelump spectrum in the QCD string model", *Nucl.Phys.* **B592** (2001) 350–368, doi:10.1016/S0550-3213(00)00592-7, arXiv:hep-ph/0003114.

[861] A. Szczepaniak, E. S. Swanson, C.-R. Ji, and S. R. Cotanch, "Glueball spectroscopy in a relativistic many body approach to hadron structure", *Phys.Rev.Lett.* **76** (1996) 2011–2014, doi:10.1103/PhysRevLett.76.2011, arXiv:hep-ph/9511422.

[862] F. Buisseret and C. Semay, "On two- and three-body descriptions of hybrid mesons", *Phys.Rev.* **D74** (2006) 114018, doi:10.1103/PhysRevD.74.114018, arXiv:hep-ph/0610132.

[863] F. Brau and C. Semay, "Semirelativistic potential model for glueball states", *Phys.Rev.* **D70** (2004) 014017, doi:10.1103/PhysRevD.70.014017, arXiv:hep-ph/0412173.

[864] C. J. Morningstar and M. J. Peardon, "The Glueball spectrum from an anisotropic lattice study",

Phys.Rev. **D60** (1999) 034509, doi:10.1103/PhysRevD.60.034509, arXiv:hep-lat/9901004.

[865] UKQCD Collaboration, "Hadrons with a heavy color adjoint particle", *Phys.Rev.* **D59** (1999) 094509, doi:10.1103/PhysRevD.59.094509, arXiv:hep-lat/9811010.

[866] G. Bali et al., "The meson spectrum in large-N QCD", *PoS* **ConfinementX** (2012) 278, arXiv:1302.1502.

[867] Hadron Spectrum Collaboration, "Toward the excited isoscalar meson spectrum from lattice QCD", *Phys.Rev.* **D88** (2013), no. 9, 094505, doi:10.1103/PhysRevD.88.094505, arXiv:1309.2608.

[868] J. J. Dudek et al., "Isoscalar meson spectroscopy from lattice QCD", *Phys.Rev.* **D83** (2011) 111502, doi:10.1103/PhysRevD.83.111502, arXiv:1102.4299.

[869] J. J. Dudek et al., "Toward the excited meson spectrum of dynamical QCD", *Phys.Rev.* **D82** (2010) 034508, doi:10.1103/PhysRevD.82.034508, arXiv:1004.4930.

[870] P. Guo et al., "Heavy quarkonium hybrids from Coulomb gauge QCD", *Phys.Rev.* **D78** (2008) 056003, doi:10.1103/PhysRevD.78.056003, arXiv:0807.2721.

[871] P. Guo et al., "Gluelump spectrum from Coulomb gauge QCD", *Phys.Rev.* **D77** (2008) 056005, doi:10.1103/PhysRevD.77.056005, arXiv:0707.3156.

[872] E. Santopinto et al., "HASPECT: HAdron SPEctroscopy CenTer", *J.Phys.Conf.Ser.* **527** (2014) 012028, doi:10.1088/1742-6596/527/1/012028.

[873] M. Battaglieri et al., "Analysis Tools for Next-Generation Hadron Spectroscopy Experiments", arXiv:1412.6393.

[874] J. R. Cudell et al., "Benchmarks for the forward observables at RHIC, the Tevatron-run II, and the LHC", *Physical Review Letters* **89** (2002), no. 20, doi:10.1103/PhysRevLett.89.201801.

[875] H1 Collaboration, "Diffractive deep-inelastic scattering with a leading proton at HERA", *Eur.Phys.J.* **C48** (2006) 749–766, doi:10.1140/epjc/s10052-006-0046-0, arXiv:hep-ex/0606003.

[876] ATLAS Collaboration, "Rapidity gap cross sections measured with the ATLAS detector in pp collisions at $\sqrt{s} = 7$ TeV", *Eur.Phys.J.* **C72** (2012) 1926, doi:10.1140/epjc/s10052-012-1926-0, arXiv:1201.2808.

[877] CMS Collaboration, "Observation of a diffractive contribution to dijet production in proton-proton collisions at $\sqrt{s} = 7$ TeV", *Phys.Rev.* **D87** (2013) 012006, doi:10.1103/PhysRevD.87.012006, arXiv:1209.1805.

[878] CMS Collaboration, "Study of exclusive two-photon production of W^+W^- in pp collisions at $\sqrt{s} = 7$ TeV and constraints on anomalous quartic gauge couplings", *JHEP* **1307** (2013) 116, doi:10.1007/JHEP07(2013)116, arXiv:1305.5596.

[879] T. L. F. P. W. Group, "LHC Foward Physics, Yellow Report in preparation",.

[880] M. Albrow et al., "CMS-TOTEM Precision Proton Spectrometer", Technical Report CERN-LHCC-2014-021. TOTEM-TDR-003. CMS-TDR-13, CERN, Geneva, Sep, 2014.

[881] "The AFP project",.

[882] L. Trentadue and G. Veneziano, "Fracture functions: An Improved description of inclusive hard processes in QCD", *Phys.Lett.* **B323** (1994) 201–211, doi:10.1016/0370-2693(94)90292-5.

[883] A. Berera and D. E. Soper, "Behavior of diffractive parton distribution functions", *Phys.Rev.* **D53** (1996) 6162–6179, doi:10.1103/PhysRevD.53.6162, arXiv:hep-ph/9509239.

[884] M. Grazzini, L. Trentadue, and G. Veneziano, "Fracture functions from cut vertices", *Nucl.Phys.* **B519** (1998) 394–404, doi:10.1016/S0550-3213(97)00840-7,

arXiv:hep-ph/9709452.

[885] J. C. Collins, "Proof of factorization for diffractive hard scattering", *Phys.Rev.* **D57** (1998) 3051–3056, doi:10.1103/PhysRevD.61.019902,10.1103/PhysRevD.57.3051,10.1103/PhysRevD.57.305110.1103/PhysRevD.61.019902, arXiv:hep-ph/9709499.

[886] ZEUS Collaboration, "A QCD analysis of ZEUS diffractive data", *Nucl.Phys.* **B831** (2010) 1–25, doi:10.1016/j.nuclphysb.2010.01.014, arXiv:0911.4119.

[887] F. Ceccopieri and L. Favart, "QCD Fits in Diffractive DIS Revisited", arXiv:1110.4829.

[888] F. A. Ceccopieri and L. Favart, "Revisiting QCD Fits in Diffractive DIS", doi:10.3204/DESY-PROC-2012-02/282, arXiv:1205.6356.

[889] H1 Collaboration, "Dijet Cross Sections and Parton Densities in Diffractive DIS at HERA", *JHEP* **0710** (2007) 042, doi:10.1088/1126-6708/2007/10/042, arXiv:0708.3217.

[890] CDF Collaboration, "Diffractive Dijet Production in $\bar{p}p$ Collisions at $\sqrt{s} = 1.96$ TeV", *Phys.Rev.* **D86** (2012) 032009, doi:10.1103/PhysRevD.86.032009, arXiv:1206.3955.

[891] CDF Collaboration, "Diffractive W and Z Production at the Fermilab Tevatron", *Phys.Rev.* **D82** (2010) 112004, doi:10.1103/PhysRevD.82.112004, arXiv:1007.5048.

[892] T. Sjostrand and M. van Zijl, "A Multiple Interaction Model for the Event Structure in Hadron Collisions", *Phys.Rev.* **D36** (1987) 2019, doi:10.1103/PhysRevD.36.2019.

[893] CMS Collaboration, "Measurement of the underlying event in the Drell-Yan process in proton-proton collisions at $\sqrt{s} = 7$ TeV", *Eur.Phys.J.* **C72** (2012) 2080, doi:10.1140/epjc/s10052-012-2080-4, arXiv:1204.1411.

[894] M. Cacciari, G. P. Salam, and S. Sapeta, "On the characterisation of the underlying event", *JHEP* **1004** (2010) 065, doi:10.1007/JHEP04(2010)065, arXiv:0912.4926.

[895] CMS Collaboration, "Study of the underlying event at forward rapidity in pp collisions at $\sqrt{s}$ = 0.9, 2.76, and 7 TeV", *JHEP* **1304** (2013) 072, doi:10.1007/JHEP04(2013)072, arXiv:1302.2394.

[896] N. Paver and D. Treleani, "Multi - Quark Scattering and Large p_T Jet Production in Hadronic Collisions", *Nuovo Cim.* **A70** (1982) 215, doi:10.1007/BF02814035.

[897] M. Rinaldi, S. Scopetta, M. Traini, and V. Vento, "Double parton correlations and constituent quark models: a Light Front approach to the valence sector", *JHEP* **1412** (2014) 028, doi:10.1007/JHEP12(2014)028, arXiv:1409.1500.

[898] Axial Field Spectrometer Collaboration, "Double Parton Scattering in pp Collisions at $\sqrt{s} = 63$-GeV", *Z.Phys.* **C34** (1987) 163, doi:10.1007/BF01566757.

[899] CDF Collaboration, "Double parton scattering in $\bar{p}p$ collisions at $\sqrt{s} = 1.8$TeV", *Phys.Rev.* **D56** (1997) 3811–3832, doi:10.1103/PhysRevD.56.3811.

[900] D0 Collaboration, "Double parton interactions in γ+3 jet events in $p\bar{p}$ collisions $\sqrt{s} = 1.96$ TeV.", *Phys.Rev.* **D81** (2010) 052012, doi:10.1103/PhysRevD.81.052012, arXiv:0912.5104.

[901] ATLAS Collaboration, "Measurement of hard double-parton interactions in $W(\rightarrow l\nu)$+ 2 jet events at $\sqrt{s}$=7 TeV with the ATLAS detector", *New J.Phys.* **15** (2013) 033038, doi:10.1088/1367-2630/15/3/033038, arXiv:1301.6872.

[902] CMS Collaboration, "Study of double parton scattering using $W + 2$-jet events in proton-proton collisions at $\sqrt{s}$ = 7 TeV", *JHEP* **1403** (2014) 032, doi:10.1007/JHEP03(2014)032, arXiv:1312.5729.

[903] M. Strikman and D. Treleani, "Measuring double parton distributions in nucleons at proton nucleus colliders", *Phys.Rev.Lett.* **88** (2002) 031801, doi:10.1103/PhysRevLett.88.031801, arXiv:hep-ph/0111468.

[904] B. Blok, Y. Dokshitser, L. Frankfurt, and M. Strikman, "pQCD physics of multiparton

interactions", *Eur.Phys.J.* **C72** (2012) 1963, doi:10.1140/epjc/s10052-012-1963-8, arXiv:1106.5533.

[905] M. Diehl, D. Ostermeier, and A. Schafer, "Elements of a theory for multiparton interactions in QCD", *JHEP* **1203** (2012) 089, doi:10.1007/JHEP03(2012)089, arXiv:1111.0910.

[906] E. Maina, "Multiple Parton Interactions in $Z + 4j$, $W^{\pm}\,W^{\pm} + 0/2j$ and $W^{+}\,W^{-} + 2j$ production at the LHC", *JHEP* **0909** (2009) 081, doi:10.1088/1126-6708/2009/09/081, arXiv:0909.1586.

[907] Pierre Auger Collaboration, "Measurement of the Depth of Maximum of Extensive Air Showers above 10^{18} eV", *Phys.Rev.Lett.* **104** (2010) 091101, doi:10.1103/PhysRevLett.104.091101, arXiv:1002.0699.

[908] Y. Itow et al., "Proposal; Precise measurements of very forward particle production at RHIC", arXiv:1409.4860.

[909] Y. Itow et al., "Letter of intent; Precise measurements of very forward particle production at RHIC", arXiv:1401.1004.

[910] W. Scandale et al., "Observation of focusing of 400 GeV/c proton beam with the help of bent crystals", *Phys.Lett.* **B733** (2014) 366–372, doi:10.1016/j.physletb.2014.05.010,10.1016/j.physletb.2014.05.051.

[911] J. Lansberg et al., "A Fixed-Target ExpeRiment at the LHC (AFTER@LHC) : luminosities, target polarisation and a selection of physics studies", *PoS* **QNP2012** (2012) 049, arXiv:1207.3507.

[912] W. Scandale et al., "Optimization of the crystal assisted collimation of the SPS beam", *Phys.Lett.* **B726** (2013) 182–186, doi:10.1016/j.physletb.2013.08.028.

[913] M. di Mauro, F. Donato, A. Goudelis, and P. D. Serpico, "A new evaluation of the antiproton production cross section for cosmic ray studies", arXiv:1408.0288.

[914] R. Kappl and M. W. Winkler, "The Cosmic Ray Antiproton Background for AMS-02", *JCAP* **1409** (2014), no. 09, 051, doi:10.1088/1475-7516/2014/09/051, arXiv:1408.0299.

[915] M. Ackermann et al., "Fermi-LAT Observations of the Diffuse γ-Ray Emission: Implications for Cosmic Rays and the Interstellar Medium", *Astrophysical J.* **750** (May, 2012) 3, doi:10.1088/0004-637X/750/1/3, arXiv:1202.4039.

[916] IceCube-PINGU Collaboration, "Letter of Intent: The Precision IceCube Next Generation Upgrade (PINGU)", arXiv:1401.2046.

[917] KM3NeT Collaboration, "The ORCA Option for KM3NeT", *PoS* (2014) arXiv:1402.1022.

[918] CDF Collaboration, "Precise measurement of the W -boson mass with the Collider Detector at Fermilab", *Phys.Rev.* **D89** (2014), no. 7, 072003, doi:10.1103/PhysRevD.89.072003, arXiv:1311.0894.

[919] D0 Collaboration, "Measurement of the W boson mass with the D0 detector", *Phys.Rev.* **D89** (2014), no. 1, 012005, doi:10.1103/PhysRevD.89.012005, arXiv:1310.8628.

[920] ATLAS Collaboration, "Re-evaluation of the LHC potential for the measurement of Mw", *Eur.Phys.J.* **C57** (2008) 627–651, doi:10.1140/epjc/s10052-008-0774-4, arXiv:0805.2093.

[921] V. Buge et al., "Prospects for the precision measurement of the W mass with the CMS detector at the LHC", *J.Phys.* **G34** (2007) N193–N220, doi:10.1088/0954-3899/34/5/N02.

[922] U. Baur and D. Wackeroth, "Electroweak radiative corrections to $p\bar{p} \to W^{\pm} \to \ell^{\pm}\nu$ beyond the pole approximation", *Phys.Rev.* **D70** (2004) 073015, doi:10.1103/PhysRevD.70.073015, arXiv:hep-ph/0405191.

[923] U. Baur et al., "Electroweak radiative corrections to neutral current Drell-Yan processes at hadron colliders", *Phys.Rev.* **D65** (2002) 033007, doi:10.1103/PhysRevD.65.033007,

arXiv:hep-ph/0108274.

[924] S. Dittmaier and . Kramer, Michael, "Electroweak radiative corrections to W boson production at hadron colliders", *Phys.Rev.* **D65** (2002) 073007, doi:10.1103/PhysRevD.65.073007, arXiv:hep-ph/0109062.

[925] A. Arbuzov et al., "One-loop corrections to the Drell-Yan process in SANC. I. The Charged current case", *Eur.Phys.J.* **C46** (2006) 407–412, doi:10.1140/epjc/s2006-02505-y,10.1140/epjc/s10052-007-0225-7, arXiv:hep-ph/0506110.

[926] C. Carloni Calame, G. Montagna, O. Nicrosini, and A. Vicini, "Precision electroweak calculation of the charged current Drell-Yan process", *JHEP* **0612** (2006) 016, doi:10.1088/1126-6708/2006/12/016, arXiv:hep-ph/0609170.

[927] C. Carloni Calame, G. Montagna, O. Nicrosini, and A. Vicini, "Precision electroweak calculation of the production of a high transverse-momentum lepton pair at hadron colliders", *JHEP* **0710** (2007) 109, doi:10.1088/1126-6708/2007/10/109, arXiv:0710.1722.

[928] R. Gavin, Y. Li, F. Petriello, and S. Quackenbush, "W Physics at the LHC with FEWZ 2.1", *Comput.Phys.Commun.* **184** (2013) 208–214, doi:10.1016/j.cpc.2012.09.005, arXiv:1201.5896.

[929] S. Catani et al., "Vector boson production at hadron colliders: a fully exclusive QCD calculation at NNLO", *Phys.Rev.Lett.* **103** (2009) 082001, doi:10.1103/PhysRevLett.103.082001, arXiv:0903.2120.

[930] G. Bozzi et al., "Transverse-momentum resummation: A Perturbative study of Z production at the Tevatron", *Nucl.Phys.* **B815** (2009) 174–197, doi:10.1016/j.nuclphysb.2009.02.014, arXiv:0812.2862.

[931] C. Balazs and C. Yuan, "Soft gluon effects on lepton pairs at hadron colliders", *Phys.Rev.* **D56** (1997) 5558–5583, doi:10.1103/PhysRevD.56.5558, arXiv:hep-ph/9704258.

[932] S. Berge, P. M. Nadolsky, F. Olness, and C.-P. Yuan, "Transverse momentum resummation at small x for the Tevatron and CERN LHC", *Phys.Rev.* **D72** (2005) 033015, doi:10.1103/PhysRevD.72.033015, arXiv:hep-ph/0410375.

[933] T. Ahmed, M. Mahakhud, N. Rana, and V. Ravindran, "Drell-Yan production at threshold in N^3LO QCD", *Phys.Rev.Lett.* **113** (2014) 112002, doi:10.1103/PhysRevLett.113.112002, arXiv:1404.0366.

[934] S. Catani et al., "Threshold resummation at N^3LL accuracy and soft-virtual cross sections at N^3LO", *Nucl.Phys.* **B888** (2014) 75–91, doi:10.1016/j.nuclphysb.2014.09.012, arXiv:1405.4827.

[935] S. Alioli, P. Nason, C. Oleari, and E. Re, "NLO vector-boson production matched with shower in POWHEG", *JHEP* **0807** (2008) 060, doi:10.1088/1126-6708/2008/07/060, arXiv:0805.4802.

[936] S. Frixione, F. Stoeckli, P. Torrielli, and B. R. Webber, "NLO QCD corrections in Herwig++ with MC@NLO", *JHEP* **1101** (2011) 053, doi:10.1007/JHEP01(2011)053, arXiv:1010.0568.

[937] S. Hoche, F. Krauss, M. Schonherr, and F. Siegert, "Automating the POWHEG method in Sherpa", *JHEP* **1104** (2011) 024, doi:10.1007/JHEP04(2011)024, arXiv:1008.5399.

[938] M. Guzzi, P. M. Nadolsky, and B. Wang, "Nonperturbative contributions to a resummed leptonic angular distribution in inclusive neutral vector boson production", *Phys.Rev.* **D90** (2014) 014030, doi:10.1103/PhysRevD.90.014030, arXiv:1309.1393.

[939] W. Giele and S. Keller, "Determination of W boson properties at hadron colliders", *Phys.Rev.* **D57** (1998) 4433–4440, doi:10.1103/PhysRevD.57.4433, arXiv:hep-ph/9704419.

[940] G. Ferrera arXiv:https://indico.cern.ch/event/340393/contribution/1/material/slides/0.pdf.

[941] J. Rojo and A. Vicini, "PDF uncertainties in the extraction of the W mass at LHC: a Snowmass Whitepaper", arXiv:1309.1311.

[942] G. Bozzi, L. Citelli, and A. Vicini, "PDF uncertainties on the W boson mass measurement from the lepton transverse momentum distribution", arXiv:1501.05587.

[943] C. Bernaciak and D. Wackeroth, "Combining NLO QCD and Electroweak Radiative Corrections to W boson Production at Hadron Colliders in the POWHEG Framework", *Phys.Rev.* **D85** (2012) 093003, doi:10.1103/PhysRevD.85.093003, arXiv:1201.4804.

[944] S. Dittmaier, A. Huss, and C. Schwinn, "Mixed QCD-electroweak $\mathcal{O}(\alpha_s\alpha)$ corrections to Drell-Yan processes in the resonance region: pole approximation and non-factorizable corrections", *Nucl.Phys.* **B885** (2014) 318–372, doi:10.1016/j.nuclphysb.2014.05.027, arXiv:1403.3216.

[945] S. Dittmaier, A. Huss, and C. Schwinn, "$O(\alpha_s\alpha)$ corrections to Drell-Yan processes in the resonance region", *PoS* **LL2014** (2014) 045, arXiv:1405.6897.

[946] L. Barzè et al. arXiv:https://indico.cern.ch/event/340393/contribution/4/material/slides/0.pdf.

[947] P. Golonka and Z. Was, "PHOTOS Monte Carlo: A Precision tool for QED correctio ns in Z and W decays", *Eur.Phys.J.* **C45** (2006) 97–107, doi:10.1140/epjc/s2005-02396-4, arXiv:hep-ph/0506026.

[948] S. Gieseke et al., "Herwig++ 2.5 Release Note", arXiv:1102.1672.

[949] K. Arnold et al., "Herwig++ 2.6 Release Note", arXiv:1205.4902.

[950] J. Bellm et al., "Herwig++ 2.7 Release Note", arXiv:1310.6877.

[951] T. Sjostrand, S. Mrenna, and P. Z. Skands, "PYTHIA 6.4 Physics and Manual", *JHEP* **0605** (2006) 026, doi:10.1088/1126-6708/2006/05/026, arXiv:hep-ph/0603175.

[952] T. Gleisberg et al., "SHERPA 1. alpha: A Proof of concept version", *JHEP* **0402** (2004) 056, doi:10.1088/1126-6708/2004/02/056, arXiv:hep-ph/0311263.

[953] CDF, D0 Collaboration, "Combination of CDF and D0 W-Boson Mass Measurements", *Phys.Rev.* **D88** (2013) 052018, doi:10.1103/PhysRevD.88.052018, arXiv:1307.7627.

[954] S. Brensing, S. Dittmaier, . Kramer, Michael, and A. Muck, "Radiative corrections to W^- boson hadroproduction: Higher-order electroweak and supersymmetric effects", *Phys.Rev.* **D77** (2008) 073006, doi:10.1103/PhysRevD.77.073006, arXiv:0710.3309.

[955] S. Dittmaier and M. Huber, "Radiative corrections to the neutral-current Drell-Yan process in the Standard Model and its minimal supersymmetric extension", *JHEP* **1001** (2010) 060, doi:10.1007/JHEP01(2010)060, arXiv:0911.2329.

[956] A. Arbuzov et al., "One-loop corrections to the Drell–Yan process in SANC. (II). The Neutral current case", *Eur.Phys.J.* **C54** (2008) 451–460, doi:10.1140/epjc/s10052-008-0531-8, arXiv:0711.0625.

[957] W. Placzek and S. Jadach, "Multiphoton radiation in leptonic W boson decays", *Eur.Phys.J.* **C29** (2003) 325–339, doi:10.1140/epjc/s2003-01223-4, arXiv:hep-ph/0302065.

[958] D. Bardin et al., "Implementation of SANC EW corrections in WINHAC Monte Carlo generator", *Acta Phys.Polon.* **B40** (2009) 75–92, arXiv:0806.3822.

[959] C. Carloni Calame et al., "Comparisons of the Monte Carlo programs HORACE and WINHAC for single W boson production at hadron colliders", *Acta Phys.Polon.* **B35** (2004) 1643–1674, arXiv:hep-ph/0402235.

[960] TeV4LHC-Top and Electroweak Working Group Collaboration, "Tevatron-for-LHC Report: Top and Electroweak Physics", arXiv:0705.3251.

[961] C. Buttar et al., "Standard Model Handles and Candles Working Group: Tools and Jets Summary Report", arXiv:0803.0678.

[962] C. Buttar et al., "Les houches physics at TeV colliders 2005, standard model and Higgs working group: Summary report", arXiv:hep-ph/0604120.

[963] Y. Li and F. Petriello, "Combining QCD and electroweak corrections to dilepton production in FEWZ", *Phys.Rev.* **D86** (2012) 094034, doi:10.1103/PhysRevD.86.094034, arXiv:1208.5967.

[964] L. Barze et al., "Neutral current Drell-Yan with combined QCD and electroweak corrections in the POWHEG BOX", *Eur.Phys.J.* **C73** (2013), no. 6, 2474, doi:10.1140/epjc/s10052-013-2474-y, arXiv:1302.4606.

[965] G. Cullen et al., "G$OSAM$-2.0: a tool for automated one-loop calculations within the Standard Model and beyond", *Eur.Phys.J.* **C74** (2014), no. 8, 3001, doi:10.1140/epjc/s10052-014-3001-5, arXiv:1404.7096.

[966] G. Bevilacqua et al., "HELAC-NLO", *Comput.Phys.Commun.* **184** (2013) 986–997, doi:10.1016/j.cpc.2012.10.033, arXiv:1110.1499.

[967] V. Hirschi et al., "Automation of one-loop QCD corrections", *JHEP* **1105** (2011) 044, doi:10.1007/JHEP05(2011)044, arXiv:1103.0621.

[968] A. Denner, L. Hofer, A. Scharf, and S. Uccirati, "Electroweak corrections to lepton pair production in association with two hard jets at the LHC", arXiv:1411.0916.

[969] S. Frixione et al., "Weak corrections to Higgs hadroproduction in association with a top-quark pair", *JHEP* **1409** (2014) 065, doi:10.1007/JHEP09(2014)065, arXiv:1407.0823.

[970] S. Frixione et al., "Electroweak and QCD corrections to top-pair hadroproduction in association with heavy bosons", arXiv:1504.03446.

[971] S. Kallweit et al., "NLO electroweak automation and precise predictions for W+multijet production at the LHC", *JHEP* **1504** (2015) 012, doi:10.1007/JHEP04(2015)012, arXiv:1412.5157.

[972] S. Boselli et al., "Higgs boson decay into four leptons at NLOPS electroweak accuracy", arXiv:1503.07394.

[973] P. Ciafaloni and D. Comelli, "Sudakov enhancement of electroweak corrections", *Phys.Lett.* **B446** (1999) 278–284, doi:10.1016/S0370-2693(98)01541-X, arXiv:hep-ph/9809321.

[974] M. Beccaria et al., "Logarithmic expansion of electroweak corrections to four-fermion processes in the TeV region", *Phys.Rev.* **D61** (2000) 073005, doi:10.1103/PhysRevD.61.073005, arXiv:hep-ph/9906319.

[975] M. Ciafaloni, P. Ciafaloni, and D. Comelli, "Bloch-Nordsieck violating electroweak corrections to inclusive TeV scale hard processes", *Phys.Rev.Lett.* **84** (2000) 4810–4813, doi:10.1103/PhysRevLett.84.4810, arXiv:hep-ph/0001142.

[976] M. Ciafaloni, P. Ciafaloni, and D. Comelli, "Electroweak Bloch-Nordsieck violation at the TeV scale: 'Strong' weak interactions?", *Nucl.Phys.* **B589** (2000) 359–380, doi:10.1016/S0550-3213(00)00508-3, arXiv:hep-ph/0004071.

[977] M. Ciafaloni, P. Ciafaloni, and D. Comelli, "Bloch-Nordsieck violation in spontaneously broken Abelian theories", *Phys.Rev.Lett.* **87** (2001) 211802, doi:10.1103/PhysRevLett.87.211802, arXiv:hep-ph/0103315.

[978] V. S. Fadin, L. Lipatov, A. D. Martin, and M. Melles, "Resummation of double logarithms in electroweak high-energy processes", *Phys.Rev.* **D61** (2000) 094002, doi:10.1103/PhysRevD.61.094002, arXiv:hep-ph/9910338.

[979] W. Stirling and E. Vryonidou, "Electroweak corrections and Bloch-Nordsieck violations in 2-to-2 processes at the LHC", *JHEP* **1304** (2013) 155, doi:10.1007/JHEP04(2013)155,

arXiv:1212.6537.

[980] A. Denner and S. Pozzorini, "One loop leading logarithms in electroweak radiative corrections. 1. Results", *Eur.Phys.J.* **C18** (2001) 461–480, doi:10.1007/s100520100551, arXiv:hep-ph/0010201.

[981] A. Denner and S. Pozzorini, "One loop leading logarithms in electroweak radiative corrections. 2. Factorization of collinear singularities", *Eur.Phys.J.* **C21** (2001) 63–79, doi:10.1007/s100520100721, arXiv:hep-ph/0104127.

[982] M. Chiesa et al., "Electroweak Sudakov Corrections to New Physics Searches at the LHC", *Phys.Rev.Lett.* **111** (2013), no. 12, 121801, doi:10.1103/PhysRevLett.111.121801, arXiv:1305.6837.

[983] M. Ciafaloni, P. Ciafaloni, and D. Comelli, "Towards collinear evolution equations in electroweak theory", *Phys.Rev.Lett.* **88** (2002) 102001, doi:10.1103/PhysRevLett.88.102001, arXiv:hep-ph/0111109.

[984] P. Ciafaloni and D. Comelli, "Electroweak evolution equations", *JHEP* **0511** (2005) 022, doi:10.1088/1126-6708/2005/11/022, arXiv:hep-ph/0505047.

[985] J.-y. Chiu, F. Golf, R. Kelley, and A. V. Manohar, "Electroweak Sudakov corrections using effective field theory", *Phys.Rev.Lett.* **100** (2008) 021802, doi:10.1103/PhysRevLett.100.021802, arXiv:0709.2377.

[986] J.-y. Chiu, F. Golf, R. Kelley, and A. V. Manohar, "Electroweak Corrections in High Energy Processes using Effective Field Theory", *Phys.Rev.* **D77** (2008) 053004, doi:10.1103/PhysRevD.77.053004, arXiv:0712.0396.

[987] K. Mishra et al., "Electroweak Corrections at High Energies", arXiv:1308.1430.

[988] S. Jadach, E. Richter-Was, B. Ward, and Z. Was, "Monte Carlo program BHLUMI-2.01 for Bhabha scattering at low angles with Yennie-Frautschi-Suura exponentiation", *Comput.Phys.Commun.* **70** (1992) 305–344, doi:10.1016/0010-4655(92)90196-6.

[989] S. Jadach et al., "Upgrade of the Monte Carlo program BHLUMI for Bhabha scattering at low angles to version 4.04", *Comput.Phys.Commun.* **102** (1997) 229–251, doi:10.1016/S0010-4655(96)00156-7.

[990] M. Cacciari, G. Montagna, O. Nicrosini, and F. Piccinini, "SABSPV: A Monte Carlo integrator for small angle Bhabha scattering", *Comput.Phys.Commun.* **90** (1995) 301–310, doi:10.1016/0010-4655(95)00102-L, arXiv:hep-ph/9507245.

[991] C. Carloni Calame et al., "Large angle Bhabha scattering and luminosity at flavor factories", *Nucl.Phys.* **B584** (2000) 459–479, doi:10.1016/S0550-3213(00)00356-4, arXiv:hep-ph/0003268.

[992] G. Balossini et al., "Matching perturbative and parton shower corrections to Bhabha process at flavour factories", *Nucl.Phys.* **B758** (2006) 227–253, doi:10.1016/j.nuclphysb.2006.09.022, arXiv:hep-ph/0607181.

[993] G. Balossini et al., "Photon pair production at flavour factories with per mille accuracy", *Phys.Lett.* **B663** (2008) 209–213, doi:10.1016/j.physletb.2008.04.007, arXiv:0801.3360.

[994] Working Group on Radiative Corrections and Monte Carlo Generators for Low Energies Collaboration, "Quest for precision in hadronic cross sections at low energy: Monte Carlo tools vs. experimental data", *Eur.Phys.J.* **C66** (2010) 585–686, doi:10.1140/epjc/s10052-010-1251-4, arXiv:0912.0749.

[995] S. Jadach, B. Ward, and Z. Was, "The Monte Carlo program KORALZ, version 4.0, for the lepton or quark pair production at LEP / SLC energies", *Comput.Phys.Commun.* **79** (1994) 503–522, doi:10.1016/0010-4655(94)90190-2.

[996] S. Jadach, B. Ward, and Z. Was, "The Precision Monte Carlo event generator K K for two fermion final states in e+ e- collisions", *Comput.Phys.Commun.* **130** (2000) 260–325, doi:10.1016/S0010-4655(00)00048-5, arXiv:hep-ph/9912214.

[997] G. Montagna et al., "On a semianalytical and realistic approach to e^+e^- annihilation into fermion pairs and to Bhabha scattering within the minimal Standard Model at LEP energies", *Nucl.Phys.* **B401** (1993) 3–66, doi:10.1016/0550-3213(93)90297-3.

[998] G. Montagna et al., "TOPAZ0: A Program for computing observables and for fitting cross-sections and forward - backward asymmetries around the Z0 peak", *Comput.Phys.Commun.* **76** (1993) 328–360, doi:10.1016/0010-4655(93)90060-P.

[999] G. Montagna, O. Nicrosini, G. Passarino, and F. Piccinini, "TOPAZO 2.0: A Program for computing deconvoluted and realistic observables around the Z0 peak", *Comput.Phys.Commun.* **93** (1996) 120–126, doi:10.1016/0010-4655(95)00127-1, arXiv:hep-ph/9506329.

[1000] G. Montagna, O. Nicrosini, F. Piccinini, and G. Passarino, "TOPAZ0 4.0: A New version of a computer program for evaluation of deconvoluted and realistic observables at LEP-1 and LEP-2", *Comput.Phys.Commun.* **117** (1999) 278–289, doi:10.1016/S0010-4655(98)00080-0, arXiv:hep-ph/9804211.

[1001] D. Y. Bardin et al., "A Realistic Approach to the Standard Z Peak", *Z.Phys.* **C44** (1989) 493, doi:10.1007/BF01415565.

[1002] D. Y. Bardin et al., "Dizet: A Program Package for the Calculation of Electroweak One Loop Corrections for the Process $e^+e^-f^+f^-$ Around the Z^0 Peak", *Comput.Phys.Commun.* **59** (1990) 303–312, doi:10.1016/0010-4655(90)90179-5.

[1003] D. Y. Bardin et al., "ZFITTER: An Analytical program for fermion pair production in e^+e^- annihilation", arXiv:hep-ph/9412201.

[1004] D. Y. Bardin et al., "ZFITTER v.6.21: A Semianalytical program for fermion pair production in e^+e^- annihilation", *Comput.Phys.Commun.* **133** (2001) 229–395, doi:10.1016/S0010-4655(00)00152-1, arXiv:hep-ph/9908433.

[1005] S. Actis, A. Ferroglia, M. Passera, and G. Passarino, "Two-Loop Renormalization in the Standard Model. Part I: Prolegomena", *Nucl.Phys.* **B777** (2007) 1–34, doi:10.1016/j.nuclphysb.2007.04.021, arXiv:hep-ph/0612122.

[1006] S. Actis and G. Passarino, "Two-Loop Renormalization in the Standard Model Part II: Renormalization Procedures and Computational Techniques", *Nucl.Phys.* **B777** (2007) 35–99, doi:10.1016/j.nuclphysb.2007.03.043, arXiv:hep-ph/0612123.

[1007] S. Actis and G. Passarino, "Two-Loop Renormalization in the Standard Model Part III: Renormalization Equations and their Solutions", *Nucl.Phys.* **B777** (2007) 100–156, doi:10.1016/j.nuclphysb.2007.04.027, arXiv:hep-ph/0612124.

[1008] W. Beenakker et al., "WW cross-sections and distributions", arXiv:hep-ph/9602351.

[1009] D. Y. Bardin et al., "Event generators for WW physics", arXiv:hep-ph/9709270.

[1010] M. S. Carena et al., "Higgs physics at LEP-2", arXiv:hep-ph/9602250.

[1011] A. Denner, S. Dittmaier, M. Roth, and D. Wackeroth, "O(alpha) corrections to $e^+e^- \to WW \to$ four fermions (+ γ): First numerical results from RACOON W W", *Phys.Lett.* **B475** (2000) 127–134, doi:10.1016/S0370-2693(00)00059-9, arXiv:hep-ph/9912261.

[1012] A. Denner, S. Dittmaier, M. Roth, and D. Wackeroth, "RACOONWW1.3: A Monte Carlo program for four fermion production at e+ e- colliders", *Comput.Phys.Commun.* **153** (2003) 462–507, doi:10.1016/S0010-4655(03)00205-4, arXiv:hep-ph/0209330.

[1013] A. Denner, S. Dittmaier, M. Roth, and L. Wieders, "Complete electroweak $\mathcal{O}(\alpha)$ corrections to charged-current $e^+e^- \to 4$ fermion processes", *Phys.Lett.* **B612** (2005) 223–232,

doi:10.1016/j.physletb.2005.03.007,10.1016/j.physletb.2011.09.020, arXiv:hep-ph/0502063.

[1014] A. Denner, S. Dittmaier, M. Roth, and L. Wieders, "Electroweak corrections to charged-current $e^+e^- \to 4$ fermion processes: Technical details and further results", *Nucl.Phys.* **B724** (2005) 247–294, doi:10.1016/j.nuclphysb.2011.09.001,10.1016/j.nuclphysb.2005.06.033, arXiv:hep-ph/0505042.

[1015] CMS Collaboration *Phys. Rev. Lett.* **111** (2013) 101804.

[1016] CMS Collaboration, "CMS reach in B[s] to dimuon and B to dimuon branching fractions for the new LHC runs", Technical Report CMS-PAS-FTR-13-022, CERN, Geneva, 2013.

[1017] L. Lellouch, "Phenomenology from lattice QCD", *Nucl.Phys.Proc.Suppl.* **117** (2003) 127–144, doi:10.1016/S0920-5632(03)01415-4, arXiv:hep-ph/0211359.

[1018] S. Aoki et al., "Review of lattice results concerning low-energy particle physics", *Eur.Phys.J.* **C74** (2014), no. 9, 2890, doi:10.1140/epjc/s10052-014-2890-7, arXiv:1310.8555.

[1019] http://www.top500.org/.

[1020] S.Sharpe, talk given at the workshop: *Lattice QCD: Present and Future*, Orsay (France), April 14-16 2004, http://events.lal.in2p3.fr/conferences/lqcd/.

[1021] L. Del Debbio et al., "QCD with light Wilson quarks on fine lattices (I): First experiences and physics results", *JHEP* **0702** (2007) 056, doi:10.1088/1126-6708/2007/02/056, arXiv:hep-lat/0610059.

[1022] M. Clark, "The Rational Hybrid Monte Carlo Algorithm", *PoS* **LAT2006** (2006) 004, arXiv:hep-lat/0610048.

[1023] S. Borsanyi et al., "Ab initio calculation of the neutron-proton mass difference", arXiv:1406.4088.

[1024] G. de Divitiis et al., "Isospin breaking effects due to the up-down mass difference in Lattice QCD", *JHEP* **1204** (2012) 124, doi:10.1007/JHEP04(2012)124, arXiv:1110.6294.

[1025] RM123 Collaboration, "Leading isospin breaking effects on the lattice", *Phys.Rev.* **D87** (2013), no. 11, 114505, doi:10.1103/PhysRevD.87.114505, arXiv:1303.4896.

[1026] MILC Collaboration, "Finite-volume effects and the electromagnetic contributions to kaon and pion masses", *PoS* **LATTICE2014** (2014) arXiv:1409.7139.

[1027] T. Ishikawa et al., "Full QED+QCD low-energy constants through reweighting", *Phys.Rev.Lett.* **109** (2012) 072002, doi:10.1103/PhysRevLett.109.072002, arXiv:1202.6018.

[1028] S. Aoki et al., "1+1+1 flavor QCD + QED simulation at the physical point", *Phys.Rev.* **D86** (2012) 034507, doi:10.1103/PhysRevD.86.034507, arXiv:1205.2961.

[1029] T. Blum et al., "Electromagnetic mass splittings of the low lying hadrons and quark masses from 2+1 flavor lattice QCD+QED", *Phys.Rev.* **D82** (2010) 094508, doi:10.1103/PhysRevD.82.094508, arXiv:1006.1311.